Hashemite Kingdom of Jordan

Jordan Journal of Biological Sciences

An International Peer-Reviewed Scientific Journal

Financed by the Scientific Research and Innovation Support Fund

This title is indexed in Scopus

http://jjbs.hu.edu.jo/

المجلة الأردنية للعلوم الحياتية
Jordan Journal of Biological Sciences (JJBS)
http://jjbs.hu.edu.jo

Jordan Journal of Biological Sciences (JJBS) (ISSN: 1995–6673 (Print); 2307-7166 (Online)): An International Peer- Reviewed Open Access Research Journal financed by the Scientific Research and Innovation Support Fund, Ministry of Higher Education and Scientific Research, Jordan and published quarterly by the Deanship of Scientific Research , The Hashemite University, Jordan.

Submission Address
Professor Atoum, Manar F
The Hashemite Universit y
P.O. Box 330127, Zarqa, 13115, Jordan
Phone: +962-5-3903333 ext.4147
E-Mail: jjbs@hu.edu.jo

المجلة الاردنية للعلوم الحياتية
Jordan Journal of Biological Sciences (JJBS)
http://jjbs.hu.edu.jo

International Advisory Board (Arranged alphabetically)

Instructions to Authors

Scopes

Study areas include cell biology, genomics, microbiology, immunology, molecular biology, biochemistry, embryology, immunogenetics, cell and tissue culture, molecular ecology, genetic engineering and biological engineering, bioremediation and biodegradation, bioinformatics, biotechnology regulations, gene therapy, organismal biology, microbial and environmental biotechnology, marine sciences. The JJBS welcomes the submission of manuscript that meets the general criteria of significance and academic excellence. All articles published in JJBS are peer-reviewed. Papers will be published approximately one to two months after acceptance.

Type of Papers

The journal publishes high-quality original scientific papers, short communications, correspondence and case studies. Review articles are usually by invitation only. However, Review articles of current interest and high standard will be considered.

Submission of Manuscript

Manuscript, or the essence of their content, must be previously unpublished and should not be under simultaneous consideration by another journal. The authors should also declare if any similar work has been submitted to or published by another journal. They should also declare that it has not been submitted/ published elsewhere in the same form, in English or in any other language, without the written consent of the Publisher. The authors should also declare that the paper is the original work of the author(s) and not copied (in whole or in part) from any other work. All papers will be automatically checked for duplicate publication and plagiarism. If detected, appropriate action will be taken in accordance with International Ethical Guideline. By virtue of the submitted manuscript, the corresponding author acknowledges that all the co-authors have seen and approved the final version of the manuscript. The corresponding author should provide all co-authors with information regarding the manuscript, and obtain their approval before submitting any revisions. Electronic submission of manuscripts is strongly recommended, provided that the text, tables and figures are included in a single Microsoft Word file. Submit manuscript as e-mail attachment to the Editorial Office at: JJBS@hu.edu.jo. After submission, a manuscript number will be communicated to the corresponding author within 48 hours.

Peer-review Process

It is requested to submit, with the manuscript, the names, addresses and e-mail addresses of at least 4 potential reviewers. It is the sole right of the editor to decide whether or not the suggested reviewers to be used. The reviewers' comments will be sent to authors within 6-8 weeks after submission.
Manuscripts and figures for review will not be returned to authors whether the editorial decision is to accept, revise, or reject. All Case Reports and Short Communication must include at least one table and/ or one figure.

Preparation of Manuscript

The manuscript should be written in English with simple lay out. The text should be prepared in single column format. Bold face, italics, subscripts, superscripts etc. can be used. Pages should be numbered consecutively, beginning with the title page and continuing through the last page of typewritten material.

The text can be divided into numbered sections with brief headings. Starting from introduction with section 1. Subsections should be numbered (for example 2.1 (then 2.1.1, 2.1.2, 2.2, etc.), up to three levels. Manuscripts in general should be organized in the following manner:

Title Page

The title page should contain a brief title, correct first name, middle initial and family name of each author and name and address of the department(s) and institution(s) from where the research was carried out for each author. The title should be without any abbreviations and it should enlighten the contents of the paper. All affiliations should be provided with a lower-case superscript number just after the author's name and in front of the appropriate address.
The name of the corresponding author should be indicated along with telephone and fax numbers (with country and area code) along with full postal address and e-mail address.

Abstract

The abstract should be concise and informative. It should not exceed **350 words** in length for full manuscript and Review article and **150 words** in case of Case Report and/ or Short Communication. It should briefly describe the purpose of the work, techniques and methods used, major findings with important data and conclusions. No references should be cited in this part. Generally non-standard abbreviations should not be used, if necessary they should be clearly defined in the abstract, at first use.

Keywords

Immediately after the abstract, **about 4-8 keywords** should be given. Use of abbreviations should be avoided, only standard abbreviations, well known in the established area may be used, if appropriate. These keywords will be used for indexing.

Abbreviations

Non-standard abbreviations should be listed and full form of each abbreviation should be given in parentheses at first use in the text.

Introduction

Provide a factual background, clearly defined problem, proposed solution, a brief literature survey and the scope and justification of the work done.

Materials and Methods

Give adequate information to allow the experiment to be reproduced. Already published methods should be mentioned with references. Significant modifications of published methods and new methods should be described in detail. Capitalize trade names and include the manufacturer's name and address. Subheading should be used.

Results

Results should be clearly described in a concise manner. Results for different parameters should be described under subheadings or in separate paragraph. Results should be explained, but largely without referring to the literature. Table or figure numbers should be mentioned in parentheses for better understanding.

Discussion

The discussion should not repeat the results, but provide detailed interpretation of data. This should interpret the significance of the findings of the work. Citations should be given in support of the findings. The results and discussion part can also be described as separate, if appropriate. The Results and Discussion sections can include subheadings, and when appropriate, both sections can be combined

Conclusions

This should briefly state the major findings of the study.

Acknowledgment

A brief acknowledgment section may be given after the conclusion section just before the references. The acknowledgment of people who provided assistance in manuscript preparation, funding for research, etc. should be listed in this section.

Tables and Figures

Tables and figures should be presented as per their appearance in the text. It is suggested that the discussion about the tables and figures should appear in the text before the appearance of the respective tables and figures. No tables or figures should be given without discussion or reference inside the text.

Tables should be explanatory enough to be understandable without any text reference. Double spacing should be maintained throughout the table, including table headings and footnotes. Table headings should be placed above the table. Footnotes should be placed below the table with superscript lowercase letters. Each table should be on a separate page, numbered consecutively in Arabic numerals.

Each figure should have a caption. The caption should be concise and typed separately, not on the figure area. Figures should be self-explanatory. Information presented in the figure should not be repeated in the table. All symbols and abbreviations used in the illustrations should be defined clearly. Figure legends should be given below the figures.

References

References should be listed alphabetically at the end of the manuscript. Every reference referred in the text must be also present in the reference list and vice versa. In the text, a reference identified by means of an author's name should be followed by the year of publication in parentheses (e.g.(Brown,2009)). For two authors, both authors' names followed by the year of publication (e.g.(Nelson and Brown, 2007)). When there are more than two authors, only the first author's name followed by "*et al*." and the year of publication (e.g. (Abu-Elteen *et al*., 2010)). When two or more works of an author has been published during the same year, the reference should be identified by the letters "a", "b", "c", etc., placed after the year of publication. This should be followed both in the text and reference list. e.g., Hilly, (2002a, 2002b); Hilly, and Nelson, (2004). Articles in preparation or submitted for publication, unpublished observations, personal communications, etc. should not be included in the reference list but should only be mentioned in the article text (e.g., Shtyawy,A., University of Jordan, personal communication). Journal titles should be abbreviated according to the system adopted in Biological Abstract and Index Medicus, if not included in Biological Abstract or Index Medicus journal title should be given in full. The author is responsible for the sccuracy and completeness of the references and for their correct textual citation. Failure to do so may result in the paper being withdraw from the evaluation process. Example of correct reference form is given as follows:-

Reference to a journal publication:

Bloch BK. 2002. Econazole nitrate in the treatment of *Candida vaginitis*. *S Afr Med J.* , **58**:314-323.

Ogunseitan OA and Ndoye IL. 2006. Protein method for investigating mercuric reductase gene expression in aquatic environments. *Appl Environ Microbiol*., **64**: 695-702.

Hilly MO, Adams MN and Nelson SC. 2009. Potential fly-ash utilization in agriculture. *Progress in Natural Sci.*, **19**: 1173-1186.

Reference to a book:

Brown WY and White SR.1985. **The Elements of Style**, third ed. MacMillan, New York.

Reference to a chapter in an edited book:

Mettam GR and Adams LB. 2010. How to prepare an electronic version of your article. In: Jones BS and Smith RZ (Eds.), **Introduction to the Electronic Age**. Kluwer Academic Publishers, Netherlands, pp. 281–304.

Conferences and Meetings:

Embabi NS. 1990. Environmental aspects of distribution of mangrove in the United Arab Emirates. Proceedings of the First ASWAS Conference. University of the United Arab Emirates. Al-Ain, United Arab Emirates.

Theses and Dissertations:

El-Labadi SN. 2002. Intestinal digenetic trematodes of some marine fishes from the Gulf of Aqaba. MSc dissertation, The Hashemite University, Zarqa, Jordan.

Nomenclature and Units

Internationally accepted rules and the international system of units (SI) should be used. If other units are mentioned, please give their equivalent in SI.

For biological nomenclature, the conventions of the *International Code of Botanical Nomenclature, the International Code of Nomenclature of Bacteria,* and the *International Code of Zoological Nomenclature* should be followed.
Scientific names of all biological creatures (crops, plants, insects, birds, mammals, etc.) should be mentioned in parentheses at first use of their English term.

Chemical nomenclature, as laid down in the *International Union of Pure and Applied Chemistry* and the official recommendations of the *IUPAC-IUB Combined Commission on Biochemical Nomenclature* should be followed. All biocides and other organic compounds must be identified by their Geneva names when first used in the text. Active ingredients of all formulations should be likewise identified.

Math formulae

All equations referred to in the text should be numbered serially at the right-hand side in parentheses. Meaning of all symbols should be given immediately after the equation at first use. Instead of root signs fractional powers should be used. Subscripts and superscripts should be presented clearly. Variables should be presented in italics. Greek letters and non-Roman symbols should be described in the margin at their first use.

To avoid any misunderstanding zero (0) and the letter O, and one (1) and the letter l should be clearly differentiated. For simple fractions use of the solidus (/) instead of a horizontal line is recommended. Levels of statistical significance such as: $^{*}P < 0.05$, $^{**}P < 0.01$ and $^{***}P < 0.001$ do not require any further explanation.

Copyright

Submission of a manuscript clearly indicates that: the study has not been published before or is not under consideration for publication elsewhere (except as an abstract or as part of a published lecture or academic thesis); its publication is permitted by all authors and after accepted for publication it will not be submitted for publication anywhere else, in English or in any other language, without the written approval of the copyright-holder. The journal may consider manuscripts that are translations of articles originally published in another language. In this case, the consent of the journal in which the article was originally published must be obtained and the fact that the article has already been published must be made clear on submission and stated in the abstract. It is compulsory for the authors to ensure that no material submitted as part of a manuscript infringes existing copyrights, or the rights of a third party.

Ethical Consent

All manuscripts reporting the results of experimental investigation involving human subjects should include a statement confirming that each subject or subject's guardian obtains an informed consent, after the approval of the experimental protocol by a local human ethics committee or IRB. When reporting experiments on animals, authors should indicate whether the institutional and national guide for the care and use of laboratory animals was followed.

Plagiarism

The JJBS hold no responsibility for plagiarism. If a published paper is found later to be extensively plagiarized and is found to be a duplicate or redundant publication, a note of retraction will be published, and copies of the correspondence will be sent to the authors' head of institute.

Galley Proofs

The Editorial Office will send proofs of the manuscript to the corresponding author as an e-mail attachment for final proof reading and it will be the responsibility of the corresponding author to return the galley proof materials appropriately corrected within the stipulated time. Authors will be asked to check any typographical or minor clerical errors in the manuscript at this stage. No other major alteration in the manuscript is allowed. After publication authors can freely access the full text of the article as well as can download and print the PDF file.

Publication Charges

There are no page charges for publication in Jordan Journal of Biological Sciences, except for color illustrations,

Reprints

Ten (10) reprints are provided to corresponding author free of charge within two weeks after the printed journal date. For orders of more reprints, a reprint order form and prices will be sent with article proofs, which should be returned directly to the Editor for processing.

Disclaimer

Articles, communication, or editorials published by JJBS represent the sole opinions of the authors. The publisher shoulders no responsibility or liability what so ever for the use or misuse of the information published by JJBS.

Indexing

JJBS is indexed and abstracted by:

DOAJ (Directory of Open Access Journals)	CABI
Google Scholar	EBSCO
Journal Seek	CAS (Chemical Abstract Service)
HINARI	ETH- Citations
Index Copernicus	Open J-Gat
NDL Japanese Periodicals Index	SCImago
SCIRUS	Clarivate Analytics (Zoological Abstract)
OAJSE	Scopus
ISC (Islamic World Science Citation Center)	AGORA (United Nation's FAO database)
Directory of Research Journal Indexing (DRJI)	SHERPA/RoMEO (UK)
Ulrich's	

المجلة الأردنية للعلوم الحياتية
Jordan Journal of Biological Sciences (JJBS)
ISSN 1995- 6673 (Print), 2307- 7166 (Online)
http://jjbs.hu.edu.jo

The Hashemite University

Deanship of Scientific Research

TRANSFER OF COPYRIGHT AGREEMENT

Journal publishers and authors share a common interest in the protection of copyright: authors principally because they want their creative works to be protected from plagiarism and other unlawful uses, publishers because they need to protect their work and investment in the production, marketing and distribution of the published version of the article. In order to do so effectively, publishers request a formal written transfer of copyright from the author(s) for each article published. Publishers and authors are also concerned that the integrity of the official record of publication of an article (once refereed and published) be maintained, and in order to protect that reference value and validation process, we ask that authors recognize that distribution (including through the Internet/WWW or other on-line means) of the authoritative version of the article as published is best administered by the Publisher.

To avoid any delay in the publication of your article, please read the terms of this agreement, sign in the space provided and return the complete form to us at the address below as quickly as possible.

Article entitled:----------

Corresponding author: ----------

To be published in the journal: Jordan Journal of Biological Sciences (JJBS)

I hereby assign to the Hashemite University the copyright in the manuscript identified above and any supplemental tables, illustrations or other information submitted therewith (the "article") in all forms and media (whether now known or hereafter developed), throughout the world, in all languages, for the full term of copyright and all extensions and renewals thereof, effective when and if the article is accepted for publication. This transfer includes the right to adapt the presentation of the article for use in conjunction with computer systems and programs, including reproduction or publication in machine-readable form and incorporation in electronic retrieval systems.
Authors retain or are hereby granted (without the need to obtain further permission) rights to use the article for traditional scholarship communications, for teaching, and for distribution within their institution.

☐ **I am the sole author of the manuscript**

☐ **I am signing on behalf of all co-authors of the manuscript**

☐ **The article is a 'work made for hire' and I am signing as an authorized representative of the employing company/institution**

Please mark one or more of the above boxes (as appropriate) and then sign and date the document in black ink.

Signed:_____ **Name printed:** _____
Title and Company (if employer representative) : _____
Date: _____

Data Protection: By submitting this form you are consenting that the personal information provided herein may be used by the Hashemite University and its affiliated institutions worldwide to contact you concerning the publishing of your article.

Please return the completed and signed original of this form by mail or fax, or a scanned copy of the signed original by e-mail, retaining a copy for your files, to:

Hashemite University
Jordan Journal of Biological Sciences
Zarqa 13115 Jordan
Fax: +962 5 3903338
Email: jjbs@hu.edu.jo

EDITORIAL PREFACE

Jordan Journal of Biological Sciences (JJBS) is a refereed, quarterly international journal financed by the Scientific Research and Innovation Support Fund, Ministry of Higher Education and Scientific Research in cooperation with the Hashemite University, Jordan. JJBS celebrated its 12th commencement this past January, 2020. JJBS was founded in 2008 to create a peer-reviewed journal that publishes high-quality research articles, reviews and short communications on novel and innovative aspects of a wide variety of biological sciences such as cell biology, developmental biology, structural biology, microbiology, entomology, molecular biology, biochemistry, medical biotechnology, biodiversity, ecology, marine biology, plant and animal biology, plant and animal physiology, genomics and bioinformatics.

We have watched the growth and success of JJBS over the years. JJBS has published 11 volumes, 45 issues and 479 articles. JJBS has been indexed by SCOPUS, CABI's Full-Text Repository, EBSCO, Clarivate Analytics- Zoological Record and recently has been included in the UGC India approved journals. JJBS Cite Score has improved from 0.18 in 2015 to 0.7 in 2019 (Last updated on 1 March, 2021) and with Scimago Institution Ranking (SJR) 0.18 (Q3) in 2019.

A group of highly valuable scholars have agreed to serve on the editorial board and this places JJBS in a position of most authoritative on biological sciences. I am honored to have six eminent associate editors from various countries. I am also delighted with our group of international advisory board members coming from 15 countries worldwide for their continuous support of JJBS. With our editorial board's cumulative experience in various fields of biological sciences, this journal brings a substantial representation of biological sciences in different disciplines. Without the service and dedication of our editorial; associate editorial and international advisory board members, JJBS would have never existed.

In the coming year, we hope that JJBS will be indexed in Clarivate Analytics and MEDLINE (the U.S. National Library of Medicine database) and others. As you read throughout this volume of JJBS, I would like to remind you that the success of our journal depends on the number of quality articles submitted for review. Accordingly, I would like to request your participation and colleagues by submitting quality manuscripts for review. One of the great benefits we can provide to our prospective authors, regardless of acceptance of their manuscripts or not, is the feedback of our review process. JJBS provides authors with high quality, helpful reviews to improve their manuscripts.

Finally, JJBS would not have succeeded without the collaboration of authors and referees. Their work is greatly appreciated. Furthermore, my thanks are also extended to The Hashemite University and the Scientific Research and Innovation Support Fund, Ministry of Higher Education and Scientific Research for their continuous financial and administrative support to JJBS.

Professor Atoum, Manar F.
March, 2021

JJBS

Volume 15, Number 4, December 2022
ISSN 1995-6673

Jordan Journal of Biological Sciences

CONTENTS

Original Articles

JJBS

Volume 15, Number 4,December 2022
ISSN 1995-6673
Pages 537 – 541
https://doi.org/10.54319/jjbs/150401

Jordan Journal of Biological Sciences

Incidence of *Helicobacter pylori* Infection among Hashimoto's Thyroiditis Patients in Amara City, Iraq

Younus JasimAbdullah[1,*], Rajwa Hasen Essa[2], and Misa Ghazi Jumaa[3]

[1]*Southern Technical University, Amara technical Institute, Amara city, Iraq.* [2]*Prof. of immunology. Almustansiriyah University, College of sciences, Biology department, Baghdad, Iraq.*[3]*Assist prof. of microbiology. Maisan University, College of Medicine, Amara city, Iraq..*

Received: Jan9, 2022; Revised: April 7, 2022; Accepted April, 7, 2022

Abstract

The association of different infections with the subsequent occurrence of autoimmunity, just like autoimmune thyroiditis, has recently been increased globally. This study aimed to determine the role of *Helicobacter pylori* (HP) infection in Hashimoto's disease. The research groups involved 50 patients with Hashimoto's disease and 50 healthy subjects. All of them were subjected to the estimation of concentrations of free triiodothyronine (FT3), free thyroxine (FT4), TSH, anti-thyroid peroxidase (anti-TPO), and anti-thyroglobulin (anti-Tg). In addition, for the diagnosis of HP, IgG, as well as anti-CagA antibodies in the serum, were detected. An independent t-test was used to test the significance of the means. Also, an odd ratio was used to clarify the association between *H. pylori* infection and HT disease. Statistical significance was detected when *P-value* is equal to or less than 0.05. The results indicated that 94% of Hashimoto's patients and 34% of the healthy subjects were seropositive for HP IgG. Also, (74%) of the HT patients were seropositive for HP IgG/anti-CagA. These results were significant at the level of 0.01 ($p< 0.001$). Hashimoto's patients with HP/CagA positive tests have significantly elevated concentrations of anti-TPO (480.69±311.29), anti-Tg (336.00±175.95), and TSH (20.43±18.98) compared with patients tested negatively to HP/CagA antibodies (358.60±281.55, 258.36±170.09 and 9.02±5.94 respectively). In conclusion, there is a relationship between *H. pylori* infection and the development of Hashimoto's thyroiditis in Iraqi patients. *H. pylori* infection, especially CagA expressing strains, could be a risk factor for the development of autoimmune hypothyroidism and to a lesser extent its progression by increasing the concentration of thyroid antibodies and TSH, which in turn leads to decreased levels of the thyroid hormones and worsening of the disease, requesting antibiotic therapy to eradicate the bacterial infection.

Keywords: Hashimoto's thyroiditis, *H. pylori infection,* correlation, anti-TPO, anti-Tg, CagA.

1. Introduction:

Autoimmune thyroid diseases (AITDs) are many distinct clinical disorders, of which Hashimoto's hypothyroidism (HT) and Graves' hyperthyroidism are the most prominent (Caturegli *et al*., 2014). They reflect examples of autoimmune organic-specific diseases which are restricted to the thyroid gland. HT is highly abundant in a female with an incidence ratio of about 8:1(Casto *et al*.,2021). However, according to the positive results of laboratory tests in women for the occurrence of autoantibodies for thyroid, about 10% of the population are suffering from HT (Machała *et al*.,2019). In the pathogenesis, the thyroid antigens may be presented by dendritic cells as foreign antigens to the T-cells leading to its proliferation and differentiation into thyroid-specific T-cells (Th1, Th2, and CD+8) producing different cytokines like IL-12, IL-17, and IFN-α which in turn mediate thyroid infiltration and cytotoxicity (Ramos-Leví, and Marazuela, 2016; Machała *et al*.,2019). Although the exact cause of AITD is unknown, they are genetically expressed and require an environmental trigger (Ragusa *et al*.,2019). Infection with *Helicobacter pylori* (HP), a gram-negative, motile, microaerophilic bacteria, is a potential environmental factor, causing persistent inflammation and immunological response in vulnerable individuals (Choi *et al*.,2017).

Studies have revealed that levels of anti-*H. pylori* cytotoxin-associated gene A product (anti-CagA) are significantly higher in HT patients than in healthy controls (Figura *et al*.,1999). CagA expressing strains of *H. pylori* have higher inflammatory activity, and they raise inflammatory cytokine levels in the stomach and throughout the body in an infected person, which may be associated with the extra-intestinal consequences of the host tissues and the subsequent development of autoimmunity (Figura *et al*., 2020). However, researchers are unable to clarify the *H. pylori-related* consequences that can cause thyroid autoimmunity. Also, the specific processes by which exposure to a microorganism induces more than one manifestation of autoimmunity (Hamid,2017; Hou *et al*., 2017). Delitala *et al* have suggested that *H. pylori* may expose the host's sequestered epitopes to the immune system leading to the development of autoimmune reaction (Delitala *et al*.,2016). In this context, the current study aimed to investigate the correlation between *H. pylori* infection and Hashimoto's thyroiditis and to evaluate if there is an effect of *H.*

* Corresponding author. e-mail: younusjasim@stu.edu.iq.

pylori on the serum levels of thyroid hormones and TSH in the patients.

2. Materials and Methods

The present study involved 100 persons (males and females) aging between (9-50 years) during the period from Dec. 2019 to Dec. 2020. Study participants were classified into two groups. The 1st group (50 patients) attended the specified center of diabetes and endocrine glands diseases in Amara city with symptoms suspected to have Hashimoto thyroiditis which was confirmed using serological tests for the detection of anti-TPO and anti-Tg. The second group (50 persons) were healthy persons of comparable age and sex and considered a control group. They were all subjected to serologic tests for the diagnosis of autoimmune thyroiditis. All of the study participants have read and signed the patient consent form, and the study has been approved by the Committee of Scientific Research Ethics / Amara Medical Institute.

3. Sample collection

Ten ml of venous blood was collected from all the study participants then centrifuged at 5000 rpm /min for 5 mins and the obtained sera were used for the serological methods for the estimation of thyroid antibodies (Anti-TPO and Anti-Tg) as well as thyroid hormones (FT3, FT4) and TSH.

4. Estimation of thyroid hormones levels in the serum

Serum levels of the thyroid hormones free triiodothyronine (fT3), free thyroxine (fT4), and thyroid-stimulating hormone (TSH) were determined on the same day of blood collection by using the electrochemiluminescence immunoassay method (Cobas, comp. Penzberg, Germany). The results were expressed in IU/mL as per the manufacturer's instruction.

5. Detection of thyroid auto-antibodies in the serum

Serum concentrations of anti-Tg and anti-TPO were evaluated using a chemiluminescent immunoassay (Mindray, China). As per the instructions of the manufacturer, the results have been recorded in IU/mL.

6. Detection of H. pylori infection

H. pylori infection in HT patients and control group has been diagnosed by using two ELISA kits (Hp-IgG, Monobind Inc. USA and anti-CagA, Sunlong Biotech. China). Biotech ELISA reader and washer (Biotech, USA) was used, and the procedure was applied; results were achieved as per the manufacturer's instructions.

7. Statistical analysis

Results of the current study were analyzed using SPSS software package ver.23 (performed by IBM Co. USA). An independent t-test was used to test the significance of the means. Also, an odd ratio was used to clarify the association between *H. pylori* infection and HT disease. Statistical significance was considered when *the P-value* is equal to or less than 0.05.

8. Results

The current study is a case-control study that involved (50) HT patients and (50) healthy controls. All of the study participants were subjected to the estimation of serum FT3, FT4, TSH, anti-TPO, and anti-Tg. The results found a significant increase in serum TSH concentrations (P <0.001) in HT patients compared to healthy subjects as shown in table (1). Serum FT4 and FT3 concentrations were also elevated in HT patients compared to the control group which is not statistically significant.

Table 1: Serum concentration of thyroid hormones in HT patients and healthy controls.

Hormones	HT group Mean ± SD	Control group Mean ± SD	*P* value
FT3 (pmol/L)	4.76±1.50	7.84±4.39	0.031*
FT4 (pmol/L)	12.07±4.27	15.57±3.58	0.056*
TSH (µIU/ml)	18.53±17.60	2.45±1.50	<0.001**

**Results are significant at 0.01 level. *Results are significant at 0.05 level. SD: standard deviation

The levels of both of anti – TPO antibodies, as well as anti - Tg antibodies, are significantly increased (*P-value* < 0.001) in HT patients against the healthy group, table (2).

Table 2: Serum concentration of thyroid auto-antibodies in the study groups.

Thyroid antibodies	HT patients Mean ± SD	Control Mean ± SD	*P* value	Reference value
Anti-TPO (IU/L)	424.79 ± 381.90	1.92 ±0.08	<0.001**	(≤ 9IU/ml)
Anti-Tg (IU/L)	56.76 ± 15.41	3.59 ±5.07	<0.001**	(≤ 4IU/ml)

**Results are significant at 0.01% level. SD: standard deviation

The incidence of *H. pylori* antibodies (IgG, CagA) among HT patients and the healthy control group is described in table (3). The HT patients with positive *H. pylori* IgG were significantly higher (47 of 50, 94%) compared to the healthy subjects (17 of 50, 34%). These results were highly significant (OR: 7.01, *P-value* < 0.001). Similarly, samples with positive results for both HP-IgG and anti-CagA represented (37%) of the HT patients and overall study groups, as all of the healthy subjects were seronegative for anti-CagA antibody. On the other hand, only (17, 34%) of the HT group showed positive *H. pylori* IgG results and negative anti-CagA against (20%) in the control group. These results were insignificant (OR: 1.83, P: 0.18).

Table 3: Incidence of HP-IgG and anti-CagA antibodies among HT patients and control group

H. pylori IgG / CagA status	HT n=50	Control n=50	*P* value	OR	95% CI
	No. (%)	No. (%)			
HP+	47(94%)	17(34%)	< 0.001**	7.01	3.00 to 16.39
HP-	3(6%)	33(%66)	< 0.001**	0.03	0.008 to 0.121
HP+/CagA+	37(74%)	0 (0%)	< 0.001**	280.55	16.16 to 4870.44
HP+ / CagA -	17(34%)	10(20%)	0.18	1.83	0.83 to 5.10

**Results are significant at 0.01% level. OR: odd ratio. 95% CI: confidence intervals.

The results of table (4) showed that TSH levels were non-significantly elevated in HT patients who had *H. pylori* IgG (HP+) in their sera in comparison with those with (HP-) sera. As a result, levels of the thyroid hormones (FT3 and FT4) were insignificantly lower in HT patients who tested positive for HP IgG compared to those who tested negative. In HT patients who tested positive for both *H. pylori* antibodies (HP+/CagA+) the levels of TSH were significantly higher (*P* value=0.008) compared to those with HP+/CagA- tests. As a consequence, there was an insignificant decrease in the levels of thyroid hormones (FT3 and FT4) in these patients compared to those with (HP+/CagA+) results, table (4).

Table 4: Serum levels of FT3, FT4 and TSH in HT patients according to the type of *H. pylori* antibodies.

Thyroid hormones (Mean± SD)	*H. pylori* antibodies					
	HP +	HP -	P value	HP+/CagA+	HP+/CagA-	P value
FT3	4.58 ± 1.44	4.76 ± 1.49	0.94	5.43 ± 1.56	4.58 ± 1.44	0.805
FT4	11.96 ± 4.42	12.00 ± 4.31	0.943	11.14 ± 4.08	11.96 ± 4.42	0.801
TSH	20.34 ± 15.98	17.93 ± 11.63	0.457	20.43 ± 18.98	9.02 ± 5.94	0.008**

*Results are significant at 0.05 level. SD: standard deviation.

In the same context, there is a considerable elevation (*P-value* =0.05) in the concentrations of anti – TPO among HT patients who tested positive for both *H. pylori* antibodies (IgG and anti-CagA) when compared with those who tested negative, table (5). Serum levels of anti – Tg on the other hand, have also been elevated in the same groups but this elevation was not statistically significant.

Table 5: Serum levels of anti-TPO and anti-Tg in HT patients according to the type of *H. pylori* antibodies.

Thyroid antibodies (IU/ml)	*H. pylori* antibodies					
	HP +	HP -	P value	HP+/CagA+	HP+/CagA-	*P* value
Anti-TPO (Mean ± SD)	443.62 ± 386.72	106.65 ± 20.40	0.05*	480.69 ± 311.29	358.60 ± 281.55	0.05*
Anti-Tg (Mean ± SD)	336.00 ± 175.95	330.00 ± 190.95	0.943	336.00 ± 175.95	258.36 ± 170.09	0.721

*Results are significant at 0.05 level. SD: standard deviation.

9. Discussion

Our results found that serum levels of TSH, thyroid autoantibodies were significantly increased in HT patients when compared with normal control. Also, thyroid hormones (FT3 and FT4) were elevated in HT patients, but this elevation was not significant. These results could be considered as an indication for the development of subclinical hypothyroidism which is characterized by elevated TSH levels and normal FT3 and FT4 levels (Machała *et al*.,2019).

For the diagnosis of HT, the current study was dependent on the estimation of serum concentrations of anti-TPO and anti-Tg antibodies; the results indicated, as shown in table (2), that the concentrations of these antibodies were significantly higher (*P*<0.001) in patients compared to the healthy controls. Elevated concentrations of the thyroid autoantibodies and TSH as well as normal levels of thyroid hormones (FT3 and FT4) indicated the development of subclinical HT disorder. Anti-TPO and anti-Tg antibodies are widely available and commonly used in clinical diagnostic laboratories for HT disease (Wang *et al*., 2018). These antibodies are the major anti-thyroid antibodies in Hashimoto's disorder, and growth in anti-TPO antibodies has been linked to clinical symptoms of illness progression in the future (Acar *et al*., 2013). Furthermore, Siriwardhane *et al*. (2019) concluded that serum levels of anti-Tg and anti-TPO can be used as markers for early prediction of the development of thyroid autoimmunity; they also recommend adding these tests to the same list of thyroid function tests which include FT3, FT4, and TSH. On the other hand, (10%) of persons with Hashimoto's disease may not have anti-TPO antibodies in their bloodstream There have been cases of negatively tested Hashimoto's hypothyroidism when thyroid antibodies production was restricted to the gland (Carbone *et al*., 2019).

Based on the results of table (3), the presence of both *H. pylori* antibodies used in this study was

significantly higher ($P<0.001$) among HT patients (94% for HP-IgG, 74% for anti-CagA) compared to the healthy subjects (17% for HP-IgG, 0% for anti-CagA). These findings indicate that there is an association between *H. pylori* infection and Hashimoto's disease, suggesting a role of the bacteria in the subsequent development of HT in Iraqi patients.

Consistence with our results, Al-Shaibani *et al* found that (94.07%) of HT patients from Baghdad city were seropositive to *H. pylori* IgG antibodies. Hamid (2017) revealed that *H. pylori* IgG was present in (57%) of HT patients in Baghdad city. Similar findings have been found by Arslan *et al*, and Elazaim *et al*, who concluded that there is an association between thyroid autoimmunity and *H. pylori* infection. This study was unable to clarify the *H. pylori-related* consequences that can cause thyroid autoimmunity, However, we agree with the opinion "The specific processes by which exposure to a microorganism induces more than one manifestation of autoimmunity are not well defined" (Hou *et al*.,2017; Hamid,2017). Furthermore, some of the thyroid proteins have recently been found to share putative conserved domains with numerous H. pylori antigens, hence *H. pylori* infection could induce HT disease through an increased inflammatory status and molecular mimicry (Figura *et al*.,2020).

The results of tables (4 and 5) showed that HT patients with positive results to HP-IgG and/or anti-CagA have significantly increased the serum levels of TSH and thyroid autoantibodies (anti-TPO and anti-Tg). The elevated levels of TSH, anti-TPO and anti-Tg especially in HT patients infected with CagA expressing strains of *H. pylori* could be due to the inflammatory response caused by *H. pylori* infection, which in turn increases the cytokines expression leading to increased infiltration of thy thyroid by the effector lymphocytes (due to the molecular mimicry). This could subsequently damage the thyroid tissues, thus increasing the disorder's progression. Our results were consistent and were confirmed by a local study (Aboud, 2011) in addition to other regional and international studies (Aghili *et al*.,2013; Shi *et al*.,2013; Korani *et al*.,2016). Otherwise, Bassi et al. concluded that the correlation between *H. pylori* and autoimmune thyroid diseases was found only with Graves's disease and not Hashimoto's. Also, Shmuely et al. couldn't clarify the importance of *H. pylori* infection in women suffering from Hashimoto's disease. We think that several factors may explain these variations in the results including the study population, size, area of study, methodology used for the diagnosis of *H. pylori* infection, types of tests used in the statistical analysis, and finally the genetic and environmental factors related to each study. However, the current study has several limitations including small sample size, and the dependence on serological methods only to diagnose *H. pylori* infection. So, more studies on the molecular level are badly required.

10. Conclusion

According to the results of the present study, it can be concluded that there is a relationship between *H. pylori* infection and the development of Hashimoto's thyroiditis in Iraqi patients. *H. pylori* infection, especially CagA expressing strains, could be a risk factor for the development of autoimmune hypothyroidism and to a lesser extent its progression increases the concentration of thyroid antibodies and TSH, which in turn leads to decreased levels of the thyroid hormones and worsening of the disease, thus requesting antibiotic therapy to eradicate the bacterial infection. Accordingly, it is reasonable to recommend the addition of thyroid antibodies (anti-TPO and anti-Tg) to the list of the thyroid function test and to examine the correlation between H. pylori infection with Graves' disease. More studies are recommended to clarify the molecular mechanism underlying the association between *H. pylori* infection and HT disease.

References

Aboud, R. S. 2011. Evaluation of anti-Helicobacter pylori IgG level in the serum of patients with autoimmune thyroid diseases.. *Iraqi J. Sci.,* **52(4)***:* 440-444.

Acar, T., Özbek, S. S., Erdogan, M., Özgen, A. G., & Demirel, S. O. 2013. US findings in euthyroid patients with positive antithyroid autoantibody tests compared to normal and hypothyroid cases. *Diagn Interv Radiol.*, **19(4)**: 265-67.

Aghili, R., Jafarzadeh, F., Ghorbani, R., Khamseh, M. E., Salami, M. A., & Malek, M. 2013. The association of Helicobacter pylori infection with Hashimoto's thyroiditis. *Acta Medica Iranica*, **51(5):** 293-296.

Al-Shaibani, A. B., Al-A'araji, S. B., & Al-Mofarji, S. T. 2014. Studying Association between Thyroid Disorders and Helicobacter pylori infection in Iraqi Patients. *Baghdad Sci.J.*, **11(4)**: 1528-1514.

Arslan, M. S., Ekiz, F., Deveci, M., Sahin, M., Topaloglu, O., Karbek, B., ... & Delibasi, T. 2015. The relationship between cytotoxin-associated gene A positive Helicobacter pylori infection and autoimmune thyroid disease. *Endocr res.*, **40(4)**: 211-214.

Bassi, V., Marino, G., Iengo, A., Fattoruso, O., & Santinelli, C. 2012. Autoimmune thyroid diseases and Helicobacter pylori: the correlation is present only in Graves's disease. *World J Gastroenterol.,* **18(10)**: 1093-1097.

Carbone A., Rotondi M., Chiovato L. 2019. Chronic Autoimmune Thyroiditis. In: Luster M., Duntas L., Wartofsky L. (eds) **The Thyroid and Its Diseases**. Springer, Cham. pp 379-397.

Casto, C., Pepe, G., Li Pomi, A., Corica, D., Aversa, T., & Wasniewska, M. 2021. Hashimoto's Thyroiditis and Graves' Disease in Genetic Syndromes in Pediatric Age. *Genes*, **12(2)**: 1-22.

Caturegli, P., De Remigis, A., & Rose, N. R. 2014. Hashimoto thyroiditis: clinical and diagnostic criteria. *Autoi rev.*, **13(4-5)**: 391-397.

Choi, Y. M., Kim, T. Y., Kim, E. Y., Jang, E. K., Jeon, M. J., Kim, W. G., ... & Kim, W. B. 2017. Association between thyroid autoimmunity and Helicobacter pylori infection. *Korean J Intern Med.*, **32(2)**: 309-313.

Delitala, A. P., Pes, G. M., Errigo, A., Maioli, M., Delitala, G., & Dore, M. P. 2016. Helicobacter pylori CagA antibodies and thyroid function in latent autoimmune diabetes in adults. *Eur. Rev. Med. Pharmacol. Sci.*, **20(19)**: 4041-4047.

Elazaim, N. A., AbdElrahman, A. M., AL Matboly, M. A. E., AbdElaziz, A. F., & Metwally, R. A. 2018. Association between Helicobacter Pylori Infection and Autoimmune Hashimoto's Thyroiditis. *Egyptian J Hospital Med.*, **73(11)**: 8007-8014.

Figura, N., Di Cairano, G., Lore, F., Guarino, E., Gragnoli, A., Cataldo, D., ... & Gennari, C. 1999. The infection by Helicobacter pylori strains expressing CagA is highly prevalent in women with autoimmune thyroid disorders. *Can J. Physiol. Pharmacol.*, **50(5)**: 817-826.

Figura, N., Di Cairano, G., Moretti, E., Iacoponi, F., Santucci, A., Bernardini, G., ... & Ponzetto, A. 2020. Helicobacter pylori infection and autoimmune thyroid diseases: the role of virulent strains. *J. Antibiot.*, **9(1)**: 1-13.

Hamid, Z. A. (2017). The possible role of helicobacter pylori infection in Hashimoto's thyroiditis. *J Fac Med Baghdad*, *59*(1), 79-82.

Hou, Y., Sun, W., Zhang, C., Wang, T., Guo, X., Wu & Liu, T. 2017. Meta-analysis of the correlation between Helicobacter pylori infection and autoimmune thyroid diseases. *Oncotarget*, **8(70)**: 115691-115700.

Korani, M., Elshayeb, E., & Sonbal, A. 2016. *Helicobacter pylori* infection: association with Hashimoto's thyroiditis. *WGJ.*, **4(5)**: 115-118.

Machała, E., Redynk, M., Iavorska, I., & Machała, P. 2019. Hashimoto's thyroiditis. *WSN.*, **128(2)**: 302-314.

Ragusa, F., Fallahi, P., Elia, G., Gonnella, D., Paparo, S. R., Giusti, C., ... & Antonelli, A. 2019. Hashimotos' thyroiditis: Epidemiology, pathogenesis, clinic and therapy. *Best Practice & Research Clinical Endocrinology & Metabolism*, **33(6)**: 1-24.

Ramos-Leví, A. M., & Marazuela, M. 2016. Pathogenesis of thyroid autoimmune disease: the role of cellular mechanisms. *Endocrinología y Nutrición*, **63(8)**: 421-429.

Shi, W. J., Liu, W., Zhou, X. Y., Ye, F., & Zhang, G. X. 2013. Associations of Helicobacter pylori infection and cytotoxin-associated gene A status with autoimmune thyroid diseases: a meta-analysis. *Thyroid*, **23(10)**: 1294-1300.

Shmuely, H., Shimon, I., & Gitter, L. A. 2016. Helicobacter pylori infection in women with Hashimoto thyroiditis: A case-control study. *Medicine*, **95(29)**: 1-5.

Siriwardhane, T., Krishna, K., Ranganathan, V., Jayaraman, V., Wang, T., Bei, K., ... & Krishnamurthy, H. 2019. Significance of anti-TPO as an early predictive marker in thyroid disease. *Autoimmune diseases*, 2019: 1-7.

Wang, S., Wu, Y., Zuo, Z., Zhao, Y., & Wang, K. 2018. The effect of vitamin D supplementation on thyroid autoantibody levels in the treatment of autoimmune thyroiditis: a systematic review and a meta-analysis. Endocrine, **59(3)**: 499-505.

JJBS

Volume 15, Number 4,December 2022
ISSN 1995-6673
Pages 543 – 551
https://doi.org/10.54319/jjbs/150402

Jordan Journal of Biological Sciences

The Use of Diet Practices, Herbs, and Supplementations for Weight Loss among Adults in Jordan: A Cross-Sectional Survey

Buthaina Alkhatib[1*], Alaa Al-Shorman[2], Lana M. Agraib[3]

[1] *Department of Clinical Nutrition and Dietetics, Faculty of Applied Medical Sciences, The Hashemite University, Zarqa.*

[2] *Msc. Human Nutrition and Dietetics, Department of Nutrition and Food Technology, Faculty of Agriculture, The University of Jordan, Amman, Jordan.* [3] *Department of Food Science and Nutrition, Faculty of Agriculture, Jerash University, Jerash, Jordan*

Received: No v22, 2021; Revised: April 17, 2022; Accepted May, 11, 2022

Abstract

Background: Obesity is a global health pandemic; several studies have indicated that people commonly seek claim diets and herbal supplementations

Aim: The study aimed to assess the prevalence of herbs and supplementation use and other weight-loss strategies among adults in Jordan.

Methods: A cross-sectional study was conducted on a sample of 689 adults (≥18 years) using a structured validated online questionnaire. Data about sociodemographic, anthropometric data, weight-loss strategies, diets, and herbs used were collected. A frequency descriptive statistic test was used to describe the sample. A p-value of < 0.05 was considered statistically significant.

Results: 28.9% of the participants reported the most common source of diets they followed to either by themselves or dietitians (26.0%). Also, 23.4% reported that they followed more than one diet. Almost three-quarters of participants (74.7%) reported that they think that weight-loss diets are unsafe to be decided by a dietitian. The majority of participants (83.5%) reported that they do not believe in the role of using herbs, and supplementations alone to reduce weight. The most commonly used single herb was green tea (43.1%). 38.2% of total participants think that using herbal supplements for weight reduction is safe. Slightly less than one-third of the participants suffered from side effects after using herbs.

Conclusions: The obese and overweight adults in Jordan seek different weight-reducing strategies, including the of use diet practices, herbs, and supplementations. More national studies with different designs are required. Also, strategies may be needed to increase national population awareness about different weight loss practices (cons and pros).

Keywords: herbs; supplementations; overweight; obesity; Jordan; fad diets; weight loss practices

1. Introduction

The prevalence of obesity has doubled in the last 40 years in more than 70 countries worldwide (GBD 2015 Obesity Collaborators *et al*., 2017). Moreover, almost 50% of the world's adult population is predicted to be overweight or obese by 2030 (Dobbs *et al*., 2014). Regarding morbidity and mortality, obesity is a global public health problem, attributed to 5.0% of deaths worldwide in 2014 (Tremmel *et al*., 2017). Additionally, it is associated with an elevated risk of several non-communicable diseases, such as diabetes mellitus (DM), dyslipidemia, cardiovascular disease (CVD), and cancer (Hruby and Hu, 2014).

This reflects the situation in Jordan; the rate of obesity is high and increasing. Hence, a national household survey study included 4056 adults (18–90 years) in Jordan. It was conducted in 2017 to determine the prevalence of obesity and associated factors and comorbidities. They found that the age-standardized prevalence of obesity was 60.4% among men and 75.6% among women, while approximately three-quarters of men and women were overweight or obese, as defined by BMI (Ajlouni *et al*., 2020).

Although the literature has approved those long-life modifications in diet and lifestyle as the best strategies to maintain a healthy weight in the long term, a good percentage of people are undertaking fad diets associated with alternative solutions with the hope of losing weight fast and easily (Kuchkuntla *et al*., 2018). There is a wide range of proposed fad diets over the last centuries. They can be categorized into several main groups, including low-/no-carbohydrate (a high intake of protein and/or fat is recommended such as the Atkins diet, the Dukan Diet, and the South Beach diet), high-carbohydrate/high-fiber (like the Ornish diet) and liquid formula diets or very low calories (Khawandanah and Tewfik, 2016). Although fad diets are simple to lose weight, many studies have indicated that such diets are unsustainable in the long term

* Corresponding author. e-mail: bkhatib@hu.edu.jo.

** **Abbreviations:** DM: Diabetes Mellitus; CVD: cardiovascular disease; BMI: body mass index; COVID-19: corona virus-19; EMR: Eastern Mediterranean region, CDC: center of disease control; JFDA: Jordan food and drug administration; SD: standard deviation

and can cause several adverse health side effects (Khawandanah and Tewfik, 2016)

Herbs are considered one of the most common alternative therapies for weight loss worldwide (Barnes *et al*., 2004). Many studies have investigated the efficacy and safety of medicinal plants in treating obesity, dyslipidemia, and diabetes mellitus (Hasani-Ranjbar *et al*., 2009; Hasani-Ranjbar *et al*., 2010; Lenon *et al*., 2012). Additionally, many plant and plant products have been shown to possess anti-obesity effects, including *Curcuma longa* (curcumin), *Zingiber officinale* (ginger), *Nigella sativa* (black seed), *Camellia sinensis* (black Chinese tea, green tea*)*, *Bidens odorata*, soybean, apple cider vinegar, castor oil, and flaxseeds (Hasani-Ranjbar *et al*., 2013; Eldalo *et al*., 2017; Alonso-Castro *et al*., 2019). In Jordan, herbs, and supplements are freely available in both pharmacies (registered approved products by JFDA) and herbal remedy traditional shops (unregistered products), using very high expectations propaganda regarding fast and safe weight loss. To date, there is not enough data to examine the practices of weight loss in the MENA region and Jordan in particular regarding the use of herbal supplementations, plant-based products, or fad diets; hence, the objective of the study was to assess the prevalence of weight-loss strategies and herbs and supplementation use among adults in Jordan.

2. Material and Methods

2.1. Design, Sampling, and Procedures

A cross-sectional survey was conducted from February to April 2021 in Jordan by the Herbal Dynasty Medical Center team, in Amman, Jordan. An online self-report questionnaire was carried out in a random sample among adults ≥ 18 years.

The study data collection was performed using a structured validated online questionnaire established using Google Forms and disseminated through internet routes (WhatsApp, Facebook, and Messenger). It was developed after an extensive review of related studies. The questionnaire included the study's purpose description and agreement to participate; self-reported sociodemographic and anthropometric data, including weight (kg) and height (cm); weight-loss strategies and herbs and supplementation use data. Informed consent for each participant was obtained on the first page of the survey, and the privacy and confidentiality of the respondents were strictly protected. Inclusion criteria included being of age ≥18, being a nonpregnant and nonlactating woman, and having the ability to read and write Arabic. The appropriate sample size for this study was calculated using Raosoft software (Raosoft, Inc. free online software, Seattle, WA, USA). In 2020, Jordan's total population is approximately 10 million, and about 7.09 million (64% of the total population) are adults, based on the Department of Statistics (Department of Statistics, 2020). A recent study estimated that approximately 75% (about 5.32 million) of the Jordanian population is either overweight or obese (Ajlouni *et al*., 2020). With a confidence interval of 5%, a confidence level of 95%, and a response distribution of 50%, a sample size of 385 was necessary. In our study, a larger same size was used in case patients refused to enroll in the study or did not match the inclusion criteria (pregnant and lactating women, who cannot write and read Arabic, and are less than 18 years old). Therefore, 689 participants completed the online questionnaire; among them, 477 were overweight and obese subjects.

The Department of Clinical Nutrition and Dietetics, Faculty of Science at Philadelphia University, Jordan, approved the study protocol. The World Medical Association Declaration of Helsinki regarding the ethical conduct of research involving human subjects was followed.

2.2. Reliability and Validity of the Questionnaire

The questionnaire was pre-tested for validity and reliability on a pilot sample of 30 participants, which was not included and excluded from the final sample. Cronbach's alpha (α) was used and calculated for the validity and reliability of the questionnaire (Noble and Smith, 2015). The results showed that the questionnaire had a Cronbach's α value equal to 0.715, indicating good reliability.

2.3. Self-reported Measurements

Participants reported their weight and height; their BMI was calculated and categorized as follows: underweight (<18.5 kg/m^2), normal weight (18.5 to 24.9 kg/m^2), overweight (25 to 29.9 kg/m^2), and obese (over 30 kg/m^2) (Center of Disease Control (CDC), 2020); the excess weight group included overweight and obese participants. Additionally, self-reported sociodemographic data, including sex, age, educational level, and marital status, were reported. In addition, they were asked about weight loss strategies that were followed, the name of herbs they were using for weight loss, form, usage duration, beliefs about efficiency, and by whom it was described (families or friends, media, or health care providers) and obtaining method in the past three to five years from data collection.

2.4. Statistical Analysis

Analyses were carried out using SPSS software (IBM SPSS Statistics for Windows, Version 22.0. Armonk, NY: IBM Corp). Frequencies, means, and standard deviation ranges were calculated using frequency descriptive statistical tests to describe the sample. The chi-square test was used to assess differences in proportions. The *p-value* of < 0.05 was considered statistically significant.

3. Results

3.1. Participant General Characteristics

A total of 689 participants responded to this questionnaire. More than four-fifths of the participants (82.7%) were female. Mean± SD of participants' BMI was 28.0±6.3 kg/m^2. Slightly more than three-quarters of the participants were 18–40 years old (77.4%). Seventy-one percent of the participants were living in middle Jordan (71%), and the majority reported having excess weight (69.1%) (Table 1).

Table 1. Demographic characteristics of participants (n=689).

Characteristic	Values[1]
BMI (kg/m^2), mean ± SD	28.0 ± 6.3
Sex	
Females	570 (82.7)
Males	119 (17.3)
Age (years)	
18-40	533 (77.4)
41-65	155 (22.5)
65 <	1 (0.1)
Living areas	
North Jordan	96 (14)
Central Jordan	489 (71)
South Jordan	104 (15)
Marital status	
Married	247 (35.8)
Single	395 (57.3)
Other[2]	47 (6.9)
Educational level	
Secondary education	105 (15.2)
College or university	493 (71.6)
Postgraduate education	91 (13.2)
Weight Categories	
Normal weight	213 (30.9)
Excess weight[3]	476 (69.1)

BMI, Body mass index
[1] Values are n (%) unless otherwise noted.
[2] others, including the divorced, widowed, engaged, and complicated relationship
[3] excess weights, a group including overweight and obese participants

3.2. Participants' Self-Image and Weight Reduction AttitBelieveieves

Table 2 shows that almost two-thirds (69.3%) of respondents reported that they think their weight is not healthy. The percentage of participants with normal weight who reported that they thought their weight was healthy was significantly higher than those with excess weight (53.3% and 5.2%, respectively; p value<0.001). Of all the participants, 16.7% reported that they believe that they had excess weight for less than a year. In comparison, 20.3% of excess weight participants reported that they were diagnosed less than a year, significantly (p value<0.001) more than the participants with a normal weight (8.5%). Moreover, (28.9%) of the participants reported the most common source of diets they followed was by themselves or by dietitians (26.0%). Normal weight participants reported that the most common source of diet they followed was themselves (27.4%), followed by dietitians (17.0%), which had a significantly lower reported percentage than participants with excess weight (29.6% vs. 30.0%, respectively; p value<0.001). Regarding the type of diets followed, 19.4% of participants did not follow any weight-reducing diet, 23.8% of total participants reported that they followed a low-calorie diet, 15.4% followed an intermittent fasting diet, and 23.4% followed more than one diet. The percentages of excess weight participants who reported following a low-calorie diet, an intermittent fasting diet, and more than one diet were higher than those of participants with normal weight, with values of 24.9% vs. 21.2%, 15.5% vs. 15.1%, and 26.0% vs. 17.5%, respectively. Almost three-quarters of participants (74.7%) reported that they thought that weight-loss diets were not safe and needed to be decided by professionals.

Table 2. Participant's self-image and weight reduction attitude beliefs.

Total (n=689)		Weight categories		*p*-value
		Normal (n=212)	Excess (n=477)	
Self-image and weight beliefs:				
Do you believe your weight is healthy?				
Yes	138 (20.0)	113 (53.3)	25 (5.2)	<0.001
No	477 (69.3)	59 (27.8)	418 (87.6)	
Maybe	74 (10.7)	40 (18.9)	34 (7.2)	
If you believe you have excess weight, for how long do you think you suffer from it?				
Less than a year	115 (16.7)	18 (8.5)	97 (20.3)	<0.001
For five years	60 (8.7)	3 (1.4)	57 (11.9)	
5-10 years	59 (8.6)	3 (1.4)	56 (11.7)	
11-15 years	12 (1.7)	1 (0.5)	11 (2.3)	
Over 15 years	24 (3.5)	0 (0.0)	24 (5.0)	
I don't think I am obese	419 (60.8)	187 (88.2)	232(48.6)	
Participants' Attitude and knowledge toward diet for weight loss:				
If you have followed a weight loss diet, who has prescribed it to you?				
I did not follow a diet	108 (15.7)	62 (29.2)	46 (9.6)	<0.001
Physician	11 (1.6)	3 (1.4)	8 (1.7)	
Dietitian	179 (26.0)	36 (17.0)	143 (30.0)	
Friend or family member	53 (7.7)	20 (9.4)	33 (6.9)	
Internet	130 (18.9)	28 (13.2)	102 (21.4)	
By myself	199 (28.9)	58 (27.4)	141 (29.6)	
All sources mentioned	8 (1.2)	0 (0.0)	1 (0.2)	
Others	1 (0.1)	5 (2.4)	3 (0.6)	
If you have followed a diet, what was it?				
I did not follow any kind of diet	134 (19.4)	66 (31.1)	68 (14.3)	<0.001
Low calories diet	164 (23.8)	45 (21.2)	119 (24.9)	
Low carbohydrates diet	54 (7.8)	7 (3.3)	47 (9.9)	
ketogenic diet	8 (1.2)	2 (0.9)	6 (1.3)	
High protein diet	19 (2.8)	7 (3.3)	12 (2.5)	
Intermittent fasting diet	106 (15.4)	32 (15.1)	74 (15.5)	
Blood type diet	2 (0.3)	1 (0.5)	1 (0.2)	
Mediterranean diet	5 (0.7)	3 (1.4)	2 (0.4)	
Others	36 (5.2)	12 (5.7)	24 (5.0)	
I followed more than one diet	161 (23.4)	37 (17.5)	124 (26.0)	
Do you think following a weight loss diet by yourself is safe, and there is no need to be prescribed by a professional?				
Yes	158 (22.9)	41 (19.3)	117 (24.5)	0.267
No	515 (74.7)	167 (78.8)	348 (73.0)	
Sometimes	16 (2.4)	4 (1.9)	12 (2.5)	

3.3. Participants' Beliefs, Knowledge, and Consumption of Herbs and Supplementations for Weight Reduction

Table 3 shows that the majority of participants (83.5%) reported that they did not believe in the role of using herbs and supplementations alone to reduce weight, while 77.9% of participants reported that they believed in the role of using herbs and supplementations along with diet and exercises for weight reduction. A total of 32.2% of participants reported that they did not use herbs for weight reduction. In an attempt to lose weight, the practice of taking 2–3 and 4–6 different herbs together was used by 23.9% and 18.7% of the participants, respectively. The most commonly used single herb was green tea (*Camellia sinensis*) (7.7%). The excess weight participants significantly had a higher percentage of using 2–3 (27.5%) and 4–6 (23.1%) different herbs together compared to normal weight participants (16.0% and 9.0%, respectively). The most common herbal advisors for the participants who used herbs for weight reduction were the internet (22.1%), themself (21.3%), and dietitians (10.9%). Only 1.7% and 0.7% of participants reported that their herbal advisors were herbalists and physicians, respectively. For normal weight participants, the most common herbal advisor was by themselves (16.0%), followed by the internet (11.3%), while for excess weight participants, it was the internet (26.8%), followed by themselves (23.7%), and dietitians (12.6%). A total of 58.6% of participants (33.5% of normal-weight participants and 69.8% of excess-weight participants) reported that they prepared herbs by mixing them with boiling water. More than half of the total participants (58.1%; 30.7% of normal-weight participants, and 70.2% of excess-weight participants) reported that they used herbs daily (one, two, or three times a day).

Table 3. Participants' beliefs and attitudes toward herbs and supplementation use for weight reduction.

Total (n=689)		Weight categories		*p*-value
		Normal (n=212)	Excess (n=477)	
Do you believe in the role of herbs alone in losing weight?				
Yes	36 (5.2)	15 (7.1)	21 (4.4)	
No	575 (83.5)	174 (82.1)	401 (84.1)	0.344
I don't Know	78 (11.3)	23 (10.8)	55 (11.5)	
Do you believe in the role of herbs in losing weight, along with diet and exercise?				
Yes	537 (77.9)	159 (75.0)	378 (79.2)	
No	77 (11.2)	25 (11.8)	52 (10.9)	0.375
I don't Know	75 (10.9)	28 (13.2)	47 (9.9)	
Have you used any of the following herbs or foods to lose weight?				
I did not use herbs	222 (32.2)	126 (59.4)	96 (20.1)	
Apple vinegar	9 (1.3)	0 (0.0)	9 (1.9)	
Senna Makki	5 (0.7)	2 (0.9)	3 (0.6)	
Green tea	53 (7.7)	15 (7.1)	38 (8.0)	
Flaxseed	8 (1.2)	1 (0.5)	7 (1.5)	
Bran	3 (0.4)	1 (0.5)	2 (0.4)	
Curcumin	2 (0.3)	0 (0.0)	2 (0.4)	
Cumin	3 (0.4)	0 (0.0)	3 (0.6)	
Green coffee	5 (0.7)	2 (0.9)	3 (0.6)	<0.001
Lemon	7 (1.0)	0 (0.0)	7 (.5)	
Honey	12 (1.7)	4 (1.9)	8 (1.7)	
Chia seed	1 (0.1)	0 (0.0)	1 (0.2)	
Ginger	11 (1.6)	4 (1.9)	7 (1.5)	
Matcha tea	5 (0.7)	3 (1.4)	2 (0.4)	
Others	10 (1.5)	1 (0.5)	9 (1.9)	
Used 2-3 herbs	165 (23.9)	34 (16.0)	131 (27.5)	
Used 4-6 herbs	129 (18.7)	19 (9.0)	110 (23.1)	
Used more than 6 herbs	39 (5.7)	0 (0.0)	39 (8.2)	
Who prescribed herbs to you?				
I did not use herbs	224 (32.5)	124 (58.5)	100 (21.0)	
Physician	5 (0.7)	1 (0.5)	4 (0.8)	
Dietitian	75 (10.9)	15 (7.1)	60 (12.6)	
herbalist	12 (1.8)	0 (0.0)	12 (2.5)	<0.001
Friends or family member	73 (10.6)	14 (6.6)	59 (12.4)	
Internet	152 (22.1)	24 (11.3)	128 (26.8)	
By myself	147 (21.3)	34 (16.0)	113 (23.7)	
All of them	1 (0.1)	0 (0.0)	1 (0.2)	
How many times per day did you take herbs for weight loss?				
I did not use herbs	221 (32.1)	124 (58.5)	97 (20.3)	
Once-daily	207 (30.0)	41 (19.3)	166 (34.8)	
Twice daily	145 (21.0)	19 (9.0)	126 (26.4)	
3 times daily	48 (7.0)	5 (2.4)	43 (9.0)	<0.001
Once a week	17 (2.5)	4 (1.9)	13 (2.7)	
Twice a week	14 (2.0)	5 (2.4)	9 (1.9)	
3 times per week	26 (3.8)	6 (2.8)	20 (4.2)	
Other	11 (1.6)	8 (3.8)	3 (0.6)	
In which form do you take the herbs?				
I did not use herbs	222 (32.2)	123 (58.0)	99 (20.8)	
Powder	33 (4.8)	10 (4.7)	23 (4.8)	
Capsules	17 (2.5)	7 (3.3)	10 (2.1)	<0.001
Boiled as a tea	404 (58.6)	71 (33.5)	333 (69.8)	
Other forms	13 (1.9)	1 (0.5)	12 (2.5)	

Table 4 shows the most commonly used type of herbs and supplementations alone or combined with other herbs reported by the participants. The reported use of green tea (*Camellia sinensis*), lemon (*Citrus*), ginger (*Zingiber officinale*), apple vinegar and cumin (*Cuminum cyminum*) by excess weight participants was significantly higher than normal-weight participants (50.9% vs. 25.5%; 41.3% vs. 14.6%; 37.7% vs. 13.7%; 25.2% vs. 3.8%, and 26.2% vs. 5.7%, respectively) with *p* value<0.001.

Table 4. The percentage of commonly used herbs for weight reduction.

Herbs	All participants (n=689)	Normal weight (n=212)	Excess weight (n=477)	*p*-value
Green tea	297 (43.1)	54 (25.5)	243 (50.9)	<0.001
Lemon	228 (33.1)	31 (14.6)	197 (41.3)	<0.001
Ginger	209 (30.3)	29 (13.7)	180 (37.7)	<0.001
Apple vinegar	128 (18.6)	8 (3.8)	120 (25.2)	<0.001
Cumin	137 (19.9)	12 (5.7)	125 (26.2)	<0.001

Note: data presenting herbs alone or combined with others

3.4. Participants Believe and Knowledge Toward Herbs and Supplementations Use Safety for Weight Reduction

As shown in Table 5, slightly more than one-third (38.2%) of all participants thought that using herbs and supplementations for weight reduction was safe. Among normal-weight participants, 34.1% do not know if herbs and supplementations for weight reduction are safe, while 33.2% of them think it is not safe, only 32.7% of normal-weight participants think using the herb for weight reduction is safe. In contrast, 40.7% of excess weight participants thought that using herbs and supplementations for weight loss was safe, 25.8% did not think that, and 33.5% did not know if it was safe. Of participants who reported using herbs and supplementations for weight loss, 6.1% reported feeling a change in their weight in the beginning and then the effect stopped, 19.4% reported that they did not feel any change in their weight, and only 14.7% reported feeling a change in their weight. Based on weight, the participant with the normal weight used herbs for weight loss and reported a weight change (9.4%) or feeling a change, in the beginning, then the effect stopped (2.8%). Slightly less than one-third (27.3%) of the total participants suffered from the side effects of herbal medicine, (62.8%) of them reported one symptom, (21.8%) reported two symptoms, and (9.6%) and (5.9%) reported three and four symptoms, respectively. The most commonly reported side effects were diarrhea (42.1%), and headache (33.7%). From the studied group, (34.7%) of participants reported that they would use herbal medications again composed of (24.5%) of normal weight and (39.2%) of excess weight. On the other hand, (20.5%) of all participants would not use herbal medications again for weight loss, composed of (25.0%) of normal weight and (18.4%) of excess weight, *p value*= 0.001). Almost half of the participants (46.0%) reported that they would recommend herbs and supplements to their friends/relatives to lose weight.

Table 5. Participants' beliefs and knowledge about the safety of herbs and supplementations use for weight loss.

	Total (n=689)	Weight categories		*p*-value
		Normal (n=212)	Excess (n=477)	
Do you think that using herbs to lose weight is safe?				
Yes	263 (38.2)	69 (32.7)	194 (40.7)	
No	193 (28.1)	70 (33.2)	123 (25.8)	0.071
I don't Know	232 (33.7)	72 (34.1)	160 (33.5)	
Did you feel that your weight changed after using the herbs?				
Did not use herbs	215 (31.2)	119 (56.1)	96 (20.1)	
Yes	101(14.7)	20 (9.4)	81 (17.0)	
No	134 (19.4)	28 (13.2)	106 (22.2)	<0.001
I don't Know	197 (28.6)	39 (18.4)	158 (33.1)	
In the beginning and then the effect stopped	42 (6.1)	6 (2.8)	36 (7.5)	
Have you experienced unpleasant symptoms or side effects during using herbs for weight loss?				
Did not use herbs	216 (31.3)	121 (57.1)	95 (19.9)	
Yes	188 (27.3)	30 (14.2)	158 (33.1)	<0.001
No	285 (41.4)	61 (28.8)	224 (47.0)	
If you experience any side effects, how many did you have it?				
Had one symptom	118 (62.8)	18 (60)	100 (63.3)	
Had two symptoms	41 (21.8)	9 (30)	32 (20.3)	0.451
Had three symptoms	18 (9.6)	1 (3.3)	17 (10.8)	
Had four symptoms	11 (5.9)	2 (6.7)	9 (5.7)	

Headache				
Yes	64 (33.7)	8 (25.0)	56 (35.4)	0.254
No	126 (66.3)	24 (75.0)	102 (64.6)	
Diarrhea				
Yes	80 (42.1)	13 (40.6)	67 (42.4)	0.852
No	110 (57.9)	19 (59.4)	91 (57.6)	
Interrupted period				
Yes	27 (14.2)	3 (9.4)	24 (15.2)	0.390
No	163 (85.8)	29 (90.6)	134 (84.8)	
Other symptoms				
Yes	11 (5.7)	2 (5.9)	9 (5.7)	0.960
No	182 (94.3)	32 (94.1)	150 (94.3)	
Are you going or intend to use the herbs again to lose weight?				
Yes	239 (34.7)	52 (24.5)	187 (39.2)	
No	141 (20.5)	53 (25.0)	88 (18.4)	0.001
I don't Know	309 (44.8)	107 (50.5)	202 (42.3)	
Will you recommend herbs and supplementations to your friends /relatives to lose weight				
Yes	317 (46.0)	92 (43.4)	225 (47.2)	0.359
No	372 (54.0)	120 (56.6)	252 (52.8)	

4. Discussion

In the Eastern Mediterranean Region (EMR), high alarming prevalence rates of obesity have been recorded in many countries due to changes in food consumption and increases in sedentary lifestyles (Rahim *et al*., 2014). Based on GBD 2015 Eastern Mediterranean Region Obesity Collaborators, the prevalence of obesity in adults increased from 15.1% in 1980 to 20.7% in 2015 (GBD 2015 Eastern Mediterranean Region Obesity Collaborators, 2018). According to our study population, 69.1% were either overweight or obese as defined by BMI; this matches the result of a recent study indicating that over three-quarters of Jordanian men or women were either overweight or obese (Ajlouni *et al*., 2020).

Weight stigma and social pressure encourage people to lose weight, which pushes people, especially obese people, to use medications, including drugs and/or herbs, to lose weight (Tomiyama *et al*., 2018). Interestingly, over 80% of the participants followed one weight loss diet or more (23.4%). Also, 55.7% of the sample followed a weight loss diet from a friend or family member, internet searching, or on their own, although 74% think that it is not safe to follow a weight loss diet without professional guidance. Physicians and herbalists have a low role in herbal prescription. This was consistent with previous studies. For example, Issa reported that the majority of Jordanian university students (70.2%) depend on homemade herbs whereas the remnant students discuss with pharmacists before using them (Issa, 2018). Moreover, excess weight Saudi participants in Taif have relied on friends (35.8%) and herbalists (31.0%) (Eldalo *et al*. 2017). Also, Mexican overweight and obese adults have rested on family/friends, and personal prescriptions (67%, and 33% respectively) (Alonso-Castro *et al*., 2019). Obesity self-treatment was also stated in Colombia (Amariles *et al*., 2006), India (Sushama and Nandita 2012), and Brazil (Martin *et al*. 2006).

In the present findings, the excess weight participants seek to follow a low-calorie diet, intermittent fasting, and more than weight-reducing diet practice. Despite the scientific facts about fad/claim diets for weight reduction, recent data have shown that excess weight subjects seek different diets such as low carbohydrate, ketogenic, high protein, intermittent fasting, single food item, skipping food group/s, and blood grouping (Khawandanah and Tewfik, 2016; Al-Bakheit, 2019). In Jordan, Al-Bakheit (2019) found that the three most common fad diets used by excess weight subjects were the high-protein diet (31.3%), fruits and vegetable diets (21.9%), and liquid diets (18.3%) (Al-Bakheit, 2019). Accordingly, Al-Kurd and Faris (2011) found that 22% of Jordanians tend to follow weight loss fad diets (Al-Kurd and Faris, 2011).

In a national cross-sectional self-report survey, to assess the prevalence, utilization, and attitude toward herbal medicines among Jordanian adults, Abdel-Qader and colleagues (2020) found that 23.6% of study participants were using herbs for weight reduction and obesity. In our study, 67.8% of the participants used one or more herbs and supplements to lose weight. This inconsistency between the results of studies could be related to the data collection period conditions; as the data of this study were collected during the COVID-19 curfew in Jordan, there was a partial ban and prohibition of movement in the evening hours, as well as a general closure of all parks and gyms. Action plans for COVID-19 quarantine have been linked closely with obesogenic practices, especially increasing food consumption, lower physical activity, and eating patterns shifted to unhealthy eating habits (Al Hourani *et al*., 2021). This has increased the tendency of people to search for quick solutions to lose weight or maintain weight.

Internationally, several studies have investigated the prevalent use of herbal supplementation and reported that the prevalence of using herbal supplementation was 98.1% in a study in Saudi Arabia (Eldalo *et al*., 2017), 24.1% in Turkey (Bellikci Koyu *et al*., 2020), 32.3% in Iran (Eldalo *et al*., 2017), and 36% in the United States (Bertisch *et al*., 2008). A population-based study conducted in the United States showed that herbal supplementation for weight loss purposes is more prevalent among people with excess

weight (Blanck *et al*., 2007). Likewise, in the current study, almost 80% of excess weight participants used herbal supplementation compared to 40.6% of normal-weight participants.

Taking a mixture of herbal supplementation of two to more 6 products was more frequent among the study participants. Other studies have reported the same (Blanck *et al*., 2007; Bellikci Koyu *et al*., 2020). As a part of the herbal mixture, green tea was the most commonly used herbal plant for weight loss among the study population, with slightly more than 43% of all participants and 50% overweight and obese, followed by lemon and ginger. This is similar to another study from Saudi Arabia, which reported that the use of green tea was the most frequent, with 88.4% (Eldalo *et al*., 2017). Hursel *et al*. (2009) reported in their meta-analysis that green tea has a positive effect on weight loss and weight maintenance; however, the effect was modest. Moreover, Jurgens and colleagues (2012) concluded that the impact of green tea has a small, statistically, and clinically nonsignificant impact on weight loss in overweight or obese adults. However, studies have reported that lemon and lemon juice might have favorable effects on weight loss (Tejpal *et al*., 2018) and hypocholesterolemic effects (Khan *et al*., 2010). Moreover, a systematic review and meta-analysis of randomized controlled trials conducted by Maharlouei and colleagues (2018) demonstrated that ginger intake reduces body weight, waist-to-hip ratio, hip ratio, fasting glucose, and HOMA-IR and increases serum HDL cholesterol levels but does not affect insulin, BMI, triglycerides, or total and LDL cholesterol levels.

In the current study, participants mostly started using herbs based on information from the internet, themselves, friends or family members, and herbalists, but the percentage of taking herbs from health professionals (dietitians and physicians) was very low (11.6%). Similar findings have been reported elsewhere (Samojlik *et al*., 2013; Bellikci Koyu *et al*., 2020). Using herbs might lead to several health risks (Pittler *et al*., 2005). Moreover, in the current study, over (27.3%) of all participants had unpleasant symptoms; however, 46.0% of the sample recommended using herbs for weight loss for friends or relatives. Therefore, it might be vital for health professionals to check and monitor if their patients use herbs and supplements.

Only 2.5% of the sample used herbs in the form of capsules, which indicates that the majority of the sample purchases herbal supplements from herbalists or local markets but not pharmacies. To gain a good quality of the product, the whole process from harvesting to storage should be well monitored. Poor manufacturing and storage practices might result in contamination with metal residues, fungi, pesticides, parasites, or insects (Posadzki *et al*., 2012). In addition, imitation and adulteration related to the safety of herbs (Bellikci Koyu *et al*., 2020) and sibutramine intoxication have been proposed in a few case reports (Bertholee *et al*., 2013; Pamukcu Gunaydin *et al*., 2015). For such reasons, it is critical to control herbs and their selling places in Jordan.

This study has many limitations; there was a lack of anthropometric measurement standardization, as it was self-reported by online questionnaires. Medication intake, herb-medicine interactions, period of commitment or use of diet practices, herbs, or supplements (extended period…or limited…), and participant disease history were not recorded in the survey. Additionally, data collection occurred during the COVID-19 quarantine, when many behaviors and attitudes changed. Finally, accessibility in sampling was the rural adults, and those who do not have access to technology were not included.

5. Conclusion

The obese and overweight adults in Jordan seek different weight-reducing strategies, including the use of diet practices, herbals, and supplements. The current study suggests that the use of herbs and supplementations for weight loss purposes is very frequent in Jordan, especially among those with excess weight. The results also reported that the most herbs used for weight reduction is green tea, and most of the participants think using herbs is safe. It is highly recommended to train health professionals about herbs during clinical practice and their possible side effects and drug interactions. Besides, national community awareness programs are needed to educate people about safe methods of losing and maintaining weight and the possible risks and benefits of using herbal supplementations.

Ethical Approval and Consent to Participate

The study protocol of this study was approved by the Department of Clinical Nutrition and Dietetics, Faculty of Science at Philadelphia University, Jordan. The World Medical Association Declaration of Helsinki regarding the ethical conduct of research involving human subjects was followed**.**

Consent for Publication

not applicable.

Availability of Data and Material

The datasets used and/or analyzed during the current study are available through the corresponding author on reasonable request.

Competing Interest

The authors declare no conflict of interests.

Funding

This research received no external funding**.**

Acknowledgments

Our deep gratitude goes to The Herbal Dynasty Medical Center for help in completing data collection, specially Afnan Alhilo and Nada Hammad. We would like to thank all the participants for their help with this work.

References

Abdel-Qader DH, Albassam A, Ismael NS, Aljamal MS, Chen LC, Mansoor K, Al Meslamani AZ. 2020. Herbal medicine use in the Jordanian population: a nationally representative cross-sectional survey. *J Pharm Pharmacogn Res*, **8**:525-536.

Ajlouni K, Khader Y, Batieha A, Jaddou H, El-Khateeb M. 2020. An alarmingly high and increasing prevalence of obesity in Jordan. *Epidemiol Health*, e2020040.

Al Hourani H, Alkhatib B, Abdullah M. 2021. Impact of COVID-19 Lockdown on Body Weight, Eating Habits, and Physical Activity of Jordanian Children and Adolescents. *Disaster Med Public Heal Prep,*1-9.

Al-Bakheit, A. 2019. Food Faddism in a Sample from Al-Balqa Governorate in Jordan. *Journal of Nutrition, Fasting and Health*, **7(2)**: 76-83.

Al-Kurd RA, Faris MAE. 2011. Nutritional and Health Quality of a Group of Popular Weight-Reducing Diets in Jordan. *Pak J Nutr*. **10(9)**: 814-22.

Alonso-Castro A, Ruiz-Padilla A, Ramírez-Morales M *et al*. 2019. Self-treatment with herbals for weight-loss among overweight and obese subjects from central Mexico. *J Ethnopharmacol*, **234**:21-26.

Amariles, Pedro, Laura I González, and Nubia A Giraldo. 2006. 'Prevalence of self-treatment with complementary products and therapies for weight loss: a randomized, cross-sectional study in overweight and obese patients in Colombia', *Current therapeutic research*, **67**: 66-78.

Barnes P, Powell-Griner E, McFann K, Nahin R. 2004. Complementary and alternative medicine use among adults: the United States, 2002. *Sem in Integr Med*, **2**:54-71.

Bellikci Koyu E, Şarer Yürekli BP, Seçkiner S, Özdemir N, Büyüktuncer Z. 2020. Use of herbals for weight loss in Turkey. *Progr Nutr*, **22**.

Bertholee D, ter Horst PG, Wieringa A, Smit JP. 2013. Life-threatening psychosis caused by using sibutramine-contaminated weight-loss coffee. *Nederlands Tijdschrift Voor Geneeskunde*, **157**: A6676-A6676.

Bertisch S, Wee C, McCarthy E. 2008. Use of Complementary and Alternative Therapies by Overweight and Obese Adults. *Obesity*, **16(7)**:1610-1615.

Blanck H, Serdula M, Gillespie C *et al*. 2007. Use of Nonprescription Dietary Supplements for Weight Loss Is Common among Americans. *J Am Diet Assoc*,**107(3)**:441-447.

Center for Disease Control (CDC). 2020. About adult BMI. https://www.cdc.gov/healthyweight/assessing/bmi/adult_bmi/index.html

Department of Statistics, Directorate of Family and Population Surveys. (2020). http://dosweb.dos.gov.jo/DataBank/Population_Estimares/PopulationEstimatesbyLocality.

Dobbs R, Sawers C, Thompson F, Manyika J, Woetzel J, Child P, Spatharou A. 2014. Overcoming obesity: An initial economic analysis. McKinsey & Company: www. McKinsey. com/mg, 1-106.

Eldalo AS, Alotaibi MN, Alenazi TO, Albogami HA, Mohamed KM. 2017. Use of herbal medicines in the treatment of obesity in Taif, Saudi Arabia. *Saudi J Med Med Sci*, **5**:149-154.

GBD 2015 Obesity Collaborators. Health Effects of Overweight and Obesity in 195 Countries over 25 Years | NEJM. *New Eng J Med*. https://www.nejm.org/doi/10.1056/NEJMoa1614362. Published 2021. Accessed June 27, 2021.

Hasani-Ranjbar S, Jouyandeh Z, Abdollahi M. 2013. A systematic review of anti-obesity medicinal plants - an update. *J Dia Meta Dis*, **12(1).**

Hasani-Ranjbar S, Larijani B, Abdollahi M. 2009. A Systematic Review of the Potential Herbal Sources of Future Drugs Effective in Oxidant-Related Diseases. *Infla & Allergy-Drug Targ*, **8**:2-10.

Hasani-Ranjbar S, Nayebi N, Moradi L, Mehri A, Larijani B, Abdollahi M. 2010. The Efficacy and Safety of Herbal Medicines Used in the Treatment of Hyperlipidemia; A Systematic Review. *Curr Pharm Des*. **16**:2935-2947.

Hruby A, Hu F. 2014. The Epidemiology of Obesity: A Big Picture. *Pharmacoeconomics*, **33(7)**:673-689.

Hursel R, Viechtbauer W, Westerterp-Plantenga M. 2009. The effects of green tea on weight loss and weight maintenance: a meta-analysis. *Int J Obes*, **33**:956-961.

Issa, Reem. 2018. 'Research Article Use of Herbal Remedies, Conventional Medicine, Diet and Exercise for Weight Loss: Case Study of University Students in Jordan', *Pak. J. Nutr*, **17**: 76-88.

Jurgens T, Whelan A, Killian L, Doucette S, Kirk S, Foy E. 2012. Green tea for weight loss and weight maintenance in overweight or obese adults. *Coch Data of Sys Rev*, **12**: 3-21.

Khani, Khan RA, Afroz S, Siddiq A. 2010. Evaluation of the hypolipidemic effect of citrus lemon. *J Basic and App Sci*, **6**: 39-43.

Khawandanah J, and Tewfik I. 2016. Fad diets: lifestyle promises and health challenges. *Journal of Food Research*, **5(6):** 80.

Khawandanah J, Tewfik I. 2016. Fad Diets: Lifestyle Promises and Health Challenges. *J Food Res*, **5(6)**:80.

Kuchkuntla A, Limketkai B, Nanda S, Hurt R, Mundi M. 2018. Fad Diets: Hype or Hope?. *Curr Nutr Rep*, **7**:310-323.

Lenon G, Li K, Chang Y, *et al*. 2012. Efficacy and Safety of a Chinese Herbal Medicine Formula (RCM-104) in the Management of Simple Obesity: A Randomized, Placebo-Controlled Clinical Trial. *Evidence-Based Comp and Alter Med*, **2012**:1-11.

Maharlouei N, Tabrizi R, Lankarani K *et al*. 2018. The effects of ginger intake on weight loss and metabolic profiles among overweight and obese subjects: A systematic review and meta-analysis of randomized controlled trials. *Crit Rev Food Sci Nutr*, **59**:1753-1766.

Martin, S, B Schneider, L Heinemann, V Lodwig, H-J Kurth, H Kolb, and WA Scherbaum. 2006. 'Self-monitoring of blood glucose in type 2 diabetes and long-term outcome: an epidemiological cohort study', *Diabetologia*, **49**: 271-78

Noble H, Smith J. 2015. Issues of validity and reliability in qualitative research. *Evid Base Nur*, **18**:34-35.

Pamukcu Gunaydin G, Dogan N, Levent S, Kurtoglu Celik G. 2015. Herbal Weight Loss Pill Overdose: Sibutramine Hidden in Pepper Pill. *Case Rep Emerg Med*, 2015:1-3.

Pittler M, Schmidt K, Ernst E. 2005. Adverse events of herbal food supplements for bodyweight reduction: systematic review*. *Obes Rev*, **6**:93-111.

Posadzki P, Watson L, Ernst E. 2012. Contamination and adulteration of herbal medicinal products (HMPs): an overview of systematic reviews. *Eur J Clin Pharmacol*, **69**:295-307.

Rahim H, Sibai A, Khader Y *et al*. 2014. Non-communicable diseases in the Arab world. *The Lancet*, **383**:356-367.

Samojlik I, Mijatović V, Gavarić N, Krstin S, Božin B. 2013. Consumers' attitude towards the use and safety of herbal medicines and herbal dietary supplements in Serbia. *Int J Clin Pharm*, **35**:835-840.

Sushama, Sharma, and Thakur Nandita. 2012. 'Study on self-medication and self diet-management by women of Indore city, India', *Res J Recent Sci . ISSN*, **2277**: 2502.

Tejpal S, Bastie C, Seetharaman J. 2018. Lemon Juice: A potential source of Angiotensin-Converting Enzyme antagonism for weight loss and insulin resistance. *Proc of the Nutr Soc*, **77**(OCE4).

Tomiyama A, Carr D, Granberg E *et al*. 2018. How and why weight stigma drives the obesity 'epidemic' and harms health. *BMC Med*, **16**(1).

Tremmel M, Gerdtham U, Nilsson P, Saha S. 2017. Economic Burden of Obesity: A Systematic Literature Review. *Int J Environ Res Public Health*,**14**:435.

JJBS

Volume 15, Number 4,December 2022
ISSN 1995-6673
Pages 553 – 559
https://doi.org/10.54319/jjbs/150403

Jordan Journal of Biological Sciences

Characterizing New Genomic and Proteomic Variations among SARS-CoV-2 Strains

Nzar A. A. Shwan[1,*], Sarkar S. Aziz[2], Bahra K. Hamad[1], Omar A. Hussein[3]

[1] Medical Laboratory Technology Department, Erbil Technical Health and Medical College, Erbil Polytechnic University, Erbil, Iraq
[2] Medical Laboratory Technology Department, Soran Technical College, Erbil Polytechnic University, Erbil, Iraq [3] Medical Laboratory Technology Department, Shaqlawa Technical College, Erbil Polytechnic University, Erbil, Iraq

Received: Jan 15, 2022; Revised: April 24, 2022; Accepted May, 11, 2022

Abstract

Since its emergence, COVID-19 has caused severe health problems, and reached more than 220 countries. The viral genome is prone to mutations leading to the appearance of new variants that might be more infectious. Many new genomic sequences of SARS-CoV-2 are uploaded to the public database; monitoring these sequences for possible variations can significantly help in the process of vaccine development and prevention plans. This study aimed to explore whole genome sequences of SARS-CoV-2 that are recently submitted to global databases from different geographical areas for possible new mutations. For this purpose, forty complete genomic sequences of SARS-CoV-2 from 20 countries were downloaded from GISAID (12 Dec 2020 -20 Mar 2021) and converted to their corresponding amino acid sequences using Expasy online software. Both the DNA and amino acid sequences were aligned with the reference genome (Accession number; NC_045512) by the multiple-sequence alignment tool Clustal Omega. The aligned sequences were then examined for any change compared to the reference genome.

The results showed a total of 1264 nucleotide variations; 93.43% were SNPs, 6.49% deletions, and 0.08% insertions. About 59% were non-synonymous mutations and 41% were synonymous mutations. Most of the non-synonymous mutations that lead to amino acid changes were in the Spike (36.63%) and Nucleocapsid (15.60%) genes. Among these changes 24 unique amino acid variations were repeated more than five times, dispersed among the following proteins NSP3, NSP6, NSP12, Spike, ORF3a, and Nucleocapsid.

The analysis in this study revealed an increase in the number of variations accumulated throughout the pandemic, and most of the non-synonymous mutations were in the Spike and Nucleocapsid genes. Sustained molecular surveillance of SARS-CoV-2 is essential to identify new variants and their impact on control measures of the pandemic and also important in the process of vaccine production.

Keywords : COVID-19, SARS-CoV-2 Sequences, Variations, Bioinformatics

1. Introduction

The recent pandemic, Coronavirus Disease-2019 (COVID-19) caused by Severe Acute Respiratory Syndrome-Coronavirus2 (SARS-CoV-2) has made a threatful health problem since its appearance in Wuhan City, China(Wu *et al.*, 2020, Li *et al.*, 2020). This pandemic has reached 220 countries, infected at least 206,987,517 individuals, and caused 4,358,629 deaths. In Iraq, the number of cases has reached 1,761,143 and 19,541 deaths, as of 10th May 2021 (Worldometer, 2021).

Coronaviruses (CoVs) are members of a diverse family of enveloped, positive-sense, single-stranded RNA-viruses, called Coronaviridae(Alluwaimi *et al.*, 2020). The CoVs include four genera, the α- and β-CoV infect mammals, whereas γ- and δ-CoV are related to birds (Worldometer, 2021, Guo *et al.*, 2020). Seven species of CoVs are capable of infecting humans. The α-CoVs HCoV-229E, HCoV-NL63, β-CoVs HCoV-HKU1, and HCoV-OC43 give rise to mild respiratory symptoms similar to the common cold (Guo *et al.*, 2020, Liu *et al., 2021*), while the β-CoVs, SARS-CoV, and Middle East Respiratory Syndrome-Coronavirus (MERS-CoV) lead to severe and possibly fatal respiratory tract infections (Guo *et al.*, 2020). The results of whole genome sequencing analysis have revealed that the SARS-CoV-2 is 96.2% similar to bat CoV (RaTG13), 79.5% to SARS-CoV, and 50% to MERS (Guo *et al.*, 2020, Hu *et al.*, 2021).

The genome size of SARS-CoV-2 is 29903 nucleotides, which contains 12 open reading frames (ORFs) encoding 27 proteins (Rahimi *et al.*, 2021, Gordon *et al.*, 2020, Wu *et al.*, 2020). It starts with 265 nucleotides, 5′ UTR, and ends with 358 nucleotides, 3′ UTR. The first ORF spans over 67% of the viral genome encoding 16 non-structural proteins (NSPs); these NSPs are mainly involved in the transcription and replication processes of the viral genome. Followed by the structural genes; membrane (M), Spike glycoprotein (S), Nucleocapsid (N), and Envelope (E) genes respectively. The other accessory proteins are

* Corresponding author. Tel.: +0-000-000-0000 ; fax: +0-000-000-0000 ; e-mail: author@institute.xxx .

encoded by the remaining ORFs dispersed between the structural genes (Kumar *et al.*, 2020).

Variations in the nucleotides and amino acid sequences are necessary for the viruses to adapt and evolve in the environment or the host. These variations enable viruses to evade the host immune system (Agudelo-Romero *et al.*, 2008). Furthermore, some variations might alter the pathogenicity or the rate of infectivity of the virus (Abdullahi *et al.*, 2020). For instance, mutations in the furin cleavage site have made SARS-CoV-2 more contagious than SARS-CoV (Huang *et al.*, 2020).

Due to the rapid spread of the disease, several studies have been conducted seeking changes in the viral genome. Koyama *et al.* (2020) analyzed 10,022 SARS CoV-2 genomes from 68 countries; most of the genome sequences were isolated in the United States of America, the United Kingdom, and Australia. Overall, their analysis showed 5,775 distinct genome variants (Koyama *et al.*, 2020).

Analysis of further genomic sequences in a wider range of countries (28 countries) has shown variants correlated with increased transmissibility, infectivity, and fatality rate (Dumonteil *et al.*, 2021, Toyoshima *et al.*, 2020).

Since its emergence, many genomic sequences of SARS-CoV2 were uploaded to the global databases from diverse geographic areas and at different times (NCBI, 2021, Gisaid.org, 2021). It is crucial to monitor these genomic sequences for possible variations to understand and trace the evolution and spread of the virus; in turn, this will have a significant contribution to versatile planning in the prevention and development of therapeutic vaccines for the virus, as well as self and community protective measures. This study aimed to analyze genomic and proteomic sequences of SARS-CoV-2, specifically those newly submitted to global databases from different geographical areas and explore the mutation rate and the effect of these mutations on the proteins produced by the virus.

2. Methodology

2.1. *Whole genomic sequences*

Forty genomic sequences of SARS-CoV-2 were downloaded from the GISAID (Gisaid.org, 2021) from 20 countries as FASTA format file (Mexico, Bulgaria, France, Italy, Belgium, Ukraine, Botswana, Brazil, Spain, Indonesia, Russia, Romania, Ghana, USA, Czech Republic, Monaco, Austria, Cameroon, England, and Scotland) (Table 1). The reference sequence of SARS-CoV2 (Accession number; NC_045512, Dec/2019) was obtained from NCBI (NCBI, 2021).

Table 1 The continents where the genomic sequences of SARS-CoV-2 were downloaded from.

Continents	*No. of countries*	*No. of sequences*
Asia	1	2
Europe	13	29
North America	2	5
South America	1	1
Africa	3	3
Sum	20	40

The downloaded sequences in this study were originally uploaded to GISAID (Gisaid.org, 2021) between 12/Dec/2020 to 20/Mar/2021. For the bioinformatic analysis only high-quality and full-length sequences with known collection date were included in this study. Incomplete and low coverage sequences with more than 5% ambiguous bases (Ns) were excluded.

2.2. *Sequence processing and alignment*

Before we proceed with the analysis, a single FASTA format file was created, including all the 40 genomic sequences along with the reference genome. This file was then used to convert the genomic sequences to their relevant amino acid sequences by the online bioinformatic software Expasy (Duvaud *et al.*, 2021). Then, both the nucleotide and amino acid reference sequences were annotated by SnapGene software (V 5.1.5) to determine and highlight the exact position of the genes and proteins, based on the information provided by the reference sequence of SARS-CoV2 on NCBI (NCBI, 2021).

Finally, the FASTA files for both the genomic sequences and the amino acid sequences were used in the multiple-sequence alignment tool (Clustal Omega) to align both nucleotide and amino acid sequences in two separate runs (Sievers *et al.*, 2011, Gasteiger *et al.*, 2003).

2.3. *Result visualization*

The results of the alignments were visualized by the UGENE software (V.37). The nucleotide and amino acid variations were observed in the aligned sequences when compared to the reference sequences. The observed variations in the genomes and proteins were recorded in Microsoft Excel (V. Professional plus 2016), which then were analysed accordingly.

3. Results

Forty genomic and proteomic sequences of SARS-CoV2 derived from twenty countries downloaded were compared and analyzed with the reference sequence (Accession number; NC_045512). The total number of nucleotide variations was 1264, of which 1181 (93.43%) variations were SNPs, 82 (6.49%) deletions and 1 (0.08%) insertion. The average nucleotide variation per sequence was 31.6, as shown in (Figure 1).

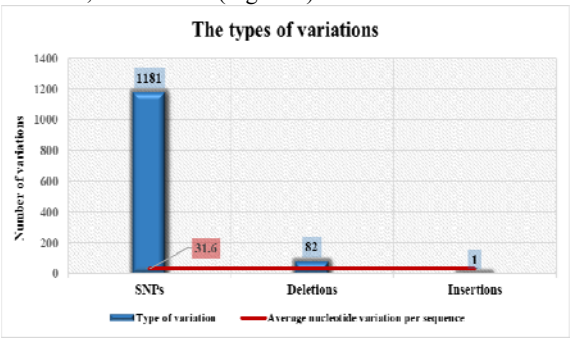

Figure 1. The types of variations. Of the total 1264 variations observed, 1181 (93.43%) are SNPs, 82 (6.49%) deletions, and 1 (0.08%) insertion (Blue columns). The average nucleotide variation per sequence (Redline) is 31.6.

Of these 1264 nucleotide variations, 745 (59%) had changed amino acid sequences (non-synonymous mutations), while the other 519 (41%) were synonymous, which had not altered the codon sequences in a manner to change the corresponding amino acid compared to the reference sequence (Figure 2).

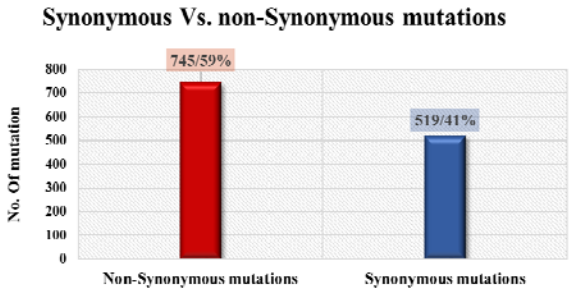

Figure 2: Synonymous Vs. Non-synonymous mutations. 59% of the observed variations changed the amino acid sequence (Non-synonymous mutations shown as red column), while the remained 41% were silent mutations that didn't alter the amino acid sequence (Synonymous mutations shown as blue column).

Based on the type of the nucleotide change, the most frequent nucleotide conversion was Cytosine (C) changed to Thymine (T) (521 /44.1%) (Figure 3), followed by Adenine (A) to Guanine (105/ 8.9%), G to T (90/ 7.63%), T to C (86/ 7.28%), G to A (80/ 6.77%), and A to T (79/ 6.7%). C to A and G to C both 74 times (6.265%), T to A (28/ 2.38%), T to G (27/ 2.28%), A to C (11/ 0.93%) and C to G with the least number (6/ 0.5%). The C substitution to other nucleotides was about 50.8%. The G substitution to other nucleotides was 20.6%, T to other nucleotides was 11.9%, and A to other nucleotides was 16.5%.

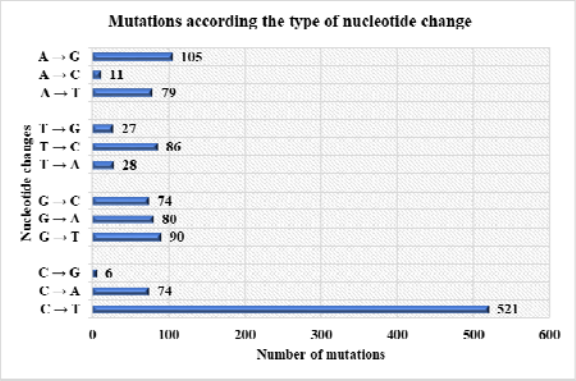

Figure 3: Types of nucleotide changes. The C substitution to other nucleotides is the most frequent nucleotide change with 50.8%. The C → T change shown at the bottom of the graph is the most prominent nucleotide change (44.1%). Other mutations are close to each other in distribution (The C substitutions: 20.6%, T substitutions: 11.9%, and A substitutions: 16.5%).

On the protein level, the most variations were located in the spike protein with 273 (36.63%) of the total 745 amino acid variations (Figure 4). Oppositely, the lowest number of variations was 1(0.12%) in NSP8 and Envelope protein, and 0 in the NSP1, NSP15, ORF6, and ORF7b. Other proteins were NSP7 and ORF7a with 2 (0.29%) variations, NSP16 (3/ 0.40%), NSP14 and ORF10 (4/ 0.53%), Membrane protein and NSP5 (5/ 0.67%), NSP9(8/ 1.10%), NSP4 (10/ 1.34%), NSP13 (18/ 2.40%), NSP2(20/ 2.69%), ORF3a (23/ 3.08%), NSP6 (32/ 4.28%), NSP12 (53/ 7.11%), ORF8 (71/ 9.52%), NSP3 (92/ 12.33%) and Nucleocapsid protein with 116 variations (15.60%). The average amino acid variation was 18.625.

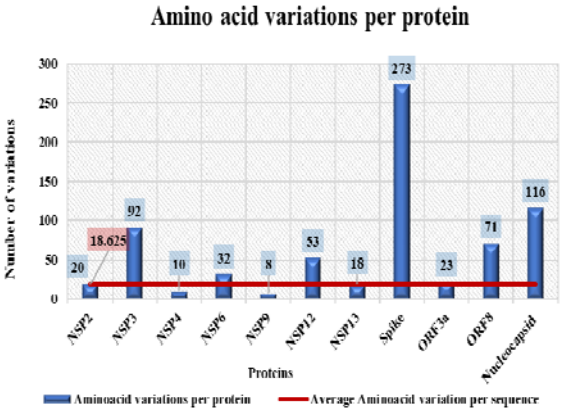

Figure 4: Amino acid variations of proteins for SARS-CoV-2 (Blue columns). The highest number of variations have been recorded in the spike protein (273), followed by Nucleocapsid (116) and to a lesser extent in NSP3 (92). Proteins with a low number of variations (NSP8, Envelope protein, NSP1, NSP15, ORF6, ORF7b, NSP7, ORF7a, NSP16, NSP14, ORF10, Membrane Protein, NSP5) are not shown here. The average amino acid variation per sequence is 18.6 (Red line).

Finally, this study showed the presence of significant amino acid variations revealed by their high frequency. In the analysis, twenty-four amino acid variations were repeated more than five times for 7 different proteins (Figure 5). Of these, three variations were from NSP3, T183I, A890D, and I1412T, all found in 19 different aligned sequences. 106-108 Del from NSP6 has been repeated 21 times. There were 39 times repetitions of P323L at NSP12. In the spike protein, there were nine amino acid variations which are 68-70 Del and A570D with both 20 times, P681H (22 times), D614G (39 times), N501Y (23 times), 144 Del (19 times), and 19 times repetition for T716 I, S982A and D1118H. ORF3a contained one such variation, which is Q57H that is repeated seven times. The Q27, R52 I, and Y73C with the frequency of 19, and K68 with nine presented in ORF8. Five frequent variations were found in the N protein; these are R203K, and G204R shared in 26 sequences, T205I found in 6 sequences, S235F, and D3L repeated in 19 sequences. The remaining amino acid variations with frequencies lower than five were neglected.

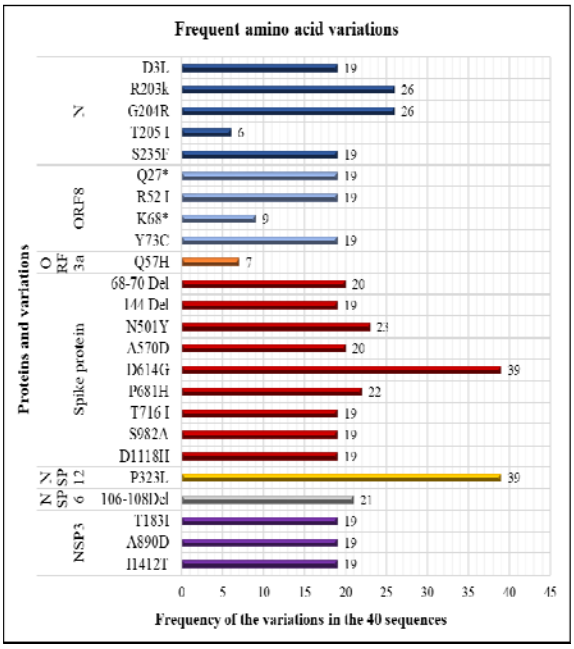

Figure 5: Frequency of highly repeated amino acid variations (more than five times) within the 40 SARS-Cov-2 genome sequences. D614G in spike protein and P323L in NSP12 (39 times), with R203S and G204R in Nucleocapsid protein, are the most repeated changes among the frequent amino acid variation.

4. Discussion

This study analysis showed a high number of nucleotide variations, with an average of 31.6 from 40 genomic sequences when compared to the reference sequence (Accession number; NC_045512). The predominant type of variation was SNPs. This phenomenon is suggested to be associated with the error-prone viral RNA-dependent RNA polymerase or by mechanisms of the host cell RNA editing enzymes as a defense mechanism (Mercatelli and Giorgi, 2020).

The type of nucleotide change (shown in Figure 3) showed C→T change to score the highest value. The average nucleotide variation in this study was higher than in the study by (Mercatelli and Giorgi, 2020). It might be caused by the higher number of mutations accumulated over time, and a lower number of sequences analyzed in this study. The reason for this mutational bias toward C→T is not completely understood, but there are two possible explanations, the codon usage bias, and the RNA editing host enzyme APOBEC (Pollpeter *et al.*, 2018, Ghosh and Chakraborty, 2020). However, it has been observed that the translational preference of a few codons is strongly correlated with the mutational bias imposed by genome compositional constraint and influenced by natural selection, especially in the second and third codon position, which is more biased towards the AT/U content. This is determined by the relative synonymous codon usage (RSCU) value with an average of 64.19% at the second position and 65.24% at the third position, respectively (Ghosh and Chakraborty, 2020).

Of the 1264 nucleotide variations, there were more non-synonymous mutations in comparison to synonymous mutations (shown in Figure 2). Analysis of 3067 SARS-CoV-2 whole genome sequences isolated from 55 countries revealed 782 variant sites, 65.98% non-synonymous, and 28.39% synonymous mutations. The remaining 5.63% was in the intergenic regions of the genome (Laamarti *et al.*, 2020). Despite the higher number of sequences included in the study, the number of variations is lower compared to the current study. These differences might be due to different submission dates of the downloaded sequences. Furthermore, Laamarti *et al.* (2020) analyzed sequences from the first three months of the emergence of the disease, while the sequences analyzed in this study were after twelve months (December 2020); for this reason, a higher number of variations potentially accumulated since the emergence of the virus in Wuhan, China at December 2019 (Laamarti *et al.*, 2020).

Non-synonymous mutation distribution (shown in Figure 4) shows the predominance of variants in S and N proteins. Other proteins contained a lower number of variations, and some of them had no variation at all. The high mutation rate in the spike protein is due to its receptor-binding properties and immunogenicity, and it is supposed to be the major target for antibodies (Singh *et al.*, 2020). The N protein is also one of the critical targets for B cells to be targeted by antibodies, the most abundant protein in coronaviruses, and highly immunogenic (Oliveira *et al.*, 2020). Both proteins are under immune system pressure (Forni *et al.*, 2020).

We only recorded the most repeated mutations, equal to or more than five-time frequency. Of these recorded mutations, the 68-70 Del, A570D, P681H, D614G, N501Y, 144 Del, T716 I, S982A, and D1118H were in the S protein (shown in Figure 5). Similar mutations were found in VOC belonging to B.1.1.7 from the viral sequences in Czech Republic, France, Ukraine, Ghana, Italy, England, Bulgaria, Spain, Belgium and Botswana (Davies *et al.*, 2020, Ramirez *et al.*, 2021, ASSESSMENT, 2020).

Some preliminary data on the effect of 68-70 Del, N501Y, D614G, and P681H has been discovered. The G614 variant, which has emerged as a predominant clade in Europe and is spreading worldwide, predominates over time in locales where it is found, implying that this change enhances viral transmission. This mutation increases the entry to ACE2-expressing cells more efficiently due to the decreased shedding of the S1-domain and higher incorporation of S-protein into the virion (Zhang *et al.*, 2020, Isabel *et al.*, 2020). The N501Y mutation appears to increase the affinity of interaction with murine and human ACE2, as it is one of the key residues in the receptor-binding domain of Spike protein (Ramirez *et al.*, 2021, Gu *et al.*, 2020, Starr *et al.*, 2020). The P681H is placed immediately in the spike furin cleavage site (Peacock *et al.*, 2021, Kemp *et al.*, 2020). However, the functional effect of this mutation is not well understood. The 69-70 deletion-mutation has been determined to increase the viral infectivity in vitro, associated with immune evasion in immunocompromised patients, and has also been shown to be related to the problems in the SARS-CoV-2 RT-PCRs assays targeting the S gene (Ramírez *et al.*, 2021, Kemp *et al.*, 2020b). However, the exact impacts of these mutations on transmissibility, infectivity, and clinical severity are not known up to this time and remain to be fully elucidated.

The N protein contained five frequent variations, R203K and G204R (Russia, Brazil, Cameroon, Mexico,

France, Ukraine, Ghana, Italy, England, Bulgaria, Spain, and Belgium), T205I (USA, Indonesia, Monaco, and Botswana), S235F and D3L (France, Ukraine, Ghana, Italy, England, Bulgaria, Spain, and Belgium). It has been shown that R203K and G204R increase positively charged site, and might increase local rigidity with the removal of Gly204. (Garvin *et al*., 2020). The exact role of mutations in the N beyond RNA and protein interaction interfaces in the pathogenesis of the virus requires further investigations (Singh *et al*., 2021).

The NSP3 follows the N protein based on the number of mutations per protein with 92 mutations. Three variations were frequent in our results in the NSP3, which are T183I, A890D, and I1412T (Bulgaria, Italy, Belgium, Ukraine, Spain, France, Ghana, and England). Loconsole *et al.* (2021) identified these mutations from a patient traveling back to the Apulia Region in Italy from London, UK (Loconsole *et al*., 2021). The functional effect remains to be explored.

Four recurrent mutations, Q27*, R52I, Y73C, and K68*, were identified in ORF8 (France, Ukraine, Ghana, Italy, England, Bulgaria, Spain, and Belgium). The functional effect of Q27* and K68* is the truncation in the protein structure(Pereira, 2021). These mutations do not seem to have a harmful effect on the virus, as the morbidity and mortality rates have not decreased despite the presence of these mutations in the circulating variants (Pereira, 2021).

The P323L mutation in NSP12 had a frequency of 39 times (Bulgaria, Italy, Belgium, Ukraine, Italy, Spain, France, Ghana, Monaco, England). The P323L is unlikely to influence polymerase enzymatic activity directly as it is located distal to the NSP12 catalytic core. Instead, this residue is located at the surface of NSP12, near one of the binding sites for NSP8. However, this mutation could modify the NSP8 interaction or interaction with a yet unknown viral or host factor (Peacock *et al.*, 2021). Also, P323L is associated with epitope loss, which could influence the pathogenesis of antibody escape variants (Hasan *et al*., 2021). However, Hasan *et al.* (2020) describe that this mutation might affect the proofreading activity of RNA-dependent RNA polymerase (RdRp), provoking other changes (Pachetti *et al*., 2020).

The amino acid deletions 106–108 in NSP6 known as the 'SGF deletion (Bulgaria, Italy, Belgium, Ukraine, Italy, Spain, France, Ghana, Monaco, England), identically found in B.1.1.7 lineage, the P.1 lineage, and several isolates from the B.1.351 lineage. NSP6 is a multi-pass transmembrane protein that is thought to be involved in autophagy and antagonism of innate immune responses, but the influence of this deletion on virus phenotype remains unclear (Peacock *et al*., 2021). The three successive amino acid deletion 106–108 has caused these variants (P.1, B.1.1.7, and B.1.351) more transmissible than previous circulating variants with possible increased risk of hospitalization, severity, and mortality in the (B.1.1.7). No impact was reported in-hospital mortality (B.1.351), and the effect on (P.1) is under investigation (WHO, 2021).

The Q57H is located in ORF3a (US, Indonesia, Monaco, France, Botswana), which codes for a protein that regulates inflammation, antiviral responses, and apoptosis in the infected cells (Joshi *et al*., 2021). Q57H mutation might affect inflammasome activation (Hassan *et al*., 2020). Other proteins had fewer variations and did not attract much of the study's attention, although they did not contain variations repeated five or more times.

5. Conclusions

The analysis in this study showed an increased number of mutations accumulated over time, revealed by the average number of mutations per sequence (31.6) in comparison to the studies mentioned previously, in the course of the pandemic, a year after the onset. A higher number of non-synonymous mutations were recorded compared to the silent mutations. Most of these mutations were located in the Spike and Nucleocapsid proteins due to their immunogenic properties as being major targets of B cells. Our results also showed some major amino acid variations that have been shown to increase viral entry to ACE2 expressing cells.

The amino acid variations have the possibility to either positively or negatively alter proteins, subsequently changing the phenotype of the virus such as infectivity, virulence, and tissue tropism. Moreover, it can also affect the decision on the process of vaccine development.

Having applied restricted criteria for the collected sequences, one limitation of our study could be a low number of whole genome sequences included in the analysis. Including further genomic sequences and restricting the analysis on the structural genes is the ideal starting point for future analysis. Finally, continued molecular observation of the SARS-CoV-2 genome is necessary to identify new emerging variants and their impact on the control measures and prevention plans of the pandemic.

References

Abdullahi, I. N., Emeribe, A. U., Ajayi, O. A., Oderinde, B. S., Amadu, D. O. & Osuji, A. I. 2020. Implications of SARS-CoV-2 genetic diversity and mutations on pathogenicity of the COVID-19 and biomedical interventions. *J Taibah Univ Med Sci,* **15,** 258-264.

Agudelo-Romero, P., Carbonell, P., Perez-Amador, M. A. & Elena, S. F. 2008. Virus Adaptation by Manipulation of Host's Gene Expression. *PLoS One,* **3,** e2397.

Alluwaimi, A. M., Alshubaith, I. H., Al-Ali, A. M. & Abohelaika, S. 2020. The Coronaviruses of Animals and Birds: Their Zoonosis, Vaccines, and Models for SARS-CoV and SARS-CoV2. *Front Vet Sci,* **7,** 655.

Assessment, R. R. 2020. Risk related to spread of new SARS-CoV-2 variants of concern in the EU/EEA.

Davies, N.G., Abbott, S., Barnard, R.C., Jarvis, C.I., Kucharski, A.J., Munday, J.D., Pearson, C.A., Russell, T.W., Tully, D.C., Washburne, A.D. and Wenseleers, T., 2021. Estimated transmissibility and impact of SARS-CoV-2 lineage B. 1.1. 7 in England. Science, 372(6538), p.eabg3055.

Dumonteil, E., Fusco, D., Drouin, A. & Herrera, C. 2021. Genomic Signatures of SARS-CoV-2 Associated with Patient Mortality. *Viruses,* **13,** 227.

Duvaud, S., Gabella, C., Lisacek, F., Stockinger, H., Ioannidis, V. and Durinx, C., 2021. Expasy, the Swiss Bioinformatics Resource Portal, as designed by its users. *Nucleic Acids Res*, **49(W1)**, pp.W216-W227.

Forni, D., Cagliani, R., Pontremoli, C., Mozzi, A., Pozzoli, U., Clerici, M. and Sironi, M., 2021. Antigenic variation of

SARS-CoV-2 in response to immune pressure. *Mol Ecol*, 30(14), pp.3548-3559.

Garvin, M. R., Prates, E. T., Pavicic, M., Jones, P., Amos, B. K., Geiger, A., Shah, M. B., Streich, J., Gazolla, J. G. F. M. & Kainer, D. 2020. Potentially adaptive SARS-CoV-2 mutations discovered with novel spatiotemporal and explainable AI models. *Genome Biol,* **21,** 1-26.

Gasteiger, E., Gattiker, A., Hoogland, C., Ivanyi, I., Appel, R. D. & Bairoch, A. 2003. ExPASy: The proteomics server for in-depth protein knowledge and analysis. *Nucleic Acids Res,* **31,** 3784-8.

Ghosh, S. & Chakraborty, S. 2020. Phylogenomics analysis of SARS-CoV2 genomes reveals distinct selection pressure on different viral strains. *Biomed Res Int,* 2020.

Global Initiative on Sharing Avian Influenza Data.Org. 2021. *GISAID - Initiative* [Online]. Available: https://www.gisaid.org/ [Accessed].

Gordon, D. E., Jang, G. M., Bouhaddou, M., Xu, J., Obernier, K., White, K. M., O'meara, M. J., Rezelj, V. V., Guo, J. Z., Swaney, D. L., Tummino, T. A., Hüttenhain, R., Kaake, R. M., Richards, A. L., Tutuncuoglu, B., Foussard, H., Batra, J., Haas, K., Modak, M., Kim, M., Haas, P., Polacco, B. J., Braberg, H., Fabius, J. M., Eckhardt, M., Soucheray, M., Bennett, M. J., Cakir, M., Mcgregor, M. J., Li, Q., Meyer, B., Roesch, F., Vallet, T., Mac Kain, A., Miorin, L., Moreno, E., Naing, Z. Z. C., Zhou, Y., Peng, S., Shi, Y., Zhang, Z., Shen, W., Kirby, I. T., Melnyk, J. E., Chorba, J. S., Lou, K., Dai, S. A., Barrio-Hernandez, I., Memon, D., Hernandez-Armenta, C., Lyu, J., Mathy, C. J. P., Perica, T., Pilla, K. B., Ganesan, S. J., Saltzberg, D. J., Rakesh, R., Liu, X., Rosenthal, S. B., Calviello, L., Venkataramanan, S., Liboy-Lugo, J., Lin, Y., Huang, X. P., Liu, Y., Wankowicz, S. A., Bohn, M., Safari, M., Ugur, F. S., Koh, C., Savar, N. S., Tran, Q. D., Shengjuler, D., Fletcher, S. J., O'neal, M. C., Cai, Y., Chang, J. C. J., Broadhurst, D. J., Klippsten, S., Sharp, P. P., Wenzell, N. A., Kuzuoglu-Ozturk, D., Wang, H. Y., Trenker, R., Young, J. M., Cavero, D. A., Hiatt, J., Roth, T. L., Rathore, U., Subramanian, A., Noack, J., Hubert, M., Stroud, R. M., Frankel, A. D., Rosenberg, O. S., Verba, K. A., Agard, D. A., Ott, M., Emerman, M., Jura, N., *et al.* 2020. A SARS-CoV-2 protein interaction map reveals targets for drug repurposing. *Nature,* **583,** 459-468.

Gu, H., Chen, Q., Yang, G., He, L., Fan, H., Deng, Y.-Q., Wang, Y., Teng, Y., Zhao, Z. & Cui, Y. 2020. Adaptation of SARS-CoV-2 in BALB/c mice for testing vaccine efficacy. *Science,* **369,** 1603-1607.

Guo, Y.-R., Cao, Q.-D., Hong, Z.-S., Tan, Y.-Y., Chen, S.-D., Jin, H.-J., Tan, K.-S., Wang, D.-Y. & Yan, Y. 2020. The origin, transmission and clinical therapies on coronavirus disease 2019 (COVID-19) outbreak – an update on the status. *Mil Med Res,* **7,** 11.

Hasan, M. M., Das, R., Rasheduzzaman, M., Hussain, M. H., Muzahid, N. H., Salauddin, A., Rumi, M. H., Rashid, S. M., Siddiki, A. Z. & Mannan, A. 2021. Global and local mutations in Bangladeshi SARS-CoV-2 genomes. *Virus Res,* **297,** 198390.

Hassan, S. S., Attrish, D., Ghosh, S., Choudhury, P. P. & Roy, B. 2021. Pathogenic perspective of missense mutations of ORF3a protein of SARS-CoV-2. *Virus Res,* **300,** 198441.

Hu, B., Guo, H., Zhou, P. & Shi, Z.-L. 2021. Characteristics of SARS-CoV-2 and COVID-19. *Nat Rev Microbio.,* **19,** 141-154.

Huang, Y., Yang, C., Xu, X. F., Xu, W. & Liu, S. W. 2020. Structural and functional properties of SARS-CoV-2 spike protein: potential antivirus drug development for COVID-19. *Acta Pharmacol Sin*, **41**, 1141-1149.

Isabel, S., Graña-Miraglia, L., Gutierrez, J. M., Bundalovic-Torma, C., Groves, H. E., Isabel, M. R., Eshaghi, A., Patel, S. N., Gubbay, J. B. & Poutanen, T. 2020. Evolutionary and structural analyses of SARS-CoV-2 D614G spike protein mutation now documented worldwide. *Sci Rep,* **10,** 1-9.

Joshi, M., Puvar, A., Kumar, D., Ansari, A., Pandya, M., Raval, J., Patel, Z., Trivedi, P., Gandhi, M., Pandya, L., Patel, K., Savaliya, N., Bagatharia, S., Kumar, S., & Joshi, C. 2021. Genomic Variations in SARS-CoV-2 Genomes From Gujarat: Underlying Role of Variants in Disease Epidemiology. *Front Genet, **12***, 586569.

Kemp, S.A., Collier, D.A., Datir, R.P., Ferreira, I.A., Gayed, S., Jahun, A., Hosmillo, M., Rees-Spear, C., Mlcochova, P., Lumb, I.U. and Roberts, D.J., 2021. SARS-CoV-2 evolution during treatment of chronic infection. *Nature*, *592*(7853), pp.277-282.

Meng, B., Kemp, S.A., Papa, G., Datir, R., Ferreira, I.A., Marelli, S., Harvey, W.T., Lytras, S., Mohamed, A., Gallo, G. and Thakur, N., 2021. Recurrent emergence of SARS-CoV-2 spike deletion H69/V70 and its role in the Alpha variant B. 1.1. 7. *Cell Rep*, *35*(13), p.109292.

Koyama, T., Platt, D. & Parida, L. 2020. Variant analysis of SARS-CoV-2 genomes. *Bull World Health Organ,* **98,** 495-504.

Kumar, S., Nyodu, R., Maurya, V.K., Saxena, S.K. 2020. Morphology, Genome Organization, Replication, and Pathogenesis of Severe Acute Respiratory Syndrome Coronavirus 2 (SARS-CoV-2). In: Saxena, S. (Eds). **Coronavirus Disease 2019 (COVID-19). Medical Virology: From Pathogenesis to Disease Control**. Springer, Singapore, pp. 21-23.

Laamarti, M., Alouane, T., Kartti, S., Chemao-Elfihri, M., Hakmi, M., Essabbar, A., Laamarti, M., Hlali, H., Bendani, H. & Boumajdi, N. 2020. Large scale genomic analysis of 3067 SARS-CoV-2 genomes reveals a clonal geo-distribution and a rich genetic variations of hotspots mutations. *PloS one,* **15,** e0240345.

Li, H., Liu, S.-M., Yu, X.-H., Tang, S.-L. & Tang, C.-K. 2020. Coronavirus disease 2019 (COVID-19): current status and future perspectives. *Int J Antimicrob Agents,* **55,** 105951.

Liu D.X., Liang J.Q., Fung T.S. 2021. Human Coronavirus-229E, -OC43, -NL63, and -HKU1 (Coronaviridae). In: Bamford, D. H. and Zuckerman, M, (eds). **Encyclopedia of Virology**, Academic Press, United States, pp. 428–440.

Loconsole, D., Sallustio, A., Accogli, M., Centrone, F., Capozzi, L., Del Sambro, L., Parisi, A. & Chironna, M. 2021. Genome sequence of a SARS-CoV-2 VUI 202012/01 strain identified from a patient returning from London, England, to the Apulia Region of Italy. *Microbiol Resour Announc,* **10,** e01487-20.

Mercatelli, D. & Giorgi, F. M. 2020. Geographic and genomic distribution of SARS-CoV-2 mutations. *Front Microbiol,* **11,** 1800.

National Center for Biotechnology Information, N. C. F. B. I. 2021. *NCBI Virus* [Online]. Available: https://www.ncbi.nlm.nih.gov/labs/virus/vssi/#/. [Accessed].

Oliveira, S. C., De Magalhães, M. T. & Homan, E. J. 2020. Immunoinformatic analysis of SARS-CoV-2 Nucleocapsid protein and identification of COVID-19 vaccine targets. *Front Immunol,* **11,** 2758.

Pachetti, M., Marini, B., Benedetti, F., Giudici, F., Mauro, E., Storici, P., Masciovecchio, C., Angeletti, S., Ciccozzi, M. & Gallo, R. C. 2020. Emerging SARS-CoV-2 mutation hot spots include a novel RNA-dependent-RNA polymerase variant. *J Transl Med,* **18,** 1-9.

Peacock, T.P., Goldhill, D.H., Zhou, J., Baillon, L., Frise, R., Swann, O.C., Kugathasan, R., Penn, R., Brown, J.C., Sanchez-David, R.Y. and Braga, L., 2021. The furin cleavage site in the SARS-CoV-2 spike protein is required for transmission in ferrets. *Nat Microbiol*, *6*(7), pp.899-909.

Peacock, T. P., Penrice-Randal, R., Hiscox, J. A. & Barclay, W. S. 2021. SARS-CoV-2 one year on: evidence for ongoing viral adaptation. *J Gen Virol,* **102,** 001584.

Pereira, F. 2021. SARS-CoV-2 variants combining spike mutations and the absence of ORF8 may be more transmissible and require close monitoring. *Biochem Biophys Res Commun,* **550,** 8-14.

Pollpeter, D., Parsons, M., Sobala, A. E., Coxhead, S., Lang, R. D., Bruns, A. M., Papaioannou, S., Mcdonnell, J. M., Apolonia, L. & Chowdhury, J. A. 2018. Deep sequencing of HIV-1 reverse transcripts reveals the multifaceted antiviral functions of APOBEC3G. *Nat Microbiol,* **3,** 220-233.

Rahimi, A., Mirzazadeh, A. & Tavakolpour, S. 2021. Genetics and genomics of SARS-CoV-2: A review of the literature with the special focus on genetic diversity and SARS-CoV-2 genome detection. *Genomics,* **113,** 1221-1232.

Ramírez, J. D., Muñoz, M., Patiño, L. H., Ballesteros, N. & Paniz-Mondolfi, A. 2021. Will the emergent SARS-CoV2 B. 1.1. 7 lineage affect molecular diagnosis of COVID-19? *J Med Virol,* **93,** 2566-2568.

Sievers, F., Wilm, A., Dineen, D., Gibson, T. J., Karplus, K., Li, W., Lopez, R., Mcwilliam, H., Remmert, M., Söding, J., Thompson, J. D. & Higgins, D. G. 2011. Fast, scalable generation of high-quality protein multiple sequence alignments using Clustal Omega. *Mol Syst Biol,* **7,** 539.

Singh, J., Samal, J., Kumar, V., Sharma, J., Agrawal, U., Ehtesham, N. Z., Sundar, D., Rahman, S. A., Hira, S. & Hasnain, S. E. 2021. Structure-function analyses of new SARS-CoV-2 variants B. 1.1. 7, B. 1.351 and B. 1.1. 28.1: clinical, diagnostic, therapeutic and public health implications. *Viruses,* **13,** 439.

Singh, P. K., Kulsum, U., Rufai, S. B., Mudliar, S. R. & Singh, S. 2020. Mutations in SARS-CoV-2 leading to antigenic variations in spike protein: a challenge in vaccine development. *J Lab Physicians,* **12,** 154-160.

Starr, T. N., Greaney, A. J., Hilton, S. K., Ellis, D., Crawford, K. H. D., Dingens, A. S., Navarro, M. J., Bowen, J. E., Tortorici, M. A., Walls, A. C., King, N. P., Veesler, D. & Bloom, J. D. 2020. Deep Mutational Scanning of SARS-CoV-2 Receptor Binding Domain Reveals Constraints on Folding and ACE2 Binding. *Cell,* **182,** 1295-1310 e20.

Toyoshima, Y., Nemoto, K., Matsumoto, S., Nakamura, Y. & Kiyotani, K. 2020. SARS-CoV-2 genomic variations associated with mortality rate of COVID-19. *J Hum Genet,* **65,** 1075-1082.

World Health Organization. 2021. *COVID-19 Weekly Epidemiological Update* [Online]. Available: https://www.who.int/docs/default-source/coronaviruse/situation-reports/20210309_weekly_epi_update_30.pdf [Accessed March 7 2021].

Worldometer. 2021. *COVID-19 Coronavirus Pandemic* [Online]. Available: https://www.worldometers.info/coronavirus/ [Accessed May 10 2021].

Wu, P., Duan, F., Luo, C., Liu, Q., Qu, X., Liang, L. & Wu, K. 2020. Characteristics of Ocular Findings of Patients With Coronavirus Disease 2019 (COVID-19) in Hubei Province, China. *JAMA ophthalmol,* **138,** 575-578.

Zhang, L., Jackson, C. B., Mou, H., Ojha, A., Peng, H., Quinlan, B. D., Rangarajan, E. S., Pan, A., Vanderheiden, A. & Suthar, M. S. 2020. SARS-CoV-2 spike-protein D614G mutation increases virion spike density and infectivity. *Nat Commun,* **11,** 1-9.

JJBS

Volume 15, Number 4,December 2022
ISSN 1995-6673
Pages 561 – 567
https://doi.org/10.54319/jjbs/150404

Jordan Journal of Biological Sciences

Artificial Intelligence Derived Artemisinin Drug Compound Acts as an Effective Candidate against SARS-CoV-2 Receptors: An In-Silico Study to Combat COVID-19

Padma K.R.and Josthna.P*

Assistant Professor, Department of Biotechnology, Sri Padmavati Mahila VisvaVidyalayam (Women's) University, Tirupati, AP

Received: Dec 25, 2021; Revised: May 14, 2022; Accepted May, 20, 2022

Abstract

Background: Global outburst of coronavirus has challenged the whole world to discover drugs to combat the current pandemic. Repurposing drugs is a promising approach as it provides new openings to challenge the emerging COVID-19. However, in the epoch of big data, artificial intelligence (AI) technology offers to leverage computational methods for finding new candidate drugs through an In-silico approach.

Aim and Objectives: The aim and objectives of our present work basically are the designing of a plant-derived compound against the COVID-19 receptors which might act as effective therapy along with predicting the outcome of the disease with a deep learning program language that is python (anaconda) 2.7 version.

Methodology: Artificial Intelligence technology helps in understanding the interactions of coronavirus with receptors through the computer-aided drug designing process (CADD). The ligand-protein interactions were prepared with the Maestro (Schrödinger) program which aids to study the docking pose of artemisinin compound with SARS-CoV-2 receptors like 7CTT, a nonstructural protein (NSP) and 7MY3 Spike glycoprotein. Thus, Artificial Intelligence technology examines the drug-target interaction with Neural Networking built with a deep learning machine algorithm and predicts the outcome of the disease with python program language.

Results: Artemisinin exhibited the highest antiviral activity against the SARS-CoV-2 receptors like 7CTT and 7MY3. The three-dimensional structures of the ligands and SARS-CoV-2 receptors were retrieved from the PubChem Open Chemistry Database. The ligand-protein interactions were performed with the help of the Maestro (Schrödinger) program, which revealed MM/GBSA values of 7CTT interaction with derivative ligands of antimalarial compounds such as D95 (-45.424), artemisinin (-35.222), MPD (-31,021), MRD (-21.952) and 6FGC (-34.089), whereas with 7MY3 spike glycoprotein interactions MMGBSA values for D95 (-26.304), MPD(-18.658), MRD(-28.03) and 6FGC (-13.47) binding affinities have followed Lipinski rule of 5 and further predicted the outcome with random forest decision tree with an accuracy of about 75% with python program.

Conclusion: Repurposing of the drug through an In-silico approach against the SARS-CoV-2 virus revealed its antiviral actions. The docking studies approach has shown the XP score, gliding energy, and MMGBSA values which were predicted with a deep learning program built with Artificial Intelligence technology.

Keywords: Artemisinin, SARS-CoV-2, Lipinski rule, Protein-ligand interactions, Random Forest decision tree, Artificial Intelligence

1. Background

Coronavirus belongs to the viral family Coronaviridae which is mainly accountable for instigating pneumonia-like symptoms and hence regarded as a worldwide menace ever since its first outburst in 2002 (Jabeer Khan 2020). The variants of Severe Acute Respiratory Syndrome Disease (SARS), and Middle East Respiratory Syndrome (MERS) materialized in the years 2002 & 2013, correspondingly leading to elevated gastrointestinal and pulmonary dysfunction (Hilgenfeld and Peiris, 2013). Nevertheless, the third outbreak of SARS-COV-2 was in 2019 with symptoms ranging from the common cold to more severe acute respiratory failure (Kong WH. *et al.,* 2020). WHO (World Health Organization) has announced this malady as a pandemic and revealed that it continually spread the virus to more than 20 million populace (Worldometer, 2020). Nevertheless, it is currently acknowledged as the greatest materialization of communal health.

Literature reports from various studies have recognized the incubation periods for COVID-19 to be one week from day one of contact (Lauer *et al.,* 2020; Backer *et al.,* 2020). However, in accordance with China's Novel Coronavirus Pneumonia Diagnosis & Treatment Plan (Seventh Edition Trial) based on the signs and symptoms. Nevertheless, COVID-19 patients are classified into trivial, modest, severe, and critical based on their signs & symptoms. Nevertheless, several scientists are underway on a number of clinical trials such as cell therapy, antiviral therapy, immunotherapy, and the use of Chinese herbal medicine approved by the Food and Drug Administration (FDA) against COVID-19 (Jean *et al.,* 2020). Various, antiviral

* Corresponding author. e-mail: penchalanenijosthna@gmail.com.

compounds such as lopinavir & ritonavir have not revealed antiviral efficacy in contrast to standard therapy (Guan 2020). The antimalarial agents such as chloroquine and hydroxychloroquine are confrontational. Nonetheless, limited clinical trials have revealed that hydroxychloroquine has failed to treat COVID-19 (Tang 2019). The National Institute of Health has counselled suspending the clinical trials involving hydroxychloroquine since it is harmless, and many reports displayed its ineffectiveness (National Institute of Health).

Naturally occurring substances found in phytomedicines have been shown to have therapeutic potential but differing mechanistic activities against SARS-CoVRSCoV-2 based on prior reports on their safety profiles (Huang *et al.,* 2020). The angiotensin-converting enzyme 2 (ACE2), heat shock protein A5 (HSPA5), and substrate-binding domain (SBD) of SARSCoV-2 are involved in the attachment of the virus to human cells, but Kumar *et al*., (2020) and Elfiky (2020) have demonstrated that natural products have the capacity to impair this attachment. Several other studies also demonstrated that the SARS-CoV-2 papain-like protease (PLpro) was inhibited by plant-based compounds obtained from various plant species, including ginger and Alpinia officinarum (Goswami *et al.,* 2020).

However, the idea of repurposing a medicine is widely used nowadays to identify the likely treatments for the current pandemic sickness.. It has acquired greater perceptiveness for the capability to recycle already existing drugs (Jin *et al.,* 2020; Kandeel and Al-Nazawi, 2020). In contrast, artificial intelligence algorithms built with machine learning plus big data are regarded as supporting tools for molecular level discern. The AI developments and latest advancements in all fields of science and engineering have grasped the attention of all researchers to study the interactions of plant-derived compounds with receptors which might produce very less side effects and prolong the life span of the human species for many years. However, entire drugs predicted by employing AI technology in drug discovery were found to be potential against coronavirus (Ho, 2020). Currently, artificial intelligence machinery has been exercised broadly for exploiting drug research contrary to COVID-19. Moreover, the Artificial Intelligence platform was ascertained to be more helpful for the recognition of potentially available drugs with inhibitory activities on human coronavirus (HCoV) by employing several learning datasets (Ke *et al.,* 2020). However, the organically available plant flora rich in Phyto-constituents offer a beneficial and influential source of chemical compounds indicating antiviral activity.

In order to expand vision on the mode of action of artesunate, the most potential malarial compound was examined by Yuyong Zhou *et al.,* (2021) and carried out a time-of addition assay in the A549-hACE2 in-vitro cell line. However, Cao *et al.,* (2020) investigated artemisinin, artesunate, and its derivatives for efficacy against SARS-CoV-2 on the A549-hACE2 cell line. Further studies on its interaction and the binding potential need to be evaluated before conducting clinical trials. Furthermore, chemical alteration of these structures, directed by computer-based docking simulations, might enhance their potentiality and selectivity (Chen *et al.,* 2018). Hence, our CADD study with help of the Artificial Intelligence technology approach is regarded as a boon to the present situation, where the whole world is facing the dreadfulness of the pandemic disease outburst. Although, vaccines are available at present naturally derived products are always effective in comparison to vaccines. Therefore, have adopted Graphical Neural Network into the bio-medical complex which assists the amalgamation of multimodal and composite relationships. Currently, GNN has revealed an immense assurance in predicting interactions (e.g., drug-drug adverse interactions, PPIs, & target-drug interactions) and in the detection of the latest molecules (Muhammad *et al.,* 2020). GNN can also promote the repurposing of drugs by characterizing the intricate interaction between drugs and maladies.

Thus, our work basically aims in the designing of the plant derived compound against the covid-19 receptors which acts as effective therapy along with predicting the outcome of the disease with a deep learning program language that is python (anaconda) 2.7 version. However, at present state, no accurate medicines are available which alarms the prospects of repurposing existing drugs which is effective. We have studied the docking pose of artemisinin compound with SARS-CoV-2 receptors like 7CTT, a non-structural protein (NSP), and 7MY3 Spike glycoprotein and predicted the outcome of the disease with python program language through a random forest decision tree approach to identify ideal and effective ligand-protein interactions which further support in future clinical trials investigation. Thus, AI-based tools helped to investigate the in-silico potentiality of the artemisinin compound against coronavirus.

2. Materials and Methods

2.1. Protein-ligand Structure preparation

For the preparation of protein-ligand Maestro11.1, Schrodinger in silico tool was utilized to examine the ligand-target interaction for current studies (Schrodinger, 2017). Nevertheless, two objectives were preferred for the study 1) 7CTT, a nonstructural protein (NSP) and 2) 7MY3 Spike glycoprotein both SARS- CoV-2 receptor-binding domain (RBD) interfacing with artemisinin compound and its derivatives.

2.2. Drug-target docking

The artemisinin and its derivatives were obtained from RCBS PDB Protein Data Bank (www.rcsb.org). All drug compounds and their derivatives were docked with 7CTT & 7MY3 SARSCoV-2 receptor using the Maestro 11.1 module of the Schrodinger software. The ligands were prepared using Protein Preparation Wizard using default settings followed by pH 7.4, whereas drug compounds and their derivatives such as D95, artemisinin, MPD, MRD, and 6FGC with a default setting of receptor grid box range of z were 25.754 and 270.701 and grid box range of x is 10. The interaction with protein-ligand and its glide scores were examined thoroughly. However, greater negative values propose a more encouraging drug-protein interaction. Therefore, compounds with a score of -2 or above were contemplated as better candidates for inhibiting SARS-CoV-2 (Shah *et al*., 2020).

2.3. Data Analysis

Correlation between features of the dataset that is the interaction of drug compounds and their derivatives against SARS CoV-2 affords significant information about their features and the degree of influence they have over the target value. The heat map of Pearson Correlation between the ligands and proteins of the dataset is analyzed, which distinctively revealed a relatively stronger outcome.

2.4. Data Pre-processing

The dataset contains data columns with the Date, String, along with Numeric types. However, we have categorical variables provided in the dataset. Machine learning language involves all input data to be passed in the numeric form. The input data to be performed is label-encoded, and this assigns a unique number to each and every categorical value in the column.

3. Results

3.1. Investigation of Artemisinin compounds' interaction with SARS-CoV-2

On docking, Artemisinin and its derivative compounds displayed the greater antiviral activity against the SARS-CoV-2 receptors like 7CTT and 7MY3. However, the 3D structures of the ligands and SARS-CoV-2 receptors were obtained from the (https://www.rcsb.org/) protein data bank. The ligand-protein interactions were performed with help of Maestro (Schrödinger) program, which has shown XP GScore and MM/GBSA values of 7CTT interaction with derivative ligands of antimalarial compounds such as D95 (-6.911) (-45.424), artemisinin (Pubchem ID 159028) (-2.605), (-35.222), MPD (-5.088), (-31,021), MRD (-3.044) (-21.952) and 6FGC (-9.617) (-34.089), whereas with 7MY3 spike glycoprotein interactions MMGBSA values for D95 (-2.208) (-26.304), MPD (-2.59), (-18.658), MRD (-2.581), (-28.03) and 6FGC (-5.082), (-13.47) binding affinities has followed Lipinski rule of 5. (Table-1)

Table 1. Molecular docking parameters of Artemisinin Antimalarial drug compound and its derivatives against SARSCOV-2 receptors such as 7CTT (NSP) and 7MY3 (spike glycoprotein) with its binding affinities and following Lipinski rule of 5 with grid box range 10

S.No	Compound Name	Receptor	RMSD	XP Gscore	MM/GBSA	Lipinski rule of 5	Grid box z range	Grid box X range
1	D95	7CTT	0.006	-6.911	-45.424	0	25.754	10
2	Artemisinin		0.033	-2.605	-35.222	0		
3	MPD		0.001	-5.088	-31,021	0		
4	MRD		0.018	-3.044	-21.952	0		
5	6FGC		0.005	-9.617	-34.089	2		
6	D95	7MY3	0.006	-2.208	-26.304	0	270.701	10
7	MPD		0.001	-2.59	-18.658	0		
8	MRD		0.018	-2.581	-28.03	0		
9	6FGC		0.005	-5.082	-13.47	2		

Moreover, it is observed that the interaction of 7CTT which is a non-structural protein revealed notable interaction with artemisinin and its derivative D95 with (XP GScore and MM/GBSA values = (-2.605) (-35.222) & (-6.911) (-45.424)). Furthermore, in 7MY3 spike glycoprotein also revealed good interaction as shown in table-1 and displayed good binding interactions (as shown in figures 1&2).

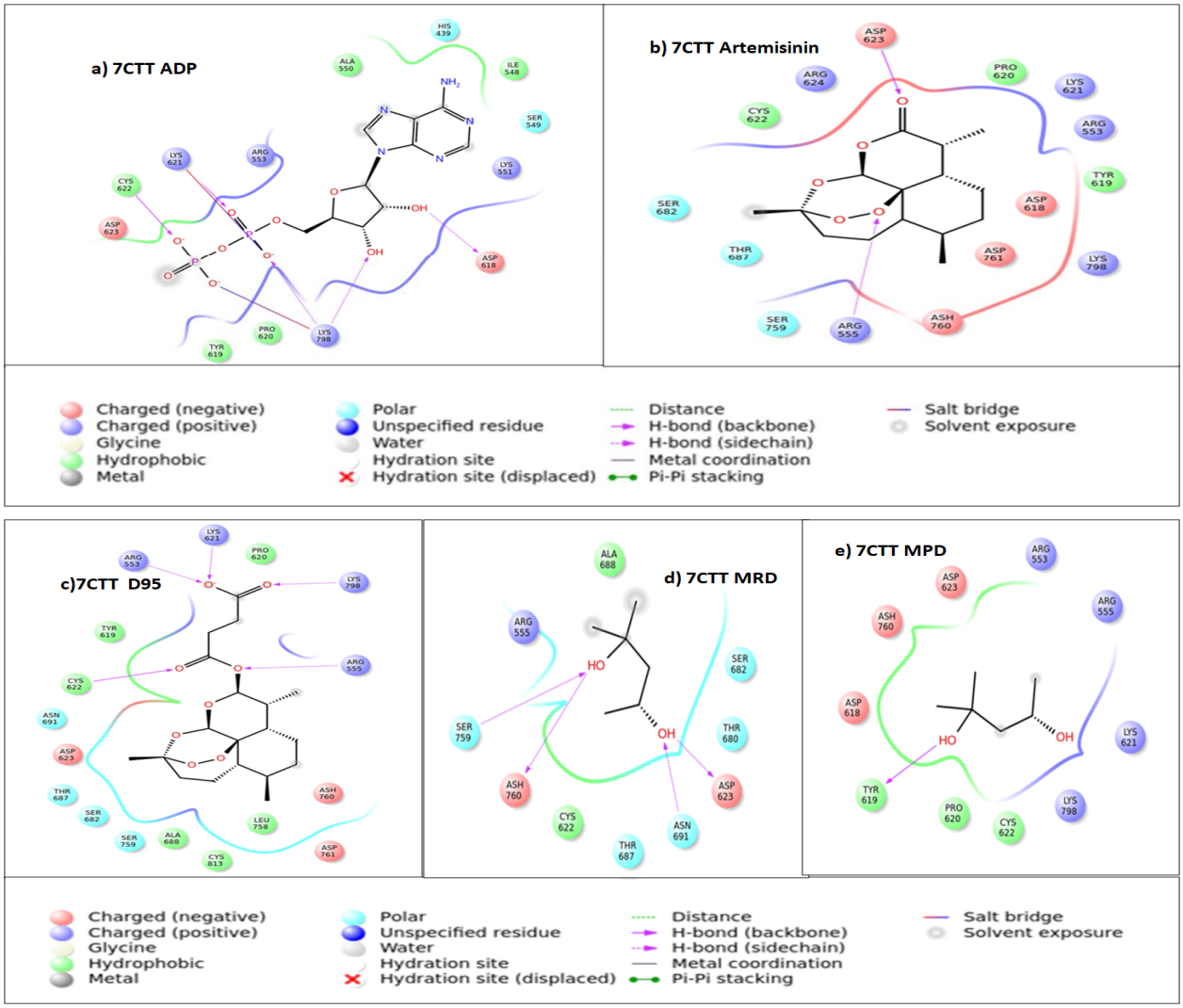

Figure-1A: 7CTT non-structural protein interacting with artemisinin and its derivatives and examined with ligplot+ a) Interaction of 7CTT with Adenosine-5'-Diphosphate, His-439, Lys-551, Asp-618, Cys-622, Lys-798,Arg-553,Tyr-619 and Pro-620. b) Interaction of 7CTT with Artemisinin residues that is Ser-682, Thr-687, Arg-555, Lys-551, Tyr-619 and Pro-620 c) Interaction of 7CTT with D95 residues such as Arg-553, Lys-798, Asp-623, Thr-687, Tyr-619 and Pro-620 d) 7CTT interaction with MRD, Asp-623, Thr-687,Arg-555, Cys-622 and Ala-688 e) 7CTT interaction with MPD, Lys-798, Arg-555,Asp-618,Cys-622, Tyr-619 and Pro-620. f) Docking of 7CTT with Artemisinin compound following Lipinski rule of 5.

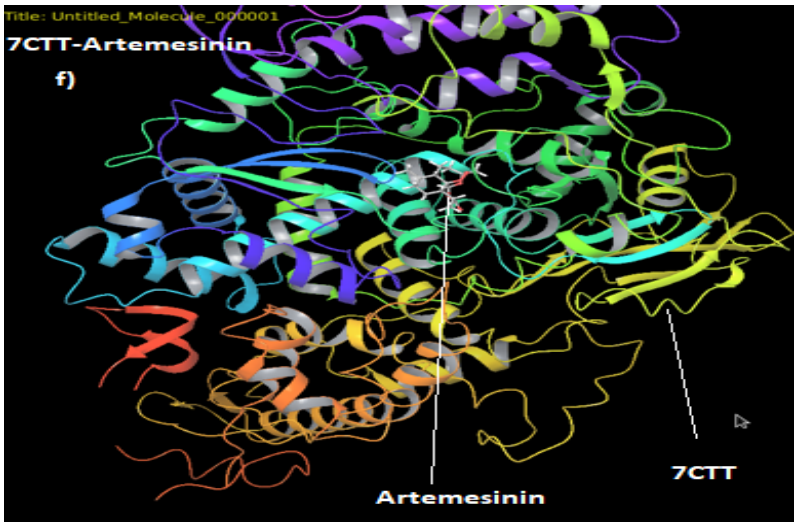

Figure-1B: 7CTT non-structural protein interacting with artemisinin is shown in this figure, and the interaction points are vision in ribbion structure.

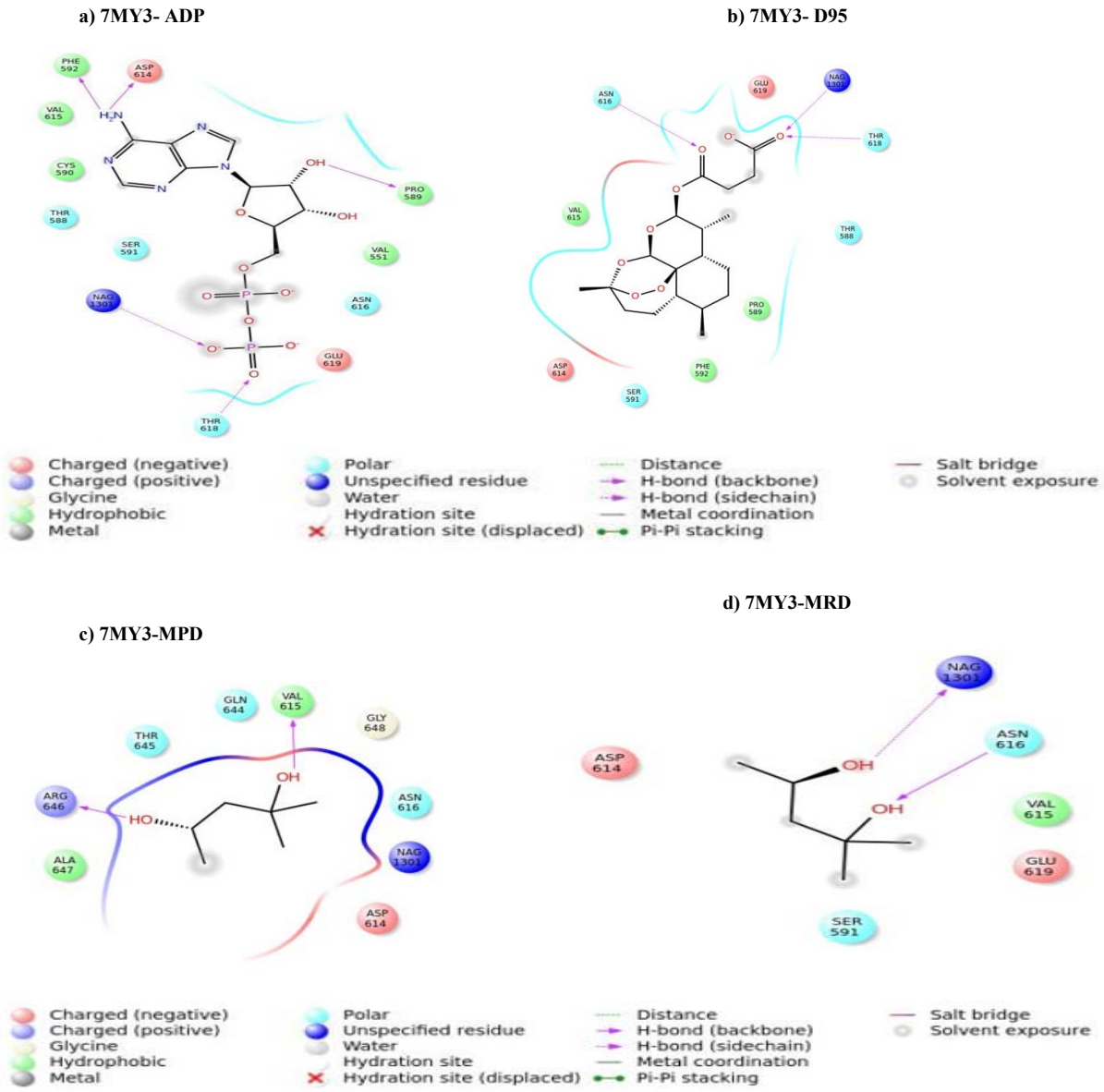

Figure 2: 7MY3 interaction with Artemisinin and its derivatives and examined with Ligplot+ a) Interaction of 7MY3 with Adenosine-5'-Diphosphate that is NAG-1301, Glu-619, Thr-618, Asn-616, Cys-590, Ser-591, Val-615, Phe-592, Pro-589 b) Interaction of 7MY3 with D95 NAG-1301, Asn-616, Val-615, Thr-618, Phe-592, Glu-619, and Pro-589 c) Interaction of 7MY3 with MPD residues such as NAG-1301, Arg-646, Gln-644, Asn-616, Thr-645, Val-615 and Ala-647 d) 7CTT interaction with MRD, NAG-1301, Asp-614, Ser-591,Glu-619, Val-615, and Asp-614.

3.2. Random Forest Decision Approach for predicting the outcome of docking interactions

RF (or Bagged DTs) is a machine learning approach that involves building multiple confusion matrixes via bootstrap aggregation. We have used two receptors of SARSCOV-2 to interact with the artemsinin and its derivatives compounds and predict its accuracy of binding. Furthermore, RF is utilized in remote sensing for predicting the accuracy/classification of data. The decision tree helps to improve the predictions. (Shown in Figure-3a &b).

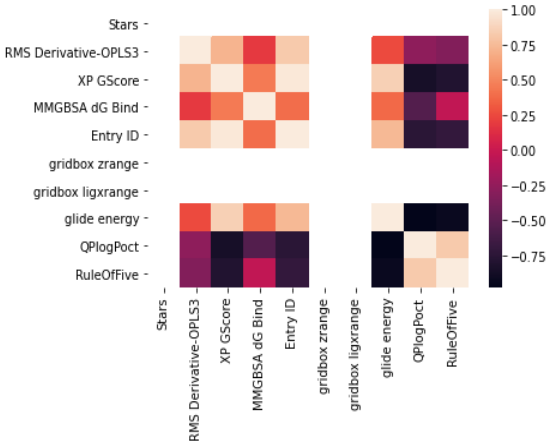

Figure-3a: Correlation between ligand protein interactions features

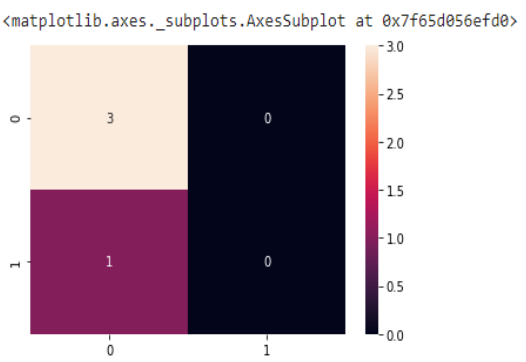

Figure-3b: Correlation matrix heatmap for the ligand-protein interactions

4. Discussion

SARS-CoV-2 was spread globally by the pandemic outbreak from December 2019 to the present (Hui *et al.,* 2020; Phan 2020), and COVID-19 is responsible for more than 3.9 million deaths (Huang, C. *et al.,* 2020; Paules 2020 and Lu *et al.,* 2020). This feverish, highly contagious respiratory systemic illness put many people's lives in danger. Remdesivir was given FDA approval as an antiviral drug for COVID-19 treatment. Additionally, new research have questioned its clinical effectiveness (Beigel, JH *et al.*,2020; Pan 2020; Dyer 2020). As a result, it was determined that using repurposed medications to treat the current pandemic outbreak was a successful method because the medications were already licensed for the treatment of other diseases. A. annua plant bioactive components with a lot of activity were used in the repurposed medications to treat malaria (Klayman 1985; Ferreira *et al.,* 2010). The primary active pharmaceutical ingredients (API) against COVID-19 showed better pharmacokinetic characteristics. The corona virus spread is regarded as an international problem globally. Currently, artificial intelligence has been utilized considerably for drug research against pandemic outbreaks. The employment of Artificial Intelligence is prominent for its intense potentiality for novel drug discovery (Coldeway, 2019; Segler *et al.,* 2018). The Artificial Intelligence platform has displayed significant inhibitory activity with contemporarily available drugs (Walters and Murcko, 2020). However, further study on artemisinin's interactions with two SARSCoV-2 receptors has been prompted in light of the antiviral efficacy of artemisinin and its derivatives in prior findings on herpes as well as on hepatitis B and C viruses (Ho *et al.,* 2014). But a number of studies have shown artemisinin's pharmacological qualities in addition to its additional mechanisms, such as its anti-inflammatory, anticancer, and antimalarial effects (Cao *et al.,* 2020; Kshirsagar & Rao, 2021). Artemisinin and its variants, among antimalarial drugs, were found to be effective against SARS-CoV-2. However, the docking of the artemisinin compound and its derivatives against two SARSCoV-2 receptors revealed the important functional groups and active residues with better G scores and **followed** Lipinski rule of 5.

Nonetheless, among the screened drugs (artemisinin, D95) against two SARS-CoV-2 receptors that is 7CTT & 7MY3, have shown better GScore values of -2.605, -6.911 in Table-1 displaying greater potent binding energy affinity. Docking pose of artemisinin and their derivatives investigated with Maestro Schrödinger Program on two receptors of SARSCOV-2, revealed significant functionally active residues Ser-682, Thr-687, Arg-555, Lys-551, Tyr-619, Pro-620 Glu-619, Thr-618, Asn-616, Cys-590, Ser-591, Val-615, Phe-592, Pro-589 as the best active binding sites with the MM/GBSA values of artemisinin, D95 -35.222 & 45.424 respectively.

The correlation matrix as a heat map with random forest decision tree predicted the accuracy of docking interactions of ligand-protein with an accuracy of 75%. Thus, our studies provide hypothetical evidence that utilization of artemisinin as repurposed drugs could potentially inhibit the binding of SARCOV-2 on ACE-2 receptor.

5. Conclusion

The current study showed that machine learning and deep learning programmes used to create artificial intelligence had a significant impact on the treatment of coronavirus. By preventing SARSCOV-2 from binding to two different types of SARSCOV-2 receptors, the artemisinin molecule and its derivatives were identified as an effective treatment candidate using an in-silico approach. The docking contacts' binding affinities and G scores adhered to the Lipinski rule of 5. Artificial intelligence technology is therefore viewed as a blessing and a useful tool for discovering repurposed medications that require clinical studies for validation.

Acknowledgements

The authors express their appreciation to Sri Padmavathi Mahila Visvavidyalayam (Women's) University for providing access to the research facilities and for actively participating in the study; also thanks go to the faculty, staff, and students from the Mahila University for their assistance in the research studies.

Funding

These studies were supported by DST-CURIE, AI for providing financial support in project by releasing funds timely.

Competing interests

The authors declare that they have no competing interests1

Consent for publication

Not applicable.

References

Backer JA , Klinkenberg D , Wallinga J 2020.. Incubation period of 2019 novel coronavirus (2019- nCoV) infections among travellers from Wuhan, China, 20–2. Eurosurveillance 25:20 0 0 062.

Beigel, JH. *et al.* 2020. Remdesivir for the treatment of Covid-19—Final report. *N. Engl. J. Med.* https:// doi. org/ 10. 1056/ NEJMo a2007 764.

Cao R, Hu H, Li Y, Wang X, Xu M, Liu J, Zhang H, Yan Y, Zhao L, Li W, et al. 2020. Anti-SARSCoV- 2 Potential of Artemisinins in vitro. ACS Infect Dis. 6(9):2524–2531.

Chen H., Engkvist O., Wang Y, Olivecrona,M., and Blaschke T. 2018. The rise of deep learning in drug discovery. Drug Discov. Today 23, 1241–1250. doi: 10.1016/j.drudis.2018.01.039.

Coldeway D. 2019. Molecule. One Uses Machine Learning to Make Synthesizing New Drugs a Snap. TechCrunch, 3October.

Dyer O. 2020. Covid-19: Remdesivir has little or no impact on survival, WHO trial shows. *BMJ* . https:// doi. org/ 10. 1136/ bmj. m4057.

Elfiky AA. 2020. Natural products may interfere with SARS-CoV-2 attachment to the host cell. J. Biomol. Struct. Dyn. doi:10.1080/07391102. 2020.1761881.

Ferreira JFS., Luthria DL., Sasaki T. & Heyerick A. 2010. Flavonoids from *Artemisia annua* L. as antioxidants and their potential synergism with artemisinin against malaria and cancer. *Molecules* **15**, 3135–3170. https:// doi. org/ 10. 3390/ molec ules1 50531 35.

Guan W , Ni Z , Hu Y , Liang W , Ou C , He J , et al. 2020. Clinical characteristics of coronavirusdisease 2019 in China. N Engl J Med 2020;382:1708–20 .

Hilgenfeld R., and Peiris M. 2013. From SARS to MERS: 10 years of research on highly pathogenic human coronaviruses. Antivir. Res. 100, 286–295. doi: 10.1016/j.antiviral.2013.08.015.

Ho D, 2020. Addressing COVID-19 drug development with artificial intelligence. Advanced Intelligent Systems 2, 2000070.

Ho WE, Peh HY, Chan TK, Wong WSF. (2014). Artemisinins: pharmacological actions beyond antimalarial. Pharmacol Ther. 142(1):126–139.

Huang, J, Tao G, Liu J., Cai J., Huang Z, and Chen JX. 2020. Current prevention of COVID-19: natural products and herbal medicine. Front Pharmacol. 11, 588508. doi:10.3389/fphar.2020.588508.

Huang, C. *et al.,* 2020. Clinical features of patients infected with 2019 novel coronavirus in Wuhan, China. *Lancet* **395**, 497–506. https://doi. org/ 10. 1016/ S0140- 6736(20) 30183-5.

Hui, D. S. *et al.* 2020.The continuing 2019-nCoV epidemic threat of novel coronaviruses to global health—the latest 2019 novel coronavirus outbreak in Wuhan, China. *Int. J. Infect. Dis.* **91**, 264–266. https:// doi. org/ 10. 1016/j. ijid. 2020. 01. 009.

Jabeer Khan R., Kumar Jha R., Muluneh Amera G., Jain M., Singh E., Pathak A., et al. 2020. Targeting novel coronavirus 2019: a systematic drug repurposing approach to identify promising inhibitors against 3C like proteinase and 2'-O-ribose methyltransferase: a systematic drug repurposing approach to identify promising inhibitors against 3C like proteinase and 2'-O-ribose methyltransferase. ChemRxiv [Preprint]. doi: 10.26434/chemrxiv.11888730.v1.

Jean S-S, Lee P-I, Hsueh P-R. 2020. Treatment options for COVID-19: The reality and challenges. J Microbiol Immunol Infec 2020;53:436–43.https://doi.org/10.1016/ j.jmii.2020.03.034 .

Jin Z., Du X., Xu Y, Deng Y, Liu M., Zhao Y., et al. 2020. Structure of Mpro from COVID-19 virus and discovery of its inhibitors. bioRxiv [Preprint]. doi: 10.1101/2020.02.26.964882.

Kandeel M., and Al-Nazawi M. 2020. Virtual screening and repurposing of FDA approved drugs against COVID-19 main protease. Life Sci. 251:117627. doi: 10.1016/j.lfs.2020.117627.

Ke YY., Peng TT, Yeh, TK., Huang WZ., Chang S.E., Wu S.H., Hung H.C., Hsu T.A., Lee, S.J., Song J.S., 2020. Artificial intelligence approach fighting COVID-19 with repurposing drugs. Biomed. J. https://doi.org/10.1016/ j.bj.2020.05.001.

Klayman DL. 1985. Qinghaosu (artemisinin): An antimalarial drug from China. *Science* **228**,1049–1055. https:// doi. org/ 10. 1126/ science. 38875 71.

Kong,WH., Li Y., Peng,MW., Kong D.G., Yang XB.,Wang L et al.2020.SARS-CoV-2 detection in patients with influenza-like illness. Nat. Microbiol. 5, 675–678. doi: 10.1038/s41564-020-0713-1.

Kshirsagar SG, Rao RV. 2021. Antiviral and immunomodulation effects of Artemisia. Medicina(Kaunas.). 57(3):217.

Kumar V., Dhanjal J. K., Bhargava P., Kaul A.,Wang J., Zhang, H. et al. 2020. Withanone and Withaferin-A are predicted to interact with transmembrane protease serine 2 (TMPRSS2) and block entry of SARS-CoV-2 into cells. J. Biomol. Struct. Dyn. doi:10.1080/07391102.2020.1775704.

Lauer SA , Grantz KH , Bi Q , Jones FK , Zheng Q , Meredith HR , et al. 2020. The incubation period of coronavirus disease 2019 (COVID-19) from publicly reported confirmed cases: estimation and application. Ann Intern Med 2020;172:577–82 .

Lu H., Stratton CW. & Tang YW. 2020. Outbreak of pneumonia of unknown etiology in Wuhan, China: The mystery and the miracle.*J. Med. Virol.* **92**, 401–402. https:// doi. org/10. 1002/ jmv. 25678.

Muhammad LJ, Islam MM, Usman SS, Ayon SI. Predictive data mining models for novel coronavirus (COVID-19) infected 'patients' recovery. SN Comput Sci. 2020;1:206. https://doi.org/10.1007/s4297 9-020-00216 –w.

NIH.https://www.nih.gov/news-events/news-releases/nih-halts-clinical-trial- hydroxychloroquine . n.d.

Paules CI., Marston HD & Fauci AS. 2020. Coronavirus infections—more than just the common cold. *JAMA* **323**, 707–708. https://doi. org/ 10. 1001/ jama. 2020. 0757.

Pan H. *et al.* 2020.Repurposed antiviral drugs for COVID-19–interim WHO SOLIDARITY trial results. *NEJM* https:// doi. org/ 10. 1056/NEJMo a2023 184.

Phan LT. *et al.* 2020. Importation and human-to-human transmission of a novel coronavirus in Vietnam. *N. Engl. J. Med.* **382**, 872–874.https:// doi. org/ 10. 1056/ NEJMc 20012 72

Schro¨dinger .2017. Maestro11.1 (LigPrep, Protein Preparation Wizard, SiteMap, Receptor Grid Generation, Glide, XP Visualizer.) Schro¨dinger LLC, New York, NY.

Segler, M.H., Preuss, M., Waller, M.P., 2018. Planning chemical syntheses with deep neural networks and symbolic AI. Nature 555, 604–610.

Shah B, Modi P, and Sagar SR. 2020. In silico studies on therapeutic agents for COVID-19: Drug repurposing approach. Life Sci 252, 117652.

Tang W , Cao Z , Han M , Wang Z , Chen J , Sun W , et al. 2019. Hydroxychloroquine in patients with mainly mild to moderate coronavirus disease: open label, randomised controlled trial. BMJ 2020:369 .

Walters WP., Murcko M., 2020. Assessing the impact of generative AI on medicinal chemistry. Nat. Biotechnol. 38, 143–145.

Worldometer 2020. Coronavirus Cases.Worldometer. Available onlineat: https://www.worldometers.info/coronavirus/coronaviruscases/#daily-cases (accessed April 27, 2020).

Yuyong Zhou, Kerry Gilmore, Santseharay Ramirez, Eva Settels, Karen A. Gammeltoft, Long V. Pham, Ulrik Fahnøe, Shan Feng, Anna Offersgaard Jakob Trimpert, Jens Bukh, Klaus Osterrieder, Judith M. Gottwein & Peter H. Seeberger 2021. In vitro efficacy of artemisinin-based treatments against SARS-CoV-2. www.nature.com/scientificreports.(2021) 11:14571 https://doi.org/10.1038/s41598-021-93361-y.

JJBS

Volume 15, Number 4,December 2022
ISSN 1995-6673
Pages 569 – 577
https://doi.org/10.54319/jjbs/150405

Jordan Journal of Biological Sciences

Genetic Polymorphisms of Inhibin-Ba (Inhβa) Gene and their Association with Twin Production Trait in Egyptian Small Ruminants

Hassan R. Darwish , Mohamad M. Aboelenin *, Kamilia B. Abd El-Aziz, Ibrahim M. Farag

Cell Biology Department, National Research Centre, Giza, Egypt

Received: June 4, 2021; Revised: January 16, 2022; Accepted: February 2, 2022

Abstract

Reproductive traits are regulated by several genes, and genetic polymorphism within these genes which have a role on the reproductive performance could be used in marker assisted selection breeding programs. Several variants of inhibin βA (INHβA) gene affect the litter size in small ruminant. Therefore, different single nucleotide polymorphisms (SNPs) within this gene could be used as a genetic marker to improve the reproductive efficiency (specially litter size) of sheep and goats. The objective of this study is to find out INHβA subunit-encoding gene polymorphisms by employing PCR-SSCP assay and subsequent analyses of nucleotide sequence, as well as to investigate the potential association of these genetic polymorphisms with twin yield in Egyptian goats and sheep breeds. One hundred and thirty-nine females were chosen, 113 of them were mothers at the 1st., 2nd., 3rd and 4th parity, and the remaining 26 females were young at sexual maturity age. Blood samples were collected for genomic DNA extraction and PCR amplification were performed using five specific primers spanning the entire INHβA CDS partial 5`UTR. Four out of the five PCR amplicons displayed different genetic polymorphisms, and the subsequent nucleotide sequence analyses showed many nucleotide substitutions. In sheep, the amplified fragment 1 showed 3 different genotypes A, C and A/C. The sequence analysis for the 3rd amplicon showed two different genotypes, A and G. Also, the 5th amplicon reveals 3 different genotypes, A, G and A/G. In goats, the sequence analysis of the 4th amplified fragment showed different three genotypes, G, A and A/G. The statistical analysis proposed that the genotype AA (in sheep) could be favorable gene markers for twin production. The present study suggested that the genetic polymorphisms of INHβA gene might have effects on fecundity traits in Egyptian small ruminants.

Keywords: INHβA gene, PCR-SSCP, Genetic polymorphism, Twin production, Egyptian Sheep and Goats.

1. Introduction

Egyptian sheep and goats are considered as one of the earliest domesticated farm animals. They have played a crucial part in animal husbandry due to their extensive uses in many disciplines, such as meat, milk, wool, hair and skin production. So, it is important to improve the reproductive traits of such species to meet people's increasing need of different animal products. Also, the enhancement of reproduction performance will ultimately pave the way for the economic benefit of farmers (Tudu *et al.*, 2015; Mishra *et al.*, 2017).

Reproductive traits are polygenic in nature and controlled by many genes (Ray *et al.*, 2016). The identification of important genetic variations of the genes responsible for reproductive traits in farm animal populations will help to reveal marker assisted selection in a more precise manner (Ahlawat *et al.*, 2015). The inhibin beta A subunit encoding gene (INHβA) may be suitable candidate that may affect the litter size in small ruminant species (Zi *et al.*, 2012). The identification of single nucleotide polymorphisms (SNPs) of such gene and studying their association with fecundity traits may be helpful for enhancing the reproductive efficiency (especially litter size) of sheep and goat animals (Chu *et al.*, 2007; Zi *et al.*, 2012). Several studies showed that the inhibin is considered to be a glycoprotein hormone, and it belongs to the superfamily called transforming growth factor-beta (TGF-β). This superfamily and its related cell-surface receptors are important intra-ovarian regulatory factors of ovarian follicular development and ovulation rate (Ling *et al.*, 1985; Rivier *et al.*, 1985; Robertson *et al.*, 1985; Woodruff *et al.*, 1996). Inhibin was found to consist of two subunits, α and β linked by disulfide bonds (Mason *et al.*, 1985). It was revealed to engaged in the regulation, synthesis and secretion of the pituitary follicle-stimulating hormone, steroidogenesis and maturation of follicles (Leyhe *et al.*, 1994; Hiendleder *et al.*, 1996b; Chu *et al.*, 2007). Also, Phillips (2005) reported that the inhibin is expressed in different organs of the body including testis, ovary, uterus in human, pig, sheep and mouse. However, a previous study in sheep, Rodgers *et al.* (1989) observed that follicles are considered to be the major source of inhibin; Moreover, Medan *et al.* (2003) reported that the

* Corresponding author. e-mail: Mohamed2000mail@yahoo.com.

inhibin is a major factor that controls the ovulation rate in domestic and laboratory animals.

INHβA ovine gene was revealed to be located on chromosome 4q26 (Brunner *et al.*, 1995). Some studies showed that INHβA gene has a main role in controlling the reproductive performance in sheep and goats: In sheep, Fleming *et al.* (1992) revealed that Booroola ewes have significant high level of inhibin-βA mRNA in follicles of homozygous FecB gene-carriers as compared to control. Also, in different sheep breeds, Vanmontfort *et al.* (1998) found significant breed differences in circulating β-inhibin concentrations with different reproductive performances. Moreover, Leyhe *et al.* (1994), Hiendleder *et al.* (1996a), Hiendleder *et al.* (1996b) and Chu et al. (2007) reported that in sheep, the polymorphisms of inhibin-βA gene have had obvious significant impact on the litter size in different breeds. In goats, Zi *et al.* (2012) studied cDNA sequences and mRNA expression of INHβA gene in prolific (lezhi black) and nonprolific (Tibetan) goat breeds; and they have analyzed sequences of 1,360 base pairs that encode an assumed peptide of 425 amino acids. The comparison between the two breeds showed three base changes in INHβA (A to G at positions: 318, 831 and 1109), resulting in a substitution of one amino acid (Asp to Gly). These authors suggested that the presence of base changes in INHβA gene that resulted in amino acid substitution might be influencing the regulatory mechanism of differential fertility in these breeds. Since the studies on genetic variations in INHβA of Egyptian small ruminant species were lack, the objective of this study was to identify the polymorphism in INHβA gene and to investigate the association of these SNPs with enhancing litter size in local sheep and goat breeds.

2. Materials and Methods

2.1. Animals

The sheep and goats used in this study included 139 females. These females consisted of 95 of sheep breeds (Barki, Osseimi, Rahmani, Saudanez and Awase) and 44 of goat breeds (Zaraiby, Damascus, Boer, Saanine and Barki). 83 of sheep and 30 of goats were mothers at first, second, third and fourth parity, and they were used for the association of identified genotypes in INHβA gene with the twin production or with the litter size. The remaining 26 females (12 of sheep and 14 of goats) were young and at an age of sexual maturity. For the same reproductive trait (twin production), these young females were conducted to select the animals that carry favorable gene markers (alleles) for their utilizing in successful breeding program. The animal breeds were sourced from Animal Production Farms belonging to Faculty of Agriculture (Cairo University), Nubaria belonging to National Research Centre and Governmental Halayieb, Egypt. The animals were not subject to any treatments during this study and only blood samples were collected from sheep and goats under veterinary supervision. Since the studied animals were a part of the herds of the farms mentioned above at the time of blood collection and were not subject to any treatments, the animals were kept in the same herds after blood sampling for this study.

2.2. Blood sample collection and DNA extraction

The samples of blood were collected. Genomic DNA was extracted from the whole blood samples according to the method described previously (Aboelenin *et al.*, 2017a; Aboelenin *et al.*, 2017b; Mahrous *et al.*, 2020c). DNA concentration and quality were assessed and stored at -20°C before use.

2.3. Primers and PCR amplification

Primers sequences were shown in table 1. These primers were cited by Chu *et al.* (2007) and used for identification of genetic polymorphisms in INHβA gene by using PCR-SSCP technique and nucleotide sequence analysis. The annealing temperature of each pair was optimized using a conventional PCR to exclude the presence of unspecific products or primer dimer, and the PCR products were analyzed by 2% agarose gel electrophoresis as described previously (Madkour et al., 2020; Mahrous et al., 2020a; Mahrous et al., 2020b; Mahrous et al., 2020d; Sroor et al., 2020; Madkour et al., 2021a; Madkour et al., 2021b; Mahrous et al., 2021; Sroor et al., 2022). The Polymerase chain reaction had been carried out in 25µl volume involving 2.5 µl of 10 x PCR buffer (50 mmol/L KCL, 10 mmol/L Tris-HCl (pH 8.0), 0.1% Triton X-100) 1.5 mmol/L $MgCl_2$, 200µmol/L each dNTP, 1µmol/L each primer, 50 ng genomic DNA, and 1 U Taq DNA polymerase. The conditions of PCR were as follows: firstly, denaturation at 94ºC for 6 min; followed by 32 cycles of denaturation at 94ºC for 30s, annealing at 55-62ºC for 30s, extension at 72ºC for 30s; with a final extension at 72ºC for 10 min.

Table 1. The sequences of primers and product size of PCR amplification of INHβA gene.

Primer	Primer sequence (5'→3')	Product size	Amplified region	Reference sequence
Primer 1	F: CAGGATGCCCTTGCTTT R: CATCGGGTCTCTTCTTCAA	224 bp	Exon 1 (1351-1574)	U16238
Primer 2	F: CACTTGAAGAAGAGACCCG R: CACCTGATTCCGCGAAC	193 bp	Exon 1 (1553-1745)	
Primer 3	F: GGCACAGCCAGGAAGACG R: CGTATGTCCAGGGAGCTCTTG	335 bp	Exon 2 (398-732)	
Primer 4	F: ATACGGATTGCCTGTG R: CTCACAGTAGTTGGCGT	333 bp	Exon 2 (728-1060)	U16239
Primer 5	F: GCTACCACGCCAACTACTGT R: TCTCTGGACCATCTCGCTC	293 bp	Exon 2 (1038-1330)	

2.4. Single-strand conformational polymorphism (SSCP)

For performing the SSCP analysis, the PCR products had been resolved. 10 ul of PCR product had been diluted in denaturing solution that consisted of A and B types. "A" type solution involved 95% of Formamide, 10 mM NaOH, 0.05% Xylene-Cyanol and 0.05% bromophenol blue. "B" type solution same as "A" solution, plus 20 mM of EDTA (pH 8.0). About 10% SSCP gel mixture (30 ml) had been prepared through acrylamide- -bisacrylamide (37.5: 1), TEMED (30 ul) and 10% ammonium persulfate (0.8 ml) in a 1x TBE (90 mM Tris-borate at pH 8.3, 4 mM EDTA), and a voltage of 300 V, running time (6- 8 h) and running temperature at 4°C. Each PCR reaction had been diluted in denaturing solution, denatured at 95°C for 5 min, chilled on ice and resolved on non-denaturing polyacrylamide gel. Electrophoresis was performed in a vertical unit (Hoefer Scientist SE600, 160 x 140 x 1 mm) in a 1x TBE buffer. The gels had been stained with 0.1% silver nitrate and visualized through 2% NaOH solution (containing 0.1% formaldehyde). Homozygous and Heterozygous genotypes from different SSCP patterns in different breeds had been photographed and analyzed using Gel Documentation system.

2.5. Sequence analysis

In order to clarify the nucleotide analysis in the SSCP patterns that were given of tested gene (INHβA) in the present study, PCR product were purified and sequenced by special company (Macrogen Incorporation, Seoul, Korea). Sequence analysis and alignment were performed by cluster wide analysis using CodonCode Aligner software, CodonCode Corporation, USA.

2.6. Statistical analysis

The obtained data for PCR-SSCP patterns had been statistically analyzed by one way ANOVA followed by two-way ANOVA. The differences among pattern groups were determined significantly according to the method of Waller and Duncan (Waller *et al.*, 1969). Also, the allele frequencies that were revealed in this study had been statistically analyzed using T-test.

The values are expressed as mean ± SE. All statements of significance were based on probability of ($P \leq 0.05$).

3. Results

3.1. PCR amplification of INHβA gene:

Genomic DNA of 139 animals of different sheep and goat breeds had been used to amplify the entire CDS and partial 5`UTR of INHβA gene using five primers pairs spanning 1326 bp. PCR amplicons were run on a 2% agarose gel and the five PCR amplicons sizes were 224 bp, 193bp, 335bp, 333bp and 293bp, respectively (Figurers 1 to 5). The first primer has had amplified the first 224 bp stretch of the INHβA gene (1 to 224), the second primer amplified the stretch from 203 to 395, the third one covered the distance from 396 to 730, the fourth one amplified the distance from 726 to 1058 and the fifth primer covered the distance from 1036 to 1328. These amplified products found to be consistent with the target regions with high specificity were used directly in SSCP assay.

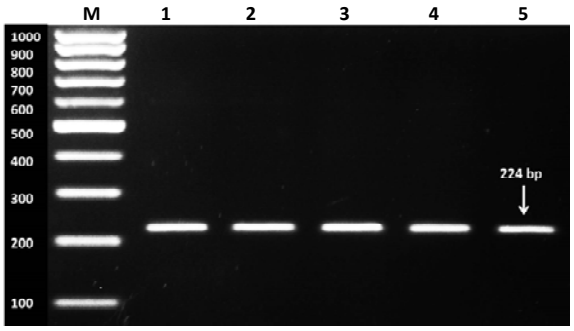

Figure 1. PCR product (lanes 1-5) of primer 1 of INHβA gene at size 224 bp. Lane M: 100 bp ladder.

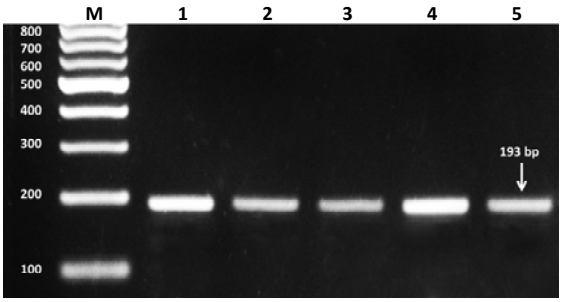

Figure 2. PCR product (lanes 1-5) of primer 2 of INHβA gene at size 193 bp. Lane M: 100 bp ladder.

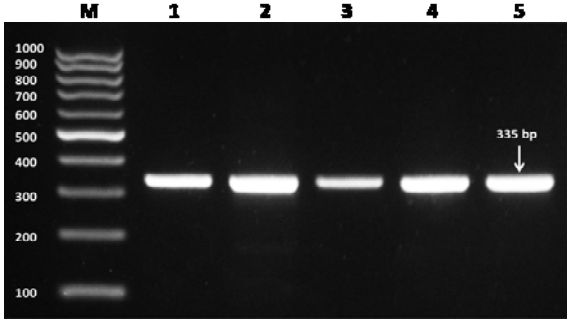

Figure 3. PCR product (lanes 1-5) of primer 3 of INHβA gene at size 335 bp. Lane M: 100 bp ladder.

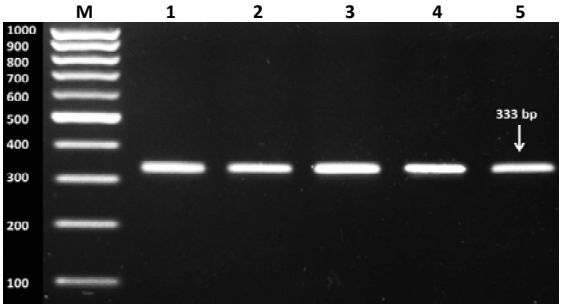

Figure 4. PCR product (lanes 1-5) of primer 4 of INHβA gene at size 333 bp. Lane M: 100 bp ladder.

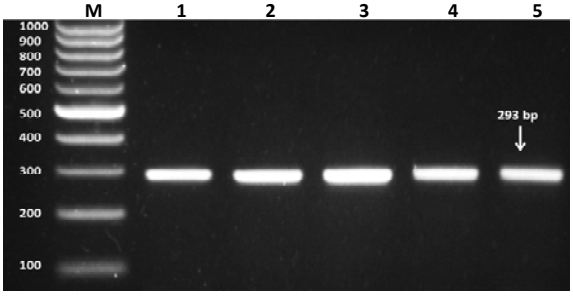

Figure 5. PCR product (lanes 1-5) of primer 5 of INHβA gene at size 293 bp. Lane M: 100 bp ladder.

3.2. PCR-SSCP analysis:

3.2.1. PCR-SSCP of primer 1 of INHβA gene:

PCR-SSCP analyses of the first amplicon (224bp) were shown in Figure 6 and Table 2. The results revealed three different banding patterns (P_1, P_2 and P_3) in sheep. However, in goats, only one pattern was found, and all goats were subjected to pattern (P_1) as that of sheep, and they were monomorphic on gel.

In sheep, 62 animals classified as pattern one, comprise 59 mothers and 3 females were at puberty, whereas 29 animals were classified as pattern two involving 21 mothers and 8 females at puberty. Only 4 animals were classified as pattern three, and consisted of 3 mothers and one female at puberty. Statistical analysis revealed that P1-mothers have high rates of litter size as compared with that of P3, while there is a significant increase in lambing mean number when compared to that of P2 or P_3. Consequently, P1-genotype is deemed to be a prolificacy gene marker.

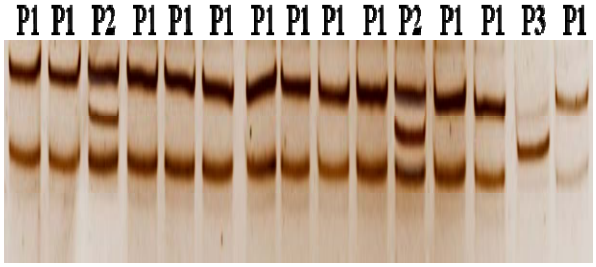

Figure 6. Shows three SSCP different patterns using primer 1 of INHβA gene.

Table 2. Shows genetic polymorphisms (SSCP patterns) of INHβA gene using primer 1 and their effects on litter size in different Egyptian sheep and goat breeds:

Species	No. of animals	SSCP Patterns (Ps)	No. of animals at age of sexual maturation	No. of mothers	No. of single births (S.b)	No. of twin births (T.b)	Mean No. of S.b	Mean No. of T.b	Mean No. of lambing	Mean No. of litter size (Twin production)
Sheep	95	P1	3	59	61	42	1.03	0.71	2.45 ± 0.4^{c}	1.74 ± 0.1^{b}
		P2	8	21	22	7	1.04	0.33	1.71 ± 0.14^{b}	1.47 ± 0.24^{ab}
		P3	1	3	3	0.0	1.00	0.00	1.00 ± 0.23^{a}	1.00 ± 0.49^{a}
Goats	44	P1	14	30	29	35	0.97	1.16	3.30 ± 0.12^{d}	2.13 ± 0.32^{c}

Data expressed as mean ± SE. Values followed by different superscript letters are significantly different from one another within the same columns ($P\leq 0.05$).

3.2.2. PCR-SSCP of primer 2 of INHβA gene:

The second fragment (193bp) revealed just one pattern as shown in Figure 7. No polymorphisms were found, and both sheep and goats were monomorphic.

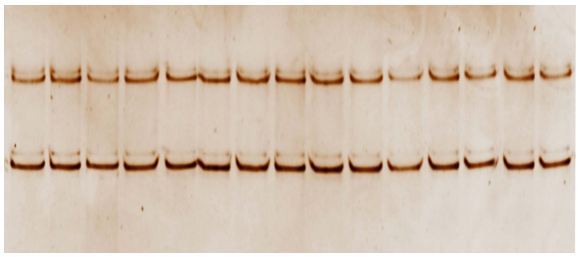

Figure 7. Shows SSCP pattern (monomorphic) using primer 2 of INHβA gene.

3.2.3. PCR-SSCP of primer 3 of INHβA gene:

PCR-SSCP analysis of the third fragment (335 bp) was shown in Figure 8 and Table 3. The results detected polymorphisms in sheep by the presence of two banding patterns, pattern 1 (P_1) and pattern 2 (P_2). However, the banding patterns in all goats were monomorphic, and they were classified as pattern 1 as that of sheep. In sheep, 70 animals were classified as pattern 1, 63 of them were mothers and the remaining 7 animals were at puberty; whereas 25 females including 20 mothers and 5 animals were at puberty were classified as pattern 2. Statistical data showed that P_1-mothers had a significant high rates of litter size and increase of mean number of lambing as compared to P_2-mothers. So, the polymorphism of this site could be considered a prolificacy gene marker.

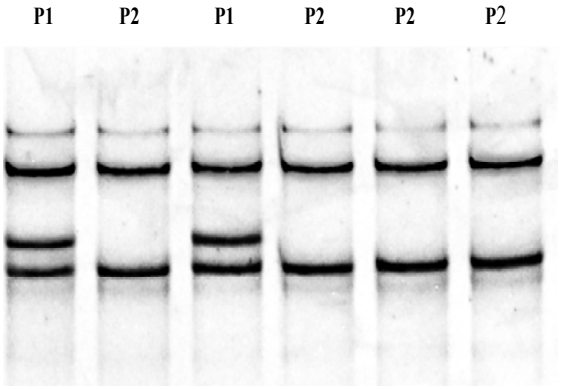

Figure 8. Shows two SSCP different patterns using primer 3 of INHβA gene.

Table 3. Shows genetic polymorphisms (SSCP patterns) of INHβA gene using primer 3 and their effects on litter size in different Egyptian sheep and goat breeds.

Species	No. of animals	SSCP Patterns (Ps)	No. of animals at age of sexual maturation	No. of mothers	No. of single births (S.b)	No. of twin births (T.b)	Mean No. of S.b	Mean No. of T.b	Mean No. of lambing	Mean No. of litter size (Twin production)
Sheep	95	P1	7	63	67	44	1.06	0.69	2.46±0.15^{b}	1.75±0.19^{b}
		P2	5	20	19	5	0.95	0.25	1.45±0.16^{a}	1.20±0.7^{a}
Goats	44	P1	14	30	29	35	0.97	1.17	3.30±0.2^{c}	2.14±0.19^{b}

Data expressed as mean ± SE. Values followed by different superscript letters are significantly different from one another within the same columns (P≤ 0.05).

3.2.4. PCR-SSCP of primer 4 of INHβA gene:

PCR-SSCP analyses of the fourth fragment of INHβA gene (333 bp) were shown in figure 9 and table 4. Three banding patterns (P_1, P_2 and P_3) were identified in goats. However, in sheep, the genetic polymorphisms were not detected, and all sheep females were subjected to pattern 1 as that of goats and they were monomorphic.

In goats, pattern 1 (P1) was investigated in 32 females, 22 of them were mothers and the remaining 10 females were at puberty, whereas P2 was observed in 10 animals including 6 mothers and 4 females at sexual maturity age. Moreover, pattern 3 (P3) was only detected in two mothers. The results showed that P2 had elevated lambing mean number and high litter size rates when compared to P1-mothers, but no statistical significance was found.

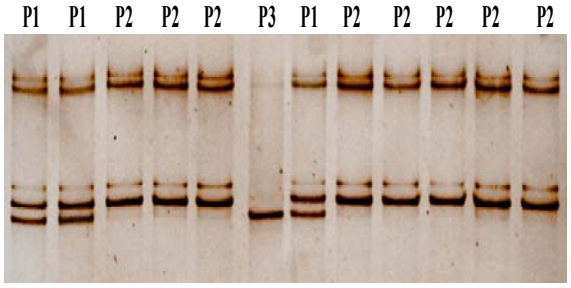

Figure 9. Shows three SSCP different patterns using primer 4 of INHβA gene.

Table 4. Shows genetic polymorphisms (SSCP patterns) of INHβA gene using primer 4 and their effects on litter size in different Egyptian sheep and goat breeds:

Species	No. of animals	SSCP Patterns (Ps)	No. of animals at age of sexual maturation	No. of mothers	No. of single births (S.b)	No. of twin births (T.b)	Mean No. of S.b	Mean No. of T.b	Mean No. of lambing	Mean No. of litter size (Twin production)
Sheep	95	P1	12	83	86	49	1.04	0.59	2.22±0.19^{a}	1.63±0.2^{a}
		P1	10	22	24	22	1.09	1.00	3.09±0.27^{ab}	2.09±0.28^{b}
Goats	44	P2	4	6	4	9	0.67	1.50	3.67±0.33^{bc}	2.17±0.18^{b}
		P3	0.0	2	1	4	0.50	2.00	4.50±0.5^{c}	2.5±0.5^{c}

Data expressed as mean ± SE. Values followed by different superscript letters are significantly different from one another within the same columns (P≤ 0.05).

3.2.5. PCR-SSCP of primer 5 of INHβA gene:

PCR-SSCP analyses of the fifth fragment of the inhibin beta A gene (293bp) were shown in figure 10 and table 5. The results detected genetic polymorphisms in sheep animals. These polymorphisms were represented by the presence of 3 banding patterns (P_1, P_2 and P_3). However, in goats, the genetic polymorphisms were absent. All goat animals were subjected to pattern 2 (P_2) as in sheep and they were monomorphic. In sheep, pattern 1(P_1) was found only in 3 mothers, while pattern 2 (P_2) was found in 39 animals involving 34 mothers and 5 females at sexual maturity age. Pattern 3 (P_3) was found in 53 females including 46 mothers and 7 females at puberty. The P3-mothers showed high litter size rates, which was insignificant in comparison with the mothers of P1 or P2 genotype. The mothers of pattern 3 showed a statistically significant increase in lambing rate number in comparison with P1-ewes. So, P3 or P2 genotypes could be considered as a potential fecundity gene marker.

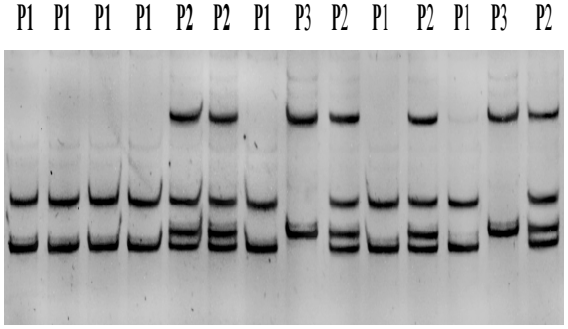

Figure 10. Shows three SSCP different patterns using primer 5 of INHβA gene.

Table 5. Shows genetic polymorphisms (SSCP patterns) of INHβA gene using primer 5 and their effects on litter size in different Egyptian sheep and goat breeds:

Species	No. of animals	SSCP Patterns (Ps)	No. of animals at age of sexual maturation	No. of mothers	No. of single births (S.b)	No. of twin births (T.b)	Mean No. of S.b	Mean No. of T.b	Mean No. of lambing	Mean No. of litter size (Twin production)
Sheep	95	P1	0.0	3	3	0.0	1.00	0.0	1.00±0.57[a]	1.00±0.23[a]
		P2	5	34	40	16	1.18	0.47	2.12±0.15[b]	1.65±0.18[ab]
		P3	7	46	43	33	0.93	0.72	2.37±0.11[b]	1.65±0.17[ab]
Goats	44	P2	14	30	29	35	0.97	1.17	3.30±0.15[c]	2.14±0.18[b]

Data expressed as mean ± SE. Values followed by different superscript letters are significantly different from one another within the same columns (P≤ 0.05).

3.3. Nucleotide Sequence Analyses of INHβA Gene:

Genetic polymorphisms in INHβA gene were detected in three amplified fragments (1, 3 and 5) in sheep, while the fourth amplified fragment was polymorphic in goats; on the other hand, no genetic polymorphisms were detected in the amplified fragment 2 in both sheep and goats. The nucleotide sequence analysis of PCR amplicon1 revealed the presence of a SNP in the position 113 (Fig.11). P_1 discriminated with "A" nucleotide (A/A), while P_2 discriminated with "C" nucleotide (C/C). P_3 ewes had both alleles with "C" and "A" nucleotide (A/C). Figure 12 shows sequence analysis of monomorphic type of PCR-SSCP analysis by using primer 2.

The primer 3 showed two patterns (P_1 and P_2) in INHβA gene. Nucleotide sequence analyses of the third amplicon showed differences between the two patterns in position of 157 on charts (Fig.13). In this location, pattern 1 discriminated with "A" nucleotide "(A/A), while P2 had "G" nucleotide (G/G) in the same location on the chart.

There were three different patterns of the fourth amplicon using primer 4 (P1, P2 and P3). Nucleotide sequence analysis identified differences between the three patterns in the position of 123 on charts (Fig.14) where pattern 1 discriminated with nucleotide "G"(G/G), while pattern 2 discriminated with nucleotide "A" (A/A). P3-animals had both alleles (A/G), where they had both G and A nucleotide at the position 123.

Moreover, using primer 5 showed three patterns. Nucleotide sequence analysis proved differences between the three patterns in the position 222 on charts (Fig.15). Pattern 1 discriminated with "G" nucleotide (G/G), while pattern 2 had both alleles with “G” and “A” nucleotides (A/G). Furthermore, pattern 3 was discriminated with "A" nucleotide (A/A).

Table 6 shows the detected alleles and genotypes of INHβA gene in local domestic sheep and goats in Egypt.

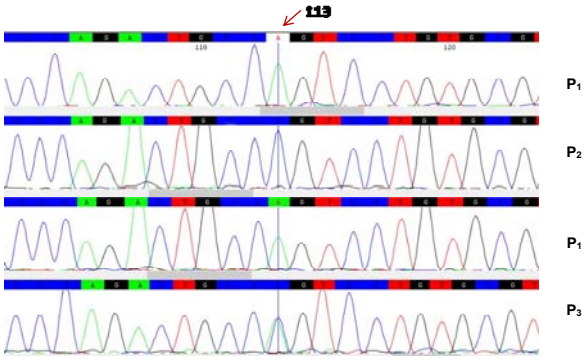

Figure 11. Sequence analysis of PCR-SSCP patterns (P_1, P_2 and P_3) of INHβA gene using primer 1.

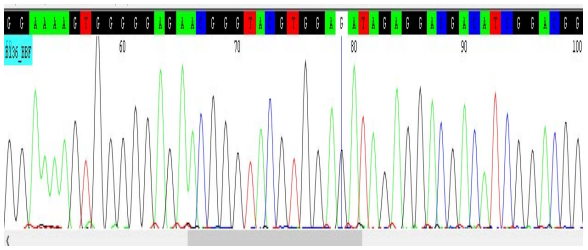

Figure 12. Sequence analysis of monomorphic (showed no any of SNPs) type of PCR-SSCP analysis of INHβA gene using primer 2.

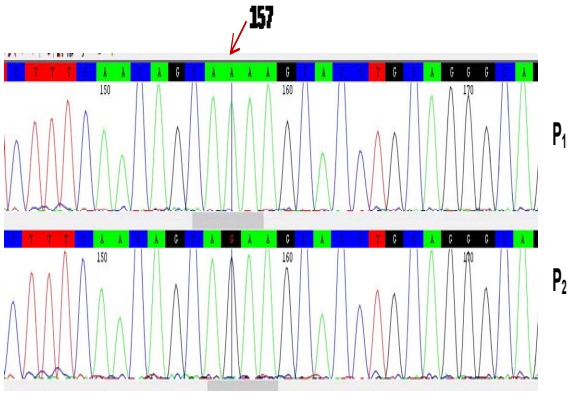

Figure 13. Sequence analysis of PCR-SSCP patterns (P_1 and P_2) of INHβA gene using primer 3.

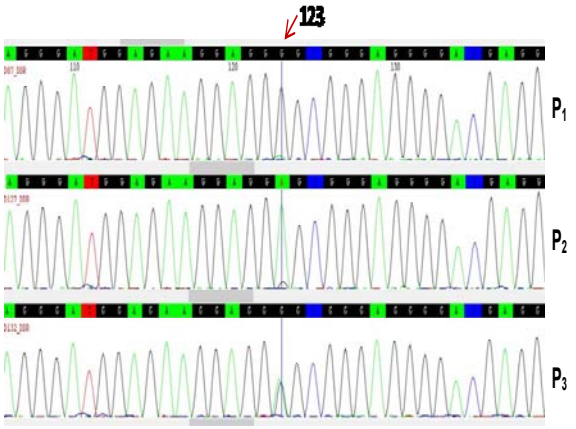

Figure 14. Sequence analysis of PCR-SSCP patterns (P_1, P_2 and P_3) of INHβA gene using primer 4.

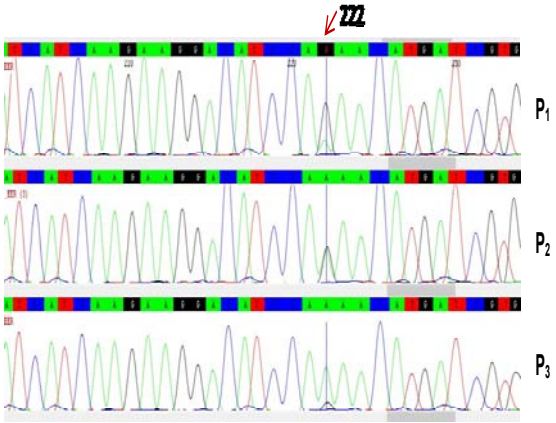

Figure 15. Sequence analysis of PCR-SSCP patterns (P_1, P_2 and P_3) of INHβA gene using primer 5.

Table 6. Nucleotide sequence analysis of INHβA gene in Egyptian sheep and goats showing relative genotype and allele frequencies.

The used primer	Species	No. of animals	Type of patterns (Ps) of SSCP analysis	Genotype	No. of Animals with SSCP pattern	Relative genotype frequency	Relative allele frequency
Primer 1	Sheep	95	P1	AA	62	0.65	A(0.67 ± 0.01)[b] C(0.33 ± 0.09)[a]
			P2	CC	29	0.31	
			P3	AC	4	0.04	
	Goats	44	P1	AA	44	1.00	A(1.00 ± 0.09)[b] C(0.0 ± 0.0)[a]
Primer 3	Sheep	95	P1	AA	70	0.74	A(0.74 ± 0.126)[b] G(0.26 ± 0.118)[a]
			P2	GG	25	0.26	
	Goats	44	P1	AA	44	1.00	A(1.00 ± 0.0009)[b] G(0.0 ± 0.0)[a]
Primer 4	Goats	44	P1	GG	32	0.73	A(0.25 ± 0.12)[a] G(0.75 ± 0.11)[b]
			P2	AA	10	0.23	
			P3	AG	2	0.04	
	Sheep	95	P1	GG	95	1.00	A(0.0 ± 0.0)[a] G(1.00 ± 0.01)[b]
Primer 5	Sheep	95	P1	GG	3	0.03	A(0.76 5± 0.1)[b] G(0.235 ± 0.11)[a]
			P2	AG	39	0.41	
			P3	AA	53	0.56	
	Goats	44	P2	AG	44	1.00	A(50 ± 0.04)[a] G(50 ± 0.04)[a]

Data expressed as mean ± SE. Values followed by different superscript letters are significantly different from one another within the same columns ($P \leq 0.05$).

4. Discussion

The present results by using SSCP and nucleotide sequence analyses detected different genetic polymorphisms in INHβA gene of Egyptian sheep and goat breeds. Some of these genetic polymorphisms were shown to be associated with increasing the litter size mean number and the lambing mean number in the local sheep and goats. The current results are consistent with that revealed by Chu *et al.* (2007). These authors studied the genetic polymorphisms in INHβA gene in eight sheep breeds, including two high fertile breeds (Small Tail Han and Hu sheep) and six low fertile breeds (Chinese Merino, Corriedale Dorest, German Mutton Merion, South African Mutton Merion, Texel, sheep). Their results determined 21 single nucleotide polymorphisms (SNPs) in the entire coding region and partial 3`UTR. These SNPs formed 12 genotypes and 9 alleles. 17 SNPs of 21 were from Hu breed; this breed is discriminated with early sexual maturity, year-round estrus and high prolificacy. Furthermore, the Small Tail Han KL-genotype mothers had more lambs than those with KK-genotype ewes. Also, the present findings are in coincidence with those revealed in several previous studies on ovine INHβA gene polymorphisms, where Hiendleder *et al.* (1992) observed allelic presence in Merino landschafe, Booroola Merino X Merino landschafe and East friesian Milk sheep (1.9 for A1 and 1.5 for A2). The frequency of alleles was 0.18 (A1) and 0.82 (A2). Moreover, Hiendleder *et al.* (1996b) studied the genetic polymorphism in INHβA gene of five sheep breeds (Merino landschaf, East Friesian Milk sheep,

Rhoenschaf, Romanov and Heidschnucke) with different reproductive performance and compared with wild sheep (O. musimon, O. ammon, O. vignei) breeds; TaqI RFLP were identified. Nucleotide sequence analysis had revealed variable SNPs at positions 21 (A /G), 25 (C/T), 80 (A/G), 119 (C/T), 165 (C/T), 216 (C/T), 260 (A/T), 310 (C/G) and 372 (A/G) between domestic and wild sheep; 3 of them led to changes in the inferred sequences of the amino acid structure. They found that the frequencies of INHβA TaqI alleles significantly differed between breeds, and allele A has a positive effect on the average litter sizes. Moreover, in 4 sheep breeds (East Friesian Milk sheep, Romanov, Merino landschaf and Rhoenschaf), Leyhe *et al.* (1994) observed 2 TaqI alleles of INHβA gene, these breeds were found to be significantly different in TaqI allele frequencies with different reproductive performance. Hiendleder *et al.* (1996a) pointed the different alleles of ovine INHβA gene (by using genomic cloning and comparative sequence analysis) and studied their effects on the litter size in East Friesian and Merino landschaf Milk sheep mothers. They identified that the nucleotide substitution had influenced the fertility rate. On the other hand, Fleming *et al.* (1992) observed high significant levels of INHβA mRNA in follicles that carry FecB gene when comparing with control. Also, Jaeger *et al.* (1994) examined 1,000 lambing records and observed that the genetic polymorphism had clear effect on litter size in sheep, which confirms the fact that reproductive traits are polygenic in nature (Ray *et al.*, 2016; Farag *et al.*, 2018).

5. Conclusions

In conclusion, the present study demonstrated that INHβA is a potent candidate gene that affect fecundity trait in local small ruminants in Egypt. So, the polymorphisms in such genes are favorable genetic markers that could be investigated before starting breeding programs and could be utilized for improving twin production in Egyptian sheep and goat breeds.

Acknowledgements

We acknowledge the financial support of the National Research Center to cover all the materials which was provided as a “Internal project (No. 11020104) and under title”: “Use of gene markers and Ca2+ regime for improving production of twins in Egyptian domestic sheep and goats”, PI: Dr. Ibrahim Farag.

Ethics approval and consent to participate

Blood samples were collected form sheep and goats under veterinary supervision and comply with local and international guidelines, international recommendations for the care and use of animals. The Blood samples were collected (after a written approval) from Animal Production Farm in Faculty Agriculture, Cairo University and Nubaria Farm belonging to National Research Centre, and in cooperating with the Governmental Halayieb Farm, Egypt). The all procedures carried out on the animals were approved by the Institutional Animal Care and Use Committee (IACUC), Faculty of Science, Cairo University, Egypt with Permit (Reference) Number: CUFS F Mol. Biol. 50 15.

References

Aboelenin MM, Mahrous KF, Elkerady A and Rashed MA. 2017a. Molecular characterization of cytochrome p450 aromatase (cyp19) gene in Egyptian river buffaloes. *Egypt J Genet Cytol*, **46**: 305-311.

Aboelenin MM, Mahrous KF, Rashed MA and Sallam MA. 2017b. Molecular characterization of tumor necrosis factor- A (TNFA) gene in Egyptian river buffaloes. *Arab Univ J Agric Sci*, **25**: 367-375.

Ahlawat S, Sharma R, Maitra A and Tantia MS. 2015. Current status of molecular genetics research of goat fecundity. *Small Rumin Res*, **125**: 34-42.

Brunner RM, Goldammer T, Hiendleder S, Jager C and Schwerin M. 1995. Mapping of the gene encoding for inhibin-beta A (INHBA) to chromosome 4q26 in sheep. *Mamm Genome*, **6**: 308-309.

Chu M, Xiao C, Fu Y, Fang L and Ye S. 2007. PCR-SSCP Polymorphism of Inhibin βA Gene in Some Sheep Breeds. *Asian-Aust J Anim Sci*, **20**: 1023-1029.

Farag I, Darwish H, Aboelhassan D, Aboelenin M and Shakweer W. 2018. Study of genetic polymorphism in BMPRIB gene and its association with improving twin production in Egyptian sheep and goats. *Res. J Anim Vet Sci*, **10**: 1-5.

Fleming JS, Tisdall DJ, Greenwood PJ, Hudson NL, Heath DA and McNatty KP. 1992. Expression of the genes for alpha inhibin, beta A inhibin and follistatin in the ovaries of Booroola ewes which were homozygotes or non-carriers of the fecundity gene FecB. *J Mol Endocrinol*, **8**: 265-273.

Hiendleder S, Lewalski H, Jaeger C, Pracht P and Erhardt G. 1996a. Genomic cloning and comparative sequence analysis of different alleles of the ovine βA-inhibin/activin (INHBA) gene as a potential QTL for litter size. *Anim. Genet.*, **27**: 119.

Hiendleder S, Leyhe B, Jaeger C, Erhardt G and Wassmuth R. 1996b. Molecular characterization of ovine a-, bA and bB-inhibin/activin alleles. *J Anim Breed Genet*, **113**: 363-372.

Hiendleder S, Leyhe B, Jaeger C and Wassmuth R. 1992. A TaqI polymorphism at the ovine beta A-inhibin (INHBA) locus. *Anim Genet*, **23**: 291.

Jaeger C and Hiendleder S. 1994. Cosmid cloning and characterization of the coding regions and regulatory elements of the ovine α-(INHA), βA -(INHβA) and BB-inhibin (INHβB) genes. *Anim Genet*, **25**: 33.

Leyhe B, Hiendleder S, Jaeger C and Wassmuth R. 1994. Pronounced differences in the frequency of TaqI beta A-inhibin alleles between sheep breeds with different reproductive performance. *Anim Genet*, **25**: 41-43.

Ling N, Ying SY, Ueno N, Esch F, Denoroy L and Guillemin R. 1985. Isolation and partial characterization of a Mr 32,000 protein with inhibin activity from porcine follicular fluid. *Proc Natl Acad Sci USA*, **82**: 7217-7221.

Madkour M, Aboelenin MM, Aboelazab O, Elolimy AA, El-Azeem NA, El-Kholy MS, Alagawany M and Shourrap M. 2021a. Hepatic expression responses of DNA methyltransferases, heat shock proteins, antioxidant enzymes, and NADPH 4 to early life thermal conditioning in broiler chickens. *Ital J Anim Sci*, **20**: 433-446.

Madkour M, Aboelenin MM, Shakweer WME, Alfarraj S, Alharbi SA, Abdel-Fattah SA and Alagawany M. 2021b. Early life thermal stress modulates hepatic expression of thermotolerance related genes and physiological responses in two rabbit breeds. *Ital J Anim Sci*, **20**: 736-748.

Madkour M, Aboelenin MM, Younis E, Mohamed MA, Hassan H, Alagawany M and Shourrap M. 2020. Hepatic acute-phase response, antioxidant biomarkers and DNA fragmentation of two rabbit breeds subjected to acute heat stress. *Ital J Anim Sci*, **19**: 1568-1576.

Mahrous KF, Abd El - Kader HAM, Mabrouk DM, Aboelenin MM, Osman NM, Khalil WKB and Hassanane MS. 2020a. Molecular characterization and expression analysis of hepc1 and hepc2 in three tilapia species collected from Lake Manzala. *Bull Natl Res Cent*, **44**: 36.

Mahrous KF, Aboelenin MM, Abd El-Kader HAM, Mabrouk DM, Gaafar AY, Younes AM, Mahmoud MA, Khalil WKB and Hassanane MS. 2020b. Piscidin 4: Genetic expression and comparative immunolocalization in Nile tilapia (Oreochromis niloticus) following challenge using different local bacterial strains. *Dev Comp Immunol*, **112**: 103777.

Mahrous KF, Aboelenin MM, Rashed MA, Sallam MA and Rushdi HE. 2020c. Detection of polymorphism within leptin gene in Egyptian river buffalo and predict its effects on different molecular levels. *J Genet Eng Biotechnol*, **18**: 6.

Mahrous KF, Mabrouk DM, Aboelenin MM, Abd El-Kader HAM, Gaafar AY, Younes AM, Mahmoud MA, Khalil WKB and Hassanane MS. 2020d. Molecular characterization and immunohistochemical localization of tilapia piscidin 3 in response to Aeromonas hydrophila infection in Nile tilapia. *J Pept Sci*, **26**: e3280.

Mahrous KF, Mabrouk DM, Aboelenin MM, Abd El kader HAM and Hassanane MS. 2021. Identification and characterization of antimicrobial peptide genes in Clarias gariepinus and Chelon ramada. *Jordan J Biol Sci*, **14**: 51-64.

Mason AJ, Hayflick JS, Ling N, Esch F, Ueno N, Ying SY, Guillemin R, Niall H and Seeburg PH. 1985. Complementary DNA sequences of ovarian follicular fluid inhibin show precursor structure and homology with transforming growth factor-beta. *Nature*, **318**: 659-663.

Medan MS, Watanabe G, Sasaki K, Nagura Y, Sakaime H, Fujita M, Sharawy S and Taya K. 2003. Ovarian and hormonal response of female goats to active immunization against inhibin. *J Endocrinol*, **177**: 287-294.

Mishra C, Rout M, Mishra S, Sahoo S, Nayak G and Patra R. 2017. Genetic polymorphism of prolific genes in goat-A brief review. *Explor Anim Medical Res*, **7**: 132-141.

Phillips DJ. 2005. Activins, inhibins and follistatins in the large domestic species. *Domest Anim Endocrinol*, **28**: 1-16.

Ray S, Dash S, Dhal S, Nayak G and Parida A. 2016. Genetic studies on reproductive performance of indigenous goats in northern Odisha. *Explor Anim Medical Res*, **6**: 192-198.

Rivier J, Spiess J, McClintock R, Vaughan J and Vale W. 1985. Purification and partial characterization of inhibin from porcine follicular fluid. *Biochem Biophys Res Commun*, **133**: 120-127.

Robertson DM, Foulds LM, Leversha L, Morgan FJ, Hearn MT, Burger HG, Wettenhall RE and de Kretser DM. 1985. Isolation of inhibin from bovine follicular fluid. *Biochem Biophys Res Commun*, **126**: 220-226.

Rodgers RJ, Stuchbery SJ and Findlay JK. 1989. Inhibin mRNAs in ovine and bovine ovarian follicles and corpora lutea throughout the estrous cycle and gestation. *Mol Cell Endocrinol*, **62**: 95-101.

Sroor FM, Aboelenin MM, Mahrous KF, Mahmoud K, Elwahy AHM and Abdelhamid IA. 2020. Novel 2-cyanoacrylamido-4,5,6,7-tetrahydrobenzo[b]thiophene derivatives as potent anticancer agents. *Arch Pharm (Weinheim)*, **353**: e2000069.

Sroor FM, Othman AM, Aboelenin MM and Mahrous KF. 2022. Anticancer and antimicrobial activities of new thiazolyl-urea derivatives: gene expression, DNA damage, DNA fragmentation and SAR studies. *Med Chem Res*.

Tudu N, Pyne S and Ghosh N. 2015. Comparative biometrics and performances of three colour varieties of Bengal goats in their home tract. *Explor Anim Medical Res*, **5**: 183-189.

Vanmontfort D, Peeters R, Buys N, Rombauts L, Verhoeven G, Charlet-Renard C, Franchimont P and Decuypere E. 1998. Circulating levels of inhibin and FSH during the oestrous cycle in 4 genotypes of sheep with different reproductive performances. *Small Rumin Res*, **29**: 213-224.

Waller RA and Duncan DB. 1969. A Bayes Rule for the Symmetric Multiple Comparisons Problems. *J Am Stat Assoc*, **64**: 1484-1503.

Woodruff TK, Besecke LM, Groome N, Draper LB, Schwartz NB and Weiss J. 1996. Inhibin A and inhibin B are inversely correlated to follicle-stimulating hormone, yet are discordant during the follicular phase of the rat estrous cycle, and inhibin A is expressed in a sexually dimorphic manner. *Endocrinology*, **137**: 5463-5467.

Zi XD, Xu HW and Wang Y. 2012. Variation in sequences and mRNA expression levels of inhibin subunits alpha (INHA) and betaA (INHBA) genes between prolific and nonprolific goat breeds. *Mol Reprod Dev*, **79**: 238.

JJBS

Volume 15, Number 4,December 2022
ISSN 1995-6673
Pages 579 – 592
https://doi.org/10.54319/jjbs/150406

Jordan Journal of Biological Sciences

In Vitro Antioxidant, Antihyperglycemic and Antiglycation Properties of Bulbs, Flower Buds and Flowers Extracts of *Lilium* Species and their Chemometric Profiling

The Su Moe [1, 2], Mingfang Zhang [1], Jing Xue [1], Mya Thida [3], Yixin Liu [1], Mohammad Sayyar Khan [1, 4], Yunpeng Du [1*] and Xiuhai Zhang [1,*]

[1]Beijing Agro-Biotechnology Research Center（Beijing Key Laboratory of Agricultural Genetic Resources and Biotechnology, Beijing Engineering Technology Research Center of Functional Floriculture）, Beijing Academy of Agriculture and Forestry Sciences, Beijing 100097, P.R. China; [2] Pharmaceutical Research Laboratory, Biotechnology Research Department, Ministry of Education, Mandalay Division, Kyaukse 05151, Myanmar;[3]Cell Culture Laboratory, Biotechnology Research Department, Ministry of Education, Mandalay Division, Kyaukse 05151, Myanmar;[4]Genomics and Bioinformatics Division, Institute of Biotechnology and Genetic Engineering (IBGE), the University of Agriculture, Peshawar 25000 Khyber Pakhtunkhwa, Pakistan

Received: June 28, 2021; Revised: January 11, 2022; Accepted: January 31, 2022

Abstract

This objective of this study was to explore the antioxidant, antihyperglycemic, and antiglycation properties of 13 methanolic extracts from 8 different *Lilium* species by various *in vitro* assays and their chemometric profiles to provide the evidence-based information for further exploration. Chemometric profiling was performed using the MetaboAnalyst and GNPS: Global Natural Products Social Molecular Networking platforms to explore and identify the metabolites from *Lilium* metabolomics profiles. *In vitro* bioactivity studies showed that flower bud extract of *L. lancifolium* was the most active extract with the strongest radical scavenging activity against DPPH and SO radicals, reducing activity of ferric ions and highest total phenolic contents among tested extracts. Univariate and multivariate statistical analysis revealed that the chemical variation between the sample classes: parts used (bulb vs flower); bioactivity (active vs inactive) and studied species. 13 bioactive metabolites were putatively identified and some of them were confirmed by comparing the MS/MS spectrums with the standards. Results suggest that metabolite profiling along with the bioactivity study could be useful to explore the chemical compositions, functional and developmental potentials of valuable plant species, and lay the foundation for identification, separation and assessment of their potential medicinal applications and species classification.

Keywords: *Lilium*; antioxidant; antihyperglycemic; antiglycation; chemometric profiling

1. Introduction

The genus *Lilium* from the family Liliaceae, consisting of about 280 genera and 4,000 species(Carr), was comprised of 110-115 species. It is a rich source of chemical diversity and substantial natural resources that have great ornamental, medicinal, and edible value. Among them, 55 species and 18 varieties originated from China, which had a noticeable history for the richness of *Lilium* resources(Tang *et al.*, 2010). Lily flowers and bulbs are regularly consumed as food and medicine all over the world, particularly in Asia(Munafo JrGianfagna, 2015). In China, the flowers and bulbs of some *Lilium* species are used for culinary and/or medicinal purposes. Local people believed that dried bulbs are potent for the lung diseases, have tonic properties, and are commonly used to flavor and thicken the soup(Royal Botanic Gardens, 1889). Moreover, specialized metabolites from some *Lilium* species showed the potential biological activities such as anti-inflammatory (Francis *et al.*, 2004), hepatoprotective (Tang *et al.*, 2015), antidiabetic (Tang, *et al.*, 2015), antioxidant (Guo *et al.*, 2014), antifungal (Uhlig *et al.*, 2014), antitumor (Shimomura *et al.*, 1987), antibacterial activities (Li, 2007) and cardiac disease(Zhou *et al.*, 2012) by various *in vitro* and *in vivo* assays. Due to these great potentials and traditional knowledge of *Lilium*, it has drawn an interest for commercial purposes.

On the other hand, taxonomic classification is critical for the plant species to recognize and effectively exploit their effectiveness for different purposes. Morphological (ViscosiCardini, 2011), physiological (Dunlop *et al.*, 1999), genetics(Du *et al.*, 2015), and chemical characterization(Rivière *et al.*, 2012) has been used to classify the plant species by comparing the difference characteristics between them. Among these taxonomic classification methods, chemical characterization or chemotaxonomy became a useful tool for the plant taxonomy. It is a method based on the dissimilarity of the chemical constituents of the plant species to classify according to their phylogeny(Kim *et al.*, 2012). Since the *Lilium* species are extremely related, several researches

* Corresponding author. e-mail: duyunpeng@baafs.net.cn ; zhangxiuhai@baafs.net.cn.

have been carried out to classify the *Lilium* species with different approaches such as floral morphology(Gao *et al*., 2015), SSR molecular markers(Du, *et al*., 2015), RAPD analysis(Ikinci, 2010) and DNA barcoding(Zheng *et al*., 2014). However, chemical characterization has not been utilized to understand the differences of chemometric profiles of *Lilium* species so far.

In recent years, metabolomics approaches has been broadly used to discover the chemical diversity of bioactive natural products, especially for the targeted isolation of structurally or biologically noble bioactive compounds(Raterink *et al*., 2014). Metabolomics is an approach that can characterize and quantify the primary and secondary metabolites or low molecular weight molecules present in the complex biological samples. Characterization of primary and secondary metabolites by metabolomics approach can be used to explore the relationship between the chemometric profiles of the studied species and identify the differences associated with the underlying study question and generate the new hypotheses(BoufridiQuinn, 2016).

In this research, bioactivities such as antioxidant activity, antihyperglycemic and antiglycation properties of bulbs, flower buds and flowers extracts of *Lilium* species were investigated by various *in vitro* assays to determine the potential application of different varieties of lily and provide the evidence-based information for further development of research and innovation. MetaboAnalyst and Global Natural Products Social Molecular Networking (GNPS) platform were used to explore the *Lilium* chemometric profiles mainly based on their bioactivity and studied species, and to facilitate the identification of MS spectra in the complex metabolomics datasets of selected *Lilium* species.

2. Materials and Methods

2.1. Chemicals and reagents

Analytical grade chemicals such as 2,2-Diphenyl-1-(2,4,6-trinitrophenyl)-hydrazyl (DPPH), ascorbic acid, gallic acid, sulphanilic acid, glacial acetic acid, sodium nitroprusside, N-(1-naphthayl) ethylenediamine dihydrochloride, ethylenediamine tetra-acetic acid (EDTA), Folin-Ciocalteu's reagent, sodium carbonate, riboflavin, nitro blue tetrazolium (NBT), potassium ferricyanide, trichloroacetic acid , ferric chloride, acarbose, α-Glucosidase, p-Nitrophenyl- α-D-Glucopyranoside (PNPG), fructose, bovine serum albumin (BSA) and sodium azide were purchased from companies such as Sigma Chemicals Co. (St. Louis, USA), and TCI Development Co. Ltd (Shanghai, China). Acetonitrile, dimethyl sulfoxide (DMSO), methanol and formic acid were purchased from Thermo Fisher Scientific, USA. Standards used for the compound identification were purchased from VEGSCI, Inc., China.

2.2. Plant materials

Lilium bulbs, flower buds and flowers used in this study were grown and collected form the greenhouses at the germplasm conservation center at the Beijing Academy of Agriculture and Forestry Sciences. The selected *Lilium* species used in this study are shown in Table 1.

Table 1. Selected *Lilium* species

Sample code	Botanical name	Family name	Parts used	Yield %
ZDM1	*L. lechtlinii var. maximowiczii*	Liliaceae	Bulb	16.96
ZDM2	*L.A.hybrids* 'Tresor'	Liliaceae	Bulb	11.99
ZDM3	*L. lancifolium*	Liliaceae	Bulb	10.49
ZDM4	*L. regale*	Liliaceae	Bulb	17.99
ZDM5	*L. pumilum*	Liliaceae	Bulb	10.46
ZDM6	*L. davidii*	Liliaceae	Bulb	14.03
ZDM7	*L. brownie*	Liliaceae	Bulb	12.65
ZDMF1	*L. davidii*	Liliaceae	Flower	35.65
ZDMF2	*L. henryi*	Liliaceae	Flower	31.64
ZDMF3	*L. lancifolium*	Liliaceae	Flower bud	26.32
ZDMF4	*L. lancifolium*	Liliaceae	Flower	36.18
ZDMF5	*L.A.hybrids* 'Tresor'	Liliaceae	Flower bud	40.98
ZDMF6	*L.A.hybrids* 'Tresor'	Liliaceae	Flower	53.76

2.3. Extraction

A grinding machine (BJ-800A, China) was used to crush freeze-dried plant samples into a fine powder. Samples were soaked for one week in 95 percent methanol then filtered, and solvents were removed using a rotary vacuum evaporator (RE 52AA, China). This step was repeated three times to get the maximum yield. Yield % was calculated using the formula: Yield % =Weight of the dry extract x 100/ Weight of the dry plant (Table 1). After removing the solvents, crude extracts were freeze-dried and stored at -80˚C for further experimentation.

2.4. Biological activity assays

2.4.1. In vitro antioxidant activity assays

Free radical-scavenging activity of the extracts was explored using the stable DPPH free radicals as mentioned by Lee et al.(Lee *et al*., 1998). The detailed experimental protocol could be seen on this previous publication of Moe et al. (2018). The optical density (OD_{515}) was measured using a Thermo Scientific Multiskan FC microplate reader. DMSO was used as the blank, and ascorbic acid was used as a positive control. Inhibition rate (%) was calculated through comparison to the blank.

Nitric oxide (NO) radical scavenging assay was performed as mentioned by Hertog et al.(Hertog *et al*., 1993). The detailed experimental protocol could be seen on this previous publication of Moe et al. (2018). The optical density (OD_{540}) was measured using a Thermo Scientific Multiskan FC microplate reader.

The extracts' free radical scavenging activity was also determined using a superoxide (SO) radical scavenging assay modified from Patel Rajesh's methodology.(Patel RajeshPatel Natvar, 2011). The detailed experimental protocol could be seen on this previous publication of Moe et al. (2018). The optical density (OD_{560}) was measured using a Thermo Scientific Multiskan FC microplate reader. In both NO and SO assays, ascorbic acid was useed as a positive control.

To assess the reducing activity of each extract, ferric reducing antioxidant power (FRAP) assay described by

Takashi Kuda et al. was used with slight modifications (Kuda *et al.*, 2005). 200 µL of extracts (10 mg/mL in DMSO), 200 µL of 0.2M Sodium Phosphate Buffer (pH 6.6) and 200 µL of 1% Potassium ferricyanide [K3Fe (CN)6] were mixed in a 2 ml micro-capped tubes and incubated at 50 ˚C for 30 min. Then, the mixture was cooled down, and 200 µL of 10% trichloroacetic acid was added to the reaction mixture. After that, 125 µL of this mixture were transferred to a 96-well microplate, and 20 µL of 0.1% Ferric chloride (FeCl3-6H2O) was added to each well. The optical density (OD_{620}) was measured using a Thermo Scientific Multiskan FC microplate reader. Gallic acid was used as a positive control.

2.4.2. In vitro antihyperglycemic activity assay

α-glucosidase inhibitory assay protocol described by Peyman Salehi et al. was used to detect the antihyperglycemic potentials of *Lilium* extracts (Salehi *et al.*, 2013). 10 µL of the extracts (0.4 mg/mL in DMSO), 120 µL of 0.1 M phosphate buffer (pH 6.9) and 20 µl of α-glucosidase (0.5 unit/ml) were mixed in a 96-well microplate and incubated at 37°C for 15 min. Subsequently, 20 µL of 5 mM p-nitrophenyl-α-D-glucopyranoside was added to initiate the enzymatic reaction, and the reaction mixture was incubated at 37°C for 15 min. After that, the reaction was neutralized with 80 µL of 0.2 M sodium carbonate solution, and optical density (OD_{405}) was measured using a Thermo Scientific Multiskan FC microplate reader. The reaction mixture without plant extracts was used as control, and that of without enzyme was used as blank for correcting the background absorbance. Acarbose was used as a positive control.

All the assays mentioned above were carried out in at least triplicate for each sample and positive controls, and inhibition rates for all the above tested assays were calculated using the following formula:

Inhibition rate (%) = [1 – (OD tested / OD control)] × 100

2.4.3. In vitro antiglycation activity assay

The ability of the extracts to inhibit the formation of advanced glycation end products (AGE) was measured to explore the i*n vitro* antiglycation activity of the extracts as described by Choudhary (Choudhary *et al.*, 2011). The detailed experimental protocol could be seen on this previous publication of Moe et al. 2018. AGEs formation was measured at the excitation of 340 nm and emission of 440 nm fluorescence's intensity by using an Agilent Cary Eclipse Fluorescence spectrophotometer (G9800, US). Rutin (1mM) was used as a positive control. The reaction mixture without fructose was used as the negative reaction control and that of without extracts as positive reaction or glycated control. Inhibition rate (%) was calculated by using the following formula:

Inhibition rate (%) = [1 - (fluorescence of tested sample / fluorescence of positive control)] × 100

2.4.4. Total phenolic content measurements

The measurement of total phenolic content present in each plant extract was done using the method described by Andrew L. Waterhouse with a few modifications(Waterhouse, 2002). Briefly, 2 µL of the extracts (1mg/mL in 70% methanol) or Gallic acid in different concentrations (0, 0.5, 1, 1.5, 2, 2.5, 5 µg/ml in 70% methanol) were put into the 96 well microplate. 148 µL of the distilled water and 20 µL of 1N Folin-Ciocalteu's reagent were added. The reaction mixtures were mixed thoroughly and incubated at room temperature for 5 min. Then, the reaction was neutralized by adding 30 µL of 0.2 g/ml sodium carbonate. After that, the samples were incubated at 40°C for 30 min, and the OD_{765} was measured with Thermo Scientific Multiskan FC microplate reader. For each sample, at least three replicate assays were performed. The total phenolic content (TPC) was represented as Gallic acid equivalent (GAE) in mg/g of extract using the equation generated from the Gallic acid standard curve ($y = 0.0007x$, $R^2 = 0.9995$).

2.5. Sample preparation for UHPLC-LTQ-XL-IT-MS/MS analysis

20 mg of each extract was dissolved in 1 mL of 70 % methanol and filtered through a 0.2 µm PTFE (polytetrafluoroethylene) filter, prior to ultrahigh performance liquid chromatography LTQ XL linear ion trap mass spectrometry/mass spectrometry (UHPLC-LTQ-XL-IT-MS/MS) analysis. Pierce™ LTQ ESI positive ion calibration solution was used to calibrate the LCMS system to check the system performance. 70% Methanol was employed in the LC-MS analysis as a blank sample for background subtraction.

2.6. UHPLC-LTQ-XL-IT-MS/MS analysis

UHPLC-LTQ-IT-MS/MS analysis was performed using the method adapted from Lee et al. with a few modification (Lee *et al.*, 2015b). Thermo Fischer Scientific LTQ XL linear ion trap mass spectrometry equipped with electrospray interface (Thermo Fischer Scientific, San José, CA, USA), DIONEX UltiMate 3000 RS Pump, RS Auto sampler and RS Column Compartment (Dionex Corporation, Sunnyvale, CA, USA) was used for metabolite profiling of the *Lilium* extracts. Samples were separated on a Thermo Scientific Hypersil GOLD C18 column with 1.9 µm particle size. The mobile phase consisted of A (0.1% (v/v) formic acid in water) and B (0.1% (v/v) formic acid in acetonitrile) and the gradient conditions were increased from 10% to 100% of solvent B. Scanning was set to start after 1 min to source. Solvent gradient time was set over 19 min, and re-equilibrated to the initial condition for 4 min by setting the divert valve to waste. The flow rate was set at 0.3 mL/min and the injection volume was 10 µL. Temperature of the column during measurement was maintained at 35 ˚C. Ion trap was performed in positive and full-scan ion modes within a range of 150–1000 m/z. The operating parameters were as follows: source voltage; ±5 kV, capillary voltage; 39 V, capillary temperature; 275 ˚C, auxiliary gas flow rate; 10−20 arbitrary units, sheath gas flow rate; 40−50 arbitrary units, spray voltage; 4.5 kV. Tandem MS (MS/MS) analysis was performed by scan-type turbo data-dependent scanning (DDS) under the same conditions used for MS scanning for the six most intense ions. MS data was acquired by Xcalibar software, Thermo Fischer Scientific(Khan *et al.*, 2020).

2.7. Data pre-processing

The UHPLC-LTQ-IT-MS/MS data were acquired with Xcalibar software (version 2.00, Thermo Fischer Scientific). The raw data files were converted from the Xcalibar standard data-format to .mzXML format using

the MSConvert software, part of the ProteoWizard package version 3.0.19140 (Chambers *et al*., 2012). All .mzXML were pre-processed using MZmine 2.51 for mass detection, chromatogram building and deconvolution, deisotoping and peak alignment (Pluskal *et al*., 2010). The aligned peak list files were exported using the built-in options "Export to MetaboAnalyst file".

2.8. Statistical analysis and putative identification of metabolites

For the LC-MS data analysis, .csv file created by MZmine 2.51 with feature lists (m/z, RT), sample name, group and the area of each peak was uploaded to MetaboAnalyst and statistical analysis was performed using unsupervised (principal components analysis - PCA and hierarchical cluster analysis - HCA) and supervised (Partial Least Squares - Discriminant Analysis - PLS-DA) methods. Samples were classified into three different groups: parts used (bulb vs flower), species names and bioactivity (inactive vs active). Analysis was performed based on the sample groups. Then the univariate and multivariate statistical analysis was processed using MetaboAnalyst 4.0 (Chong *et al*., 2019). The data integrity check was done by default, data filtering was performed by mean intensity value and auto scaling was used for the normalization. Principal component analysis (PCA) and partial least-square discriminant analysis (PLS-DA) were performed to explore the metabolite differences between samples. The most significant metabolites were selected based on variable importance in the projection (VIP) score.

After statistical analysis, metabolites were identified by using the standard compounds by comparing both mass spectra and retention time. If the standard compounds could not purchase, putative identification was done by the GNPS public spectral database which comprised of the library containing the natural product compounds from user contributions and third party databases such as Massbank, ReSpect, HMDB, CASMI and Sumner Spectral Libraries (http://gnps.ucsd.edu) (Wang *et al*., 2016b). mzXML files converted from the raw LC-MS files were uploaded to GNPS and molecular network was created with the MSCluster algorithm enabled(Frank *et al*., 2008) using the default parameters. The spectra in the network were then searched against GNPS' spectral libraries. The library spectra were filtered in the same manner as the input data. All matches kept between network spectra and library spectra were required to have a score above 0.6 and at least 4 matched peaks. Blank Spectra were also uploaded and filtered before networking. MASST Search (Mass Search Tool) was also used to search single MS/MS spectrum of interest against all public spectral libraries on GNPS (Wang *et al*., 2020).

For the bioactivity assays, all data were expressed as mean ± standard error mean of at least triplicate experiments. One-way analysis of variance (ANOVA) and Dunnett's or Tukey's multiple comparison tests were performed to compare the difference between the plant extracts and standard control or between the tested plants extracts. In each analysis, $P < 0.05$ was considered to be statistically significant. Correlation analysis was also performed to evaluate the correlations between DPPH radical scavenging assay and the rest of tested bioactivity assays using GraphPad Prism version 7.00 for Windows, GraphPad Software, La Jolla California USA, www.graphpad.com.

3. Results

3.1. In vitro antioxidant, antihyperglycemic and antiglycation activities of Lilium extracts

In this research work, potential antioxidant, antihyperglycemic and antiglycation activity of 13 methanolic extracts of bulbs, flower buds and flowers from 8 different *Lilium* species were explored by using the various *in vitro* assays for evidence-based validation. Comparison between the bioactivities of each plant extract and the standard or comparison between the samples was carried out to distinguish the potentially bioactive plant extract for further study and samples that were significantly different ($P< 0.05$) from the standard or from each other were also stated.

ZDMF3 (flower bud extract of *L. lancifolium*) emerged as the most active plant extract in four of the seven bioassays that were evaluated. It demonstrated the highest ferric ion reducing activity with the maximum absorbance value of 2.02±0.08 and the highest radical scavenging activity against DPPH and SO radicals with inhibition rates of 91.54±0.38 %, 82.35 ± 1.25%, respectively (Table 2) and highest total phenolic contents of 112.74 mg GAE/g of extract (Figure 1). While many other extracts had significantly lower activity than the standard for these assays, ZDMF3 was comparable to the standard and could be a potential source of antioxidants and valuable for reducing oxidative stress.

Table 2. *In vitro* antioxidant activities of selected *Lilium* extracts

Sample code	Inhibition rate (%)			
	DPPH free radical scavenging activity	Nitric oxide radical scavenging activity	Superoxide radical scavenging activity	FRAP activity (Absorbance)
ZDM1	0.00*	28.02±3.72*	12.93±1.92*	0.18±0.002*
ZDM2	0.00*	35.92±2.66*	15.61±3.49*	0.20±0.002*
ZDM3	44.02 ± 4.49*	54.54±0.24*	69.21±3.38*	0.85±0.025*
ZDM4	57.96 ± 0.80*	60.19±1.44*	80.26±2.12	0.89±0.020*
ZDM5	3.80 ± 3.52*	36.60±2.52*	2.77±6.67*	0.32±0.003*
ZDM6	0.85 ± 0.33*	37.46±3.75*	11.28±5.21*	0.21±0.001*
ZDM7	8.66 ± 3.15*	20.38±6.91*	36.66±4.22*	0.16±0.002*
ZDMF1	23.14 ± 3.73*	45.64±2.17*	42.57±6.56*	1.22±0.017*
ZDMF2	17.90 ± 0.47*	36.60±3.90*	51.44±2.42*	0.39±0.015*
ZDMF3	91.54 ± 0.38	56.48±1.95*	82.35±1.25	2.02±0.089*
ZDMF4	68.05 ± 1.29*	52.46±0.32*	68.59±4.68*	1.29±0.028*
ZDMF5	60.56 ± 2.17*	36.51±1.12*	53.07±3.37*	0.94±0.011*
ZDMF6	26.51 ± 0.73*	21.10±5.51*	45.59±2.97*	1.24±0.020*
Ascorbic Acid	97.48 ± 0.16	74.88±0.86	89.56±0.58	-
Gallic Acid	-	-	-	3.82±0.031

Results were shown as the average of at least triplicates of experiments ± standard error of mean.*P < 0.05, extract *vs* standard in each group. DPPH: 1, 1-diphenyl-2-picrylhydrazyl; FRAP: Ferric Reducing Antioxidant Power; GAE: gallic acid equivalent.

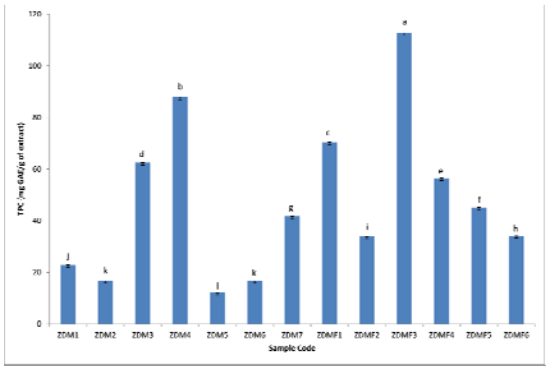

Figure 1. TPC of *Lilium* extracts determined by the Folin-Ciocalteu's assay and calculated as GAE in mg/g extract based on dry weight. Results were the average of triplicates ± standard error of the mean. Different letters (a–l) indicated significant difference (P < 0.05) from each group. GAE: gallic acid equivalent; TPC: total phenolic content

For the inhibition of NO radicals, ZDM4 (bulb extract of *L. regale*) exhibited the best activity against NO radicals among the tested samples. The inhibition rate was 60.19±1.44%, while the standard ascorbic acid showed the inhibition rate of 74.88±0.86% (Table 2). ZDM4 also has the moderate activity for antihyperglycemic activity through α-glucosidase inhibition assay with the rate of 61.51±9.66% (Table 3). It also possesses the second highest total phenolic contents of 87.86 mg GAE/g of extract (Figure 1). The highest activity of α-glucosidase inhibition among the tested extracts was to be possessed by ZDM7 (bulb extract of *L. brownii*) with the inhibition rate of 63.38±2.33%.

Table 3. *In vitro* antihyperglycemic and antiglycation activities of selected *Lilium* extracts

Sample code	Inhibition rate (%)	
	Antihyperglycemic activity	Antiglycation activity
ZDM1	29.16±2.36*	27.92±12.52*
ZDM2	15.35±2.96*	12.84±2.68*
ZDM3	38.38±9.99*	84.26±4.62
ZDM4	61.51±9.66*	22.06±9.88*
ZDM5	34.72±5.18*	29.33±6.06
ZDM6	0.00*	20.17±1.92*
ZDM7	63.38±2.33*	22.88±6.02*
ZDMF1	28.88±1.24*	9.22±7.44*
ZDMF2	38.13±2.91*	0.00*
ZDMF3	19.56±2.54*	0.00*
ZDMF4	10.45±5.67*	5.30±12.36*
ZDMF5	41.60±1.80*	0.00*
ZDMF6	43.95±6.92*	27.98±4.28*
Acarbose	98.67±0.33	-
Rutin	-	56.73±3.35

Results were shown as the average of at least triplicates of experiments ± standard error of mean.*P < 0.05, extract *vs* standard in each group.

Then the inhibition of AGE formation was evaluated by a non-enzymatic glycation reaction. Among all the tested samples, ZDM3 (bulb extract of *L. lancifolium*) revealed the highest antiglycation activity with inhibition rate of 84.26±4.62% (Table 3). Its activity was remarkably higher than the standard, rutin, with that of 56.73±3.35% at the tested concentration.

3.2. Metabolite Profiling of Lilium Extracts by MetaboAnalyst workflow

We analyzed the *Lilium* extract metabolomics data by classifying the samples based on their plant parts (bulb vs flower) to determine whether the samples are correctly classified using this statistical model. As shown in Figure 2, PCA score plot clearly distinguished the metabolites from the bulb and flower extracts. In the PCA plot, 2

components account for 34 % of the variance. With the exception of one bulb extract, ZDM4 (*L. regale*), which clustered into the flower extract, hierarchical clustering analysis (Figure 3) likewise clearly distinguished between the two groups: one group comprising the flower extracts and the other group including the bulb extracts. *L. regale* bulb: purple in color, was different from all the other tested bulb extracts, which were all white. These color giving metabolites from ZDM4 extracts might be quite similar to that of the flower extracts, and this could be the reason that ZDM4 was clustered into the flower extracts. As per the result obtained, MetaboAnalyst platform was considered to be suitable for the analysis of *Lilium* metabolomic data sets.

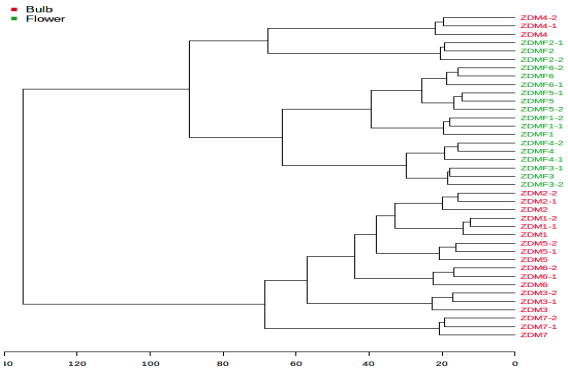

Figure 3. Dendrogram showing the hierarchical clustering pattern of *Lilium* metabolomics data based on the class defined by parts used (Bulb vs Flower).

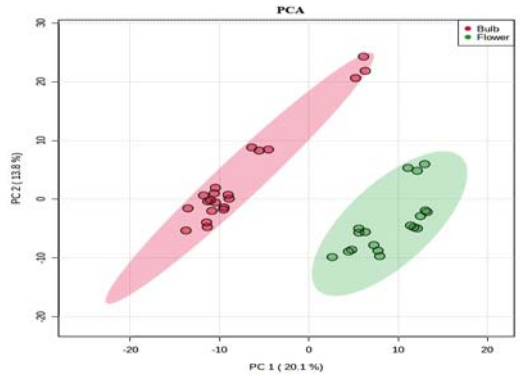

Figure 2. PCA scores plot for the unsupervised analysis of *Lilium* metabolomics data based on the class defined by part used (Bulb vs Flower).

We then investigated the *Lilium* metabolomics data sets by classifying the sample class information based on their bioactivities: active vs inactive extracts to understand the metabolites separation between them. Bioactivity was classified based on the DPPH radical scavenging activity as this activity was positively correlated with the other antioxidant activities, such as NO radical scavenging activity(r= 0.45), SO radical scavenging activity(r= 0.79), FRAP activity(r= 0.74) and total phenolic contents(r= 0.71). Extracts with ≥50 % of the inhibition rate of DPPH radicals were considered as active extracts, and those with < 50% were regarded as inactive extracts. For this analysis, 2 components account for 36% of the variance in PCA score plot (Figure 4A), and active extracts were clearly separated from the inactive extracts with 2 components account for 29% of the variance in PLS-DA plot (Figure 4B). The metabolites that separated the active and inactive extracts can be seen in Figure 4C. As we can see in the dendrogram, almost all the active extracts are from the flower parts. As we previously mentioned, one bulb extract ZDM4 that revealed as bioactive appeared clustering into the flower extract (Figure 5A). PLS-DA analyses allow us for selecting the most important features or metabolites that differentiate between groups through its VIP score in the sPLS plot [23]. Of the 15 most important features of group separation, four metabolites were putatively identified as solasodine, chlorogenic acid, hydroferuloylglucose and 15-Oxospirosolan-3-yl 2-O-(6-deoxy- alpha-L-mannopyranosyl) -beta- D-Glucopyranoside (Steroidal saponins) by the GNPS public spectral database (Table 4).

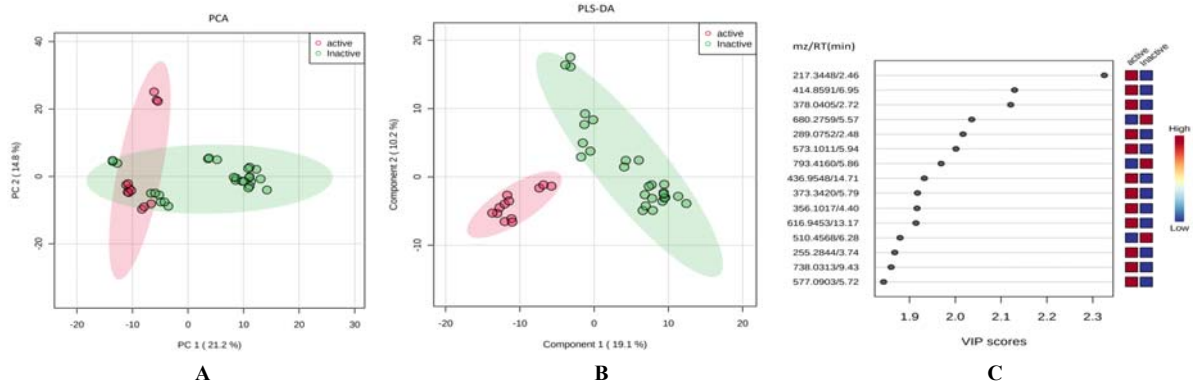

A **B** **C**

Figure 4. Unsupervised and supervised analysis of *Lilium* metabolomics data based on their bioactivity: (A) PCA scores plot; (B) PLS-DA scores plot and (C) PLS-DA loadings for the 15 most important variables (metabolites) that could discriminate between the active and inactive extracts.

Table 4. Discriminant metabolites from bioactivity-based grouping

No.	Parent ion (mz)	Retention Time (min)	Proposed Identity	Molecular Formula	Identifier	GNPS library ID
1	217.3448	2.46	NI	-	GNPS	-
2	414.8591	6.95	Solasodine	C27H43NO2	GNPS/Standard	CCMSLIB00004690970
3	378.0405	2.72	Chlorogenic acid	C16H18O9	GNPS	CCMSLIB00003139010
4	680.2759	5.57	NI	-	GNPS	-
5	289.0752	2.48	NI	-	GNPS	-
6	573.1011	5.94	NI	-	GNPS	-
7	793.4160	5.86	NI	-	GNPS	-
8	436.9548	14.71	NI	-	GNPS	-
9	373.3420	5.79	Hydroferuloylglucose	C16H20O10	GNPS	CCMSLIB00000209861
10	356.1017	4.40	NI	-	GNPS	-
11	616.9453	13.17	NI	-	GNPS	-
12	510.4568	6.28	NI	-	GNPS	-
13	255.2844	3.74	NI	-	GNPS	-
14	738.0313	9.43	15-Oxospirosolan-3-yl 2-O-(6-deoxy-alpha-L-mannopyranosyl)-beta-D-Glucopyranoside	C39H63NO12	GNPS	CCMSLIB00000852029
15	577.0903	5.72	NI	-	GNPS	-

NI: Not Identified

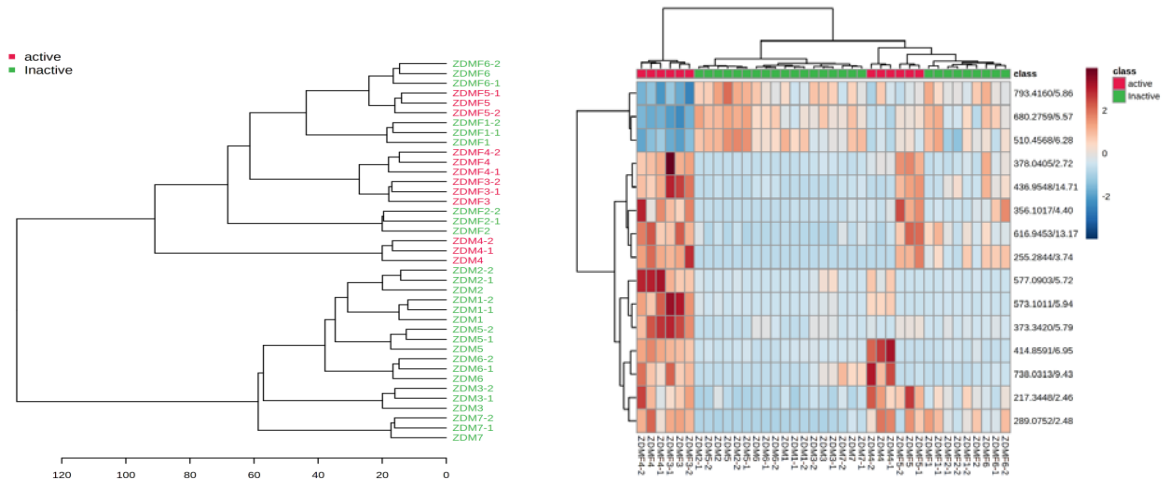

A B

Figure 5. Clustering pattern of *Lilium* metabolomics data based on the class defined by bioactivity: (A) Dendrogram; (B) Heatmap (distance measure using euclidean, and clustering algorithm using ward.D).

We also studied metabolomic data of the *Lilium* bulb samples by classifying the samples based on their species to discover if the chemical characterization could differentiate the bulbs of these closely related *Lilium* species. For the unsupervised analysis, 2 components account for 45% of the variance in PCA score plot. As shown in the Figure 6A, *Lilium* species were closely related and three species such as *L.brownii*, *L. lancifolium* and *L. regale* were separated from the area in which the rest species are grouping into close manner. However, as shown in the Figure 6B, supervised analysis could discriminate the species with 2 components account for 41% of the variance. The top 15 significant metabolites that discriminate these species and their relative concentration can be seen in the PLS-DA loading plot (Figure 6C). Among these 15 most important metabolites, relative concentration of 3 metabolites such as 534.5637mz/14.08min, 517.0777mz /14.08min, and 532.5118mz /13.13min were found to be highest in *L.brownii* than the rest of the species. The concentration of 7 metabolites such as 485.4668mz/13.29min, 696.6569mz/12.85 min, 694.7240mz/11.73min, 589.8393mz /12.52min, 522.9131mz /14.26min (PC(0:0/18:0)), 613.9326mz /11.75 min, and 502.0174mz /13.29min were highest in *L.A.hybrids* 'Tresor'. The rest five most important metabolites appeared as 332.0139 mz /4.76 min, 234.1394mz /12.28 min, 397.3256mz /1.58min, 453.9508mz /4.60min, and 579.2074mz /5.88min (2-(hydroxymethyl)-6-(2,20,21-trihydroxydocosan-3-yloxy)oxane-3,4,5-triol) were relatively highest in concentration in *L.regale*.

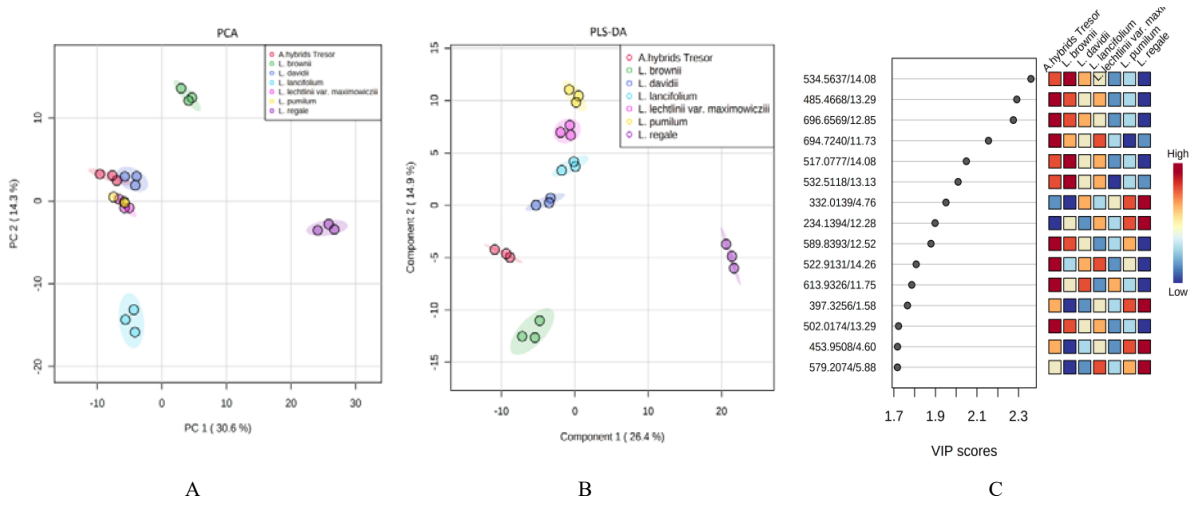

Figure 6. Unsupervised and supervised analysis of metabolomics data of *Lilium* bulb samples based on species: (A) PCA scores plot; (B) PLS-DA scores plot and (C) PLS-DA loadings for the 15 most important variables (metabolites) that could discriminate between the closely related *Lilium* species.

3.3. Chemical Interpretation of Lilium Extracts by GNPS workflow

After the identification of discriminant metabolite, the bioactive compounds were further explored to get the more comprehensive chemical information into the metabolomics profiles of the methanol extracts of *Lilium*. As the classic untargeted metabolomics study with the statistical analysis was hindered by metabolite annotation due to its big and complexity data type and the availability of the chemical standards for the structural identification, classic molecular networking from GNPS was applied to identify the bioactive compounds present in the *Lilium* metabolomics profiles. Molecular network of the methanol extracts of *Lilium* was created on GNPS platform which organizes the metabolomics data by the relatedness of the structures through the similarity between fragmentation patterns (MS/MS) of precursor ions. The created molecular network can be found at the GNPS website via the following links:

https://gnps.ucsd.edu/ProteoSAFe/status.jsp?task=42a7896ae4094dbf8d745f525b0e8b90.

The molecular network was generated for the spectra with a minimum of four shared fragment ions, and by merging all identical spectra into individual consensus nodes. Blank spectra from the solvent control were filtered before the networking. In the created *Lilium* molecular network, 7597 nodes were produced from the 91681 MS/MS spectra establishing the 788 molecular families, which were formed based on the structural relatedness. MS/MS spectra which do not have any similarity with others formed as the self-loop single node. 47.3 % of the molecular families composed of 2824 nodes were putatively identified by GNPS spectral libraries with the unique compound names of 966 in total and the lists can be browsed at the link provided above. All the structural annotations were level 2 annotations according to the 2007 Metabolomics Standards Initiative (MSI) (Sumner *et al.*, 2007). Among them, 13 metabolites which were previously found in the Liliaceae genus could be detected in this *Lilium* network by the GNPS spectral library matching (Table 5). In order to determine the presence of some compounds in the Lilium extracts, several reference compounds were purchased, their MS/MS spectra were generated using the same method as the crude extracts, and they were submitted to the GNPS website for data analysis. Ten bioactive compounds were confirmed to be present in *Lilium* species by comparing the MS/MS spectral data with standards. Retention time and spectral data of these compounds can be seen in Table 5.

Table 5. LC-MS characteristics of metabolites to be present in selected *Lilium* extracts

No	Proposed Identity	Retention Time (min)	Parent ion (mz)	MS2 ions	Molecular formula	Identifier	GNPS library ID
1	Regaloside C	2.16	417.08	255,163,399,325	C18H24O11	Standard	CCMSLIB00005720288
2	Gallic acid	2.71	172.47	125,144,150,121	C7H6O5	Standard/ GNPS	CCMSLIB00005720302
3	Chlorogenic acid	2.75	355.48	163	C16H18O9	GNPS	CCMSLIB00000221163
4	Rutin	4.69	611.49	303,465	C27H30O16	GNPS	CCMSLIB00005435850
5	Daucosterol	5.89	579.11	399,416	C35H60O6	Standard	CCMSLIB00005720278
6	Stigmasterol glucoside	6.48	574.28	530,681,737,482, 624,511,455	C35H58O6	Standard	CCMSLIB00005720298
7	Solasodine	9.52	414.89	397,253,271,158	C27H43NO2	Standard/ GNPS	CCMSLIB00005720295
8	Quercetin	10.72	301.44	240	C15H10O7	Standard	CCMSLIB00004705497
9	Quercetrin	11.77	448.49	304,416,286	C21H20O11	Standard/ GNPS	CCMSLIB00005720287
10	Diosgenin/Spirost-5-en-3-ol, (3beta,25R)-	12.70	415.65	272,253,283	C27H42O3	GNPS	CCMSLIB00000855694
11	Gibberellic acid GA3	13.08	346.43	329,311,285	C19H22O6	Standard/ GNPS	CCMSLIB00005720279
12	Riboflavin	13.50	413.70	396,354	C17H20N4O6	Standard	CCMSLIB00004689658
13	Isopimaric acid	17.92	303.47	257,285,179,247, 123	C20H30O2	Standard/ GNPS	CCMSLIB00005720283

4. Discussion

In China, *Lilium* species are considered as commercially important and widely used as edible and medicinal purposes. Many researches demonstrated that *Lilium* species have a wide range of biological activities including antioxidant and antidiabetic activities. Plant extracts or compounds which have the antioxidant, antihyperglycemic and anti-glycation activities might have great therapeutic potential for treating diabetic complications (Chinchansure *et al.*, 2015). Zhang et al. studied that polysaccharides extracted from one of the *Lilium* species, *Lilium davidii var. unicolor* Salisb has certain antiglycation activity at different stages of non-enzymatic glycosylation process(Zhang *et al.*, 2018). However, very few researches have been carried out for the evidence-based validation, especially for antidiabetic potentials of *Lilium* species through glycation inhibition activity. The advanced glycation end-products (AGEs) formation is significantly increased in hyperglycemic conditions(Moe *et al.*, 2018). Therefore, inhibition of AGEs is essential to prevent AGEs related biological disorders. Many researches have been carried out to search the natural or synthetic compounds, which can inhibit the AGEs. As anti-glycemic agents like metformin, amino guanidine and irbesartan have some side effects, compounds isolated from natural resources have been considered safer and cheaper options for the inhibition of AGEs formation(Kaewnarin *et al.*, 2014).

Among the studied species, we could have presumed that different parts of *L. lancifolium* could be useful for different purposes, as its flower bud extract was active for antioxidant activity when we tested its activity with four different *in vitro* assays such as DPPH, SO, FRAP and TPC, and its bulb extract was active for antidiabetic activity through glycation inhibition properties. This might be due to the specialized metabolite localization being different between the plant parts, and bioactivities could differ with the choice of the part used. Since the oxidative stress and non-enzymatic protein glycation was linked to various diseases such as Alzheimer's disease, rheumatoid arthritis, diabetes and atherosclerosis(Perera *et al.*, 2013, RahbarFigarola, 2003), *L. lancifolium* could be a promising plant species with therapeutic potential that merits further investigation, or could be used to develop the functional components or nutraceutical products using its different parts.

Following the investigation of bioactivities of selected *Lilium* species, we further explore the chemical information that could give us the background information for different type of sample presenting the bioactivity in different ways. Hence, chemometric profiling of crude extracts of *Lilium* species was performed to explain this purpose. UHPLC-LTQ-IT-MS/MS analysis with data-dependent scanning (DDS) mode was done and MetaboAnalyst platform (https://www.metaboanalyst.ca) was used to explore the metabolite characteristics of selected *Lilium* species.

MetaboAnalyst is an extensive web-based platform for analysis of complex metabolomics datasets: particularly for data pre-processing, statistical analysis, and functional interpretation which requires little statistical or computational background (XiaWishart, 2016). The parent ion mass and retention time information can help the analyst to locate the target compounds in a complicated metabolomic data set even if the MetaboAnalyst platform is unable to annotate the identification of the discriminant features (Demarque et al., 2020). Finding the known metabolites within complex biological samples—a process sometimes referred to as dereplication—is one of the main obstacles to finding the noble bioactive compound. It is crucial to identify the MS spectra of the metabolites of complex metabolomics dataset by spectral database matching or standard compound comparison. Therefore, in order to search for compound identity using the spectral database, the information provided by MetaboAnalyst is crucial. Moreover, by using the grouping or class

information, it could also provide the information to determine whether the samples are correctly classified as it should be or the chemical information of discriminant compounds, which could be used as biomarker based on the studied questions. From this exploratory statistical analysis, we could detect the pattern of the significant metabolites based on the predefined grouping information. For instance, the metabolites that distinguish between the parts used are distinct from those that distinguish between groups based on bioactivity or species. Hence, we could extract the important chemical information using this exploratory statistical analysis. Even though the selected *Lilium* species belong to one genus, the chemical constituents were mainly related to different parts of the species, this may be due to the fact that the metabolites have different functions at different stages of the plant growth or plant parts based on the demand of metabolism and protective system of the plant (Kadhim *et al.*, 2019).

Among the identified important features of bioactivity-based group separation, solasodine detected in the *Lilium* extracts is bioactive alkaloid, and previous studies indicated that it has antimicrobial, anti-oxidant, neuroprotection, anticonvulsant and central nervous system depressant activities (Chauhan *et al.*, 2011, Kumar *et al.*, 2009, Lecanu *et al.*, 2011, Niño *et al.*, 2009, Sharma *et al.*, 2014). Solasodine, iridoid glycoside, is a typical Solanaceae metabolite. In addition to Solanaceae, other plant families such as Asparagaceae, Compositae, Smilacaceae, Rhamnaceae, and Rosaceae, were examined for the presence of iridoid glycosides(Chi *et al.*, 1981). However, there is no previous report that Liliaceae can biosynthesize the iridoid glycosides. Even though the presence of solasodine was confirmed by comparing the MS2 spectra with the standard in this current research, it is still needed to confirm its presence in this species by the targeted isolation. As shown in the Figure 5B, the relative concentration of this bioactive compound tentatively identified as solasodine was higher in *L. regale* extracts than the rest of the extracts. NO radical scavenging activity and antihyperglycemic activity of *L. regale* extracts might be due to the presence of this compound.

Hydroferuloylglucose, which was putatively identified by the GNPS library matching, was also found to have similar MS2 fragmentation pattern of that reported in the work of Ma et.al (Figure 7) (Ma *et al.*, 2007). Ma et.al reported that Hydroferuloylglucose, one of the plant phenols, phenylpropanoid glycosides type compound could be one of the responsible compounds for the biological activity of ethanolic extract of *Ananas comosus* L. leaves, which exhibited the antidiabetic, antihyperlipidemic and antioxidative effects. The presence of this compound may have influenced the antioxidant and antidiabetic properties of *Lilium* species.

The metabolites which are specifically found to be highest concentration in particular plant species may serve as potential biomarkers for discriminating the closely related species. Therefore, the metabolites, showed up as important features for species based group separation (Table 6), could be used as biomarkers to distinguish *L.brownii*, *L.A.hybrids* 'Tresor' and *L.regale* from the rest of the species, as the relative concentration of these 15 metabolites were quite low in the rest species. However, only two metabolites were putatively identified as PC (0:0/18:0) and 2-(hydroxymethyl)-6-(2, 20, 21-trihydroxydocosan-3-yloxy) oxane-3, 4, 5-triol by the GNPS public spectral database. With the help of GNPS library matching, some of the discriminant metabolites were able to identify putatively. However, many of them were still needed for the identification.

Table 6. Discriminant metabolites from species-based grouping for the Lily bulbs

No.	Parent ion (mz)	Retention Time (min)	Proposed Identity	Molecular Formula	Identifier	GNPS library ID
1	534.5637	14.08	NI	-	GNPS	-
2	485.4668	13.29	NI	-	GNPS	-
3	696.6569	12.85	NI	-	GNPS	-
4	694.7240	11.73	NI	-	GNPS	-
5	517.0777	14.08	NI	-	GNPS	-
6	532.5118	13.13	NI	-	GNPS	-
7	332.0139	4.76	NI	-	GNPS	-
8	234.1394	12.28	NI	-	GNPS	-
9	589.8393	12.52	NI	-	GNPS	-
10	522.9131	14.26	PC(0:0/18:0)	C26H55NO7P	GNPS	CCMSLIB00003121778
11	613.9326	11.75	NI	-	GNPS	-
12	397.3256	1.58	NI	-	GNPS	-
13	502.0174	13.29	NI	-	GNPS	-
14	453.9508	4.60	NI	-	GNPS	-
15	579.2074	5.88	2-(hydroxymethyl)-6-(2,20,21-trihydroxydocosan-3-yloxy)oxane-3,4,5-triol	C28H56O9	GNPS	CCMSLIB00000847180

NI: Not Identified

As the classic untargeted metabolomics study with the statistical analysis was hindered by metabolite annotation due to its big and complexity data type and the availability of the chemical standards for the structural identification,

classic molecular networking from GNPS was applied to identify the bioactive compounds present in the *Lilium* metabolomics profiles. Molecular network of the methanol extracts of *Lilium* was created on the GNPS platform which organizes the metabolomics data by the relatedness of the structures through the similarity between fragmentation patterns (MS/MS) of precursor ions.

Among the identified metabolites which were involved in the *Lilium* molecular network created by GNPS, regaloside C is a glycerol glucoside, isolated from the bulbs of *Lilium* genus and its biological activities involve anti-inflammatory and cardiomyocyte protective activity (Qiu *et al.*, 2020). Some bioactive phenolic acids such as gallic acid and chlorogenic acid were found to be present in the *Lilium* molecular network. Gallic acid is well known bioactive metabolite, which is present in a variety of fruits and a number of plants, and showed several biological activities such as antioxidant, anti-inflammatory, hepatoprotective, antimicrobial, antidepressant, antiparkinson, antidiabetic, antimalarial, diuretic, cardioprotective, antiviral, antifungal, wound healing, anthelmintic, and anxiolytic (Kahkeshani *et al.*, 2019, Nayeem *et al.*, 2016). Chlorogenic acid also plays several biological and pharmacological roles, such as anti-microbial, antioxidant, anti-inflammatory, antipyretic, hepatoprotective, cardioprotective, neuroprotective, anti-obesity, antiviral, anti-hypertension and as a central nervous system (CNS) stimulator and modulator for many metabolic disorders such as diabetes, hepatic steatosis, cardiovascular disease and obesity (Naveed *et al.*, 2018).

Some phytosterol were also detected in the *Lilium* molecular network. A phytosterol, namely daucosterol, was among them and it possesses some biological activities, such antimicrobial, antiproliferative, neuroprotective, anti-cancer, and apoptotic effects by several *in vitro* assay results (Jiang *et al.*, 2015, Lee *et al.*, 2015a, Lee *et al.*, 2009, SultanaAfolayan, 2007, Wang *et al.*, 2016a, Zhao *et al.*, 2015). Another phytosterol, Stigmasterol glucoside, was also present in this network. Khatun et. al discussed the possible biological activity of plant sterols, and they assumed that glucose moiety of the sterol glucoside may prevent the esterification of cholesterol, and this might inhibit the entry of cholesterol into the blood vessel (Khatun *et al.*, 2012). Quercetin, a medicinally important flavonoid, and its derivatives, quercetrin and rutin, were identified in this molecular network. Many studies reported several beneficial health effects on quercetin such as antioxidant, antidiabetic, antiviral, anti-inflammatory, cardioprotective, neuroprotective, hepatoprotective and antimicrobial through various *in vitro* assays (Pejin *et al.*, 2015). Moreover, it's derivative, bioactive rutin, was previously reported to be present in the bulb extract of *L. lancifolium* (Jin *et al.*, 2012), and it had been identified in this *Lilium* molecular network. As rutin has wide range of bioactivities such as anticancer (Alonso-Castro *et al.*, 2013), antidiabetes (Niture *et al.*, 2014), antihypertensive (Olaleye *et al.*, 2014), anti-inflammation (Choi *et al.*, 2014) and antioxidant (Sikder *et al.*, 2014), the presence of this compound could contribute the antioxidant and antiglycation activity of *Lilium* species. Zhang et.al reported that quercetrin inhibited colorectal cancer cell growth and facilitated apoptosis, and might be potential candidate for colorectal cancer chemotherapy (Zhang *et al.*, 2017). Diosgenin or Spirost-5-en-3-ol, (3beta,25R), a well-known plant steroid sapogenin compound found in this species, also has numerous pharmacological potentials such as anti-diabetes, anticancer, immunomodulatory, estrogenic, cardiovascular protective, neuroprotective and skin protective effects (Chen *et al.*, 2015). Gibberellic acid GA3: plant growth hormone and vitamin B2 were also detected. A widely available tricyclic diterpenoid, isopimaric acid, which has interesting biological and pharmaceutical properties, such as antimicrobial, antiviral, antiallergenic, and anti-inflammatory activities, was also present in the *Lilium* network.

5. Conclusions

It could be concluded that *L. lancifolium* showed most promising activities among the studied species as its flower bud extract was active for antioxidant activity in four different *in vitro* assays, and its bulb extract was active for antidiabetic activity through glycation inhibition property. *L. lancifolium* may therefore be a promising plant species with potential therapeutic properties and is deserving of additional in-depth study for targeted isolation of compound of interest. Two MS2-based untargeted metabolomics approaches, MetaboAnalyst and GNPS, assist to explore the specialized metabolite profiles of selected *Lilium* species. To our knowledge, this study was the first to explore the specialized metabolite profile of *Lilium* species by these approaches. Using these methods, it was possible to recover the chemical information of 13 previously identified bioactive chemicals as well as some of the discriminant molecules that may be utilized as biomarkers for *Lilium* species. Many compounds present in the *Lilium* extracts could not confirm their identities through the public database searches. This could be for a number of reasons: either these metabolites were potentially new and noble compounds that required isolation and identification using various chromatographic techniques, or their spectra were already known but not included in this public database for spectral matching. It's also possible that commercially available spectral databases could identify more metabolites than the public database we used. Although the selected *Lilium* species belong to one genus, their chemical composition was mainly related to the choice of the plant parts. Since the metabolites have different functions at different stages of the plant growth, or depend on the demand of metabolism and protective system of the plant, the chemical composition of the specific parts of the plant might be different. It appeared that the major metabolites detected in this study seem to have potential therapeutic uses. However, further studies are still needed for the practical usage, as most studies are based on *in vitro* assays, and their effects on humans still need to go through clinical trials. From the current work of our research, metabolite profiling of selected *Lilium* species along with the bioactivity study will further pave the way for the targeted isolation of structurally or biologically noble bioactive compounds, and will provide evidence-based information of antioxidant and antidiabetic activity for further development and application of these *Lilium* species for therapeutic uses. Moreover, we expect that our study could be an invaluable proof to promote the

exploration and research on this and other edible and medicinal plants.

6. Supplementary Materials

TIC chromatograms of each sample can be available as supplementary materials. (Figure S1. TIC chromatogram of methanolic extract of ZDM1, Figure S2. TIC chromatogram of methanolic extract of ZDM2, Figure S3. TIC chromatogram of methanolic extract of ZDM3, Figure S4. TIC chromatogram of methanolic extract of ZDM4, Figure S5. TIC chromatogram of methanolic extract of ZDM5, Figure S6. TIC chromatogram of methanolic extract of ZDM6, Figure S7. TIC chromatogram of methanolic extract of ZDM7, Figure S8. TIC chromatogram of methanolic extract of ZDMF1, Figure S9. TIC chromatogram of methanolic extract of ZDMF2, Figure S10. TIC chromatogram of methanolic extract of ZDMF3, Figure S11. TIC chromatogram of methanolic extract of ZDMF4, Figure S12. TIC chromatogram of methanolic extract of ZDMF5, Figure S13. TIC chromatogram of methanolic extract of ZDMF6.)

Acknowledgments

This research work has been financially supported by Ministry of Science and Technology of the People's Republic of China through Talented Young Scientist Program (TYSP), which is greatly appreciated by the authors. The authors are also grateful to Beijing Agro-Biotechnology Research Center, Beijing Academy of Agriculture and Forestry Sciences, Beijing, China for supporting this research work.

Conflict of Interests

We declare that we have no conflict of interests.

References

Alonso-Castro AJ, Domínguez F, García-Carrancá A. 2013. Rutin exerts antitumor effects on nude mice bearing SW480 tumor. *Arch Med Res*. **44(5)**:346-351.

Boufridi A, Quinn RJ. 2016. Turning metabolomics into drug discovery. *J Braz Chem Soc*. **27(8)**:1334-1338.

Carr GG. Liliaceae. http://www.botany.hawaii.edu/faculty/carr/lili.htm.

Chambers MC, Maclean B, Burke R, Amodei D, Ruderman DL, Neumann S, Gatto L, Fischer B, Pratt B, Egertson J. 2012. A cross-platform toolkit for mass spectrometry and proteomics. *Nat Biotechnol*. **30(10)**:918.

Chauhan K, Sheth N, Ranpariya V, Parmar S. 2011. Anticonvulsant activity of solasodine isolated from *Solanum sisymbriifolium* fruits in rodents. *Pharm Biol*. **49(2)**:194-199.

Chen Y, Tang YM, Yu SL, Han YW, Kou JP, Liu BL, Yu BY. 2015. Advances in the pharmacological activities and mechanisms of diosgenin. *Chin J Nat Med*. 2015/08/01/**13(8)**:578-587.

Chi HJ, Kim HS, Lee SY. 1981. Iridoid-containing Korean Medicinal Plants (I). *Korean Journal of Pharmacognosy*. **12(1)**:19-22.

Chinchansure AA, Korwar AM, Kulkarni MJ, Joshi SP. 2015. Recent development of plant products with anti-glycation activity: a review. *RSC Adv*. **5(39)**:31113-31138.

Choi KS, Kundu JK, Chun KS, Na HK, Surh YJ. 2014. Rutin inhibits UVB radiation-induced expression of COX-2 and iNOS in hairless mouse skin: p38 MAP kinase and JNK as potential targets. *Arch Biochem Biophys*. **559**:38-45.

Chong J, Wishart DS, Xia J. 2019. Using metaboanalyst 4.0 for comprehensive and integrative metabolomics data analysis. *Curr Protoc Bioinformatics*. **68(1)**.

Choudhary MI, Abbas G, Ali S, Shuja S, Khalid N, Khan KM, Atta-ur-Rahman, Basha FZ. 2011. Substituted benzenediol Schiff bases as promising new anti-glycation agents. *J Enzyme Inhib Med Chem*. **26(1)**:98-103.

Demarque DP, Dusi RG, de Sousa FDM, Grossi SM, Silvério MRS, Lopes NP, Espindola LS. 2020. Mass spectrometry-based metabolomics approach in the isolation of bioactive natural products. *Sci Rep*. **10(1)**:1051-1051.

Du F, Jiang J, Jia H, Zhao Xy, Wang Wh, Gao Qk, Mao Wh, Wu Y, Zhang L, Grierson D. 2015. Selection of generally applicable SSR markers for evaluation of genetic diversity and identity in *Lilium*. *Biochem Syst Ecol*. **61**:278-285.

Dunlop PJ, Bignell CM, Brooker M, Brophy JJ, Hibbert DB. 1999. Use of gas chromatograms of essential leaf oils to compare eight taxa of genus *Angophora* (Myrtaceae): possible relationships to the genus *Eucalyptus*. *Biochem Syst Ecol*. **27(8)**:815-830.

Francis JA, Rumbeiha W, Nair MG. 2004. Constituents in Easter lily flowers with medicinal activity. *Life Sci*. **76(6)**:671-683.

Frank AM, Bandeira N, Shen Z, Tanner S, Briggs SP, Smith RD, Pevzner PA. 2008. Clustering millions of tandem mass spectra. *J Proteome Res*. **7(01)**:113-122.

Gao Y-D, Harris AJ, He X-J. 2015. Morphological and ecological divergence of *Lilium* and *Nomocharis* within the Hengduan Mountains and Qinghai-Tibetan Plateau may result from habitat specialization and hybridization. *BMC Evol Biol*. **15(1)**:147.

Guo H, Zhang Y, Niu L, Jiao H, Lei J, Luo J. 2014. Phenolic compounds and antioxidant property of petal extracts of six *Lilium* species native to China. *Asian Journal of Chemistry*. **26(18)**.

Hertog MG, Hollman PC, Van de Putte B. 1993. Content of potentially anticarcinogenic flavonoids of tea infusions, wines, and fruit juices. *J Agric Food Chem*. **41(8)**:1242-1246.

Ikinci N. 2010. Genetic diversity in two *Lilium* (Liliaceae) species from different regions of Greece based on a random amplified polymorphic DNA (RAPD) analysis. *J Med Plant Res*. **4(18)**:1888-1894.

Jiang Lh, Yuan Xl, Yang Ny, Ren L, Zhao Fm, Luo Bx, Bian Yy, Xu Jy, Lu Dx, Zheng Yy. 2015. Daucosterol protects neurons against oxygen–glucose deprivation/

reperfusion-mediated injury by activating IGF1 signaling pathway. *J Steroid Biochem Mol Biol*. **152**:45-52.

Jin L, Zhang Y, Yan L, Guo Y, Niu L. 2012. Phenolic compounds and antioxidant activity of bulb extracts of six Lilium species native to China. *Molecules*. Aug 3**17(8)**:9361-9378.

Kadhim NJ, Al-Rekaby LS, Redha AA, Chappell J. Chemical composition and antioxidant capacity of eggplant parts during vegetative and flowering stage. Proceedings of the J Phys Conf Ser; 2019: IOP Publishing.

Kaewnarin K, Niamsup H, Shank L, Rakariyatham N. 2014. Antioxidant and antiglycation activities of some edible and medicinal plants. *Chiang Mai Journal of Science*. **41(1)**:105-116.

Kahkeshani N, Farzaei F, Fotouhi M, Alavi SS, Bahramsoltani R, Naseri R, Momtaz S, Abbasabadi Z, Rahimi R, Farzaei MH, et al. 2019. Pharmacological effects of gallic acid in health and diseases: a mechanistic review. *Iran J Basic Med Sci*. **22(3)**:225-237.

Khan MS, Gao J, Zhang M, Chen X, Du Y, Yang F, Xue J, Zhang X. 2020. Isolation and characterization of plant growth-promoting endophytic bacteria Bacillus stratosphericus LW-03 from Lilium wardii. *3 Biotech*. **10(7)**:1-15.

Khatun M, Billah M, Quader MA. 2012. Sterols and sterol glucoside from *Phyllanthus* species. *Dhaka University Journal of Science*. **60(1)**:5-10.

Kim YM, Lee J, Park SH, Lee C, Lee JW, Lee D, Kim N, Lee D, Kim HY, Lee CH. 2012. LC–MS-based chemotaxonomic classification of wild-type *Lespedeza sp.* and its correlation with genotype. *Plant Cell Rep*. **31(11)**:2085-2097.

Kuda T, Tsunekawa M, Hishi T, Araki Y. 2005. Antioxidant properties of dried `kayamo-nori', a brown alga *Scytosiphon lomentaria* (Scytosiphonales, Phaeophyceae). *Food Chem*. 2005/03/01/**89(4)**:617-622.

Kumar P, Sharma B, Bakshi N. 2009. Biological activity of alkaloids from *Solanum dulcamara* L. *Nat Prod Res*. **23(8)**:719-723.

Lecanu L, Hashim A, McCourty A, Giscos-Douriez I, Dinca I, Yao W, Vicini S, Szabo G, Erdélyi F, Greeson J. 2011. The naturally occurring steroid solasodine induces neurogenesis *in vitro* and *in vivo*. *Neuroscience*. **183**:251-264.

Lee J, Weon JB, Yun BR, Eom MR, Ma CJ. 2015a. Simultaneous determination three phytosterol compounds, campesterol, stigmasterol and daucosterol in *Artemisia apiacea* by high performance liquid chromatography-diode array ultraviolet/visible detector. *Pharmacogn Mag*. **11(42)**:297.

Lee JY, Lee JH, Park JH, Kim SY, Choi JY, Lee SH, Kim YS, Kang SS, Jang EC, Han Y. 2009. Liquiritigenin, a licorice flavonoid, helps mice resist disseminated candidiasis due to *Candida albicans* by Th1 immune response, whereas liquiritin, its glycoside form, does not. *Int Immunopharmacol*. **9(5)**:632-638.

Lee S, Oh DG, Lee S, Kim G, Lee J, Son Y, Bae CH, Yeo J, Lee C. 2015b. Chemotaxonomic metabolite profiling of 62 indigenous plant species and its correlation with bioactivities. *Molecules*. **20(11)**:19719-19734.

Lee SK, Mbwambo Z, Chung H, Luyengi L, Gamez E, Mehta R, Kinghorn A, Pezzuto J. 1998. Evaluation of the antioxidant potential of natural products. *Comb Chem High Throughput Screen*. **1(1)**:35-46.

Li H. 2007. Study on the nutrients, bioactive materials and cultivation characteristics of *Lilium lancifolium* Thunb.PhD dissertation, Northwest University of Science and Technology.

Ma C, Xiao Sy, Li Zg, Wang W, Du Lj. 2007. Characterization of active phenolic components in the ethanolic extract of *Ananas comosus* L. leaves using high-performance liquid chromatography with diode array detection and tandem mass spectrometry. *J Chromatogr A*. **1165(1-2)**:39-44.

Moe TS, Win HH, Hlaing TT, Lwin WW, Htet ZM, Mya KM. 2018. Evaluation of *in vitro* antioxidant, antiglycation and antimicrobial potential of indigenous Myanmar medicinal plants. *J Integr Med*. **16(5)**:358-366.

Munafo Jr JP, Gianfagna TJ. 2015. Chemistry and biological activity of steroidal glycosides from the *Lilium* genus. *Nat Prod Res*. **32(3)**:454-477.

Naveed M, Hejazi V, Abbas M, Kamboh AA, Khan GJ, Shumzaid M, Ahmad F, Babazadeh D, FangFang X, Modarresi-Ghazani F, et al. 2018. Chlorogenic acid (CGA): A pharmacological review and call for further research. *Biomed Pharmacother*. 2018/01/01/**97**:67-74.

Nayeem N, Asdaq S, Salem H, AHEl-Alfqy S. 2016. Gallic acid: a promising lead molecule for drug development. *Journal of Applied Pharmacy*. **8(2)**:1-4.

Niño J, Correa Y, Mosquera O. 2009. Biological activities of steroidal alkaloids isolated from *Solanum leucocarpum*. *Pharmaceutical Biology*. **47(3)**:255-259.

Niture NT, Ansari AA, Naik SR. 2014. Anti-hyperglycemic activity of rutin in streptozotocin-induced diabetic rats: an effect mediated through cytokines, antioxidants and lipid biomarkers. *Indian J Exp Biol*.

Olaleye M, Crown O, Akinmoladun A, Akindahunsi A. 2014. Rutin and quercetin show greater efficacy than nifedipin in ameliorating hemodynamic, redox, and metabolite imbalances in sodium chloride-induced hypertensive rats. *Hum Exp Toxicol*. **33(6)**:602-608.

Patel Rajesh M, Patel Natvar J. 2011. *In vitro* antioxidant activity of coumarin compounds by DPPH, super oxide and nitric oxide free radical scavenging methods. *Journal of Advanced Pharmacy Education and Research*. **1**:52-68.

Pejin B, Ciric A, Markovic JD, Glamoclija J, Nikolic M, Stanimirovic B, Sokovic M. 2015. Quercetin potently reduces biofilm formation of the strain *Pseudomonas aeruginosa* PAO1 *in vitro*. *Current pharmaceutical biotechnology*. **16(8)**:733-737.

Perera P, Ekanayaka S, Ranaweera K. 2013. *In vitro* study on antiglycation activity, antioxidant activity and phenolic content of *Osbeckia octandra* L. leaf decoction. *J Pharmacogn Phytochem*. **2(4)**.

Pluskal T, Castillo S, Villar-Briones A, Orešič M. 2010. MZmine 2: modular framework for processing, visualizing, and analyzing mass spectrometry-based molecular profile data. *BMC Bioinformatics*. **11(1)**:395.

Qiu K, Li Z, Li C, Huang H, Zhu W. 2020. Protective effect of total glycosides from lily on H2O2-induced H9C2 cells mitochondrial damage and characterization of the chemical profiles by UHPLC-LTQ-Orbitrap-MSn. *J Funct Foods*. 2020/08/01/**71**:104036.

Rahbar S, Figarola JL. 2003. Novel inhibitors of advanced glycation endproducts. *Arch Biochem Biophys*. **419(1)**:63-79.

Raterink R-J, Lindenburg PW, Vreeken RJ, Ramautar R, Hankemeier T. 2014. Recent developments in sample-pretreatment techniques for mass spectrometry-based metabolomics. *Trends Analyt Chem*. **61**:157-167.

Rivière C, Pawlus AD, Mérillon J-M. 2012. Natural stilbenoids: distribution in the plant kingdom and chemotaxonomic interest in *Vitaceae*. *Nat Prod Res*. **29(11)**:1317-1333.

Royal Botanic Gardens K, Springer. 1889. Lily Flowers and Bulbs Used as Food. www.jstor.org/stable/4113224.

Salehi P, Asghari B, Esmaeili MA, Dehghan H, Ghazi I. 2013. α-Glucosidase and α-amylase inhibitory effect and antioxidant activity of ten plant extracts traditionally used in Iran for diabetes. *J Med Plant Res*. **7(6)**:257-266.

Sharma T, Airao V, Panara N, Vaishnav D, Ranpariya V, Sheth N, Parmar S. 2014. Solasodine protects rat brain against ischemia/reperfusion injury through its antioxidant activity. *Eur J Pharmacol*. **725**:40-46.

Shimomura H, Sashida Y, Mimaki Y, Minegishi Y. 1987. Jatropham glucoside from the bulbs of *Lilium hansonii*. *Phytochemistry*. **26(2)**:582-583.

Sikder K, Kesh SB, Das N, Manna K, Dey S. 2014. The high antioxidative power of quercetin (aglycone flavonoid) and its glycone (rutin) avert high cholesterol diet induced hepatotoxicity and inflammation in Swiss albino mice. *Food Funct*. **5(6)**:1294-1303.

Sultana N, Afolayan A. 2007. A novel daucosterol derivative and antibacterial activity of compounds from *Arctotis arctotoides*. *Natural product research*. **21(10)**:889-896.

Sumner LW, Amberg A, Barrett D, Beale MH, Beger R, Daykin CA, Fan TWM, Fiehn O, Goodacre R, Griffin JL, et al. 2007. Proposed minimum reporting standards for chemical analysis Chemical Analysis Working Group (CAWG) Metabolomics Standards Initiative (MSI). *Metabolomics*. **3(3)**:211-221.

Tang W, Munafo Jr JP, Palatini K, Esposito D, Huang MT, Komarnytsky S, Ho CT, Gianfagna TJ. 2015. Hepatoprotective activity of easter lily (*Lilium longiflorum* Thunb.) bulb extracts. *J Agric Food Chem*. **63(44)**:9722-9728.

Tang Y, Liu X, Gituru RW, Chen L. 2010. Callus induction and plant regeneration from *in vitro* cultured leaves, petioles and scales of *Lilium leucanthum* (Baker) Baker. *Biotechnol Biotechnol Equip*. **24(4)**:2071-2076.

Uhlig S, Hussain F, Wisløff H. 2014. Bioassay-guided fractionation of extracts from Easter lily (*Lilium longiflorum*) flowers reveals unprecedented structural variability of steroidal glycoalkaloids. *Toxicon*. **92**:42-49.

Viscosi V, Cardini A. 2011. Leaf morphology, taxonomy and geometric morphometrics: a simplified protocol for beginners. *PLoS One*. **6(10)**:e25630.

Wang GQ, Gu JF, Gao YC, Dai YJ. 2016a. Daucosterol inhibits colon cancer growth by inducing apoptosis, inhibiting cell migration and invasion and targeting caspase signalling pathway. *Bangladesh J Pharmacol*. **11(2)**:395-401.

Wang M, Carver JJ, Phelan VV, Sanchez LM, Garg N, Peng Y, Nguyen DD, Watrous J, Kapono CA, Luzzatto-Knaan T. 2016b. Sharing and community curation of mass spectrometry data with Global Natural Products Social Molecular Networking. *Nat Biotechnol*. **34(8)**:828.

Wang M, Jarmusch AK, Vargas F, Aksenov AA, Gauglitz JM, Weldon K, Petras D, da Silva R, Quinn R, Melnik AV, et al. 2020. Mass spectrometry searches using MASST. *Nat Biotechnol*. 2020/01/01**38(1)**:23-26.

Waterhouse AL. 2002. Determination of total phenolics. *CPFAC*. **6(1)**:I1. 1.1-I1. 1.8.

Xia J, Wishart DS. 2016. Using MetaboAnalyst 3.0 for comprehensive metabolomics data analysis. *Curr Protoc Bioinformatics*. Sep 7**55**:14.10.11-14.10.91.

Zhang X, Teng G, Zhang J. 2018. Ethanol/salt aqueous two-phase system based ultrasonically assisted extraction of polysaccharides from *Lilium davidiivar. unicolor* Salisb: physicochemical characterization and antiglycation properties. *J Mol Liq*. **256**:497-506.

Zhang Y, Guo Y, Wang M, Dong H, Zhang J, Zhang L. 2017. Quercetrin from *Toona sinensis* leaves induces cell cycle arrest and apoptosis via enhancement of oxidative stress in human colorectal cancer SW620 cells. *Oncol Rep*. **38(6)**:3319-3326.

Zhao C, She T, Wang L, Su Y, Qu L, Gao Y, Xu S, Cai S, Shou C. 2015. Daucosterol inhibits cancer cell proliferation by inducing autophagy through reactive oxygen species-dependent manner. *Life Sci*. **137**:37-43.

Zheng SH, Li YK, Ren WG, Huang LF. 2014. Molecular identification in genus of *Lilium* based on DNA barcoding. *Acta pharmaceutica Sinica*. **49(12)**:1730-1738.

Zhou ZL, Feng ZC, Fu CY, Zhang HL, Xia JM. 2012. Steroidal and phenolic glycosides from the bulbs of *Lilium pumilum* DC and their potential Na+/K+ ATPase inhibitory activity. *Molecules*. **17(9)**:10494-10502.

JJBS

Volume 15, Number 4,December 2022
ISSN 1995-6673
Pages 593 – 601
https://doi.org/10.54319/jjbs/150407

Jordan Journal of Biological Sciences

Molecular Analysis of Human Pegivirus (GBV-C) Infecting Hemodialysis Patients in Baghdad, Iraq: A Single Center Study

Hayder Ahmed Kadhim (MSc)[1], Arwa Mujahid Al-Shuwaikh (PhD)[2,*], and Ismail Ibrahim Latif (MBChB, PhD)[3]

[1]College of Nursing, Al-Bayan University, [2]Microbiology Department, College of Medicine, Al-Nahrain University, [3]Microbiology Department, College of Medicine, University of Diyala,.

Received: June 28, 2021; Revised: January 7, 2022; Accepted: January 31, 2022

Abstract

Patients undergoing hemodialysis are at an increased risk of contracting viral infections. The aims of this study were to determine the prevalence of GBV-C infections and to evaluate their clinical importance in hemodialysis patients. This one center cross-section study was carried out for 100 patients attending Al-Kindy center for hemodialysis in Baghdad, Iraq. Serum samples were tested by reverse transcription nested polymerase chain reaction (nested RT-PCR) for GBV-C detection and for liver function evaluation. GBV-C RNA was detected in 35% of hemodialysis patients, 17/48 (35.4%) in HCV positive patients, while 18/52 (34.6%) without HCV. GBV-C infection had no significant association with HCV status among hemodialysis patients, and also no significant association with age, sex and liver enzyme. Patients who have GBV-C have a much longer hemodialysis period than those who do not have GBV-C. Furthermore, phylogenetic analysis showed that ten GBV-C local isolates were related to GBV-C genotype 2; however, two pairs of the local isolates were completely identical (100%), which could be an indicator for nosocomial transmission among hemodialysis unit. In conclusion, GBV-C did not seem to contribute to increasing the level of liver enzyme or the severity of HCV infection in hemodialysis patients, and so mandatory screening for GBV-C is not recommended for hemodialysis patients at this time.

Keyword: HPgV, GBV-C, ALT, AST, hemodialysis, one step nested RT-PCR, phylogenic tree.

1. Introduction

Patients undergoing hemodialysis (HD) therapy are at an increased risk of contracting viral infections. This is due to their underlying impaired cellular immunity, which makes them more susceptible to infection. Furthermore, the HD process necessitates prolonged blood exposure to infectious materials via extracorporeal circulation, which increases the likelihood of nosocomial infection exposure (Bernieh, 2015). Patients undergoing long-term hemodialysis are particularly vulnerable to parenterally transmitted agents, making them an important population for studying the clinical and epidemiological implications of newly discovered agents (Forns, 1999). Hepatotropic or other hepatitis-associated viruses, such as hepatitis B virus (HBV), hepatitis C virus (HCV), torque teno virus (TTV), SEN Virus (SENV), and hepatitis G virus (HGV) are responsible for some of the most common viral infections in hemodialysis patients (Forns, 1999; Ozdarendeli *et al.*, 2005; Abd El-Hady *et al.*, 2006; Abdullah *et al.*, 2012; Abdullah *et al.*, 2014; Khudair *et al.*, 2019).

Human pegivirus (HPgV) or GB virus C (GBV-C), previously known as hepatitis G virus (HGV), was discovered in 1995 and belongs to the Flaviviridae family. It is an enveloped, icosahedral, single-stranded RNA positive-sense virus (9.4 kb) (Ibrahim and Hamdani 2015; Rinonce *et al.*, 2017). GBV-C is classified into seven genotypes with unique distribution depending on the geographic area. Genotypes 1 and 5 are mainly found in Africa, genotype 3 is more prevalent in Asian, in European and North American populations, genotype 4 in the Philippines and Southeast Asia, genotype 6 in China and Japan and 7 is found solely in China. Sometimes, multiple GBV-C genotypes that display a propensity to recombine may infect the same person (Slavov *et al.*, 2019; dos Santos Bezerra *et al.*, 2020). Vertical, parental and sexual transmission of GBV-C have been reported (Sathar *et al.*, 2000). The frequency and occurrence of the GBV-C infection are higher in risk groups that are vulnerable to sexually transmitted or blood-borne infections (Scallan *et al.*, 1998; Christensen *et al.*, 2003).

The clinical significance of GBV-C infection in humans has yet to be determined, and there is a paucity of data in HD patients. The prevalence of GBV-C infection among patients with end-stage renal disease and chronic HD was ranged from 6% to 44% in different countries (Ozdarendeli *et al.*, 2005; Bernieh, 2015). However, none of the studies found that GBV-C infection causes any increase in liver enzymes or hepatic failure, although co-infection with other hepatitis viruses may increase morbidity and mortality rates (Eslamifar *et al.*, 2007;

* Corresponding author. e-mail: arwa_alshwaikh_2004@yahoo.com;arwa.mujahid@gmail.com.

** **List of abbreviation**: HPgV= human pegivirus, GBV-C= GB virus type C, ALT= alanine transaminase, AST= aspartate aminotransferase, HD= hemodialysis.

Dadmanesh *et al.*, 2015). The aim of the present study was to determine the prevalence, risk factors and clinical implications of GBV-C infection in hemodialysis patients and to evaluate any possible association with HCV.

2. Materials and Methods

2.1. Study population

The study covered the period from December 2020 to February 2021.This cross-sectional study was conducted on 100 hemodialysis patients in one center at Al-Kindy hospital in Baghdad, Iraq. The participants in this study comprised two groups: those who had HCV antibodies and those who did not.

2.2. Specimen collection

Prior to beginning hemodialysis sessions, 5 ml blood sample was collected from patients as part of the hospital routine work, and sera were isolated from left over blood samples. Blood samples were allowed to clot at room temperature for 20 minutes before being centrifuged at 3,000 rpm for 10 minutes within 2 hours of blood sampling. Aliquots of each sample were made and stored at -20ºC and -70ºC until they were used for biochemical tests (ALT and AST) and reverse-transcriptase nested PCR, respectively. This study was approved by College of Medicine, University Diyala and Ministry of Health (No. 86229 on 8 December 2020).

2.3. RNA Extraction

The serum samples were allowed to thaw at room temperature. For the isolation and purification of RNA, the Viral Nucleic Acid Extraction Kit II (Cat. #VR00, Geneaid, Taiwan) was used. The procedure was carried out following the manufacturer's instructions.

2.4. GBV-C virus RNA Amplification

RNA was converted to cDNA and amplified in the same tube using the SuperScript™ III One-Step RT-PCR System with Platinum™ Taq DNA Polymerase (Invitrogen, USA). The RT-PCR reaction mixture (25 µL) was prepared using 5 µL of RNA, 1 µl of each of G58 (outer forward primer) and G75 (outer reverse primer) (Table 1), 1 µl of SuperScript™ III RT/Platinum™ Taq Mix, 12.5 µl of the master mix and 4.5 µl nuclease-free water. RNA was transformed to cDNA at 50°C for 30 minutes and then RNA/cDNA hybrid was denatured during the 2-minute incubation at 94°C, followed by 30 cycles of denaturation at 94˚C for 30-second, annealing at 55˚C for 30-second, and extension at 72˚C for 30-second, and final extension for 2-minute at 72˚C. For the second-round reaction, RT-PCR products were further amplified using nested PCR with primers specific for 5-untranslated region (G134 and G131). The reaction mixture (25 µL) was prepared using 5 µL of amplified cDNA from the first PCR run, 1 µl of each of G134 (inner forward primer) and G131 (inner reverse primer), 12.5 µl of the master mix and 5.5 µl nuclease-free water. The cycling conditions for the second-round reaction were performed as following (94˚C for 2-minute, followed by 40 cycles, denaturation at 94˚C for 30-second, annealing at 55˚C for 30-second, and extension at 72˚C for 30-second, and final extension for 2-minute at 72˚C. The PCR products (208 bp) were detected in 3% agarose gel (Figure 1) after electrophoresis for 1 hour at 80 volts.

Table 1. The primers used in nested RT-PCR (Egawa *et al.*, 1996; AbuOdeh *et al.*, 2015).

Primer Name	Product size (bp)	Primer Sequence (5' to 3')
G58 (outer; forward)	242	CAGGGTTGGTAGGTCGTAAATCC
G75 (outer; reverse)	242	CCTATTGGTCAAGAGAGACAT
G134 (inner; forward)	208	GGTCAYCYTGGTAGCCACTATAGG
G131 (inner; reverse)	208	AAGAGAGACATTGWAGGGCGACGT

2.5. Quality control

Samples that previously tested positive were used as positive control samples; they were further confirmed by sequencing, while the negative control consisted of the reagents used to prepare the PCR amplification mixture without GBV-C RNA.

2.6. Sequencing and phylogenetic analysis

Ten PCR products of second-round PCR of GBV-C and G134 (inner; forward) primer were sent for Sanger sequencing by Microgen Corporation (Korea). The results were analyzed using Bio Edit v7.2.5. The phylogenetic relationships between the ten GBV-C samples were reconstructed in the form of a Neighbor-Joining tree by Mega Xv.10.2.5+NCBI and based on the Jukes-Cantor (JC) model. Genotypes of GBV-C were provisionally estimated from the tree based on the clustering with the reference GBV-C isolates from GenBank (GenBank acc. AB013206.1, AF095693.1, GQ227348.1, GQ380413.1, Y18156.1, JX494215.1, AY269959.1, AF075218.1, AF058742.1, AY196904.1, AF078055.1, AJ000584.1, AF172512.1, AB033840.1, AB022539.1, JF832375.1, U86113.1, AF073743.1, AF015876.1). Our isolates were deposited at GenBank under the acc. MW962987.1, MW962988.1, MW962989.1, MW962990.1, MW962991.1, MW962992.1, MW962993.1, MW962994.1, MW962995.1 and MW962996.1.

2.7. Statistical Analysis

All data were analyzed using the statistical package for social sciences (SPSS), version 26. Data were expressed as means ± S.D. The chi-squared test ($\chi 2$) was used to determine the frequency difference, and Student's t-test was used to evaluate the mean differences. ANOVA test was used to compare the means of more than two independent groups. The level of significance in all cases was set at a two-tailed ($p<0.05$).

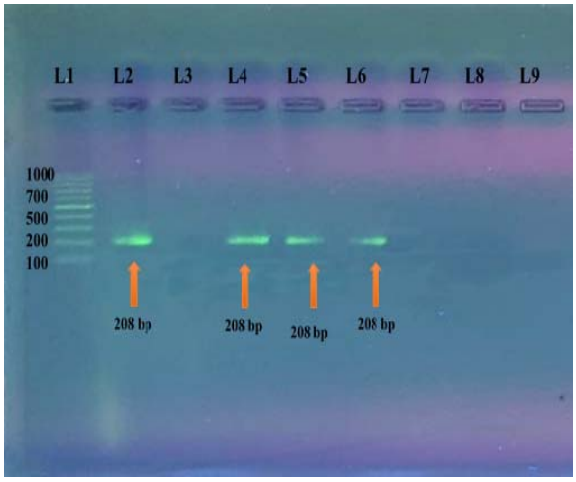

Figure 1. Gel electrophoresis of GBV-C second round PCR product using 3% agarose in TBE buffer, L1 was (100-1000 bp) ladder. L2, L4, L5, and L6 were positive samples (208 bp), while L3, L7, L8, and L9 were negative samples.

3. Result

This study included 100 hemodialysis patients with a mean age of 51.17 years (±15.69 SD). Forty-eight (48) were HCV positive, while 52 were HCV negative, with mean ages of 49.9 years (±15.097 SD) and 51.6 years (±16.635 SD), respectively. Males made up 60% of the population, while females made up 40%. GBV-C was found in 35 out 100 (35%) hemodialysis patients, 17 out 48 (35.4%) HCV positive patients, and 18 out 52 (34.6%) HCV negative patients. There was no significant association (p> 0.05) between GBV-C infection and HCV status among the hemodialysis patients (Table 2). In addition, there was no statistically significant difference (p> 0.05) between GBV-C positive and GBV-C negative individuals in terms of liver enzyme levels (Table 3).

Table 2. Occurrence of GBV-C among hemodialysis patients with respect to HCV status.

GBV-C RNA Status*	HCV status		Total hemodialysis patients (n=100)	Statistic
	HCV Positive (n=48)	HCV Negative (n=52)		
GBV-C Positive	17 (35.4%)	18 (34.6%)	35 (35%)	
GBV-C Negative	31 (64.6%)	34 (65.4%)	65 (65%)	p= *0.933*
Total	48 (100%)	52 (100%)	100 (100%)	

*Using Chi-square test at 0.05 level

Table 3. Serum ALT and AST level (U/L) in relation to GBV-C status in hemodialysis patients (n=100).

Biochemical tests*	GBV-C		Statistic
	Positive (n=35)	Negative (n=65)	
ALT (U/l)**	5.460 ± 5.093	6.605 ± 6.101	p= 0.619
AST (U/l)**	7.111±5.437	8.875 ±7.296	p= 0.213

**Normal values: AST 15-37 U/L, ALT 12-78 U/L

*Using T- test at 0.05 level.

Concerning the demographic data, clinical characteristics and risk factors of participants, there is no significant statistical difference (p>0.05) between the GBV-C positive and negative individuals. However, the duration of hemodialysis is significantly (p<0.05) longer in GBV-C positive patients than in GBV-C negative patients (Table 4).

For GBV-C genotyping, ten GBV-C positive samples were successfully sequenced using the 5'-untranslated region (5'-UTR). The sequences of the current study were compared with GBV-C reference sequences from the GenBank database. The sequences of the local GBV-C isolates were 96-99% similar to that of the reference GBV-C genotype 2 and clustered in a common group with the sequences of GBV-C isolated from Bolivia, United Kingdom, Brazil, Canada, Belgium, Venezuela, France, China, Hong Kong, USA, Singapore, Germany, South Africa, Yamagata, Japan, Colombia, Sweden, Greece and Italy (Table 5)

Nucleotide sequence alignment showed 99% similarity between local isolate sequences in current study with Bolivian isolate GenBank Accession number (AB013206.1). However, these local isolates (GB virus C IRAQ:3, 4, 5, 14, 19, 37, 46, 60, 62 and 76) showed some variations summarized in the table (6).

Phylogenetic trees of GBV-C (5-UTR) detected in hemodialysis patients were constructed using Neighbor joining (NJ) tree based on the Jukes-Cantor (JC) model and evaluated using the interior branch test method with (MEGA version 10.2.5). All local GBV-C (5-UTR) sequences were grouped in the same cluster with 99% similarity (Figure 2). These sequences belong to genotype 2 and were clustered in a common group (Figure 3) with GBV-C sequences from: Bolivia (AB013206.1), United Kingdom (AF095693.1) and Belgium (Y18156.1) with 99%, 98%, 97% similarity, respectively.

Table 4. Comparison of clinical characteristics and risk factors according to GBV-C status in hemodialysis patients (n=100).

Risk factors*		GBV-C		Total	Statistic
		Positive	Negative		
Age (mean±SD)**		50.94±13.70	51.29±16.77	51.17±15.69	p=0.198
Sex	Female	14 (39.6%)	26 (40.4%)	40 (40%)	p=1.000
	Male	21(60.4%)	39 (59.6%)	60 (60%)	
Diabetes Mellitus	Presence	14(40%)	19(29.2%)	33 (33%)	p=0.275
	Absence	21(60%)	46(70.8%)	67 (67%)	
	Total	35(100%)	65(100%)	100(100%)	
Hypertension	Presence	26(74.29%)	52 (80%)	78 (78%)	p=0.629
	Absence	9 (25.71%)	13 (20%)	22 (22%)	
	Total	35 (100%)	65 (100%)	100(100%)	
History of blood transfusion	Presence	30(85.71%)	47 (72.3%)	77 (77%)	p=0.499
	Absence	5 (14.29%)	18 (27.7%)	23 (23%)	
	Total	35 (100%)	65 (100%)	100(100%)	
History of kidney transplantation	Presence	1 (2.85%)	1 (1.56%)	2 (2%)	p=0.653
	Absence	34(97.15%)	64(98.44%)	98 (98%)	
	Total	35 (100%)	65 (100%)	100(100%)	
History of surgery	Presence	21 (60%)	37(56.92%)	58 (58%)	p=0.504
	Absence	14 (40%)	28(43.08%)	42 (42%)	
	Total	35 (100%)	65 (100%)	100(100%)	
History of multiple sexual partners	Presence	30(85.71%)	57(87.69%)	87 (87%)	p=0.738
	Absence	5(14.29%)	8(12.31%)	13 (13%)	
	Total	35 (100%)	65 (100%)	100(100%)	
History of Tattooing	Presence	4 (11.42%)	7 (10.76%)	11 (11%)	p=0.920
	Absence	31(88.58%)	58(89.24%)	89 (89%)	
	Total	35 (100%)	65 (100%)	100(100%)	
Hemodialysis duration	< 1 y	6(17.14%)	29(82.86%)	35 (35%)	p=0.02
	1-2 y	8 (36.36%)	14(63.64%)	22 (22%)	
	2-4 y	9 (60%)	6 (40%)	15 (15%)	
	> 5 y	12 (42.85%)	16 (57.15%)	28 (28%)	
No. of blood transfusions	0-2 time	21(32.3%)	44 (67.7%)	65 (65%)	p=0.71
	2-4 time	10 (41.66%)	14(58.34%)	24 (24%)	
	> 5 time	4 (36.36%)	7 (63.64%)	11 (11%)	

*Using Chi-square test.

**Using T-test at 0.05 level, S.D: Standard deviation

Table 5. The similarity of the local GBV-C sequence with that of isolates from different countries

No.	Accession	Country	Similarity
1	ID: AB013206.1	Bolivia	99%
2	ID: AF095693.1	United Kingdom	98%
3	ID: GQ227348.1	Brazil	98%
4	ID: GQ380413.1	Canada	98%
5	ID: Y18156.1	BELGIUM	97%
6	ID: JX494215.1	Venezuela	97%
7	ID: AY269959.1	France	97%
8	ID: AF075218.1	China	97%
9	ID: AF058742.1	Hong Kong	97%
10	ID: AY196904.1	USA	97%
11	ID: AF078055.1	Singapore	97%
12	ID: AJ000584.1	GERMANY	97%
13	ID: AF172512.1	South Africa	96%
14	ID: AB033840.1	Yamagata	96%
15	ID: AB022539.1	Japan	96%
16	ID: JF832375.1	Colombia	96%
17	ID: U86113.1	Sweden	96%
18	ID: AF073743.1	Greece	96%
19	ID: AF015876.1	Italy	96%

Table 6. Local GBV-C gene 5'UTR point mutation comparing with Bolivian isolate (AB013206.1).

No	Local isolate	Type of substitution	Location	Nucleotide	Similarity
1	1-3 GB virus C IRAQ	Transition	160	C\T	99%
		Transition	198	G\A	
2	2-4 GB virus C IRAQ	Transition	144	A\G	99%
		Transition	198	G\A	
3	3-5 GB virus C IRAQ	Transition	144	A\G	99%
		Transition	198	G\A	
4	4-14 GB virus C IRAQ	Transvertion	72	C\A	98%
		Transition	160	C\T	
		Transvertion	184	T\A	
		Transition	198	G\A	
5	5-19 GB virus C IRAQ	Transition	144	A\G	98%
		Transvertion	152	A\T	
		Transvertion	184	T\A	
		Transition	198	G\A	
6	6-37 GB virus C IRAQ	Transition	49	C\T	99%
		Transition	71	C\T	
		Transition	144	A\G	
7	7-46 GB virus C IRAQ	Transvertion	152	A\T	98%
		Transvertion	184	T\A	
		Transition	198	G\A	
8	8-60 GB virus C IRAQ	Transition	49	C\T	98%
		Transvertion	61	C\A	
		Transition	164	C\T	
		Transition	198	G\A	
9	9-62 GB virus C IRAQ	Transvertion	45	G\C	99%
		Transition	160	C\T	
		Transition	198	G\A	
10	10-76 GB virus C IRAQ	Transition	160	C\T	99%
		Transvertion	184	T\A	
		Transition	198	G\A	

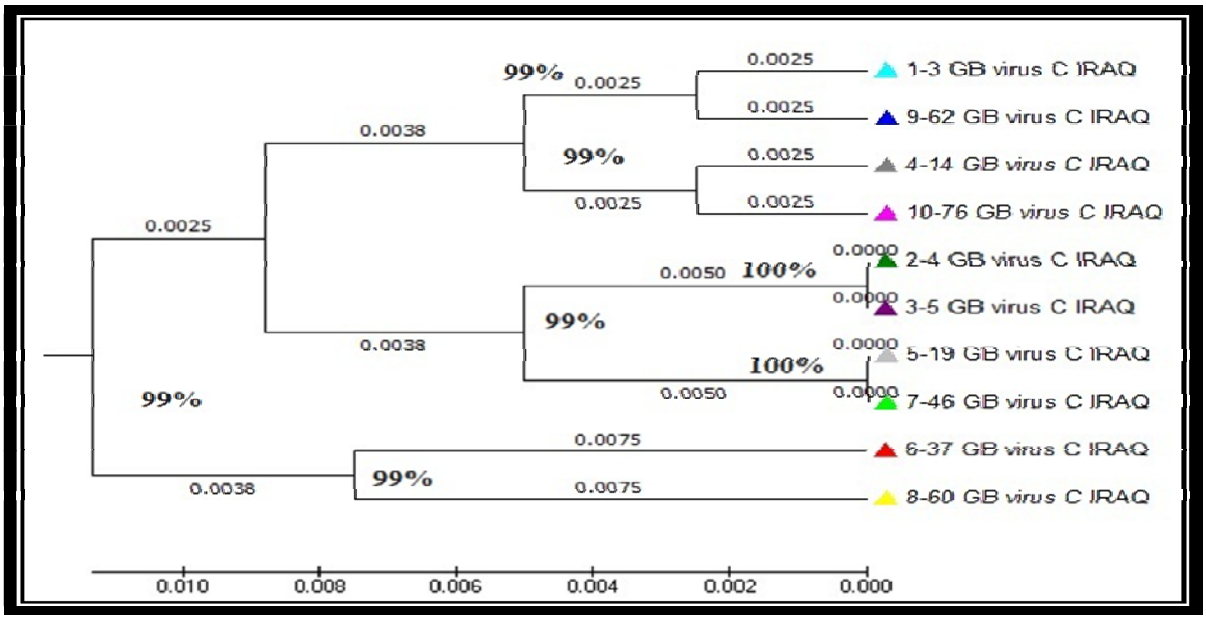

Figure 2. Phylogenetic trees for 5'UTR of 10 local isolates of GBV-C constructed by the neighbor joining method.

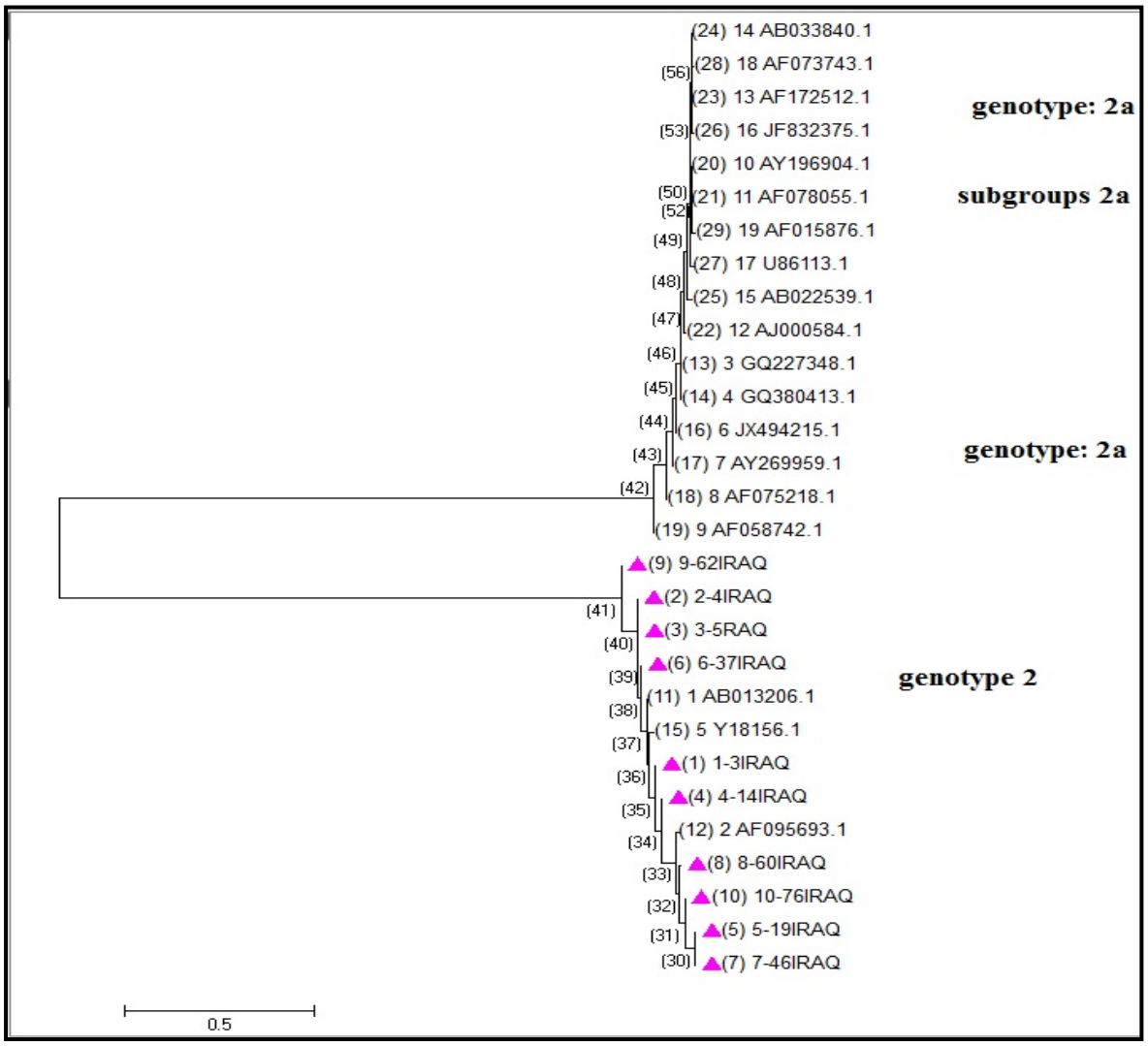

Figure 3. Phylogenetic trees for 5'UTR of 10 local isolates of GBV-C and 19 reference isolates constructed by the neighbor joining method. Local isolates were flagged with pink colored triangle. The scale bar under the tree indicates 0.5 nucleotide substitutions per site.

4. Discussion

In the current study, GBV-C was found in 35 (35%) of hemodialysis patients, 17 (35.4%) of whom were HCV positive and 18 (34.6%) were HCV negative, Table (2). This prevalence is within the range reported in other countries including Indonesia (55%) (Handajani *et al.*, 2000), Germany (50%) (Sanchooli *et al.*, 2018), Turkey (25%) (Akcali *et al.*, 2006), Italy (24%) (De Filippi *et al.*, 2001), Iran (10%) (Sanchooli *et al.*, 2018), and Pakistan (3.6%) (Qureshi *et al.*, 2020). Variable rates of blood transfusion, surgical procedure and adherence to universal precautions may explain these disparities in GBV-C prevalence. The variation in GBV-C prevalence around the world could be attributed to variation in amplified target region and primers used (Sanchooli *et al.* 2018). In Iraq, the rate of GBV-C infection among healthy people was 0%, hemodialysis was 20.3%, and thalassemia was 14.8% (Hasan *et al.*, 2018). Another study found that HGV infection was detected in 25% of blood donors, 30% of chronic hepatitis C and 25% of chronic hepatitis B (Al-Obeidy *et al.,* 2010).

According to Table (3), there was no significant association between the levels of ALT and AST in hemodialysis patients with or without GBV-C infection, indicating that GBV-C infection did not cause more serious liver damage in those patients and that GBV-C did not appear to influence liver enzyme levels. Salama and Selim (2009), on the other hand, showed a significant difference in ALT and AST values between GBV-C positive and negative patients. There have been many debates about the pathogenicity of GBV-C since it was identified; several studies have shown that GBV-C can cause acute, chronic and even fulminant hepatitis (Zhu et al. 2003). Paradoxically, GBV-C infection has been shown to have little significance in causing liver damage in humans (Zhu et al. 2003; Alhetheel and El-Hazmi 2014; Nasidi and Rogo 2017). The current findings support the findings of Alhetheel and El-Hazmi (2014), who stated that there were no significant differences in liver enzyme (ALT and AST) levels among HBV or HCV infected patients who were also infected with GBV-C.

This study found no statistically significant difference in diabetes mellitus (DM), hypertension, history of blood transfusion, history of kidney transplantation, history of surgery, history of multiple sexual partners, history of tattooing, or number of blood transfusions between GBV-C positive and negative individuals ($p>0.05$). Hemodialysis duration is significantly ($p<0.05$) longer in

GBV-C positive individuals (Table 4). In the current study, 40% of GBV-C positive patients had DM and 74.29% had hypertension; however, there was no significant association between infection of GBV-C and DM or hypertension. Other studies reported a lower percentage (13.1-15%) of DM and (21.3%) hypertension (Izumi *et al.*, 2019; Savassi-Ribas *et al.*, 2020). This disparity could be attributed to differences in the study population, their underlying medical condition, age, and sample size. In addition, there was no significant association between GBV-C infection and a history of blood transfusion, despite the fact that 85.71% of hemodialysis patients who were GBV-C positive had a history of blood transfusion, and 73.96% had blood transfusions frequently. This is consistent with the findings of Ibrahim and Hamdani (2015), who found no significant differences in the prevalence of GBV-C RNA among age groups, sex, or frequency of blood transfusion. Also, Salama and Selim (2009) reported that there was no significant association between blood transfusion or products of blood, with or without GBV-C infection.

Kheirabad *et al.* (2016) demonstrated a significant association between the prevalence of viruses, such as HCV and HIV in HD patients and GBV-C. Recently, the following strategies have emerged to reduce the risk of infections following blood transfusion: (1) careful donor selection, (2) regular screening of blood donors for HBV, HCV, HIV, human T-cell viruses, and cytomegalovirus (in high-incidence areas), and (3) virus removal and inactivation, particularly double inactivation of blood products and plasma derivatives, excluding complete blood or RBC components (Ghanbari *et al.*, 2010; Kelishadi *et al*., 2019). The history of kidney transplantation and history of surgery also had no significant differences in prevalence of GBV-C, which is in agreement with Rinonce *et al.* (2017). In contrast, Vogt *et al.* (2006) reported that there was a higher correlation between the infection of GBV-C and the number of operating surgery and blood transfusion. In addition, there was no significant association between GBV-C infection and the history of multiple sexual partners and tattooing, which is in consistence with that reported by Rinonce *et al.* (2017). But the high incidence of GBV-C-RNA in intravenous drug users and their heterosexual partners supports that sexual contact may help virus spread in some groups, in addition, the presence of identical sequences in both husband and wife, suggesting that one person was the source of the transmission, however, it is unknown if the transmission occurred sexually or through other unidentified means (Mphahlele *et al.,* 1998).

Many studies have reported that the duration of hemodialysis was a risk factor for GBV-C infection supporting patient-to-patient transmission (Hasan *et al.*, 2018; Sanchooli *et al.,* 2018), which is consistent with the current study finding. This could be attributed to nosocomial infections as a result of hemodialysis units failure to adhere to strict infection control procedures. Although the frequency of GBV-C was only 35%, the current study may have underestimated the true prevalence of GBV-C because E2 antibodies were not used to assess the history of GBV-C infection, and only active GBV-C infection was measured based on viral RNA amplification (Rinonce *et al.,* 2017). Other studies found no significant difference between the long hemodialysis duration and infection with GBV-C (Hosseini-Moghaddam *et al.,* 2008; Rinonce *et al.,* 2017).

Alignment of local isolates 5'-UTR sequences demonstrated that these sequences were sharing (96-99%) similarity with GBV-C reference sequences from Bolivia, United Kingdom, Brazil, Canada, Belgium, Venezuela, France, China, Hong Kong, USA, Singapore, Germany, South Africa, Yamagata, Japan, Colombia, Sweden, Greece and Italy, as shown in (Table 5). However, the results show that all local isolates are very similar, at least using the 5'-UTR, to the Bolivian reference isolate sequence (GenBank accession number AB013206.1), although some substitution mutations (transition and/or transversion) were seen (Table 6). A significant amount of research on this virus revealed some genomic diversity, particularly when the 5'-UTR region of the gene which was employed for phylogenetic analysis (Ibrahim and Hamdani 2015; Slavov *et al.,* 2019)**.** RNA viruses are known to develop a variety of subtypes (quasi-species) providing advantage for viruses to evade host defense mechanisms. Indeed, the variability of 5′-UTR areas in GBV-C greatly contributes to genotype diversity in this virus (Vitrenko *et al.,* 2017).

There is little variation, at least in the 5'-UTR, amongst local isolates themselves. The ten local strains clustered together in the phylogenetic tree with (99%) similarity. The high similarity between the ten GBV-C local isolates sequences in the current study (Figure 2) might be due to the nature of the 5'-UTR selected for amplification and sequencing; this is a highly conserved region with few genomic variations (Chivero and Stapleton, 2015). In addition, the amplified fragment was relatively short (208 bp), which puts a limitation on phylogenetic information that help distinguish the amplified sequences. The epidemiological profile of studied group (hemodialysis patients) may also have influenced this high similarity between the sequences. The 5'-UTR region of GBV-C was chosen because it is well conserved among isolates and easy to amplify (Da Mota *et al.*, 2019; Rinonce *et al.*, 2017).

All ten GBV-C local isolates in the current study were related to genotype (2), and all our isolates clustered with the Bolivian isolate (AB013206.1), United Kingdom isolate (AF095693.1) and Belgian isolate (Y18156.1) with 99%, 98%, 97%, respectively, as shown in (Figure 3). GBV-C isolates belonged to genotype 2, which is common in North America/Europe. This genotypic profile is similar to that reported in other previous studies in blood donors from Kuwait, Jordan and Emirati (AbuOdeh *et al.,* 2015), and in Iraqi thalassemia patients (Ibrahim and Hamdani, 2015), which also clustered with genotype 2. As a result, it appears that many regions in the Middle East have a similar genetic pattern of GBV-C to North America and Europe, which might be due to reciprocal immigration and traveling between these countries. Therefore, the predominance of genotype 2 in the current study could suggest patient-to-patient transmission owing to the predominance of this genotype in the general population. Interestingly, two pairs were completely identical (100%), particularly in the 5'-UTR sequences (2-4 GB virus C IRAQ and 3-5 GB virus C IRAQ) and (5-19 GB virus C IRAQ and 7-46 GB virus C IRAQ) among local isolates, as shown in figure 2, which could be due to nosocomial

transmission among patients in hemodialysis unit as reported by Rinonce *et al.*, (2017).

In conclusion, GBV-C did not seem to contribute to increases in the level of liver enzyme or the severity of HCV infection in hemodialysis patients. Based on phylogenetic analysis of the 5'-UTR, the current study found that local isolates were closely similar to each other and to similar reference known strains, suggesting that GBV-C infection of genotype 2 is one of the prevalent genotypes in Iraq. The limitation of current study is that only 10 PCR products of positive samples were sequenced; however, it is considered as a preliminary study on GBV-C genotyping that could pave the way for further studies with larger samples size from different regions of Iraq to shed light on the actual GBV-C prevalence of different genotypes in our country.

Acknowledgment

The authors would like to thank all the workers at the Al-Kindy dialysis center in Al-Kindy hospital for their assistance with sample collection.

Author contributions

As part of his MSc, Hayder A. Kadhim performed all laboratory work, statistical analysis and wrote the draft of this paper. This work was designed, supervised and reviewed by Dr. Arwa M. Al-Shuwaikh and Dr. Ismail I Latif. The final version of this manuscript was read and approved by the authors.

Conflict of Interests

The authors state that they do not have any conflicting interests.

Funding

Self-funded.

References

Abd El-Hady SI, Zaki SMI, El-Sayed AA, Ezz El-Din MA and El-Salamouny NMA 2006. Prevalence of SEN virus (SEN-V) infection among patients on maintenance hemodialysis in Egypt. *Egypt J Med Microbiol*., **15(1):** 99-112.

Abdullah AM, Ahmed AH and Latif II. 2014. Hepatitis C virus prevalence in hemodialysis patients from three centers in Baghdad, Iraq: a survey by polymerase chain reaction and serological methods. *Science Journal of University of Zakho*, **2(1):** 116-123.

Abdullah AM, Hardan A-R and Latif II. 2012. Genotyping of hepatitis C virus isolates from Iraqi hemodialysis patients by reverse transcription-PCR and one step nested RT-PCR. *Diyala Journal of Medicine*, **3(1):** 9-18.

AbuOdeh RO, Al-Absi E, Ali NH, Khalili M, Al-Mawlawi N, Hadwan TA, Althani AA and Nasrallah GK. 2015. Detection and phylogenetic analysis of human Pegivirus (GBV-C) among blood donors and patients infected with hepatitis B virus (HBV) in Qatar. *J Med Virol.,* **87(12):**2074–81.

Akcali S, Sanlidag T and Ozbakkaloglu B. 2006. Prevalence of GBV-C/hepatitis G virus viremia among chronic hepatitis B, chronic hepatitis C and hemodialysis patients in Turkey. *Ann Saudi Med*., **26(1)**, 68-69.

Alhetheel A and El-Hazmi MM. 2014. Hepatitis G virus in Saudi blood donors and chronic hepatitis B and C patients. *J Infect Dev Ctries.*, 8(01):110-5.

Al-Obeidy ES, Abdullah SF and Mukhlis FA. 2010. Hepatitis G virus infection among Iraqi patients with chronic liver diseases. *J Fac Med Baghdad.,* **52(3):**301–5.

Bernieh B. 2015. Viral hepatitis in hemodialysis: An update. *J Transl Int Med*., **3(3):** 93-105.

Chivero ET and Stapleton JT. 2015. Tropism of human Pegivirus (Formerly Known as GB Virus C/Hepatitis G Virus) and host immunomodulation: insights into a highly successful viral infection. *J Gen Virol.,* **96(7):**1521–32.

Christensen PB, Fisker N, Mygind LH, Krarup HB, Wedderkopp N, Varming K and Georgsen J. 2003. GB virus C epidemiology in Denmark: different routes of transmission in children and low- and high-risk adults. *J Med Virol.,***70(1):**156–62.

Da Mota LD, Finger-Jardim F, Silva CM, Germano FN, Nader MM, Gonçalves CV, Da Hora VP, Silveira J, Basso RP, Soares MA and Martínez AM. 2019. High prevalence and autochtonous transmission of human Pegivirus (HPgV-1) in blood donors in the extreme southern of Brazil. *J Med Viro.l,* **91(1):**31–37.

Dadmanesh M, Hosseinzadeh M, Keyvani H, Ghorban K, Rahimi M, Hosseinzadeh M, *et al.* 2015. Evaluation of prevalence and risk factors of hepatitis G virus infection among hemodialysis patients referred to Iranian army hospitals in Tehran during 2012-2013. *Hepat Mon*., **15(1):** e18322.

De Filippi F, Lampertico P, Soffredini R, Rumi MG, Lunghi G, Aroldi A, *et al.* 2001. High prevalence, low pathogenicity of hepatitis G virus in kidney transplant recipients. *Dig Liver Dis*., **33(6):**477-9.

dos Santos Bezerra R, Santos EV, Silveira RM, Pinto AC, Covas DT, Kashima S and Slavov SN. 2020. Molecular prevalence and genotypes of human Pegivirus-1 (HPgV-1) and SENV-like viruses among multiply transfused patients with beta-thalassemia. *Transfus Apher Sci.,* **59(2):**102697.

Egawa K, Yukawa T, Arakawa S, Nakao H, Inoue T, Tanaka T, Tsuda F, Okamoto H, Miyakawa Y and Mayumi M. 1996. Infection with GB virus C in leprous patients in Japan. *J Med Virol*., **49(2):** 110–114.

Eslamifar A, Hamkar R, Ramezani A, Ahmadi F, Gachkar L, Jalilvand S, *et al.* 2007. Hepatitis G virus exposure in dialysis patients. *Int Urol Nephrol*., **39(4):**1257-63.

Forns X, Hegerich P and Darnell A, Emerson SU, Purcell RH and Bukh J. 1999. High prevalence of TT virus (TTV) infection in patients on maintenance hemodialysis: frequent mixed infections with different genotypes and lack of evidence of associated liver disease. *J Med Virol*., **59:**313–317.

Ghanbari R, Ravanshad M, Hosseini SY, Yaghobi R and Shahzamani K. 2010. Genotyping and infection rate of GBV-C among Iranian HCV-infected patients. *Hepa Mon.,* **10(2):**80–87.

Handajani R, Lusida MI, Suryohudoyo P, Adi P, Setiawan PB.Soetjipto, *et al.* 2000. Prevalence of GB virus C/Hepatitis G virus infection among various populations in Surabaya, Indonesia, and identification of novel groups of sequence variants. *J. Clin Microbiol*., **38(2)**:662-8.

Hasan AS, Noaman NG and Hasan ME. 2018. Hepatitis G virus infection among high risk population in diyala province. *Iraqi J Community Med.,* **31(4):**153–58.

Hosseini-Moghaddam SM, Keyvani H, Samadi M, Alavian SM, Mahdavimazdeh M, Daneshvar S and Razzaghi Z. 2008. GB virus type C infection in hemodialysis patients considering co-infection with hepatitis C virus. *J Med Virol*., **80(7):**1260–63.

Ibrahim MS, Al Hamdani AH and Faeq A. 2015. Hepatitis G virus infection and genotypes in Iraqi thalassemia patients. *Iraqi J Hematol.,* **4(1):**67–81.

Izumi T, Sakata K, Okuzaki D, Inokuchi S, Tamura T, Motooka D, Nakamura S, Ono C, Shimokawa M, Matsuura Y, Mori M, Fukuhara T and Yoshizumi T. 2019. Characterization of human pegivirus infection in liver transplantation recipients. *J Med Virol.,* **91(12):**2093–2100.

Kelishadi M, Hashemi P, Ashrafi GH, Behnampour N and Tabarraei A. 2019. Presence of GB virus C in whole-blood derivatives: a pilot study. *Med Lab J.,* **13(5):**26–31.

Kheirabad AK, Bahri F, Kargar M, Ghasemzadeh I. 2016. Hepatitis C and G virus infection prevalence among hemodialysis patients and associated risk factors in the hormozgan province of southern Iran. *Hepat Mon.,* **16(10):**e40375.

Khudair EA, Al-Shuwaikh AM and Farhan, NM. 2019. Detection and genotyping of SEN virus among patients with hepatitis and healthy blood donors from Baghdad, Iraq. *Jordan J Biol Sci*., **12(3):** 355–360.

Mphahlele MJ, Lau GK and Carman WF. 1998. HGV: The identification, biology and prevalence of an orphan virus. *Liver,* **18(3):**143–55.

Nasidi F and Rogo L. 2017. Biology of hepatitis G virus: a review. *Sokoto J Med Lab Sci.,* **2(1):**21–38.

Ozdarendeli A, Toroman ZA, Kalkan A, Kilic SS, Ozden M and Doymaz MZ. 2005. Prevalence and genotypes of hepatitis G virus among hemodialysis patients in eastern Anatolia, Turkey. *Med PrincPract.,* **14(2):**102–6.

Qureshi L, Shaikh NA, Tunio IA, Ambwani J, Bhatti N and Ghumro PB. 2020. Prevalence of hepatitis-g virus infection in patients with liver diseases in district larkana, Pakistan. *RMJ.,* **45(4):**755–57.

Rinonce HT, Yano Y, Utsumi T, Heriyanto DS, Anggorowati N, Widasari DI, Ghozali A, Utoro T, Lusida MI, Prasanto H and Hayashi Y. 2017. Prevalence and genotypic distribution of GB virus C and Torque Teno virus among patients undergoing hemodialysis. *Mol Med Rep.,* **15(5):**2843–52.

Salama KM and Selim OE. 2009. Hepatitis G virus infection in multitransfused Egyptian children. *Pediatr Hematol Oncol*., **26(4):**232–39.

Sanchooli A, Makvandi M, Nisi N and Samiei RN. 2018. Prevalence of hepatitis G virus and co-infection with hepatitis B virus and hepatitis C virus among hemodialysis patients in Ahvaz, Iran. *Jundishapur J Chronic Dis Care.,* **7(2):**2–7.

Sathar MA, Soni PN and York D. 2000. GB Virus C/Hepatitis G Virus (GBV-C/HGV): still looking for a disease. *Int J Exp Pathol*., **81**: 305-322

Savassi-Ribas F, Pereira JG, Horta MA, Wagner TC, Matuck TA, Monteiro de Carvalho DB, Mello FC, Varella RB and Soares CC. 2020. Human Pegivirus-1 infection in kidney transplant recipients: a single-center experience. *J Med Virol.,* **92(12):**2961–68.

Scallan MF, Clutterbuck D, Jarvis LM, Scott GR and Simmonds P. 1998. Sexual transmission of GB virus C/hepatitis G virus. *J Med Virol.,* **55(3):**203–8.

Slavov SN, Silveira RM, Rodrigues ES, Diefenbach CF, Zimmermann AM, Covas DT and Kashima S. 2019. Human Pegivirus-1 (HPgV-1, GBV-C) RNA prevalence and genotype diversity among volunteer blood donors from an intra-hospital hemotherapy service in Southern Brazil. *Transfus Apher Sci.,* **58(2):**174–78.

Vitrenko Y, Kostenko I, Kulebyakina K and Sorochynska K. 2017. Prevalence of human Pegivirus-1 and sequence variability of its E2 glycoprotein estimated from screening donors of fetal stem cell-containing material. *Virol J.,* **14(1):**1–11.

Vogt M, Klostermann B, Braun S, Busch R, Hess J, Frösner G and Lang T. 2006. Prevalence and clinical role of GBV-C infection after cardiac surgery in childhood: a study on 414 patients. *J Infect.,* **53(1):**43–48.

Zhu WF, Yin LM, Li P, Huang J and Zhuang H. 2003. Pathogenicity of GB virus C on virus hepatitis and hemodialysis patients. *World J Gastroenterol.,* **9(8):**1739–42.

JJBS

Volume 15, Number 4,December 2022
ISSN 1995-6673
Pages 603 – 609
https://doi.org/10.54319/jjbs/150408

Jordan Journal of Biological Sciences

Nutritional and Endophytic Composition of Edible Tubers of Tiger nut (*Cyperus esculentus* L.)

Omotayo O. Oyedara[1,2,*], Abdulfatai B. Rufai[3], Gideon O. Okunlola[3], Folasade M. Adeyemi[1]

[1]*Department of Microbiology, Faculty of Basic and Applied Sciences, Osun State University, Osogbo, Nigeria;* [2]*Departamento de Microbiología e Inmunología, Facultad de Ciencias Biológicas, Universidad Autónoma de Nuevo León, San Nicolás de los Garza, 66450, Nuevo León, Mexico;* [3]*Department of Plant Biology, Faculty of Basic and Applied Sciences, Osun State University, Osogbo, Nigeria*

Received: July 6, 2021; Revised: January 22, 2022; Accepted: January 31, 2022

Abstract

In this study, different parameters including phytochemical, nutritional, anti-nutritional compositions, and endophytic microbial populations that can play roles in the health benefits of tiger nut (*Cyperus esculentus* L.) tubers were determined in tiger nut tuber samples obtained from three different local markets situated in Osogbo, Ile-Ife, and Ado-Ekiti in the Southwestern part of Nigeria. Tannins (127.33-620.1 GAE/100 g), alkaloids (0.5-18%), flavonoids (4.5-9.5%), terpenoid, and cardiac glycoside were present in all the samples. The most and least abundant elements in the tiger nuts were Potassium (0.255-0.345%) and Copper (0.0007-0.0009%), respectively. The anti-nutrients found in the tiger nut tubers were oxalate (0.42-1.08 mg/100 g), tannin (0.42-0.98 mg/100 g), and phytic acid (0.56-1.64%). By molecular techniques, *Lactococcus lactis*, *Bacillus cereus*, *Enterobacter cloacae*, *Bacillus licheniformis*, *Bacillus aryabhattai*, and *Enterobacter roggenkampii* were identified as the endophytic bacteria in the tiger nut tubers, while the endophytic fungi isolated were *Saccharomyces cerevisiae* and *Candida tropicalis*. The presence of reportedly pharmacologically active phytochemicals, essential elements, endophytic bacterial and fungal strains with probiotic potentials, and negligible amounts of anti-nutrients in the study tiger nut samples supports the nutritional and health benefits of tiger nut tubers.

Keywords: Tiger nut tuber, phytochemicals, anti-nutrients, elements, endophytes

1. Introduction

Tiger nut (*Cyperus esculentus* L) is a sedge plant belonging to the same genus as the papyrus plant (*Cyperus papyrus* L.) of the family "Cyperaceae". Tiger nut tuber (Plate 1), also known as "Aya", "Imumu", and "Aki-hausa" among the Hausa, Yoruba, and Igbo tribes respectively in Nigeria, is either eaten raw or processed into different products such as milk, flour, bread, and beverages (Oladele and Aina, 2007; Aguilar *et al*., 2015). The consumption of tiger nut or its derived products are associated with health benefits, and reports have shown that tiger nut has medicinal and nutritional properties (Sabah *et al*., 2019; Bazine and Arslanoğlu, 2020). It is useful medically for the prevention and management of diseases such as thrombosis, heart cancer, erectile dysfunction, obesity, diabetes, and high blood pressure (Adejuyitan, 2011).

For centuries, humans have used plants for several medicinal purposes. The nutritional content, phytochemical composition, presence of beneficial and pharmacologically relevant endophytes in plants contribute to their medicinal and nutritional characteristics. Phytochemicals, for instance, contribute to plant potentials to promote good health and cure diseases (Barbieri *et al*., 2017). Furthermore, plants also contain anti-nutritional compounds that can adversely affect humans by interfering with metabolic processes such as nutrient absorption (Kunatsa *et al*., 2020). Hence, knowledge of anti-nutrients in a plant or its product can provide information on its nutritional significance.

Similar to phytochemicals, endophytic microbes defend plants against pathogens and aid their growth (Nayak *et al*., 2017; Bind and Nema, 2019; Yasser *et al*., 2020). When consuming plant materials including, fruits and leaves, animals also ingest endophytes. According to Martínez-Romero *et al*. (2020), microbes associated with plants form part of herbivores' gut microbiota.

Endophytes aid the degradation of complex plant materials such as cellulose, and antimetabolites in animals. Furthermore, endophytic *Lactobacillus plantarum* has probiotic potential to protect humans against bacterial and viral infections (Martínez-Romero *et al*., 2020).

With limited information on endophytic microbes associated with tiger nut tuber, this study examined tiger nut tubers purchased from three local markets in the South-Western part of Nigeria for the endophytic bacterial and fungal composition alongside parameters including phytochemicals, nutritional elements, anti-nutrients that can play roles in the health benefits.

* Corresponding author. e-mail: omotayo.oyedara@uniosun.edu.ng.

Plate 1. A picture of the tiger nut tubers (*Cyperus esculentus* L.)

2. Materials and methods

2.1. Sample collection

Fresh tiger nut tubers were purchased from three different local markets Ile-Ife (7.52 ºN and 4.28 ºE), Osogbo (7.77 ºN and 4.57 ºE), and Ado-Ekiti (7.62 ºN and 5.22 ºE) in the Southwestern part of Nigeria. The tiger nuts were then transported to the laboratory for processing and analysis. Before analysis, a taxonomist at the Forest Herbarium Ibadan (FHI), Forestry Research Institute of Nigeria, Ibadan, Nigeria, identified and confirmed the tiger nut tubers.

2.2. Phytochemical, Elemental, and Anti-nutritional analysis

The tiger nuts were qualitatively and quantitatively analyzed for the presence of terpenoids, saponins, alkaloids, steroids, flavonoids, cardiac glycosides, and tannins according to the method described by Harbone (1984). The mineral contents were analyzed using colorimetric or spectrophotometric, or titrimetric methods where applicable (AOAC, 2005). The tiger nut samples were analyzed to determine the content of sodium (Na), potassium (K), calcium (Ca), iron (Fe), magnesium (Mg), zinc (Zn), manganese (Mn), copper (Cu), phosphorus (P), total nitrogen (T.N), and organic matter (O.M). The atomic absorption spectrophotometer was used to evaluate the anti-nutritional compounds, tannin, and oxalate contents of the tiger nut samples in triplicate, according to the standard methods of AOAC, (2005). The phytate contents were estimated using the solvent extraction gravimetric method (Onwuka, 2005).

2.3. Isolation of Endophytic bacteria and fungi

The tiger nut tubers were carefully inspected visually to select ones without superficial damages. The surfaces of selected tiger nuts (100 g) were sterilized, following the process described by Afzal *et al*. (2019), with slight modifications. Briefly, tiger nuts were washed thoroughly three times with sterile distilled water and then soaked in 5% sodium hypochlorite (NaOCl) for 5 minutes. The tiger nuts were later washed twice in sterile distilled water to remove the sterilizing agent (NaOCl) and thrice in 96% ethanol to ensure the total removal of epiphytic microbes on the surface of the tiger nuts. This was then followed by rinsing the tiger nuts in sterile distilled water eight times, and the last rinse water was cultured on nutrient and potato dextrose agar to confirm the removal of the epiphytic microorganisms. The processed tiger nuts were grinded with sterile mortar and pestle, and the resulting milky extract was serially diluted in sterile phosphate buffer and inoculated on sterile nutrient and potato dextrose agar plate to isolate the endophytic bacteria and fungi, respectively. The plates were incubated at 30 ºC for 24-72 h and 5 days for bacterial and fungal isolation, respectively.

2.4. Molecular Identification of Endophytic bacteria and fungi

DNA was extracted from isolated endophytic bacteria using the NIMR Biotech (Lagos, Nigeria) DNA Purification Kit according to the manufacturer's instruction, while fungal DNA was extracted using the "Bust n' Grab" method described by Harju *et al*. (2004). Molecular identification of endophytic bacterial isolates were based on the Polymerase Chain Reaction (PCR) amplification of the 16S rRNA gene fragment using universal primers; 27F: 5′-AGAGTTTGATCCTGGCTCAG-3′ and 1492R:5′-GGTTACCTTGTTACGACTT-3′ (Chen *et al*., 2015) that amplified 1500 bp of the gene fragment. The rDNA internal transcribed spacer (ITS) region of the fungal isolates was amplified using primers sets (ITS1, 5′-TCCGTAGGTGAACCTGCGG-3′) and (ITS4, 5′-TCCTCCGCTTATTGATATGC-3′) that amplified the 600 bp of the ITS region. The PCR amplified products were sequenced by Inqaba Biotech West Africa Ltd (IITA, Ibadan, Nigeria), and the nucleotide sequences obtained were edited using FinchTV software. The edited sequences were subjected to similarity search against nucleotides in the NCBI database using BLASTn program for bacterial and fungal identification. Phylogenetic tree showing the relationship between isolated endophytes and sequences retrieved from the GenBank was inferred using the Maximum Likelihood method of the MEGA7 software (Kumar *et al*., 2016) based on the Tamura-Nei model (Tamura and Nei, 1993) with 1000 pseudoreplicates to obtain the bootstrap values.

3. Results

3.1. Phytochemical, Elemental, and Anti-nutritional analysis

The result of the qualitative analysis of the phytochemicals in the tiger nut samples is presented in Table 1. Saponins, steroids, and phenols were absent in all the samples. Meanwhile, anthraquinone was found only in samples purchased from Ado-Ekiti. The quantity of tannin in the tiger nut samples ranged between 127.33 and 620.1 (Table 2), with tiger nut samples from Ado-Ekiti having the lowest amount (127.3 GAE/100 g). The highest quantity of flavonoids was found in the tiger nut tubers from Osogbo (9.5%), followed by Ado-Ekiti (4.5%) and Ile-Ife (5%). The alkaloid contents in the tiger nut samples from Ile-Ife, Ado-Ekiti, and Osogbo were 18%, 4%, and 0.5%, respectively. The mineral composition of the tiger nut samples is presented in Table 3. While slight variations

were observed in percentage of minerals; Na (0.021-0.020%), Ca (0.030-0.040%), Mg (0.101-0.112%), K (0.255-0.345%), Mn (0.001-0.0001%), Cu (0.0007-0.0009%), Fe (0.0045-0.0048%), Zn (0.0024-0.0025%), and P (0.108-0.166%) in the tiger nuts purchased from the different markets, the organic matter and total nitrogen content were low in tiger nut samples from Ile-Ife (69.48% and 3.47%, respectively) compared to tiger nuts from Ado-Ekiti (84.65% and 4.23%, respectively) and Osogbo (85.99% and 4.30%, respectively). The amount of oxalate, which is one of the anti-nutrients tested in the tiger nut sample, ranged from 1.02 to 0.42 mg/100 g, with tiger nuts from Osogbo having the highest amount followed by samples from Ile-Ife (0.88 mg/100 g) and Ado-Ekiti (Table 4). The phytic acid (1.64%) and tannin (0.98 mg/100 g) compositions were highest in Osogbo tiger nut samples. The amounts of phytic acid and tannin in the tiger nut samples purchased from the Ile-Ife market were 1.45% and 0.42 mg/100 g, respectively. Meanwhile, tiger nuts from Ado-Ekiti had 0.56% and 0.44 mg/100 g of phytic acid and tannin, respectively.

Table 1: Qualitative analysis of phytochemical compounds in tiger nut samples obtained from the three different markets.

Phytochemical	Method of analysis	Sample A (Ile-Ife)	Sample B (Ado-Ekiti)	Sample C (Osogbo)
Alkaloid	Dragenduff	+	+	++
	Mayer	+	+	++
	Wagner	+	+	++
Flavonoid	Ethyl acetate/Ammonia	+	+	+
Saponin	Frothing	-	-	-
Tannin	Ferric chloride	+	+	+
Anthraquinone	Borntrager	-	+	-
Terpenoid	Salkowski	++	+	+
Cardiac Glycoside	Keller-Killiani	+	++	+
Steroid	Liebermann-Burchard	-	-	-
Phenol	Lead acetate	-	-	-

Keys: ++: present in high concentration; +: present in trace amount; -: absent

Table 2: Quantitative analysis of phytochemical compounds in tiger nut samples obtained from the three different markets

Phytochemical	Sample A (Ile-Ife)	Sample B (Ado-Ekiti)	Sample C (Osogbo)
Tannin (GAE/100 g)	620.1	127.33	413.74
Flavonoid (%)	5	4.5	9.5
Alkaloid (%)	18	4	0.5

Keys: GAE - Gallic Acid Equivalent

Table 3: The mineral composition of tiger nut samples obtained from the three different markets

Mineral (%)	Sample A (Ile-Ife)	Sample B (Ado-Ekiti)	Sample C (Osogbo)
Sodium (Na)	0.020	0.021	0.021
Calcium (Ca)	0.030	0.040	0.030
Magnesium (Mg)	0.101	0.102	0.112
Potassium (K)	0.345	0.255	0.285
Manganese (Mn)	0.001	0.001	0.0001
Copper (Cu)	0.0007	0.0009	0.0008
Iron (Fe)	0.0048	0.0048	0.0045
Zinc (Zn)	0.0025	0.0024	0.0025
Phosphorus (P)	0.144	0.166	0.108
Organic matter	69.48	84.65	85.99
Total Nitrogen	3.47	4.23	4.30

Table 4: The anti-nutritional constituents of tiger nut samples obtained from the three different markets

Phytochemical	Sample A (Ile-Ife)	Sample B (Ado-Ekiti)	Sample C (Osogbo)
Oxalate (mg/100g)	0.88	0.42	1.02
Phytic acid (%)	1.45	0.56	1.64
Tannin (mg/100g)	0.42	0.44	0.98

3.2. Molecular Identification of Endophytic bacteria and fungi

A total of twenty-one endophytic bacteria were isolated from the tiger nut samples. However, six PCR amplicons were successfully sequenced, and based on the BLASTn search and molecular phylogenetic analysis (Figure 1), the sequences shared similarities with *Lactococcus lactis*, *Bacillus cereus*, *Enterobacter cloacae*, *Bacillus licheniformis*, *Bacillus aryabhattai*, and *Enterobacter roggenkampii* with percentage identity ranging from 90.90 to 99.80% (Table 5). Two endophytic fungi successfully identified include *Saccharomyces cerevisiae* and *Candida tropicalis* (Figure 2). The bacterial 16S rRNA and fungal ITS sequences obtained in this study were submitted to the National Center for Biotechnology Information (NCBI) GenBank database under the accession numbers MZ452337-MZ452342 for bacterial isolates and MZ42353, MZ452354, and MZ452357 for fungal isolates (Table 5).

Table 5: The BLAST hit identification of endophytic bacteria and fungi isolated from tiger nut samples

Isolate code	BLAST hit Homologue Sequence (Accession number)	Percentage Identity (%)	E-value	Accession number of deposited sequence
TG1	*Lactococcus lactis* strain IMAU98440 (MW135286.1)	90.90	0.0	MZ452337
TG2	*Bacillus cereus* strain Q21 (MH915663.1)	98.29	0.0	MZ452338
TG3	*Enterobacter cloacae* strain BY56 (MN133903.1)	99	0.0	MZ452339
TG4	*Bacillus licheniformis* strain QT445 (MT065669.1)	97.99	0.0	MZ452340
TG5	*Enterobacter roggenkampii* strain CCI9 (LC529204.1)	99.19	0.0	MZ452341
TG6	*Bacillus aryabhattai* strain 3595 (MT538470.1)	98.34	0.0	MZ452342
TGY1	*Saccharomyces cerevisiae* strain XZFM7F3 (MW710205.1)	99.75	0.0	MZ452353
TGY3	*Saccharomyces cerevisiae* strain XZFM7F3 (MW710205.1)	99.38	0.0	MZ452354
TGY4	*Candida tropicalis* isolate ZA030 (JN606259.1)	99.80	0.0	MZ452357

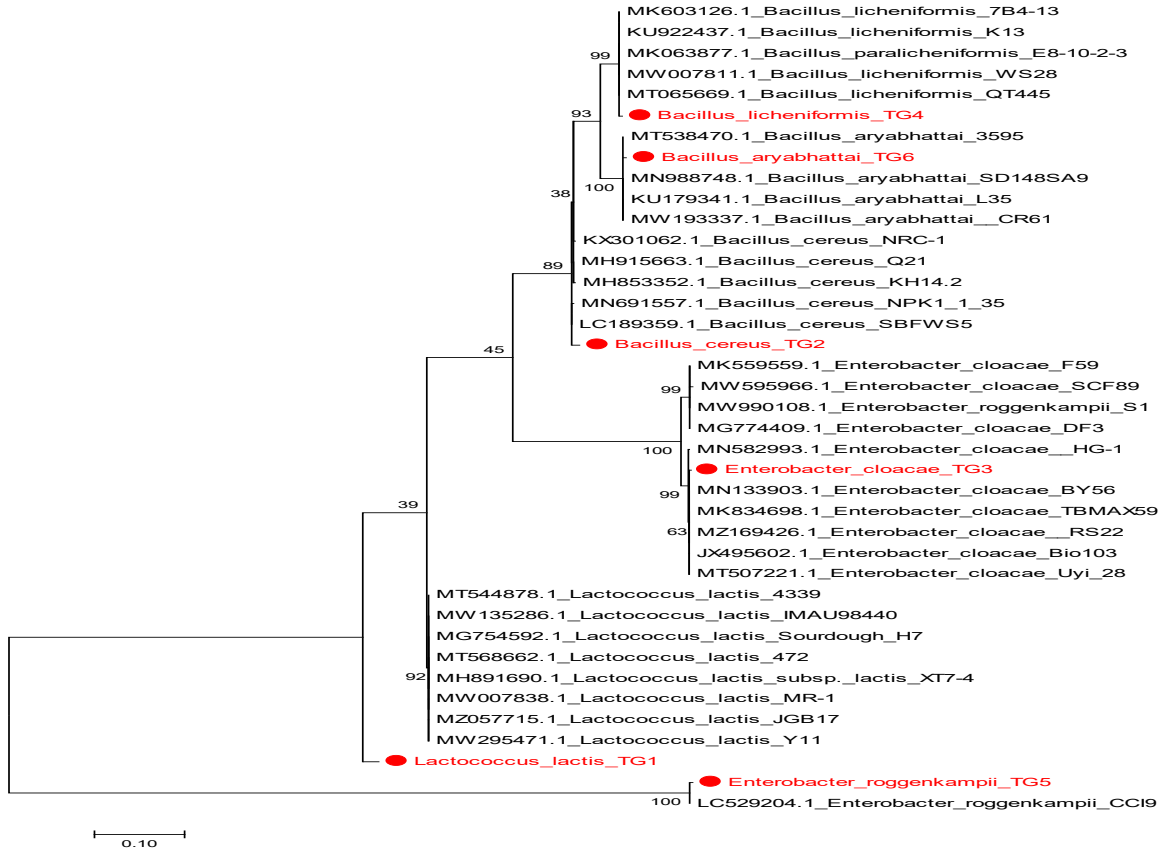

Figure 1. Molecular Phylogenetic relationship of the isolated endophytic bacteria by Maximum Likelihood method.

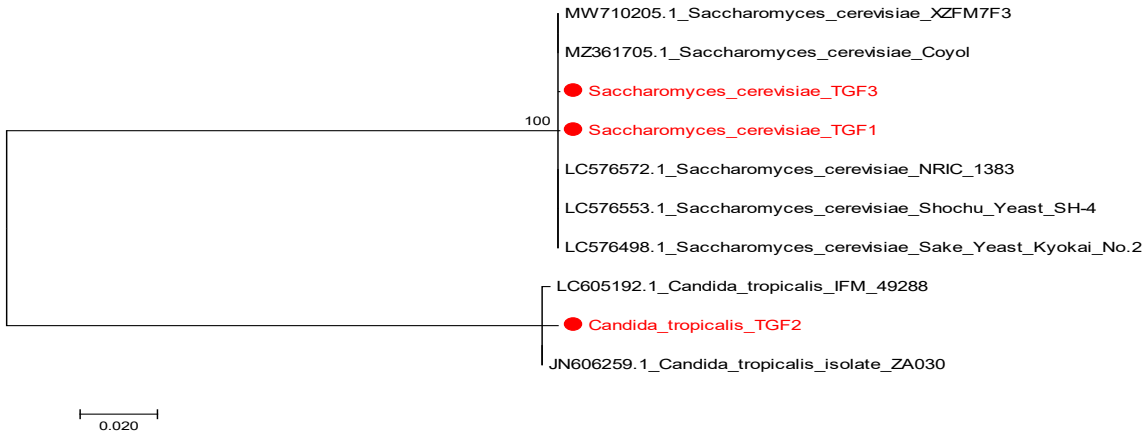

Figure 2. Molecular Phylogenetic relationship of the isolated endophytic fungi by Maximum Likelihood method.

4. Discussion

This study analyzed the properties such as phytochemical, elemental, anti-nutritional, and endophytic microbial constituents that can play roles in the beneficial importance of tiger nuts when consumed. The results obtained in this study revealed alkaloids, flavonoids, tannins, terpenoids, and cardiac glycosides as the phytochemical compounds present in the tiger nuts purchased from the three markets. Quantitatively, tiger nuts purchased from Ile-Ife had the highest quantities of tannin (620.1 GAE/100 g) and alkaloids (18%). Meanwhile, the tiger nuts bought in the Osogbo market had the highest amount of flavonoids (9.5%). The variations observed in the phytochemical components of the tiger nuts bought from the different locations could be because of some factors, which may include, the cultivation conditions, a difference in the period between harvest and purchase, period of exposure, and preservation methods (Asante *et al*., 2014; Bado *et al*., 2015). Phytochemicals reported in this study have different pharmacological properties, hence supporting the nutritional and medicinal values of tiger nut tubers. The phytochemicals have hepatoprotective, anti-sickling, aphrodisiac, antimicrobial, anti-inflammatory, and antioxidant properties (Da Silva *et al*., 2012; Rehman *et al*., 2015; Dermane *et al*., 2018; Yang *et al*., 2020). Furthermore, anthroquinone, a phytochemical compound known to have a laxative effect and relevant in the cure for constipation (Lombardi *et al*., 2020), was identified, in tiger nut samples purchased from the Ado-Ekiti market. Similar to the report of Aduwamai *et al*., (2018), saponin was not detected in any of the tiger nut tubers analyzed in this study.

The result of the mineral composition showed that the study tiger nuts were rich in organic matter. The abundance of elements in the tiger nut samples was in the following order: K > P > Mg > Ca > Na > Fe > Zn > Mn > Cu. The high amount of potassium (0.255-0.345%) and magnesium (0.101-0.112%) to sodium (0.020-0.021%) in tiger nut makes it suitable as a diet formulation for individuals with high blood pressure. Phosphorus, a component of Adenosine triphosphate (ATP) which is an energy rich molecule in the body, was the second most abundant element in the tiger nut samples. The least abundant elements in the tiger nut samples were iron (0.0045-0.0048%), zinc (0.0024-0.0025%), and copper (0.0007-0.0009%). Zinc plays a vital role in alleviating neurodegenerative disorder-related problems in the elderly (Prasad, 2014). Hence, tiger nut consumption can be a source of zinc to improve the health conditions of the elderly. Tiger nut can also be a good food supplement to prevent anemic conditions because it contains iron, a component of hemoglobin. Furthermore, Fe, Cu, Zn, and Ca present in the tiger nut samples have been reported as essential elements in male fertility and sexual function (Shinohara and Watanabe, 1996).

Anti-nutrients are substances that prevent the efficient utilization of food nutrients by the body. They are sometimes toxic, and their effects may result from their metabolic products (Okoye and Ene, 2018). Phytic acid, oxalate, and tannin were the anti-nutrients identified in the tiger nut samples. High amounts of oxalate, phytic acid, and tannin in food samples can reduce calcium absorption (Bello *et al*., 2008), cause mineral deficiencies (Phillippy *et al*., 2004), and have interaction that is detrimental to humans with dietary protein (Cirkovic Velickovic and Stanic-Vucinic, 2018), respectively. The amount of tannins (0.42-0.98 mg/100 g) observed in this study is tolerable and may not cause any adverse effects considering the recommended amount of tannins daily intake for a man, which is 560 mg/100 g (Bello *et al*., 2008). Overall, the low amount of anti-nutrients observed for the tiger nuts in this study supported its usage as a medicinal, beneficial, and functional food that can improve the health status of consumers.

This study, to our knowledge, is the first report on the endophytic bacteria associated with tiger nut tuber. The endophytic bacteria isolated include the genera *Lactococcus*, *Bacillus*, and *Enterobacter*, which have been reported as endophytes of several plants (McCulloch *et al*., 2014; Hu *et al*., 2017; Yaish, 2017; Guo *et al*., 2020; Panigrahi *et al*., 2020). *Lactococcus lactis* belongs to the group of lactic acid bacteria with the status of "generally regarded as safe" (GRAS) and probiotic potential (Oliveira *et al*., 2017). *Bacillus* species promote plant growth by producing auxins, siderophores, gibberellin, and indole acetic acid that protect plants against phytopathogens and adverse conditions, such as drought (Suhandono *et al*., 2016). Macedo-Raygoza *et al*. (2019) also reported the nitrogen-fixation and phosphorus solubilization potentials of *Enterobacter cloacae*. There are reports on the probiotics potentials of genera *Bacillus*, strains of *L. lactis*, and *E. cloacae* in human, aquatic, and poultry nutrition (Gao *et al*., 2018; Girijakumari *et al*., 2018; Yerlikaya, 2019; Zhao *et al*., 2019), hence suggesting the application of tiger nut as a probiotic functional food in these different areas.

The two species of endophytic fungi isolated in this study (*S. cerevisiae* and *C. tropicalis*) have been reported to be implicated in the spoilage of exposed tiger nut milk (Onovo and Ogaraku, 2007). Similar to *B. cereus*, *C. tropicalis* is a potential pathogen of humans. However, studies have reported *S. cerevisiae* and *B. cereus* as important endophytic microorganisms (Pennacchi *et al*., 2008; Cutting, 2011). Further work is to examine the biological activities of the endophytic bacteria and fungi isolated from the tiger nut tubers for possible beneficial applications.

5. Conclusion

This study provided information on the different parameters that can play roles in the health benefits of tiger nut, perhaps as a functional food. This study has revealed that tiger nut tubers have important pharmacologically active phytochemicals, nutritional elements, negligible amount of anti-nutrients, and endophytic bacterial and fungal strains previously reported by several authors to have probiotic potentials.

References

Adejuyitan JA. 2011. Tigernut processing: its food uses and health benefits. *Am. J. Food Technol*., **6(3)**: 197-201.

Aduwamai UH, John UI, Aminu A and Isaac UK. 2018. Influence of different processing methods on proximate and anti-nutritional

value of tigernuts (*Cyperus esculentus* L.). *GSC biol. pharm. Sci*., **3(3)**: 029–034.

Afzal I, Shinwari ZK, Sikandar S and Shahzad S. 2019. Plant beneficial endophytic bacteria: Mechanisms, diversity, host range and genetic determinants. *Microbiol. Res.*, **221**: 36-49.

Aguilar N, Albanell E, Miñarro B, Guamis B and Capellas M. 2015. Effect of tiger nut-derived products in gluten-free batter and bread. *Food Sci. Technol*., **21(5)**: 323-331.

AOAC. 2005. The Official Method of Analysis. 17th Ed. Association of Official Analytical Chemists, Washington D.C. U.S.A.

Asante FA, Oduro I, Ellis WO and Saalia FK. 2014. Effect of Planting Period and Site on the Chemical Composition and Milk Acceptability of Tigernut (*Cyperus Esculentus* L) Tubers in Ghana. *Am. J. Food Nutri*., **2(3)**: 49-54.

Bado S, Bazongo P, Son G, Kyaw MT, Forster BP, Nielen, S, Lykke AM, Ouédraogo A and Bassolé, IHN. 2015. Physicochemical characteristics and composition of three morphotypes of *Cyperus esculentus* tubers and tuber oils. *J Anal Methods Chem.*, **2015**:1-8.

Barbieri R, Coppo E, Marchese A, Daglia M, Sobarzo-Sánchez E, Nabavi SF and Nabavi SM. 2017. Phytochemicals for human disease: An update on plant-derived compounds antibacterial activity. *Microbiol. Res*., **196**: 44-68.

Bazine T and Arslanoğlu F. 2020. Tiger Nut (*Cyperus esculentus*); Morphology, Products, Uses and Health Benefits-Review. *BSJ Agri*., **3(4)**: 324-328.

Bello MO, Falade OS, Adewusi SRA and Olawore NO. 2008. Studies on the chemical compositions and anti-nutrients of some lesser known Nigeria fruits. *Afr. J. Biotechnol*., **7(21)**: 3972-3979.

Bind M and Nema S. 2019. Isolation and molecular characterization of endophytic bacteria from pigeon pea along with antimicrobial evaluation against *Fusarium udum*. *Appl Microbiol*., **5(2)**: 19.5.163.

Chen YL, Lee CC, Lin YL, Yin KM, Ho CL and Liu T. 2015. Obtaining long 16S rDNA sequences using multiple primers and its application on dioxin-containing samples. *BMC bioinform*., **16(18)**: 1-11.

Cirkovic Velickovic TD and Stanic-Vucinic DJ. 2018. The role of dietary phenolic compounds in protein digestion and processing technologies to improve their antinutritive properties. *Compr. Rev. Food Sci. Food Saf*., **17(1)**: 82-103.

Cutting SM. 2011. Bacillus probiotics. *Food Microbiol*., **28(2)**: 214-220.

Da Silva CV, Borges FM and Velozo ES. 2012. Phytochemistry of some Brazilian plants with aphrodisiac activity. *Phytochemicals-A Global Perspective of Their Role in Nutrition and Health*, 307-326.

Dermane A, Kpegba K, Metowogo K, Joppa MK, Eklu-Gadegbeku K, Aklikokou, AK and Gbeassor, M. 2018. Evaluation of the anti-sickling activity of *Newbouldia laevis* P. Beauv extracts. *Int. J. Chem. Biol. Sci*., **12(6)**: 2808-2817.

Gao X, Zhang M, Li X, Han Y, Wu F and Liu Y. 2018. Effects of a probiotic (*Bacillus licheniformis*) on the growth, immunity, and disease resistance of *Haliotis discus hannai* Ino. *Fish Shellfish Immunol*., **76**: 143-152.

Girijakumari NR, Ethiraja K and Marimuthu PN. 2018. *In vitro* and *in vivo* evaluation of probiotic properties of *Enterobacter cloacae* in Kenyi cichlid, *Maylandia lombardoi*. *Aquac Int*., **26(4)**: 959-980.

Guo DJ, Singh RK, Singh P, Li, DP, Sharma A, Xing YX., Song XP, Yang LT and Li YR. 2020. Complete Genome Sequence of *Enterobacter roggenkampii* ED5, a Nitrogen Fixing Plant Growth Promoting Endophytic Bacterium with Biocontrol and Stress Tolerance Properties, Isolated from Sugarcane Root. *Front. Microbiol*, **11**:2270.

Harbone JB, 1984. Phytochemical Methods: A Guide to Modern Techniques of Plant Analysis, 3rd Ed. Chapman and Hall, London, New York, 3rd edition, 21-29.

Harju S, Fedosyuk H and Peterson KR. 2004. Rapid isolation of yeast genomic DNA: Bust n'Grab. *BMC Biotechnol*., **4(1)**: 1-8.

Hu HJ, Chen YL, Wang YF, Tan, YY, Chen SL and Yan SZ. 2017. Endophytic *Bacillus cereus* effectively controls *Meloidogyne incognita* on tomato plants through rapid rhizosphere occupation and repellent action. *Plant Dis.*, **101(3)**: 448-455.

Kumar S, Stecher G and Tamura K. 2016. MEGA7: molecular evolutionary genetics analysis version 7.0 for bigger datasets. *Mol. Biol. Evol*., **33(7)**: 1870-1874.

Kunatsa Y, Chidewe C and Zvidzai CJ. 2020. Phytochemical and anti-nutrient composite from selected marginalized Zimbabwean edible insects and vegetables. *J. Agric. Food Res*., **2**: 100027.

Lombardi N, Bettiol A, Crescioli G, Maggini V, Gallo E, Sivelli F, Sofi F, Gensini GF, Vannacci A and Firenzuoli F. 2020. Association between anthraquinone laxatives and colorectal cancer: protocol for a systematic review and meta-analysis. *Syst. Rev*., **9(1)**: 1-6.

Macedo-Raygoza GM, Valdez-Salas B, Prado FM, Prieto KR, Yamaguchi LF, Kato MJ, Canto-Canché BB, Carrillo-Beltrán M, Di Mascio P, White JF, Beltrán-García MJ. 2019. *Enterobacter cloacae*, an endophyte that establishes a nutrient-transfer symbiosis with banana plants and protects against the black Sigatoka pathogen. *Front Microbiol*., **10**: 804.

Martínez-Romero E, Aguirre-Noyola JL, Bustamante-Brito R, González-Román P, Hernández-Oaxaca D, Higareda-Alvear V, Montes-Carreto LM, Martínez-Romero JC, Rosenblueth M and Servín-Garcidueñas LE. 2020. We and herbivores eat endophytes. *Microb. Biotech*., **14(4)**: 1282-99.

McCulloch JA, de Oliveira VM, de Almeida Pina AV, Pérez-Chaparro PJ, de Almeida L., de Vasconcelos JM, de Oliveira LF, da Yang, DEA, Rogez HLG., Cretenet M and Mamizuka EM. 2014. Complete genome sequence of *Lactococcus lactis* strain AI06, an endophyte of the Amazonian açaí palm. *Genome Announc*., **2(6)**: e01225-14.

Nayak S, Mukherjee A and Samanta S. 2017. Endophytic microorganisms of tropical tuber crops: Potential and perspectives. *J. Appl. Nat. Sci*., **9(2)**: 860-865.

Okoye JI and Ene GI. 2018. Effects of processing on the nutrient and anti-nutrient contents of tiger nut (*Cyperus esculentus* Lativum). *J. Food Sci. Technol.*, **1(1)**: 1-7.

Oladele AK and Aina JO. 2007. Chemical composition and functional properties of flour produced from two varieties of tiger nut (*Cyperus esculentus*). *Afr. J. Biotechnol*, **6(21)**: 2473-2476

Oliveira LC, Saraiva TD, Silva WM, Pereira UP, Campos BC, Benevides LJ, Rocha FS, Figueiredo HC, Azevedo V, Soares SC. 2017. Analyses of the probiotic property and stress resistance-related genes of . *Lactococcus lactis* subsp. lactis NCDO 2118 through comparative genomics and in vitro assays. *PLoS One* 12(4): e0175116.

Onovo JC and Ogaraku AO. 2007. Studies on some microorganisms associated with exposed Tigernut milk. *J. Biol. Sci*., **7(8)**: 1548–1550.

Onwuka GI. 2005. Food Analysis and Instrumentation: Theory and Practice. Lagos, Nigeria: Naphtali print. **5**:133-135.

Panigrahi S, Mohanty S and Rath CC. 2020. Characterization of endophytic bacteria *Enterobacter cloacae* MG00145 isolated from

Ocimum sanctum with Indole Acetic Acid (IAA) production and plant growth promoting capabilities against selected crops. *S. Afr. J. Bot*, **134**: 17-26.

Pennacchia C, Blaiotta G, Pepe O and Villani F. 2008. Isolation of *Saccharomyces cerevisiae* strains from different food matrices and their preliminary selection for a potential use as probiotics. *J. Appl. Microbiol*., **105(6)**: 1919-1928.

Phillippy BQ, Lin M and Rasco B. 2004. Analysis of phytate in raw and cooked potatoes. *J. Food Compos. Anal*., **17(2)**: 217-226.

Prasad AS. 2014. Zinc is an antioxidant and anti-inflammatory agent: its role in human health. *Front Nutr.,* **1(14)**: 1-10.

Rehman JU, Aktar N, Khan MY, Ahmad K, Ahmad M, Sultana S and Asif HM. 2015. Phytochemical screening and hepatoprotective effect of *Alhagi maurorum Boiss* (Leguminosae) against paracetamol-induced hepatotoxicity in rabbits. *Trop. J. Pharm. Res*., **14(6)**: 1029-1034.

Sabah MS, Shaker M and Moursy I. 2019. Nutritional Value of Tiger Nut (*Cyperus esculentus* L.) Tubers and Its Products. *Environ. Sci*., **14(1)**: 301-318.

Shinohara A and Watanabe H. 1996. Role of essential trace elements on sexual function and its disorder. *Nihon rinsho. Japanese J. Clin. Med*., **54(1)**: 155-161.

Suhandono S, Kusumawardhani MK, Aditiawati P. 2016. Isolation and molecular identification of endophytic bacteria from Rambutan fruits (Nephelium lappaceum L.) cultivar Binjai. *HAYATI J. Biosci*., 23(1): 39-44.

Tamura K and Nei, M. 1993. Estimation of the number of nucleotide substitutions in the control region of mitochondrial DNA in humans and chimpanzees. *Mol. Biol. Evol*., **10(3)**: 512-526.

Yaish MW, 2017. Draft genome sequence of the endophytic *Bacillus aryabhattai* strain SQU-R12, identified from *Phoenix dactylifera* L. roots. *Genome Announc*., **5(32)**: e00718-17.

Yang L, Zhu Y, He Z, Zhang T, Xiao Z, Xu R. and He J. 2020. Plantanone D, a new rare methyl-flavonoid from the flowers of *Hosta plantaginea* with anti-inflammatory and antioxidant activities. *Nat. Prod. Res*., **35(22)**: 4331-4337.

Yasser MM, Marzouk MA, El-Shafey NM and Shaban SA. 2020. Diversity and Antimicrobial Activity of Endophytic Fungi from the Medicinal Plant *Pelargonium graveolens* (geranium) in Middle Egypt. *Jordan J. Biol. Sci*., **13(12)**: 197-205.

Yerlikaya O. 2019. Probiotic potential and biochemical and technological properties of *Lactococcus lactis* ssp. *lactis* strains isolated from raw milk and kefir grains. *J. Dairy Sci*., **102(1)**: 124-134.

Zhao Y. Zeng D. Wang H. Qing X. Sun N, Xin J, Luo M, Khalique A, Pan K, Shu G and Jing B. 2019. Dietary Probiotic *Bacillus licheniformis* H2 Enhanced Growth Performance, Morphology of Small Intestine and Liver, and Antioxidant Capacity of Broiler Chickens Against *Clostridium perfringens*–Induced Subclinical Necrotic Enteritis. *Probiotics Antimicrob Proteins*, **12**:883-895.

JJBS

Volume 15, Number 4,December 2022
ISSN 1995-6673
Pages 611 – 619
https://doi.org/10.54319/jjbs/150409

Jordan Journal of Biological Sciences

Microbial Biomass Integrated with Sugarcane Wastes is a Proper Nutritive Supply for Nile Tilapia

Sayeda M. Ali[1,*], Ahmad M. Aboseif [2], Alkhateib Y. Gaafar[3], Ahamed D. El-Gamal[4] and Ahmed K. El-hammady[2]

[1] *Hydrobiology Department, Microbiology Laboratory, National Institute of Oceanography and Fisheries, NIOF, Aswan Research Station, Egypt ;*[2]*Fish nutrition Department, National Institute of Oceanography and Fisheries, NIOF, El-Qanater Research Station, Egypt;*[3]*Hydrobiology Department, Veterinary Research Division, National Research Center, Egypt ;*[4]*Botany Dept., Faculty of Science (boys), Al-Azhar University, Cairo, Nasr City, Egypt.*

Received: July 21, 2021; Revised: January 22, 2022; Accepted: February 9, 2022

Abstract

Single-cell proteins have a potential source for partial replacement of protein and lipids in animal feed. Also, using microorganisms in fish feed enhanced feed efficiency, growth performance, and disease resistance. The purpose of this study is to see if combining several microorganisms (*Azotobacter chroococcum*, *Chlamydomonas reinhardtii*, and baker's yeast) with sugarcane by-products may produce a low-cost fish feed formulation. A total of twelve treatments were completed (consisting of various microbial biomass combined with sugarcane by-products, and integrated with commercial fish feed in different levels, 0, 25, 50, 75, and 100 % w.w^{-1}). Nile tilapia (*Oreochromis niloticus*) were evaluated for growth performance, proximate composition, and histopathological examination. Results showed that using low amounts of the experimented formulations (25% and not more than 50% w.w^{-1}) increased fish productivity (weight gain and specific growth rate) and proximate compositions of fish without putting fish at risk. On the other hand, using higher levels from the combined diet (75, 100%) caused fish mortality. Although all the fish experimental treatments showed normal histological structure, the mortality of fish may be due to a lack of nutrients. In conclusion, this study is important for both the environment and the economy. More research is needed to extend the safe application of this study in aquaculture through the evaluation of fish in the field and for prolonged viability.

Keywords: Fish fodder, Sugarcane by-products, *Oreochromis niloticus*, *Azotobacter chroococcum*, *Chlamydomonas reinhardtii*, and baker's yeast.

1. Introduction

Aquaculture has become an important economic activity, particularly in developing countries (such as Egypt), to manage the shortage of protein food supplies (Gutierrez-Wing and Malone, 2006). Many factors limit aquaculture's expansion, including rising artificial feed prices due to the use of artificial substrates (organic and inorganic) and expensive protein sources (Delgado *et al.,* 2003). Therefore, many researchers have used alternative and complementary ingredients in feed formulations to reduce feed costs such as mango residue meal (Lima *et al.,* 2011), cassava sweep (Boscolo *et al.,* 2002), Pizzeria by-product (De Sousa *et al.,* 2019), and fenugreek seeds to improve the growth and immunity parameters in the *O. niloticus* (Abbas *et al*., 2019).

In a world where sugarcane industries remain one of the most popular agricultural industries, reusing sugarcane industrial by-products in aquaculture is critical. In Egypt, Egyptian sugar and integrated industries are considered the oldest and widespread industries. Actually, there are eight sugar factories distributed throughout the country from north to south, such as Abu Kerkas at Minya governorate, Gerga at Sohag governorate, Naga Hammadi, Deshna, Kous and Arment at Qena governorate, Edfu and Kom Ombo at Aswan governorate. The main product of these companies is sugar, and there are other related products such as ethanol, vinegar, glacial acetic acid, fodder yeast, solvents, animal feed, paper, and wood. In Egypt, Sugar factories operate intensively around six months from December to June in juicing, refining and sugar crystallization. During the other six months, the plants convert bagasse into wooden boards. The main by-products are bagasse, press mud (filter mud or clay industry), molasses, fly ash (produced during the burning of bagasse and causing air pollution), and wastewater effluent (discharged through the drainage pipe into a channel that finally reaches the Nile). Estimated amounts of by-products from sugarcane are 31% bagasse, 3.5% pressed clay (mud) and 4.5% molasses. According to Egyptian cultivated sugarcane, there are three million tons of bagasse, 316 thousand tons of filter mud and 370 thousand tons of molasses are generated annually (Nakhla and El Haggar, 2014). In fact, these by-products are used for different purposes; molasses is used in fermentation processes to produce fodder yeast, carbon dioxide, alcohol, vinegar, perfumes and medical solutions (Ryoheiet *al.,* 2003; Fadel *et al.,* 2013). In addition molasses, press mud and bagasse are used as a fertilizer in agriculture (Bento *et al.,* 2019) and aquaculture (Keshavanath and Shivanna, 2006; Raul *et al.,* 2020).

In addition, beneficial microorganisms serve a variety of roles in aquaculture productivity. They can be consumed directly or indirectly as food (Duncan and Moriarty, 1997), and they may help fish with their enzymatic digestion (Burford *et al.,* 2008). Microbes may also break down organic materials and transform nitrogenous compounds into microbial protein (Mishra *et al.,* 2008). Furthermore, some microorganisms can enhance the immune response of fish, such as *Azotobacter chroococcum* (Ali *et al.,* 2011) and *Saccharomyces cerevisiae* (Tukmechi *et al.,* 2011; Abdel-Tawwab *et al.,* 2020).

This study looks into the possibilities of making low-cost fish fodders by combining sugarcane industrial by-products with microbes, and the possibility of substituting a portion of the commercial diet. Consequently, this study aims to reduce both the environmental and economic problems of sugarcane and aquaculture industries.

2. Materials and Methods

2.1. Collection and chemical analysis of the sugarcane industry by-products

The Egyptian Sugar and Integrated Industries Company, Kom Ombo, Aswan, Egypt, provided the industrial waste, where all samples were obtained from inside the factory except wastewater effluent collected from the drainage tube. Pith was kept at room temperature, and industrial clay (press mud) was air-dried for 2-3 days before being packed and maintained at room temperature; molasses was kept in the refrigerator, and wastewater effluent was kept frozen. Chemical analyses for pith and press mud are presented in Table (1), where electrical conductivity (EC), pH, and total dissolved solids (TDS) were measured using CRISON multimeter (MM40+). Organic Carbon was determined using the method of Walkley-Black (Walkley, 1982). Nitrogen and ash content were determined according to the Association of Official Analytical Chemists, AOAC, (1995). Colorimetric methods were used to determine phosphorus (APHA, 1998). Heavy metals were determined using atomic absorption spectrometry (Perkin-Elmer 3110, USA) (APHA, 1998).

Table 1. Chemical composition of sugarcane solid wastes (pith and press mud)

Parameters	Pith	Press mud
pH	5.52	5.63
EC (dSm^{-1})	390	2910
Total dissolved solids (mgl^{-1})	250	1867
Moisture (%)	5.5	73.6
Total solids (%)	94.5	26.4
Ash (%)	6.4	4.9
Organic carbon (%)	20.7	9.5
Nitrogen (%)	3.3	4.2
Phosphorus (%)	1.0	1.4
Mn (ppm)	18.6	139.2
Zn (ppm)	34.5	65.4
Cu (ppm)	0.8	30.3
Fe (ppm)	460.5	627.3

2.2. Tested microorganisms

Three microorganisms were used: *Azotobacter chroococcum* isolated from the beach of Lake Nasser, microalgae *Chlamydomonas reinhardtii* isolated from soil sample collected from industrial zones of 6th October City and Baker's yeast obtained from an Egyptian market an accessible source of *Saccharomyces cervaicae*.

2.3. Fish experimental diets (preparation, composition and treatments)

Experimental diets (treatments) consisted of microbial biomass integrated with sugarcane by-products and mixed with commercial diet. Table (2) shows the experimental diets. The highest microbial biomass was obtained using batch culture technique. And culture media were prepared using sugarcane industrial wastewater effluent amendment with molasses and/or press mud as described in Ali *et al.* (2022). Briefly, *C. reinhardtii* was grown in the sugarcane wastewater effluent amendment with 1% molasses and 0.5% clay factor, *C. reinhardtii* batch culture were incubated at room temperature (30-32ºC) under continuous fluorescent light for 96 hours. *A. chroococcum* was grown in sugarcane wastewater effluent amendment with 1% molasses, 1% press mud and $0.5gl^{-1}$ $CaCO_3$, *A. chroococcum* batch culture were incubated in a rotary shaker of 100 rpm at 35 ± 2°C for 72 hours. Baker's yeast was grown in sugarcane wastewater effluent amendment with 5% molasses, baker's yeast batch culture were incubated in a rotary shaker of 100 rpm at 32 ± 2°C for 48 hours (Fig. 1A). After that, microbial biomass was mixed with sugarcane solid wastes (equal proportion of pith and dehydrated press mud was mixed well (Fig. 1B)); microbial cultures were added as 5 ml to each gram of the mixed sugarcane solid wastes, and mixed well (Fig.1C), to produce three basic mixtures. Mixture (1): containing only *A. chroococcum* integrated with sugarcane by-products (Azotobacter-integrated); mixture (2): containing microbial mix (*A. chroococcum*, *C. reinhardtii* and baker's yeast) integrated with sugarcane by-products (microbial mix integrated), and mixture (3): containing only sugarcane byproducts (only sugarcane byproducts). Microorganisms are estimated at about 10^7*Azotobacter* cells/g, 0.003 mg algal mass/g and 0.005 mg yeast mass/g. Then, each of the three previous mixtures was dried at room temperature (30-35°C) for 48 hours. Following that,

each of the three dried previous mixtures was combined with a commercial diet in different percentage (0, 25, 50, 75 and 100 % w.w^{-1}) as shown in Table (2). Proximate composition of the different experimental treatments is shown in Table (3).

Table 2. Treatment description for experimental diets.

Treatments	Treatment description
Control	100% commercial diet
Diets containing *A.chroococcum* integrated with sugarcane by-products (Azotobacter-integrated)	
25 % Azotobacter-integrated	Diet containing 25 % Azotobacter-integrated and 75% commercial diet.
50 % Azotobacter-integrated	Diet containing 50 % Azotobacter-integrated and 50 % commercial diet.
75 % Azotobacter-integrated	Diet containing 75 % Azotobacter-integrated and 25% commercial diet.
100 % Azotobacter-integrated	Diet containing 100 % Azotobacter-integrated.
Diets containing microbial mix integrated with sugarcane by-products (microbial mix-integrated)	
25 % microbial mix-integrated	Diet containing 25 % microbial mix-integrated and 75% commercial diet.
50 % microbial mix-integrated	Diet containing 50 % microbial mix-integrated and 50% commercial diet.
75 % microbial mix-integrated	Diet containing 75 % microbial mix-integrated and 25% commercial diet.
100 % microbial mix-integrated	Diet containing 100 % microbial mix-integrated
Diets containing only sugarcane byproducts (only sugarcane byproducts)	
25 % only sugarcane by-products	Diet containing 25 % only sugarcane by-products and 75% commercial diet.
50 % only sugarcane by-products	Diet containing 50 % only sugarcane by-products and 50% commercial diet.
75 % only sugarcane by-products	Diet containing 75 % only sugarcane by-products and 25% commercial diet.
100 % only sugarcane by-products	Diet containing 100 % only sugarcane by-products.

Table 3. Proximate composition for different experimental treatments

Treatments	CP%	EE%	Ash %
Control	24.85	11.95	7.97
25 % Azotobacter-integrated	21.42	10.90	11.74
50 % Azotobacter-integrated	17.99	9.85	15.50
75 % Azotobacter-integrated	14.56	8.80	19.27
100 % Azotobacter-integrated	11.13	7.75	23.03
25 % microbial mix-integrated	21.55	10.81	11.64
50 % microbial mix-integrated	18.25	9.67	15.31
75 % microbial mix-integrated	14.95	8.52	18.97
100 % microbial mix-integrated	11.65	7.38	22.64
25 % only sugarcane by-products	21.26	10.70	11.20
50 % only sugarcane by-products	17.66	9.46	14.43
75 % only sugarcane by-products	14.07	8.21	17.65
100 % only sugarcane by-products	10.47	6.96	20.88

CP%, crude protein % and EE%, ether extract %

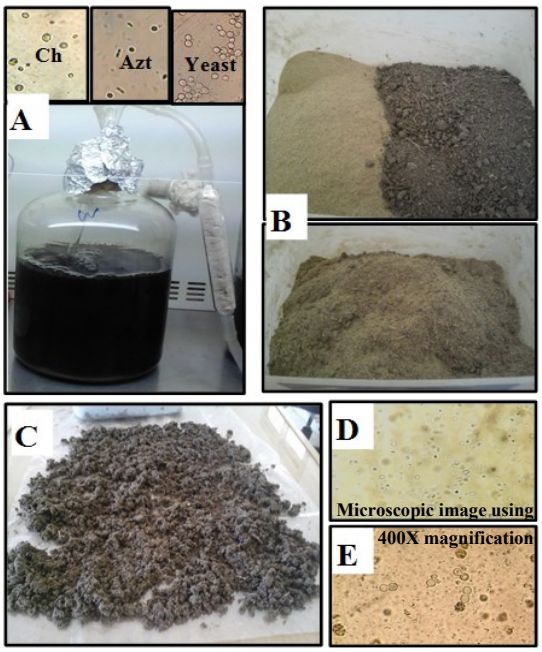

Figure 1.Preparation of experimental diets; (A) microbial biomass production (*Chlamydomonas reinhardtii* (Ch), *Azotobacter chroococcum* (Azt) and yeast) was obtained by using batch culture technique and sugarcane industrial wastewater effluent amendment with molasses and/or press mud, (B) equal ratio of pith and dehydrated press mud was mixed well, (C) microbial cultures were added as 5 ml to each gram of the mixed sugarcane solid wastes and mixed well. Three basic mixtures were produced; (D) diets containing *A. chroococcum* integrated with sugarcane by-products (Azotobacter-integrated), (E) diets containing microbial mix (Ch, Azt and yeast) integrated with sugarcane by-products (microbial mix-integrated) and diets containing only sugarcane byproducts (only sugarcane byproducts). After that, each of the previous three mixtures (after air drying) was mixed with a commercial diet in different percentage (0, 25, 50, 75 and 100 % $w.w^{-1}$) as shown in Table (2).

2.4. Fish feeding

One thousand Nile tilapia (*Oreochromis niloticus*) fingerlings with an average body weight of 0.5 ± 0.4 g (mean ± SE) were obtained from the General Authority for Fish Resources Development, Aswan, Egypt, and transferred to Aswan Research Station, National Institute of Oceanography and Fisheries, Aswan, Egypt. Fish were acclimated in glass aquaria (80 x 60 x 50 cm) for seven days, with two daily feedings of a basic diet.The aquaria were filled with clean, dechlorinated water with continuous aeration. The water temperature ranged from 28 to 30 °C, pH 7, and the dissolved oxygen was 7±1 mg/l. During the experimental period, the water was changed by 10 % daily. Fish were fed at 5% of their body weight daily in the first week, then 3 % of their body weight daily until the experiment ended. The experiment was conducted for 45 days, and fish samples were collected every two weeks.

2.4.1. Ethics Statement

The dealing with the experimental fish followed the National Institute of Oceanography and Fisheries institutional ethical guidelines of humane dealing with experimental animals. With no more than the least number of fish per group used, fish were anesthetized with eugenol either before sample collection or euthanized.

2.4.2. Fish analysis

2.4.2.1. Fish growth performance

Fish growth parameters (fish length and weight) were recorded for each treatment and control every 15 days. Total length was measured from the head to the end of the tail. Also, weight was measured in grams on a digital scale. Growth indices (weight gain (WG), specific growth rate (SGR), feed conversion efficiencies (FCE), the condition factor (CF), and the percentage of survival were calculated according to the following formula (Priestley *et al.*, 2006):

$$WG = \text{Final weight} - \text{Initial weight}$$

$$SGR = 100 \times \frac{(\ln \text{Final weight} - \ln \text{Initial weight})}{\text{Days of feeding}}$$

$$FCE = 100 \times \frac{(\text{Final weight} - \text{Initial weight})}{\text{Dry feed intake}}$$

$$CF = 100 \times \frac{\text{Total weight}}{\text{Total length}^3}$$

$$\text{Survival (\%)} = 100 \times \frac{\text{Final number of fish}}{\text{initial number of fish}}$$

2.4.2.2. Proximate composition

Diets and fish carcass samples were analyzed for dry matter (DM) and ash content, and crude protein (N x 6.25) using a Kjeltech auto-analyzer in accordance with AOAC guidelines (1995). Crude fat was measured according to Bligh and Dyer (1959). Nitrogen-free extract (soluble carbohydrate) was calculated by subtracting the difference.

2.4.2.3. Histopathological examination

Five fish were fixed whole for 24 hours in 10% phosphate-buffered formalin, then dehydrated with increasing concentrations of ethanol (70 %, 80 %, 90 %, 95 %, and 100 %), embedded in paraffin, and finally sectioned at 5 µm thick. Tissue sections were stained with Hematoxylin and Eosin (Presnell *et al.*, 1997) and examined by light microscopy (CX 41, Olympus, Japan), according to Roberts (2012).

2.5. Statistical Analysis:

Data were statistically analyzed using analysis of variance (ANOVA) using the STATISTICA computer programs.

3. Results

3.1. Fish growth performance

Figure (2) shows the effects of experimental diets on *O. niloticus* weight gain (WG), specific growth rate (SGR), feed conversion efficiencies (FCE), and condition factor. After 15 days of fish feeding, the treatment fed with 25% microbial mix–integrated diets had a higher WG (0.29 g) than the control (0.25 g), and after 30 days of fish feeding, the treatment fed with 25% Azotobacter–integrated diets had a higher WG (0.52 g) than the control (0.46 g). Moreover, after 45 days of fish feeding, several treatments recorded significantly higher WG values compared to control. In details, the treatment fed with 25, 50, 75% Azotobacter-integrated diets recorded 0.99, 1.18, 0.99 g WG respectively; the treatment fed with 25, 50% microbial mix-integrated diets recorded 0.99, 1.15g WG

respectively, and the treatment fed with 25% only sugarcane byproducts diets recorded 0.86 g WG, while control recorded 0.79 g WG (Fig. 2).

Statistically, the best SGR was recorded for 25 % microbial mix-integrated diets (2.95 SGR %), compared to control (2.58 SGR %) after 15 days of feeding, and 25 % Azotobacter-integrated diets (2.28 SGR %) and 25 % microbial mix-integrated diets (2.19 SGR %), compared to control (2.09 SGR %) after 30 days of feeding. After 45 days of feeding, the highest values were recorded in 25, 50, 75 % Azotobacter-integrated diets (2.36, 2.62, 2.69 SGR %, respectively); 25, 50 % microbial mix-integrateddiets (2.16, 2.58 SGR %, respectively) and 25 % only sugarcane byproducts mixed diet (2.36 SGR %) compared to control (2.04 SGR %).

Feed conversion efficiencies (FCE) values of fishes were improved, where after 15 days of fish feeding, the treatment fed with 25 % microbial mix-integrated diet recorded higher FCE (5.3 %) compared to control (4.5 %). In addition, after 30 days of fish feeding, the treatment fed with 25 % Azotobacter-integrated diet, and the treatment fed with 25 % microbial mix-integrated diet recorded higher FCE (12.9 and 12.2 % respectively) compared to control (11.4 %). Also after 45 days of fish feeding, significant increases ($P \leq 0.05$) in FCE in many treatments were recorded compared to control (19.8 %), such as FCE in 25, 50, 75 % Azotobacter-integrated diets (24.9, 29.5, 24.7 %, respectively); 25, 50 % microbial mix-integrated diets (24.8, 28.8 %, respectively).

Furthermore, Figure (2) showed that using experimental diets improved condition factor, particularly after 45 days of feeding, a phenomenon seen in all treatments except the highly concentrated one (100 % treatments), where 25, 50, 75% Azotobacter-integrated diets recorded 2.1, 3.1, 2.4 $gm.cm^{-3}$ respectively; 25, 50, 75% microbial mix-integrated diets treatments recorded 2.4, 2.1, 2.1 $gm.cm^{-3}$respectively, and 25, 50, 75% only sugarcane byproducts diets recorded 2.1, 1.7, 2.4 $gm.cm^{-3}$respectively, compared to control (1.1 $gm.cm^{-3}$).

Lower concentrations of experimental diets (25, 50%) had considerably higher values in both WG and SGR, regardless of time, but higher concentrations (75, 100%) were deemed unsuitable for fish feeding (Table 4). Also, *A. chroococcum*- integrated and microbial mix-integrated diets had a significant effect on weight gain and specific growth rate compared to the only sugarcane byproducts mixed diets. In addition, all treatments except highly concentrated ones (100% treatments) recorded higher condition factor values compared to control (Table 4).

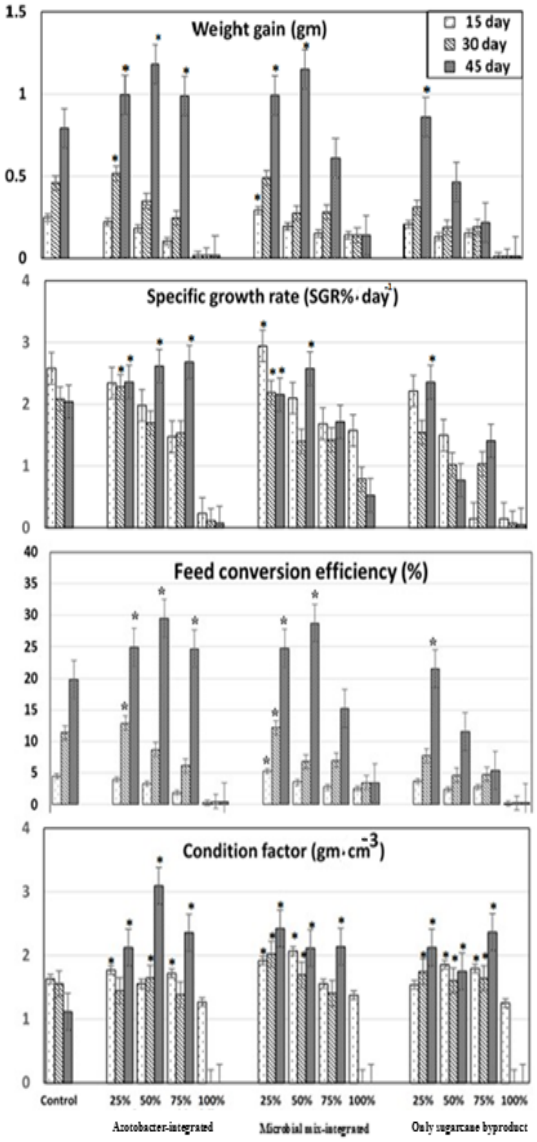

Figure 2. Growth performance (weight gain, specific growth rate, feed conversion efficiency and condition factor) for *Oreochromis niloticus* fingerlings feeding on *A. chroococcum* integrated with sugarcane by-products (Azotobacter-integrated) or microbial mix integrated with sugarcane by products (microbial mix-integrated) or only sugarcane byproducts after 15, 30 and 45 days of fish feeding.

Significant increases ($P \leq 0.05$), more than the control, at the same time are indicated by asterisks (*).

Table 4. Combined statistical analysis (regardless of sampling time) of weight gain, specific growth rate, feed conversion efficiencies and condition factor for different experimental treatments.

Treatments	WG (gm)	SGR (%)	FCE (%)	CF(gm. cm^{-3})
Control	0.50 ^{e}	2.24 ^{c}	11.91 ^{e}	1.43 ^{e}
25 % Azotobacter-integrated	0.58 ^{b}	2.33 ^{b}	13.92 ^{b}	1.78 ^{cd}
50 % Azotobacter-integrated	0.57 ^{c}	2.10 ^{d}	13.86 ^{c}	2.10 ^{a}
75 % Azotobacter-integrated	0.45 ^{g}	1.90 ^{f}	10.91 ^{g}	1.82 ^{c}
100 % Azotobacter-integrated	0.02 ^{l}	0.14 ^{k}	0.42 ^{l}	0.42 ^{f}
25 % microbial mix-integrated	0.59 ^{a}	2.43 ^{a}	14.10 ^{a}	2.12 ^{a}
50 % microbial mix-integrated	0.54 ^{d}	2.03 ^{e}	13.05 ^{d}	1.96 ^{b}
75 % microbial mix-integrated	0.35 ^{h}	1.61 ^{g}	8.34 ^{h}	1.70 ^{d}
100 % microbial mix-integrated	0.14 ^{k}	0.96 ^{i}	3.18 ^{k}	0.46 ^{f}
25 % only sugarcane by-products	0.46 ^{f}	2.04 ^{e}	10.98 ^{f}	1.80 ^{c}
50 % only sugarcane by-products	0.26 ^{i}	1.10 ^{h}	6.23 ^{i}	1.74 ^{d}
75 % only sugarcane by-products	0.19 ^{j}	0.86 ^{j}	4.34 ^{j}	1.93 ^{b}
100 % only sugarcane by-products	0.01 ^{m}	0.09 ^{l}	0.27 ^{m}	0.42 ^{f}

(WG) weight gain, (SGR) specific growth rate, (FCE) feed conversion efficiencies and (CF) condition factor

At the same column, means followed by the differ letter are significantly different ($P \leq 0.05$).

3.2. Proximate analysis of fish

Final proximate compositions of fish significantly affected by the treatments (Figure 3). Crude protein recorded significantly higher values in fish fed with 25, 50, 75% Azotobacter-integrated diets (65.7, 63.6, 67.3 % respectively), and 25, 50% microbial mix-integrated diets (65.1, 66.5% respectively), and 50, 75% only sugarcane byproducts diets (65.4, 65.2% respectively), compared with control (62.4%), while crude lipid concentrations in all treatments were lower than control (22.5%). Fish fed with 25% microbial mix-integrated diet and fish fed with 25% only sugarcane byproducts diet (21.4 and 20.7% respectively) did not significantly differ from control. The maximum nitrogen-free extract (soluble carbohydrate) was recorded in fish fed with 25% only sugarcane byproducts diet (3.7%), 50% microbial mix-integrated diet (2.9 %), 50% only sugarcane byproducts diet (2.7 %) and 50% Azotobacter-integrated diets (2.6 %), comparing to control (2.4%). Fortunately, lower ash content was recorded in fish fed with 25% microbial mix-integrated diet (11.4 %) compared to control (12.8 %), while fish fed with 100 % integrated diets recorded higher ash content (Fig. 3).

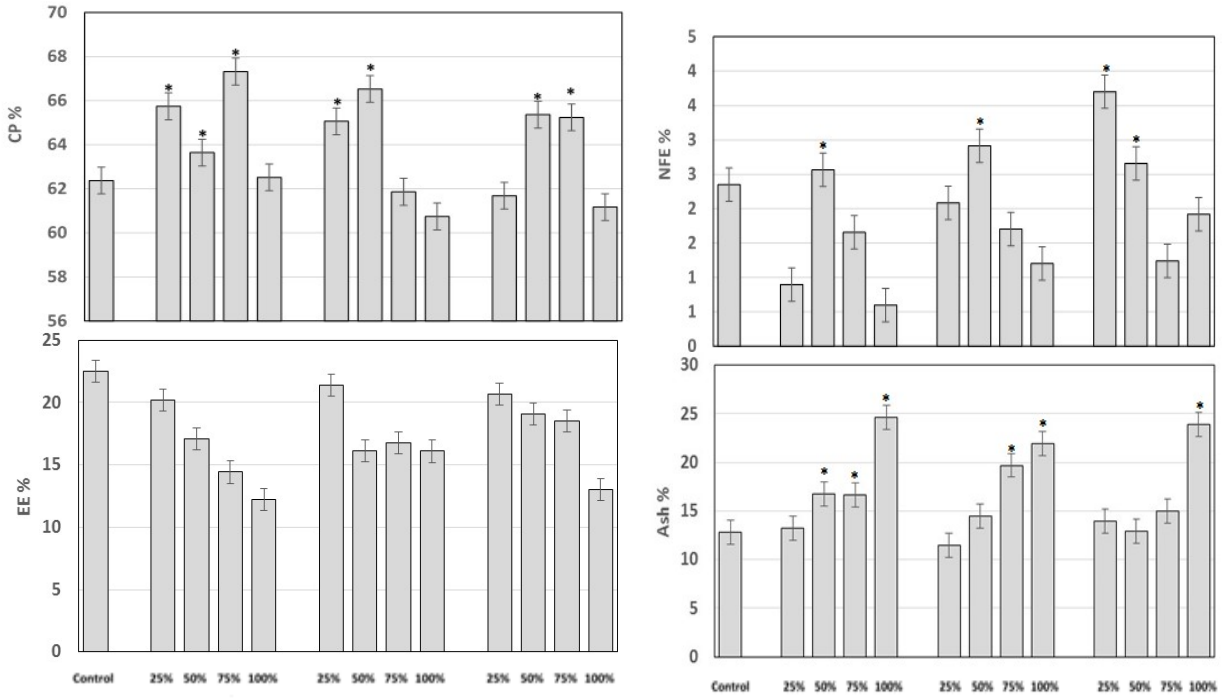

Figure 3. Final proximate compositions for *Oreochromisniloticus* fingerlings feeding on *A. chroococcum* integrated with sugarcane by-products (Azotobacter-integrated) or microbial mix integrated with sugarcane by-products (microbial mix-integrated) or only sugarcane byproducts after 45 days of fish feeding.

CP, crude protein; EE, ether extract; NFE, nitrogen free extract. Significant increases ($P \leq 0.05$), more than the control, are indicated by asterisks (*).

3.3. Histopathological examination

There were no significant differences in the histopathological picture of the different treatments as compared to the control. The majority of the tissues evaluated had normal histological structure (Fig. 4).

Although all experiment diets had no visible negative effects on fish health, there is a discernible effect on fish color (Fig. 5). As the amount of the experimental diet was increased, the blackness of the fish increased. The fishes that received 100 % of the experimental diet showed more darkness than those that received 75 % of the experimental diet. Moreover, fishes receiving 25 % of the experimental diets were more white and similar to the control (Fig. 5A, and 5B). This is related to the color of water (Fig. 5C and 5D), where the darkness of water increased with increasing the amount of the experimental diet (Fig. 5E).

Furthermore, the percentage of fish that survived was inversely proportional to the increase in the content of the experimental diets. It was higher in individuals who were given a 25% or 50% experimental diet, which is similar to a control diet (100 % survival rate). On the contrary, fishes receiving a 100 % experimental diet recorded more mortality than the others receiving 75 % experimental diet, and the mortality began in the 11th day of feeding. The lowest mortality was recorded in fishes fed with Azotobacter-integrated diets (Fig. 6).

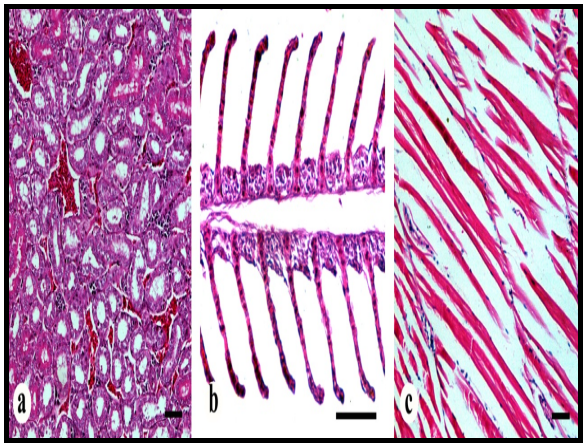

Figure 4. An example histopathological picture of *Oreochromis niloticus* fingerlings showing: (a) posterior kidney showing normal renal structure with moderate congestion, (b) Primary gill lamella showing normal structure, (c) musculature showing normal myofilamentos structure.

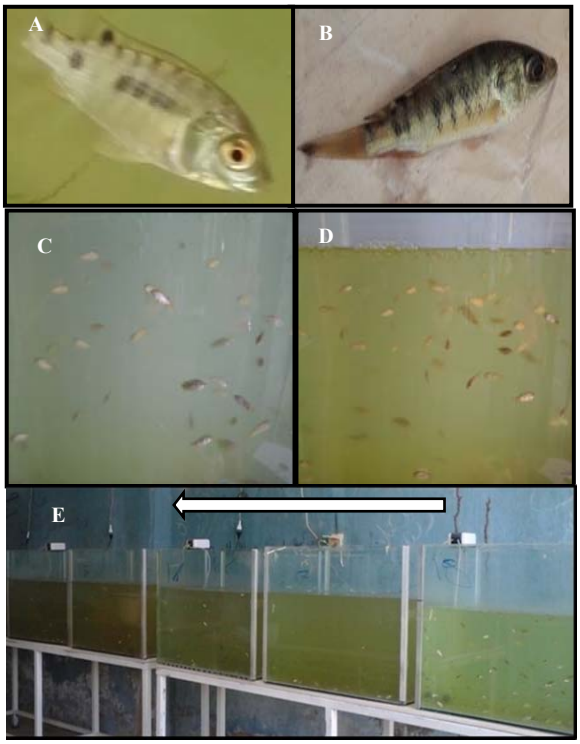

Figure 5. Photo image showing external color for *Oreochromis niloticus* fingerlings and water color for fish aquaculture. A, shows light and normal color of fish; B, shows dark color of fish, C, shows normal color of water aquaculture; D, shows dark color of water aquaculture which received high experimental diet; E, shows darkness of water aquaculture increased with increasing the amount of the experimental diet (with the direction of arrow).

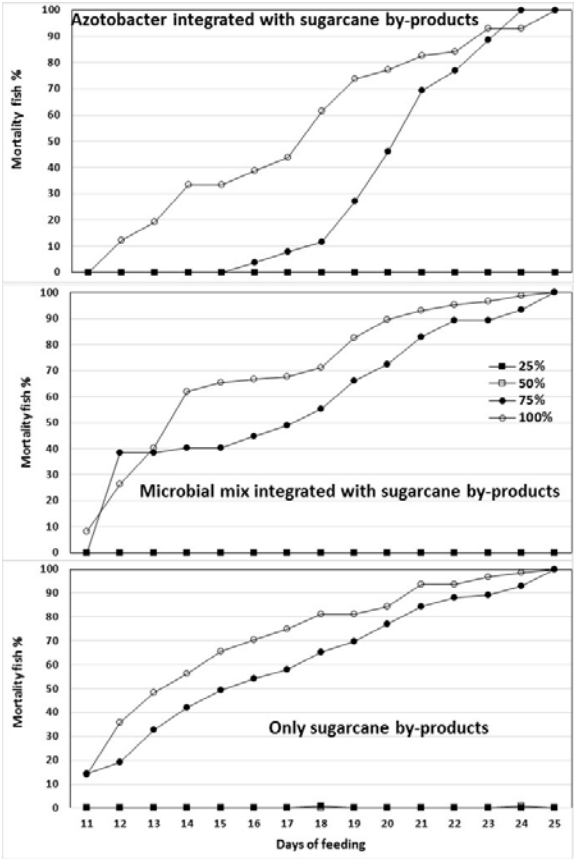

Figure 6. *Oreochromis niloticus* fingerlings mortality (%) from the eleventh day until the twenty-fifth day of feeding.

4. Discussion

Fish farming is an important industry, especially with the growing number of population and increasing food shortages. Using low-cost fish diets either in their ingredients or in their preparation is important to reduce the production cost and consequently increase fish productivity. In aquaculture, microorganisms play an important and useful role as nitrogen-fixing bacteria can raise net primary productivity, increase plankton production, and thereby increase fish biomass (Tripathy and Ayyappan, 2005; Ali *et al.,* 2015). Furthermore, nitrogen-fixing bacteria are used in controlling pathogens and improving the fish immunity system (Decamp *et al.,* 2008; Ali *et al.,* 2011).

The effect of sugarcane by-products on aquacultures have been studied by a number of researchers, such as Aderolu *et al*. (2013) who used molasses in the feed of catfish, and Gangadhar and Keshavanath (2012) who demonstrated that sugarcane bagasse can be applied in tank bottom as a substrate to increase rohu fish production.

The objective of this study is to provide low-cost, high-effective fish diets to lower fish production costs. The use of minor additions from the combination diet (25, 50%) considerably improved fish growing parameters, indicating that microbial biomass integrated with sugarcane wastes can replace a portion of the commercial fish diet (Table 4). On the other hand, using large amounts of combination diet (75, 100%) in fish feeding reduced fish growth performance, which could be due to a lack of accessible nutrients, as assessed by the approximation analysis (Table 3).

Furthermore, using microbial biomass integrated with sugarcane wastes increased fish growth performance more than using sugarcane by-products without microorganisms (only sugarcane byproducts), which indicates that microorganisms provided essential nutrients, such as essential amino acids, vitamins, and un-identified growth factors, increased digestibility of the raw materials, and catabolized anti-nutritional factors by the action of the produced enzymes. These results are compatible with the results of Keshavanath and Shivanna, 2006; Gangadhar and Keshavanath, 2012.

Moreover, the highest values for condition factor (used as an index to evaluate the aquatic ecosystem in which fish live) were found in fishes fed with 50% Azotobacter-integrated diets, which confirms that *Azotobacter* improved the water quality of aquaculture (Ali *et al.,* 2012). Additionally, the fish that were fed with 25% of microbial mix-integrated diets recorded higher carcass amounts of crude protein and lipid, which could be related to the high lipid content of *C. reinhardtii*cells (Yang *et al.,* 2018).

Despite the fact that there were no visible histological changes in fish tissues, the proportion of fish mortality increased with increasing amount of experimental diets. Fishes fed with 100 % integrated diets recorded higher mortality than those fed with 75 % integrated diet (Fig. 6). Furthermore, fish fed Azotobacter-integrated diets had a lower mortality rate than fish fed alternative treatments, although using higher amounts of the integrated diet (75 and 100 %) caused fish mortality and increased fish dark color. All of the fish samples from all of the experimental treatments lacked histological abnormalities in their tissues, indicating that nutrient deficiency was the cause of death.

5. Conclusion

It can be concluded that microbial mix–integrated sugarcane byproducts can be applied in Nile tilapia feeding after mixing with a commercial diet in between 25-50 %. Also, fodder factories must be complementary with sugarcane factories to reduce pollution and increase economic value. Further research is needed to confirm the safety and applicability of using such integrated diets in fish feeding and also to reduce feed cost through investigating the proper supplementary additions, especially with higher concentrations of integrated diets.

6. Declarations

Ethics approval and consent to participate: All applicable international, national, and/or institutional guidelines for the care and use of animals were followed by the authors. All the contributing authors consent to participate in this study.

Competing interests: The authors have no conflicts of interest to declare.

Authors Contributions SMA and ADE contributed to the study design and material preparation for microbial growth experiments. SMA and AKE contributed to the study design and material preparation for aquaculture experiments. AMA performed the proximate composition. AYG performed the histopathological examination.

SMA collected, analyzed and interpreted data and was a major contributor in writing the manuscript. All authors read and approved the final manuscript.

Funding

Not applicable.

Consent to participate

Not applicable.

Consent for publication

Not applicable.

Code availability

Not applicable.

Data availability

All data generated or analyzed during this study are included in this published article.

Acknowledgments

We would like to thank the General Authority for Fish Resources Development, Aswan, Egypt for providing the required fish. Thanks are also due to Mr. Ahmad El-Badry and Mr. Hassan El-Badry for their sincere efforts during the experiment.

References

Abbas WT, Abumourad IMK, Mohamed LA, Abbas HH, Authman MMN, Soliman WSE and Elgendy MY. 2019. The Role of the Dietary Supplementation of Fenugreek Seeds in Growth and Immunity in Nile Tilapia with or without Cadmium Contamination. *Jordan J Biol Sci*., **12 (5)**: 649 – 656.

Abdel-Tawwab M, Adeshina I and Issa ZA. 2020. Antioxidants and immune responses, resistance to *Aspergilus flavus* infection, and growth performance of Nile tilapia, *Oreochromis niloticus*, fed diets supplemented with yeast, *Saccharomyces serevisiae*. *Anim. Feed Sci. Technol*., **263**:114484.

Aderolu AZ, Aarode OO and Bello RA. 2013. Inclusion effect of graded levels of molases in the diet of *Clarias gariepinus* juvenile. *Int. J. Fish. Aquac.*, **5 (7)**: 172-176.

Ali SM, Aboseif AM, El-Gamal AD and El-hammady A. 2022. Microbial biomass production using sugarcane industrial by-products and their application to Nile tilapia aquaculture. *Res. J. Biotechnol*., 17 (5): 130 -142.

Ali SM, Nasr HS and Abbas MT. 2015. Using diazotrophic bacteria for biomass production of microalgae. *EJER,* **3**: 41-52.

Ali SM, Nasr HS and Abbas WT. 2012. Enhancement of *Chlorella vulgaris* growth and bioremediation ability of aquarium wastewater using diazotrophs. *Pakistan J Biol Sci*, **15 (16)**: 775-782.

Ali SM, Wafa MIA and Abbas WT. 2011. Evaluation of *Azotobacter* and *Azospirillum* biofertilizers as a probiotics in *Oreochromis niloticus* aquaculture. *J Fish Aquat Sci*, **6 (5)**: 535-544.

AOAC, Association of Official Analytical Chemists. 1995. **Official Methods of Analysis**. 16th Edition, Washington DC.

APHA, American Public Health Association. 1998. **Standard methods for the examination of water and wastewater,** 20th edition. American Public Health Association, Washington, DC.

Bento LR, Castro AJR, Moreira AB, Ferreira OP, Bisinoti MC and Melo CA. 2019. Release of nutrients and organic carbon in different soil types from hydrochar obtained using sugarcane bagasse and vinasse. *Geoderma*, **334**: 24–32.

Bligh EG and Dyer WJ. 1959. A rapid method for total lipid extraction and purification. *Can. J. Biochem. Physiol.* **37**: 911-917.

Boscolo WR, Hayashi C and Meure F. 2002. Farinha de Varredura de Mandioca (*Manihot esculenta*) na Alimentacao de Alevinos de Tilapia do Nilo (*Oreochromis niloticus* L.). *R. Bras. Zootec*. **31**: 546–551.

Burford MA, Alongi DM, McKinnon AD and Trott LA. 2008. Primary productivity in a tropical macrotidal estuary, Darwin Harbour, Australia. *Estuar. Coast. Shelf Sci.* **79**: 440-448.

De Sousa AA, Pinho SM, Rombenso AN, de Mello GL and Emerenciano MGC. 2019. Pizzeria by-product: A complementary feed source for Nile tilapia (*Oreochromis niloticus*) raised in biofloc technology?. *Aquaculture* **501**: 359–367.

Decamp O, Moriarty DJW and Lavens P. 2008. Probiotics for shrimp larviculture: review of field data from Asia and Latin America. *Aquac. Res.* **39**: 334–338.

Delgado LC, Wada N, Rosegrant WM, Meijer Sand Ahmed M. 2003. Fish to 2020: Supply and Demand in Changing Global Markets. *IFPRI*, Washington, D.C. pp. 237

Duncan T and Moriarty S. 1997. **Driving Brand Value: Using Integrated Marketing to Drive Stakeholder Relationships**. New York: McGraw-Hill.

Fadel M, Keera AA, Mouafi FE and Kahil T. 2013. High level ethanol from sugar cane molasses by a new thermotolerant *Saccharomyces cerevisiae* strain in industrial scale. *Biotechnol. Res. Int.*, Article ID 253286, 6 pages.http://dx.doi.org/10.1155/2013/253286

Gangadhar B and Keshavanath P (2012). Growth performance of rohu, Labeo rohita (Ham.) in tanks provided with different levels of sugarcane bagasse as periphyton substrate. *Indian J. Fish*. **59 (3)**: 77-82.

Gutierrez-Wing MT and Malone R. 2006. Biological filters in aquaculture: Trends and research directions for freshwater and marine applications. *Aquac. eng.* **34 (3)**:163-171.

Keshavanath P and Shivanna GB. 2006. Evaluation of sugarcane by-product pressmud as a manure in carp culture. *Bioresour. Technol.* **97**: 628–634.

Lima MR, Ludke MCMM, Neto FFP, Pinto BWC, Torres TR and Souza EJO. 2011. Farelo de residuo de manga para tilapia do Nilo. *Anim. Sci*. **33**: 65–71.

Mishra VK, Upadhyay AR, Pandey SK and Tripathi BD. 2008. Concentrations of heavy metals and aquatic macrophytes of Govind Ballabh Pant Sagar an anthropogenic lake affected by coal mining effluent. *Environ. Monit. Assess.* **141**: 49–58.

Nakhla DA and El Haggar S. 2014. Environmentally balanced sugarcane industry in Egypt. http://uest.ntua.gr/conference2014/pdf/nakhla.pdf

Presnell JK, Schreibman MP and Humason GL. 1997. **Humason's animal tissue techniques**. Johns Hopkins University Press.

Priestley SM, Stevenson AE and Alexander LG. 2006. Growth rate and body condition in relation to group size in black widow tetras (*Gymnocorymbus ternetzi*) and common goldfish (*Carassiusauratus*). *J. Nutr*. **136**: 2078S-2080S.

Raul C, Bharti VS, Dar Jaffer Y, Lenka S and Krishna G. 2020. Sugarcane bagasse biochar: Suitable amendment for inland aquaculture soils. *Aquac. Res.* https://doi.org/10.1111/are.14922

Roberts RJ. 2012. Fish pathology. John Wiley & Sons

Ryohei UENO, Naoko HS and Naoto U. 2003. Fermentation of molasses by several yeasts from hot spring drain and phylogeny of the unique isolate producing ethanol at 55°C. *J. Tokyo Univ. Fish.* **90**: 23-30.

Tripathy PP and Ayyappan S. 2005. Evaluation of *Azotobacter* and *Azospirillum* as biofertilizers in aquaculture. *World J. Microbial. Biotechnol*. **21**: 1339-1343.

Tukmechi A, Andani HRR, Manaffar R and Sheikhzadeh N. 2011. Dietary administration of beta-mercapto-ethanol treated *Saccharomyces cerevisiae* enhanced the growth, innate immune response and disease resistance of the rainbow trout, *Oncorhynchus mykiss*. *Fish Shellfish Immunol* **30 (3)**: 923-928.

Walkley A. 1982. Walkley-Black method. In: Page AL (Ed.) **Methods of soil analysis. Part 2. Chemical and microbiological properties.** Madison: American Society of Agronomy Inc., Soil Science Society of America Inc.; 1982. p. 570–1.

Yang LCJ, Qin SZM, Jiang Y, Hu L, Xiao P, Hao W, Hu Z, Lei A and Wang J. 2018. Growth and lipid accumulation by different nutrients in the microalga *Chlamydomonas reinhardtii*. *Biotechnol. Biofuels* **11**: 40.

JJBS

Volume 15, Number 4,December 2022
ISSN 1995-6673
Pages 621 – 627
https://doi.org/10.54319/jjbs/150410

Jordan Journal of Biological Sciences

Consolidated Bioethanol Production using *Trichoderma asperellum* B1581

Mona Fatin Syazwanee Mohamed Ghazali, Muskhazli Mustafa*, Nur Ain Izzati Mohd Zainudin and Nor Azwady Abd Aziz

Department of Biology, Faculty of Science, Universiti Putra Malaysia, 43400 UPM Serdang, Selangor, Malaysia

Received: July 21, 2021; Revised: December 30, 2021; Accepted: January 31, 2022

Abstract

Consolidated bioprocessing (CBP) is an alternative commercial process that combines all essential processes in a single bioreactor for the conversion of lignocellulosic biomass into ethanol. The challenge in the development of CBP is to find microorganisms with crucial properties for the utilisation of lignocellulosic materials to produce bioethanol. Also, it can be difficult to determine the optimal culture conditions for all processes to occur simultaneously. Therefore, this study focused on the potential of *Trichoderma asperellum* B1581 to produce ethanol and optimised the physicochemical parameters required for paddy straw waste conversion via CBP. Six parameters (days of saccharification, saccharification temperature (°C), days of fermentation, fermentation temperature (°C), medium level (%, v/v), and substrates loading (%, w/v)) were optimised in one-factor-at-a-time (OFAT) analysis via Response Surface Methodology (RSM). The numerical optimisation was statistically validated by comparing the volume of ethanol produced to the volume predicted by the RSM. *T. asperellum* B1581 produced 0.94 g/L bioethanol in CBP and is a more convenient, manageable and cost-effective process as all the crucial steps were performed by only one organism.

Keywords: Bioethanol production; Consolidated bioprocessing; Fermentation; Optimization; Paddy straw; Response surface method; Saccharification.

1. Introduction

Non-renewable fossil fuels such as coal, oil and natural gas have been known to be the primary sources of energy for many decades (Lugani *et al.*, 2020). With the growing of human population as well as urbanization in the 21st century and to continue pursuing current development goals, energy availability has emerged as one of the key problems that needs to be resolved. (Awogbemi *et al.*, 2021). Several alternatives have been considered by researchers, particularly biofuels which primarily depend on the type of biomass (Afolalu *et al.*, 2021). Biofuels can be categorized into four generations: (1) food-based crops containing starch, (2) lignocellulosic-based biofuels, (3) algal biomass and (4) genetically modified algae with high lipid content (Robak and Balcerek, 2020). Since the first-generation biofuels faced major controversy due to the food versus fuel issue, the direction of research interest has been shifted towards the second-generation biofuels by utilizing lignocellulosic biomass as renewable feedstock for biofuel production (Dey *et al.*, 2020). Lignocellulosic biomass is one of the most abundantly available bioresource with an annual global yield of 1.3 billion tons, and hydrolysis of this material would result in the release of valuable reducing sugars which are crucial for the production of biofuels such as bioethanol and biogas (Baruah *et al.*, 2018). Bioethanol is a high-energy substitute fuel to gasoline with an excellent clean-burning system and commonly blended with conventional gasoline for the use in automobile as an effort to reduce greenhouse gases emissions (Chang *et al.*, 2018). In bioethanol production, several processes such as pretreatment, saccharification and fermentation are the predominant steps that need to be executed in an efficient way (Kumar *et al.*, 2020). Four significant process configurations are required for efficient lignocellulose-based biofuel production: separate hydrolysis and fermentation (SHF), simultaneous saccharification and fermentation (SSF), simultaneous saccharification and co-fermentation (SSCF), and consolidated bioprocessing (CBP) (Parisutham *et al.*, 2014).

The consolidated process involves the integration of both saccharification and fermentation into one bioreactor, hence reducing the number of stages in the bio-refinery (Zoglowek *et al.*, 2016). The resulting process is like SSF, but without the addition of exogenous enzyme (Teter *et al.*, 2014). CBP also involves the use of a microorganism or a group of compatible microorganisms for substrate hydrolysis and fermentation within a single reactor (Olson *et al.*, 2012; Ho *et al.*, 2012). However, the most difficult step in CBP is the selection of an appropriate microorganism or microbial consortium that secretes the hydrolytic enzyme required for the lignocellulosic material to produce ethanol (Paulova *et al.*, 2015). A study by Bech *et al*. (2015) proved the ability of *T. asperellum* to hydrolyse pretreated duckweed, producing up to 60% glucose yield, and hence this fungus is a potential

* Corresponding author. e-mail: muskhazli@upm.edu.my.

organism for on-site enzyme production. *Trichoderma asperellum* has also been used in several biochemical processes due to its impressive features to boost cellulose production and cause less catabolite suppression (Nava-Cruz *et al.*, 2016). *Trichoderma asperellum* B1581 was chosen as a subject for this study based on a previous study by Syazwanee *et al.* (2019) in which the strain was identified as the best producer of exoglucanase (at 2.37 ± 0.34 U/mL) and β-glucosidase (3.00 ± 0.15 U/mL). Exoglucanase, also known as cellobiohydrolase (CBH), is a primary exocellulase that converts cellulose into cellobiose where its high production is crucial because it makes up 60% of the enzyme cocktail (Brady et al., 2015). β-glucosidase also plays a significant role in bioethanol production to eliminate cellobiose inhibition (Wang *et al.*, 2012) and has become a conundrum in producing bioethanol.

Besides selecting a productive strain, optimising the culture conditions is crucial to systematically improve the efficiency of ethanol production by adding or eliminating components from the formulation, which also results in more stability and reproducible culture conditions (Dong *et al.*, 2012). Therefore, this study was designed to determine the effectiveness of *T. asperellum* B1581 as single culture in producing ethanol, as well as optimising the physicochemical parameters for paddy straw waste conversion based on one-factor-at-a-time (OFAT) analysis and Response Surface Methodology analysis (RSM).

2. Materials and Methods

2.1. Fungal isolates

Trichoderma asperellum B1581 was obtained from the Mycology Laboratory, Faculty of Science, Universiti Putra Malaysia and grown on Potato Dextrose Agar (PDA) at 28°C ± 2°C for 7 days.

2.2. Culture conditions

The culture medium was prepared by using 1% (w/v) pretreated paddy straw (Syazwanee *et al.*, 2018) mixed into 25 mL of 10% (v/v) basal medium ($(NH_4)2SO_4$ 1.4 g/L; KH_2PO_4 2.0 g/L; $CaCl_2$ 0.3 g/L; $MgSO_4.7H_2O$ 0.3 g/L; $CoCl_2$ 2.0 g/L) with 1 mL of trace element ($MnSO_4.H_2O$ 1.56 g/L; $FeSO_4.7H_2O$ 5.0 g/L; $ZnSO_4.7H_2O$ 1.4 g/L), then sterilised at 121 ± 0.5°C for 15 min. The medium was inoculated with fungal spore suspensions once cooled.

The spore suspensions of *T. asperellum* B1581 was prepared from well sporulated colonies and were suspended in sterilized water. The concentrations of the spore suspensions were calculated using haemocytometer, and the concentrations were adjusted to 1 x 10^6 spore/mL (Mauch *et al.*, 1988).

2.3. One-Factor-At-a-Time (OFAT) analysis

In order to determine dynamic variables, one-factor-at-a-time (OFAT) analysis was design to investigate one factor while other variables were kept constant (Abou-Taleb and Galal, 2018). The CBP culture conditions were based on a preliminary study, 150 rpm, 30°C ± 0.5°C for saccharification and fermentation processes, 3 days of saccharification and 3 days of fermentation. The effect of six parameters on ethanol production, days of saccharification, saccharification temperature (°C), days of fermentation, fermentation temperature (°C), medium level (%, v/v), and substrates loading (%, w/v) were assessed using the Megazyme® ethanol assay kit in triplicates (Cutzu and Bardi, 2017). The data obtained from OFAT was analysed by using mean ± standard deviation at 95% confidence limit ($p < 0.05$) (Wahid and Nadir, 2013).

2.4. Response Surface Methodology (RSM)

The optimisation of RSM was performed using a Central Composite Design (CCD) via Design-Expert software Version 6.0.8 (Stat-Ease Inc., Minneapolis, MN, USA) with full expression of the quadratic model. In Central Composite Design (CCD), all factors were studied in five levels (-α, -1, 0, +1, +α). The coded variables were used to explain the ranges used in CCD such as extreme predicted point (±α), central point (0) and axial point (±1). For each response, optimum points were predicted based on the variables input and followed the second-order polynomial in the quadratic model. The amount of ethanol was quantified for each set-up and was subjected to analysis of variance (ANOVA) by evaluating the goodness-of-fit and significance of each parameter in the regression model (Said and Amin, 2015).

The prediction of model on each species of fungi producing ethanol was based on the response of the independent variables and the interactions were developed from the following equation (Eq. 1):

$$Y = \beta_0 + \beta_1 A + \beta_2 B + \beta_3 C + \beta_4 D + \beta_5 E + \beta_6 F + \beta_{11} A^2 + \beta_{22} B^2 + \beta_{33} C^2 + \beta_{44} D^2 + \beta_{55} E^2 + \beta_{66} F^2 + \beta_{12} AB + \beta_{13} AC + \beta_{14} AD + \beta_{15} AE + \beta_{16} AF + \beta_{23} BC + \beta_{24} BD + \beta_{25} BE + \beta_{26} BF + \beta_{34} CD + \beta_{35} CE + \beta_{36} CF + \beta_{45} DE + \beta_{46} DF + \beta_{56} EF \quad \text{(eq. 1)}$$

The equation of Y is the amount of ethanol produced, β_0 is the interception of coefficient, $\beta_1, \beta_2, \beta_3, \beta_4, \beta_5, \beta_6$ were linear coefficients, $\beta_{11}, \beta_{22}, \beta_{33}, \beta_{44}, \beta_{55}, \beta_{66}$ were quadratic coefficients, $\beta_{12}, \beta_{13}, \beta_{14}, \beta_{15}, \beta_{16}, \beta_{23}, \beta_{24}, \beta_{25}, \beta_{26}, \beta_{34}, \beta_{35}, \beta_{36}, \beta_{45}, \beta_{46}, \beta_{56}$ represent interactive coefficients and symbols A, B, C, D, E and F were hours of saccharification, temperature of saccharification, hours of fermentation, temperature of fermentation, medium level and substrate level respectively.

3. Results

3.1. One-Factor-At-A-Time (OFAT) analysis

The OFAT analysis was conducted in sequence with the temperature of fermentation was the first parameter tested from 25°C to 45°C with an interval of 5°C. The most ethanol (0.06 ± 0.02 g/L) was produced at 30°C for fermentation after 3 days of saccharification and 3 days of fermentation with the other parameters remaining constant. The fermentation at other points of temperature failed to produce any ethanol. Throughout the evaluation, the most optimum days for both saccharification and fermentation processes by *T. asperellum* B1581 were 2 days (48 h) respectively; making a total of 4 days (96 h) for both processes to complete. The amount of ethanol produced during this period was 0.05 ± 0.01 g/L. Pertain to medium and substrates loading, *Trichoderma asperellum* B1581 produced up to 1.35 ± 0.02 g/L and 1.41 ± 0.07 g/L with 3% (w/v) substrate loading and 10% (v/v) basal medium. Generally, the amount of ethanol produced by *T. asperellum* B1581 decreased as the substrate loading increased over 3 % (w/v) and the volume of medium increased more than 10% (v/v). The final parameter analysed was the temperature of saccharification and as for

T. asperellum B1581, the volume of ethanol produced was the highest during saccharification at 30°C. The OFAT analysis managed to identify a compromise temperature for both saccharification and fermentation processes in CBP, which was 30°C ± 0.5°C. The summary of OFAT analysis is shown in Table 1.

Table 1. The pre-determine ranges for each of the parameters in one-factor-at-a-time (OFAT) and the optimum point for the highest ethanol production by *Trichoderma asperellum* B1581

No.	Parameters	Control setting	Ranges	Optimum point
1.	Temperature of fermentation	30 ± 0.5°C	25°C - 45 ± 0.5°C	30°C
2.	Days of saccharification	3 days	1 day – 5 days	2 days
3.	Days of fermentation	3 days	1 day – 5 days	2 days
4.	Substrates loading (w/v)	1%	1% - 7%	3%
5.	Medium level (v/v)	10%	10% - 90%	10%
6.	Temperature of saccharification	30 ± 0.5°C	25°C - 45 ± 0.5°C	30°C

3.2. Response Surface Methodology (RSM) analyses for optimisation

In RSM, the period of saccharification and fermentation was converted into hours for a more precise value. Five-level and six factors were used in a fractional factorial design to evaluate the effects of synthesis parameters, including hours of saccharification (h), saccharification temperature (°C), hours of fermentation (h), fermentation temperature (°C), medium level (%, v/v) and substrates loading (%, w/v). The optimum point from the OFAT analysis was used as the centre point in the CCD. There were 86 settings, including a 10-centre point set-up generated by the software and experiments were carried out on *T. asperellum* B1581. The adequacy of the model was validated by checking the statistical properties listed in the fit summary table such as ANOVA, lack-of-fit, R-squared, adjusted R-squared, predicted R-squared and adequate precision. The F-value for *T. asperellum* B1581 at 7.92 (Table 2) implied that the significant value, with only a 0.01% chance, happened due to noise. The validity of the null hypothesis was significant with a Probable F-value of <0.05, indicating less than 5% possibility, in which regression parameters were zero.

Table 2. Statistical summary of ethanol production by *T. asperellum* B1581

Source	Value
Std. dev.	0.19
Mean	0.26
R-Squared (R^2)	0.79
Adjusted R-Squared	0.69
Predicted R-Squared	0.39
PRESS	5.98
Adequate Precision	11.82

A regression model displays lack-of-fit when it is unable to adequately describe the functional relation between the experimental factors and the response variable. The lack-of-fit for *T. asperellum* B1581 was 2.11 with 0 pure error. The R-square (R^2) value varied between 0 and 1, with the value closer to 1, accounting for a larger proportion of the variance by the model. The quadratic regression model showed that the value of the determination coefficient (R^2) was 0.79 with the fit explaining 79% of the total variation in the data.

The ratio for *T. asperellum* B1581 was 11.82, indicating an adequate signal. Despite the inadequacy in the predicted R^2 value for the *T. asperellum* B1581 model, the ratios in adequate precision proved these models could be used to navigate the design space, and thus effectively navigate three dimensional (3D) structures (Figure 1).

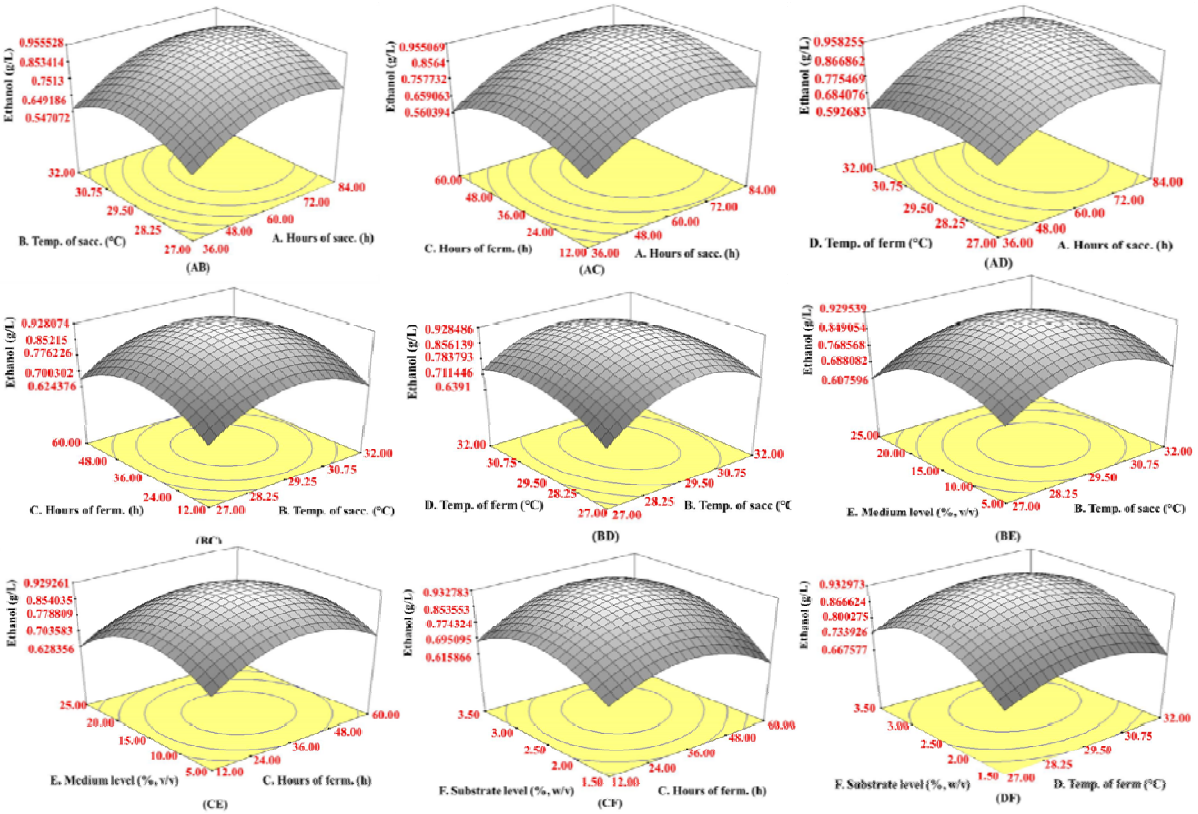

Figure 1. The development of 3D surface plot-based response of ethanol production produced by *T. asperellum* B1581 with interaction among parameters. (A) hours of saccharification, (B) temperature of saccharification, (C) hours of fermentation, (D) temperature of fermentation, (E) medium level and lastly (F) substrates loading.

The amount of ethanol produced by *T. asperellum* B1581 can be expressed by Equation (Y_1):

Y_1 = + 0.93 + 0.11A + 0.021B + 0.016C + 0.019 D - 0.031 E + 0.048 F - 0.12A2 - 0.14B2 - 0.13C2 - 0.082D2 - 0.13E2 - 0.12F2 + 0.013AB + 0.010AC + 0.036AD - 0.031AE + 0.042AF - 2.703E-003BC - 0.029BD - 6.719E-004BE - 0.020BF + 2.516E-003CD - 5.453E-003CE + 0.034CF - 0.010DE + 9.547E-003DF - 0.037EF (eq. 2)

Symbols A, B, C, D, E, F represent the coded variables used in CCD: (A) hours of saccharification, (B) saccharification temperature, (C) hours of fermentation, (D) fermentation temperature, (E) medium level and lastly (F) substrates loading. The positive and negative signs in these equations represent the synergy and antagonistic effects among the variables, respectively. The predicted ethanol production (0.96 g/L) was compared to the actual ethanol production (0.94 g/L) for validation purposes (Table 3), with no significant difference in production. The settings of OFAT analysis were also compared with the optimization set-up generated by RSM software to observe the differences between the set-up as well as the amount of ethanol produced. The response of ethanol production by *T. asperellum* B1581 using optimized set-up was rather low (0.94 g/L) compared to the value of ethanol produced in OFAT analysis (1.35 g/L).

Table 3: The optimization settings recommended by RSM with comparison to settings produced by OFAT analysis

	Saccharification		Fermentation		Basal medium		Ethanol (g/L)	
	Hours (h)	Temp. (°C)	Hours (h)	Temp. (°C)	Medium (%,v/v)	Substrate (%, w/v)	Predicted	Actual
RSM Set-up	67.72	29.58	32.9	29.79	12.42	2.84	0.96	0.94
OFAT analysis	48	30	48	30	10.00	3.00	1.35	

4. Discussion

One of the main challenges of consolidated bioprocessing (CBP) is the difficulty of establishing optimum culture conditions for microbial growth, saccharification and fermentation processes. Thus, the culture (medium and substrate loading), saccharification (temperature and days) and fermentation (temperature and days) were evaluated to determine the maximum ethanol production by lignocellulolytic fungi in aerobic conditions via CBP. The main problem in CBP is that the temperature needs to be a compromise between the optimal temperature for saccharification of biomass and fermentation to take place. Even though the saccharification temperature is best at 50°C (Amarasekara,

2013), the current findings with saccharification temperature at 30°C are essential for efficient ethanol production via CBP in tropical countries, helping to reduce the cooling and water costs during fermentation, subsequently reducing the total production costs (Murata *et al.*, 2015). Other parameters that influence the cost of production is the incubation period, with the optimum period for both saccharification and fermentation by *T. asperellum* B1581 being 2 days respectively, thus a total of 4 days for both processes to produce approximately 0.05 ± 0.01 g/L ethanol. Four days for CBP was reported previously (Nadeem *et al.*, 2015), and a longer incubation exceeding the optimum period will result in a low amount of ethanol due to nutrient depletion and diminished growth conditions (Fahrizal *et al.*, 2013).

Regarding medium and substrates loading, this study had observed the similar trend reported previously that high substrate concentrations severely limit the ethanol yield commercially, increasing the cost of processing, especially in downstream distillation (Zhao *et al.*, 2015). In order to create more economical process, substrate concentrations need to be optimized as the increasing of viscosity material may lead to end-product inhibition, reducing enzyme mobility and prevent hydrolysis process to take place (Mardawati *et al.*, 2019). In the context of medium volume, further increment will cause a high degree of aerobic metabolism, which utilizes sugar substrate but zero ethanol production (Arifa and Sarwar, 2012). Thus, optimisation of the fermentation or cultural conditions is a crucial step to achieve an optimum ratio of the metabolite production and cost before semi-pilot/pilot production plans (Shaymaa *et al.*, 2019).

The OFAT analysis developed a setting for optimisation of bioethanol production using *T. asperellum* B1581. However, the weakness of OFAT analysis was their incapability to establish interactions between factors that lead to inaccurate optimal conditions, particularly when interactions among different factors are significant (Humbird and Fei, 2016). Unlike the multivariate approach which offers global knowledge in its whole experimental area, OFAT only gives local knowledge where the experiment is performed (Ashgar *et al.*, 2014). Shaymaa *et al.* (2019) had shown the effectiveness of combination between Plackett–Burman design and Box-Behnken design as tools for the RSM. However, Central Composite Design (CCD) was chosen for this study as a statistical strategy rather than Plackett-Burman or Box-Behnken designs because CCD has axial points outside the region of interest to make up for OFAT's drawbacks.

Generally, different strains of fungi have their own optimal growth conditions, and this has led to the need to find the closest optimal condition for both strains to mutually co-exist for bioethanol production. In order to explore the relationships between several explanatory operating variables, Response Surface Methodology (RSM) has been extensively used for optimizing parameters for the production of ethanol from different substrates (Dasgupta *et al*., 2013). Besides, RSM is able to minimize the number of experiments required to develop a statistical relationship between factors and response, thus reducing the time consumption for optimization process. As seen in the RSM model produced in this study, the models provided an adequate fit for estimation with stability. A previous study reported that a combination of 5:1 *Aspergillus niger* B2484 and *Trichoderma asperellum* B1581 produced the most ethanol (1.03 g/L). The single culture organism is more economically efficient, reducing the risk of contamination or any possible complication during consortium development (Syazwanee *et al.*, 2021). A single microbial community can produce all the necessary enzymes to convert sugars into ethanol in a single reactor, thus reducing the overall costs (Sarabana *et al.*, 2015).

Industrial yeasts like *Saccharomyces cereviseae* have been used to produce alcohol for hundreds of years and have been extensively researched as the main strain for sugar-based bioethanol industries. The fermentation process for ethanol typically requires multiple setups for saccharification and fermentation and typically takes several hours to complete. On the overhand, CBP offers a combination of enzyme secretion, saccharification, and fermentation process in the same bioreactor has been known for economical manufacturing of bioethanol (Hasunuma *et al*., 2013). The key to cost reduction in CBP comes from either fermentative organisms that secrete vital cellulolytic enzymes for the breakdown of biomass, or from fermentative cellulolytic organisms that do not require a separate step for enzyme production (Linger and Darzins, 2013).

The effort to use *T. asperellum* B1581 crude enzyme in CBP for direct fermentation of ethanol has not been reported in any previous reports, and this study has become the first to investigate their potentials. Therefore, RSM is a valuable tool to plan the strategy in developing and optimizes the setup for CBP. Even though the RSM set-up produces a lower ethanol yield compared to OFAT set-up, the setting generated by RSM was still chosen over OFAT because the RSM analysis tends to overlook the overall interactions between physical and other factors affecting fermentation (Zambare and Christopher, 2012). Lower ethanol output may be caused by the fact that the filamentous fungi in CBP require several days to complete the fermentation process and usually consume the ethanol it produces (Anasontzis and Christakopoulos, 2014). Lower ethanol output in optimization setup by RSM was believed due to several drawbacks: (i) the productivity and ethanol yields are low and the fermentation process is time–consuming, (ii) optimum rate for hydrolysis of cellulases is usually greater than the ethanol producing microorganisms, (iii) unclear number of cellulase genes to be introduced into a single strain of host organism to become a viable CBP organism, and (iv) some of the secretory cellulolytic proteins may not fold properly (Jouzani and Taherzadeh, 2015). Although ethanol concentrations produced by filamentous fungi such as *T. asperellum* B1581 are unexpectedly high for organisms normally considered non-fermentative, the amount of ethanol produced is still too low for industrial bioethanol production and further analysis on the CBP setup is expected.

5. Conclusion

The OFAT analysis revealed that the optimum culture conditions of *T. asperellum* B1581 were 2 days of both saccharification and fermentation at 30°C with 3% (w/v) substrates loading and 10% (v/v) medium level. The optimised physicochemical conditions (67.7 h

saccharification, 32.9 h fermentation, 2.8% (w/v) substrate, 12.4% (v/v) medium level, 30°C for both processes) generated through RSM achieved ethanol production of 0.94 g/L, indicating the potential of *T. asperellum* B1581 as a single culture for bioethanol production in consolidated bioprocessing (CBP).

Acknowledgements

The authors would like to thank Universiti Putra Malaysia for the financial support through Grant No. GP-IPS/2016/9485600 and all staff of the Plant Systematic and Microbe Laboratory, Biology Department, Universiti Putra Malaysia for their efforts.

Conflict of Interest Statement

There are no conflicts of interest in this publication.

References

Abou-Taleb KA and Galal GF. 2018. A comparative study between one-factor-at-a-time and minimum runs resolution-IV methods for enhancing the production of polysaccharide by *Stenotrophomonas daejeonensis* and *Pseudomonas geniculate*. *Ann Agric Sci.*, **63**: 173-180.

Afolalu SA, Yusuf OO, Abioye AA, Emetere ME, Ongbali SO and Samuel OD. 2021. Biofuel; a sustainable renewable source of energy-a review. *IOP Conf Ser: Earth Environ Sci.,* **665**: 012040.

Amarasekara AS. 2013. Fermentation 1 – Microorganism. In: Amarasekara AS. (Ed.), **Handbook of Cellulosic Ethanol**. Scrivener Publishing, United States of America, pp. 283-338.

Anasontzis GE and Christakopoulos P. 2014. Challenges in ethanol production with *Fusarium oxysporum* through consolidated bioprocessing. *Bioengineered*, **5**: 393-395.

Arifa T and Sarwar S. 2012. Effect of cultural condition on production of ethanol from rotten apple waste by *Saccharomyces cerevisiae* straining. *Can J App Sci.*, **2**: 12-21.

Ashgar A, Abdul Rahman AA and Wan Daud WMA. 2014. A comparison of central composite design and Taguchi method for optimizing fenton process. *Sci World J.,* **2014**, 1-14.

Awogbemi O, Kallon DVV, Onuh EI and Aigbodion VS. 2021. An overview of the classification, production and utilization of biofuels for internal combustion engine applications. *Energies*, **14**: 5687.

Baruah J, Nath BK, Sharma R, Kumar S, Deka RC, Baruah DC and Kalita E. Recent trends in the pretreatment of lignocellulosic biomass for value-added products. *Front. Energy Res.*, **6**: 141.

Bech L, Herbst FA, Grell MN, Hai Z and Lange L. 2015. On-site enzyme production by *Trichoderma asperellum* for the degradation of duckweed. *Fungal Genom Biol.,* **5**: 1-10.

Brady SK, Sreelatha S, Feng Y, Chundawat SPS and Lang MJ. 2015. Cellobiohydrolase 1 from *Trichoderma reesei* degrades cellulose in single cellobiose steps. *Nat Commun.,* **6**: 10149-10158.

Chang YH, Chang KS, Chen CY, Hsu CL, Chang TC and Jang HD. 2018. Enhancement of the efficiency of bioethanol production by *Saccharomyces cerevisiae* via gradually batch- wise and fed-batch increasing the glucose concentration. *Fermentation*, **4**: 45.

Cutzu R and Bardi L. 2017. Production of bioethanol from agricultural wastes using residual thermal energy of a cogeneration plant in the distillation phase. *Fermentation*, **3**:24.

Dasgupta D, Suman SK, Pandey D, Ghosh D, Khan R, Agrawal D, Jain RK, Vadde VT and Adhikari DK. 2013. Design and optimization of ethanol production from bagasse pith hydrolysate by a thermotolerant yeast *Kluyveromyces* sp. IIPE453 using response surface methodology. *SpringerPlus*., **2**: 1-10.

Dey P, Pal P, Kevin JD and Das DB. 2020. Lignocellulosic bioethanol production: prospects of emerging membrane technologies to improve the process – a critical review. *Rev Chem Eng.*, **36**: 333-367.

Dong HN, Zhao XM, Ma YY and Zhang MH. 2012. Optimization of a synthetic medium for ethanol production by xylose-fermenting *Zymomonas mobilis* using response surface methodology. *Chin Sci Bull.,* **57**: 3782-3789.

Fahrizal F, Abubakar A, Muzaifa M and Muslim M. 2013. The effects of temperature and length of fermentation on bioethanol production from arenga plant (*Arenga pinnata* MERR). *Int J Adv Sci Eng Inf Technol.,* **3**: 54-57.

Ho CY, Chang JJ, Lee SC, Chin TY, Shih MC, Li WH and Huang CC. 2012. Development of cellulosic ethanol production process via co-culturing of artificial cellulosomal *Bacillus* and kefir yeast. *Appl Energy.,* **100**: 27-32.

Humbird D and Fei Q. 2016. Scale-up considerations for biofuels. In: Eckert CA and Trinh CT. (Eds.), **Biotechnology for Biofuels Production and Optimization.** Elsevier, Netherlands, pp. 513-537.

Hasunuma T, Okazaki F, Okai N, Hara KY, Ishii J and Kondo A. 2013. A review of enzymes and microbes for lignocellulosic biorefinery and the possibility of their application to consolidated bioprocessing technology. *Bioresour Technol.,* **135**: 513–522.

Jouzani SJ and Taherzadeh MJ. 2015. Advances in consolidated bioprocessing systems for bioethanol and butanol production from biomass: a comprehensive review. *Biofuel Res J*., **2**: 152-195.

Kumar SPJ, Kumar NSS and Chintagunta AD. 2020. Bioethanol production from cereal crops and lignocelluloses rich agro-residues: prospects and challenges. *SN Appl Sci.*, **2**: 1673.

Linger JG and Darzins A. 2013. Consolidated bioprocessing. In: Lee JW (Ed.), **Advance Biofuels and Bioproducts**. Springer, United States of America, pp. 267-280.

Lugani Y, Rai R, Prabhu AA, Maan P, Hans M, Kumar V, Kumar S, Chandel AK and Sengar RS. 2020. Recent advances in bioethanol production from lignocelluloses: a comprehensive review with a focus on enzyme engineering and designer biocatalysts. *Biofuel Res J.*, **28**:1267-1295.

Mardawati E, Putri AV, Yuliana T, Rahimah S, Nurjanah S and Hanidah I. 2019. Effects of substrate concentration on bioethanol production from oil palm empty fruit bunches with simultaneous saccharification and fermentation (SSF). *IOP Conf Ser: Earth Environ Sci.*, **230**: 012079.

Mauch F, Mauch-Mani B and Boller T. (1988). Antifungal hydrolases in pea tissue and inhibition of fungal growth by combinations of chitinase and β-1,3-glucanase. *Plant Physiol.*, **88**: 936-942.

Murata M, Nitiyon S, Lertwattanasakul N, Sootsuwan K, Kosaka T, Thanonkeo P, Limtong S and Yamada M. 2015. High-temperature fermentation technology for low-cost bioethanol. *J Japan Ins Energy.,* **94**: 1154-1162.

Nadeem M, Aftab MU, Irfan M, Mushtaq M, Qadir A and Syed Q. 2015. Production of ethanol from alkali-pretreated sugarcane bagasse under the influence of different process parameters. *Front Life Sci*., **8**: 358-362.

Nava-Cruz NY, Contreras-Esquivel JC, Aguilar-González MA, Nuncio A, Rodrìguez-Herrera R and Aguilar CN. 2016. Agave atrovirens fibers as substrate and support for solid-state

fermentation for cellulase production by *Trichoderma asperellum*. *Biotech 3.,* **6**: 115-122.

Olson DG, McBride JE, Shaw AJ and Lynd LR. 2012. Recent progress in consolidated bioprocessing. *Curr Opin Biotechnol*., **23**: 396-405.

Parisutham V, Kim TH and Lee SK. 2014. Feasibilities of consolidated bioprocessing microbes: From pretreatment to biofuel production. *Bioresour Technol.,* **161**: 431–440.

Paulova L, Patakova P, Branska B, Rychtera M and Melzoch K. 2015. Lignocellulosic ethanol: Technology design and its impact on process efficiency. *Biotechnol Adv.,* **33**: 1091–1107.

Robak K and Balcerek M. 2020. Current state-of-the-art in ethanol production from lignocellulosic feedstocks. *Microbiol Res.*, **240**: 126534.

Said KAM and Amin MAM. 2015. Overview on the response surface methodology (RSM) in extraction processes. *J Appl Sci Process Eng.*, **2**: 8-17.

Sarabana SSH, El-Gabry KIM and Eldin AM. 2015. Optimizing growth conditions provoked ethanol production by fungi grown on glucose. *Middle East J Appl Sci.,* **5**: 1222-1231.

Shaymaa AI, Serwa A, Abood A, Fayed B, Ismail SA and Hashem AM. 2019. A Study of the Use of Deep Artificial Neural Network in the Optimization of the Production of Antifungal Exochitinase Compared with the Response Surface Methodology. *Jordan J Biol Sci.*, **12**: 543551.

Syazwanee MMF, Shaziera AN, Izzati MNA, Azwady AN and Muskhazli M. 2018. Improvement of delignification, desilication and cellulosic content availability in paddy straw via physico-chemical pretreatments. *Annu Res Rev Biol.,* **26**: 1-11.

Syazwanee MMF, Izzati MNA, Azwady AN and Muskhazli M. 2019. Screening of lignocellulolytic fungi for hydrolyzation of lignocellulosic materials in paddy straw for bioethanol production. *Malays J Microbiol.,* **15**: 379 -386.

Syazwanee MMF, Izzati MNA, Azwady AN and Muskhazli M. 2021. Improvement of bioethanol production in consolidated bioprocessing (CBP) via consortium of *Aspergillus niger* B2484 and *Trichoderma asperellum* B1581. *Pertanika J Sci Technol.,* **29**: 301 – 316.

Teter SA, Sutton KB and Emme B. 2014. Enzymatic processes and enzyme development in biorefining. In: Waldron K (Ed.), **Advances in Biorefineries: Biomass and Water Supply Chain Exploitation.** Woodhead Publishing, United Kingdom, pp. 199-226.

Wahid Z and Nadir N. 2013. Improvement of one factor at a time through design of experiments. *World Appl Sci J.*, 21: 56-61.

Wang M, Li Z, Fang X, Wang L and Qu Y. 2012. Cellulolytic Enzyme Production and Enzymatic Hydrolysis for Second-Generation Bioethanol Production. In: Bai FW, Liu CG, Huang H and Tsao G. (Eds.), **Biotechnology in China III: Biofuels and Bioenergy. Advances in Biochemical Engineering Biotechnology.** Springer, Germany, pp. 1-24.

Zambare VP and Christopher LP. 2012. Optimization of enzymatic hydrolysis of corn stover for improved ethanol production. *Energ Explor Exploit.,* **30**: 193-205.

Zhao X, Moates GK, Elliston A, Wilson DR, Coleman MJ and Waldron KW. 2015. Simultaneous saccharification and fermentation of steam exploded duckweed: Improvement of the ethanol yield by increasing yeast titre. *Bioresour Technol.,* **194**: 263–269.

Zoglowek M, Hansen GH, Lübeck PS and Lübeck M. 2016. Fungal consortia for conversion of lignocellulose into bioproducts. In: Silva, R.N. Sharjah (Ed.), **Mycology: Current and Future Developments (Vol. 1) Fungal Biotechnology for Biofuel Productions**. Betham Science Publisher, United Arab of Emirates, pp. 329-365.

JJBS

Volume 15, Number 4,December 2022
ISSN 1995-6673
Pages 629 – 634
https://doi.org/10.54319/jjbs/150411

Jordan Journal of Biological Sciences

Potential of *Pasteurella multocida* (serotype A1) Isolated from Diseased Chicken to Establish Infection in African Catfish (*Clarias gariepinus*)

Victor O. Omeje[1,*], Chijioke C. Unachukwu [1], Calistus C. Okolo[1] and Chuka Ezema[2]

[1]*Department of Veterinary Medicine and* [2]*Department of Animal Health and Production, Faculty of Veterinary Medicine, University of Nigeria, Nsukka, Enugu State, Nigeria.*

Received: September 18, 2021; Revised: January 17, 2022; Accepted: February 14, 2022

Abstract

In integrated poultry cum fish systems, the droppings and offals from the chicken are used to fertilize the pond and feed the fish. These droppings and offals may sometimes harbour pathogenic microorganisms such as *Pasteurella multocida*. This study aimed to ascertain if *P. multocida* of *avian* origin can establish and cause infection in *Clarias gariepinus.* One hundred and twenty, apparently healthy 6 weeks old *C. gariepinus* juveniles were divided into three treatment groups and used for the study. Serotype A1 *P. multocida* isolated from infected chicken was homogenized in a sterile phosphate buffered saline and the turbidity adjusted to correspond to 0.5 McFarland's turbidity standard. Treatment group A consists of fish infected by immersion in homogenized bacterial inoculums administered at 1 ml/ liter of water while group B were injected intraperitoneally with 0.2ml of the bacterial inoculums. Group C were injected with sterile buffered saline to serve as control. Monitoring of the experimental fish for any clinical sign of disease was carried out daily. Blood samples were collected from 12 fish per treatment group for determination of haematological parameters and blood chemistry analysis. No clinical signs of disease were observed in all the groups for 28 days post infection; the growth rates and morphometric parameters did not differ significantly among treatment groups. There was also no significant change ($p>0.05$) in haematological and serum biochemical parameters. This study has demonstrated that serotype A1 *Pasteurella multocida* did not establish an infection in *C. gariepinus;* hence, it did not result in any haemato-biochemical alteration in the fish.

Keywords: Avian; Catfish; Clarias gariepinus**;** Pasteurella multocida; poultry

1. Introduction

African catfish is a very popular fish species among consumers in Nigeria and other Sub-Saharan African countries (Adah *et al*., 2021). As a result of increase in demand, most farmers operate integrated farms where they keep birds and fishes. Integrated fish cum livestock husbandry is practiced with a view to bringing together normally exclusive farming systems. In such farming system, waste from one enterprise (livestock) becomes input for the other subsystem (fish), thereby maximizing input utilization (Delmendo, 1980; Shoko *et al*., 2019). In Asia and other countries where integrated farming is widely practiced, integration of fish with chicken and duck are the most popular (Sahoo and Singh, 2015). The fish cultured in such system benefits from abundant nutrients arising from natural food which develops from the fertilization of the pond with the livestock manure (Bashir *et al*., 2020). In some integrated poultry cum fish farms, the poultry house overlays the ponds, and the droppings from the birds are used to fertilize the pond. Some farmers also pour poultry faeces and offals, especially intestine, into the fish pond as feed for fish. These droppings and offals from chicken may sometimes harbour pathogenic microorganisms that cause various diseases in chickens such as *Pasteurella multocida, Escherichia coli, Salmonella enteritidis* and parasites. These parasites and microorganisms may sometimes be a source of infection to susceptible fishes cultured in such integrated farms.

Pasteurella multocida is one of the bacterial infections commonly encountered in poultry industry in Sub-Saharan Africa. The *P. multocida* was first discovered in 1878 in birds exhibiting signs of cholera while Louis Pasteur first isolated it in 1880. *Pasteurella multocida* is small, penicillin-sensitive, Gram-negative, non-motile coccobacilli (Zhao *et al*., 2021). The bacterium causes infections in humans through the bites and scratches of cats or dogs (Kannangara *et al*., 2020). In humans, *P. multocida* has been associated with numerous primary or secondary respiratory syndromes (Pak *et al*., 2018) indicating that the organism is of zoonotic importance. The organism is a normal microbiota of the upper respiratory tract of mammals and birds such as cats, dogs, rabbits, cows, swine and chicken. The bacteria are present in a wide range of environments including aquatic habitat.

Pasteurella multocida causes fowl cholera, an acute septicemic infection in birds that results in significant economic losses to the poultry industry, especially in turkey production (Mostaan *et al*., 2020). Pasteurellosis of

* Corresponding author. e-mail: okonkwo.omeje@unn.edu.ng.

fishes, especially those caused by *Pasteurella piscida*, have existed for a long time. In 1963 at Chesapeake Bay, USA, the disease was reported to have caused heavy losses in white perch (*Roccus americanus*) and striped bass (*M. saxatilis*) production (Snieszko *et al.,* 1964). Also in Japan in 1964 and 1972, it was reported to be responsible for massive mortality of cage-cultured yellowtails (*Seriola quinqueradiata*) in excess of 340 metric tons (Matsusato, 1975). Recently, the incidence of pasteurellosis that caused significant economic losses has been reported in lumpsuckers (*Cyclopterus lumpus* L) in Norway affecting fishes of all life stages (Ellul *et al*., 2019). *Pasteurella* infections have been variously described as bacterial tuberculosis and pseudotuberculosis (Egusa, 1983).

There is a need to study the transmission and pathogenicity of *P. multocida* in fish since poultry manure is used as organic fertilizers in fish ponds. From the literature reviewed, there is no record of *P. multocida* infection among *Clarias gariepinus*. Therefore, this study aimed to ascertain if *P. multocida* of *avian* origin can cause infection in *C. gariepinus* and its effects on the haematological parameters, serum biochemistry, growth and survival of the fish species.

2. Materials and Methods

2.1. Experimental animals and culture system maintenance

The study was undertaken at the Aquaculture Research Facilities, Department of Veterinary Medicine, University of Nigeria, Nsukka situated at latitude 6°45' and 7°N and longitude 7°12' E. The climate is considered as being tropical, with marked periods of rainfall and dry seasons with minimum temperature (16^0C) in December/ January and maximum temperature (34^0C) in March/ April (Source: World Climate Online). One hundred and twenty apparently healthy 6weeks old *Clarias gariepinus* juveniles were procured from a reliable farm in Nsukka, Enugu state. Prior to the commencement of the experiment, the experimental fish were acclimatized for two weeks, during which 2mm fish basal diet was provided at the rate of 3% of their body weight twice daily (Sarka and Rahid, 2012). Borehole water was used for the experiment, and the culture water was changed once in 2 days by gradual removal and addition to ensure adequate oxygenation. The experiment was carried out in 6 tarpaulin fish ponds, constructed with metallic framework. Each of the ponds is 52x48x58.3cm (LxWxH) and has a capacity of 145.5L. Uneaten food and solid wastes were removed from the culture water by siphoning. Water quality parameters such as dissolved oxygen, temperature and pH were monitored weekly. Portable dissolved oxygen meter JPB – 607 A was used to monitor the dissolved oxygen and the water temperature while pocket-sized pH meter manufactured by Hanna instruments was used to monitor the pH of the culture water. The water quality parameters obtained include mean dissolved oxygen 5.6 ± 0.7, mean temperature 25.3 ± 1.38^0 and mean pH of 6.5 ± 0.12. All the parameters measured were within the tolerable limits for fish culture (Timmons and Losordo, 1994).

2.2. Bacterial strains

Serotype 1 characterized *Pasteurella multocida* isolate was obtained from Department of Pathology and Microbiology, National Veterinary Research Institute, Vom Plateau state, Nigeria. Upon arrival, it was sub-cultured on a blood agar at the laboratory of the Department of Veterinary Medicine, University of Nigeria, Nsukka. Biochemical test such as citrate test, H_2S test and methyl red test were performed to re-confirm the organism.

2.3. Infection of Catfish

120 African catfish (*Clarias gariepinus*) used for the study were randomly assigned into three treatment groups (A, B and C) of 40 catfish per group. Each group was further subdivided into two replicates and the stocking density were 20 fish per replicate for ease of handling and reared in tarpaulin pond of 145.5L capacity with iron framing at the 4 sides as stated above. *Pasteurella multocida* was homogenized in a sterile phosphate buffered saline and the turbidity was adjusted to correspond to 0.5 McFarland's turbidity standard (equivalent to 1 x 10^8 colony forming units/ml) in accordance with Zapata and Ramirez-Arcos (2015). Fish in group A were infected by immersing them in appropriate tank containing 1ml/liter of bacterial inoculums for 5 minutes while group B were injected intraperitoneally with 0.2ml of the bacterial inoculums. Group C were injected with sterile buffered saline only to serve as control.

2.4. Observation of critical outcomes and sampling frequency

The infected fish were monitored daily for signs of ill health: sluggishness, off feed, skin lesions, morbidity and mortality. At the end of the experimental period of 4 weeks, the weight and lengths (total and standard) of 6 fish per replicate (12 fish per treatment group) were determined. Tissue samples were taken from 6 fish per replicate for bacteriological assay. Isolation and identification of *P. multocida* using ovine blood agar selective media and *P. multocida* specific PCR methods (Dziva *et al*., 2008) were also employed for detection of the bacterium in fish samples from each treatment group. Also, blood samples were collected from 6 fish per replicate for determination of haematology and blood chemistry analysis.

Sampling and taking of the morphometric (total length, standard length and weight) of a representative sample in each replicate was undertaken every week, and the sample size was 6 fish per replicate. The final sampling and taking of the morphometric of a representative sample in each replicate was undertaken at the 28^{th} day, and the mortality in each treatment was recorded so as to calculate the survival rate.

Condition factor, growth and mortality rates were determined.

The condition factor (K) of each fish was calculated using the formula:

$$K = \frac{100W}{L^3}$$ (Ighwela *et al*., 2011)

Where L = standard length (cm) and W = Body weight (g)

Specific growth rate was calculated using the formula:

$$SGR = \frac{LnW_f - LnW_i}{T \text{ (days)}} X100$$

(Gharaei *et al*., 2020)

Where W_f = final weight and W_i= initial weight

$$\text{Survival rate} = \frac{\text{Final number of fish}}{\text{Initial number of fish}} X100$$

2.5. Gross pathology

Fish in all the groups were examined for presence of skin lesions. Three fishes from each group were selected and sacrificed 4 weeks post infection. Following death, the fishes were dissected, and the internal organs were examined for the presence of gross lesions.

2.6. Determination of Haematological Parameters

Six fishes were randomly selected from each replicate for haematology and serum biochemistry. Universal bottles treated with ethylene diamine tetra acetic acid (EDTA) were used for blood collection for haematological determination. Blood samples were collected from the caudal circulation (Lawrence *et al*., 2020) with the aid of heparinized 3ml disposable plastic syringes and a 21 gauge disposable hypodermic needle. Collected blood was mixed well with the anticoagulant, and the following haematological studies were carried out on the blood sample. The packed cell volume (PCV) was determined by the micro-heamatocrit method (Schalm *et al.,* 1975). The haemoglobin concentration (Hb) was determined by the cyanometmoglobin method (Kachmar, 1970). The erythrocyte count was determined by haemocytometer method (Dacie and Lewis, 1991). The total white blood count was determined by the haemacytometer method (Dacie and Lewis, 1991). Smears for the differential white blood cell count were prepared on clean slides and studied by the Leishman technique (Schalm *et al.,* 1975).

2.7. Serum biochemistry determination

Non-heparinized blood samples were collected from the caudal circulation from six fish per replicate for the serum chemistry analysis. The collected bloods were allowed to clot, and the clotted blood meant for serum biochemistry was separated from clear serum by centrifugation. All serum biochemistry determination was carried out following standard procedures. Serum Aspartate aminotransferase (AST) and Serum alanine aminotransferase (ALT) were determined using the standard colorimetric method of Reitman and Frankel (1957). This is an in-vitro method of determining AST and ALT using Randox Glutamic-oxaloacetic transaminase test kit and Randox Glutamic-pyruvic transaminase test kit respectively. Total proteins were determined by the direct Biuret method (Lubran, 1978) for the in-vitro determination of total protein in serum or plasma using the total proteins test kit while Albumin was determined using the Bromocresol Green method (Reinhold, 1953)**.** Serum urea nitrogen was determined by the modified Berthlot-Searcy method for the in-vitro determination of urea in serum or plasma using urea test kit.

2.8. Analysis of data

Clinical outcome, morbidity and mortality rates were determined and presented in tables. Data on absolute body weight, condition factor, specific growth rate, survival rate, haematology and serum biochemistry among the four experimental groups were compared using one way analysis of variance (ANOVA). Significant difference was accepted at $p<0.05$.

3. Results

3.1. Clinical signs

No clinical sign of disease was observed in all the groups for 28 days post infection of the *Clarias gariepinus* with *Pasteurella multocida* as shown in Table 1. There were also no gross pathological lesions observed in all the organs examined at the end of the experimental period. Tissue samples taken from each treatment group at the end of the experimental period for bacteriological assay yielded no *P. multocida* isolates.

Table 1. Clinical signs of infection in *Clarias gariepinus* infected with *Pasteurella multocida*.

	Experimental group		
Clinical parameter	A (*P. multocida* injected I.P	B (*P. multocida* infected in water)	C (Unifected Control)
Sluggish Movement	Absent	Absent	Absent
Anorexia	Absent	Absent	Absent
Morbidity rate	Absent	Absent	Absent
Curdling together	Absent	Absent	Absent
Emaciation	Absent	Absent	Absent
Growth rate	Good	Good	Good
Mortality rate	0%	0%	0%

3.2. Changes in Morphometric, Haematologic and Serum biochemistry paremeters

The mean weight of the fish infected with *Pasteurella multocida* are presented in Table 2. Fish in group C gave the least mean weight of 245.64±24.55 twenty eight days post infection. Fish in group A gave a lower mean weight of 254.94±48 compared to those in group B which gave 261.04±9.9 twenty eight days post infection. The results gotten from calculation of the condition factor and specific growth rate also showed that both morphometric parameters did not vary significantly ($p>0.05$) 28 days post infection.

The result of the haematology as outlined in Table 3 showed that there was no significant change ($p>0.05$) in haematological parameters of *Clarias gariepinus* infected with type A1 *Pasteurella multocida*.

Also, the result of the serum biochemistry as outlined in Table 4 showed that there was no significant change ($p>0.05$) in the serum biochemistry parameters of *Clarias gariepinus*.

Table 2: Effect of *Pasteurella multocida* infection on the mean (± SD) morphometric parameters and specific growth rate of *Clarias gariepinus*

Parameter	Day 0 post infection			Day 14 post infection			Day 28 post infection		
	Group A	Group B	Group C	Group A	Group B	Group C	Group A	Group B	Group C
Weight (g)	152.90±11.7	179.60±11.8	181.50±22.5	235.81±19.5	235.47±15.2	235.34±29.2	254.94±5	261.04±9.9	245.64±24.5
Standard length (cm)	27.05±0.74	28.85±0.43	28.52±0.35	30.71±0.92	30.60±0.70	30.31±1.14	30.79±1.22	32.00±0.67	31.25±0.71
Condition factor	0.67±0.09	0.77±0.03	0.78±0.11	0.90±0.08	0.83±0.04	0.82±0.04	0.81±0.10	0.80±0.03	0.71±0.05
Specific growth Rate							0.68±0.26	0.48±0.09	0.68±0.21

Table 3: Effect of *Pasteurella multocida* infection on the mean (± SE) Haematological parameters of *Clarias gariepinus*

Parameters	Group A	Group B	Group C	Group A	Group B	Group C	Group A	Group B	Group C
RBC ($\times10^6$/µL)	2.25±0.10	2.27±0.15	2.32±0.22	1.73±0.6	1.55±0.10	1.76±0.16	1.78±0.15	1.42±0.16	1.50±0.88
WBC ($\times10^9$/µL)	11.46±0.15	11.87±0.20	11.90±0.11	12.14±0.32	12.02±0.29	12.32±0.24	12.50±0.35	12.49±0.40	12.77±0.35
HG (g/dl)	8.56±0.35	8.56±0.40	8.40±0.47	8.03±0.49	8.83±0.22	8.64±0.35	8.13±0.24	8.71±0.38	7.83±0.60
PCV (%)	36.63±3.81	38.00±4.06	39.13±4.58	25.75±5.73	34.25±3.74	40.00±6.34	36.13±5.20	24.25±4.71	36.88±3.96
Lymphocyte (%)	91.00±1.85	91.50±2.60	93.13±2.03	91.00±2.10	89.88±2.56	90.79±1.14	90.00±1.85	90.50±2.60	92.13±2.03
Neutrophils (%)	6.38±1.22	6.13±1.50	4.88±1.36	6.13±1.36	6.63±1.69	5.50±1.10	7.38±1.22	7.00±1.22	5.88±1.36
Eosinophils (%)	1.63±0.53	1.00±0.50	1.00±0.46	2.13±0.64	2.88±0.88	1.75±0.53	1.88±0.61	1.25±0.73	1.38±0.65
Monocytes (%)	0.99±0.27	1.37±0.82	0.99±0.59	0.74±0.64	0.61±0.22	1.96±0.5	0.74±0.25	1.25±0.65	0.61±0.30
MCH(pg)	38.04±3.86	37.71±4.23	36.21±4.42	46.24±3.54	56.97±4.93	49.09±2.45	45.67±3.68	61.34±6.34	52.20±4.23
MCV(fl)	162.8±10.22	167.4±8.23	168.66±12.54	148.83±13.11	220.97±13.00	227.27±13.12	202.98±9.31	170.77±14.12	245.87±12.21
MCHC(g/dl)	23.37±2.74	22.53±3.74	21.47±4.12	31.18±3.11	25.78±3.11	21.60±2.30	28.00±4.23	22.13±2.20	35.92±4.23S

The Mean parameters determined did not vary significantly (p>0.05) among the group

Table 4: Effect of *Pasteurella multocida* infection on the mean (± SE) blood serum chemistry of *Clarias gariepinus*

Parameters	Group A	Group B	Group C	Group A	Group B	Group C	Group A	Group B	Group C
Total protein(g/dl)	4.45±0.19	3.70±0.39	5.27±0.33	4.56±0.48	4.54±0.46	4.13±0.20	3.81±0.36	4.92±0.16	4.78±0.29
Albumin(g/dl)	0.83±0.22	1.21±0.34	0.48±0.19	1.69±0.37	0.44±0.14	0.37±0.12	0.68±0.32	0.61±0.16	0.91±0.17
Globulin(g/dl)	3.62±0.08	2.49±0.21	4.79±0.52	2.870±0.21	4.10±0.25	3.76±0.08	3.13±0.12	4.31±0.13	3.87±0.21
Alb/ Glo ratio	0.23±0.08	0.49±0.10	0.10±0.03	0.59±0.06	0.11±0.08	0.10±0.02	0.18±0.03	0.14±0.08	0.24±0.07
ALT (IU/L)	13.00±2.22	13.38±7.41	15.13±2.39	20.75±3.06	13.50±2.76	18.00±2.97	15.13±4.11	15.13±3.27	16.25±3.56
AST (IU/L)	54.75±8.81	53.37±8.88	60.50±6.70	65.37±11.90	53.37±8.88	60.00±9.43	55.50±7.79	53.00±8.96	56.25±8.48
Urea (mg/	4.58±0.68	6.12±0.71	4.94±0.63	5.17±0.81	4.66±0.51	4.98±0.86	5.49±0.67	3.95±0.84	5.70±0.65

The Mean parameters determined *did not vary significantly (p>0.05) among the group*

4. Discussion

Establishment of bacterial infection in fish results in specific signs and symptoms severity of which is dependent on the virulence and pathogenicity of the bacterium involved (Omeje *et al*., 2019). In this study, *Clarias gariepinus* experimentally infected with serotype A1 *P. multocida* of poultry origin were investigated in order to evaluate its infectivity and haemato-biochemical effect on the fish. There was total absence of common clinical signs of bacterial disease, which may include sluggish movement, anorexia, morbidity, curdling together, and emaciation in the group infected by immersion which indicates that they were not diseased. The same observance was made on Group A in which the fish was infected by injecting 0.02ml/g of the organism intraperitoneally. Supposedly, the fish in this group should have a greater influence of the bacterium because intraperitoneal infection -which is a parenteral route- ensures prompt absorption of injected material into the liver through the mesenteric vessels (Al Shoyaib *et al*., 2020). Although intravenous injection is quicker in eliciting response, intraperitoneal injection was used because intravenous access will be challenging for the juvenile fish being used for the experiment. For both groups, the morbidity and the mortality rates were zero; there was absence of observable clinical signs of infection throughout the 28 days post infection which was the same as uninfected control group C. Bacteriological assay employing normal bacteria isolation in blood agar and specific PCR methods yielded no *P. multocida* isolates, which indicates that the bacterium did not establish an infection in *Clarias gariepinus*. The results of the study also indicated that the specific growth rate (SGR) and the Condition Factor (CF) of the fish in the groups were normal and did not differ significantly ($p>0.05$) in the three groups 28 days post infection. This result is in agreement with Nizan and Hammerschlag (1993) who reported that *Pasteurella multocida* has been isolated from Tilapia hybrids (*Oreochromis spp)* with no clinical sign which showed that the infection was subclinical and the source of infection was suggested to be the poultry manure used as organic fertilizer in the ponds. However, *Pasteurella piscicida* was reported to cause Pasteurellosis in fish species such as sea bass, white bass, yellowtail, striped bass and gilthead sea-bream (Thune *et al.,* 1993). In poultry industry pasteurellosis due to *P. multocida* has been recognized as one of the diseases of veterinary importance. A variety of domestic livestock including mammals and birds are susceptible to *P. multocida* (Abdulrahman and Davies, 2021), but there has not been any reported case of *P. multocida* infection in African catfish (*Clarias gariepinus).* Although they isolated *P. multocida* from natural pond water, Prince and Brand (1984) suggested that it may be due to the presence of waterfowl carcasses which shed the bacteria. A research done by Backstrand and Botzler (1986) showed that even though the capability of water in transmitting *P. multocida* organism from infected to susceptible avian host (waterfowl) is not in doubt, they postulated that the concentration of the organism declines rapidly in water. The low survival of *P. multocida* in water hypothesized by these scientists was reflected in the Group B of this study which was infected by immersing the fish into a tank containing 1 ml/ litre of the bacterial inoculum.

Changes in blood parameters are known to occur in fishes under disease, agitation or nutritive stress (Blaxhall, 1972; Dossou *et al*., 2018). The result of the haematology showed that the bacterium, *Pasteurella multocida* did not induce changes in haematological parameters. The packed cell volume, haemoglobin concentration, red blood cell count, white blood cell count, eosinophils, neutrophils and lymphocytes did not differ significantly on days 0, 14 and 28 post infections for the three groups. This may also suggest the absence of any other infection (parasitism, allergy, dermatitis). This is in agreement with the work of Adedeji *et al* (2000) who reported that haematological parameters are crucial and serve as a possible indicator of physiological or pathological changes in disease investigation and fishery management.

Plasma enzymes are useful as appropriate markers of tissue (organ) damage (Ramesh *et al*., 2018). An elevated level of plasma enzyme may suggest damage to tissue or organ. Damage to the liver may cause poor detoxification and deamination, which can lead to poor feed conversion, loss of weight and mortality. Based on the result of serum biochemistry, there were no significant differences in the plasma enzymes (alanine aminotransferase and aspartate aminotransferase) analyzed, after 28 days post infection for the group A, B and C. This is indicative that there was no gross pathological change or damage in the liver of the fish since the *P. multocida* organism did not establish to cause infection in the *C. gariepinus*. The serum total protein, total albumin and blood urea nitrogen also did not differ significantly ($p>0.05$).

5. Conclusion

This study has demonstrated that type 1 *Pasteurella multocida* did not establish an infection in *Clarias gariepinus.* Hence, it did not result in any haemato-biochemical alteration in *Clarias gariepinus*.

Acknowledgement

The authors express their appreciation to the Nigerian Tertiary Education Trust Fund (TETFUND) for providing the funding via Institution Based Research Intervention (TETFUND/ DESS/UNI/NSUKKA/2018/RP/VOL.1) for the present study.

Ethical Statements

All experiments in this study associated with fish complied with animal welfare ethical approval (FVM-UNN-IACUC-2019-0925) obtained from Faculty of Veterinary Medicine Institutional Animal Care and Use Committee, University of Nigeria, Nsukka.

Conflict of Interests

The authors declare that there is no conflict of interests.

References

Abdulrahman RF and Davies RL. 2021. Diversity and characterization of temperate bacteriophages induced in *Pasteurella multocida* from different host species. *BMC microbial.*, **21(1)**: 1-20.

Adah DA, Saidu L, Oniye SJ, Kazeem HM, Adah SA. 2021. Prevalence and Risk Factors Associated with *Aeromonas hydrophila* infection in *Clarias gariepinus* and Pond Water from Fish Farms in Kaduna State, Nigeria. *Jordan J Bio Sci*., **14(3)**: 477-484

Adedeji OB, Taiwo VO and Agbede SA. 2000. Comparative haematology of five Nigerian freshwater fish species. *Nig Vet J*., **21**: 75-84

Al Shoyaib A, Archie SR and Karamyan VT. 2020. Intraperitoneal Route of Drug Administration: Should it Be Used in Experimental Animal Studies? *Pharmaceu Res*., **37(1)**: 1-17

Backstrand JM and Botzler RG. 1986. Survival of *Pasteurella multocida* in soil and water in an area where avian cholera is enzootic. *J wildlife dis*., **22(2)**: 257-259

Bashir MA, Liu J, Geng Y, Wang H, Pan J, Zhang D and Liu H. 2020. Co-culture of rice and aquatic animals: An integrated system to achieve production and environmental sustainability. *J Cleaner Product.*, 249: 119310.

Blaxhall PC. 1972. The haematological assessment of the health of freshwater fish: A review of selected Literature. *J Fish Bio.,* **4(4)**: 593-604.

Dacie SIV, Lewis SM. 1991. *Practical haematology* (7th edition) J. and A. Churchill Ltd. Livingston, London Melborne and New York, pp: 67

Delmendo MN. 1980. A review of Integrated livestock-fowl-fish farming system p. 59-71 Inc Integrated Agriculture – agriculture farminig systems, Pullin, R.S.V. and Shehadeh, Z.H., (eds), Proceedings of the ICLARM-SEARCA conference, Manila, Philippines, 6-9 August, 1979. 258 pp

Dossou S, Koshio S, Ishikawa M, Yokoyama S, Dawood MA, El Basuini MF. et al., 2018. Growth performance, blood health, antioxidant status and immune response in red sea bream (*Pagrus major*) fed *Aspergillus oryzae* fermented rapeseed meal (RM-Koji). *Fish shellfish immunol.*, **75**: 253-262

Dziva F, Muhairwa AP, Bisgaard M and Christensen H. 2008. Diagnostic and typing options for investigating diseases associated with *Pasteurella multocida*. *Vet microbiol.*, **128(1)**: 1-22.

Egusa S. 1983. Disease problems in Japanese yellowtail, *Seriola quinqueradiata*, culture: a review. *Rapp. P.-V. Reun.-Cons In. Explor. Mer*, **182**: 10-18.

Ellul RM, Walde C, Haugland GT, Wergeland H and Rønneseth A. 2019. Pathogenicity of Pasteurella sp. in lumpsuckers (*Cyclopterus lumpus* L.). *J Fish Dis.*, **42(1)**: 35-46.

Gharaei A, Shafiei M, MirdarHarijani J, Hassanein P, Arshadi A. 2020. Immune Responses and Haematological Parameters Changes of Rainbow Trout (*Oncorhynchus mykiss*) under Effects of Dietary Administration of Sumac (RhuscoriariaL.). *J Agr Sci Tech.,* **22(1)**: 173-186

Ighwela KR, Ahmed AZ, Abol-Munafi AB. 2011. Condition Factor as an Indicator of Growth and Feeding Intensity of Nile Tilapia Fingerlings (*Oreochromis niloticus*) Feed on Different Levels of Maltose. *American-Eurasian J Agric Environ Sci*., **11(4)**: 559-563

Kachmar JF. 1970. Determination of blood haematology by the cyanomethaemoglobin procedure in: Tietz NW ED, Fundamentals of Clinical Chemistry, W. B. Sanders company, Philadelphia, pages 268-269

Kannangara DW, Pandya D and Patel P. 2020. *Pasteurella multocida* Infections with Unusual Modes of Transmission from Animals to Humans: A Study of 79 Cases with 34 Nonbite Transmissions. *Vector-Borne Zoon Dis.*, **20(9)**: 637-651.

Lawrence MJ, Raby GD, Teffer AK, Jeffries KM, Danylchuk AJ, Eliason EJ, Hasler CT, Clark TD. and Cooke SJ. 2020. Best practices for non-lethal blood sampling of fish via the caudal vasculature. *J Fish Bio*., **97(1)**: 4-15

Lubran MM. 1978. The measurement of total serum proteins by the Biuret method. *Annals Clin. Lab. Sci*., **8(2)**: 106-206

Matsusato T. 1975. Bacterial tuberculosis of cultured yellowtail. Proceedings of the 3rd US-Japan meeting on aquaculture, Tokyo, Japan, pp. 115-118

Mostaan S, Ghasemzadeh A, Sardari S, Shokrgozar MA, Brujeni GN, Abolhassani M and Karam MRA. 2020. *Pasteurella multocida* vaccine candidates: A systematic review. *Avicenna J Medical Biotechn*.., **12(3)**: 140.

Nizan S, Hammerchlag E. 1993. First report of *Pasteurellosis* in fresh water hybrid tilapia (*Oreochromis aureus ×O. noloticus)* in Isreal. *Bull Europ Assoc Fish Pathol.,* **13**: 179-180

Omeje VO, Okolo CC, Eze DC. 2019. Pathogenicity (LD_{50}) and antibiotics sensitivity tests of *Aeromonas hydrophila* isolated from fishes of the Kainji Lake area. *Internat J Fisher Aquat Stud.,* **7(6):** 190-196.

Pak S,Valencia D, Decker J, Valencia V and Askaroglu Y. 2018. *Pasteurella multocida* pneumonia in an immuno-competent patient: Case report and systematic review of literature. Lung India. **35(3)**: 237-240.

Ramesh M, Anitha S, Poopal RK and Shobana C. 2018. Evaluation of acute and sublethal effects of chloroquine (C18H26CIN3) on certain enzymological and histopathological biomarker responses of a freshwater fish *Cyprinus carpio*. *Toxicol Reports*, **5:** 18-27

Reinhold, JG. 1953. Standard Methods of Clinical Chemistry. Academic Press New York, pp: 256.

Reitman S and Frankel S. 1957. A colorimeter method for determination of serum glutamic oxaloacetic and Glutamic pyruvic transaminases. *American J Clin Pathol.,* **28**: 56-62.

Sahoo UK, Singh SL. 2015. Integrated Fish-Pig and Fish-Poultry Farming in East Kalcho, Saiha District of Mizoram, North-East India: An Economic Analysis. *Int J. Agric Forest*., **5(5)**: 281-286.

Sarkar MJA and Rashid MM. 2012. Pathogenicity of the bacterial isolates *Aeromonas hydrophila* to catfishes, carps and perch. *J Fish.*, **44(4)**: 393-397.

Schalm OW, Jain NC and Carol EJ. 1975. Veterinary Haematology, 3rd ed. Lea and Febiger, Philadelphia, pp 19-25

Shoko AP, Limbu SM, Lamtane HA, Kishe-Machumu MA, Sekadende B, Ulotu EE, Masanja JC and Mgaya YD. 2019. The role of fish-poultry integration on fish growth performance, yields and economic benefits among smallholder farmers in sub-Saharan Africa, Tanzania, *Afr J Aquat Sci*., **44(1)**: 15-24.

Snieszko SF, Bullock GL, Hollis E and Boone JG. 1964. Pasteurella sp. from an epizootic of white perch (*Roccus americanus*) in Chesapeake Bay tidewater areas. *J Bacteriol.*, **88(6)**: 1814.

Timmons MB and Losordo TM (1994). *Aquaculture water re-use systems: Engineering design and management*, New York: Elsevier science B.V.

Zapata A and Ramirez-Arcos S. 2015. A comparative study of McFarland turbidity standards and the Densimat photometer to determine bacterial cell density. *Current Microbiol.*, **70(6):** 907-909.

Zhao X, Shen H, Liang S, Zhu D, Wang M *et al.* 2021. The lipopolysaccharide outer core transferase genes *pcgD* and *hptE* contribute differently to the virulence of *Pasteurella multocida* in ducks. *Vet. Res.,* **52(1):** 37.

JJBS

Volume 15, Number 4,December 2022
ISSN 1995-6673
Pages 635 – 642
https://doi.org/10.54319/jjbs/150412

Jordan Journal of Biological Sciences

The Biological Effect of ZnO Nanoparticles Produced by Using *Petroselinum crispum* Extract against *Candida* spp

Laith Z. Fadhel[1,*], Sabah M. Hadi[1], Mahmood K. H. Al-Mashhadani[2], Hamid H. Murbat[3]

[1] *Department of Biology, College of Science, University of Baghdad, Iraq;* [2] *Department of Chemical Engineering, College of Engineering, University of Baghdad, Iraq;* [3]*Department of physics, college of Sciences for women, University of Baghdad, Iraq*

Received: September 16, 2021; Revised: February 23, 2022; Accepted: April 1, 2022

Abstract

Non-thermal or cold plasma create many reactive species and charged particles when brought into contact with plant extracts. The major constituents involve reactive oxygen species, reactive nitrogen species and plasma ultra-violets. These species can be used to synthesize biologically important nanoparticles. The current study addressed the effect of the green method-based preparation approach on the volumetric analysis of Zn nanoparticles. Under different operating conditions, the traditional thermal method and the microwave method as well as the plasma generation in dielectric barrier discharge reactor were adopted as a preparation approach in this study. The results generally show that the type of method used plays an important role in determining the size of the zinc particles produced. The traditional and microwave method stimulated the formation of clusters and agglomerates of Zn nanoparticles by effect of temperature parameter. As an example, it was noted that the lowest average diameter was obtained at 50 °C, which was 18.77 nm compared with 30.07, 23, 31, and 25.27 nm in diameter for particles generated with other temperatures of 30, 60, 70, and 80 °C respectively. These formations can occur at relatively low temperature at the expense of the formation of irregular particles. However, the weights of pre-prepared *Petroselinum crispum* seeds, and the ratio of the extract of *P. crispum* seeds to the salt, are factors that may play an important role in determining the size of the Zn nanoparticles. The current study has also shown that the highest percentage of generated nanoparticles was obtained with the cold plasma method under moderate operating conditions with the advantage of the economic factor. In addition, the Zn nanoparticles synthesized by cold plasma method in 10 min in all concentrations showed more inhibition effect as antifungal against *Candida albicans*.

Keywords : Zinc nanoparticles, *P. crispum*, plasma , microwave

1. Introduction

The importance of nanoparticles (NPs) lies in the fact that the diameter of their particles is less than 100 nanometers, which gives them nanoscale properties different from the corresponding bulk materials. These unique properties are their possession of high surface energy and quantum confinement in addition to nanoparticles' specifically large surface area. Thus, this technology can have wide applications in several fields including treatment of waste/water, sensing and catalyzing, corrosion prevention, conduction, oil recovery, electronics, clean energy, and drug delivery (Singh *et al.,* 2015; Sharma *et al*., 2020 and EL-Seedi *et al.,* 2019).

The utilization of biological synthesis methods to make nanoparticles has grown increasingly popular, owing to the fact that they are non-toxic and non-polluting to the environment. Plants, yeasts, algae, bacteria, and fungi were used to make nanoparticles; however, the preparation of nanoparticles from plants had **attracted wide interest in comparison with other methods** (Daphedar and Taranath, 2018; Paul and Sinha, 2014 and Thi *et al*., 2020)

Because zinc oxide nanoparticles are distinct from other nanoparticles as a unique material, they have attracted the attention of a large number of researchers, prompting them to conduct a large number of studies on them due to the diversity of its environmentally friendly applications in a variety of fields. Anti-microorganisms and nanomedicine, UV blocking, biosensors, phytochemical activities, drug carriers, and cosmetics are examples of these applications (Gunalan *et al*., 2012, Senthilkumar and Sivakumar**,** 2014 and Thi *et al.,* 2020).

ZnNPs is an inorganic semiconducting material that has three crystalline structures: zinc blende, rock salt and wurtzite (Thi *et al.,* 2020). Its nanostructure is distinct from the rest of the metal oxides since it contains an abundance of diverse nanostructures in its shapes, properties, and attributes such as nanotubes, nanorods, and nanospheres (Yahya *et al*., 2013). The nature of ZnNPs gave it a catalytic efficiency and a high adsorption capacity, which led to its employment in a variety of promising industrial applications, including adding ingredients to paints, sunscreens synthesis, the rubber and ceramic sector, sewage treatment, and fungicides (Gunalan *et al*., 2012).

* Corresponding author. e-mail: laithzuhair2018@gmail.com.

There are many methods to prepare zinc nanoparticles. Physical methods, for example, include melt mixing, laser ablation, electric deposition, ball milling, physical vapour deposition, sputter deposition, and ion implantation (Rahayu *et al.,* 2020). While Sol-gel, chemical-mechanical synthesis, microwave method, thermal evaporation, hydrothermal technique, vapor transport synthesis, and precipitation method are some chemical methods used to make nano-zinc oxide (Sabir *et al.,* 2014). The chemical approaches necessitate the employment of organic compounds that act as redactors and capping agents, and it is one of the most widely used methods, requiring the employment of a wide range of catalytic precursors under various reaction circumstances of time, temperature, and reactant concentrations. The difference in the reaction conditions leads to the difference in the size and shape of the resulting zinc nanoparticles (Sabir *et al*., 2014 and Thi *et al*., 2020).

Recently, green synthesis has been preferred over physical and chemical methods in the manufacture of nano-zinc oxide because of its low costs and not requiring high temperatures or specialized devices or the use of toxic organic compounds as reducing agents or solvents during the synthesis process, and thus no toxic or dangerous compounds are produced from the reaction. The green method is one of the environmentally friendly methods because it reduces the risks of pollution. The properties of the resulting nano-zinc oxide depend on the exact structure and structural characteristics, which are determined according to the chosen method of manufacture. (Sabir *et al*., 2014 and Lakshmeesha *et al*., 2019).

Use of plants or plant extracts as row materials was due to its ease of work, the availability of plants in abundance, and the presence of chemical compounds, which are considered as reducing agents. In fact, (Fakhari *et al*., 2019) proved that the zinc raw material plays a key role in the internal structure and external morphology of zinc nanoparticles by using two types of primers, which are zinc nitrate and zinc acetate, and in the presence of the aqueous extract of the leaves of *Laurus nobilis* plant (Fakhari *et al*., 2019).

The precursor concentration of zinc nitrate has a significant impact on the production of nano-ZnO when *Aloe vera* extract is employed according to (Rasli *et al.,* 2020). These compounds include enzymes, proteins, flavonoids, phenols, alkaloids, tannins, soaps, and others, which play a key role in the reduction process of particles (Lakshmeesha *et al*., 2019 and Rahayu *et al.,* 2020). In addition, using zinc acetate compound as a starting material and adding *Ixora coccinea* leaf extract, (Yedurkar *et al.,* 2016) were able to generate spherical zinc oxide nanoparticles with a high degree of stability.

The species *Petroselinum crispum*, or as known locally parsley, is one of the herbal and aromatic plants that belong to the Apiaceae family. The chemical composition of parsley has revealed the presence of flavonoids, terpenes, coumarins, furanocoumarins, essential oils, and fatty acids as secondary compounds (Chaves *et al.,* 2011, Liberal *et al.,* 2020). Parsley belongs to the Mediterranean herb whose leaves have a high content of Vitamin C (ascorbic acid). This high content of vitamin C in parsley leaves can play an essential role as a strong reducing agent in this synthesis of nanoparticles (Roy *et al.,* 2015).

The present study is a serious attempt at the investigation of effective methods of chemical green synthesis on nanoparticle sizes. The current investigation was adopted on the hypothesis that says that the size of particles that can be produced with this method is restricted by the details of the preparation as well. Therefore, the conventional thermal method, the microwave method, and the plasma method have been covered in this study. The comparison was made by analyzing the size of the measured particles, using atomic force microscopy. The biological activity of ZnO NPs nanoparticles was evaluated by using well diffusion method for pathogenic fungi like *Candida albicans*, *Candida guiller*, *Candida zeylenoid* and *Candida kruse*.

2. Material and methods

2.1. Preparation of the aqueous extract of the Petroselinum crispum

P. crispum seeds were purchased from a local market in Baghdad and ground for 5-7 minutes in an electrical grinder. 10 g of *P. crispum* seeds powder was mixed with 100 mL of boiling distilled water. The mixture was placed in a magnetic stirrer for 2-3 hours and left for 24 hours. Then the mixture was filtered by using Whitman paper No.1, and the filtrate was stored at 4 °C. The methods of (Trease and Evans, 1989 and Harborne, 1973) were used to identify active phytoconstituents (Table-1).

2.2. Preparation of zinc nanoparticles

The Zn nanoparticle was prepared by three methods:

2.2.1. Preparation of zinc nanoparticles by using magnetic stirrer

ZnNPs was synthesized by adding 45 mL of $1*10^{-3}$ M of $ZnSO_4$ (Sigma-Aldrich) solution in a flask placed on the magnetic stirrer device (AL- Shaheen *et al*., 2020). After the temperature stabilized at 60 °C, added 5 mL of *P. crispum* seeds hot aqueous extract with continuous stirring for half an hour. The final solution was stored at 4 C° (Rasli *et al*., 2020).

2.2.2. Preparation of Zinc nanoparticles using Microwave:

The nanostructured zinc solution was prepared by adding 45 mL of ZnSO4 at a concentration of $1*10^{-3}$ M in a flask with the addition of 5 mL of *P. crispum* hot aqueous seeds extract. Then the mixture was placed in the microwave for 50 seconds (500-1000) watts, after which it was stored at 4 °C (Chikan and McLaurin, 2016).

2.2.3. Preparation of Zinc nanoparticles using Cold Plasma:

Dielectric barrier discharge reactor was used to generate the cold plasma. The generation system was designed in accordance with the nature of the used models and to achieve the largest plasma package that can be generated as can be seen in Figure (1). After numerous tests, the optimum distance between the electrode and the model surface was from a half to one centimeter. Four solutions of ZnNPs were prepared in four flasks, added to each solution 45 mL of $1*10^{-3}$ M ZnSO4 then added 5 mL from *P. crispum* hot aqueous seeds extract in every flask. The solutions were exposed directly to the plasma device with a difference in the exposure time of the plasma for

every solution which is (1, 3, 5, and 10) minutes; then the solutions were stored at 4 °C (Primc *et al*., 2021).

2.3. Identifying the best circumstances for synthesis zinc nanoparticles

2.3.1. Determine the optimum temperature for the synthesis of ZnNPs

The optimal temperature for synthesis ZnNPs was established by mixing 45 mL of $1*10^{-3}$ M ZnSO4 solution in a flask with 5 mL of *P. crispum* hot aqueous seeds extract then put on a magnetic stirrer device at varied temperature (30, 40, 50, 60, 70 and 80 °C) every time. After that, all the solutions were kept at 4 °C (Verma and Mehata, 2016).

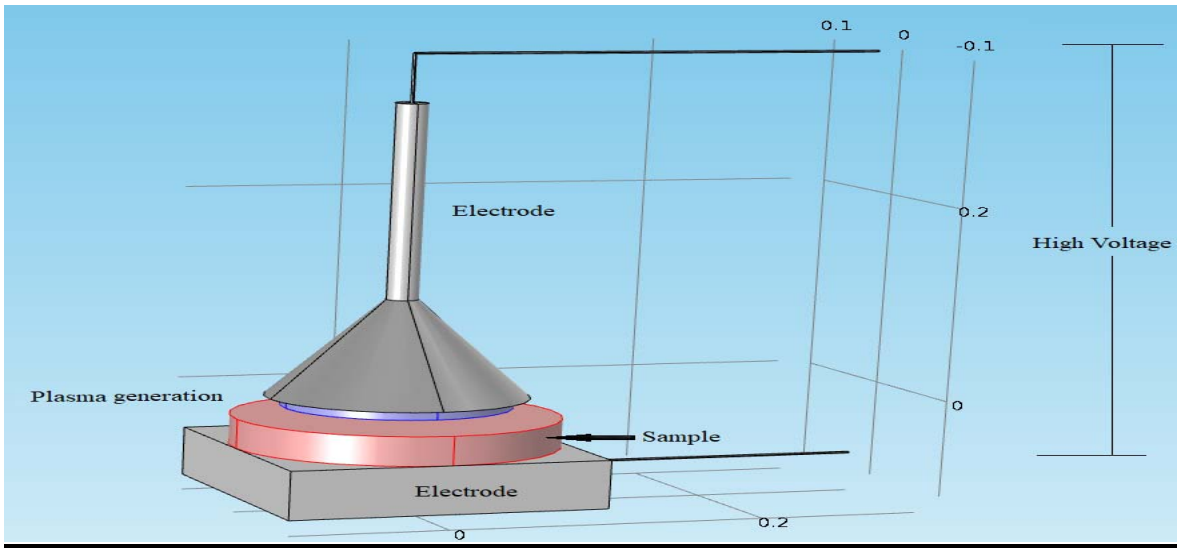

Figure 1: Schematic diagram of Plasma generation in dielectric barrier discharge (DPD) reactor used in the current study

2.3.2. The effect of variance in plant material weight in extraction of P. crispum seeds hot aqueous extract in ZnNPs synthesis:

The hot aqueous extracts were prepared using different weights of powdered *P. crispum* seeds, which are (4, 7, 10, 13, and 16 g) per 100 mL of boiling distilled water, and the extracts were placed on the magnetic stirrer device for 2 - 3 hours for homogenization then left for 24 hours. The mixtures were then filtered and kept in 4 °C (Sithara *et al*., 2017).

2.3.3. Evaluate the use of different volumes from P. crispum seeds hot aqueous extract and ZnSO4 solution in ZnNPs manufacturing.

Different volumes of seeds hot aqueous extract and ZnSO4 solution were used in manufacture of ZnNPs by adding (45, 25 and 5) mL of $1*10^{-3}$ M ZnSO4 with (5, 25 and 45) mL of seeds hot aqueous extract respectively (Ahmed *et al.,* 2016 and Javad *et al*., 2017).

2.4. Characterization of ZnNPs

2.4.1. Atomic Force Microscopy (AFM) measurement

The surface morphology of ZnNPs was investigated using AFM (Angstrom AA2000, contact mode, atmospheric circumstances, USA) pictures, which provide clear topological images of surface morphology at high magnification. A 0.5 mL sample of ZnNPs was centrifuged for 5 minutes at 10000 rpm in an eppendrof tube. Using atomic force microscopy, a few droplets of the sample were deposited on the slide, air dried, and described (Altaee *et al*., 2020).

2.4.2. UV spectrophotometer measurement

UV-vis spectroscopy was used to do preliminary characterization of the ZnNPs. The optical behavior of the biosynthesized ZnNPs was studied using a spectrophotometer (UV-Spectrophotometer - Shimadzu UV-1800) in a quartz cuvette with a 1 cm optical path at ambient temperature. Aliquots of ZnNPs were examined in the wavelength range of (200 - 700 nm) (Malarkodi *et al*., 2014).

2.5. Biological activity of ZnNPs

The agar well diffusion assay method was used to test the antifungal activity of ZnNPs synthesized by magnetic stirrer, microwave and cold plasma in 10 minutes. Stock cultures of *Candida albicans*, *Candida guiller*, *Candida zeylenoid*, and *Candida kruse* were freshly cultured in a petri dish at 25 °C for 24 - 48 hours in an incubator (Memmert, Germany) on Sabouraud Dextrose Agar (SDA) medium (Hi Media, India) (Mahdavi *et al*., 2013). A loop full of cells were transferred from the agar to a test tube with 5 mL of Sabouraud Dextrose broth (Hi Media, India), then incubated at 30 °C with shaking for 12 - 16 hours (Bensizerara *et al*., 2013). SDA agar plates were inoculated with Candida strains under aseptic conditions and wells were filled with 50 µL with various concentrations of ZnNPs (100, 75, 50 and 25) % and incubated at 25 °C for 24 - 48 hours. The inhibition zones were measured in millimeter (well size 6 mm) (Devi and Bhimba, 2014). Antifungal nystatin (50 mcg) was selected as a positive control, by using a disc diffusion method against *Candida albicans*, *Candida guiller*, *Candida zeylenoid*, and *Candida Kruse*. The standard antifungal disc was purchased from Hi-Media, India (Deabes *et al*., 2020).

3. Results and Discussions

The Differences in chemical and physical conditions such as weight of plant material, volumes of reactants, temperature and the kind of reaction method have significantly affected the size, form and the morphology of ZnNPs in this study.

3.1. The visual observation and pH value of Zn nanoparticles

The reaction between *P. crispum* extract and ZnSO4 solution was transparent at the beginning of the reaction; however, the change in color was noticed after that as it turned into a light yellow color after of Zn nanoparticle formation, while the pH value of ZnNPs was 7 and remained constant during the reactions and after the formation of Zn nanoparticles and did not change during the period of storage.

3.2. Characterization of the zinc nanoparticles by UV–vis spectrophotometric analysis

Zinc oxide nanoparticles were synthesized according to decided protocol using seeds aqueous extract from *P. crispum*. After the addition of seeds extract to the zinc sulphate solution, a slight color change will appear. It indicates the completion of the reaction, which is due to the excitement of plasmon vibrations in the zinc nanoparticles. Zinc sulphate solution alone without extract has no color; the intensity of color will steadily increase after the addition of seeds of the aqueous extract with an increase in the incubation period and the temperature. The ZnNPs exhibited slight yellow color, which may due to the excitement of the surface plasmon resonance (SPR) effect and the reduction of zinc sulphate. The reduction of seeds aqueous extract by zinc ions and the formation of ZnNPs was emphasized using UV–vis spectroscopy. A wavelength scanning process in the UV–vis spectra revealed an absorption peak at approximately 338 nm for ZnNPs (Figure 2).

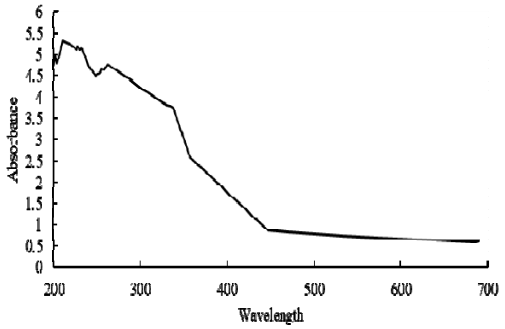

Figure 2: UV-Vis spectrum of manufactured ZnNPs by the reaction between ZnSO4 10^{-3} M with *P. crispum* seeds extract.

These results were similar to the results of (Salem *et al*., 2015) which revealed an absorption peak at 340 nm for zinc nanoparticles synthesized by green method using leaf and fruit extracts from *C. procera*. Through Table (1), which shows the detection of secondary metabolites in plant seed extract *P. crispum*, the presence of metabolic compounds in appropriate quantities such as phenols, flavonoids and tannins can interact with zinc molecules as reduction agents and help in the synthesis and stability of zinc nanoparticles.

Table 1: Qualitative Phytochemical Analysis of *P. crispum* seeds extract

Phytoconsitituents	Reagents	Aqueous extract
Alkaloids	Mayer's + Wagner's	-
Saponins	Gelatin	-
Tannins	Ferric chloride	+
Phenols	Iron chloride	+ +
Flavonoids	Alkaline Reagent	+ +
Glycosides	Borntrager's	-

3.3. The effect of experimental conditions on the formation of Zn nanoparticles

The results showed the formation of zinc nanoparticles in all different experimental conditions, such as weight of plant material, volumes of reactants, temperature as well as at different manufacturing methods such as are magnetic stirrer, microwave and cold plasma. Generally, the sizes of the Zn-nanoparticles ranged between 18.77 and 75 nm.

3.3.1. The effect of different temperatures in ZnNPs synthesis

Effect of thermal treatment was addressed in the current study. The influence of 30, 40, 50, 60, 70, and 80 °C on the preparation of zinc oxide nanoparticles (Zn-NPs) was adopted in the current investigation. Figure (3) and Figure (4) show the volume percentage of the diameters of Zn-NPs formed using Atomic Force Microscopy at different temperatures. The figures show that the temperature has a clear effect on the particle size of the Zn-NPs produced. Lowest average diameter (18.77 nm) was obtained at 50 °C. This diameter began to increase with the rise in temperature to be 23, 31, 25.27, and 30.07 nm in diameter for particles generated in temperatures of 60, 70, 80, and 30 °C respectively. In fact, these experimental data of Zn-NPs were due to the formation of clusters and agglomerates. In addition, increase in the temperature increases the acceleration of the rates of nucleation. This interpretation was also supported by (Bandeira *et al*., 2020; Parra and Haque, 2014; Dhadapani *et al*., 2014; Manzoor *et al*., 2015 and Shaziman *et al*., 2015). They emphasized that the temperature and exposure time can determine the structure and size of nanoparticles form by green method. On the other hand, the reduction in the temperature gives irregular shapes while keeping the clusting rates low. This study, and through a set of experiments, found that the temperature of 50, 60 and 80 °C gave the lowest diameter, so the average temperatures between them was 60 C°, which was adopted in the subsequent experiments. In fact, it appears that this increase in particle size with increasing temperature is not limited to zinc oxide, but many other mineral particles have had the same effect. For example, the average diameter of silver particles increases with increasing temperature, and for the same reasons above (Liu *et al*., 2020).

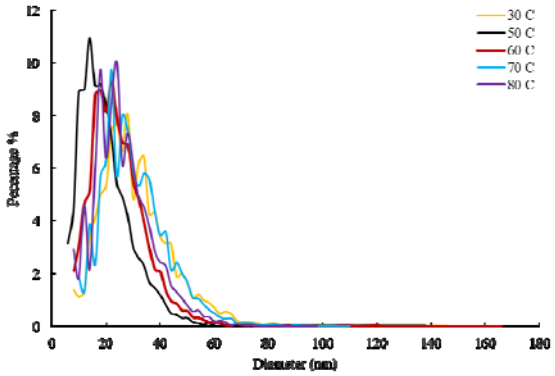

Figure 3: Granularity Distribution of Zn NPS at different temperatures (30, 50, 60, 70and 80 ºC).

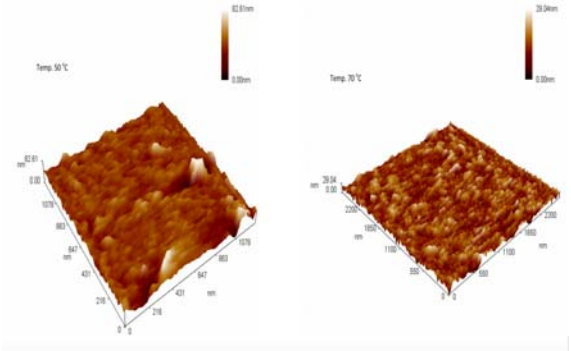

Figure 4: 3D-response of Granularity Distribution of zinc oxide nanoparticles at 50 and 70 ºC using Atomic Force Microscopy

3.3.2. The effect the different plant weights of P. crispum seeds extracts in ZnNPs synthesis

The effect of different group of weights of *P. crispum* seeds powder (4, 7, 10, 13 and 16) g, on the size of the nanoparticles generated by using green method was studied, as shown in Figure 5 and 6. The experimental data showed the variation in the average diameter of the nanoparticles and at a temperature of 60 °C and within the generated particles. The lowest diameter ratio of nanoparticles was obtained at 10 g weight compared to other weights, since the average diameter was 23.62 nm at a weight of 10 g, compared to the other weights that ranged between 64 and 75 nm.

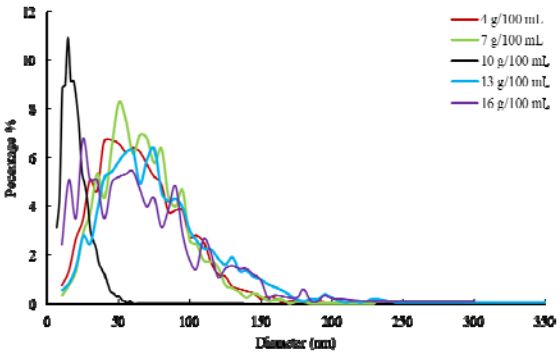

Figure 5: Granularity Distribution of zinc nanoparticles at different weight of *P. crispum* seeds (4, 7, 10, 13, and 16 g / 100 mL)

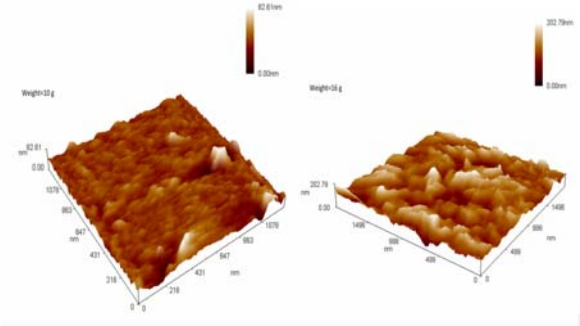

Figure 6: 3D-response of Granularity Distribution of ZnNPs at 50 and 70 ºC using Atomic Force Microscopy

3.3.3. Effect of different volume ratio of P. crispum seeds extract and ZnSO4 solution in ZnNPs synthesis

The effect of the ratio of the extract of *P. crispum* seeds to the salt on the diameter of the generated particles was verified in the present study. The results showed that the half-weights (50 % for each one) achieved the lowest possible diameter than other percentages as shown in Figure 7 and 8. 43.36 nm was achieved at 50 % volume of the extract with 50 % volume of salt pulse 50 % of the extract, while 49.62 nm and 70.16 nm were achieved at 20 % volumes of extract pulse 80 % of the extracted solution as well as 80 % volumes of extract pulse 20 % of salt, respectively. However, in the form of a single digit, the quantity that achieved less than 40 nanometers was greater in the first percentage compared to the average.

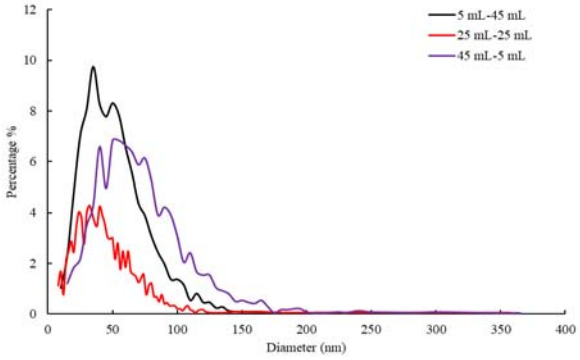

Figure 7: Granularity Distribution of ZnNPs at different volume ratio of *P.crispum* seeds extract and ZnSO4 solution

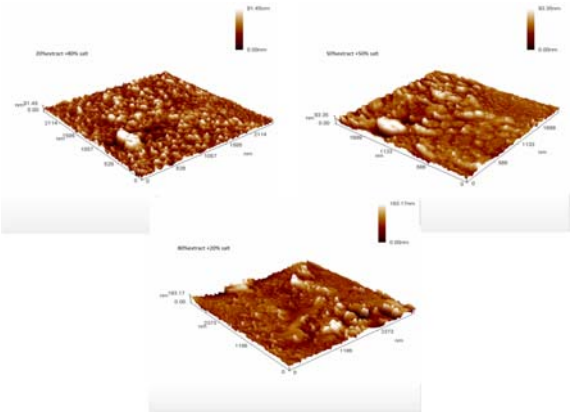

Figure 8: 3D-response of Granularity Distribution of ZnNPs at different extract solution of *P.crispum* seeds to salts ratio using Atomic Force Microscopy.

3.4. owave device in synthesis of ZnosThe effect of using cold plasma in synthesis of ZnNPs

The use of cold plasma as an alternative to the heating stage in preparing nanoparticles was also present in this investigation. Figure 9 shows a complete analysis of the size of the generated fine particles. The time factor was the important variable that was adopted in this study. The results showed that the exposure of the solution to a time of 3 minutes was the best in terms of the quantity and size of the generated particles. The reduction in time was apparently not sufficient to achieve the required particle size, whereas the increased exposure time of the models to plasma radiation may cause some of the particles to agglomerate to form larger particles. Periods 3-5 minutes led to the production of nanoparticles size. This is consistent with (AL- Azawi *et al.,* 2019) in the production of Silica NPs at a concentration of 18 nm using cold plasma for five minutes.

In fact, the cold plasma method used in the current study causes three regions to occur, which include (gas phase region, interface region, and liquid phase region). Each of these regions undergoes a specific reaction that consumes or produces electrons (Humud and Dawood, 2016 and Kaushik *et al.,* 2019). The main driver of these reactions is the plasma generated to generate hydrogen peroxides [OH^+] in the gas phase and interface regions (Milosavljevic and Micic, 1978). In the liquid phase, these generated peroxides react to produce enough electrons to form the zinc with zero ions [Zn^0].

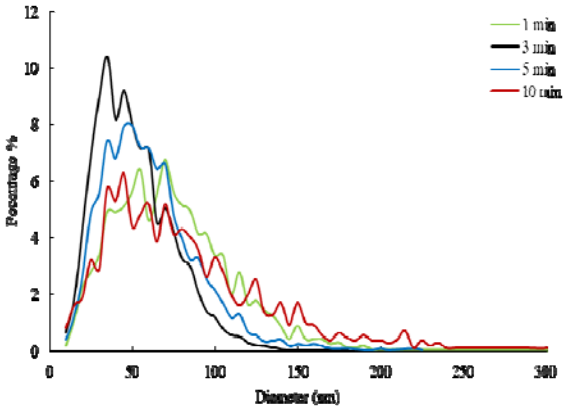

Figure 9: Granularity Distribution of zinc oxide nanoparticles using plasma approach method

3.5. The effect of using the microwave device in synthesis of Zn NPs

The use of microwave devices as another means of preparing the heat required for the formation of nanoparticles has also been adopted in the current study. The exposure time to microwave waves was selected as an independent variable in the current study. As for determining the time of exposure of the laboratory samples to those microwaves, they were restricted by the amount of heat and the temperature that the samples would reach. Fifty degrees Celsius and sixty degrees Celsius were determined after several experiments on the condition that the temperature does not reach more than the required temperature. Figure 10 shows the numerical percentage of nanoparticles formed by using this method. The results showed that this percentage of nanoparticles formed after fifty seconds is higher than that obtained after the passage of sixty seconds. The results here support previous studies that showed the contribution of heat gradient-free to improving the size of the microparticles generated (Gerbec *et al.,* 2005). More clearly, 7 % represented the numerical percentage of nanoparticles formed at 50 °C, compared to 4 % at exposure time of 60 °C. These results were consistent with what was obtained using the conventional method. However, the difference between the two methods is the short period of time for the training phase with the cost factor.

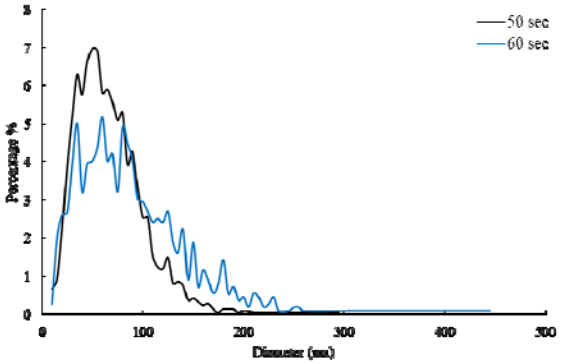

Figure 10: Granularity Distribution of zinc oxide nanoparticles using microwave approach methods.The biological activity of Zn NPs samples

Antifungal activity of Zn NPs samples was studied against four types of Candida as *Candida albicans*, *Candida guiller*, *Candida zeylenoid,* and *Candida kruse*. The results presented in table 2 show that the synthesis method of Zn nanoparticles and their concentration also the kinds of Candida under study have a great effect on the zone size of inhibition for fungi as reported by (Gunalan *et al*., 2012). The Zn nanoparticles that were synthesized by cold plasma showed a high inhibition effect unlike the ZnNPs that were synthesized by using the magnetic stirrer method, and the microwave method did not show any inhibitory effect against any *Candida* species. Table 2 shows ZnNPs synthesized by cold plasma method in the concentrations (100, 75, 50, and 25) %. The results illustrated that the highest inhibition effect against both *C. albicans* and *C. zeylenoid* was more than that with the positive control (nystatin). ZnNPs achieved a high inhibition effect in 100% concentration, compared with the positive control for *C. Kruse*. All the concentrations of ZnNPs showed a low inhibition effect than positive control of *Candida guiller*. The antimicrobial activity differences may derive from the electrostatic attraction between the negatively charged microbial cell membrane and the positively charged zinc nanoparticles (Hamouda *et al*., 2001), and this is due to difference in the synthesis method of ZnNPs. The synthesis method of zinc nanoparticles affected the interaction of zinc ions with microbial cells and inhibited their growth, as the nanoparticles formed in each way were different in terms of size and orientation (Gunalan *et al*., 2012 and Wang *et al*., 2007).

Table 2: The antifungal activity of ZnO NPs which synthesized by using three methods and the concentrations (100, 75, 50 and 25) % against Candida

Fungi	Positive Control Nystatin (mm)	Zone of inhibition (mm)				Synthesis method of ZnNPs				Concentration of ZnNPs (%)			
		Cold plasma method (10 min)				Magnetic stirrer method				Microwave method			
		100	75	50	25	100	75	50	25	100	75	50	25
Candida albicans	16	35	30	27	24	0.0	0.0	0.0	0.0	0.0	0.0	0.0	0.0
Candida guiller	18	12	17	15	0.0	0.0	0.0	0.0	0.0	0.0	0.0	0.0	0.0
Candida zeylenoid	18	25	22	20	0.0	0.0	0.0	0.0	0.0	0.0	0.0	0.0	0.0
Candida kruse	19	20	16	17	0.0	0.0	0.0	0.0	0.0	0.0	0.0	0.0	0.0

The Figure 11 showed that ZnNPs synthesized by cold plasma method in the concentrations (100, 75, 50 and 25) % have the highest inhibition effect against *C. albicans*., followed by *C. zeylenoid* that showed a good effect in the concentrations (100, 75 and 50) % of Zn nanoparticles; both *C. zeylenoid* and *C. kruse* have achieved almost the same inhibition effects against using the nanoparticles in the same concentrations, while the concentration 25 % of zinc nanoparticles did not show any inhibitory effect on fungi except for *C. albicans*. That may be due to proper diffusion of Zn nanoparticles in the agar medium. The results showed an increase in the percentage of fungi inhibition by increasing the concentration of zinc nanoparticles, and this is consistent with what has been achieved by both (Gunalan *et al*., 2012 and Navale *et al.,* 2015). The difference in the inhibitory effect of zinc nanoparticles on fungi may be due to difference in their individual response and their genotypic characters (Senthilkumar and Sivakumar, 2014).

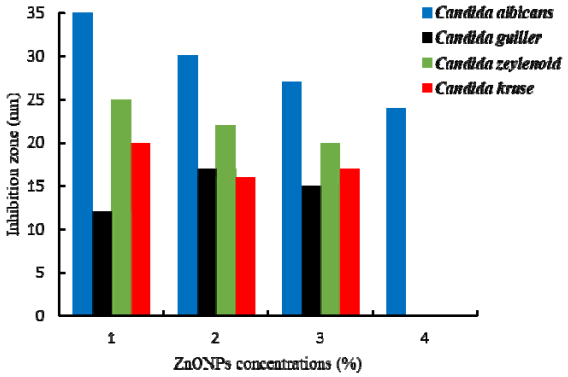

Figure 11: The effect of ZnO nanoparticles that synthesized by using cold plasma method for 10 min on the biological activity for pathogenic fungi by using different concentrations (1) 100%, (2) 75%, (3) 50%, (4) 25%.

4. Conclusions

The effect of the preparation method on the size of the zinc-nanoparticles was verified in the current study under different operating conditions. The study concluded the importance of those conditions as well as the method used in the preparation process, whether it was the traditional thermal method, microwave oven or plasma, on the size analysis of generated particles. High temperatures, in addition to being economically costly, also increase the size of zinc nanoparticles generated in the microwave and thermal method, while the use of the Plasma generation in dielectric barrier discharge (DPD) reactor has achieved the best percentage of formed particles of nano sizes with the associated operational and economic factor. The zinc nanoparticles that were prepared by using cold plasma also achieved the highest inhibition zone against fungi, especially *Candida albicans*.

References

AL-Azawi MT, Hadi SM and Mohammed CH. 2019. synthesis of silica nanoparticles via green approach by using hot aqueous extract of *Thuja orientalis* leaf and their effect on biofilm formation. Iraqi *J Agric Sci*, **50**:245-255.

Ahmed S, Ahmad M, Swami BL and Ikram S. 2016. A review on plants extract mediated synthesis of silver nanoparticles for antibacterial application: A green expertise. *J of Advs Res*, **7**:17-28

Al-Shaheen MAS, Owaid MN and Muslim RF. 2020. Synthesis and characterization of zinc nanoparticles by natural organic compounds extracted from licorice root and their influence on germination of Sorghum bicolor seeds. *JJBS,* **13 (4)**: 559-565.

Altaee MF, Yaaqoob LA and Kamona ZK. 2020. Evaluation of the biological activity of nickel oxide nanoparticles as antibacterial and anticancer agents. *Iraqi J Sci,* **61 (11)**: 2888-289.

Bandeira M, Giovanela M, Roesch-ely M, Devine DM. & DA Silva Crespo J. 2020. Green synthesis of zinc oxide nanoparticles: A review of the synthesis methodology and mechanism of formation. *Sustainable Chem Pharm,* **15:** 100223.

Bensizerara D, Menasria T, Melouka M, Cheriet L. and Chenchouni H. 2013. Antimicrobial activity of zerophytic plant (Cotula cinerea Delile) extracts against some pathogenic bacteria and fungi. *JJBS*, **6 (4)**: 266-271.

Chaves Douglas SA, Flavia SF, Mariane A, Ana Paula DE, Russolina B. and Zingalib and Sonia SC 2011. Phenolic chemical composition of Petroselinum *crispum* extract and its effect on haemostasis. *NPC*, **6 (7)**: 961-964.

Daphedar A. And Taranath, TC. 2018. Green synthesis of zinc nanoparticles using leaf extract of *Albizia saman* (Jacq.) Merr. and their effect on root meristems of *Drimia indica* (Roxb.) Jessop. *Caryologia*, **71:**93-102.

Deabes MM, Allayeh AK, Seif MM, Rasmey AM and Nagiub KM. 2020. Antiviral, antifungal, and antibacterial potential activities of *Ephedra Sinica in Vitro*. *JJBS*, **13**:313-320.

Devi JS. And Bhimba BV. 2014. Antibacterial and antifungal activity of silver nanoparticles synthesized using *Hypnea muciformis*. *Biosci Biotechnol Res. Asia*, **11 (1)**: 235-238.

Dhandapani P, Siddarth AS, Kamalasekaran, S, Maruthamuthu S. And Rajagopal G. 2014. Bio-approach: Ureolytic bacteria mediated synthesis of ZnO nanocrystals on cotton fabric and evaluation of their antibacterial properties. *Carbohydr. Polym,* **103:** 448-455.

El-Seedi HR, EL-Shabasy R M, Khalifa SAM, Saeed A, Shah A, Shah R, Iftikhar, F J, Abdel-Daim, MM, Omri A, Hajrahand N.H, Sabir JSM, Zou X, Halabi MF, Sarhan W. And Guo W. 2019. Metal nanoparticles fabricated by green chemistry using natural extracts: biosynthesis, mechanisms, and applications. *RSC Advances,* **9:**24539-24559.

Fakhari S, Jamzad M. And Fard HK. 2019. Green synthesis of zinc oxide nanoparticles: a comparison. *Green Chem Lett Rev,* **12:**19-24.

Gerbec JA, Magana D, Washington A. and Strouse GF. 2005. Microwave-Enhanced reaction rates for nanoparticle synthesis. *J Am Chem Soc*, **127**: 15791-15800.

Gunalan S, Sivaraj R. and Rajendran V. 2012. Green synthesized ZnO nanoparticles against bacterial and fungal pathogens. *Pro Nat Sci-Mater,* **22:** 693-700.

Hamouda T, Myc A, Donovan B, Shih AY, Reuter JD. and Baker JR, 2001. A novel surfactant nanoemulsion with a unique non-irritant topical antimicrobial activity against bacteria, enveloped viruses and fungi. *Microbiol. Res***, 156 (1)**:1–7.

Harborne JB. 1973. **Phytochemical methods**, Chapman and Hull Ltd, London, pp.:49-188.

Humud HR and Dawood MM. 2016. Effect of Ag nanoparticles on R6G laser dye hosted by PMMA polymerized by plasma jet. *Iraqi J Physics*, **14**: 27-36.

Javad S, Akhter I, Aslam K, Tariq A, Ghaffar N, Iqbal S and Naseer I. 2017. Antibacterial activity of plant extract and zinc nanoparticles obtained from *Syzigium aromaticum* L. *Pure Pure Appl Biol*, **6 (4)**: 1079-1087.

Kaushik NK, Kaushik N, Linh NN, Ghimire B, Pengkit A, Sornsakdanuphap J, Lee SJ. And Choi EH. 2019. Plasma and nanomaterials: fabrication and biomedical applications. *J. Nanomater*, https://doi.org/10.3390/nano9010098. (Jan. 14,2019).

Lakshmeesha TR, Kalagatur NK, Mudili V, Mohan CD, Rangappa S, Prasad BD,

Ashwini BS, Hashem A, Alqarawi AA, Malik JA, Abd_Allah EF, Gupta VK, Siddaiah CN. And Niranjana SR. 2019. "Biofabrication of zinc oxide nanoparticles with syzygium aromaticum flower buds extract and finding Its novel application in controlling the growth and mycotoxins of *Fusarium graminearum*". *Front. Microbiol,* https://doi.org/10.3389/fmicb.2019.01244. (Jun. 12,2019).

Liberal Â, Fernandes Â, Polyzos N, Petropoulos SA, Dias MI, Pinela J, Petrovi´c J,

Sokovi´c M, Ferreira ICFR. And Barros L. 2002. Bioactive properties and phenolic compound profiles of turnip-rooted, plain-leafed and curly-leafed parsley cultivars. *Mol,*

25: 1-17.

Liu H, Zhang H, Wang J. And Wei J. 2020. Effect of temperature on the size of biosynthesized silver nanoparticle: Deep insight into microscopic kinetics analysis. *Arab J Chem,* **13:** 1011-1019.

Mahdavi V, Saber M, Dastjerdi HR. And Mehrvar A. 2013. Susceptibility of the Hymenopteran Parasitoid, Habrobracon hebetor (Say) (Braconidae) to the Entomopathogenic Fungi *Beauveria bassiana* Vuillemin and *Metarhizium anisopliae* Sorokin. *JJBS*, **6 (1)**: 17-20

Malarkodi C., Rajeshkumar S, Paulkumar K, Vanaja M, Gnanajobitha G. And Annadurai G. 2014. Biosynthesis and antimicrobial activity of semiconductor nanoparticles against oral pathogens. *Bioinorg Chem Appl*, **2014**: 1-10

Manzoor U, Tuz Zahra F, Rafique S, Moin MT. And Mujahid M. 2015. "Effect of synthesis temperature, nucleation time, and postsynthesis heat treatment of ZnO nanoparticles and its sensing properties". *J Nanomater,* https://doi.org/10.1155/2015/189058. (Jan. 12, 2015)

MIilosavljevic BH. And Micic OI. 1978. Solvated electron reactions in water-alcohol solutions. *J Phys Chem*, **82**: 1359-1362.

Navale GR, Thripuranthaka M, Late DJ. And Shinde SS, 2015. Antimicrobial activity of ZnO nanoparticles against pathogenic bacteria and fungi. *Nanotechnol Nanomed Sci-Medcentral*,

3 (1): 1033-1042

Parra MR. And Haque FZ. 2014. Aqueous chemical route synthesis and the effect of calcination temperature on the structural and optical properties of ZnO nanoparticles. *Journal J. Mater. Res. Technol,* **3:** 363-369.

Paul D. and Sinha SN. 2014. Extracellular synthesis of silver nanoparticles using *Pseudomonas aeruginosa* KUPSB12 and its antibacterial activity. *JJBS*, **7 (4)**: 245-250.

Primc G, Brencic K, Mozetic M. And Gorjanc M. 2021. Recent advances in the plasma-assisted synthesis of zinc oxide nanoparticles. *J Nanomater*, **11(1191):** 1-19.

Rahayu E, Wonoputri V. And Samadhi TW. 2020. "Plant extract-assisted biosynthesis of zinc oxide nanoparticles and their antibacterial application". *IOP Con Ser.: Mater Sci Eng,* https://doi.org/10.1088/1757-899X/823/1/012036. (Oct, 2019).

Rasli NI, Basri H. And Harun Z. 2020. Zinc oxide from *Aloe vera* extract: two-level factorial screening of biosynthesis parameters. *Heliyon,* **6:** 1-8.

Roy K, Sarkar CK. and Ghosh CK. 2015. Plant-mediated synthesis of silver nanoparticles using parsley (Petroselinum crispum) leaf extract: spectral analysis of the particles and antibacterial study. *Appl Nanosci*, **5**:945–951.

Sabir S, Arshad M. and Chaudhari SK. 2014. Zinc oxide nanoparticles for revolutionizing agriculture: Synthesis and applications. *Sci. World J,* **2014:** ID 925494.

Salem W, Leitner DR, Zingl FG, Schratter G, Prassl R, Goessler W, Reidl J. & Schild S. 2015. Antibacterial activity of silver and zinc nanoparticles against *Vibrio cholerae* and enterotoxic *Escherichia coli*". *Int. J. Med. Microbiol. Suppl,* **305:** 85-95.

Senthilkumar SR. & Sivakumar T. 2014. Green tea (*Camellia sinensis*) mediated synthesis of zinc oxide (Zno) nanoparticles and studies on their antimicrobial activities. *Int. j. pharm,*

6: 461-465**.**

Sharma R, Garg R. & Kumari A. 2020. A review on biogenic synthesis, applications and toxicity aspects of zinc oxide nanoparticles. *EXCLI J,* **19:** 1325-1340.

Shaziman S, Ismailrosdi AS, Mamat MH. & Zoolfakar AS. 2015. "Influence of growth time and temperature on the morphology of ZnO nanorods via hydrothermal". *IOP Con Ser.: Mater Sci Eng,* http://dx.doi.org/10.1088/1757-899X/99/1/012016. (Nov, 2015).

Singh A, Singh NB, Hussain I, Singh H. & Singh SC. 2015. Plant-nanoparticle interaction: An approach to improve agricultural practices and plant productivity. *Int. J. Pharm. Sci. Invent*, **4:** 25-40.

Sithara R, Selvakumar P, Arun C, Anandan S and Sivashanmugam P. 2017. Economical synthesis of silver nanoparticles using leaf extract of *Acalypha hispida* and its application in the detection of Mn(II) ions. *J Adv Res*, **8**: 561-568.

Thi UUD, Nguyen TT, Thi YD, Thi KHT, Phan BT. & Pham KN. 2020. Green synthesis of ZnO nanoparticles using orange fruit peel extract for antibacterial activities. *R. Soc. Chem.,* **10:** 23899-23907.

Trease GE. and Evans WC. 1989. **Textbook of Pharmacognosy**, 13 edn. Nottingham, England.

Verma A and Mehata MS. 2016. Controllable synthesis of silver nanoparticles using Neem leaves and its microbial activity. *J Radiat Res Appl Sci*, **9**:109-115

Viktor Chikan, V. and Emily J. McLaurin, EJ. 2016. Rapid nanoparticle synthesis by magnetic and microwave heating. *J Nanomater*, **6 (85)**: 1-9.

Wang X, Yang F, Yang W. and Yang X. 2007. A study on the antibacterial activity of one-dimensional ZnO nanowire arrays: effects of the orientation and plane surface, *ChemComm*, **42**: 4419–4421.

Yahya N, Puspitasari P. & Latiff, NRA. 2013. Hardness improvement of dental amalgam using zinc oxide and aluminum oxide nanoparticles. characterization and development of biosystems and biomaterials, *Ads Struct Mater,* **29:** 9-32

Yedurkar S, Maurya, C. & Mahanwar P. 2016. Biosynthesis of zinc oxide nanoparticles using *Ixora Coccinea* Leaf Extract—A Green Approach. *OJSTA* , **5**: 1-14.

JJBS

Volume 15, Number 4,December 2022
ISSN 1995-6673
Pages 643 – 647
https://doi.org/10.54319/jjbs/150413

Jordan Journal of Biological Sciences

Some Experimental Studies on the Anticoagulant Activity of the Synthetic Coumarin Derivatives

Ilir Mazreku[1], Ibrahim Rudhani[2*], Luiza Lajqi[3], Mimoza Hadergjonaj[3], Hamide Ibrahimi[3], Arben Haziri[3**]

[1]*Department of Biology, Faculty of Natural Science, University of Prishtina "Hasan Prishtina", Kosovo;* [2]*Department of Intern Medicine and Nephrology, Faculty of Medicine, University of Prishtina "Hasan Prishtina", Kosovo;* [3]*Department of Chemistry, Faculty of Natural Science, University of Prishtina "Hasan Prishtina", Kosovo*

Received: October 16, 2021; Revised: January 8, 2022; Accepted: January 19, 2022

Abstract

Intensive research efforts have been devoted to the design and synthesis of 4-hydroxycoumarin derivatives as anticoagulants. The main purpose of this study was to report the synthesis of some coumarin-type derivatives, including, 4-aryl-1,2-dihydro-6-(4-hydroxy-2-oxo-2H-chromene-3-yl)-2-oxopyridin-3-carbonitrile (3, 4). The structure of the synthesized compounds has been verified on the basis of literature data and spectroscopic measurements such as NMR, MS and IR. In addition, there were two objectives for the study: first, to test these synthetic derivatives *in vivo* for their anticoagulant effects in the laboratory male mice (*Mus musculus swiss albino*). Second, to compare between the *in vivo* activity of these synthetic derivatives and that of Warfarin (CAS 81-81-2), which is the most commonly used anticoagulant. Prothrombin time (PT) was used as the value to compare the anticoagulant properties of the synthesized compounds (1, 3, 4) and warfarin. The time for plasma to solidify following the addition of warmed thrombokinase suspension was taken as the PT. Results of this study revealed that the most potent compound of the synthesized derivatives was 4-(3-bromo-phenyl)-6-(4-hydroxy-2-oxo-2H-chromene-3-yl)-2-oxo-1,2-dihydro-pyridine-3-carbonitrile (4), which shows higher anticoagulant activity ($PT_{(s)}$ 21.30) than warfarin ($PT_{(s)}$ 14.60). However, Anticoagulant activity was also associated with toxicity by the all synthesized compounds. Conclusion and practical importance: Synthesized coumarins (3 and 4) increased PT when compared to saline treated control group and other coumarins. They are potentially antithrombotic drug candidates for further elaboration. Compounds 3 and 4 need to be further tested for the side effects so that they can be introduced into clinical trials.

Keywords: Coumarine derivatives, Hyroxycoumarin, Warfarin, Anticoagulant activity

1. Introduction

Coumarins are one of the most significant families of natural product compounds and can be found in many plants as secondary metabolites. Chemically, coumarins belong to the subgroup of lactones (Nikhil *et al*., 2012). There is a large number of coumarin derivatives, namely natural and synthetic coumarin, which associated with various types of biological activities, such as anti-inflammatory, anticancer, antioxidant, anti-HIV, as well as anti-coagulant (Murray *et al*., 1982; Kostova, 2005; Kontogiorgis and Hadjipavlou-Litina, 2005; Yuce *et al*., 2009; Fernanda *et al*., 2015). Coumarins and their derivatives are principal oral anticoagulants, and this is attributed to their competitive inhibition effect on vitamin K in the biosynthesis of prothrombin (Beillerot*et al*., 2008; Ozkan*et al*., 2010). Clinically, coumarine derivatives are the precursors of several anticoagulants, particularly warfarin, which is the most commonly used oral anticoagulant medication. All of the above information has been the motivation to conduct the current study. Chemically, coumarins are extremely variable in structure due to the different types of substitutions in their basic structure. In this context, the aims of this study were to report the synthesis of some coumarin derivatives, including, 4-aryl-1,2-dihydro-6-(4-hydroxy-2-oxo-2H-chromene-3-yl)-2-oxopyridine-3-carbonitriles and then to evaluate their anticoagulant activities, in comparison to that of commercially anticoagulant drug warfarin.

2. Metarial and Method

All reactions were performed under an atmosphere of argon in oven-dried glassware. Anhydrous solvents for reactions were obtained by filtration through activated alumina or by storage over molecular sieves (4 Å). Phenol (Sigm-Aldrich, Switzerland), 4-hydroxy-coumarin (Sigm-Aldrich, Switzerland), oxychloride-phosphorus (Sigm-Aldrich, Switzerland), chloride-zinc anhydride (Sigm-Aldrich, Switzerland), malonic acid (Sigm-Aldrich, Switzerland), glacial acetic acid (Sigm-Aldrich, Switzerland), sodium carbonate (Sigm-Aldrich, Switzerland), 3-nitrobenzaldehyde (Sigm-Aldrich, Switzerland), 3-bromobenzaldehyde (Sigm-Aldrich, Switzerland), ethyl cyanoacetate (Sigm-Aldrich,

* Corresponding author. e-mail: ibrahim.rudhani@uni-pr.edu
** Corresponding author. e-mail: arben.haziri@uni-pr.edu.

Switzerland), ammonium acetate (Sigm-Aldrich, Switzerland), ethanol (Sigm-Aldrich, Switzerland), methanol (Sigm-Aldrich, Switzerland) and warfarin (Merck & Co, Germany) were used as reagents in the chemical reactions. IR spectra were recorded with the IR spectrophotometer (IR Perkin Elmer 297). The naming of the structures was done by the ChemDraw program, 545.^{1}H-NMR spectra were recorded on a 300 MHz NMR spectrometer instrument (Bruker AC 300). Mass spectra were recorded on an AutoSpeq Q VG with ionization energy of 70ev.

*2.1. Synthesis of 4-hydroxycoumarin (**1**)*

Firstly, phenol (0.01 mol), malonic acid (0.01 mol), oxy-chloride phosphorus (40 ml) and zinc chloride-anhydride (30 g) were heated in a water bath at 70 °C for 12 hours. Thereafter, this reacted mass was cooled and poured into ice. Then, the solid cooled mass was dissolved in 10% sodium carbonate and filtered. 4-Hydroxycoumarine, white precipitate, was obtained by acidification of the filtrate. The reaction yield was 98%. The melting point of the synthesized compound corresponds to the literature data 211 – 213 ^{0}C (Naveen *et al*., 2006).

*2.2. Synthesis of 3-acetyl-4-hydroxy-coumarin (**2**)*

12.5 ml of $POCl_3$ was added to the 8.1 ml solution of 4-hydroxy-coumarin in 45 ml of glacial acetic acid. The mixture was refluxed for 2 hours. After cooling, a voluminous white precipitate was obtained which was filtered and dried. The precipitate was recrystallized from methanol and 3-acetyl-4-hydroxycoumarine was obtained as a white to yellow substance with needle-shaped crystals, as shown in Figure 1. The melting point corresponds to the data in the literature 210 ^{0}C (Al-ayed, 2011; Dholakia *et al*., 1968). Yields 80%.

Figure 1. Crystals of compound **2**.

*2.3. Synthesis of 6-(4-hydroxy-2-oxo-2H-chromene-3-yl)-4-(3-nitro-phenyl)-2-oxo-1,2-dihydropyridin-3-carbonitrile (**3**)*

3-Acetyl-4-hydroxy-coumarin (1g, 5mmol) was mixed with 0.75g (5 mmol) 3-nitro-benzaldehyde in 20 ml ethanol. In this mixture, 0.57ml ethyl acetate and 0.75g (10mmol) ammonium acetate were added. The mixture was refluxed for 4hours. The yellow precipitate (Figure 2) was recrystallized from ethanol or methanol. Melting point 223 ^{0}C. Yields 72%. IR (KBr, ʊ cm^{-1}): 3450. 3300. 3030, 2950, 2200, 2000, 1750, 1520, 1340.^{1}H-NMR (300 MHz, DMSO): δ 5.63 (s, 1H, C-H), 7.20-8.23 (m, 9H), 13.33 (s, 1H, OH). HRMS (ESI): m/z [M + H]$^{+}$ calcd for $C_{21}H_{12}N_3O_6$ 402.0681, found 402.0683.

Figure 2. Crystals of compound **3**.

*2.4. Synthesis of 4-(3-bromo-phenyl)-6-(4-hydroxy-2-oxo-2H-chromene-3-yl)-2-oxo-1,2-dihydropyridin-3-carbonitrile (**4**)*

3-Acetyl-4-hydroxy-coumarin (1g, 5 mmol) was mixed with 3-bromo-benzaldehyde (0.95g, 5 mmol) in 20 ml ethanol, and another 0.57 ml ethyl acetate and 0.75g (10 mmol) ammonium acetate was added in the mixture. The mixture was refluxed for 5 hours. White precipitates were recrystallized from ethanol to obtain white crystals as in Figure 3. Melting point 215 ^{0}C. Yields 64%. IR (KBr, ʊ cm^{-1}): 3450, 3030, 2950, 2240, 1750, 750-800.^{1}H-NMR (300 MHz, DMSO): δ 5.71 (s, 1H, C-H), 7.19-8.20 (m, 9H), 13.50 (s, 1H, OH). HRMS (ESI): m/z [M + H]$^{+}$ calcd for $C_{21}H_{12}BrN_2O_4$434.9903, found 434.9969.

Figure 3. Crystals of compound **4**.

2.5. Animals and treatment protocol

Male laboratory mice of the type *Mus musculus swiss albino* aged 12-17 weeks (Figure 4A) were used to measure the anticoagulant effect of the synthesized compounds. Male laboratory rats weighing 130–160 g were obtained from the Experimental Animals Unit of the Departament of Biology at the University of Prishtina. The study was approved by the Prishtina University Committee. The animals were housed in stainless steel cages in a room at 23 ± 2 ^{0}C under 12 h dark/light cycles. After arrival, all the rats were fed standard rat chow for 7 days. Rats were given free access to food and water.

The synthesized compounds were mixed with 0.9% NaCl solution. Gastric tube was used for oral adminestration of prepared -solutions of warfarinë (1 mg/kg) and synthesized compounds **3** and **4** (20 mg/kg), respectivly (Figure 4B). The rats were then allowed to stand for 24 h in order for the substances to achieve the desired effect before analysis.

A

B

Figure 4. **A**) Mice (*Mus musculus Swiss albino*), **B**) Treatment with intragastric tube.

Then the rats were randomly divided into 5 groups as; Group I: 4-hydroxy coumarin (**1**) (n = 5), Group II: 6-(4-hydroxy-2-oxo-2H-chromene-3-yl)-4-(3-nitro-phenyl)-2-oxo-1,2-dihydropyridin-3-carbonitrile (**3**) (n = 5), Group III: 4-(3-bromo-phenyl)-6-(4-hydroxy-2-oxo-2H-chromene-3-yl)-2-oxo-1,2-dihydropyridin-3-carbonitrile (**4**) (n = 5), Group IV: warfarin (n = 5), Group V: control (n = 5).

2.6. Drug administration and prothrombin time

Drugs dissolved in saline were administered to the coumarin treated groups (Groups I, II and III) and warfarin treated group (Group IV) by oral gavage route for a single time with a dose of 20 mg/kg and 1 mg/kg, respectively (Figure 4B). For the control group (Group V), the vehicle used was saline solution. After 24 h, the animals were anaesthetized with ethyl ether by inhalation and blood samples were immediately collected through cardiac puncture into a tube containing 1:9 volume 3.8% g sodium citrate. The blood was then centrifuged (Denley DJB Labcare Ltd., BS 400, Buckinghamshire, UK) for 15 min. The separated plasma was transferred to a test tube kept in a water bath (Clifton Nickel-Electro Ltd., Digital Shaker Bath, North Somerset, UK) at 37 ^{0}C. The anticoagulant activity of coumarins was determined by using Stago-Neoplastine CI Plus Kit (Diagnostica Stago, Asnieres, France). The time for plasma to solidify following the addition of warmed thrombokinase suspension was taken as the prothrombin time (PT), as described by Ozkan,*et al*. (2010).

2.7. Statistics Analysis

All statistical analysis was carried out using GraphPad Prism 4.0 (GraphPad Software, San Diego, CA. USA). Groups of data were compared with two-tailed t test. Values of $p < 0.05$ or $p < 0.01$ were regarded as significant or highly significant, respectively.

3. Results and Discussion

3.1. Synthesis of coumarine derivatives

4-Hydroxycumarine derivatives are synthesized according to scheme 1, using procedure described by Abdelhafez, *et al*., (2010). Structure of the synthesized compounds has been verified on the basis of data obtained from the NMR, MS and IR spectra.

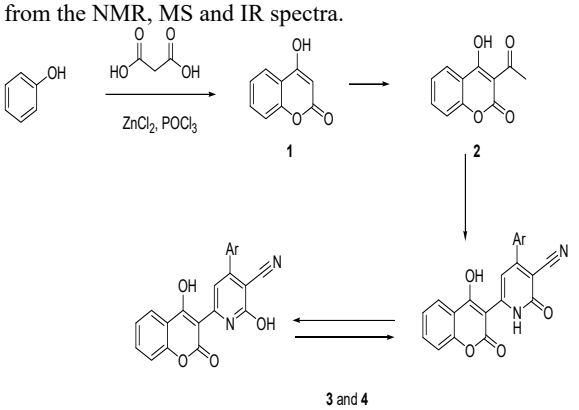

Scheme 1. The strategy for the synthesis of coumarin derivatives with anticoagulant properties.

By reaction of phenol with malonic acid in the presence of oxychloride-phosphorus and anhydride zinc chloride, compound **1** was obtained. The structure of the synthesized compound **1** is verified by the melting point. The melting point corresponds to the literary data 211-213 ^{0}C (Naveen *et al*., 2006). By reaction of 4-hydroxycoumarin with glacial acetic acid in the presence of $POCl_3$, a white to yellow precipitate of **2** was obtained according to the above reaction (Scheme 1). Also, the melting point of **2** corresponds to the literary data 210 ^{0}C (Al-ayed, 2011; Dholakia *et al*., 1968). In the IR spectrum of this compound, a characteristic signal in the interval 3100-2500cm^{-1} has appeared which has resulted from the stretching vibrations of the group ט (-OH). The stretching vibrations ט (C-H) of the aromatic system and the ט (C-H) stretching vibrations of the methylene group are displayed with weak intensities at 2750 cm^{-1} and 2550 cm^{-1}. In the range 1800-2000cm^{-1}, a series of weak absorptions have appeared resulting from overtones that are characteristic of the aromatic ring. Also, the peak in the range 1600cm^{-1} is characteristic of the stretching vibrations ט (C=C). At 1750 cm^{-1}, a characteristic adsorption of the (C=O) group of carbonyl compounds has been shown, whereas the peak in the range 1250 cm^{-1} is characteristic of the stretching vibrations of the C-O bond.

The reaction of the compound **2** with 3-nitro-benzaldehyde in the presence of ethylcyanoacetate, a compound **3** as yellow precipitate was obtained according to the reaction shown in Scheme 2.

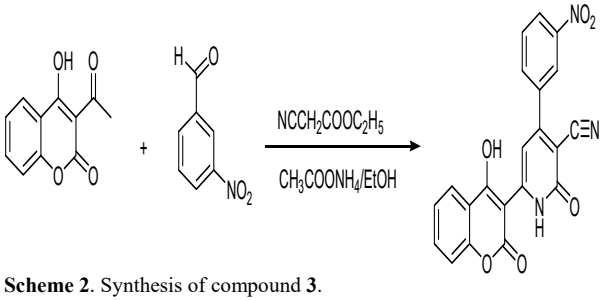

Scheme 2. Synthesis of compound **3**.

In the IR spectrum of this compound these characteristic absorptions have appeared. At 3450 cm^{-1} the absorption peak for vibration of N-H group is shown, while at 3300 cm^{-1} the absorption peak of the OH group is shown. Aromatic ט (C-H) stretching vibrations are displayed at 3030 cm^{-1} and aliphatic stretching (CH) vibrations at 2950 cm^{-1}. At 2200 cm^{-1} a weak peak has appeared as a result of (C≡N) stretching vibrations. At 1750-2000 cm^{-1} the characteristic overtones for the aromatic system have appeared. Vibrations ט (NO_2) asymmetric stretching and ט (NO_2) symmetrical stretching are shown at 1520 cm^{-1} and 1340 cm^{-1}.

By reaction of **2** with 3-bromo benzaldehyde in the presence of ethylcyanoacetate, ammonium acetate and ethanol a new product **4** with crystal structure was obtained according to the reaction shown in Scheme 3.

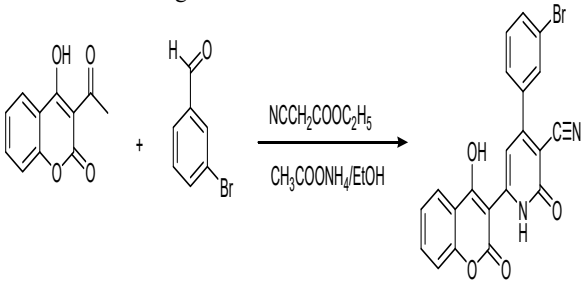

Scheme 3. Synthesis of compound **4.**

In the IR spectrum of this compound, these characteristic absorptions have appeared. At 3450 cm^{-1} a peak with average intensity characteristic for the ט (N-H) stretching vibrations of the secondary amines is shown. At 3030 cm^{-1} ט (C-H) aromatic stretching vibrations appeared and at 2950 cm^{-1} (C-H) aliphatic vibrations. At 2240cm^{-1} an intense peak has appeared resulting from (C≡N) stretching vibrations. At 1725 cm^{-1} a characteristic peak for stretching vibration (C=O) has appeared, whereas two symmetrical signals in the range 750 -800 cm^{-1} are characteristic of monosubstituted aromatic ring.

3.2. Prothrombin time

PT values for the groups are given in Table 1. PT was higher in all groups when compared to control; however, it was significantly higher in the **4** treated and warfarin treated groups than in the control group ($p < 0.01$).

Thromboembolism is an important cause of morbidity and mortality. To prevent vascular death ensuing from thrombosis, oral administration of anticoagulant drugs is one of the most important treatments. Vitamin K antagonists such as warfarin, acenocoumarol and phenprocoumarin are the main anticoagulant drugs producing an anticoagulant effect by interfering with the cyclic inter-conversion of vitamin K and its 2,3-epoxide (D'Andrea*et al*., 2008). Warfarin is the most widely used coumarin oral anticoagulant because its onset and duration of action are predictable. The maintenance dosage of warfarin varies between 1 and 30 mg/kg daily (Hirsch *et al*., 1992). After 24–48h of starting warfarin, the INR (International Normalized Ratio) begins to rise (Gage and Milligan, 2005). Coumarins exert their effects *in vivo* only after a latent period of 4–12 h, and their effect lasts for 1.5–5 days (Hirsch and Fuster, 1995). The anticoagulant activity of coumarins blocking the prothrombin biosynthesis by inhibition of vitamin K-epoxide reductase is closely dependent on the presence of a hydroxyl group in position 4 and a highly lipophilic substituent in position 3 of the benzopyrano moiety (Manolov and Danchev, 1995). On the other hand, despite the lack of the aforementioned structural requirements, a similar mechanism of action is reported to take place for the anticoagulant 1,3-indandione derivatives (Bruno *et al*., 2006; Arora and Mathur, 1963).

From the preliminary anti-thrombotic activity screening studies done in our laboratory, we decided to use a single dosage of 20 mg/kg and blood samples were collected 24h after the administration of the synthesized coumarins. As shown in Table 1, the PT of all groups increased. However, the PT was significantly higher in the **4** treated group when compared to the warfarin group.

Table 1: Effect of the coumarins derivatives on prothrombin time of the rats 24 h after single oral administration.

	Group I	**Group II**	**Group III**	**Group IV**	**Group V**
Prothrombin time (PT) (s)	11.30	20.80*	21.30*	14.60*	9.16
Standard deviation/ Standard error	0.63/0.30	0.54/0.24	0.38/0.15	0.39/0.16	0.15/0.07

Values are given as mean and standard deviation (SD), standard error (SE). Group I was treated with 4-hydroxycoumarin (20 mg/kg), Group II with 6-(4-hydroxy-2-oxo-2H-chromene-3-yl)-4-(3-nitro-phenyl)-2-oxo-1,2-dihydropyridin-3-carbonitrile (**3**) (20 mg/kg),4-(3-bromo-phenyl)-6-(4-hydroxy-2-oxo-2H-chromene-3-yl)-2-oxo-1,2-dihydropyridin-3-carbonitrile (**4**) (20 mg/kg), Group IV with warfarin (1 mg/kg), while Group V was treated with saline (control).* Significant difference between control and treated sample: $p < 0.01$ (by 2-tailed t-test); $n = 5$.

Compound **4** is a potential compound as an antithrombotic drug for further elaboration.

After injection of synthesized compound **3** in mice, we have seen stereotypical behavior (increased locomotors activity repeated in uninterrupted series) as shown in Figure 5A. Also, in animals, treated with compound **3**, changes in the intestinal tract were observed, which appeared with diarrhea (liquid feces) (Figure 5B). The increased secretion of the eye and edema of the eyelids was observed as another symptom. Mice treated with compound **3** had milky white secretion from the tear duct and increased eyelid edema up to total eye closure (Figure 5C).

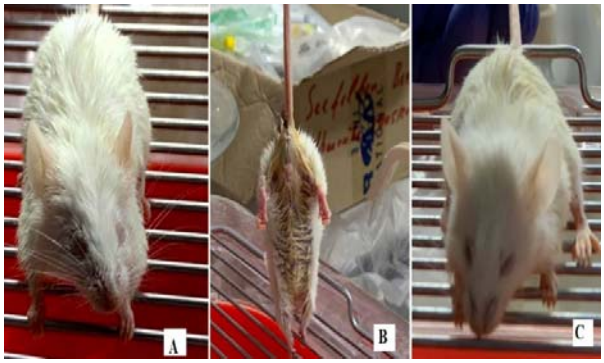

Figure 5. Some of the toxic effects presented in the tested mice, **A**) edema of the eyelids, **B**) diarrhea, **C**) increased secretion in the eye.

Mice treated with compound **4** had almost identical intestinal symptoms. All other behavioral or visual system-related symptoms were not present in mice treated with compound **4**.

The commercial drug, warfarin, had the same symptomatology as that of the group of mice treated with compound **3**, except that the symptoms were not as high. In particular, no changes in behavior were recorded.

Based on these results as well as the results obtained from Table 1, we see that these derivatives show *in vivo* anticoagulant potential. On the other hand, in addition to anticoagulant activity, these derivatives have been associated with high toxic effects, which is another problem that requires further study.

4. Conclusion

In conclusion, the PT value of 6-(4-hydroxy-2-oxo-2H-chromene-3-yl)-4-(3-nitro-phenyl)-2-oxo-1,2-dihydropyridin-3-carbonitrile (**3**) and 4-(3-bromo-phenyl)-6-(4-hydroxy-2-oxo-2H-chromene-3-yl)-2-oxo-1,2-dihydropyridin-3-carbonitrile (**4**) were higher than that of warfarin. Based on the anticoagulant activity, they are a potentially antithrombotic drug candidate for further elaboration. As a result of this work, we concluded that these derivatives showed satisfactory anticoagulant potential, but that anticoagulant ability was closely related with toxicity. We recommend working on these derivatives by changing their structures with the aim to decrease their toxic effects.

References

Abdelhafez M, Amin M, Batran R., Maher J, Nada S and Sethumadhavan S. 2010.Synthesis, anticoagulant and PIVKA-II induced by new 4-hydroxycoumarin derivatives. *Bioorg Med Chem.,* **18 (10)**: 3371-3378.

Al-ayed AS. 2011. Synthesis of New Substituted Chromen[4,3-c]pyrazol-4-ones and Their Antioxidant Activities. *Molecules.*, **16 (12)**: 10292-10302.

Arora RB and Mathur CN. 1963. Relationship between structure and anticoagulant activity of coumarin derivatives. *Br J Pharmacol Chemother*., **20**: 29-35.

Beillerot A, Dominguez J, Kirsch G and Bagrel D. 2008. Synthesis and protective effects of coumarin derivatives against oxidative stress induced by doxorubicin. *Bioorg Med Chem.*, **18**: 1102-1105.

Bruno O, Brullo C, Schenone S, Bondavalli F, Ranise A and Tognolini M. 2006. Synthesis, antiplatelet and antithrombotic activities of new 2-substitued benzopyrano[4,3-d]pyrimidin-4-cycloamines and 4-amino/cycloamino-benzopyrano [4,3-d]pyrimidin-5-ones. *Bioorg Med Chem.*, **14**: 121-130.

D'Andrea G, D'Ambrosia R and Margaglione M. 2008. Oral anticoagulants: pharmacogenetics relationship between genetic and non-genetic factors. *Blood Review*., **22**: 127-140.

Dholakia VN, Parekh MG, and Trivedi NK. 1968. Improved and rapid synthesis of new coumarinyl chalcone derivatives and their antiviral activity. *Aust J Chem*., **22**: 345-2347.

Fernanda GM,Joaquın GM, Mariana MA, Magdalena CG, Ivan CG, Ariana GG and Soraya OR. 2015. Coumarin heterocyclic derivatives: chemical synthesis and biological activity. *Nat Prod Rep.*, 1-35.

Gage B and Milligan P. 2005. Pharmacology and pharmacogenetics of warfarin and other coumarins when used with supplements. *Thromb Res*., **117**: 55-59.

Hirsch J, Dalen J, Deykin D and Poller L. 1992. Oral anticoagulants. *Chest*., **102**:312S–326S.

Hirsch J and Fuster V. 1995. Guide to anticoagulant therapy. Part 2: Oral anticoagulants. *Circulation*. **91 (2)**: 1469-1480.

Kontogiorgis C and Hadjipavlou-Litina D. 2005. Synthesis and antiinflammatory activity of coumarin derivatives. *J Med Chem*., **48 (20)**: 6400-6408.

Kostova I. 2005. Synthetic and natural coumarins as cytotoxic agents. *Curr Med Chem Anticancer Agents*., **5 (1)**: 29-46.

Manolov I and Danchev ND. 1995. Synthesis, toxicological and pharmacological assessment of some 4-hydroxycoumarin derivatives. *Eur J Med Chem*., **30**: 531-535.

Murray RDH, Mendez J and Brown SA. 1982. **The Natural Coumarins: Occurrence**, **Chemistry and Biochemistry**. Chichester, New York, John Whiley.

Naveen S, Adlakha P, Upadhyay K, Shah A, Anandalvar S and Prasad S. 2006. Crystal structure of 3-nitro-4-hydroxycoumarine. *X-Ray structure Analytical Online.,* **22 (4)**: x103-x104.

Nikhil B, Shikha B, Anil P and Prakash NB. 2012. Diverse pharmacological activities of 3-substituted coumarins: A review. *Int Res J Pharm*., **3**: 24-29.

Ozkan D, Basak Y, Cihan G, Ayse O, Goksel S, Mustafa B and Aysen Y. 2010. *Arzneimittelforschung*., **60 (10)**: 617-620.

Yuce B, Danis O, Ogan A, Sener G, Bulut M and Yarat A. 2009. Antioxidative and lipid lowering effects of 7,8-dihydroxy-3-(4-methylphenyl) coumarin in hyperlipidemic rats. *Arzneimittelforschung*., **59 (3)**:129-134.

JJBS

Volume 15, Number 4,December 2022
ISSN 1995-6673
Pages 649 – 657
https://doi.org/10.54319/jjbs/150414

Jordan Journal of Biological Sciences

Kinetic, Catalytic and Thermodynamic Properties of Immobilized *B.Circulans* 25 Milk Clotting Enzyme on Activated Chitosan Polymer and Its Ability to Form Milk Curds

Samia A. Ahmed*, Mohamed A. Abdel-Naby and Ahmed F. Abdel-Fattah

Chemistry of Natural and Microbial Products Department, National Research Centre, Dokki, Giza, Egypt

Received: October 16, 2021; Revised: January 8, 2022; Accepted: January 19, 2022

Abstract

Enzymes immobilization has been widely used to increase their shelf life which is essential for the world's industries. Therefore, milk clotting enzyme (MCE) from *Bacillus circulans* 25 was immobilized by covalent binding, ionic binding and entrapment methods using various carriers. MCE covalently immobilized on activated chitosan polymer with the bifunctional agent glutaraldehyde (Ch-MCE) exhibited highest immobilization yield (74.6 %) and highest retained activity (77 %). The effect of temperature and pH on the enzyme activity was evaluated, and the results showed that Ch-MCE had higher optimum reaction temperature by 10°C and higher optimum pH by 1.0. Compared to the native MCE, Ch-MCE exhibited lower activation energy by 1.4-fold. In addition, Ch-MCE exhibited higher half-life time, lower deactivation rate constant and higher energy for denaturation than the free enzyme. After immobilization, V_{max}, K_M, specificity constant, turnover number, and catalytic efficiency of the enzyme were significantly changed. Furthermore, thermodynamic parameters for denaturation (enthalpy, entropy and Gibbs free energy) confirmed that the immobilization improved the catalytic properties of MCE. The reusability of Ch-MCE was also assessed, and 90.4% of its activity was retained after 7 catalytic cycles, confirming its suitability for industrial applications. Immobilization helps to overcome the limitations of reducing MCE catalytic activity associated with changes in temperature, pH and inhibitors, which makes it useful in industrial applications and biotechnological processes.

Keywords: Milk clotting enzyme, immobilization, stability, thermodynamic, catalytic, kinetics, reusability.

1. Introduction

Microbial rennin is more acceptable in cheese production as an alternative to chymosin from newborn ruminants due to ethical problems and increased demand for cheese making (da Silva, 2017). Rennin acts in two stages for milk protein coagulation by specific hydrolysis of peptide bond (Phe_{105}-Met_{106}) of κ-casein (da Silva, 2017). Recently, there have been additional applications of proteases in dairy technology to accelerate the ripening of cheese which is the most complex and important process for the development of favorable flavor and texture (Afroz et al., 2015). Industrial applications of enzymes have been restricted by several factors such as the high cost, instability at high pH and temperature, and their availability in small amounts (Duman and Bayer, 2021). In addition, the use of soluble enzymes has some drawbacks that increase the consumption of enzymes as inactivation, reduction of catalytic stability and difficulty of removal from the mixtures. These problems can be overpowered by immobilizing the enzyme on insoluble solid support. Enzyme immobilization is considered an effective technique which not only stabilizes enzymes under operating conditions but also allows enables reuse and continuous use (Wehaidy et al., 2018). A proper enzyme immobilization is a powerful tool to improve enzymatic properties, such as resistance to drastic reaction conditions, enhanced enzyme activity, improvement of enzyme specificity, and may even be coupled to purification. Enzymes can be immobilized by adsorption, entrapment, covalent binding and ionic binding methods. However, immobilization by covalent binding is the most effective procedure in establishing enzymes and preventing enzyme leakage due to the formation of irreversible covalent bond between support and the enzyme (Eskandarloo and Abbaspourrad, 2018). Covalent binding consists of two steps: first one, activation of functional groups found on the support surface by a specific reagent as glutaraldehyde (GA); and the second, adding enzyme to form covalent bond with activated support. In the coupling reaction, these activated groups will react with strong electron donating nucleophiles, such as the amino group (NH_2) and functional groups of certain amino acids on the surface of most enzymes (such as carboxylic group (COOH) of aspartic acid, amino groups (NH_2) of lysine, hydroxyl group (OH) of serine, and sulfhydryl group (SH) of cysteine). Immobilization can be performed using different supports whose properties play an important role in enzyme behavior. Desired properties of the insoluble supports include low-cost, non-toxic, high surface area, reusable and good stability (Narwal et al., 2016). Since

* Corresponding author. e-mail: dr_sa_ahmed@yahoo.com.

there is no universal support suitable for all enzymes and all applications, it is important to examine different supports using different methods of enzyme immobilization. Chitosan is one of natural polymer (polysaccharides) derived from chitin by deacetylation process and has excellent biocompatibility, no toxicity, cheapness, high mechanical strength, and a susceptibility to chemical modifications (Salazar-Leyva et al., 2017; Yandri et al., 2020). One common approach for enzyme immobilization on chitosan is through multipoint covalent binding between the functional groups present on the surface of an activated chitosan by cross-linking agents such as GA and the surface functional groups of the enzyme protein. When an enzyme becomes immobilized through many surface residues on a rigid support through very short spacer arms, important stabilizing effects may be achieved. Thermodynamics act as a key tool to understand the thermal deactivation process. Estimation of the thermodynamic parameters of the enzyme as enthalpy (ΔH^*), entropy (ΔS^*), and the Gibbs free energy (ΔG^*) can provide useful information as enzyme behavior, activity and thermostability. The suitability of enzymes for industrial application is judged by their thermodynamic parameters (Zaboli et al., 2019). Using free rennet to make cheese is not successful due to enzyme loss in whey, poor enzyme distribution, low yield, and poor cheese quality. So, the present study reports the immobilization of *B.circulans* 25 MCE and characterization of its catalytic, kinetics and thermodynamic parameters. Finally, evaluate the ability and reusability of Ch-MCE to form milk curds.

2. Materials and methods

2.1. Materials

Chitosan, Chitin, Dowex 1x4, Dowex 50W, Amberlite IR-120, Alumina, DEAE- sephadex A-25 and DEAE-cellulose DE-52 were obtained from Sigma Chemical Co., USA. Sodium alginate was supplied from BDH Chemical Ltd., Poole, England. Ceramic, wool and chicken bones were collected from the local market in Egypt. Skim milk powder spray dried (heat treated grade) was made in USA and obtained from the Ministry of Agriculture, Giza. Egypt. Other chemical reagents used were of analytical grade.

2.2. Methods

2.2.1. Enzyme production

MCE from *B.circulans* 25 has been produced according to the previous work (Ahmed et al., 2018). The medium used for MCE production had the following composition (g/L): lactose 20, yeast extract 1, peptone 1, K_2HPO_4 2 and $MgSO_4.7H_2O$ 0.25, and the pH was adjusted to 6.0 prior to sterilization. One mL of cell suspension of 24 h-old slant (OD600~0.3) was transferred to 50 mL sterile medium in 250-mL Erlenmeyer flask. The flasks were incubated at 35°C and 180 rpm for 24 h. The broth media after incubation was centrifuged at 6000 x g and 4°C for 15 min and the cell free filtrate was considered as source of crude enzyme.

2.2.2. Milk clotting activity and protein determination

Milk clotting activity was estimated according to Narwal et al. (2016) method. Enzyme solution (2.5 mL) or certain weight of Ch-MCE was incubated with 10 mL skim milk (12 g dry skim milk/100 mL of 0.01 M $CaCl_2$) at 40°C. The time at which the first particles were formed was recorded. The time at which the first particles were formed was recorded by a stopwatch. One unit of the MCE activity (U) was equalized to 10 mL milk clotted within 10 min. The protein content of the MCE preparation was estimated by the method of Lowry et al. (1951) using bovine serum albumin (BSA) as standard. The amount of immobilized protein was calculated by subtracting the amount of unbound protein from the amount of protein originally added for immobilization.

2.2.3. Enzyme immobilization

Immobilization yield (IY %) and immobilization efficiency (IE %) were calculated according to Abdella et al. (2020) to select the suitable carrier and method.

$$\text{Immobilization yield (\%)} = I/(A–B)\ X100 \quad (1)$$

$$\text{Immobilization efficiency (\%)} = (I/A)\ X\ 100 \quad (2)$$

Where: I (total activity of immobilized enzyme), A (total activity offered for immobilization and B (total activity of unbounded enzyme).

2.2.3.1. Immobilization of MCE by covalent- binding

Chitosan beads were prepared by shaking 0.4 g chitosan in 5 mL of 0.01 M HCl containing GA (2.5 %) at 30°C for 2 h. The beads were precipitated using 0.1 N NaOH, collected by filtration, and washed with distilled H_2O (to remove the excess GA). Then 5 mL enzyme solution (440U) was mixed with the wet beads by gently shaking. After 2 h at 30°C, the unbounded enzyme was removed by washing with distilled H_2O until no activity was detected. One gram of other carriers (chitin, wool, chicken bone, As-alumna, ceramic or PVC) was shaken in 25 mL Tris–HCl buffer (0.01 M, pH 6.0) containing 2.5 % GA at 30°C for 2 h. The carriers were filtered off, and washed with distilled H_2O to remove the excess GA. Then each treated carrier was incubated with Tris HCl buffer (5 mL, 220 U of MCE). After incubation at 30°C for 2 h, the unbounded enzyme was removed by washing with distilled H_2O (Abdel-Naby et al., 1998).

2.2.3.2. Immobilization of MCE by ionic- binding

The anion or cation exchanger (1 g) equilibrated with phosphate buffer (0.1 M, pH 6.0) or Tris-HCl (0.1 M, pH 8.0) and was incubated for 16 h at 4°C with certain volume of the enzyme solution (50 U) in the same buffer (Eskandarloo and Abbaspourrad, 2018). The unbounded enzyme was removed by washing with the same buffer.

2.2.3.3. Immobilization of MCE by alginate entrapment

In this experiment, 10 mL of different concentrations of Na-alginate solution were mixed with equal volume of enzyme solution (200 U) to obtain final concentration range of 2-8 % (w/v). The whole mixture obtained by sodium alginate was extruded drop wise through a Pasteur pipette into a gently stirred 0.1 M $CaCl_2$ solution for 2h. The resulting beads with a diameter of ~1.0-1.5 mm were collected, washed with buffer, and kept for 24 h at 4°C to remove the unbound enzyme (Dey et al., 2003).

2.2.4. Characterization of free and chitosan immobilized MCE

2.2.4.1. Optimum pH and pH stability

The effect of pH on the activity of free and Ch-MCE was investigated in 0.01 M buffer with different pH values (4.5 – 8.5). The relative activity was calculated according to Eq.3.

Relative activity (%) = (A1/A2) X 100 (3)

Where: A1 (activity detected under the certain condition and A2 (activity detected under the optimal condition).

The stability to pH was investigated by pre-incubating enzyme samples in 0.01M tris - HCl buffer with pH ranging from 5.0 to 9.0 at 25°C for 1h followed by adjusting the pH to the optimal of each enzyme form. The residual (retained) activity was assayed under the standard conditions and calculated to according to Eq.4.

Residual activity (%) = (Af / Ai) × 100 (4)

Where: Af (final activity detected) and Ai (initial activity detected).

2.2.4.2. Optimum temperature and thermal stability

The enzyme samples in 0.01M tris - HCl buffer at pH 6.0 and 7.0 (for free and Ch-MCE), respectively were subjected to different temperatures (from 30°C to 100°C). The activation energy (E_a) was estimated from the slope of Arrhenius plot of log the residual enzyme activity (%) against reciprocal of absolute temperature in Kelvin (°K) according to Eq.5.

Slope = - E_a / 2.303 R (5)

Where: E_a (activation energy) and R (gas constant 1.976 Kcal/ mol).

Temperature coefficient value (Q_{10}), the rate of an enzymatic catalysis reaction changes for every 10 °C rise in temperature, was calculated as reported by Wehaidy et al. (2018) as Eq.6.

Q_{10}= antilog E = (E x10/RT^2) (6)

Where $E = E_a$ = activation energy

For thermal stability, free and Ch-MCE were heated at different temperatures (40–80°C) in the absence of substrate for different time intervals (15–120 min). Every 15 min, a sample was removed and the residual activity was estimated under standard assay conditions. The enzyme activity without heating was taken as 100%. Deactivation rate constant (k_d) was determined according to Eq.7 from the semi logarithmic plot of residual activity (%) versus time (min) (Singh et al., 2019).

Slope = - k_d (7)

Half-life ($t_{1/2}$) value of inactivation is given according to Eq.8.

$t_{1/2}$= ln2/ k_d (8)

The energy for denaturation of enzyme (E_{ad}) was calculated from Arrhenius plot of (ln k_d) as a function of (1/T) temperature in Kelvin (°K) using the following in Eq.9.

Slope = $-E_{ad}$/ R (9)

2.2.4.3. 2.2.4.3. Effect of substrate concentration

Both the free and Ch-MCE activities were assayed with different substrate concentrations ranged from 1 to 12 % (w/v) at optimal assay conditions. Michaelis–Menten constant (K_M) and maximum velocity (V_{max}) were estimated from Lineweaver and Burke (1934). In addition, the turnover number (k_{cat}), catalytic efficiency (k_{cat} / K_M), specificity constants

(V_{max} / K_M), free energy of substrate binding ($\Delta G^*_{E–S}$) and free energy of transition state binding ($\Delta G^*_{E–T}$) were estimated according to Wehaidy et al. (2018) as Eqs. (10-15).

k_{cat} = ($k_b T$ / h) x e $^{(-\Delta H^*/RT)\ x\ e\ (\Delta S^*/R)}$ (10)

Where: k_b (Boltzmann's constant =1.38×10^{-23} J/ K), T (absolute temperature (°K), h (Planck's constant =6.626×10^{-34} Js), N (Avogadro's number =6.02×10^{23}/ mol), and R (Gas constant=8.314 J/ K/ mol).

ΔH^* (Enthalpy) = $E_a - RT$ (11)

ΔG^* (Gibbs free energy of activation) = $-RT\ ln\ (k_{cat}\ h / k_b$ x $T)$ (12)

ΔS^* (Entropy) = ($\Delta H^* - \Delta G^*$) /T (13)

$\Delta G^*_{E\text{-}S}$ (Free energy of substrate binding) = $-RT\ ln\ K_a$, where $K_a = 1/ K_M$ (14)

$\Delta G^*_{E\text{-}T}$ (Free energy for transition state formation) = $-RT\ ln\ (k_{cat} / K_M)$ (15)

2.2.4.4. Effect of metal ions

The metal ions ($ZnSO_4$, $CoCl_2$, $CaCl_2$, $MnSO_4$, $CuSO_4$, $MgSO_4$, and $HgCl_2$) were added individually (10 mM) to the reaction mixture. Both free and Ch-MCE activities were assayed under optimal assay conditions.

2.2.5. Suitability of Ch-MCE in making cheese (reusability)

A weight sample (4 g) of Ch-MCE (wet) was placed in a bag of muslin. The bag was immersed in skim milk solution (10 mL). The mixture was incubated at 85°C until forming the colt. At the end of the reaction, the bag containing Ch-MCE was removed from the colt, washed with H_2O, and re-suspended in a freshly prepared substrate (10 mL) to start a new run.

3. Result and discussion

The efficiency of enzyme immobilization was evaluated by different parameters including the residual activity (RA %), the immobilization efficiency (IE %), the loading efficiency LE (immobilized enzyme activity/gram carrier); however, the IY (%) is the key parameter that it represents the general output of the immobilization process efficiency.

3.1. Enzyme immobilization

3.1.1. Immobilization of MCE by covalent- binding

Immobilization of MCE by covalent-binding was achieved by cross-linking between the enzyme and activated carriers throughout GA as a spacer group. Abdella et al. (2020) explained that the interaction occurred between the NH_2 groups (in the enzyme protein molecule) and the free C=O group (located on GA) forming C=N– bond. In the case of chitosan, the used amount of MCE was higher than that used for other carriers due to its higher loading efficiency. The data presented in Table 1 indicated good IY and LE, especially with chitosan (74.6 % and 315.0 U/g carrier). Our result is higher than that obtained by Esposito et al. (2016) on immobilized MCE by 1.1-fold. Covalent binding is the best method regarding to the strength of the interactions, reduce protein leakage (due to the formation of stable cross- linking between the enzyme and the carrier via

spacer group). In addition, side chains of several amino acids can form covalent bonds with carriers (Nwagu et al., 2011). Moreover, covalent binding via spacer group may increase the local surface area and consequently reduced the protein crowding. Further, chitosan was preferred as a suitable carrier because it is cationic, biodegradable, inert, non-toxic and biocompatible compound (Hosseini and Varidi, 2021).

3.1.2. Immobilization of MCE by ionic- binding

A series of ion exchangers was used for the immobilization of MCE by ionic binding. The results in Table 2 showed that the most suitable ion exchanger for MCE immobilization is Dowex 50W with highest LE (19.0 U/g carrier) and highest IY (56.7 %). On the contrary, MCE immobilized on DEAE-Sephdex A-25 had no activity, which might be due to that the enzyme's active sites were involved in the fixation process. Similarly, Abdel-Naby et al. (1998) pointed to the low bound enzyme for protease immobilization by ionic binding.

Table 1. Immobilization of *B. circulans* 25 MCE by covalent-binding.

Carrier	Added enzyme (U/g)(A)	Un bounded enzyme (U/g)(B)	Immobilized enzyme (U/g)(I)	Immobilization yield (IY %)
Chitin	220.0	100.00	79.20	66.00
Wool	220.0	131.40	49.75	56.15
Chicken bones	220.0	133.30	57.75	66.61
Ceramic	220.0	122.40	51.06	52.31
As-alumina	220.0	118.32	60.16	59.17
PVC	220.0	131.92	54.89	62.32
Chitosan	440.0	17.60	315.00	74.57

Table 2. Immobilization of *B. circulans* 25 MCE by ionic-binding.

Carrier	Added enzyme (U/g)(A)	Un bounded enzyme (U/g)(B)	Immobilized enzyme (U/g)(I)	Immobilization yield (IY %)
Dowex 50 W	50.0	16.40	19.00	56.65
Dowex 1x4	50.0	17.10	8.50	25.84
Ambelite IR- 120	50.0	23.80	10.00	38.17
DEAE–Cellulose DE-52	50.0	39.80	3.30	32.35
DEAE – Sephadex A-25	50.0	26.30	-	-

3.1.3. Immobilization by alginate entrapment

The most common method to prepare hydrogels from an aqueous alginate solution is to combine the solution with ionic cross-linking agents, such as divalent cations (i.e., Ca^{2+}). MCE was immobilized by entrapment in Ca-alginate with different concentrations as presented in Table 3. The results showed that the LE was decreased from 37.2 to 18 U/10 mL gel with the gel concentration increased from 2 to 8 %. This is probably due to the decrease of the gel porosity with the increase of Na-alginate concentration, and consequently the diffusion limitation was developed. Similar observation was previously reported for entrapped proteases (Abdel-Naby et al., 1998; Lamas et al., 2001). Hosseini and Varidi (2021) reported that decreasing alginate concentration from 0.2 to 0.04% increased the rennet encapsulation efficiency. The pore size of the gel, reflected in the viscosity of the carrier due to the size of the molecule and/or its concentration, can affect the diffusion of substrates or products and limit the reaction rates of the entrapped enzyme. Narwal et al. (2016) immobilized bacterial MCE in alginate-pectate interwoven gel with higher IY (73%).

Table 3. Immobilization of *B. circulans* 25 MCE by entrapment in Ca-alginate.

Na – alginate concentration (%)	Added enzyme (U/10ml gel) (A)	Un bounded enzyme (U/10ml gel) (B)	Immobilized enzyme (U/10ml gel) (I)	Immobilization Yield (IY %)
2	200.0	9.00	37.20	19.48
4	200.0	11.60	24.30	12.89
6	200.0	13.90	21.10	11.34
8	200.0	15.30	18.00	9.74

3.2. Characterization of free and Ch-MCE

Among all preparations, chitosan- immobilized MCE (Ch-MCE) gives the highest IY and the highest LE, consequently, in the following experiments Ch-MCE was used. Chitosan is a versatile, easily easily-to- process cationic biomaterial that can be widely used in many applications such as medical, tissue engineering, antibacterial dressings, and enzyme immobilization, due to its biological and chemical properties such as biodegradability, safety, and non-toxicity (El-Shishtawy et al., 2021; Hosseini and Varidi, 2021). Much scientific literature reported that in many cases of enzyme immobilization methods the protocol leads to losses in some enzyme activity. Ch-MCE retained 77 % of the initial specific activity shown by the free enzyme. The enzyme activity may decrease due to the corresponding changes caused by the immobilization (Siar et al., 2017). Also, the decrease in the specific activity may be due to the diffusional limitation of the substrate and product flow. Although GA creates very strong bonds between enzymes and carriers, it changes the structure of some enzymes during the binding process, causing loss of their activity (Salazar-Leyva et al., 2017).

3.2.1. Effect of pH and pH stability of the free and Ch-MCE

The pH can either change the ionization of the enzyme-substrate complex or alter the protein structure of the enzyme. As illustrated in Figure 1, the immobilization shifted the optimum activity of the MCE from free 6.0 to 7.0. MCE. At higher pH values up to 8.0, the drop in activity was more pronounced with the free than that of the Ch-MCE. These effects may be due to the changes of the ionic microenvironment of the enzyme active site and /or distribution of the surface charges of the carrier after immobilization (Talbert and Goddard, 2012;

Pervez et al., 2017). These are due to the use of cationic carrier like chitosan which interacts with anionic groups on the enzyme surface. Pervez et al. (2017) reported that the pH in the immediate vicinity of enzyme molecule may change, depending upon the surface and residual charge on the solid support (chitosan is positively charged due to amino groups).

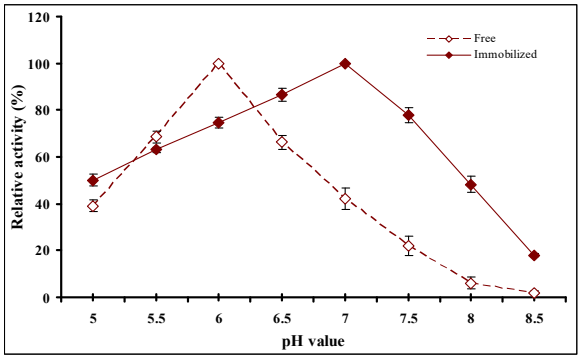

Figure 1. Effect of pH on the activity of free MCE and Ch-MCE.

The results in Figure 2 showed that the pH stability of Ch-MCE was shifted to higher pH values compared to the free MCE. These results reveal the same trend as in the shift of the optimum pH. The results showed that covalent binding maintained the MCE catalytic activity especially in the case of alkalinity. Pervez et al. (2017) reported that immobilization decreases the inhibition of enzymes either by stabilizing the enzyme structure or by eliminating the inhibitor. Moreover, multipoint covalent attachment between the enzyme molecule and an activated carrier makes the structure of the enzyme more rigid, consequently decreasing conformational changes which can be induced by extreme pH (Salazar-Leyva et al., 2017). Narwal et al. (2016) suggested that titratable acidity of milk should be between 0.19 to 0.25 % lactic acid equivalents (which correspond to pH from 5.0 to 6.5) at the time of adding an enzyme. Therefore, for industrial applications, the MCE should be stable between these pH ranges.

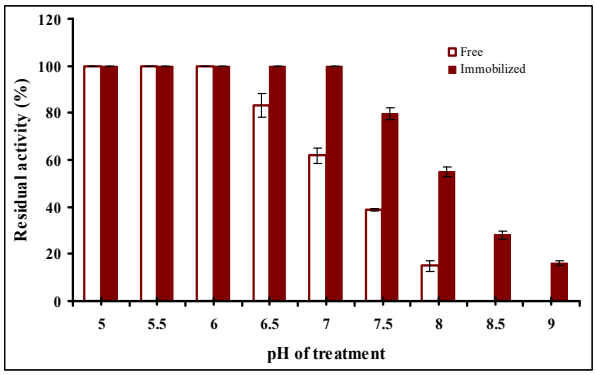

Figure 2. pH stability of free MCE and Ch-MCE.

3.2.2. Effect of temperature and thermal stability of the free and Ch-MCE

As seen in Figure 3, immobilization increases the optimum temperature by 10°C which is probably a result of the thermal stability enhanced by immobilization. Covalent binding of enzyme onto chitosan enhanced the optimum temperature and stability of the biocatalysts for thermal inhibition (Salazar-Leyva et al., 2017). Hosseini and Varidi (2021) reported that free and immobilized rennet showed the highest activity at the same temperature (40 °C), and at higher temperatures there is a sharp decrease in the activity of the free enzyme compared to the immobilized enzyme.

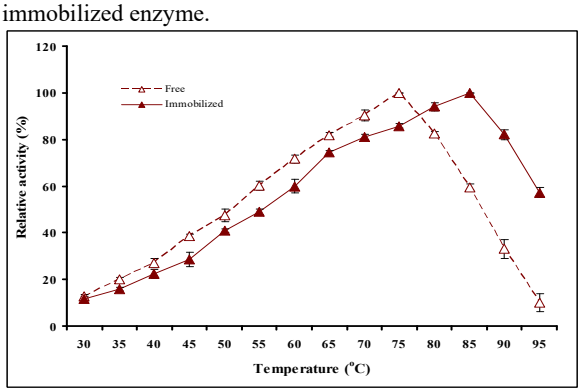

Figure 3. Effect of temperature on the activity of free MCE and Ch-MCE.

The calculated E_a (Figure 4) indicated that the energy required to form the enzyme-substrate complex for the free enzyme (36.76 kJ/mol) was 1.4-fold higher than that required for the Ch-MCE (34.31 kJ/mol), confirming that immobilization improved the catalytic efficiency of the enzyme by lowering the energy required to make the activated complex of enzyme and substrate (Wehaidy et al., 2018). This result of E_a was lower by 1.7-fold than that obtained for immobilized *Aspergillus fumigatus* protease (Hernandez-Mariinez et al., 2011).

Similar decrease in E_a was reported by El-Shishtawy et al. (2021) for the immobilization of catalase enzyme. Reduced E_a of the immobilized enzyme compared to free enzyme may be due to the mass transfer limitations (Thakrar and Singh, 2019).

Although thermostable enzymes are more suitable for industrial applications than mesophilic enzymes, stability of MCEs for long times at mild temperatures is very important for their suitability in making cheese. The results in Figure 5 showed that the immobilization improved the stability of MCE to the thermal inhibition. After heating at 60°C, the Ch-MCE was stable up to 120 min with 100 % residual activity whereas, the free MCE lost about 90.4 % of its initial activity. In addition, after heat treatment at 70°C for 90 min, the free MCE was completely inhibited; however, the Ch-MCE retained 40 % of its initial activity. The increase in enzyme stability after immobilization was possibly related to the higher rigidity of the immobilized form (Yang et al., 2017). The immobilized enzyme would be bound to the support via multipoint covalent bonds, and thus its structure would be rigid, and therefore it would be more resistant to the thermally induced denaturations which would reduce free enzyme activity (Wahba et al., 2021). In addition, the stability to heat inhibition enhancement after immobilization could be caused by the carrier that protects the enzyme from denaturation by absorbing a great amount of heat (Figueira et al., 2011).

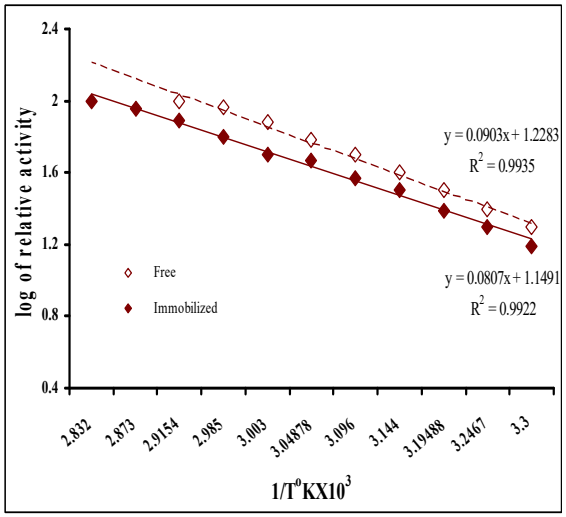

Figure 4. Arrhenius plot for temperature dependence of the activity of free MCE and Ch-MCE.

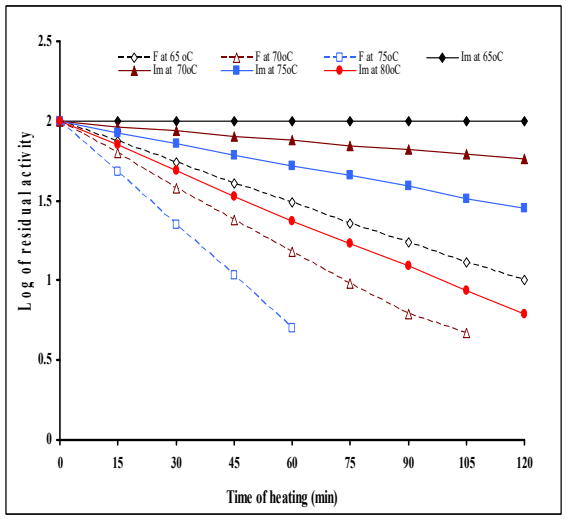

Figure 5. First-order plots of the effect of thermal inactivation of free MCE and Ch-MCE.

The calculated k_d in Table 4 indicated that the stability of the Ch-MCE to the thermal inhibition was superior to that of the free MCE (the lower k_d, the more thermo stable enzyme). For example, k_d at 70°C for the free enzyme was higher by 3-fold than that of the Ch-MCE. These results confirm the effectiveness of the MCE immobilization on chitosan for increasing the thermal stability. The decrease of k_d value is predicted because the condition of the enzyme is less flexible than in water, so the unfolding of the enzyme is decreased, and the stability of the enzyme has increased (Yandri et al., 2020). In addition, $t_{1/2}$ of the Ch-MCE at 65, and 75°C were higher by 6 and 5-fold, respectively than that of the free MCE. The binding between the enzyme and the carrier reduces conformational flexibility and thermal vibration, thus protecting the immobilized protein from denaturing and unfolding by increasing the temperature (Figueira et al., 2011).

Table 4. Thermal properties of free and Ch-MCE.

Property	Milk-clotting enzyme	
	Free	immobilized
Deactivation rate constant k_d / min, at		
60 °C	8.35 x 10^{-3}	Stable for 120 min
65 °C	13.5 x 10^{-3}	1.97 x 10^{-3}
70 °C	21.167 x 10^{-3}	4.45 x 10^{-3}
75 °C	Unstable	10.09 x 10^{-3}
Half life time $t_{½}$ (min), at		
60 °C	36.04	Stable for 120 min
65 °C	22.29	152.79
70 °C	14.22	66.88
75 °C	Unstable	29.83
Energy for denaturation E_{ad} (KJ/ mol)	217.34	378.73

The E_{ad} for Ch-MCE was greater by 161.39 kJ/ mol than that obtained for free MCE (Figure 6 and Table 4). This result indicated that immobilized form needed more energy for deactivation compared to the free form. The stability of enzymes is enhanced by the rigidification of their immobilized structure via the multipoint covalent linkages established between them and their supports (Wahba et al., 2021). The energy of thermal inactivation is an important factor to judge its thermal stability (Thakrar and Singh, 2019).

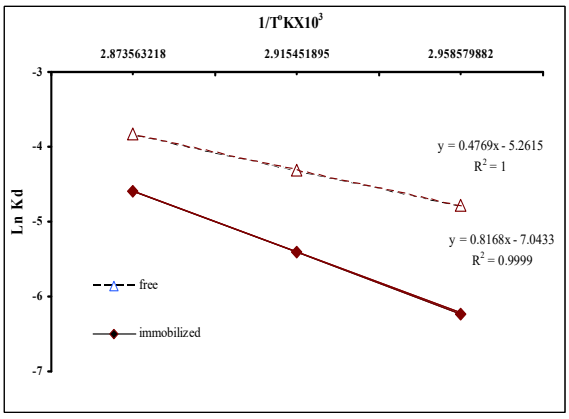

Figure 6. Arrhenius plot for activation energy of denaturation for free MCE and Ch-MCE.

3.2.3. *Effect of substrate concentration*

In order to determine the kinetic parameters of the MCE, the activity of the free and Ch-MCE was measured at different substrate concentrations and the Lineweaver-Burk was plotted. As seen in Figure 7, Ch-MCE provided K_M 1.3-fold higher and V_{max} 1.3-fold lower than the free MCE suggested that the main problem is just diffusion problems for the entry of the substrate inside the biocatalyst particle. Wahba et al. (2021) found that, the increase in K_M indicates that the affinity of an enzyme for its substrate is decreased due to the resistance to mass transfer and the reduction of the immobilized enzyme

flexibility. Furthermore, decreasing the affinity of the immobilized enzyme may be due to the changes in the enzyme structure by the immobilization process or the reduction of substrate access to the active site of the enzyme (Pervez et al., 2017; Hosseini and Varidi (2021). The decrease in V_{max} of immobilized enzymes could be attributed to the interactions between these enzymes and their respective supports which could reduce the flexibility of the enzymes (Wahba et al., 2021). In addition, the V_{max} / K_M of Ch-MCE was decreased by 1.6-fold compared to the free MCE (Table 5). Low V_{max} / K_M ratio specifies the smaller specificity of immobilized form for casein than the free MCE (Singh et al., 2019). Similar observations were reported by Cahyaningrum and Sianita (2014).

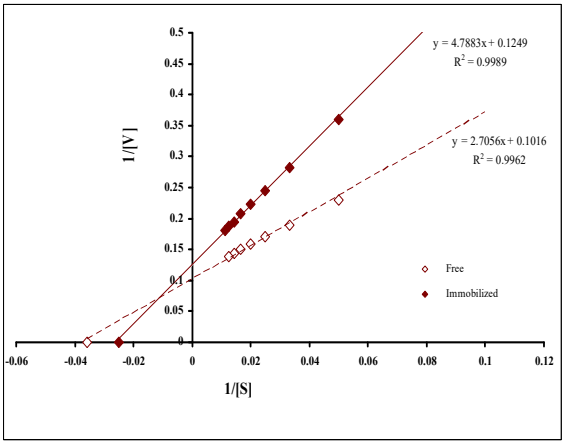

Figure 7. Lineweaver-Burk Plot for free MCE and Ch-MCE.

k_{cat} represents the maximum number of reactions catalyzed per minute. The k_{cat} of Ch-MCE was higher by 1.5-fold compared to the free MCE (Table 5). The k_{cat} / K_M of free and Ch-MCE were 0.154 and 0.174 /S mg/mL, respectively, indicating that the immobilization technique enhanced the catalytic efficiency ~ 13 %. On contrary, Mafra et al. (2019) found that the immobilized enzyme catalytic efficiency was 34 % lower than the free form. The recorded data in Table 5 showed a decrease in the Ch-MCE ΔH^* compared to the free MCE. In addition, ΔS^* for Ch-MCE was lower by 14.2 kJ/ mol than that of the free MCE. The lower ΔH^* and the negative ΔS^* values for Ch-MCE pointed to the stability and the effective transitional state of the complex of enzyme-substrate (Wehaidy et al., 2018). The ΔG^* of a substance results from the stabilizing forces present in protein's structure, such as Van der Waals interactions and hydrogen bonds. The higher ΔG^* is associated with more tolerance toward heat inactivation (Zaboli et al., 2019). As shown in Table 5, ΔG^* for the Ch-MCE was higher by 5.49 kJ/ mol than the free MCE indicating that a change of the Ch-MCE-substrate complex into products is less spontaneous in comparison with free MCE. The catalytic reaction can be evaluated by estimating ΔG^* for enzyme-substrate complex conversion into products (Riaz et al., 2007).

The ΔG^*_{E-T} for Ch-MCE was lower 1.0-fold compared to the free MCE. This result indicated that this reaction is more spontaneous for Ch-MCE than for free MCE (Ferreira et al., 2018). In addition, the ΔG^*_{E-S} confirmed that the Ch-MCE requires higher amount of free energy by 1.1-fold to form this transition state compared to the free MCE. The same behavior among soluble and conjugated MCE from *B. subtilis* KU710517 was reported by Wehaidy et al. (2018).

3.2.4. Effect of metal ions

The effects of various metal ions on the Ch-MCE activity compared to the free MCE were (data not shown). Both free and Ch-MCE were activated by Mg^{+2}, Ca^{+2} and Mn^{+2} whereas Hg^{+2} and Co^{+2} inhibited them. Cu^{+2} decrease enzymatic activity of the free MCE by 8.7 % although no lose in activity of Ch-MCE. In general, it was observed that the inhibitory effect of these investigated metal ions was less pronounced with the Ch-MCE compared to free MCE (Pandey et al., 2017). Siar et al. (2017) suggested that if multi-point covalent bond is achieved, the structure of enzyme becomes more rigid and consequently increases enzyme stability under any distorting reagent.

Table 5. kinetic and thermodynamic parameters for casein hydrolysis by free and Ch- MCE.

Parameter	Milk-clotting enzyme	
	Free	Immobilized
E_a (KJ/ mol)	36.76	34.31
V_{max} (U/ mg protein)	10.0	8.0
K_M (mg skim milk/ ml)	28.01	35.71
k_{cat} (S^{-1})	4.3	6.23
k_{cat} / K_M (/S mg/ ml)	0.1535	0.1744
Ka (1/ K_M)	0.036	0.028
ΔH^* (kJ/ mol)	33.86	31.33
ΔG^* (kJ/ mol)	96.68	102.17
ΔS^* (J/ mol /K)	-183.67	-197.87
ΔG^*_{E-T}((kJ/ mol)	5.34	5.12
ΔG^*_{E-S}((kJ/ mol)	9.48	10.5
V_{max} / K_m	0.357	0.224
Q_{10}	1.0	1.0

3.3. Suitability of Ch- MCE in forming milk curds (reusability)

One of the most important characteristics of the immobilized enzymes for both economical and industrial applications is their reusability (El-Shishtawy et al., 2021). The reusability study was carried out under optimal conditions. The Ch-MCE exhibited a very high capability to be reused, since we observed 100 and 90.4 % retained activity after being used for 5 and 7 consecutive cycles, respectively. Conversely, the immobilized proteases retained 40 % of its initial activity after the second cycle (Salazar-Leyva et al., 2017). El-Shishtawy et al. (2021) reported that immobilized enzyme onto CS/ZnO and CS/ZnO/Fe_2O_3 retained 38% and 88% of its original activity after five cycles. Multipoint covalent binding of enzymes on activated supports promotes a rigidification of its structure and reusability (Ahmed et al., 2019). Upon repeated use, gradual decrease in activity was observed (Figure 8), which was probably due to the loss of the enzyme from the carrier physically, frequent interactions between the substrate and the active site of the immobilized enzyme, distorting the active site, and resulting in activity loss (El-Shishtawy et al. (2021)

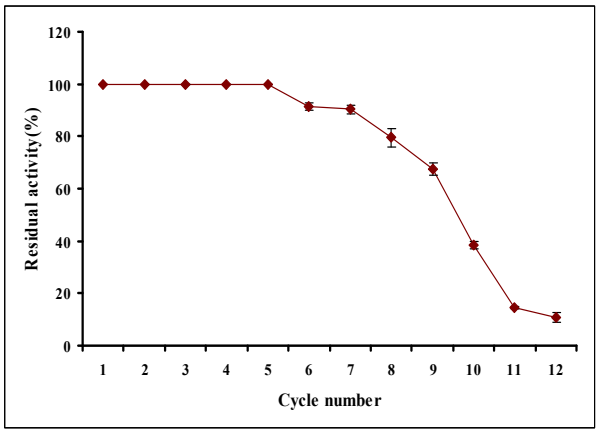

Figure 8. Suitability of Ch-MCE in the forming of milk curds (reusability).

4. Conclusion

Using rennet enzyme in making cheese is one from the largest application of enzymes in food processing. Therefore, this study has aimed to enhance the properties of MCE by immobilization and evaluate its catalytic, kinetics and thermodynamic parameters. MCE from *B. circulans* 25 was covalent-binding to activated chitosan polymer (Ch-MCE) with IY 75% and IE 72%. The Ch-MCE exhibited higher optimum temperature by 10°C and lower activation energy by 0.9- fold than the free form. Additionally, it possessed higher $t_{1/2}$, lower deactivation rate constant, and lower affinity to its substrate. Moreover, the energy for denaturation of the Ch-MCE was 1.8-fold higher than that of the free enzyme, meaning that the immobilization process increases the heat resistance of enzyme. The calculated thermodynamic parameters as enthalpy (ΔH^*), Gibbs free energy (ΔG^*), and entropy (ΔS^*) demonstrated that covalent-binding between enzyme and activated chitosan increased its thermal stability. Furthermore, it was successfully used for 7 consecutive cycles with high retaining activity (90.4 %). It can be concluded that this work helps to overcome the limitations of the reduction in MCE catalytic activity associated with changes in temperature, pH and inhibitors making it useful in industrial applications and biotechnological process.

Acknowledgements

We thank the National Research Centre, Egypt for laboratory assistance.

Competing interests

The authors declare that there is no conflict of interests.

References (please re check References fromat)

Abdella MAA, El-Sherbin GM, El-Shamy AR, Atalla SMM and Ahmed SA. 2020. Statistical optimization of chemical modification of chitosan-magnetic nanoparticles beads to promote *Bacillus subtilis* MK1 α-amylase immobilization and its application. Bull Natl Res Cent. **44**: 1-13.

Abdel-Naby MA, Ismail AMS, Ahmed SA and Abdel-Fattah AF. 1998. Production and immobilization of alkaline protease from *Bacillus mycoides*. Bioresour. Technol. **64**: 205-210.

Afroz QM, Khan KA, Ahmed P and Uprit S. 2015. Enzymes used in dairy industries. Int. j. appl. res. **1(10)**: 523-527.

Ahmed SA, Abdel-Naby MA and Abdel-Fattah AF. 2018. Applicability of wool covalent bonded *Bacillus circulans* 25 cells for milk-clotting enzyme production by batch, repeated batch and continuous process. Braz. J. Chem. Eng. **35**: 847-856.

Ahmed SA, Abdel Wahab WA and Abdel-Hameed SAM. 2019. Comparative study in kinetics and thermodynamic characteristics of immobilized caseinase on novel support from basalt by physical adsorption and covalent binding. Biocatal. Agric. Biotechnol. **18**: 101028.

Cahyaningrum SE and Sianita MM. 2014. Immobilization of pepsin onto chitosan silica nanobeads with glutaraldehyde as crosslink agent. Bull. Chem. React. Eng. Catal. **9**: 263-269. https://doi:10.9767/bcrec.9.3.7060.263-269.

da Silva RR. 2017. Bacterial and fungal proteolytic enzymes: Production, catalysis and potential applications Appl. Biochem. Biotechn. **183**: 1–19.

Dey G, Singh B and Banerjee R. 2003. Immobilization of α-amylase produced by *Bacillus circulans* GRS313. Braz. Arch. Biol. Technol. **46**: 167-176.

Duman YA and Bayer Y. 2021. Kinetics and thermodynamics of keratin degradation by partially purified and encapsulated keratinase from *Bacillus vallismortis* DSM11031. Biocatal. Biotransformati. **39**: 283-291.

El-Shishtawy, RM, Ahmed, NSE and Almulaiky, YQ. 2021. Immobilization of Catalase on Chitosan/ZnO and Chitosan/ZnO/Fe2O3 Nanocomposites: A comparative study. Catalysts. **11**, 820.

Eskandarloo, H. and Abbaspourrad, A. 2018. Production of galacto-oligosaccharides from whey permeate using β-galactosidase immobilized on functionalized glass beads. Food Chemi. **251**:115–124.

Esposito M, Pierro P D, Dejonghe W, Mariniello L and Porta R. 2016. Ezymatic milk clotting activity in artichoke (*Cynara scolymus*) leaves and alpine thistle (*Carduus defloratus*) flowers. Immobilization of alpine thistle aspartic protease, Food Chem. **204**:115–121.

Ferreira MM, Santiago FLB, da Silva NAG, Luiz JHH, Fernandéz-Lafuente R, Mendes AA and Hirata DB. 2018. Different strategies to immobilize lipase from *Geotrichum candidum*: Kinetic and thermodynamic studies. Process Biochem. **67**: 55-63.

Figueira Jde-A, Dias FFG, Sato HH and Fernandes P. 2011. Screening of supports for the immobilization of β-glucosidase. Enzyme Res. Article ID 642460.

Hernandez-Mariinez R, Gutiérrez-Sanchez G, Bergmann CW, Loera-Corral O, Rojo-Dominguez A, Huerta-Ochoa S, Regalado-Gonzalez C and Prado-Barragan LA. 2011. Purification and characterization of a thermodynamic stable serine protease from *Aspergillus fumigatus*. Process Biochem. **46**: 2001–2006.

Hosseini S and Varidi M. 2021. Optimization of Microbial Rennet Encapsulation in Alginate – Chitosan Nanoparticles. Food Chem. **352**:129325.

Lamas EM, Berros RM, Balcão VM and Malcata FX. 2001. Hydrolysis of whey protein by protease extracted from *Cynara cardunculus* and immobilized into highly activated supports. EnzymeMicrob. Technol. **28**: 642-52. .

Lineweaver H and Burke D. 1934. Determination of enzyme dissociation constants. J. Am. Chem. Soc. **56**: 658-666.

Lowry OH, Rosebrough NJ, Farr AL and Randall RJ. 1951. Protein measurement with the folin phenol reagent. J Biol Chem. **193**: 265-275.

Mafra ACO, Ulrich LG, Kornecki JF, Fernandez-Lafuente R, Tardioli PW and Ribeiro MPdeA. 2019. Combi-CLEAs of glucose oxidase and catalase for conversion of glucose to gluconic acid eliminating the hydrogen peroxide to maintain enzyme activity in a bubble column reactor. J.Catal. **9**: 1-16.

Narwal RK, Bhushan B, Pal A, Malhotra S, Kumar S and Saharan V. 2016. Inactivation thermodynamics and iso-kinetic

profiling for evaluating operational suitability of milk clotting enzyme immobilized in composite polymer matrix. Int. J. Biol. Macromol. **91**: 317-28.

Nwagu TN, Okolo BN and Aoyagi H. 2011. Immobilization of raw starch digesting amylase on silica gel: A comparative study. Afr. J. Biotechnol. **10**: 15989-15997.

Pandey G, Munguambe DM, Tharmavaram M, Rawtani D and Agrawal YK. 2017. Halloysite nanotubes-An efficient nano-support for the immobilization of α-amylase. Appl Clay Sci. **136**: 184–191.

Pervez S, Aman A and Ul Qader SA. 2016. Role of two polysaccharide matrices on activity, stability and recycling efficiency of immobilized fungal amyloglucosidase of GH15 family. Int. J. Biol. Macromol. **96**: 70–77.

Riaz M, Perveen RR, Javed MR, Nadeem H and Rashid MH. 2007. Kinetic and thermodynamic properties of novel glucoamylase from *Humicola* sp. Enzyme Microb Technol. **41**: 558-564.

Salazar-Leyva JA, Lizardi-Mendoza J, Ramirez-Suarez JC, Lugo-Sanchez ME, Valenzuela-Soto EM, Ezquerra-Brauer JM, Castillo-Ya~Nez FJ and Pacheco-Aguilar R. 2017. Catalytic and operational stability of acidic protease from *Monterey sardine* (*Sardinops sagax caerulea*) immobilized on a partially deacetylated chitin support. J. Food Biochem. **41**: e12287._.

Siar E, Zaak H, Kornecki JF, Zidouneb MN, Barbosa O and Fernandez-Lafuente R. 2017. Stabilization of ficin extract by immobilization on glyoxyl agarose. Preliminary characterization of the biocatalyst performance in hydrolysis of proteins. Process Biochem. **58**: 98-104.

Singh RS, Chauhan K and Kennedy JF. 2018. Fructose production from inulin using fungal inulinase immobilized on 3-aminopropyl-triethoxysilane functionalized multiwalled carbon nanotubes. Int. J. Biol. Macromol. **125**: 41–52.

Talbert JN and Goddard JM. 2012. Enzymes on material surfaces. Colloids Surf. B: Biointerfaces. **93**: 8–19.

Thakrar FJ and Singh SP. 2019. Catalytic, thermodynamic and structural properties of an immobilized and highly thermostable alkaline protease from a haloalkaliphilic actinobacteria, *Nocardiopsis alba* TATA-5. Bioresour. Technol. **278**: 150–158.

Wahba MI, Hassan ME and Ali KA. 2021. Chitosan-glutaraldehyde activated carrageenanalginate beads for β-D-galactosidase covalent immobilization. Biocatal. Biotransformation. **39**: 138-151.

Wehaidy HR, Abdel-Naby MA, Shousha WG, Elmallah MIY and Shawky MM. 2018. Improving the catalytic, kinetic and thermodynamic properties of *Bacillus subtilis* KU710517 milk clotting enzyme via conjugation with polyethylene glycol. Int. J. Biol. Macromol. **111**: 296–301.

Yandri, Suhartati T, Satria H, Widyasmara A and Hadi S. 2020. Increasing Stability of α-amylase Obtained from *Bacillus subtilis* ITBCCB148 by Immobilization with Chitosan. Mediterr.J.Chem. **10**: 155-161.

Yang A, Long C, Xia J, Tong P, Cheng Y, Wang Y and Chen H. 2017. Enzymatic characterization of the immobilized alcalase to hydrolyse egg white protein for potential allergenicity reduction. J Sci Food Agric. **97**: 199–206.

Zaboli M, Raissi H, Zaboli M, Farzad F and Torkzadeh-Mahani M. 2019. Stabilization of D-lactate dehydrogenase diagnostic enzyme via immobilization on pristine and carboxyl-functionalized carbon nanotubes, a combined experimental and molecular dynamics simulation study. Arch Biochem and Biophys. **661**: 178–186.

JJBS

Volume 15, Number 4,December 2022
ISSN 1995-6673
Pages 659 – 669
https://doi.org/10.54319/jjbs/150415

Jordan Journal of Biological Sciences

Identification, Aquaculture Trials and Ecological Associations of Hexacorallian Zoanthids Collected from Selected Inter-Tidal and Underwater Rocky Sites of Pakistan

Syeda Sobia Nasir[1], Nuzhat Afsar[1,*], Abdul Ghani[1]and Amjad Ali[2]

[1]*Institute of Marine Science, University of Karachi. Karachi-75270, Pakistan;*[2]*Center of Excellence in Marine Biology, University of Karachi, Karachi-75270, Pakistan*

Received: October 23, 2021; Revised: March 14, 2022; Accepted: April 21, 2022

Abstract

One intertidal (Buleji) and two diving sites (Mubarak village and Churna Island (2 stations)) were visited for the collection of zoanthids (with *morphotypes*) (*Zoanthus sansibaricus (6)*, *Z. vietnamensis (2)*, *Palythoa tuberculosa* and *P. mutuki (2)* from Buleji), while *Z. sansibaricus (morph-4)* and *P. tuberculosa* from both diving sites. Moreover, 29 intertidal (26 Molluscans and 1 Annelida, Arthropoda and Echinodermata) and 1 underwater Porite (*Tubipora musica*) associates were identified from Buleji and diving station-I of Churna Island, respectively, in order to study their ecology. All zoanthids (including morphotypes) and porite were reared in aquaria to determine their growth potentials in artificial settings. During culture, the recorded parameters ranged between 35-36.5‰ salinity, 7.3-7.7 pH, 25.4-31.0˚C temperature, 0.4-0.3ppm NO_2^-, 0.12-0.08ppm NO_2-N, 500-545mg/l Ca, 0.23-0.25mg/l NH_3 and 7-10mg/l DO_2. The *Z. sansibaricus* (morph-1c) and *Z. vietnamensis* (morph-1), *P. tuberculosa*(c), and *P. mutuki* (morph-1c & 2a) lived up to 21 weeks, showing 41, 51, 18, and 32 & 66 average growth rate or average polyp growth percentage (APG%) respectively, while *Z. sansibaricus* (morph-4a), *P. mutuki* (morph-2b) and *T. musica* were sustained up to 19, 6 and 4 weeks with APG% of 0, -92 and -93, respectively.

Keywords: Hexacorallia, Zoanthids, Buleji, Mubarak Village, Churna Island, Aquaculture, Identification, Ecology

1. Introduction

Hexacoralian zoanthids are delicate, radially symmetrical, diploblastic, and vibrant marine invertebrates attached to intertidal/deep-sea rocks (Gul, 2013; Trivedi and Vachhrajani, 2014) with basal discs (Budarf *et al.,* 2009). Mouth is surrounded by tentacles and six (paired) mesenteries, although 5th pair is complete in suborder Macrocnemina while incomplete in Brachycnemina (Khushali and Pradeep, 2013; Krishna and Gophane, 2013). Van der Land and Hartog (2001) proposed their taxonomy, although molecular grade identification is required in addition to morphological parameters (Reimer *et al*., 2007). They are famous epizoic animals (Nasir *et al*., 2018), associated with Annelida, Arthropoda, Cnidaria, Crustacea, Echinodermata, Mollusca, Porifera (Khushali, 2015), and photosynthetic algae, *Zooxanthellae* (Rabelo *et al*., 2015a). Recent anthropogenic stressors negatively affect wild zoanthids (Lin *et al.,* 2018), while their aquaculture seems to be difficult due to toxic secretion abilities (Hamade *et al.,* 2015). However, rearing experiments might conserve these species.

Pakistan possesses 990km coastline (Mangroves for the future, 2016). *Zoanthus sansibaricus* is found from Manora, Karachi (Gul, 2013; Morandini *et al.*, 2015; Nasir *et al.,* 2018), and a natural product zoanthaminone was isolated from *Zoanthus* sp (Atta-ur-Rahman, 1989). However, no published work was related to their aquaculture except Nasir *et al.*, (2018), who identified and reared *Zoanthus sansibaricus*, *Z. vietnamensis*, *Epizoanthus scotinus,* and *Palythoa tuberculosa.* Thus, the aim and objectives of this study are to provide awareness for their replenishment via aquaculture and identify not only the zoanthid species in and around Karachi coasts but also the factors affecting their normal growth rates and their ecological associations to highlight positive and negative interactions.

2. Materials and Methods

From October 2018 to April 2019, zoanthids were collected from intertidal rocks of Buleji (24^o 50’ 355” N 066^o 50’ 367” E), ~8m depth from Mubarak Village (24^o 51’ 599” N 066^o 38’ 804” E), and two stations of Churna Island (Station I: 24^o 54’ 890” N 066^o 36’ 840” E and Station II: 24^o 53’ 926” N 066^o 35’ 508” E), using SCUBA. A one-square-foot quadrate was placed randomly to collect the samples by hammer and chisel. Live samples were transferred to laboratory for rearing. The details are given below:

* Corresponding author. e-mail: nafsar@uok.edu.pk.

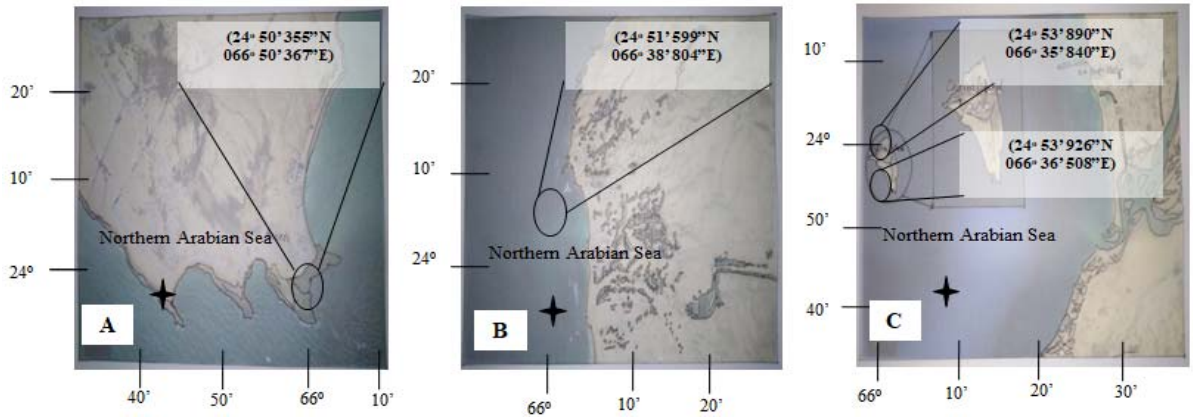

Figure 1: Maps of Collection Sites: (A) Buleji Coast, (B) Mubarak Village, (C) Churna Island Station I & II

2.1. Study Area (Fig 1)

2.1.1. Buleji:

Triangular, highly diversified, south-west to the Arabian Sea, almost 8km rocky parts, having tides-pools on west while sand/mud on east side (Nasir *et al.*, 2018).

2.1.2. Churna Island:

Arabia sea on its west, 9km away from Hub river, highly diversified rocky island (1.2x0.5km), less turbid, famous for snorkeling and SCUBA diving (Shahid, 2015; Khan, 2015).

2.1.3. Mubarak Village:

Variety of sediments from Boulders to pebbles, rocks with tidepools, caves and overhanging structures (Ali *et al.*, 2014).

2.2. Identification of Specimens

Zoanthids are identified morphologically based on the types of polyp (immersae/ liberae/ intermediae) (Reimer *et al.*, 2006), colors of polyps, tentacles and oral slits, number of tentacles, size of colonies and oral discs, and sediment encrustation inside tissue or not. The collected zoanthid and associated species were identified morphologically with the aid of online available literatures (Esper 1805; Haddon and Shackleton, 1891; Carlgren, 1900; Pax and Muller, 1957; Reimer *et al.*, 2011; Gul, 2013; Khushali, 2014; Koupaei *et al.*, 2014; Reimer *et al.*, 2014; Nasir *et al.*, 2018, and Linnaeus, 1758; Rudy *et al.*, 1983; Bosch *et al.*, 1995; Budd, 2007; Apte *et al.*, 2010; Bano *et al.*, 2011; Afsar *et al.*, 2012; Carmona *et al.*, 2014a, 2014b, Agustiadi and Luthfi, 2017; Ghani *et al.*, 2017; Ghani *et al.*, 2018a, 2018b; Kazmi *et al.*, 2018; Ghani *et al.*, 2019).

2.3. Laboratory Rearing Data Collection

The collected species were reared for 21 weeks in two aquaria containing 30L seawater, strong bio-filter aerators and 25 watts white LED bulbs. The parameters (pH, temperature, and salinity) were monitored weekly using hand-held digital pH-, thermo-, and refracto-meters, respectively, while nutrient concentrations like dissolved oxygen, calcium, nitrite-nitrogen, and ammonia were checked fortnightly with their respective kits: AQUA NITE Thailand, Merck KGaA, 84271 Darmstack, Germany, Aquacare 2000.10, PARA Test, Aquacare 2000.4, PARA Test. Lugol's iodine solution (few drops) were poured in aquaria weekly for growth nourishment and pathogens removal (Nasir *et al.*, 2018). The number of polyps counted before placing in aquaria (Polyps placed (PP)). The number of polyps grown (PG) were counted once every week (up to 21 weeks that is PG_1 to PG_{21}), to judge the increase or decrease in polyps quantity, then their sum was taken as: $(\Sigma_{PG})=PG_1+\ldots.+PG_{21}$. The average polyps grown over 21 weeks was calculated by: $APG/21wk=(\Sigma_{PG})/21$ to obtain the mean production of polyps grown throughout the production period i.e. 21 weeks. Then, Standard deviation (SD) is taken for each specimen from their (PG) of 21 weeks to analyze fluctuations in polyp number within overall observation period. The average growth rates of reared species were recorded as: Average Polyp Growth Percentage APG%=((APG/21wk-PP)/PP)*100 (Table 3).

3. Results

The findings of the research are categorized into three (3) parts: Part (I) identification of Hexacorallian zoanthids and their associated fauna, Part (II) growth patterns along collection sites, while Part (III) aquaculture trials. The details are mentioned below:

3.1. Part (I) Identification

Four species of zoanthids including their (morphotypes) were identified as *Zoanthus sansibaricus* (6), *Zoanthus vietnamensis* (2), *Palythoa tuberculosa* and *Palythoa mutuki* (2) from the intertidal rocks of the Buleji coast. Only two zoanthid species, *Zoanthus sansibaricus* (morphotype-4) and *Palythoa tuberculosa*, were collected from 8m depth of Mubarak Village and both Churna Island's stations (Table 1; Plate 1). The details are as follows:

Table 1: Morphological appearance and number of tentacles of observed in collected Zoanthids and a porite coral species

S.No	Species Names	Morph	Polyp color/ outside	Inside	Tentacles
1	*Zoanthus sansibaricus*[1]	1	Purple	Green	48
		2	Purple/Pink	Light green and few Orange	48
		3	Green	Brown	48
		4	Green	Green	48
		5	Green	Blue	40
		6	Brown	Brown and few Green	48
2	*Zoanthus vietnamensis*[2]	1	Brown	Pink	48
		2	Green	Pink ring and Brown or Grey	48
3	*Palythoa tuberculosa*[3]	Nil	Yellow/Cream	White	32 (Brown)
4	*Palythoa mutuki*[4]	1	Brown	Green	47
		2	Brown	Brown	40
1	*Tubipora musica*[5]	Nil	Bright Red	Nil	8 (Gray)

Note: [1](Carlgren, 1900; Gul, 2013; Reimer *et al.*, 2014; Koupaei *et al.*, 2014; Nasir *et al.*, 2018)

[2](Pax and Muller, 1957; Reimer *et al.*, 2011; Khushali, 2014; Nasir *et al.*, 2018)

[3](Esper, 1805; Reimer *et al.*, 2011; Koupaei *et al.*, 2014; Reimer *et al.*, 2014; Nasir *et al.*, 2018)

[4](Haddon and Shackleton, 1891; Reimer *et al.*, 2011; Koupaei *et al.*, 2014)

[5](Linnaeus, 1758; Agustiadi and Luthfi, 2017)

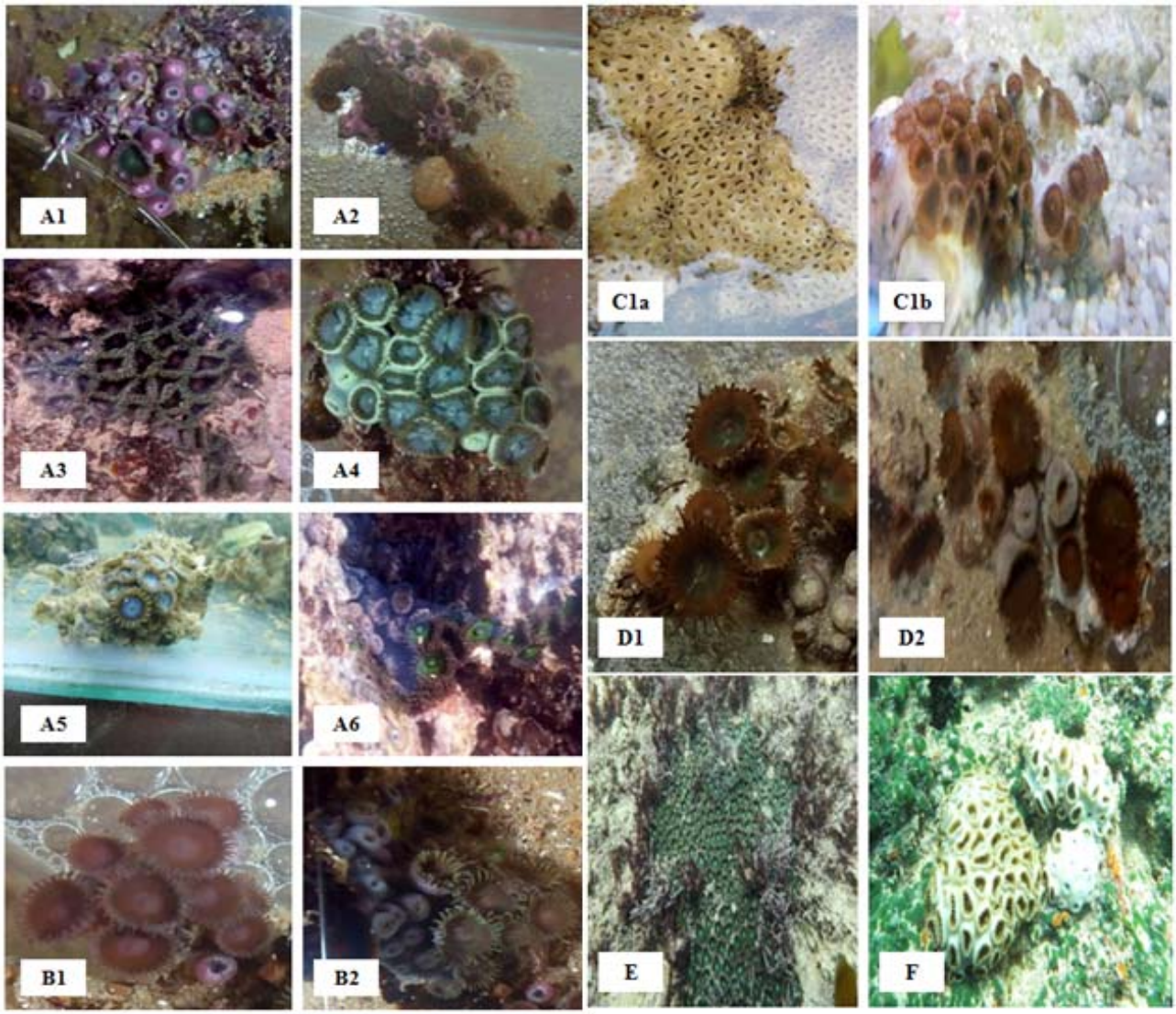

Plate 1: Intertidal Zoanthids species: *Zoanthus sansibaricus*: (A1) Morph 1, (A2) Morph 2, (A3) Morph 3, (A4) Morph 4, (A5) Morph 5 and (A6) Morph 6, *Zoanthus vietnamensis*: (B1) Morph 1 and (B2) Morph 2, *Palythoa tuberculosa*: (C1a) Closed Polyps and (C1b) Open Polyps, *Palythoa mutuki*: (D1) Morph 1 and (D2) Morph 2, Underwater Zoanthids species: (E) *Z. sansibaricus* and (F) *P. tuberculosa*

Moreover, only single species was associated with deep-water zoanthids of Churna Island (Table 1; Plate 2). However, 29 species belonging to various phyla such as Mollusca, Annelida, Echinodermata and Arthropoda, were found in association with intertidal zoanthids at Buleji coast (Table 2). It was observed that zoanthids have no negative impact with all mentioned species in (Table 2), except nudibranchs (*Baeolidia palythoae* and *Berghia* spp), which were found to be grazing on zoanthids. Additionally, an unidentified bacterial disease was observed (Plate 3). The details are mentioned below:

3.1.1. Zoanthids

Zoanthus sp. have delicate, erect and liberae polyps, do not accumulate sediments inside their tissues, gray/green/purple externally, while bright/green-brown internally. *Z. sansibaricus* are most stiff species, classified into morphotypes based on oral discs coloration like brown, green, purple, orange, yellow, red, white or fluorescent, containing about 60 tentacles (30 each row). *Z. vietnamensis,* have brown polyps with green/white/light pink tentacles, white oral slits with pink loop in their oral discs. The species of the genus *Palythoa* encrust sediments in tissues. The *P. tuberculosa* have immerse and round polyps, fused at base then extend individually, 30-34 tentacles (1/2 oral disc size). They have green-brown oral discs with creamy brown colors externally. Another species, *P. mutuki,* has 30mm long intermediae polyps (brownish apex) and 45-67 tentacles with green/brown oral discs (>1/2 tentacles' size) (Reimer, 2010; Khushali and Pradeep, 2013).

3.1.2. Associated Species

Tubipora musica (scleractinian) associated with deepwater zoanthids were collected from 1st diving station of the Churna Island (Table 1; Plate 2). Furthermore, 29 species were associated with intertidal zoanthids at Buleji, including 26 species of the phylum Mollusca (three classes: Gastropods (23 species), Bivalvia (2), and Polyplacophora (1) and one species of each phyla: Annelida, Echinodermata, and Arthropoda. The abundantly found species with zoanthids in descending order were: *Turbo bruneaus* > *Tenguella granulate* > *Trochus fultoni*. No associated species harmed zoanthids but only two nudibranchs, namely *Baeolidia palythoae* and *Berghia* spp, fed on zoanthids. On the other hand, a harmful bacterial growth over zoanthids was observed (Plate 3).

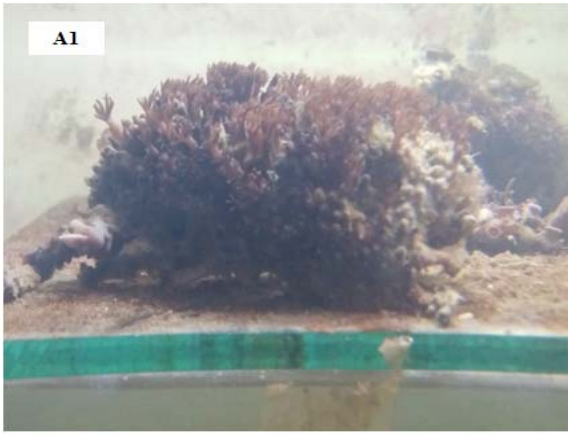

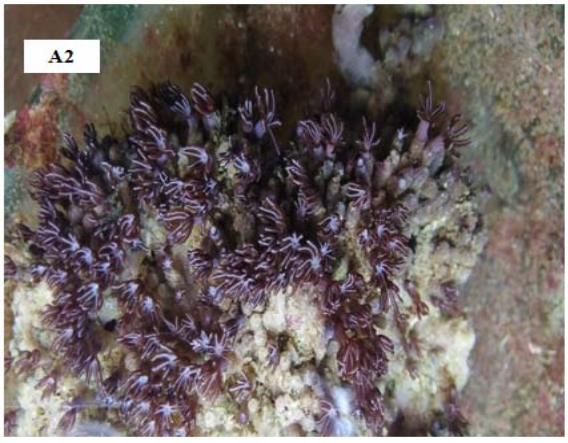

Plate 2: Underwater Zoanthids' Associates: (A1) *Tubipora musica* (Side view) and (A2) *Tubipora musica* (Top view)

Table 2: Checklist of associated fauna observed in association with zoanthids of Buleji coast, Karachi

Phylum	Class	Order	Family	Genus	Species
Mollusca	Gastropoda	Trochida	Trochidae	*Trochus*	*Trochus fultoni* (Melvill, 1898)
		Archeogastropoda	Turbinidae	*Turbo*	*Turbo bruneus* (Roding, 1798)
		Cycloneritida	Neritidae	*Nerita*	*Nerita albicilla* (Linnaeus, 1758)
		Caenogastropoda	Cerithiidae	*Cerithium*	*Cerithium caeruleum* (G. B. Sowerby II, 1855)
					Cerithium scabridum (Philippi, 1848)
				Clypeomorus	*Clypeomorus bifasciata* (G. B. Sowerby II, 1855)
		Littorinimorpha	Cypraeidae	*Naria*	*Naria turdus* (Lamarck, 1810)
			Cymatiidae	*Gyrineum*	*Gyrineum natator* (Roding, 1798)
		Neogastropoda	Muricidae	*Tenguella*	*Tenguella granulata* (Duclos, 1832)
				Purpura	*Purpura panama* (Roding, 1798)
				Drupella	*Drupella rugosa* (Born, 1778)
				Tylothais	*Tylothais savignyi* (Deshayes, 1844)
				Semiricinula	*Semiricinula tissoti* (Petit de la Saussaye, 1852)
					Semiricinula konkanensis (Melvill, 1893)
			Nassariidae	*Nassarius*	*Nassarius deshayesianus* (Issel, 1866)
			Pisaniidae	*Pollia*	*Pollia undosus* (Linnaeus, 1758)
			Olividae	*Oliva*	*Oliva bulbosa* (Roding, 1798)
			Conidae	*Conus*	*Conus namocanus* (Hwass in Bruguiere, 1792)
		Siphonariida	Siphonariidae	*Siphonaria*	*Siphonaria belcheri* (Hanley, 1858)
					Siphonaria savignyi (Krauss, 1848)
		Nudibranchia	Aeolidiidae	*Baeolida*	*Baeolidia palythoae* (Gosliner, 1985)
				Berghia	*Berghia spp* (Trinchese, 1877)
		Systellommatophora	Onchidiidae	*Peronia*	*Peronia verruculata* (Cuvier, 1830)
	Polyplacophora	Chitonida	Chitonidae	*Chiton*	*Chiton peregrines* (Thiele, 1909)
	Bivalvia	Orcida	Arcidae	*Barbatia*	*Barbatia obliquata* (Wood, 1828)
		Mytilida	Mytilidae	*Leiosolenus*	*Leiosolenus tripartitus* (Jousseaume, 1894)
Arthropoda	Malacostraca	Isopoda	Cirolanidae	*Eurydice*	*Eurydice pulchra* (Leach, 1815)
Echinodermata	Ophiuroidea	Amphilepidida	Ophiactidae	*Ophiactis*	*Ophiactis savignyi* (Muller and Troschel, 1842)
Annelida	Polychaeta	Phyllodocida	Nereididae	*Nereis*	*Nereis vexillosa* (Grube, 1851)
4	6	15	20	26	29

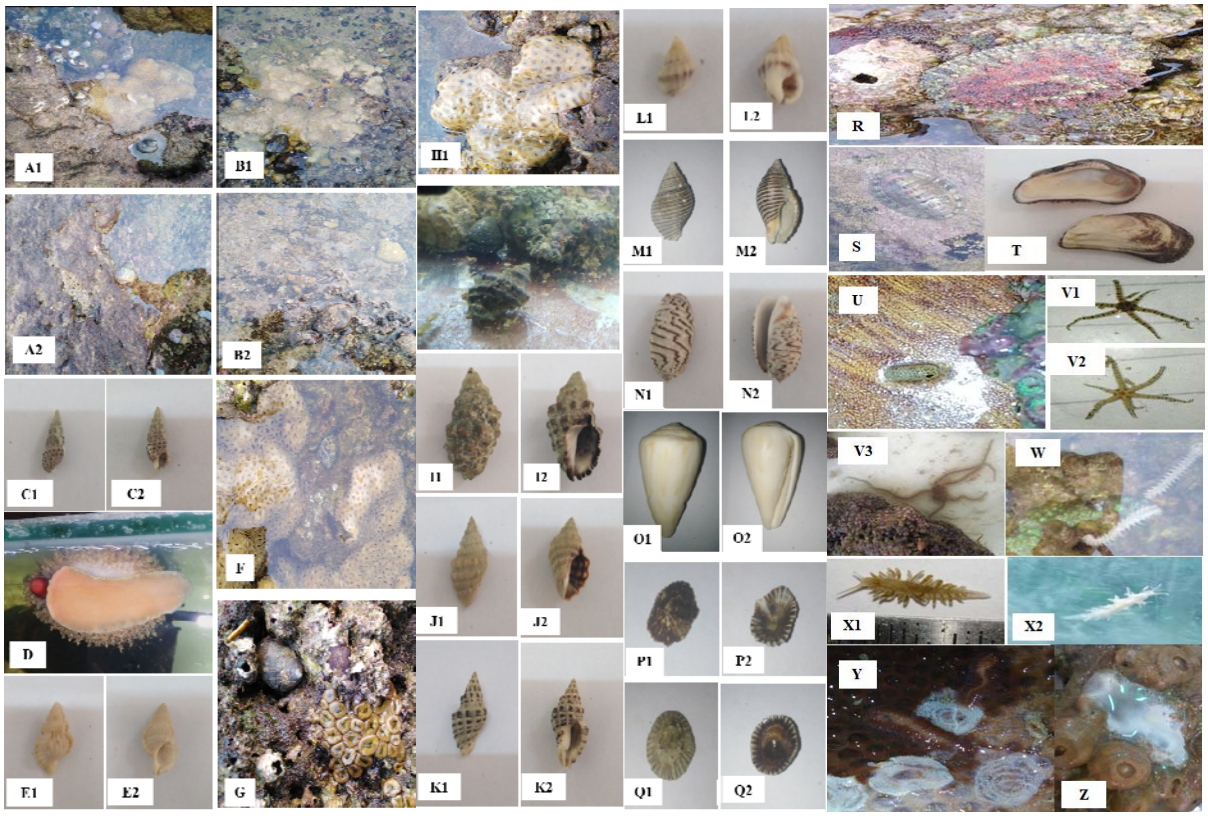

Plate 3: Intertidal Zoanthids' Associates: (A1) Trochus fultoni and Turbo bruneus with Palythoa tuberculosa, (A2) Trochus fultoni and Turbo bruneus with Zoanthus sansibaricus, (B1) Nerita albicilla, Cerithium caeruleum and Clypeomorus bifasciata with Palythoa tuberculosa, (B2) Nerita albicilla, Cerithium caeruleum, Clypeomorus bifasciata with Zoanthus sansibaricus, (C1) Cerithium scabridum (Dorsal view), (C2) Cerithium scabridum (Ventral view), (D) Naria turdus (Ventral view), (E1) Gyrineum natator (Dorsal view), (E2) Gyrineum natator (Ventral view), (F) Tenguella granulata with Palythoa tuberculosa, (G) Purpura panama with Zoanthus sansibaricus, (H1) Drupella rugosa with Palythoa tuberculosa, (H2) Drupella rugosa with Zoanthus sansibaricus, (I1) Tylothais savignyi (Dorsal view), (I2) Tylothais savignyi (Ventral view), (J1) Semiricinula tissoti (Dorsal view), (J2) Semiricinula tissoti (Ventral view), (K1) Semiricinula konkanensis (Dorsal view), (K2) Semiricinula konkanensis (Ventral view), (L1) Nassarius deshayesianus (Dorsal view), (L2) Nassarius deshayesianus (Ventral view), (M1) Pollia undosus (Dorsal view), (M2) Pollia undosus (Ventral view), (N1) Oliva bulbosa (Dorsal view), (N2) Oliva bulbosa (Ventral view), (O1) Conus namocanus (Dorsal view), (O2) Conus namocanus (Ventral view), (P1) Siphonaria belcheri (Dorsal view), (P2) Siphonaria belcheri (Ventral view), (Q1) Siphonaria savignyi (Dorsal view), (Q2) Siphonaria savignyi (Ventral view), (R) Peronia verruculata, (S) Chiton peregrines, (T) Barbatia obliquata, (U) Eurydice pulchra, (V1) Ophiactis savignyi (Dorsal view), (V2) Ophiactis savignyi (Ventral view), (V3) Ophiactis savignyi (In Aquarium), (W) Nereis vexillosa, (X1) Berghia spp (In aquarium) (X2) Berghia spp (Outside the aquarium), (Y) Baeolidia palythoae with eggs (grazing) and (Z) Bacteria (disease)

3.2. Part (II) Growth Patterns

All identified zoanthid species including *Zoanthus and Palythoa* were either totally absent or diminutive on high tide zones of Buleji. However, *Zoanthus* were more abundant at low tide, while *Palythoa* at mid tides. Only two zoanthid species, *Z. sansibaricus* (morphotype-4) and *P. tuberculosa*, were abundantly found across all diving sites at water depth of around 8m.

3.3. Part (III) Aquaculture

During aquarium trials, the average recorded parameters in aquaria varied between 35-36.5‰ salinity, 7.3-7.7 pH, and 25.4-31.0˚C temperature (Fig 2a), whereas the aggregate nutrients' concentrations were 0.3-0.4ppm NO^{2-}, 0.08-0.12ppm NO_2–N, 500-545mg/l Ca, 0.23-0.25mg/l NH_3 and 7-10mg/l DO_2 (Fig 2b). It was observed that most species lived less than one week then died completely, thus showing 0 APG/21wk and -100 APG%, namely *Z. sansibaricus* (morph-1(a, b), 2, 3, 4(b, c, d)), *P. tuberculosa*(a, b, d, e, f) and *P. mutuki* (morph-1a, b) (Table 3). A few survived about a week like *Z. sansibaricus* (morph-1d, 4e, 5, 6), *Z. vietnamensis* (morph-2), *P. mutuki* (morph-1d), hence shown -95 APG% while 5, 10, 1, 2, 13, and 5 APG/21wk respectively (Table 3, Fig 3a). *Tubipora musica* and *P. mutuki* (morph-2b) remained alive for 4 and 6 weeks, having -93 and -92 APG% with 24 and 27 APG/21wk respectively. *Z. sansibaricus* (morph-4a) lived for 19 weeks with 25 APG/21wk and 0 APG%. However, some species were successfully grown and sustained throughout the culture period of 21 weeks, for instance, *Z. sansibaricus* (morph-1c), *Z. vietnamensis* (morph-1), *P. tuberculosa*(c), *P. mutuki* (morph-1c and 2a) with 41, 51, 18, 32, 66 APG% and 189, 15, 59, 57, 28 APG/21wk respectively (Table 3, Fig 3a-c). The possible reasons of death or loss of polyps might be due to the nudibranchs grazing, bacterial disease outbreak, parameters fluctuation (including increase in salinity via evaporation), and provision of low light causing less photosynthesis. Small aquarium space available for aquaculture experiment can also be a factor for deterioration, although use of lugol's solution, removal of nudibranchs and diseased or dead polyps by hand picking, provision of freshwater bath treatment for 5 minutes, reducing salinity by adding freshwater seemed to boost the growth rates of some species. The date and site of

collections, numbers of polyps counted per square foot and collected for cultivation, APG/21wk, APG % and SD are enlisted in (Table 3; Fig 3a-c). However, the average growth rates (APG%) of successfully reared species (i.e. species who had shown growth activities from 4 to 21 weeks, either increased or decreased from or reached to their initial quantities placed in aquarium) in ascending order are: *T. musica* (-93) < *P. mutuki* Morph-2b (-92) < *Z. sansibaricus* Morph-4a (0) < *P. tuberculosa*(c) (18) < *P. mutuki* Morph-1c (32) < *Z. sansibaricus* Morph-1c (41) < *Z. vietnamensis* Morph-1 (51) < *P. mutuki* Morph-2a (66). The details are mentioned below:

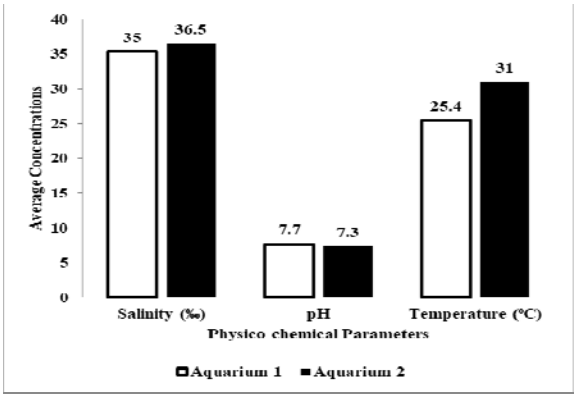

Figure 2a: Average physico-chemical parameters during culture trials

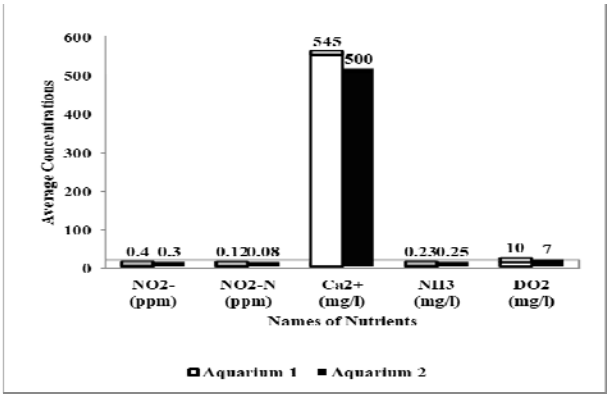

Figure 2b: Average nutrient's concentrations during aquarium trials

Table 3. Species, date and site of collection, Polyps observed per Square foot, number of polyps placed and grown over 21 weeks (all Morphotype of Zoanthids and Associated Coral species)

S.No	Species Names	Morph	Site	Date	Polyps/sq.ft	Aq #	Polyps Placed (PP)	Σ_{PG}	APG/21wk	APG%	SD (±)
1	*Z. sansibaricus*	1a	B	9/10/18	1000	1	26	0	0	-100	0
		b	B	7/11/18	1000	1	74	0	0	-100	0
		c	B	3/1/19	6432	1	134	3961	189	41	66
		d	B	18/4/19	7488	2	108	108	5	-95	24
		2	B	9/10/18	2000	1	130	0	0	-100	0
		3	B	9/10/18	1000	1	330	0	0	-100	0
		4a	B	3/1/19	3600	1	25	524	25	0	10
		b	CI I	9/3/19	3168	2	44	0	0	-100	0
		c	CI II	13/3/19	936	2	13	0	0	-100	0
		d	MV	15/4/19	1944	2	27	0	0	-100	0
		e	B	18/4/19	3600	2	206	206	10	-95	45
		5	B	18/4/19	1008	2	14	14	1	-95	3
		6	B	18/4/19	22176	2	47	47	2	-95	10
2	*Z. vietnamensis*	1	B	3/1/19	1440	1	10	318	15	51	5
		2	B	18/4/19	5760	2	273	273	13	-95	60
3	*P. tuberculosa*	0a	B	9/10/18	3000	1	132	0	0	-100	0
		b	B	7/11/18	3000	1	500	0	0	-100	0
		c	B	3/1/19	7200	1	50	1243	59	18	9
		d	CI I	9/3/19	2160	2	30	0	0	-100	0
		e	CI II	13/3/19	4536	2	63	0	0	-100	0
		f	MV	15/4/19	1440	2	20	0	0	-100	0
4	*P. mutuki*	1a	B	9/10/18	1000	1	302	0	0	-100	0
		b	B	7/11/18	10000	1	680	0	0	-100	0
		c	B	3/1/19	9456	1	43	1191	57	32	17
		d	B	18/4/19	6048	2	98	98	5	-95	21
		2a	B	3/1/19	1224	1	17	593	28	66	7
		b	B	18/4/19	1440	2	333	566	27	-92	73
5	*T. musica*	0	CI I	9/3/19	23328	1	324	500	24	-93	73

Note: B:Buleji, CI I:Churna Island Station I, CI II:Churna Island Station II, MV:Mubarak Village, Aq #:Aquarium No, Σ_{PG}=Sum of polyps grown, APG/21wk=Average Polyp Grown over 21 weeks, APG%=Average Polyp Growth Percentage, SD=Standard Deviation

APG%: -100=died completely within 1wk, -95=died after 1wk, -93=died after 4wk, -92=died after 6wk, 0=reached to initially placed quantity

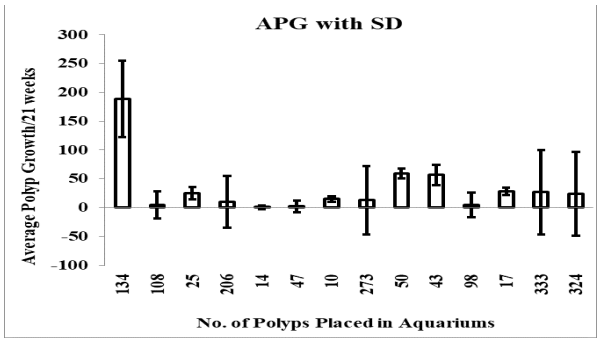

Figure 3a: Average polyp growth over 21 weeks (APG/21wk) and Standard Deviation (±SD) of Zoanthids and associated Porites reared in aquaria. **Note:** *Z. sansibaricus:* [Morph-1: 134(c) & 108(d), Morph-4: 25(a) & 206(e), Morph-5: 14, Morph-6: 47)]; *Z. vietnamensis:* [Morph-1: 10, Morph-2: 273]; *P. tuberculosa*: 50(c); *P. mutuki:* [Morph-1: 43(c) & 98(d), Morph-2: 17(a) & 333(b)] and *T. musica:* 324.

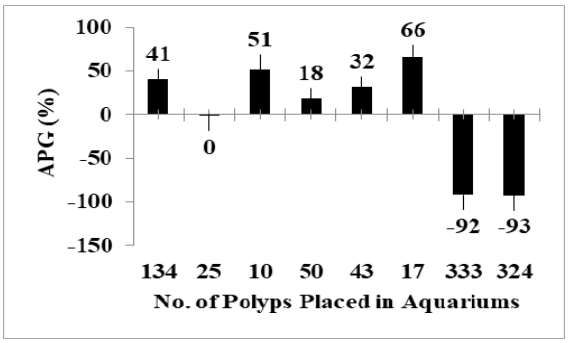

Figure 3b: Average polyp growth percentage (APG %) of Zoanthids and associated Porites reared in aquaria. **Note:** Polyp number: [**134**: *Z. sansibaricus* Morph-1(c)], [**25**: *Z. sansibaricus* Morph-4(a)], [**10**: *Z. vietnamensis* Morph-1], [**50**: *P. tuberculosa* (c)], [**43**: *P. mutuki* Morph-1(c)], [**17** & **333**: *P. mutuki* Morph-2 (a) & (b)] and [**324**: *T. musica*].

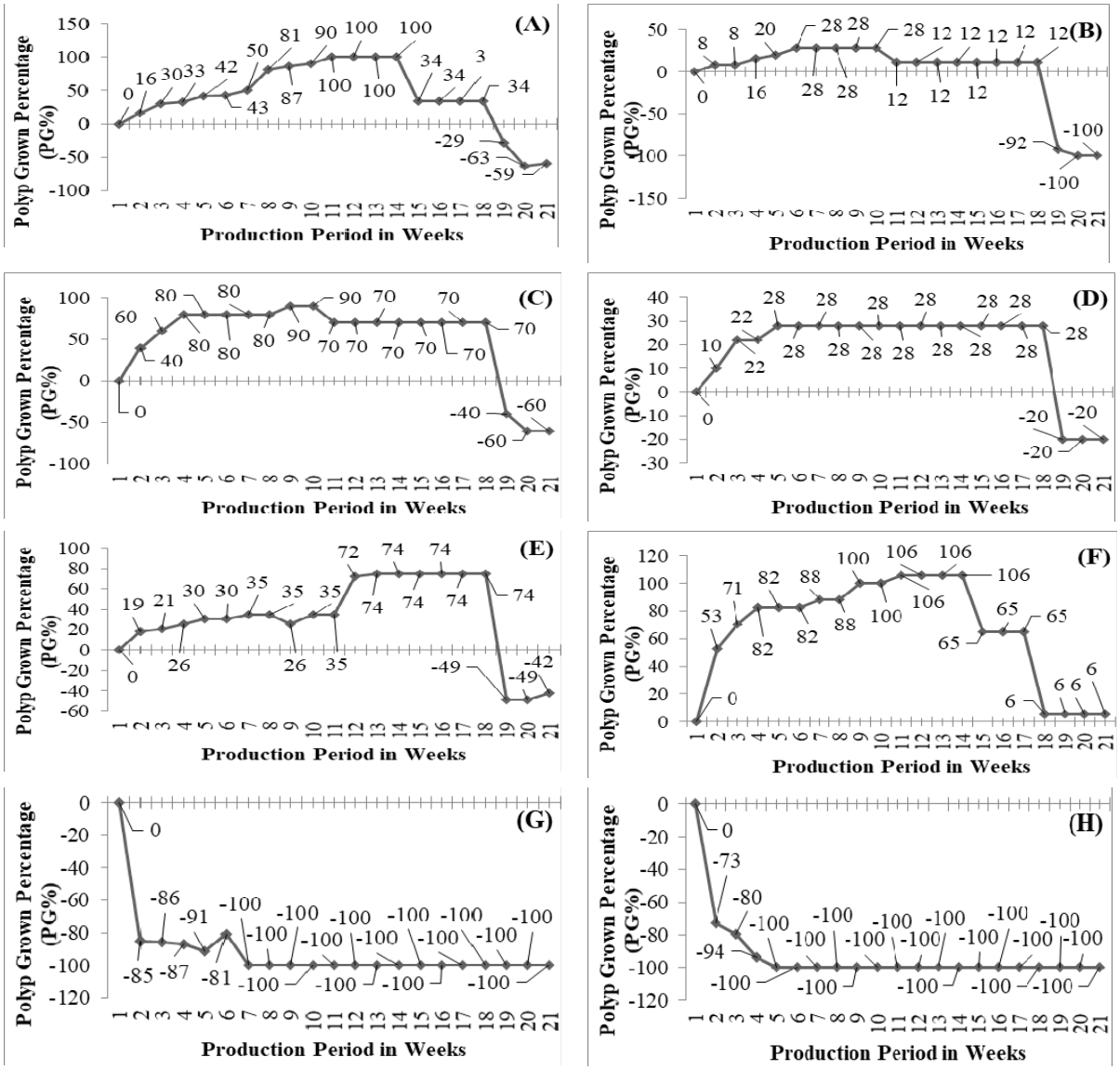

Figure 3c: Percentage of polyp grown/21 weeks (Zoanthids and Associated Coral): (A) 134 polyps of *Z. sansibaricus* (morph 1c), (B) 25 polyps of *Z. sansibaricus* (morph 4a), (C) 10 polyps of *Z. vietnamensis* (morph 1), (D) 50 polyps of *P. tuberculosa* (c), (E) 43 polyps of *P. mutuki* (morph 1c), (F) 17 polyps of *P. mutuki* (morph 2a), (G) 333 polyps of *P. mutuki* (morph 2b) and (H) 324 polyps of *T. musica.*
Note: 0 indicates quantity of polyps remains same as initially placed, the points above 0 indicates increase while below 0 indicates decline in growth rates. While -100 indicates that organisms completely died.

All grown species multiplied after 1st week of their placement in aquaria may be because they were adapting changes to new environment. *Z. sansibaricus* morph-(1c) shown peak growth rates from 11 to 14 weeks then, started diminishing and after 18th week declined sharply. However, survived up to 21 weeks (Fig 3c(A)). *Z. sansibaricus* morph-(4a) had shown growth acceleration in between 6-10 weeks, then started reducing with dominant death rates from 18th week and survived till 19th week then died completely (Fig 3c(B)). *Z. vietnamensis* morph- (1) had the shortest peak growth activities from 9 to 10 weeks, and started declining sharply after week 18 but survived to overall production period of 21 weeks (Fig 3c(C)). *P. tuberculosa* (c) multiplied with the longest growth peaks from 5-18 weeks but declined suddenly till 19th week after then nearly stable until 21 weeks (Fig 3c(D)). *P. mutuki* morph- (1c) shown peak growth rates in between 12-18 weeks, then sharp diminishing rates till 19th then slightly increased and remained alive until 21 (Fig 3c(E)), (2a) shown the highest growth rates than others from week 11 to 14, then declined twice sharply (i.e. after 14th and 17th weeks), but never died completely within 21 weeks of study period (Fig 3c(F)), and its morph (2b) had fast declining rates till 2nd week with a little multiplication at the end of the 5th week but started declining again while completely died on the 7th week thus sustained only 6 weeks (Fig 3c(G)). *T. musica* resulted almost similar to *P. mutuki* (morph-2b) but never multiplied, yet survived up to 4 weeks only, then died completely (Fig 3c(H)).

4. Discussion

In this research, the diversity of intertidal as well as deeper zoanthids in and around the Karachi coast were given. The identification of the collected zoanthids along with their intertidal and deep sea associated species was done with the help of online keys. The cultivation trials have been made to observe their growth potential in artificial media.

4.1. Identification of Zoanthid and Associated species

4.1.1. Zoanthids

An article published from Pakistan has revealed the occurrence of about four zoanthid species such as *Zoanthus sansibaricus, Zoanthus vietnamensis, Epizoanthus scotinus,* and *Playthoa tuberculosa* from Sunera, Paradise, Buleji and Manora intertidal rocks of Pakistan's Northern Arabian Sea (Nasir *et al*., 2018). Another article has evidenced the occurrence of varied morphotypes of *Z. sansibaricus*, *Z. vietnamensis*, *P. tuberculosa,* and *P. mutuki* from the Saurashtra coast of Gujarat, India. All of the aforementioned species are dominant along tropical to temperate intertidal rocky shores where corals are not abundantly present (Khushali and Pradeep, 2013). In the present study, the collected species and their morphotypes were found to be similar to that described by aforementioned literatures.

4.1.2. Associated species

Numerous studies have evidenced the symbiotic associations of zoanthids with other organisms that belong to different groups; for instance, Porifera (*Spongia officinalis*), Annelida (*Lanice conchelega*, *Nereis pelagica*, *Lepidonotus squamatus*), Polychaete larvae, Arthropoda (*Alpheus melabaricus*, *Alphaeus sp*, *Charybdis truncata*, *Menippe rumphii*, *Eurydice pulchra*, *Corophium* sps), Mollusca (*Cellana radiate*, *Cyprea tigris*, *Turbo bruneus*, *Cerithidea sps*, *Thais calvigera*, *Baeolida palythoae*), Echinodermata (*Asterias sps*, *Ophiotrix fragilis*, *Ophiocomina nigra*, *Stomopneutes variolaris* and *Tropiomera sp*) (Chakravarty *et al*., 2016). In this study, we observed almost the same associated fauna.

4.2. Growth Patterns

Zoanthids' population dynamics and their allocation patterns on inter-tidal rocks are elaborated in various studies (Trivedi and Vachhrajani, 2014). Despite this, fewer studies have been conducted in Pakistan on their growth rates and abundance (Ali *et al*., 2014). In the present study, the growth patterns of zoanthid species were found in a similar manner as described by Nasir *et al*., (2018) and Rabelo *et al*., (2015b); that is *Zoanthus* species are rich at low tides while *Playthoa* species are plentiful at mid tides. However, both are absent at high tidal levels.

5. Aquaculture

A single paper has been contributed from Pakistan on the cultivation trials of zoanthids. The article evidenced that zoanthids can be cultured successfully by just maintaining their required parameters, although the data was presented for 8 weeks only (Nasir *et al.,* 2018). Consequently, a comparative study is premeditated for 21 weeks, and freshly obtained erratic data related to the growth rates of identified zoanthids such as *Z. sansibaricus*, *Z. vietnamensis*, *P. tuberculosa,* and *P. mutuki,* including *T. musica* (deepwater zoanthid associates). The present study also revealed that zoanthids could be cultivated artificially by gratifying their requirements. However, mortalities occurred most likely due to small space, nudibranch grazing, bacterial disease outbreak. Lack of defense mechanism and internal immunity, and salinity changes due to evaporation of seawater from aquaria could also be considered. Nevertheless, few steps alleviated the growth rates of some species such as: lugol's iodine solution (few drops) controlled pathogens; nudibranchs, dead and diseased polyps were removed immediately, while freshwater bath treatment for at least 5 minutes using strong aerator (for water flushing flow) was given to remaining polyps in separate tanks, the hypersaline seawaters were mixed with freshwater in order to maintain salinity, and polyps were provided with enough space in aquarium to grow easily by placing racks and stones.

6. Conclusion

From the above research, it can be concluded that the rocky coasts of Pakistan are enriched with hexacorallian zoanthids. They form positive associations with other organisms such as molluscs, arthropods, echinoderms, annelids, scleractinians, etc., while negative with bacteria and nudibranchs. They can not only be sustained but also cultured in artificial environments if their required parameters are maintained successfully. The zoanthids species should be treated with freshwater bath including few drops of lugols iodine for ~5 min, and acclimatized before placing in aquarium, in order to get rid of

pathogens, boost immunity and eradicate hidden enemies that may come out after some time in aquarium, such as nudibranchs.

Acknowledgements

We cordially thank Dr. James Davis Reimer (Associate Professor, Department of Chemistry, Biology, and Marine Science, University of Ryukyus, Okinawa, Japan) for helping us in the identification of Zoanthids' samples.

References

Afsar N, Siddiqui G, Ayub Z. 2012. Updates of records of selected Prosobranch Gastropod species found along the coasts of Sindh and Balochistan, Pakistan. *Pak J Zool*., **44:** 267-275.

Agustiadi T and Luthfi OM. 2017. Diversity of Stoloniferan Coral (Stolonifera) at Lirang Island, Southwest Maluku (Moluccas), Indonesia. *Int J Oceans Oceanogr*., **11:** 21-30.

Ali A, Ormond R, Leujak W and Siddiqui PJA. 2014. Distribution, diversity and abundance of coral communities in the coastal waters of Pakistan. *J Mar Biolog Assoc UK*., **94:** 75–84.

Apte D, Bhave V and Parasharya D. 2010. an Annotated and Illustrated Checklist of the Opisthobranch Fauna of Gulf of Kutch, Gujarat, India, With 21 New Records for Gujarat and 13 New Records From India: Part 1. *J Bombay Nat His Soc*., **107:** 14.

Atta-ur-Rahman. 1989. Isolation and structural studies on new natural products of potential biological importance. *Pure Appl Chem*., **61:** 453-456.

Bano A, Moazzam M, Ayub Z and Siddiqui G. 2011. First Report of Siphonaria (Mollusca: Gastropoda) Species From The Rocky Coasts Off Karachi, Pakistan (Northern Arabian Sea). *Pak J Zool*., **43:** 602-604.

Bosch D, Dance SP and Fletcher N. 1995. **Seashells of eastern Arabia**. Motivate Pub, UAE.

Budarf ML, Labbé C, David G, Rioux JD. 2009. GWA studies: rewriting the story of IBD. *Trends Genet*., **25(3):** 137-46.

Budd GC. 2007. ***Eurydice pulchra* Speckled sea louse**. Marine Life Information System, United Kingdom.

Carlgren O. 1900. Ostafrikanische Actinien. Gesammelt von Herrn Dr. F. Stuhlmann 1888 und 1889. *Mitteilungen aus dem Naturhistorischen Museum*., **17:** 1-124.

Carmona L, Pola M, Gosliner TM and Cervera JL. 2014a. Review of Baeolidia, the largest genus of *Aeolidiidae* (Mollusca: Nudibranchia), with the description of five new species. *Zootaxa*., **3802:** 477–514.

Carmona L, Pola M, Gosliner TM and Cervera JL. 2014b. The atlantic mediterranean genus *berghia trinchese*, 1877 (Nudibranchia: Aeolidiidae): Taxonomic review and phylogenetic analysis. *J Molluscan Stud*., **80:** 482–498.

Chakravarty MS, Sudhan BS, Ganesh PRC, Dogiparti A. 2016. Some animal associates of zoanthids, *Palythoa mutuki* (Haddan & Shackeleton, 1891) and *Zoanthus sansibaricus* (Carlgen, 1990) along rocky shores of Visakhapatnam, India – A Checklist. *Int J Fish Aquat Stud*., **4(4):** 380-384.

Esper EJC. 1805. **Die Pflanzenthiere in Abbildungen nach der Natur mit Farben erleuchtet nebst Beschreibungen**, Nèurnberg, in der Raspischen Buchhandlung, Nürnberg.

Ghani A, Afsar N and Moazzam M. 2018b. A checklist of molluscans inhabiting Bandri beach along the Jiwani coast, Balochistan, *Pak J Mar Sci*., **27:** 61-71.

Ghani A, Afsar N and Qadir S. 2018a. New report of *Tutufa bardeyi* (Jousseaume, 1881) (Mollusca: Gastropoda) from Jiwani coast, Pakistan. *Int J Biol Biotechnol*., **15:** 163-166.

Ghani A, Afsar N and Rahman S. 2017. Quantitative Analysis of Macrobenthic Molluscan Populations Inhabiting Bandri Area of Jiwani, South West Pakistan Coast. *Jordan J Biol Sci*., **10:** 281-287.

Ghani A, Afsar N, Ahmed R, Qadir S, Saleh S, Majeed S and Imam N. 2019. Comparative study of significant molluscans dwelling at two sites of Jiwani coast, Pakistan. *Pak J Mar Sci*., **28:** 19-33.

Gul S. 2013. Occurrence of Zoanthid Colonies (Cnidaria: Hexacorallia: Zoantharia) At Karachi Coast, Pakistan: A Preliminary Report. *Int J Biol Biotechnol*., **10:** 153-154.

Haddon AC and Shackleton AM. 1891. **A Revision of the British Actiniæ. Part II: The Zoantheæ**. Volume IV (Series II). Dublin: Royal Dublin Society, London: Williams and Norgate.

Hamade AK, Deglin SE, McLaughlin JB, Deeds JR, Handy SM, Knolhoff AM. 2015. Suspected Palytoxin Inhalation Exposures Associated with Zoanthid Corals in Aquarium Shops and Homes, Alaska, 2012–2014. *Morb Mortal Wkly Rep*., **64:** 852-855.

Kazmi QB, Moazzam M and Sultana R. 2018. **Marine Molluscan fauna Of the Pakistani coastal waters**. BCC&T Press University of Karachi.

Khan MM. 2015. Churna-Kaio Islands Complex, Balochistan Coast, Pakistan. Scientific Information to Describe Areas Meeting Scientific Criteria for Ecologically or Biologically Significant Marine Areas. Marine Fisheries Department, Islamic Republic of Pakistan.

Khushali PM and Pradeep CM. 2013. Brachycnemic Zooxanthellate Zoanthids (Cnidaria: Zoantharia) of Saurashtra Coast: A Preliminary Survey. *Res J Mar Sci*., **1:** 10-13.

Khushali PM. 2014. Occurrence of Zoanthid genus Isaurus from Saurashtra coast, Gujarat, India. *Eur J Zool Res*., **3:** 1-5.

Khushali PM. 2015. Ecological Assessment and Distribution Pattern of Some Anthozoans along Saurashtra Coast Of Gujarat, India. Ph.D Thesis, Maharaja Sayajirao University of Baroda, Vadodara, India.

Koupaei AN, Mostafavi PG, Mehrabadi JF and Fatemi SMR. 2014. Molecular diversity of coral reef-associated zoanthids off Qeshm Island, northern Persian Gulf. *Int Aquat Res*., **6:** 64.

Krishna JM and Gophane A. 2013. Cnidarian from the Coast of Goa – Identified to the Species Level. *J Pharmacogn Phytochem*., **2:** 209-218.

Lin C, Zhou JM, Chong G, Wang LH, Meng PJ and Sujune T. 2018. The effects of aquarium culture on coral oocyte ultrastructure. *Sci Rep*., **8:** 15-159.

Linnaeus C. 1758. **Systema Naturae per regna tria naturae, secundum classes, ordines, genera, species, cum characteribus, differentiis, synonymis, locis**, thirteenth ed. Vindobonae, Vienna.

Mangroves for the future (MFF) Pakistan. 2016. **A Handbook on Pakistan's Coastal and Marine Resources**, MFF Pakistan, Pakistan.

Morandini AC, Gul S, Häussermann V and Pörschmann U. 2015. Checklist of cnidarians from Pakistani waters. *Check List*., **11(2):** 1-8.

Nasir SS, Khan H and Afsar N. 2018. Zoanthids (Cnidaria: Verrill, 1865) Dwelling Four Rocky Habitats along the Pakistan Coast. *Int J Biol Biotechnol*., **15:** 765-772.

Pax F and Müller I. 1957. Zoantharien aus Viet-Nam. *Mém Mus natl his nat*., **16:** 1–40.

Pax F. 1910. Studien an westindischen Actinien. *Zool Jahrb*., **11(2):** 157–330.

Rabelo EF, Rocha LL, Colares GB, Bomfim TA, Nogueira VLR, Katzenberger M, Cascon HM and Melo VMM. 2015a. Symbiodinium diversity associated with zoanthids (Cnidaria: Hexacorallia) in Northeastern Brazil. *Symbiosis*., **64(3):** 105-113.

Rabelo EF, Soares MDO, Bezerra LEA and Cascon HM. 2015b. Distribution pattern of zoanthids (Cnidaria: Zoantharia) on a Tropical reef. *Mar Biol Res*., **11(6):** 1-9.

Reimer JD, Obuchi M, Irei Y, Fujii T and Nozawa Y. 2011. Shallow-water brachycnemic zoanthids (Cnidaria: Hexacorallia) from Taiwan: a preliminary survey. *Zool Stud*., **50:** 363-371.

Reimer JD, Ono S, Iwama A, Takishita K, Tsukahara J and Maruyama T. 2006. Morphological and Molecular Revision of Zoanthus(Anthozoa: Hexacorallia) from Southwestern Japan,with Descriptions of Two New Species. *Zool Sci*., **23:** 261–275.

Reimer JD, Poliseno A and Hoeksema BW. 2014. Shallow-water zoantharians (Cnidaria, Hexacorallia) from the Central Indo-Pacific. *ZooKeys*., **444:** 1–57.

Reimer JD. 2010. Key to field identification of shallow water brachycnemic zoanthids (Order Zoantharia: Suborder Brachycnemina) present in Okinawa, Galaxea. *J Coral Reef Stud*., **12:** 23-29.

Reimer JD, Sinniger F, Fujiwara Y, Hirano S, Maruyama T. 2007. Morphological and molecular characterisation of Abyssoanthus nankaiensis, a new family, new genus and new species of deep-sea zoanthid (Anthozoa: Hexacorallia: Zoantharia) from a north-west Pacific methane cold seep. *Invertebr Syst*., **21(3)**: 255-262.

Rudy P, Rudy HL and Watson JF. 1983. **Oregon Estuarine Invertebrates: An Illustrated Guide to the Common and Important Invertebrate Animals**, third ed. Fish and Wildlife Service, US Dept of the Interior, Washington DC.

Shahid U. 2015. Churna Island, Karachi, Pakistan: Template for Submission of Scientific Information to Describe Areas Meeting Scientific Criteria for Ecologically or Biologically Significant Marine Areas. WWF-Pakistan, Pakistan.

Trivedi JN and Vachhrajani KD. 2014. Study of the Macro Faunal Associates of the Littoral Zoanthid Palythoa mutuki (Cnidaria, Anthozoa) from Saurashtra Coast, Gujarat, India. *Int J Mar Sci*., **4:** 1-9.

Van der Land J and den Hartog JC. 2001. A check-list of the marine species in Europe and a bibliography of guides to their identification. Collection Patrimoines Naturels. *Eur Regist Mar species*., **50:** 106-109.

JJBS

Volume 15, Number 4,December 2022
ISSN 1995-6673
Pages 671 – 678
https://doi.org/10.54319/jjbs/150416

Jordan Journal of Biological Sciences

Assessment of Phenotypic Diversity of Some Local Moroccan Date Palm Varieties and Clones (*Phoenix Dactylifera* L.) from the Zagora Region, Southern Morocco

Abderrahim Alahyane[1,*], Imane Elateri[1], Hassan Alahyane[3], Jamal Ayour[1], Abdelilah Meddich[1], Ahmed Ait-Oubahou[2], Mohamed Benichou[1], Mohamed Elfatihi Abderrazik[1]

[1]*Laboratory of Agro-Food, Biotechnologies and Valorization of Plant Bioresources, Department of Biology, Faculty of Sciences-Semlalia, Cadi Ayyad University, P.O. Box 2390, 40090 Marrakesh, Morocco;* [2]*Laboratory of Horticultural, Hassan II Agronomy and Veterinary Institute, P.O. Box 6202 N 10, Ait Melloul 86150, Morocco;*[3]*Laboratory "Water, Biodiversity & climate change ", Department of Biology, Faculty of Sciences, Semlalia, Cadi Ayyad University, Marrakech, P.O. Box2390, 40000, Morocco.*

Received: October 28, 2021; Revised: February 27, 2022; Accepted: April 11, 2022

Abstract

The purpose of this research was a better understanding of the phenotypic diversity of date palms (*Phoenix dactylifera* L.) in southern Morocco. To determine the total degree of polymorphism and find their distinct phenotypic attributes, 17 date palm accessions from various date palm groves in the Drâa-Tafilalet zone (Zagora) were studied. Thirty vegetative and reproductive parameters were examined, and multidimensional statistical methods were used to assess the data. These findings indicated that the date palm germplasm exhibited a high level of genetic polymorphism. The principal component analysis (PCA) revealed that leaf length and width, spine length and width, and fruit sizes were responsible for a considerable amount of the observed variability. Strong correlations were found between the studied traits, especially between fruit dimensions (length and width) and fruit and pulp weights (0.776; 0.861; 0.868; 0.719), respectively. A positive correlation was also found between petiole width at the bottom and spines (0.706), between petiole width at the bottom and leaflets number (0.765) as well as between spadice length and spadice length at the ramified part (0.673). Five phenotypic groups were identified with levels of dissimilarity ranging from 0.37 to 0.92. The first cluster had four cultivars (Bourar, Mentouj tissgharine, Khalt lohmadi and Khalt abdelghani); the second group possessed six cultivars (Khalt bheir ngli, Khalt iaach, Bouezgagh, Black bousthammi, KHL and Elmensoum); the third cluster included four cultivars (Elahmer chetoui, Elasfer eljaid, Hak feddan laaneb and Khalt khel); the fourth group contained two cultivars (Khalt zoubair ibn laouam and Mentouj lhaj lehbib); and the fifth group contained only one cultivar, 'Khalt iaissi'. In each one of these groups, the similarities observed between cultivars were based on fruit characteristics (semi-dry, dry, and soft dates). This work highlighted the most important traits that can be used for assessing the diversity of date palm trees and fruit. Leaf length and width, spine length and width, and fruit sizes had the highest discrimination value.

Keywords: Morocco; diversity; date palm; *Phoenix dactylifera* L.; cultivars, Zagora palm grove.

1. Introduction

The date palm is the most valuable arid-region crop in Morocco, and it has commercial value in all of North Africa. There are about 5.4 million palm trees in Morocco (Sedra, 2015). The annual date production is more than 117 thousand tonnes (FAOSTAT, 2012). More than 456 cultivars are known in Morocco (INRA, 2011). Plantations of date palms contribute to the construction of oasis ecosystems because they have a diverse genetic stock and help to create a suitable environment for the growth of the underlying crops. In addition, they contribute to stabilizing human populations in arid regions where the resources are limited. Urbanization, drought, salt, desertification, insect infestations, poor soils, genetic erosion, age, and diseases such as Bayoud caused by *Fusarium oxysporum f. sp. albedinis* are all potentially damaging to Morocco's oases (Botes and Zaid, 2002; Awad, 2006; Ehsine *et al.,* 2014; Meddich *et al.,* 2015). All these constraints have resulted in an abandonment of orchards by farmers who preferred migration from rural areas to urban centers, leading to degradation of these areas. From an agronomic standpoint, the best strategy for combating Fusarium wilt as well as drought and salt issues is to plant resistant date palms with high quality fruit and good production (Saaidi *et al.,* 1992). Resistant date palms can be obtained by a transfer of genetic material between genetically different palm trees (natural interbreeding), thereby changing the composition of the gene pool that provides the new population with traits of resistance to drought and parasites. As a result, selecting local palm trees that are adapted to the soil and climatic conditions of Morocco is of high interest and relevance. Trees called ‘khalts’ or ‘sairs’ which result

* Corresponding author. e-mail: alahyanerh@gmail.com.

from natural seedlings (Munier, 1973) have an interesting degree of polymorphism because of the high heterozygosity of the parental varieties (Saaidi, 1992; Sedra *et al.,* 1998). Farmers' empirical selection has resulted in the existing cultivars in each oasis. The process of denominations is local and begins at the place where the crop is grown (Elhoumaizi *et al.,* 2002). Djerbi *et al.* (1986) observed that certain 'khalts' have excellent fruit quality and have a significant resistance to *Fusarium oxysporum* f. sp. *albedinis* in date palm plantations.

The assessment of phenotypic diversity is an essential part of a breeding strategy (Brake *et al.,* 2021). There are variations in date palm genetic resources, according to several research reports. Most of them mainly focused on fruit morphology and the design of description cards (Mason, 1915; Nixon, 1950; Elhoumaizi *et al.,* 2006; Elshibli and Korpelainen, 2009; Rabei *et al.,* 2012; Zehdi-Azouzi *et al.,* 2015; Al-Khayri *et al.,* 2015). Some research, on the other hand, has emphasized the characteristics of fruit and leaves (Reynes *et al.,* 1994; Bouabidi *et al.,* 1996; Ahmen *et al.,* 2011; Elsafy *et al.,* 2015; Ennouri *et al.,* 2018).

The aim of the research reported here is to contribute to the assessment of phenotypic variability among seventeen date palm varieties and clones in Morocco's Zagora palm grove, to evaluate the degree of polymorphism among the varieties and clones investigated, and to find differences and similarities among cultivars that might be valuable in date palm classification. This will stimulate the selection of local palm trees that are productive and adaptable to the pedoclimatic conditions in Morocco in the future.

2. Material and methods

2.1. Plant materials

The 17 date palm accessions studied were obtained from different areas in the Drâa region (Zagora, Southern Morocco) (Table 1). The accessions were collected from different farmers' groves but were all growing in the Zagora oasis during the study period. These varieties and clones were available and abundant at the start of the study. During the harvest season in October 2018, the study was carried out in a field with the following GPS coordinates: 30°20' 59" N, longitude of 5°50'06" W, and elevation of 731 m, about 0.76 km from Zagora, Morocco. It was estimated that the field covered 39.04 hectares. The study region has a semi-arid environment with 61 mm of annual rainfall and a mean annual temperature of 22.9 °C. During the months of September and October 2018, sample parameters were measured. The physicochemical quality characteristics of the soil in the research area are shown in Table 2.

Table 1. Name, abbreviations and origin of date palm samples.

Accession	Label	Origin
Bourar	BRR	Tissgharine
Mentouj tissgharine	MTN	Tissgharine
Bouezgagh	BZG	Jenan lohmadi
Black bousthammi	BST	Jenan lohmadi
Khalt iaach	KHL	Jenan lohmadi
Khalt lohmadi	LHD	Jenan lohmadi
Elahmer chetoui	ECT	Aghlal elkhyat mehdia
Elasfer eljaid	EED	Aghlal elkhyat mehdia
Khalt zoubair ibn laouam	ZIE	Fedan laaneb tansita
Hak feddan laaneb	HFL	Fedan laaneb tansita
Khalt iaissi	IAS	Way hamama
Elmensoum	EMS	Way hamama
Khalt abdelghani	IAH	Bheir ingli
Iklane	IKL	Bheir ingli
Mentouj lhaj lehbib	MEL	Bheir ingli
Khalt bheir ngli	KBN	Bheir ingli
Khalt khel	KKL	Sefsafa

Table 2. Physico-chemical parameters of soils in the Zagora palm grove.

Site	**pH**	**EC** ($mS.cm^{-1}$)	**AP** ($mg.kg^{-1}$)	**TOC** ($g.kg^{-1}$)	**OM** ($g.kg^{-1}$)	**TN** ($g.kg^{-1}$)	**C/N**	**$CaCO_3$** ($g.kg^{-1}$)	**Texture**
Zagora	7.58 ±0.01	0.46 ±0.02	10.40 ±0.14	1.35 ±0.34	2.32 ±0.58	0.14 ±0.04	10.32±0.06	104.04±1.43	Sandy-loamy

Ec: Electrical conductivity; AP: Available phosphorus; TOC: Total organic carbon; OM: Organic Matter; TN: Total Kjeldahl nitrogen; C/N: Carbon/Nitrogen ratio.

Thirty criteria were examined to describe the phenotypes. The reproductive and vegetative characteristics of the date palm that were evaluated (Table 3). The measurements were carried out on the 17 date palm accessions. These samples were collected as follows: The samples were collected and characterized starting from the first week of October, which was 8 to 12 weeks after full flowering. This period varied from one cultivar to another. In order to ensure the homogeneity of the samples and the representativeness of the results, a certain number of fully developed plant material was collected from different parts of each tree.

The weight of the fruit and seeds was determined using an analytical balance. Manual measuring tape was used to measure the length and width of various reproductive and vegetative parts of the date palm (Table 3), while a digital caliper was used to assess the fruit and seed diameter.

For morphometric analysis, three individuals from each accession were selected. These characters are reported as part of standard descriptors for the date palm (IPGRI, 2005). All attributes related to fruit were measured at harvest stage.

Table 3. Measured vegetative and reproductive characters.

Character	Unit	code
Leaf		
Spinted part length	cm	P1
Petiole width at the bottom	cm	P2
Leaf length	cm	P3
Leaf width	cm	P4
Rachis thickness between the last spine and the first leaflet	cm	P5
Leafleted part length	cm	P6
Spines		
Spines number		P7
Spine width at the middle	mm	P8
Spine lengh at the middle	cm	P9
Leaflets		
Terminal leaflet length	cm	P10
Leaflets number		P11
Spacing index		P12
Terminal leaflet width	mm	P13
Leaflet width at the middle	mm	P14
Leaflet length at the middle	mm	P15
Fruit		
Fruit length	mm	P16
Fruit width	mm	P17
Fruit weight	gr	P18
Pulp weight	gr	P19
Seed length	mm	P20
Seed width	mm	P21
Seed weight	gr	P22
Seed/fruit length ratio		P23
Seed/fruit width ratio		P24
Spadice		
Spadice length	cm	P25
Spadice width at the middle	mm	P26
Spadice thickness at the middle	mm	P27
Spadice length at the ramified part	cm	P28
Spathe		
Spathe length	cm	P29
Spathe width	cm	P30

2.2. Data analysis

The data was analyzed using principal component analysis (PCA) and cluster analysis (CA) (XLSTAT, 2014). To obtain a new set of variables identified as principal components, PCA starts with a linear model and minimizes the structure of a data table (Mainley, 1994). The genetic relationship between accessions was investigated using cluster analysis with Euclidean distances as similarity metrics and the Unweighted Pair-Group Method Arithmetic Average (UPGMA).

3. Results

Mean values of the reproductive and vegetative traits studied are shown in Table 4. The data show a large variability between cultivars.

Table 4. Date palm accessions' average values for measured characteristics.

Code	P 1	P 2	P 3	P4	P5	P6	P7	P8	P9	P10	P11	P12	P13	P 14	P 15	P 16	P 17	P 18	P 19	P 20	P 21	P 22	P 23	P 24	P 25	P 26	P 27	P 28	P 29	P 30
BRR	88.7	10.5	324	118.6	2.6	231	30	6	14.8	21	163	0.48	11	18	54.7	44.30	20.83	13.25	12.36	17.37	5.00	0.82	0.39	0.06	118	42	22	28.0	94	5.7
BST	122.3	12.2	404	123.3	3	272	25	3.8	14.2	24.3	195	0.72	16	19	70.7	28.43	16.70	8.35	7.24	16.00	6.10	0.95	0.56	0.11	119	42	5	26.3	73	7.3
BZG	110	10.2	401	103	3.2	280	20	8	15.3	25	187	0.51	20	34	56.9	38.40	18.00	10.04	8.80	19.20	6.33	1.19	0.50	0.12	73	51	20	24.7	45	8.5
ECT	156	11.8	431	129	2	272.3	42	4.5	15.2	30	182	0.60	17	22	65.1	40.43	20.73	15.97	14.34	24.17	6.13	1.53	0.60	0.10	158	75	20	65.0	73	9.7
EED	157	14.7	465	148	3.3	293.3	43	7.6	16.3	13.5	199	0.60	9	30	72.4	40.20	21.43	14.27	12.45	24.77	7.47	1.70	0.62	0.12	116	64	14	52.3	84	6.3
EMN	92	3.8	355	92.3	2.5	257.3	23	6	13.7	21.7	155	0.72	19	24	61.4	22.97	14.77	4.90	3.83	14.90	6.17	1.02	0.65	0.20	87	44	5	33.0	43	8.9
HFL	144.7	9.8	403	120.6	2.3	238.3	31	4.5	13.3	16.3	162	0.67	18	33	57.5	42.57	23.03	17.36	16.01	21.37	6.40	1.28	0.50	0.07	122	52	19	60.0	64	8.2
IAH	66.7	3.2	313	87	1.6	240	14	2.6	7.8	17.6	127	0.53	12	12	45.5	28.23	18.20	7.94	6.58	17.50	6.40	1.34	0.62	0.17	126	47	13	38.7	53	7.4
IAS	186.7	7.2	369	77	2.8	177.3	26	4	13.6	20.7	142	0.66	20	25	46.9	36.77	17.47	9.79	8.68	20.67	5.37	1.06	0.56	0.11	107	53	14	33.3	43	4.1
IKL	75.7	3.2	284	54	0.6	201.2	13	4.5	7.5	17.7	113	0.55	19	24	33.1	37.07	20.20	10.49	9.25	18.80	6.00	1.16	0.51	0.11	75	53	11	30.3	58	5.2
KBN	137	6.5	423	64	2.7	276.7	20	4	8.8	20.7	170	0.54	21	15	34.3	34.70	17.40	8.90	7.54	21.37	7.03	1.33	0.62	0.15	87	51	5	33.7	64	9.2
KHL	106	9.7	433	142.6	10.2	321.3	44	5	14.8	19.2	207	0.65	16	28	80.7	27.20	21.03	11.18	9.39	17.37	7.73	1.53	0.64	0.14	88	50	15	37.7	47	10.8
KKL	106.7	5.3	302	95	1.8	190	15	3.5	6.4	16.8	117	0.53	20	16	49.7	22.50	15.27	3.96	3.08	14.90	5.60	0.88	0.66	0.22	114	43	15	39.3	53	7.0
LHD	90	9.5	360	92	2.2	269.7	24	4.8	16.7	20.2	163	0.69	13	17	45.8	33.60	17.93	8.79	6.68	22.73	7.97	2.01	0.68	0.23	119	61	15	44.7	80	8.2
MEL	80	5.8	292	71.6	1.7	211.7	25	4	5.9	21.7	157	0.55	21	24	40.6	45.23	23.97	18.48	17.09	23.07	7.30	1.70	0.51	0.09	117	56	15	34.0	44	5.5
MTN	80.3	9.5	367	119	1.6	277	20	4	11	17.3	125	0.64	18	16	45.1	32.70	19.43	11.94	10.69	17.47	6.90	1.10	0.53	0.09	115	41	16	42.0	47	8.2
ZIE	115.3	12.7	360	98.6	1.8	235	28	4	10.2	19.8	224	0.61	15	21	56.6	33.23	18.00	9.93	8.18	18.77	7.57	1.66	0.57	0.17	118	45	15	50.7	74	7.2

BRR : Bourar ; **MTN** : Mentouj tissgharine ; **BZG** : Bouezgagh ; **BST** : Black bousthammi; **KHL**: Khalt iaach; **LHD**: Khalt Lohmadi ; **ECT** : Elahmer chetoui ; **EED** : Elasfer eljaid ; **ZIE** : Khalt zoubir ibn laouam ; **HFL** : Hak feddan laaneb ; **IAS** : Khalt iaissi ; **EMS** : Elmensoum ; **IAH** : Khalt abdelghani ; **IKL** : Iklane ; **MEL** : Mentouj lhaj lehbib ; **KBN** : Khalt bheir ngli ; **KKL** : Khalt khel.

3.1. Principal component analysis

The differences in vegetative and reproductive parameters between genotypes were studied using PCA. The first component accounted 31.25 %, whereas the second and third components explained 50.28 % and 61.06 %, respectively (Table 5).

Table 5. Eigen values and levels of the variance associated with the three principal components.

Axe	1	2	3
Eigenvalues variance	9.37	5.71	3.23
Variance proportion			
Individual (%)	31.25	19.04	10.78
Cumulative (%)	31.25	50.28	61.06
Eigenvalues vectors[1]	P2 (0.269)	P6 (-0.242)	P8 (-0.265)
	P3 (0.245)	P16 (0.334)	P20 (0.279)
	P4 (0.242)	P17 (0.261)	P21 (0.316)
	P7 (0.295)	P18 (0.271)	P22 (0.402)
		P19 (0.286)	P23 (0.322)
		P24 (-0.271)	P26 (0.280)
		P30 (-0.265)	P28 (0.301)

[1] Only variable showing high weight was taken into account.

P2: Petiole width at the bottom; **P3**: Leaf length; **P4**: Leaf width; **P6**: Leafleted part length; **P7**: Spines number; **P8**: Spine width at the middle; **P16**: Fruit length; **P17**: Fruit width ; **P18**: Fruit weight ; **P19**: Pulp weight ; **P20**: Seed length; **P21**: Seed width; **P22**: Seed weight; **P23**: Seed/fruit length ratio; **P24**: Seed/fruit width ratio; **P26**: Spadice width at the middle; **P28**: Spadice length at the ramified part; **P30**: Spathe width.

Petiole width at the bottom, leaf length, leaf width, spines number and leaflets number had high positive weight in the first principal component. The attributes with high negative weight in the second component were leafleted part length, seed/fruit weight ratio, and spathe width. Positive weight was found in fruit length, fruit width, fruit weight, and pulp weight.

The most important variables influencing the third principal component were spine width in the middle, which had high negative weight, and seed length, seed width, seed weight, seed/fruit length ratio, spadice width in the middle, and spadice length at the ramified part, which had strong positive weight.

The cultivars are shown on the plot axes (1-2) and (1-3) in Figures 1 and 2, respectively. In the plot of axis (1 and 2), the first axis presents a significant contrast between Elasfer eljaid (EED) and Khalt khel (KKL); (EED) has the largest petiole width at the bottom of the leaf. The second axis shows the contrast between Mentouj lhaj lehbib (MEL), characterised by a large size fruit, and Khalt iaach (KHL), distinguished by a large rachis thickness, leafleted part length, leaflet length and spathe width (Fig. 1). In the plot of axis (1 and 3), the third axis contrasts clone Khalt lohmadi (LHD), which has large size seed, to Bouzegagh (BZG) and Bourar (BRR), which are characterised by long leafleted part, terminal leaflet, spine, and leaflet width at the middle.

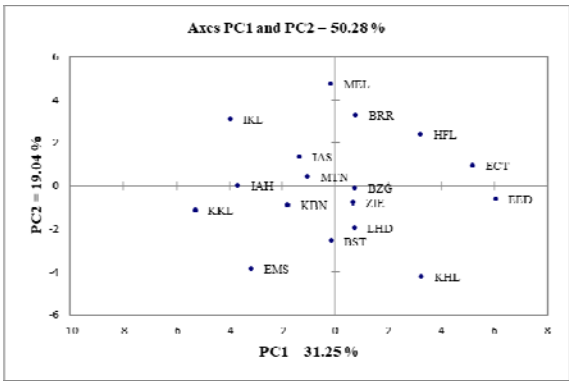

Figure 1. Representation of date palm accessions on the plan 1- 2 of PCA

BRR : Bourar ; **MTN** : Mentouj tissgharine ; **BZG** : Bouezgagh ; **BST** : Black bousthammi; **KHL**: Khalt iaach; **LHD**: Khalt Lohmadi ; **ECT** : Elahmer chetoui ; **EED** : Elasfer eljaid ; **ZIE** : Khalt zoubir ibn laouam ; **HFL** : Hak feddan laaneb ; **IAS** : Khalt iaissi ; **EMS** : Elmensoum ; **IAH** : Khalt abdelghani ; **IKL** : Iklane ; **MEL** : Mentouj lhaj lehbib ; **KBN** : Khalt bheir ngli ; **KKL** : Khalt khel.

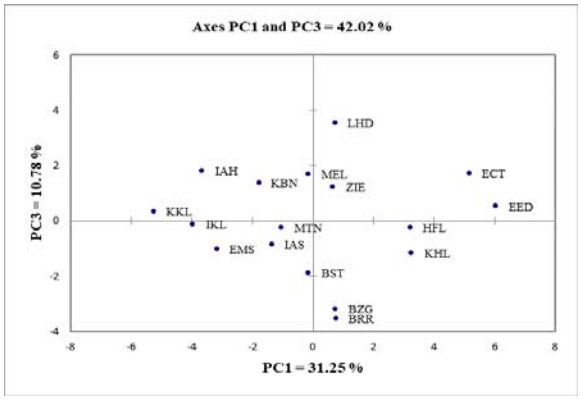

Figure 2. Representation of date palm accessions on the plan 1-3 of PCA.

BRR : Bourar ; **MTN** : Mentouj tissgharine ; **BZG** : Bouezgagh ; **BST** : Black bousthammi; **KHL**: Khalt iaach; **LHD**: Khalt Lohmadi ; **ECT** : Elahmer chetoui ; **EED** : Elasfer eljaid ; **ZIE** : Khalt zoubir ibn laouam ; **HFL** : Hak feddan laaneb ; **IAS** : Khalt iaissi ; **EMS** : Elmensoum ; **IAH** : Khalt abdelghani ; **IKL** : Iklane ; **MEL** : Mentouj lhaj lehbib ; **KBN** : Khalt bheir ngli ; **KKL** : Khalt khel.

3.2. Matrix correlation

Analysis of matrix interrelationships between the variables studied **(**Table 6**)** showed that leaf length (P3) was positively correlated to spined part length (P1) and petiole width at the bottom (P2). Leaf width (P4) was correlated to leaf length (P3) and petiole width at the bottom (P2). Leafleted part length (P6) was in correlation with leaf length (P3) and leaf width (P4).

High intercorrelations were observed between spines number (P7) and petiole width at the bottom (P2), leaf length (P3) and leaf width (P4). Spine width at the middle (P8), spines number (P7), leaf width (P4), leaf length (P3) and petiole width at the bottom (P2) were correlated with spine length at the middle (P9). High correlations were also noticed between leaflets number (P11) and petiole width at the bottom (P2), leaf length (P3) and spines number (P7). Leaflet width at the middle (P14) was correlated to spine width at the middle (P8). The correlation matrix also showed a significant intercorrelation between leaflet length at the middle (P15) and petiole width at the bottom (P2), leaf length (P3), leaf width (P4), rachis thickness between the last spine and the first leaflet (P5), spines number (P7), spine length at the middle (P9) and leaflets number (P11). Fruit width (P17) was correlated to fruit length (P16). A high correlation was observed between fruit weight (P18) and fruit sizes (P16, P17). Length, width and weight of fruit (P16, P17 and P18) were strongly correlated to pulp weight (P19). Seed length (P20) was correlated to fruit length (P16) and the weight of fruit and pulp (P18, P19). Seed weight (P22) was highly correlated to seed length and width (P20, P21).

Table 6 Coefficients of correlation between the studied characters in date palm accessions.

Variables	P1	P2	P3	P4	P5	P6	P7	P8	P9	P10	P11	P12	P13	P14	P15	P16	P17	P18	P19	P20	P21	P22	P23	P24	P25	P26	P27	P28	P29	P30
P1	**1**	0.4729	**0.6657**	0.2698	0.1441	0.0120	0.5191	0.1567	0.4169	0.1500	0.3705	0.2683	0.0889	0.4132	0.3230	0.2418	0.0219	0.2069	0.2020	0.4621	-0.1261	0.0358	0.1014	-0.2318	0.2211	0.4342	0.0356	0.3929	0.1507	-0.0441
P2		**1**	**0.6955**	**0.7626**	0.2590	0.5089	**0.7060**	0.4167	**0.6659**	0.1404	**0.7657**	0.2036	-0.4787	0.3311	**0.6330**	0.3391	0.2703	0.3975	0.3680	0.3712	0.2788	0.2909	-0.1409	-0.3180	0.3850	0.2564	0.3435	0.4091	**0.6040**	0.1675
P3			**1**	**0.6547**	0.5115	**0.7494**	**0.7075**	0.4202	**0.6810**	0.1552	**0.6841**	0.3655	-0.1825	0.4162	**0.6446**	0.0824	0.0966	0.2139	0.1798	0.3877	0.3339	0.2612	0.2366	-0.1680	0.0912	0.3837	-0.0366	0.3857	0.2333	0.5421
P4				**1**	0.5126	**0.6293**	**0.7630**	0.3834	**0.6583**	-0.0049	0.5411	0.2581	-0.5458	0.3103	**0.8729**	0.0239	0.2607	0.2873	0.2701	0.0551	0.1507	0.0744	0.0215	-0.2524	0.3906	0.1174	0.3608	0.4223	0.3647	0.4110
P5					**1**	0.5820	0.5912	0.2369	0.4055	-0.0024	0.5082	0.2251	-0.0910	0.3265	**0.6602**	-0.2260	0.1299	0.0091	-0.0161	-0.1108	0.3200	0.1379	0.2280	-0.0077	-0.2588	-0.0193	0.0075	-0.0823	-0.1339	0.5088
P6						**1**	0.5153	0.4138	0.5627	0.1388	0.5985	0.2593	-0.3180	0.1567	0.5822	-0.1106	0.0963	0.0955	0.0516	0.1330	0.5680	0.3502	0.2654	0.0067	-0.0489	0.1771	-0.0818	0.1612	0.1801	**0.7777**
P7							**1**	0.3752	**0.6367**	0.1433	**0.6936**	0.2752	-0.3653	0.4594	**0.7659**	0.3067	0.4876	0.5376	0.5047	0.4602	0.2929	0.3964	0.0517	-0.3217	0.3610	0.5067	0.3094	0.5292	0.3696	0.3121
P8								**1**	**0.6265**	0.0556	0.3983	-0.0897	-0.2389	**0.6615**	0.4078	0.2995	0.1213	0.1498	0.1432	0.2038	0.0484	0.0561	-0.2018	-0.1551	-0.3620	0.2157	0.2517	-0.0997	0.1886	0.0934
P9									**1**	0.2659	0.5396	0.4469	-0.4337	0.4250	**0.6590**	0.1481	0.0269	0.1305	0.1031	0.2316	0.0756	0.1476	0.0220	-0.1254	0.1121	0.3090	0.2280	0.1892	0.4036	0.3046
P10										**1**	0.2936	0.0360	0.3031	-0.0084	0.1460	0.1255	-0.1235	0.0795	0.0865	0.0869	-0.2134	-0.0386	-0.1074	-0.1469	0.1922	0.2908	0.0850	-0.0775	0.0019	0.2810
P11											**1**	0.2327	-0.2751	0.3906	**0.6850**	0.1403	0.1479	0.2330	0.1923	0.2603	0.4680	0.4289	0.0447	-0.0844	0.0859	0.2060	0.0383	0.2198	0.3812	0.3817
P12												**1**	0.0311	0.1531	0.3999	-0.3369	-0.1945	-0.1109	-0.1391	-0.0308	0.2767	0.1635	0.4119	0.1919	0.0973	0.0301	-0.4077	0.2222	-0.0798	0.2494
P13													**1**	0.1284	-0.3944	-0.0801	-0.1523	-0.0759	-0.0447	-0.1138	-0.1689	-0.2487	-0.0174	-0.0168	-0.3842	-0.0893	-0.2229	-0.2311	**-0.6984**	0.0645
P14														**1**	0.4321	0.3929	0.4103	0.4327	0.4290	0.3131	0.0737	0.1271	-0.2510	-0.3732	-0.2982	0.2949	0.3016	0.1419	-0.1373	0.0161
P15															**1**	-0.1727	0.0674	0.0884	0.0690	-0.0735	0.1341	0.0622	0.1735	-0.0753	0.1888	0.0967	0.1120	0.2511	0.2078	0.4294
P16																**1**	**0.7768**	**0.8617**	**0.8685**	**0.7192**	-0.0313	0.2538	**-0.6905**	**-0.7387**	0.2203	0.4684	0.5577	0.2114	0.3520	-0.3646
P17																	**1**	**0.9447**	**0.9372**	0.5938	0.2474	0.3989	-0.4895	**-0.6955**	0.2563	0.4133	0.5345	0.3620	0.1812	-0.1101
P18																		**1**	**0.9964**	**0.6909**	0.1807	0.3771	-0.5255	**-0.7663**	0.3867	0.4952	0.5423	0.4443	0.2176	-0.1018
P19																			**1**	**0.6514**	0.1091	0.3023	-0.5747	**-0.8024**	0.3759	0.4527	0.5460	0.4058	0.1968	-0.1354
P20																				**1**	0.4013	**0.7104**	-0.0056	-0.2789	0.3422	**0.8673**	0.2806	0.5368	0.3073	-0.0803
P21																					**1**	**0.8585**	0.4407	0.2952	-0.0203	0.2789	-0.1412	0.3149	0.0360	0.4146
P22																						**1**	0.3725	0.2165	0.2357	**0.6490**	0.1008	0.5012	0.2046	0.2185
P23																							**1**	**0.8154**	0.0509	0.2300	-0.4689	0.2545	-0.1673	0.4430
P24																								**1**	-0.1451	-0.0863	-0.4116	-0.0307	-0.1139	0.2556
P25																								-	**1**	0.3662	0.3688	**0.6737**	0.4458	-0.0092
P26																										**1**	0.2620	0.5775	0.2331	0.1043
P27																											**1**	0.3635	0.2031	-0.0603
P28																												**1**	0.3123	0.2836
P29																													**1**	-0.0768
P30																														**1**

Seed fruit/length ratio (P23) was negatively correlated to fruit length (P16) and correlated positively to seed/fruit weight (P24). A high negative intercorrelation was shown between seed/fruit weight ratio, fruit length and width (P16, P17) and fruit and pulp weight (P18, P19). Spadice width at the middle (P26) was correlated to spadice length at the ramified part (P28). Spathe length (P29) was positively correlated to the petiole width at the bottom (P2) and correlated negatively to the terminal leaflet width (P13). A high correlation was also found between spathe width (P30) and leafleted part length (P6).

3.3. Cluster analysis

UPGMA produced a dendogram with five phenotypic groups identified among the 17 date palm accessions (Figure 3). The level of dissimilarity ranged from 0.37 to 0.92. The BRR, MTN, LHD, and IAH cultivars were part of the first cluster. BRR and MTN originated from Tissgharine whereas LHD and IAH originated from Jenan lohmadi and Bheir ingli, respectively. The second group included six cultivars that can be divided into two subgroups: KBN and KHL from Bheir ingli; and BZG, BST and KHL from Jenan lohmadi and EMS from Way hamama. The third cluster included four cultivars: ECT and EED from Aghlal lekhyat mehdia, HFL from Fedan laaneb tansita, and KKL originating from Sefsafa. EED and KKL were closely related to the lowest registered dissimilarity level (d = 0.37). The fourth group included two cultivars: ZIE originating from Fedan laaneb tansita and MEL belonging to Bheir ingli. The single cultivar IAS from Way hamama represented the last cluster.

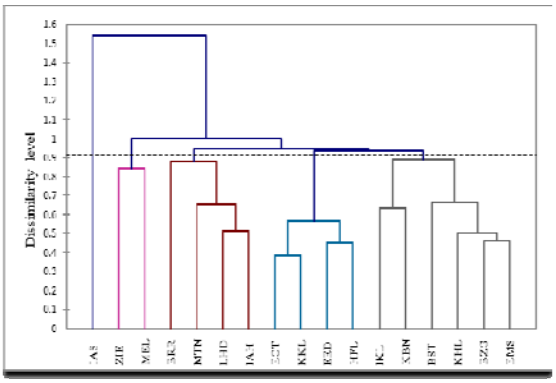

Figure 3 Cluster dendogram of Moroccan date palm accessions.

BRR : Bourar ; **MTN** : Mentouj tissgharine ; **BZG** : Bouezgagh ; **BST** : Black bousthammi; **KHL**: Khalt iaach; **LHD**: Khalt Lohmadi ; **ECT** : Elahmer chetoui ; **EED** : Elasfer eljaid ; **ZIE** : Khalt zoubir ibn laouam ; **HFL** : Hak feddan laaneb ; **IAS** : Khalt iaissi ; **EMS** : Elmensoum ; **IAH** : Khalt abdelghani ; **IKL** : Iklane ; **MEL** : Mentouj lhaj lehbib ; **KBN** : Khalt bheir ngli ; **KKL** : Khalt khel.

4. Discussion

The aim of this work was the investigation of the phenotypic diversity in reproductive and vegetative traits in 17 Moroccan date palm accessions growing in the Zagora palm grove. The date palm trees' quantitative markers have been used as morphological features to detect similarities and differences between date palm cultivars growing in different countries, e.g. Tunisia, Algeria, Morocco and Mauritania (Rhouma, 1994; Elhoumaizi *et al.,* 2002; Mohamed Ahmed *et al.,* 2011). In addition, traits related to the reproductive system were assessed. Our results are similar to Mohamed Ahmed *et al.* (2011), who studied 30 parameters associated with the plant's vegetative and reproductive systems to find a high degree of polymorphism in 23 Mauritanian date cultivars, and Elhoumaizi *et al.* (2002), who found a significant degree of polymorphism in twenty-six Moroccan date cultivars from the Figuig oasis, based on the date palm's vegetative system.

PCA showed that traits related to leaf (petiole width at the bottom, leaf length, leafleted part length), spines number, leaflets number, spathe width and fruit sizes and weight accounted for a high proportion of variability. A high correlation was observed between some characters (leaf length and leafleted part length and between leaf width and leaflet length at the middle) based on Pearson's coefficient correlation, showing that the tree is architecturally arranged, as reported by Mohamed Ahmed *et al.* (2011).

Cluster analysis revealed that the date palm germplasm studied is characterized by a continuous phenotypic diversity. This result is confirmed by the obtained topology of the dendogram and is due to the extensive transfer of plant material between different growing areas. As a consequence, geographical origin was not a determining criterion for the classification of cultivars. Similar findings were reported by Elhoumaizi *et al.* (2002).

Furthermore, the UPGMA dendogram revealed similarities between cultivars based on fruit characteristics such as half dry date in LHD and IAH, dry date in BZG and EMS, and soft date in EED and HFL. Similarities between cultivars based on fruit characteristics were noted in LHD and IAH characterised by semi-dry date, BZG and EMS with a dry date, EED and HFL exhibiting a soft date.

5. Conclusions

The present data showed that characters associated with the date palm's vegetative and reproductive organs were good discriminating traits to analyse the phenotypic diversity in date palms. The traits related to leaf length and width, spine, fruit sizes had the best differentiating value. Five clusters were obtained by a dendrogram classification and showed typical continuous phenotypic variations that differentiate the date palm varieties and clones. There was a significant phenotypic variability among date palm accessions in this research. Biochemical and molecular indicators should be investigated in order to accurately describe the phenotypic and genetic diversity of Moroccan date palm germplasm.

Acknowledgements

The authors are thankful to the president of Ennakhil Cooperative (Mohamed ELmadani) for providing infrastructures and facilities in Zagora, and the *National Center for Scientific and Technical Research* (CNRST) in Rabat for its financial support. Thanks must be given to all staff of Ennakhil Cooperative.

Data Availability

The data used to support the findings of this study are included within the article.

Conflict of Interest

The authors declared no conflict of interest.

References

Awad MA. 2006. Water spray as a potential thinning agent for date palm flowers (*Phoenix dactylifera* L.) c.v. 'Lulu'. *Sci Hortic.*, **111(1):** 44-48.

Botes A and Zaid A. 2002. The economic importance of date production and international trade. *In* "Date palm cultivation" (A. Zaid, ed.). Food and Agricultural Organisation of the United Nations Rome.

Bouabidi HMR and Rouissi M. 1996. Critères de caractérisation des fruits de quelques cultivars de palmiers dattiers (*Phoenix dactylifera* L.) du sud tunisien. *Ann. l'Institut Natl. la Rech. Agron.*, **96**: 73-87.

Brake MH, Al-Gharaibeh MA, Hamasha HR, Sakarneh NSA, Alshomali IA, Migdadi HM and Haddad NJ. 2021. Assessment of genetic variability among Jordanian tomato landrace using inter-simple sequence repeats markers. *Jordan J Biol Sci.,* **14**(1).

Djerbi M, Saaidi M and Sedra MH. 1986. A new Fusarium wilt (Bayoud like disease) on Canary Islands palm *Phoenix canariensis* in Morocco, in: The Second Symposium on Date Palm, Saudi Arabia, Al-Hassa, pp. 375-380.

Ehsine M, Belkadhi MS and Chaieb M. 2014. Seasonal and Nocturnal Activities of the *Rhinoceros Borer* (Coleoptera: Scarabaeidae) in the North Saharan Oases Ecosystems. *J Insect Sci.,* **14**: 1-5.

Elhoumaizi MA, Saaidi M, Oihabi A and Cilas C. 2002. Phenotypic diversity of date-palm cultivars (*Phoenix dactylifera* L.) from Morocco. Genet. Resour. *Crop Evol*., **49:** 483-490.

Elhoumaizi MA, Devanand PS, Fang J and Chao CCT. 2006. Confirmation of Medjool date as a landrace variety through genetic analysis of medjool accessions in Morocco. *J Am Soc Hortic Sci.,* **131:** 403-407.

Elsafy M, Gustavsson L and Mujaju C. 2015. Phenotypic diversity of date palm cultivars (*Phoenix dactylifera* L.) from Sudan estimated by vegetative and fruit characteristics. *Biodivers Int J.*, ID 610391.

Elshibli S and Korpelainen H. 2009. Biodiversity of date palms (*Phoenix dactylifera* L.) in Sudan: chemical, morphological and DNA polymorphisms of selected cultivars. *Plant Genet Resour.,* **7**: 194-203.

Ennouri K, Ayed RB, Ercisli S, Smaoui S, Gouiaa M and Triki MA. 2018. Variability assessment in *Phoenix dactylifera* L. accessions based on morphological parameters and analytical methods. *Acta Physiol Plant.*, **40**(1): 5.

FAOSTAT. 2012. **Agros-statistics**, Database. Food & Agri. Organiz. United Nations, Rome.

INRA (The National Institute of Agronomic Research). 2011. Atlas of date palm in Morocco. Rabat, Morocco.

IPGRI (Institut international des ressources phytogénétiques). 2005. **Descripteur du palmier dattier** (*Phoenix dactylifera* L.), IPGRI. ed. Rome, Italy.

Jain SM and Johnson DV. 2015. **Date palm genetic resources and utilization** (Vol. 1). J. M. Al-Khayri (Ed.). Africa and the Americas: Springer.

Mainley BFJ. 1994. **Multivariate Statistical Methods: A Primer**. Chapman Hall London Press.

Mason SC. 1915. Botanical characters of the leaves of date palm used in distinguishing cultivated varieties. United states Dep. *Agric. Bull.* 223.

Mohamed Ahmed MVO, Bouna ZEO, Mohamed Lemine FM, Djeh TKO, Mokhtar T and Mohamed Salem AO. 2011. Use of multivariate analysis to assess phenotypic diversity of date palm (*Phoenix dactylifera* L.) cultivars. *Sci Hortic.,* **127**: 367-371.

Meddich A, Oihabi A, Jaiti F, Bourzik W and Hafidi M. 2015. Role of arbuscular mycorrhizal fungi on vascular wilt and drought tolerance in date palm (*Phoenix dactylifera L.*). *Can J Bot.,* **93**: 369-377.

Munier P. 1973. **Le palmier-dattier. Techniques agricoles et productions tropicales**. Maisonneuve Larose, Paris, France.

Nixon R. 1950. Imported varieties of date palm in the United States. United states Dep. Agric. Bull. 834.

Rabei S, Said W, Rizk R and El Sharab S. 2012. Morphometric taxonomy of date palm diversity growing in Egypt. *Egypt J Bot.*, 175-189.

Reynes M and Bouabidi PG. 1994. Caractérisation des principales variétés de dattes cultivées dans la région du Djérid en Tunisie. *Fruits*., **49:** 189-198.

Rhouma A. 1994. Le Palmier Dattier en Tunisie: Le Patrimoine Génétique, vol. I., INRAT, Ara. ed. Tunis, Tunisie.

Saaidi M. 1992. Comportement au champ de 32 cultivars de palmier dattier vis-à vis du bayoud 25 années d'observations. *Agronomie.,* **12:** 359-370.

Saddoud O, Baraket G, Chatti K, Trifi M, Marrakchi M, Salhi-Hannachi A and Mars M. 2008. Morphological variability of fig (*Ficus carica* L.) cultivars. *Int J Fruit Sci.,* **8**: 35-51. https://doi.org/10.1080/15538360802365921

Salem AOM, Rhouma S, Zehdi S, Marrakkchi M and Trifi M. 2008. Morphological variability of Mauritanian date-palm (*Phoenix dactylifera* L.) cultivars as revealed by vegetative traits. *Acta Bot Croat*., **67:** 81-90.

Sedra MH, Lashermes P, Trouslot P, Combes MC and Hamon S. 1998. Identification and genetic diversity analysis of date palm (*Phoenix dactylifera* L.) varieties from Morocco using RAPD markers. *Euphytica.,* **103:** 75-82.

Sedra MH. 2015. Date palm status and perspective in Morocco. In Date palm genetic resources and utilization, Springer, Dordrecht, pp. 257-323.

Zehdi-Azouzi S, Cherif E, Moussouni S, Gros-Balthazard M, Abbas Naqvi S, Ludeña B and Si-Dehbi F. 2015. Genetic structure of the date palm (*Phoenix dactylifera*) in the Old World reveals a strong differentiation between eastern and western populations. *Ann Bot.*, **116:** 101-112.

JJBS

Volume 15, Number 4,December 2022
ISSN 1995-6673
Pages 679 – 687
https://doi.org/10.54319/jjbs/150417

Jordan Journal of Biological Sciences

Optimisation of Total Phenolic Compound Extraction and Antioxidant Activity from Dried Inflorescence of *Ammi Visnaga* Using Mixture Design and Triangular Surfaces

Zineb El Jabboury [1,2]; Smail Aazza [2], Driss Ousaaid [3,*], Oumaima Chater[1], Wafae Squalli [1], Ouafae El Ghadraoui [4] , Meryem Benjelloun[1], Lahsen El Ghadraoui [1]

[1]*Laboratory of Functional Ecology and Environmental Engineering, Faculty of Sciences and Technology, University of Sidi Mohamed Ben Abdellah, Fez, Morocco;* [2]*Laboratory of Phytochemistry, National Agency of Medicinal and Aromatic Plants (NAMAP/ANPMA)-Taounate, Morocco.;* [3]*Laboratory of Natural substances, Pharmacology Environment, Modeling, Health and quality of life. Faculty of Sciences Dhar El Mahraz, University Sidi Mohamed Ben Abdellah, Fez, Morocco.;* [4]*Department of Chemistry, Laboratory of Applied Organic Chemistry, Faculty of Science and Technology, University of Sidi Mohamed Ben Abdellah - Fez, Morocco.*

Received: December 26, 2021; Revised: March 22, 2022; Accepted: April 4, 2022

Abstract

Ammi visnaga L. (Apiaceae) is a medicinal plant widely distributed in the Mediterranean area. In Morocco, the umbel is traditionally prescribed for mouth care, toothache, and diabetes. This study was designed to examine the affinity of different solvents towards total phenolic compounds (TPC) from the dried umbels of *Ammi visnaga.* Mixture Design Response Surface Methodology was performed to maximize phenolic compounds and antioxidant activity using the selected solvents from the first step. Plant extracts were prepared using the optimized solvent mixtures. Ternary mixture with 66.67% acetone, 16.67% water, and 16.67% methanol was the most proper mixture to obtain high TPC (29.62 ± 0.60 mg EGA/g dw). Pure methanol was appropriate for TAC followed by binary mixture of 50% water and 50% acetone and ternary mixture with equal proportion of three studied solvents. Special cubic model explained the variance of the total phenolic content, and the antioxidant activity of our extracts at levels of R^2 are greater than 95%. In general, the total phenolic content and the antioxidant activity of our extracts increased with the increasing amount of water in the methanol or acetone solvent mixture. The extraction ability of phenolic compounds was also influenced positively and significantly by the water content.

Keywords: *Ammi visnaga L.*, Phenolic content, Antioxidant activity, Optimization, Extraction.

1. Introduction

Ammi visnaga L. is a widespread herb in the basin of the Mediterranean Sea, Nile Valley, West of Africa, Europe, and Asia (Khalil et al., 2020). This species belongs to the Umbellifereae family; it contains a wide range of bioactive substances. In Moroccan traditional medicine, *Ammi visnaga L* is empirically practiced to treat numerous ailments (Jouad et al., 2002). Herb presents different pharmacological effects including antihyperglycemic effect, antispasmodic effect, antiheadache, antinephritic colic, and used widely for dental hygiene (Bellakhdar et al., 1991; Ziyyat et al., 1997).

The bioactive ingredients possessed high antioxidant potential that makes them suitable for maintaining different physiological functions (Laaroussi et al., 2020; Ousaaid et al., 2020; Pejin et al., 2013). The extraction yield is profoundly associated with numerous factors such as pedoclimatic conditions, maturity of fruits, variety, extraction process, and polarity of extractor solvent.

The efficacy of the extraction method and suitability of extractor solvents affect the composition of the obtained extract, which impacts its biological properties. A successful extraction technique makes a mixture of solvents with suitable proportions. To select an extraction method, it is necessary to assess the accuracy, the stability of the extracted substances, the availability of resources, and processing costs leading towards a biological application of the extract (Oliveira et al., 2001). Within this frame, numerous techniques are coming in the forefront to reduce the amount of waste solvents and benchwork developing inventory tools including optimization studies (Cavalcanti et al., 2021). Optimized extraction constitutes a good tool to study the effect of one variable, especially solvent, on the recovered bioactive compounds and antioxidant ability (Aazza, 2021). Response surface methodology (RSM) is an accurate instrument for improving the extraction procedure (Saravana Pandian et al., 2022). In addition, it is a promoting technique for elaborating, enhancing, and optimising procedures. It can evaluate the effect of different variables, factors, and their interactions (Farris and Piergiovanni, 2009). The experimental combination design has been largely used in a variety of fields, including the development of new biofilms and for the extraction of secondary metabolites from natural products

* Corresponding author. e-mail: driss.ousaaid@usmba.ac.ma.

(Munhoz et al., 2014). The main aim of the experimental methodology is to assess how the responses are influenced by the fluctuation in the proportions of the mixture components.

Ammi visnaga L. is considered as a member of Apiaceae family. It is well known for its numerous therapeutic properties due to its high amount of biological active compounds (Kamal et al., 2022). Phytochemical analysis of *Ammi visnaga* extract using HPLC revealed the presence of numerous phenolic compounds including coumarin, apignin, kaempferol, caffeic acid, rutin, quercetin, visnagin and ferulic acid (Al-Zaidi and Khorsheed, 2021). In the same context, Ahmed et al. (2021) listed different bioactive compounds of *Ammi visnaga* such as flavonoids, coumarins and furocoumarins, isobensofurans, sesquiterpenes, phthalides, and miscellaneous. These molecules possess different pharmacological activities including antibacterial, anticancer, antidiabetic, and antihyperlipidemic activities (Afzal et al., 2021; Ahmed et al., 2021).

The current work was designed to screen the ability of the solvent to extract phenolic compounds from *Ammi visnaga* inflorescence. Secondly, we used statistical mixture design beside a simplex centroid model with acetone, methanol, and water as extractor solvents, in order to boost the extraction of the compounds and increase the phenolic activity and other antioxidant composites.

2. Material and methods

2.1. Chemicals and standards

Folin–Ciocalteu reagent, sodium carbonate (Na_2CO_3), sulphuric acid, sodium phosphate, ammonium molybdate, acetone, methanol, ethyl acetate, chloroform, dichloromethane, toluene, hexane, petroleum ether, gallic acid, and ascorbic acid were purchased from Sigme Aldriche.

2.2. Extraction procedure and sample preparation

The extractions were carried out in triplicate conferring to the following formula: 50 mg of dried and pulverized inflorescence of *Ammi visnaga* was extracted for 20 minutes by sonication with 1 mL of solvents mixture. The extracts were centrifuged for 15 minutes at 6000 rpm, and the supernatants were recuperated and stored at 4ºC (Ousaaid et al., 2020b).

2.3. Total phenolic content (TPC)

The TPC was quantified using the Folin–Ciocalteu method as previously described by (Lamuela-ravents, 1999). In brief, 50 µL of extract was mixed with 450 µL of Folin–Ciocalteu reagent (0.2 N), after 5 minutes, 450 µL of a Na_2CO_3 solution (75 g L^{-1}) was added to the mixture. All samples were incubated in the dark environment for 2 hours, and their absorbance was read at 760 nm in a Jenway 6505 UV/visible, scanning spectrophotometer. The concentration of the calibration curve (y = 1,6021x + 0,0683, R^2 = 0,997) ranged from 0.008 to 1 mg/mL of gallic acid. The experiment was prepared in triplicates, and the results are expressed as mg equivalent of gallic acid (mg EGA/g) of dried plant.

2.4. Total antioxidant capacity (TAC)

The total antioxidant capacity (TAC) of all samples was determined using the phosphomolybdenum method according to (Prieto et al., 1999). An aliquot of 25 µL of the sample solution was mixed principally with 1 mL of reagent solution (0.6M sulphuric acid, 28mM sodium phosphate, and 4mM ammonium molybdate) in a falcon of 15 mL. The falcon tubes were covered and incubated in a water bath at 95°C temperature for 90 minutes. Then, the absorbance of the mixture was measured at 695 nm, against a blank, in a Jenway 6505 UV/visible, scanning spectrophotometer. Calibration curve was prepared using aqueous ascorbic acid solution with doses varying between 5,0 to 0,0039 mg/mL (y = 0,7889x + 0,0492, R^2 = 0,996). The results are expressed as g of equivalent ascorbic acid (g EAA/g) of dried plant.

2.5. Evaluation of solvent impact by simplex axial design

Two dissimilar categories of standard designs are usually used for extraction experimentations with combinations: (i) simplex-centroid design, and (ii) simplex-lattice design. Both designs will assess the triangular reply surface at the vertices (i.e., the corners of the triangle) and then the centroids (sides of the triangle) (Montgomery, 2012).

In the simplex-centroid design, different conditions tested form a triangle, with pure components in the vertex, representing 100% of each single solvent. Central points on every side expressing permutations of the binary blends (1/2: 1/2: 0; 1/2: 0: 1/2; 0: 1/2: 1/2) and the medium point as a ternary mixture (1: 1: 1). This scheme is from time to time increased with internal points (axial ones) expressing 2/3 of one of the targeted solvents and 1/6 for the others (Figure1), also known as a Simplex Axial Design (SAD)

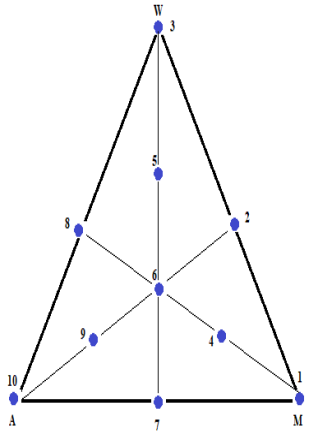

	Acetone	Water	Methanol
1	0,00	0,00	100,00
2	0,00	50,00	50,00
3	0,00	100,00	0,00
4	16,67	16,67	66,67
5	16,67	66,67	16,67
6	33,33	33,33	33,33
7	50,00	0,00	50,00
8	50,00	50,00	0,00
9	66,67	16,67	16,67
10	100,00	0,00	0,00

(Sampaio et al., 2015).

Figure 1. Simplex axial design (SAD).

To boost the extraction procedure, a mixture design was developed as presented in Figure 1. The simplex-centroid design coupled with axial points in three replicates was chosen to determine the solvent combination of water (W), methanol (M), and acetone (A) on the basis of preliminary results obtained using different solvents as presented in Table 1.

Figure 1 presents all tested conditions. This design permitted the evaluation of linear (W, E and A), quadratic (WE, WA, and EA), and special cubic (WEA) models for the response under study.

2.6. Statistical analysis

All the experiments for selection of the solvent proportion, as well as total phenolic content and total antioxidant capacity were performed in triplicate, and the results were reported as mean ± standard deviation.

Variance analysis (ANOVA) was applied to determine the fittest of the multiple regression model (p <0.05) to evaluate the significant effects of the variables and their interactions. From the regression coefficients, the response and contour surface graphs of the model were generated. The analyses were executed via the free version of STATISTICA version 10 software (StatSoft, 2011).

3. Results and discussions

3.1. Total phenolic compounds (TPC)

Different solvents of different polarities ranging from (0.1 to 10,2) have been screened for their ability to extract a high amount of TPC, and the obtained results are presented in Table 1 and Figure 2. The analysis of data revealed that the water, methanol, acetone are the suitable extractor solvents to recover the high amounts of TPC, while the lowest values were registered in petroleum ether and hexane extracts (Table 1). Our findings are in agreement with those reported by (Aourabi et al., 2019). It has been proved that the mixture of different solvents with different polarities is an effective procedure to extract the high amounts of bioactive compounds (Aazza, 2021; Aourabi et al., 2019; Saravana Pandian et al., 2022).

Table 1 .polarity index

Solvant	Polarity Index (P·)	TPC mg acid galic eq./g dry plant
Petroleum ether	0.1	0,01±0,01
Hexane	0.1	0,47±0,14
Toluene	2.4	3,80±0,58
Dichloromethan	3.1	8,10±0,37
Chloroform	4.1	10,05±0,24
Ethanol	4. 3	18,90±1,50
Ethyl Acetate	4.4	8,91±0,00
Methanol	5.1	27,06±2,37
Acetone	5.1	24,55±0,63
Water	10.2	20,74±0,64

Subtitle: W = Water, M = Methanol, A = Acetone.

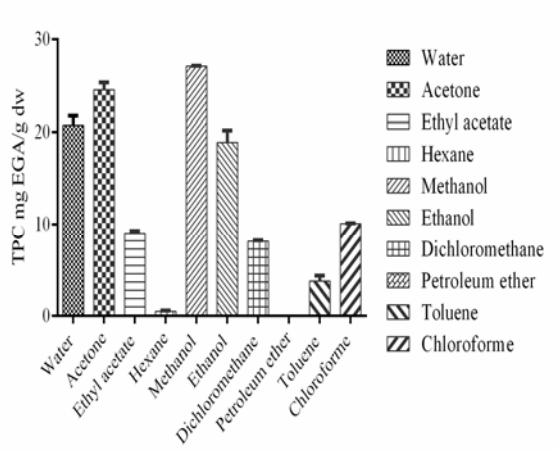

Figure 2: Total phenolic compounds based on different solvents used

3.2. Mixture design optimization of the Extraction Process

Dissimilar levels of water, methanol, and acetone have been usually used to extract phenolic content, essentially from medicinal herbs (Wang et al., 2008). In this work, we have identified the optimal values of the water, methanol, and acetone considered as independent variables, to attain the extreme response for the extraction of total phenolic content from dried inflorescence of *Ammi visnaga*. The recapture of phenolic mixtures is founded on the polarity of the solvent applied; thus, we choose methanol, water, and acetone as the most appropriate mixture which recovered the highest amount of TPC in this experiment.

The response surfaces obtained for TPC using mixture design as a function of the percentage composition of water, methanol, and acetone are illustrated in Figure 3A and contour plots are illustrated in Figure 3B.

Figure 3 A and B showed that the pure acetone has low extractor power and presented the lowest amounts of total phenolic content, followed by pure methanol, while the highest phenolic content was established in water extract.

The amount of extracted phenolic compounds is proportional to the water concentration in the solvent mixture using either both methanol and acetone. The same results have been reported by (Santos Felix et al., 2018) for *Spondias mombin* L. apple bagasse agroindustrial residues, where the lowest contents of phenolic compounds were obtained using 100% acetone, 100% alcohol or mixture of two extractor solvent (acetone (50%) and ethanol (50%), while the highest amounts were obtained only with water or mixture of three studied solvents (water, methanol, and acetone). Maximum total phenols contents can be expected from mixtures mostly rich in water. This shows that the extraction yield is highly related to the polarity of the extractor solvent. Our finding are in accordance with those reported by Rajha et al., (2014).

The highest values on the contour graph (Figure 3B) occurred between the following positions: water (100%), water/ acetone (1/2: 1/2) and water (100%), and water/methanol (1/2: 1/2). The proportions were optimized according to the response surface were (Water 70%), methanol (%5) and acetone (25%) as being the maximum inside the experimental domain, yielding maximum predicted amount of TPC (29,9197 mg EGA/g dry plant).

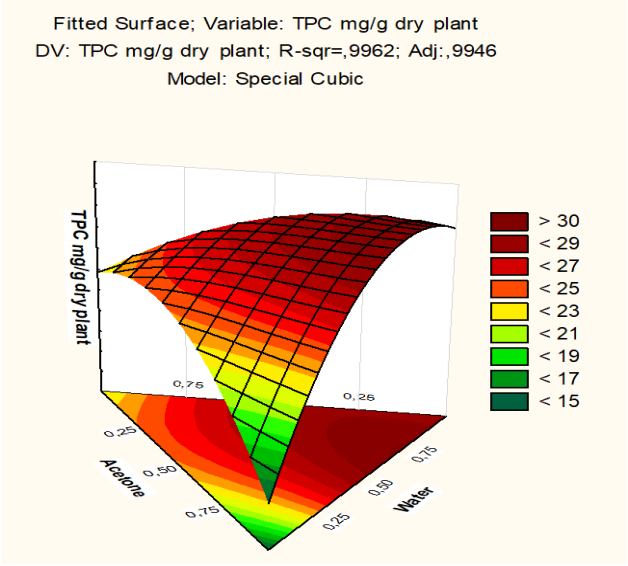

Figure 3A : Response surface contour plot of the special cubic model predicted TPC as a function of the acetone, water and methanol proportions(3D).

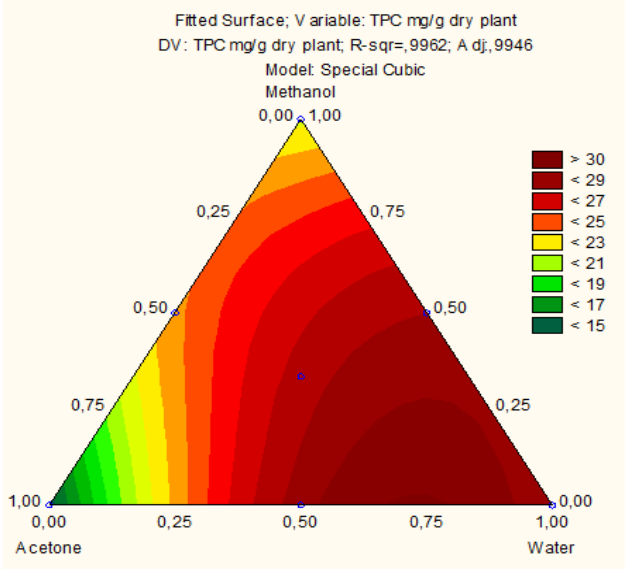

Figure 3B : Response surface plot of the special cubic model predicted TPC as a function of the acetone, water and methanol proportions(2D).

3.3. Analysis of variance (ANOVA)

In order to investigate the fitness and significance of the model, the analysis of variance (ANOVA) was performed. This analysis also shows the effects of individual parameters and interaction of variables of the mixture on response parameters as presented in Table 2.

The F-value compares the dissimilarity of the variances in the average responses at the design points and the equivalent assessed responses using the linear model (linear regression) with the predicted experimental variation as assessed from replicated design points (pure error). The model F-value of 349.14 implies that the selected model is statistically important (Table 3).

Table 2 :simplex axial design and results for mixture tested of TPC and TAC

	Acetone	Water	Methanol	TPC mg/g dry plant	TAC mg/g dry plant
1	0,00	0,00	100,00	21,69±0,26	168,09±1,23
2	0,00	50,00	50,00	27,99±0,31	94,18±1,56
3	0,00	100,00	0,00	28,01±0,13	69,87±1,16
4	16,67	16,67	66,67	21,68±0,31	111,10±1,93
5	16,67	66,67	16,67	11,59±0,00	83,76±1,31
6	33,33	33,33	33,33	27,43±0,25	130,69±1,89
7	50,00	0,00	50,00	23,71±0,75	78,26±1,09
8	50,00	50,00	0,00	28,57±0,10	142,72±2,00
9	66,67	16,67	16,67	29,62±0,60	153,43±1,30
10	100,00	0,00	0,00	14,44±0,29	45,57±1,94
All Runs				23,47±6,02	168,09±1,23

Table 3 . Analysis of variance (ANOVA) results for the mixture models

	SS	DF	MS	F	P
Model	476,04	5	95,20	349,14	0,00
Total Error	4,0904	15	0,27		
Lack of Fit	2,2870	1	2,28	17,75	0,000867
Pure error	1,8034	14	0,12		
Total adjusted	480,13	20	24,00		

The p-value (or Prob> F) is the likelihood of attaining the F-value. A value less than 0.05 designates that there is a statistically significant dissimilarity among the calculated means. A value larger than 0.10 defines that there is no dissimilarity among the calculated means, whereas the p-value (or Prob> F) is the probability of achieving the F-value. A value less than 0.05 specifies that there is a statistically significant dissimilarity among the means. A value superior than 0.10 designates that there is no difference between the calculated means (Sahu et al., 2009). Hence, in our study, the overall model p-value (probability of error value) being less than 0.0001 toughly confirms that the model is very significant.

The linear model explained that the variance in TPC content at the level of R^2 with a frequency of 62,02% and 57,87% for R^2adj. whereas, the quadratic and special cubic model explained better the variance in TPC content at the level of R^2 with an of ($R^{2:}$ 99, 15 %; R^2 Adj: 98, 86%) and ($R^{2:}$ 99,62 % 15; R^2 Adj: 99, 46%) respectively, indicating better how well fit of the model previously analysed is. Thus, the quadratic and cubic models were better in predicting the behaviour of the mixture.

The cubic model is given by the equation correlating the three variables. Hence, the analytical response is:

TPC = + 17,08 * acetone + 24,11 * water + 21,56 * methanol + 26,85 * acetone * water + 4,50 * acetone * methanol + 27,59 * water * methanol - 113,28 * acetone * water * methanol + 0,

To analyse the validity of the regression model, a raw residue analysis was performed.

A normal distribution was observed by comparing raw residue results to the expected normal values Figure 4.

The statistical analysis was carried out with the experimental values. The analysis of the main effects and their interactions in the form of analysis of variance (ANOVA) are presented in (Table 2) at the 95% confidence level ($p < 0.05$). Although the lack of fit was significant ($p < 0.05$) for the total content of polyphenols in the three extraction times, the cubic model was adjusted with significant probability ($p < 0.05$).

In order to examine the relative importance of the main effects and their interactions with statistical significance ($p < 0.05$), a standardized Pareto chart was employed (Figure 5). The main factors of different mixtures which extend beyond the reference line were significant at the level of 0.05.

Water (B) represented the most significant effect on phenolic compounds extraction followed by methanol (C) and acetone (A), and finally by the binary interaction of pure acetone with both methanol and water. Thus, the application of the mixture design was effective to establish the best proportion among the solvents for the extraction of phenolic compounds.

The desirability profile for TPC was generated with the values of 12.123 mg EGA/g – low (0.00); 21,404 mg EGA /g – intermediate (0.05); and 28.685 mg EGA /g – high (1.00). A graphic representation of the predicted values and desirability profile are shown in Figure 6. A predicted composition of the EO reference mixture and experimental data is presented in Table 4.

Table 4 .Approximate and experimentally determined percentage of inhibition (n = 8) for values obtained from desirability profile evaluation.

Data	Values measured experimentally			TPC	TAC
	Acetone	Water	Methanol		
Predicted values	33.33	33.33	33.33	27,43	130.69
Values measured experimentally				48.68	108.84

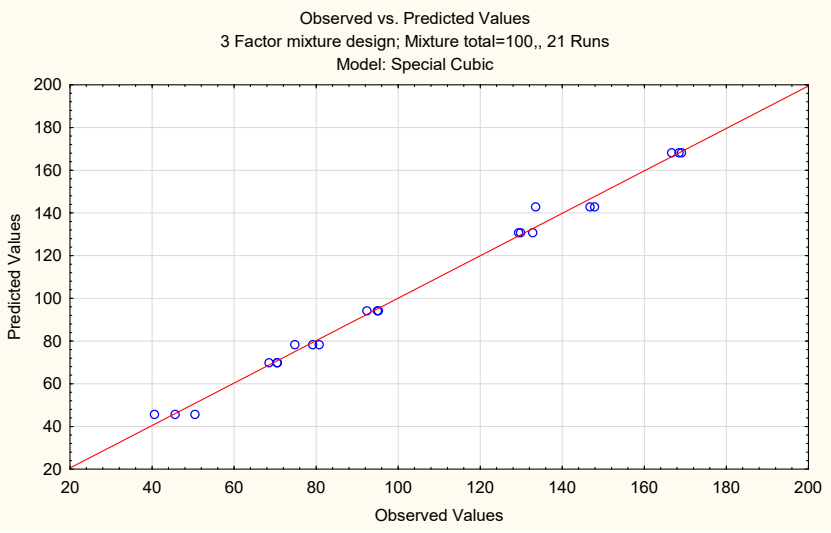

Figure 4: Predicted values (from the model) versus actual values (from experiments).

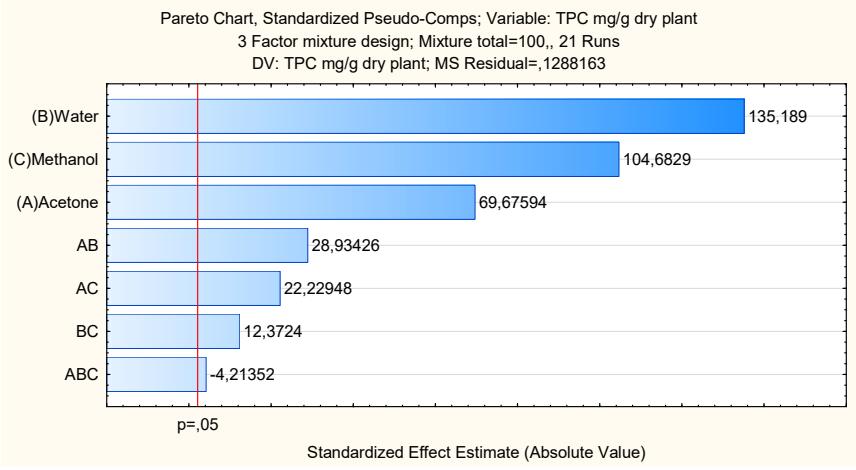

Figure 5: standardized Pareto's chart analysis of standardized effect for TPC

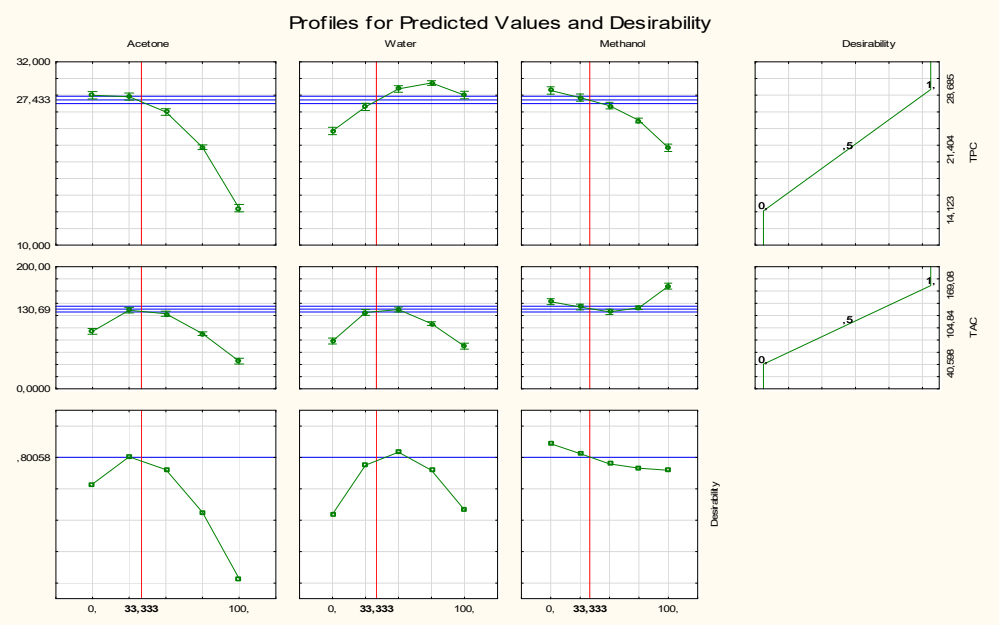

Figure 6: Desirability profile for optimization of references mixture of solvents

3.4. Total Antioxidant capacity (TAC):

Recently, the natural substances with high antioxidant ability have had a paramount importance due to their pharmacological properties (Laaroussi et al., 2020). Natural products constitute a dense source of antioxidants and are well-known for their efficacy and safety with regard to chemicals (Baj et al., 2018). Hence, the main objective of the current study was to examine the efficacy of the simplex-centroid mixture design method for the design of the most suitable extractor solvents mixture to recover high amounts of bioactive compounds with potent antioxidant properties.

Assays to measure TAC can be direct, which are founded on the capability to prevent the oxidation of a substance. On the foundation of the chemical reactions convoluted, TAC assays can also be separated into two classifications: hydrogen atom transfer (HAT) based procedures or on single electron transfer (SET) based approaches (Apak et al., 2016). The HAT-based techniques measure the aptitude of an antioxidant to quench free radicals by hydrogen contribution (Rubio et al., 2016). Response surfaces were identified for antioxidant activity as a meaning of the extraction solvent configurations. The linear, special cubic and quadratic models were experienced.

The highest antioxidant capacity values on the surface response and the contour graph are seen to occur with methanol or with equivalent proportions of water and acetone (Figure 7). The Highest antioxidant activity was achieved using the pure methanol and followed by a mixture of the studied extractor solvents (66.67/16.67/16.67). In contrary, the both solvents, water and acetone, were achieved the lowest antioxidant activity. This capacity reaches its maximum mixing the equal proportions of both solvents. The obtained results are in concordance with those reported by (Ribeiro et al., 2013). Statistical analysis indicated that the phenolic compounds are considered as the main contributors to antioxidant ability (Ousaaid et al., 2020c). The obtained results revealed that the extracts preformed using ternary solvent mixture with equal proportion and those with high proportion of methanol present high content of TPC. The combination of water and acetone exert their extraction effect synergistically, but the introduction of methanol to the mixture increases the extractable ability of the optimized procedure.

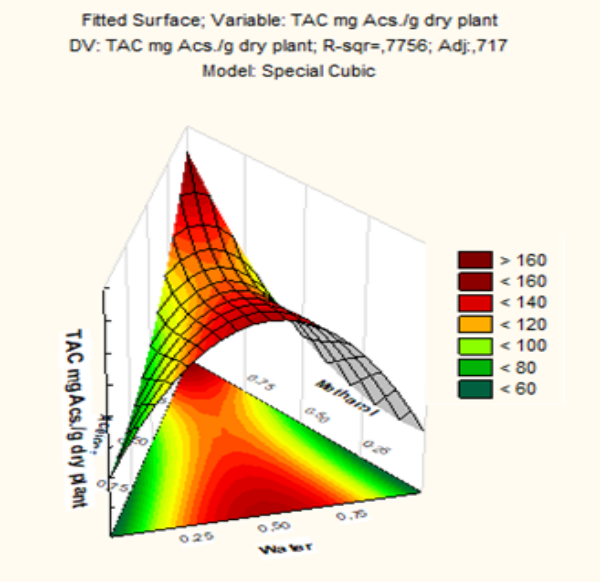

Figure 7 A: Response surface contour plot of the special cubic model predicted CAT as a function of the acetone, water and methanol proportions (3D).

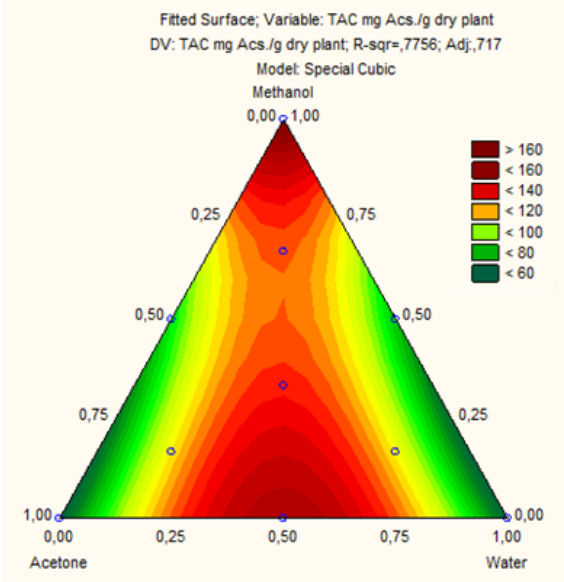

Figure 7B: Response surface plot of the special cubic model predicted CAT as a function of the acetone, water and methanol proportions (2D).

3.5. Analysis of variance (ANOVA)

ANOVA is applied to the linear, quadratic, and even special cubic models showed significant lack of fit at the 95% confidence level for total antioxidant capacity. The special cubic model is given by the following polynomial equation:

TAC = + 59,21 * acetone + 60,85 * water + 163,46 * methanol + 349,26 * acetone * water - 96,27 * acetone * methanol - 126,51 * water * methanol + 597,12 * acetone * water * methanol + 0,

In the statistical experimental design, the full cubic model, including linear and interaction terms, was chosen to describe the mixture composition. The responses and the consistent factors are optimized and modelled using ANOVA test to assess the statistical parameters via means of response surface technique (Table 5) and in order to evaluate which terms have more influence on the response variables using the *p* value (significance probability), always checking if the model was well adjusted to data by R^2 (coefficient of determination).

Table 5 : analysis of variance (ANOVA) results for the mixture models

	SS	DF	MS	F	P
Model	33727,77	6	5621,29	13,24	0,000002
Total Error	9759,45	23	424,32		
Lack of Fit	9531,47	3	3177,15	278,72	0,000000
Pure error	227,98	20	11,39		
Total adjusted	43487,23	29	1499,55		

According to Table 5, the model was significant since *p* value was lower than 0.01, and F value was high (F= 13,25). We also found a high correlation between observed and predicted values for antioxidant activity (Figure 8).

The standardized Pareto chart (Figure 9) shows that all extractor solvents and some of their interactions were significant except the binary combination of acetone-methanol and the ternary combination of the three solvents. It is worthy to note that the methanol solvent affects the extraction of antioxidant compounds from *Ammi visnaga*.

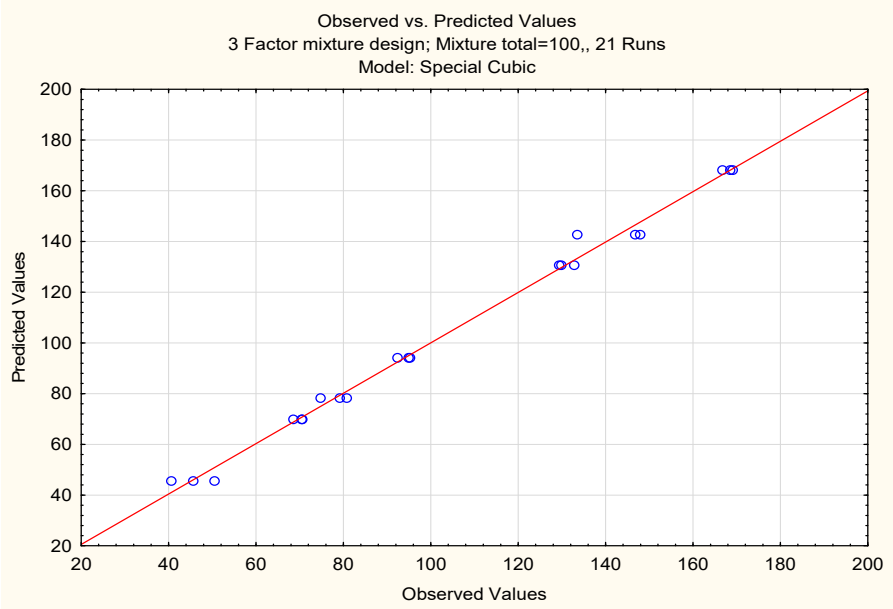

Figure 8: Predicted values (from the model) versus actual values (from experiments).

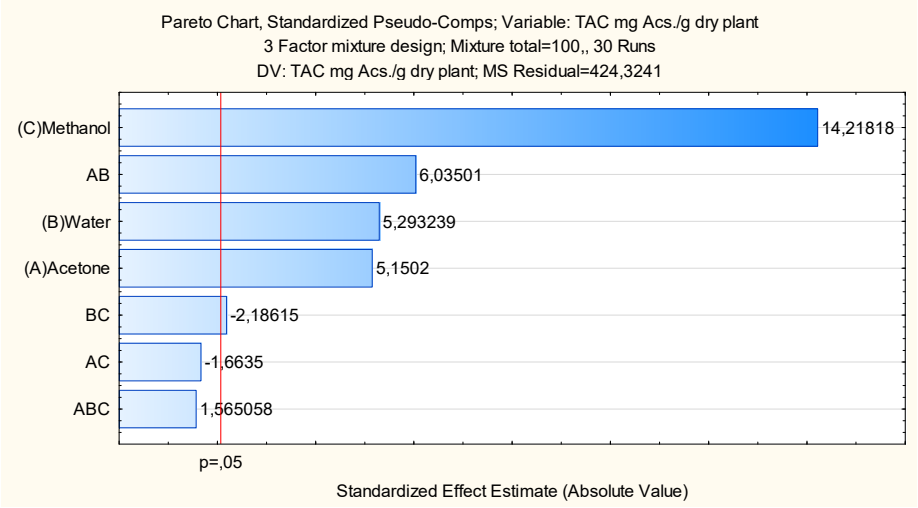

Figure 9: Analysis of Pareto chart of the standardized effects for TPC

4. Conclusion

In this work, the extraction with different solvents using simplex-centroid mixture design in order to find the optimal solvents mixture for extraction was studied. This study indicated that ternary mixture of water-acetone-methanol (66.67/16.67/16.67) was the most appropriate solvent mixture for extraction of phenolic compounds. While, the highest antioxidant activity occurs with methanol and ternary interaction between acetone, water, and methanol (66.67/16.67/16.67). Meanwhile, the pure methanol appeared to be the best extractor solvent of antioxidant compounds from *Ammi visnaga*.

5. Data Availability

The data used to support the findings of this study are included within the article.

Conflicts of interest

There are no conflicts of interest.

Funding Statement

No funding.

References:

Aazza S. 2021. Application of Multivariate Optimization for Phenolic Compounds and Antioxidants Extraction from Moroccan Cannabis sativa Waste. J Chem. **2021**, e9738656. https://doi.org/10.1155/2021/9738656

Afzal S, Ahmad HI, Jabbar A, Tolba MM, AbouZid S, Irm N, Zulfiqar F, Iqbal MZ, Ahmad S, Aslam Z. 2021. Use of Medicinal Plants for Respiratory Diseases in Bahawalpur, Pakistan. BioMed Res Int **2021**, e5578914. https://doi.org/10.1155/2021/5578914

Ahmed SST, Fahim J, Abdelmohsen UR. 2021. Chemical and biological potential of Ammi visnaga (L.) Lam. and Apium

graveolens L.: A review (1963-2020). JABPS., **4**: 160–176. https://doi.org/10.21608/jabps.2021.55949.1115

Al-Zaidi YM, Khorsheed AC. 2021. Separation and identification of many volatile oil compounds and phenolic compounds from the seeds of Ammi visnaga (L.) growing in Iraq. J Kerbala Agri Sci., **8:** 1–11.

Aourabi S, Driouch M, Sfaira M, Mahjoubi F, Hammouti B, Emran KM. 2019. Influence of phenolic compounds on antioxidant and anticorrosion activities of Ammi visnaga extracts obtained ultrasonically in three solvent systems. Int J Electrochem Sci., **14**: 6376–6393.

Apak R, Özyürek M, Güçlü K, Çapanoğlu E. 2016. Antioxidant activity/capacity measurement. 2. Hydrogen atom transfer (HAT)-based, mixed-mode (electron transfer (ET)/HAT), and lipid peroxidation assays. J Agric Food Chem., **64**: 1028–1045

Baj T, Baryluk A, Sieniawska E. 2018. Application of mixture design for optimum antioxidant activity of mixtures of essential oils from Ocimum basilicum L., Origanum majorana L. and Rosmarinus officinalis L. Ind Crops Prod., **115**: 52–61. https://doi.org/10.1016/j.indcrop.2018.02.006

Bellakhdar J, Claisse R, Fleurentin J, Younos C. 1991. Repertory of standard herbal drugs in the Moroccan pharmacopoea. J Ethnopharmacol., **35**: 123–143.

Cavalcanti VP, Aazza S, Bertolucci SKV, Rocha JPM, Coelho AD, Oliveira AJM, Mendes LC, Pereira MMA, Morais LC, Forim MR. 2021. Solvent Mixture Optimization in the Extraction of Bioactive Compounds and Antioxidant Activities from Garlic (Allium sativum L.). Molecules., **26**: 6026.

Farris S, Piergiovanni L. 2009. Optimization of manufacture of almond paste cookies using response surface methodology. J Food Process Eng., **32**: 64–87. https://doi.org/10.1111/j.1745-4530.2007.00203.x

Jouad H, Maghrani M, Eddouks M. 2002. Hypoglycemic effect of aqueous extract of Ammi visnaga in normal and streptozotocin-induced diabetic rats. J herb pharmacother., **2**: 19–29.

Kamal FZ, Stanciu GD, Lefter R, Cotea VV, Niculaua M, Ababei DC, Ciobica A, Ech-Chahad A. 2022. Chemical Composition and Antioxidant Activity of Ammi visnaga L. Essential Oil. Antioxidants., **11**: 347. https://doi.org/10.3390/antiox11020347

Khalil N, Bishr M, Desouky S, Salama O. 2020. Ammi visnaga L., a potential medicinal plant: A review. Molecules., **25**: 301.

Laaroussi H, Bakour M, Ousaaid D, Aboulghazi A, Ferreira-Santos P, Genisheva Z, Teixeira JA, Lyoussi B. 2020. Effect of antioxidant-rich propolis and bee pollen extracts against D-glucose induced type 2 diabetes in rats. Food Res Int., **138**: 109802.

Lamuela-ravents RM. 1999. 2,6-di-tert-butyl-4-hydroxytoluene, **299**: 152–178.

Montgomery DC. 2012. **Design and Analysis of Experiments** Eighth Edition. Design 41–43. https://doi.org/10.1198/tech.2006.s372

Munhoz VM, Longhini R, Souza JRP, Zequi JAC, Mello EVSL, Lopes GC, Mello JCP. 2014. Extraction of flavonoids from Tagetes patula: Process optimization and screening for biological activity. Revi Brasileira de Farmaco., **24**: 576–583. https://doi.org/10.1016/j.bjp.2014.10.001

Oliveira AL, Padilha CD, Ortega GG, Petrovick PR. 2001. (L A M .) D C . (M A R C E L A) , A S T E R A C E A E , A V A L I A Ç Ã O E S T U D O S P R E L I M I N A R E S D E O T I M I Z A Ç Ã O D A E X T R A Ç Ã O 1 33–38.

Ousaaid D, Laaroussi H, Bakour M, ElGhouizi A, Aboulghazi A, Lyoussi B, ElArabi I. 2020a. Beneficial effects of apple vinegar on hyperglycemia and hyperlipidemia in hypercaloric-fed rats. J Diabetes Res., **2020**.

Ousaaid D, Mansouri I, Laaroussi H, ElGhouizi A, Lyoussi B, ElArabi I. 2020b. Phytochemical Content and Antioxidant Activity of Flesh Fruits Rosa canina Extracts Collected from Ait Ayach Midelt. Indian J Agri Res., **54:** 373–377.

Ousaaid D, Mansouri I, Laaroussi H, Lyoussi B, El Arabi I. 2020c. Physicochemical properties and antioxidant activity of two varieties of apple cultivated in different areas in Morocco. Medi J Chemi., **10**: 371–377.

Pejin B, Bogdanovic-Pristov J, Pejin I, Sabovljevic M. 2013. Potential antioxidant activity of the moss Bryum moravicum. Nat Prod Res., **27**: 900–902. https://doi.org/10.1080/14786419.2012.665915

Prieto P, Pineda M, Aguilar M. 1999. Spectrophotometric quantitation of antioxidant capacity through the formation of a phosphomolybdenum complex: Specific application to the determination of vitamin E. Anal Biochem., **269**: 337–341. https://doi.org/10.1006/abio.1999.4019

Rajha HN, Darra N, El Hobaika Z, Boussetta N, Vorobiev E, Maroun RG, Louka N. 2014. Extraction of Total Phenolic Compounds , Flavonoids , Anthocyanins and Tannins from Grape Byproducts by Response Surface Methodology . Influence of Solid-Liquid Ratio , Particle Size , Time , Temperature and Solvent Mixtures on the Optimization Process. Food Nutr Sci., **5:** 397–409. https://doi.org/10.4236/fns.2014.54048

Ribeiro BD, Coelho MAZ, Marrucho IM. 2013. Extraction of saponins from sisal (Agave sisalana) and juá (Ziziphus joazeiro) with cholinium-based ionic liquids and deep eutectic solvents. Eur Food Res Technol., **237**: 965–975. https://doi.org/10.1007/s00217-013-2068-9

Rubio CP, Hernández-Ruiz J, Martinez-Subiela S, Tvarijonaviciute A, Ceron JJ. 2016. Spectrophotometric assays for total antioxidant capacity (TAC) in dog serum: an update. BMC Vet Res., **12**: 166. https://doi.org/10.1186/s12917-016-0792-7

Sahu JN, Acharya J, Meikap BC. 2009. Response surface modeling and optimization of chromium(VI) removal from aqueous solution using Tamarind wood activated carbon in batch process. J Hazard Mat., **172:** 818–825. https://doi.org/10.1016/j.jhazmat.2009.07.075

Sampaio CRP, Anastácio LMC, De Francisco TMG, Ribani RH. 2015. Anthocyanins and phenolic compounds in five ripening stages of byrsonima ligustrifolia after extraction optimization. J Food Nutr Res., **54**: 365–378.

Santos Felix AC, Novaes CG, Pires Rocha M, Barreto GE, do Nascimento BB, Giraldez Alvarez LD. 2018. Mixture Design and Doehlert Matrix for the Optimization of the Extraction of Phenolic Compounds from Spondias mombin L Apple Bagasse Agroindustrial Residues. Front Chem., **5**: 1–8. https://doi.org/10.3389/fchem.2017.00116

Saravana Pandian P, Sindhanaiselvan S, Subathira A, Saravanan S. 2022. A correlative algorithmic optimization study for an integrated soft computing technique in aqueous two-phase protein extraction from Litopenaeus vannamei waste. Biomass Conv. Bioref. https://doi.org/10.1007/s13399-022-02355-x

StatSoft Inc. 2011. Statistica (data analysis software system).

Wang J, Sun B, Cao Y, Tian Y, Li X. 2008. Optimisation of ultrasound-assisted extraction of phenolic compounds from wheat bran. Food Chem., **106**: 804–810. https://doi.org/10.1016/j.foodchem.2007.06.062

Ziyyat A, Legssyer A, Mekhfi H, Dassouli A, Serhrouchni M, Benjelloun W. 1997. Phytotherapy of hypertension and diabetes in oriental Morocco. J Ethnopharmacol., **58**: 45–54.

JJBS

Volume 15, Number 4,December 2022
ISSN 1995-6673
Pages 689 – 696
https://doi.org/10.54319/jjbs/150418

Jordan Journal of Biological Sciences

ERIC-PCR Genotyping and Clonal Genetic linkage Between Carbapenem-Resistant *Acinetobacter baumannii* Isolates

Rasha H. Shayea [1,*] and Munim R. Ali [2]

Department of Biology, College of Science, Mustansiriyah University, Baghdad, Iraq.

Received: December 15, 2021; Revised: March 1, 2022; Accepted: March 26, 2022

Abstract

Acinetobacter baumannii is a nosocomial bacterium that has become a global issue due to high levels of resistance to various antibiotics, notably last-resort treatments like carbapenems. The goal of this study was to use Clonal lineage and enterobacterial repetitive intergenic concensus - polymerase chain reaction (ERIC-PCR) finger-printing techniques to determine the source of the epidemic and the routes of *A. baumannii* isolates transmission. Sputum, blood, urine, burn wounds, and fluids from patients hospitalized to several hospitals in Baghdad, Iraq yielded 75 *A. baumannii* isolates. Morphological testing and PCR with *blaOXA-51* gene primers were used to identify *A. baumannii* isolates. The phenotypic results for *A. baumannii* isolate discovery were verified (100%) by molecular analysis. Twenty-nine *A. baumannii* isolates were categorized as multidrug-resistant (MDR), 36 as XDR, and eight as pan-drug resistant (PDR), whereas two isolates were responsive to most antibiotics. The lineages of the isolates were determined, with 8 belonging to group one, 6 to group two, and none to group three. 45 carbapenem-resistant *Acinetobacter baumannii* (CRAB) strains were grouped into six groups using ERIC-PCR fingerprinting genotyping analysis (selected only the 45 isolates resistant to carbapenem). The other seven strains were single strains. A significant level of genetic similarity was found amongst *A. baumannii* isolates from hospitalized patients, implying cross-transmission. The most likely explanation of the rise in *A. baumannii* occurrences in Baghdad patients was the spread of six epidemic clones, highlighting the importance of the study. To avoid nosocomial *Acinetobacter baumannii* spread, enhanced infection control methods are required. The findings further suggest that ERIC-PCR is a quick and accurate method for determining the clonal similarities of *A. baumannii* isolates from a variety of clinical samples.

Keywords: Clonal relationship, *Acinetobacter baumannii*, Genetic typing, Enterobacterial repetitive intergenic consensus – polymerase chain reaction.

1. Introduction

Acinetobacter baumannii has become one of the most difficult pathogens to control and treat among healthcare-associated illness pathogens (Szczypta *et al*.,2021). *A. baumannii* can cause a variety of infections, including bloodstream infections, surgical site infections, pneumonia, and urinary tract infections (Godziszewska *et al*.,2016). It has been discovered that it spreads in the hospital environment, causing epidemic outbreaks among hospitalized patients, due to its ability to colonize the skin, medical devices, and respiratory systems of patients and health care staff (Antunes *et al*.,2014). It can also form biofilm on surfaces that are not alive (Peleg *et al*.,2008). The ability to build biofilms and the presence of drug resistance mechanisms appear to be the greatest approaches to increase hospital mortality (Krzyciak *et al*., 2017).

Many drugs are naturally resistant to *A.baumannii*, and resistance can also be acquired by chromosomal changes and horizontal gene transfer (Pormohammad *et al*.,2019). The emergence of exceptionally drug-resistant (XDR) and multidrug-resistant (MDR) *A. baumannii* has become a public-health issue in both developed and developing countries (Salih & Shafeek,2019). Globally, resistance to last-resort antibiotics such as colistin and carbapenems is on the rise (Theriault *et al*.,2019).

Carbapenem-resistant *Acinetobacter baumannii* (CRAB) outbreaks are common in healthcare facilities, particularly in intensive care units (Ridha *et al*.,2019). These outbreaks can be enhanced by clonal transmission or the spread of genetically unrelated strains. Clonality can be examined using molecular typing methods in such contexts, and several techniques have been used to type organisms in various environments (Alnimr *et al*.,2019). In the event of an incident, PCR-based genotyping schemes such as PCR-based sequence group typing, in which *A. baumannii* has been divided into three distinct groups, designated Group 1–3, based on their csuE (part of the pilus assembly system needed for biofilm formation), ompA (outer-membrane protein A), and blaOXA-51-like genes, are quick, cheap, and simple to use instruments for typing *A. baumannii*. In the same group of isolates, all three loci contained the same combination of alleles, indicating that the outbreak strains studied belonged to three primary clonal lineages. Using sequence changes across alleles, multiplex PCRs has been designed to

* Corresponding author. e-mail: : rashahatemhatem@gmail.com.

quickly detect isolates that belong to specific genotypes or sequence groupings (Turton *et al*.,2007).

Enterobacterial repetitive intergenic consensus (ERIC) sequences are the most common repeated elements used for genetic typing (Ali & Khudhair, 2019). Non-coding transcribed areas are represented by ERIC sequences, which contain a higher central conserved inverted repeat (Yoke-Kqueen *et al*.,2013). The ERIC amplicon's sequence number and location are utilized as genetic markers to type and differentiate gram-negative bacteria (Omid *et al*., 2018). The goal of this study is to identify the origins of the outbreak and the transmission routes of *A. baumannii* isolates, which will be evaluated using clonal lineage and ERIC-PCR as a genetic typing technique.

2. Materials and Methods

2.1. Sampling

A total of 75 isolates have been taken from various hospitals in Baghdad (Central Children's Hospital, Baghdad Teaching Hospital, Burn Hospital, Children Protection Teaching Hospital (Medical City), Al-Imameen Al-Kadhimayn City Hospital) during three months from March 2021 to June 2021.The isolates included: 75 specimens taken from wounds, urine, respiratory infections (sputum), burns, and CSF of patients setting in hospitals, particularly in intensive care units. All the isolates were characterized via VITEK 2 System, the bio-chemical reactions between the bacterial isolates that have been suspended in their solutions, and media in VITEK2 Identification Cards. The specimens were transported to the laboratory (via transport media) and cultured on *A. baumannii*-selective media (Chrom agar) and MacConkey agar, incubated at a temperature of 37ºC for 24hrs under aerobic conditions. Then the colony's color, shape, edges, and texture were examined (Atlas *et al.,*1997).

2.2. Antimicrobial sensitivity test

The susceptibility of antibiotics to the antimicrobial agents listed below has been determined by using the disk diffusion approach on Mueller-Hinton agar (Merck, Germany) in accordance with the clinical and lab standards institute (CLSI 2020) Guidelines: meropenem (10µg), imipenem (10µg), cefixime (5µg), ceftazidime (30µg), cefepime (30µg), amoxicillin/clavulanate (20/10µg), amoxicillin (25µg), piperacillin-tazobactam (100/10µg), piperacillin (100µg), amikacin (30µg), gentamicin (10µg), Trimethoprim/sulphamethoxazole(25µg), ciprofloxacin (5µg), colistin sulfate (10µg) and tetracycline (30µg) were utilized. A fresh 24h bacterial lawn of the isolates was utilized for the preparation of 0.50 McFarland (1.50×10^8 CFU/ml) bacterial concentration. The bacterial growth inhibition diameter has been assessed and compared with reference tables that have been provided by the CLSI (CLSI, 2020).

2.3. DNA Extraction

Bacterial DNA extract was extracted from the Nutrient agar after 24 hours of incubation at 37ºC according to the boiling method as Annotated in Abed & Ali (Abed and Ali,2020). In a brief, 5 colonies have been thoroughly suspended in 1mL DNase- and RNase-free water and boiled for 10min. After centrifugation, five microliters of the supernatant were used as template DNA. DNA preparations were stored at - 20 C until they were needed for PCR.

2.4. Genotyping detection

It was confirmed by amplifying the blaOXA-51 gene for *A. baumannii* confirmation, detection by PCR technique in comparison with positive controls strain (Zueter & Harun, 2018; Ridha *et al*., 2019).

2.5. PCR - Based Sequence Group Typing

Multiplex PCR is used for the identification of the groups (international clones) of 1-3 organisms. This has been achieved with the use of primers given in Table 1 that were utilized for amplifying *csuE*, *ompA*, and *blaOXA-51-like* genes, which were applied for designating the sequence groups as well as the corresponding main international clones I–III as stated by Turton *et al*.(Turton *et al*.,2007). PCR was performed under the following conditions: 3 mins at 94ºC, then 30 cycles of 45sec at 94ºC, 45sec at 57ºC, and 1min at 72 ºC, followed by a 5mins extension at 72 ºC. For a strain to be classified as a member of group 1 or 2, it needed to have all three fragment amplifications in the corresponding multiplex PCR and no amplification in the other multiplex PCRs. PCR amplification of only *ompA* segment in group 2 and *csuE* and *blaOXA-51-like* fragments in group 1 was used to characterize the isolates in group 3 (Turton *et al*.,2007). The PCR products have been separated on 1% agarose gel and seen under ultraviolet light after being stained with ethidium bromide.

Table 1: Primers that have been utilized in multiplex PCRs for identifying sequence type groups

Table2: Distributions of *A. baumannii* strain specimens (n = 75)

samples	Number of isolates
Sputum	20 (26%)
Blood	18 (24%)
Burn	13 (17%)
Wound s.	10 (13%)
Urine	7 (9%)
CSF	4 (5%)
Fluid	3 (4%)
Total	75 (98%)

2.6. Genotyping of Acinetobacter baumannii by ERIC-PCR

To investigate the genetic diversity and the clonal relationship of *A. baumannii* isolates, specific ERIC-PCR primers were used to identify the number of genetic patterns of isolates. ERIC-1(5′TGTAAGCTCCTGGGGATTCAC3′) and ERIC-2 (5′AAGTAAGTGACTGGGGTGAGCG 3′) were employed for this phase, as indicated via Coudron *et al.* (Coudron *etal*.,2000). The amplification reaction volume has been 25µl, while the cycling conditions were: After 5 minutes of denaturation at 94 ° C, 35 cycles of 1 minute at 95 ° C, 1min at 52ºC, 5min at 72ºC, and a final extension of 10min at 72ºC have been completed. Furthermore, the amplified products were separated by electrophoresis and stained with ethidium bromide on a 1% agarose gel. UPGMA was used to cluster the ERIC patterns, and the coefficient of Dice similarity has been utilized to compare them (Sallman *et al*.,2018).

3. Results

Over three months, 75 isolates of *A. baumannii* were collected from various hospitals in Baghdad/Iraq and genotypically and phenotypically confirmed as *A. baumannii* (Table2).

The phenotypic test results exhibited that all the isolates showed a pinkish tint colony due to non-lactose fermentation when cultured on MacConkey, while light purple with a halo around the colonies on chrom agar.

For confirming phenotypic identification regarding the *A. baumannii* isolates, PCR testing of the blaOXA-51 gene revealed that 75 (100%) isolates had the target gene (Figure1).

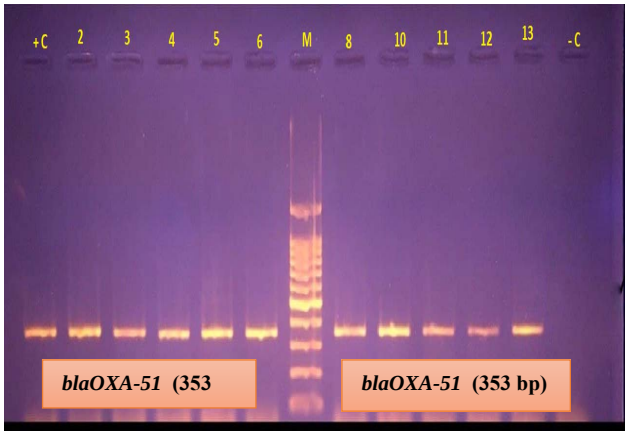

Figure 1: The blaOXA-51 gene product size (band 353 bp) was detected by using agarose gel electrophoresis (1% agarose, 7v/cm2) with Ethidium bromide staining. **Utilizing the** template DNA that was prepared with the use of the boiling method. The molecular size of the DNA ladder was 100 bp, located in the middle (M). DNA isolated from ***A. baumannii*** samples have shown positive PCR, with a positive control on the right and negative control on the left.

3.1. Antibiotic sensitivity test

The susceptibility profiles of 75 clinical isolates of *A. baumannii* to the antimicrobials studied were obtained in (Figure 2A). Among 75 *A.baumannii* with drug-resistant strains, most strains were resistant to common antimicrobial agents, although colistin was more effective. Interestingly, carbapenem appears to be a moderately effective antibiotic in this research. It is clear that *A. baumannii* isolates show a high level of resistance to piperacillin (98.66%) and amoxicillin (91%). The resistance pattern differed between samples from various sources, including 38.6 % (29/75) of *A. baumannii* isolates were classified as MDR, 48

%(36/75) as XDR, and 10.6 %(8/75) as pan-drug resistant. At the same time, two isolates 2.6% (2/75) were susceptible to fourteen of the sixteen antibiotics tested.

The dendrogram is based on the antimicrobial drug sensitivity pattern of seventy-five *A. baumannii* isolates. In this dendrogram, the isolate (63spu) was the origin of isolates responsible for resistance that utilized a 0. 4 cutoff to produce two clusters and then divided into different isolates with genetic variations. This indicated its ability to acquire different resistant genes as indicated in (Fig 2B).

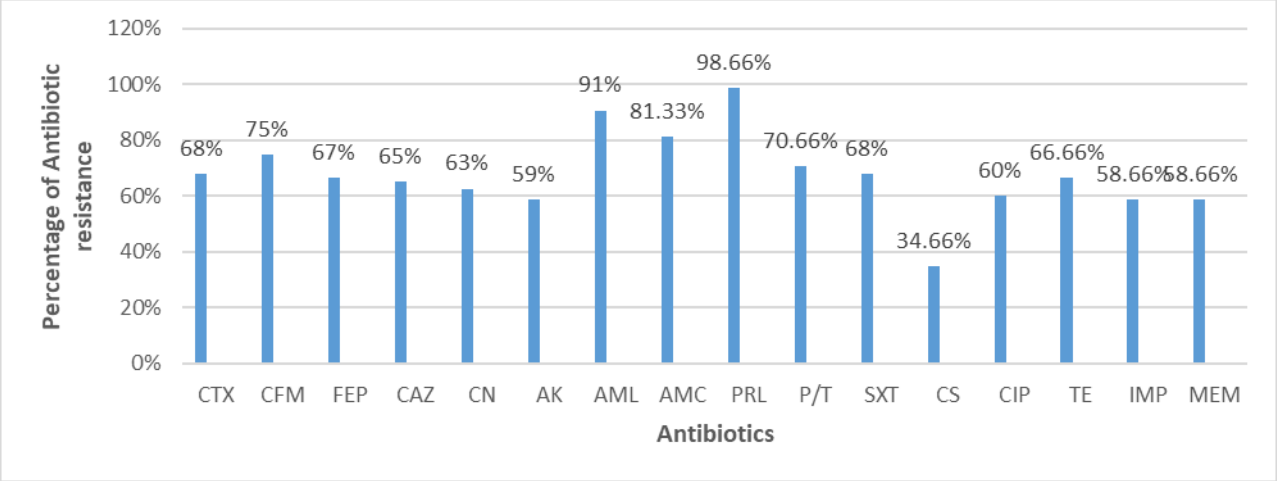

Figure 2A: **Antimicrobial resistance (%) of *A. baumannii* isolates.**

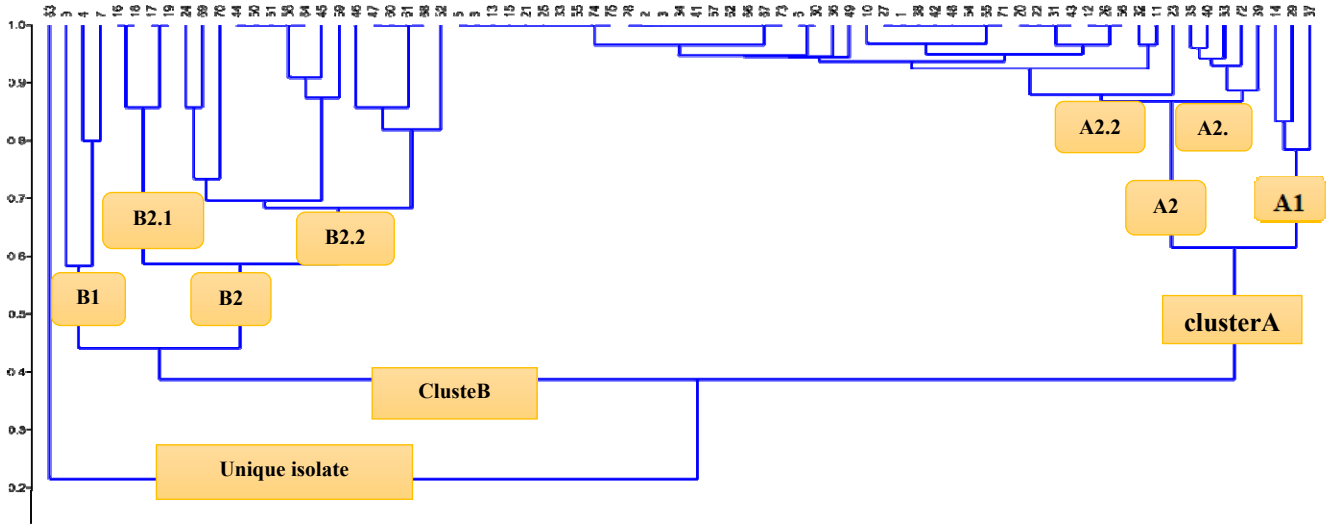

Figure 2B: Antibiogram typing analysis for 75 clinical *A. baumannii* isolates, by Dice coefficient values.

The accessions are obviously divided into two distinct clusters, A and B. Cluster A is divided into two subclusters, A1 and A2. The subcluster A1 consists of three isolates that were resistant five to eight antibiotics. The subcluster A2 is further divided into subgroups A2.1 and A2.2. The subgroup A2.1 consisted of five isolates which were resistant to three to sixteen antibiotics and subgroup A2.2 consisted of forty-three isolates which were resistant four to sixteen antibiotics. Cluster B also can be grouped into two subclusters B1 and B2. The subcluster B1 consists of three isolates which were resistant two to six isolates, while subcluster B2 is further divided into subgroups B2.1 and B2.2. The subgroup B2.1 consisted of four isolates which resist three to four isolates and the subgroup B2.2 consisted of sixteen isolates which resist two to fifteen antibiotics. Finally, all these clusters arise from a unique isolate (63 spu.) which was considered the origin of resistance.

3.2. PCR - based Sequence Group Typing

In group one of the clonal complex, all strains produced all three PCR fragments. However, there were none in group two PCR, while strains in group two gave the expected opposite results. Group 3 strains with the same ompA allele as Group2 produced the middle fragment (for ompA) in the Group2 PCR, yet the top two segments (for the other 2 loci) in Group1 PCR. Multiplex PCRs can thus be used to quickly classify outbreak strains into various sequence classes. Our findings revealed that eight isolates belonged to group one, six isolates to group two, and 39 isolates to group three. This method could not be used to type 22 isolates (Figure3) (Table 3).

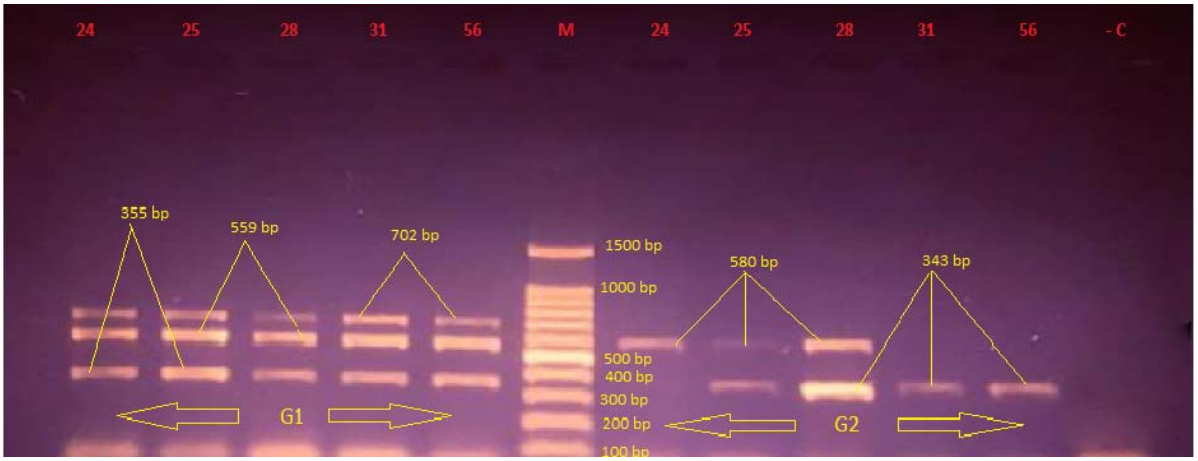

Figure3: Genetic detection of the global lineage through the multiplex PCR for 2 listed primers G1 *ompA (355 bp), csuE (702 bp) & blaOXA-51-like/ 66* (559 bp) and G2 *ompA (343 bp), csuE (580 bp) & blaOXA-51-like/66* (162 bp). Agarose Gel Electrophoresis (1% Agarose, 7V/Cm2) and Ethidium Bromide Staining to complete detection. In middle lane, molecular size DNA Ladder (100 bp DNA Ladder) and C indicate the negative control, isolates (24, 25, 28, 31 & 56) under G1 (ICI) due to harboring all G1 genes.

Table3: Determination of International Clone Types of *A. baumannii* isolates

Isolates number for each group with persentages	Isolates	Groups of international clone
22 (29.3%)	1CSF.,7 BL.,10 B.S, 14 spu.,15 BL.,16 spu.,18 W.S., 19 spu.,29 Uri.,30 spu.,34 spu.,35 BL. 36BL.,39 spu.,41 spu.,52BL.,59 B.S.,60 spu., 69Spu, 70 B.S, 71 BL., 76 B.S	G0
8 (10.6%)	12 W.S, 24 Ur., 25 BL., 28 Spu., 31 FL., 51 B.S, 56 Spu., 75 FL.	G1
6(8%)	3 Spu., 4 BL., 6 CSF, 21 BL., 45 B.S, 67 Ur.	G2
39(52%)	2 W.S, 5 B.S, 8 BL., 9 BL, 11 W.S, 13 CSF, 17 w.s, 20 BL., 22 BL., 23 Ur., 26 W.S, 27 W.S, 32 BL., 33 Spu., 37 Spu.,38 Spu. 42 Spu.,43 W.S,44 CSF, 46 Ur.,47 Ur.,48 B.S,49 FL.,50 B.S, 53Spu. 54 Spu.,55 Ur., 57 B.S,58 B.S, 61 W.S,62 B.S,63 Spu.,64 BL.,65 BL.,66 W.S, 68 W.S, 72 BL.,73 Spu.,74 BL.	G3

BL.: Blood, CSF: cerebrospinal fluid, Spu.: sputum, Uri.:urine. W.S.:wound swab, B.S: burn swab, FL.:fluid.

3.3. Amplification of DNA by ERIC – PCR

The ERIC-PCR fingerprinting technique has been utilized in order to classify *A. baumannii* strains obtained from different samples and at the same location and isolation period. It produced 17 DNA amplicon bands ranging from 100 to 1400 bp on average. Clonal diversity was discovered among 45 carbapenem-resistant *A. baumannii* isolates by detecting 13 ERIC patterns (ERIC - types), six of which were common type (A-F) that were divided into two clusters (Clusters 1–II) and seven unique types with a 97% similarity level. ERIC-type E was identified as the dominant type, with 11 isolates belonging to it (24.4%). In addition, genotype C had 5 isolates, followed by genotypes B and F (four isolates), and A and D (three isolates). Other isolates have been distributed in other patterns, revealing seven single types (between them, two isolates, 35 Flu. and 75 Flu., were considered the origin of types), and eight isolates were non-typed by ERIC PCR. Our results classified 30 (66.6%) isolates into six main genotypes (Figure4).

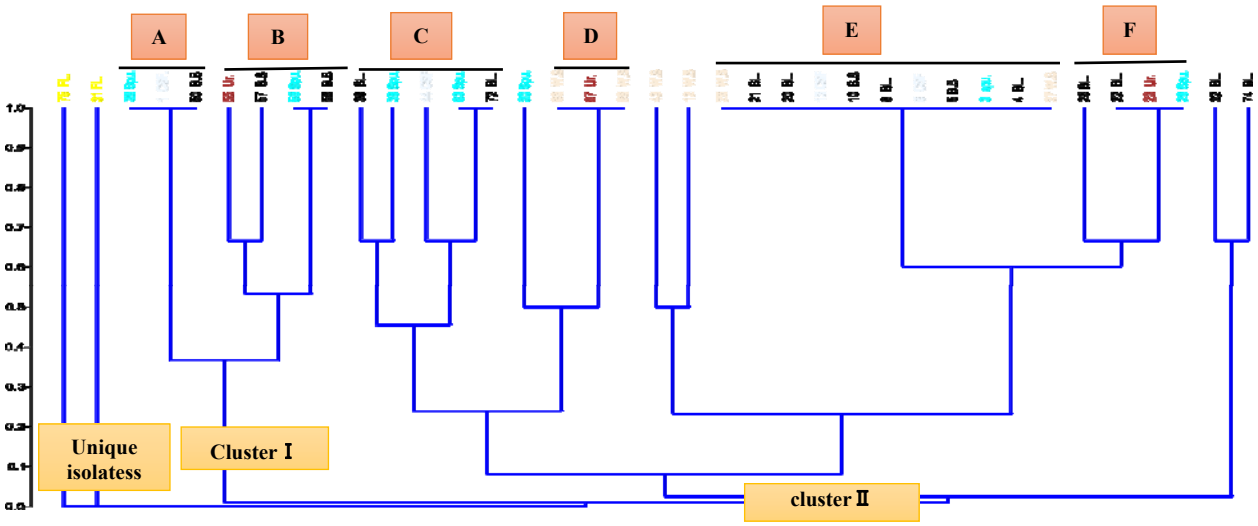

Figure 4: ERIC dendrogram utilizing the Bionumerics Fingerprint Analyst Software (Applied Maths) and unweighted pair groups, Dice technique, and arithmetic averages at 97% similarity on 45 *Acinetobacter baumannii* isolates.

4. 4. Discussion

A.baumannii is a potential nosocomial pathogen that causes a wide range of illnesses, from small soft tissue infections to more serious infections like bacteremia and ventilator-related pneumonia (Moubareck & Halat,2020). In this study, 75 *Acinetobacter baumannii* isolates were found in sputum, blood, wounds, burns, urine, fluids, and cerebrospinal fluid from patients with nosocomial infections. Our findings reveal that most isolates obtained were from sputum (26%) followed by blood (24%). This indicated that respiratory tract infections, which are typically connected with endotracheal tubes or tracheostomies, peritonitis in patients undergoing peritoneal dialysis, and catheter-related blood circulation infections were the most common types of *A. baumannii* clinical isolates. Our findings matched those of prior investigations by Saed *et al*. (2015) and Smail & Ganjo (2020). Mechanical ventilation, endotracheal intubation, and intravascular catheterization have all been linked to respiratory infections in previous research (Raka *et al*.,2009).

The rapid rise of MDR-AB and XDR-AB strains has become a serious problem in the treatment of hospital-acquired infections in recent years (Pournajaf *et al*.,2018). *A. baumannii* isolates developed resistance to the most routinely prescribed antimicrobial drugs, including aminoglycosides, cephalosporins, and extended-spectrum penicillins, in combination with -lactam inhibitors, quinolones, and carbapenems, according to our laboratory findings (Figure 3-A). The isolates were then categorized into three categories based on their antibiotic resistance pattern: MDR 38.6 % (29/75), XDR 48 % (36/75), and PDR 10.6 % (8/75) based on these findings. The drug of choice for treating the infection was carbapenems. However, *A. baumannii* resistance to carbapenem in clinical isolates has recently been identified as a serious danger, meaning that if carbapenem is misused, early treatment discontinuation will likely result in a rapid increase in resistance and treatment failure (Gango *et al*.,2016). Due to bacteria's ability to acquire antibiotic resistance genes and survive for days in the hospital environment and on the hands of health-care workers (HCWs), endemic *A. baumannii* strains may be transferred and persist in hospitals (Shalaby *et al*.,2016). Colistin is one of the most extensively used alternative medicines for carbapenem-resistant *A. baumannii*, according to Behera and his group study (Behera *et al*.,2017). Colistin is still one of the most effective single antimicrobial agents against multidrug-resistant *Acinetobacter baumannii*, and it's frequently employed as a last resort (Hatami,2018). These findings are similar to those of Xie *et al*. (2018) and El-Kazzaz *et al*. (2020).

A. baumannii is able to acquire antibiotic resistance genes and survive for days both in the hospital environment and on the hands of healthcare workers (HCWs), which could lead to possible transmission and the persistence of endemic *A. baumannii* strains in hospitals (Shalaby *et al*.,2016)

Previous studies indicated that each antimicrobial agent (except colistin) had a resistance pattern of greater than 50% against *A. baumannii* in various clinical specimens. Colistin sensitivity was determined in all clinical isolates (100 percent). Antibiotic overuse in hospitalized patients, as well as delays in discharge, organ implants, and prolonged catheter use, are all contributing to the spread of resistant bacteria among vulnerable patients (Amini *et al*.,2012)

Different molecular approaches have revealed genotypic diversity to track the incidence and evolution of drug-resistant bacteria (Khuntayaporn *et al*.,2021). Within *A. baumannii*, two molecular typing approaches, global lineage and enterobacterial repetitive intergenic consensus - polymerase chain reaction - were applied in our study (ERIC - PCR).

According to PCR analysis, all isolates were employed multiplex PCR with their stated circumstances to determine which type of clones belong to its two primer groups (Turton *et al*.,2007). Three intrinsic genes, *ompA, csuE, and blaOXA-51-like*, were targeted for this purpose.

In this study, 75 strains were divided into four groups: G1, G2, G3, and G0, with all strains from the G1 clonal complex producing all three segments in G1 PCR but none in G2 PCR, and strains from the G2 generated clonal complex producing the expected opposite results. Only the *ompA* allele, as well as *csuE* and *bla OXA-51* - alleles found in Group 1 PCR - are shared by Group 3 strains (Turton *et al*., 2007). However, the results of other strains did not reveal any of those genes, therefore they were quickly labeled as G0, which had never been documented before. As a result, the findings of the study revealed a significant prevalence of ICIII strains, with 52 % (39/75) belonging to this group. While the prevalence of each of the ICI was lower, reaching 10.6 %(8/75) for ICII and 8 % (6/75) for ICII, respectively. Finally, IC0 achieved a score of 29% (22/75). These findings contrast with those of Hamidian and Nigro, who found a greater dispersion of two major clones I and II on a large scale (Hamidian & Nigro,2019). The findings were also in contrast to those of Khuntayaporn et al. in Thailand, where recording ICII is far more common than recording ICI (Khuntayaporn *et al*.,2021). This difference in study outcomes could be attributed to a variety of factors, including geographical diversity.

Forty five carbapenem-resistant *A. baumannii* isolates were typed using ERIC-PCR. Two clusters (6 common kinds A-F) of *A. baumannii* strains with high relatedness, of which one ERIC-type predominated, were recovered from the same period of location and isolation, indicating that epidemiological relatedness has an impact on A. *baumannii* strain clustering (Fig. -4). Furthermore, the observed ERIC patterns revealed a high genetic similarity of 97 percent, as well as a higher number of DNA finger-prints among *A. baumannii* strains. Cross-transmission occurred among hospitalized patients, as evidenced by this finding. The conclusions of this study agree with those of previous studies (Hammoudi *et al*.,2015; Ying *et al*.,2015; Aljindan *et al*.,2018). Using the ERIC-PCR, researchers were also able to group *A. baumannii* strains based on genetic relatedness.

ERIC - PCR, according to our findings, is a quick and reliable method for demonstrating clonal relatedness of *A. baumannii* recovered from a variety of samples isolated from a variety of inpatients. As a result, compared to quick typing, this PCR-based target repetitive element approach is more suited, and it is also less expensive than other DNA fingerprint approaches.

5. Conclusion

A high level of genetic similarity was found amongst *A. baumannii* isolates from hospitalized patients, indicating cross-transmission. The most often discovered clonal lineage in the current investigation was international clone III (52 %, 39/75 isolates). This clone's isolates were largely linked to the *ompA* gene, which explains why 37.33 % of them carried the *ompA* gene. Furthermore, ERIC-PCR was used to indicate that the spread of six epidemic clones was the most likely source of the increase in *A. baumannii* occurrences in Baghdad patients. The findings also suggest that ERIC-PCR may be used to determine clonal similarities between *A. baumannii* isolates from a variety of clinical samples in a quick and reliable manner.

6. Ethical approval

The authors are confident that the publication of this manuscript will not raise any ethical issues.

Acknowledgment

The authors appreciate the support of Mustansiriyah University, College of Science, Biology Department, Baghdad, Iraq. for their contribution to this research work.

Conflict of interests

The authors declare that there is no conflict of interests in this publication.

References

Abed ES and Ali MR , 2020. Molecular Analysis of Efflux Pumps and Quorum Sensing Genes in MDR *Acinetobacter baumannii*. *Bioch. and Cellu. Archi.*, 20(1): 2259–2266.

Ali MR and Khudhair AM. 2019. Occurrence of Quorum Sensing Genes Amongcytotoxic and Invasive MDR *Pseudomonas auroginosa* . *Asian J. of Microbiol. Biotech. Env. Sc.* , 21(3) : 67-72.

Aljindan R, Alsamman K and Elhadi N .2018. ERIC-PCR Genotyping of *Acinetobacter baumannii* Isolated from Different Clinical Specimens. *Saudi J Med Med Sci*, 6(1): 13–17.

Alnimr A , Alamri A and Alsultan A . 2019. Genetic Diversity of Imipenem-Resistant *Acinetobacter baumannii* Infections at an Intensive Care Unit. ***Critical Care Research and Practice***, Article ID 3290316, 6 pages. https://doi.org/10.1155/2020/3290316.

Amini M, Davati A & Golestanifard M. 2012. Frequency of nosocomial infections with antibiotic-resistant strains of Acinetobacter spp. In ICU patients. *Iranian Jo. of Patho.*, 7: 241-245.

Antunes LCS, Visca P, TownerK J .2014. *Acinetobacter baumannii*: evolution of a global pathogen. *Pathog. Dis.*, 71:292–301.

Atlas RM, Brown AE and Parks LC .1997. **Laboratory Manual of Experimental Microbiology.** 1sted. Mosby, st. Louis U.S.A.

Behera I C , Swain SK & Chandra M . 2017. Incidence of colistin-resistant *Acinetobacter baumannii* in an Indian tertiary care teaching hospital. *IJAR*, 3: 283-286.

Clinical and Laboratory Standards Institute.2020. **Performance standards for antimicrobial susceptibility testing**, 30th ed CLSI supplement M100 CLSI., Wayne, PA.

Coudron PE , Moland ES & Thomson KS .2000. Occurrence and detection of AmpC beta-lactamases among *Escherichia coli*, *Klebsiella pneumoniae*, and Proteus mirabilis isolates at a veterans medical center. *J Clin Microbiol*., 38:1791–6.

El-Kazzaz W, Metwally L, Yahia R, Al-Harbi N, El-Taher A and Hetta HF. 2020. Antibiogram, Prevalence of OXA Carbapenemase Encoding Genes, and RAPD-Genotyping of Multidrug-Resistant *Acinetobacter baumannii* Incriminated in Hidden Community-Acquired Infections. *Antibiot.*, 9(9): 603.

Gango A R, Maghdid D M , Mansoor IY., Kok D J, Severin J A, Verbrugh H A, Kreft D, Fatah M, ALnakshabandi A & Dlnya A. 2016. OXA-carbapenemases present in clinical *Acinetobacter baumannii* calcoaceticus complex isolates from patients in Kurdistan region, Iraq. *Microbi. Drug Resist.*, 22: 627-637.

Godziszewska J, Guzek D, Głąbski K , Wierzbicka A. 2016. Mobile antibiotic resistance-The spread of genes determining the resistance of bacteria through food products. *Postepy Hig. Med. Dosw.* , **70**:803–810.

Hamidian M & Nigro S J . 2019. Emergence, molecular mechanisms, and global spread of carbapenem-resistant *Acinetobacter baumannii. Microbi. Genom.*, 5(10): e000306. Dio:https://dx.doi.org/10.1099%2Fmgen.0.000306

Hammoudi D , Moubareck CA ,Hakime, N, Houmani M Barakat, A, Najjar Z, et al. 2015.Spread of imipenem-resistant *Acinetobacter baumannii* co-expressing OXA-23 and GES-11 carbapenemases in Lebanon*. Int J Infect Dis*. ,36:56–61.

Hatami R .2018. The frequency of multidrug-resistance and extensively drug-resistant *Acinetobacter baumannii* in the west of Iran. *Jo. of Clinical Microb. and Infect. Diseas*., 1(1):4-8.

Khuntayaporn P, Kanathum P, Houngsaitong J , Montakantikul P , Thirapanmethee K & Chomnawang, M. T. 2021. Predominance of international clone 2 multidrug-resistant ***Acinetobacter*** *baumannii* clinical isolates in Thailand: a nationwide study. *Annals of clin. Microbiol. and antimicrob.,* 20(1): 1-11.

Krzyściak P, Chmielarczyk A ,Pobiega M, Romaniszyn D ,Wójkowska-Mach J. 2017. *Acinetobacter baumannii* isolated from hospital-acquired infection: Biofilm production and drug susceptibility. *APMIS.* , **125** :1017–1026.

Moubareck CA and Halat DH. .2020. Insights into *Acinetobacter baumannii*: A Review of Microbiological, Virulence, and Resistance Traits in a Threatening Nosocomial Pathogen. *Antibiot. (Basel),* 9(3): 119. DOI: 10.3390/antibiotics9030119

Omid Z, Shokoohizadeh L, Hossainpour H and Alikhan MY . 2018. Molecular analysis of *Pseudomonas aeruginosa* isolated from clinical, environmental, and cockroach sources by ERIC-PCR. *BMC Resear. Notes*, 11: 668.

Peleg AY, Seifert H , Paterson DL .2008. *Acinetobacter baumannii*: Emergence of a successful pathogen. *Clin. Microbiol. Rev.*, **21**:538–582.

Pormohammad A, Mehdinejadiani K, Gholizadeh P, Mohtavinejad N , Dadashi M , Karimaei S , Safari H , Azimi T .2019. Globalprevalence of colistin resistance in clinical isolates of *Acinetobacter baumannii*: A systematic review and meta-analysis. *Microb.Pathog.* [http://doi.org/10.1016/j.micpath.2019.103887] [http://www.ncbi.nlm.nih.gov/pubmed/31765766]

Pournajaf A, Rajabnia R , Razavi S , Solgi S .2018. Molecular characterization of carbapenem-resistant *Acinetobacter baumannii* isolated from pediatric burns patients in an Iranian hospital. *Trop. Jo. of Pharma. Research* ,17(1):135-141.

Raka L , Kalenc S , Budimir A , Katic S , Mulliqi-Osmani G , Zoutman D & Jaka A . 2009. Molecular epidemiology of *Acinetobacter baumannii* in central intensive care unit in Kosova teaching hospital. *Brazi. Jo. of Infect. Dises.*, **13**: 408-413.

Ridha DJ , Ali MR and Jassim KA.2019. Occurrence of Metallo-β-lactamase Genes among *Acinetobacter baumannii* Isolated from Different Clinical Samples*. J Pure Appl Microbiol*., 13(2): 1111-1119.

Ridha, D.J . ; Ali, M.R. and Jassim,K.A.(2019). Molecular analysis of multidrug-resistant *Acinetobacter baumannii* isolated in Baghdad hospital, *Int.J.Res.Pharm.Sci*.,10(3):1970-1987.

Saed S ,Yazdanpanah M, Lal-Dehghani M , Khallghi A , Honarmand M , Afrough P & Ghazvini K .2015. Emerging Trend of Acinetobacter Nosocomial Infection in Northeast of Iran. *Jo. of Med. Bacterio.*, 2: 56-61.

Salih T S and Shafeek R R .2019. In silico Detection of Acquired Antimicrobial Resistance Genes in 110 Complete Genome Sequences of *Acinetobacter baumannii*. *JJBS.* **, 12(5):** 589 – 594**.**

Sallman RS , Hussein SS and Ali M R .2018. ERIC-PCR Typing, RAPD-PCR Fingerprinting, and Quorum Sensing Gene Analysis of *Pseudomonas aeruginosa* Isolated from Different Clinical Sources. *Al-Mustansi. Jo. of Scien.*, 29(2):50-62.

Shalaby MM , Meseehah MS , Shahin AM , Abdelwahaab AM , Maklad SS .2016. Phenotypic and Genotypic Characterization of Acinetobacter Infection in Intensive Care Units in Egypt. *Jo. of Americ. Scien.*; 12(7).

Smail SB, Ganjo AR .2020. Prevalence of infections with antibiotic-resistant *Acinetobacter baumannii* in different clinical samples from hospitals in Erbil. *ZAN. Jo. of Pure and App. Scien.*, 32(3):95-100.

Szczypta A ,Talaga Ć wiertnia K , Kielar M , Krzyściak P, Gajewska A , Szura M , Bulanda M and Chmielarczyk A . 2021. Investigation of *Acinetobacter baumannii* Activity in Vascular Surgery Units through Epidemiological Management Based on the Analysis of Antimicrobial Resistance, Biofilm Formation and Genotyping. *Int J Environ Res Public Health. ,* 18(4): 1563.

Theriault N, Tillotson G and Sandrock C E . 2019. Global travel and Gram-negative bacterial resistance; implications on clinical management. Expert Rev. *Anti-Infect. Ther.* [http://doi.org/10.1080/14787210.2020.1813022]

Turton JF, Gabriel SN ,Valderrey C , Kaufmann ME & Pitt TL . 2007. Use of sequence-based typing and multiplex PCR to identify clonal lineages of outbreak strains of *Acinetobacter baumannii. Clin Microbiol Infect*., 13(8):807–15.

Xie R, Zhang X D, Zhao Q, Peng B & Zheng J .2018. Analysis of global prevalence of antibiotic resistance in *Acinetobacter baumannii* infections disclosed a faster increase in OECD countries. *Emerg. Microb. & infect.,* 7(1): 31. https://doi.org/10.1038/s41426-018-0038-9

Ying C , Li Y , Wang Y, Zheng B & Yang C .2015. Investigation of the molecular epidemiology of *Acinetobacter baumannii* isolated from patients and environmental contamination*. J Antibiot. (Tokyo)*,68:562–7.

Yoke-Kqueen C, Teck-Ee K, Son R, Yoshitsugu N and Mitsuaki N . 2013. Molecular characterization of Vibrio parahaemolyticus carrying tdh and trh genes using ERIC, RAPD, and BOX-PCR on local Malaysia bloody clam and Lala. *Internatio. Food Resear. Jo.*, 20: 3299–3305.

Zueter A M and Harun A B.2018. Development and Validation of Conventional PCR for the Detection of the sctQ Gene. *JJBS.*, **11(4):** 435 – 439.

JJBS

Volume 15, Number 4,December 2022
ISSN 1995-6673
Pages 697 – 707
https://doi.org/10.54319/jjbs/150419

Jordan Journal of Biological Sciences

Phytochemical Composition, Antioxidant Potential and α-Amylase Inhibitory Activity of Different Extracts from *Aaronsohnia pubescens* (Desf.)

Chouaib Kandouli[1,*], Zineb Leulmi[1], Laid Bahri[2], Karima Oufroukh[3], Ala Abdessemed[3] and Aicha Mechakra[1]

[1]*Biology and Environment Laboratory, Faculty of Nature and Life Sciences, University of frères Mentouri, Constantine 1, Road Ain El Bey, Constantine 25017, Algeria;* [2]*Laboratory of Applied Biochemistry, Faculty of Natural and Life Sciences, University of frères Mentouri, Constantine 1, Algeria;*[3]*National Research Center of Biotechnology, Constantine, Algeria.*

Received: August 31, 2021; Revised: November 24, 2021; Accepted: December 18, 2021

Abstract

The medicinal plant *Aaronsohnia pubescens* is currently used in the algerian phytotherapy to treat several disorders. In order to investigate the potential influence of *A. pubescens*, six extracts were screened for their antioxidant and anti-amylase capacities. Antioxidant ability was evaluated by different assays as well as scavenging effect of free radicals (DPPH, ABTS, GOR and hydroxyl radical), metal chelating, reducing power, CUPRAC and total antioxidant capacity. Total phenolic and flavonoid contents in these extracts were also measured. Phenolic compounds in different extracts were identified using the HPLC-DAD analysis. The total phenolic contents of these extracts ranged from 70 to 335.9 mg GAE/g. Generally, the highest amounts of total phenolic and flavonoid contents were observed in ethyl acetate and *n*-butanol extracts, which may explain their strong antioxidant activity. All extracts demonstrated a significant inhibitory activity on α-amylase. Based on these findings, *A. pubescens* could serve as a source of natural compounds for oxidative damage and diabetes mellitus management.

Keywords: *Aaronsohnia pubescens*, antioxidant activity, flavonoid content, phenolic content, ethyl acetate extract, *n*-butanol extract.

1. Introduction

Reactive oxygen species (ROS) are constantly produced in cells and involved in many physiological processes such as host defense and cellular signaling (Ray *et al.,* 2012). Cell is equipped with antioxidant systems to eliminate ROS and preserving redox homeostasis. Excessive ROS production can cause cell death and contribute to disease development (Liguori *et al.,* 2018). For a long time, herbal medicine was the main or even the only resource of our ancestors for their health conditions. However, despite the growth of pharmaceutical industries, the use of medicinal plants and plant products has never been totally abandoned and people continue to resort to traditional medicine.

During the last decades, the antioxidant therapy research has increased tremendously with the aim to prevent or remediate oxidative stress damages. Recently, considerable attention has been devoted to naturally occurring antioxidants in medicine industry as an alternative to synthetic antioxidants, which are gradually restricted due to their possible side effects such as the dysfunction of reproductive system (Naresh and Nidhi, 2019). Plant extracts possess pools of biologically active molecules including antioxidants. Natural antioxidants "carotenoids, phenolic acids, flavonoids, coumarins, etc." are generally of low toxicity at their bioavailable dose, and furthermore they can act synergistically (Kancheva and Kasaikina, 2013).

Aaronsohnia pubescens (Desf.) K. Bremer & Humphries, syn. *Matricaria pubescens* (Desf.) called Ouazouaza in arabic, is a medicinal plant that belongs to the Asteraceae family. It is largely distributed in the northern and central Algerian Sahara (Benchelah *et al.,* 2000 and Makhloufi *et al.,* 2015). In Algeria, *A. pubescens* is widely used in folk medicine as an antiseptic, antirheumatic, antiarthritic, antidiarrheal and to treat digestive complications. It is also used as a condiment and as an aromata in the preparation of some traditional dishes (Cherif *et al.,* 2017 and Hammiche and Maiza, 2006). Several studies of *A. pubescens* chemical composition revealed its richness in terpenoids (e. g., *α*-pinine, Z-β-ocimene *α*-curcumene and 6-oxo-cyclonerolido), and phenolic compounds such as apigenin, luteolin, quercetin and herniarin (Boutaghane *et al.,* 2011; Makhloufi et *al.,* 2015 and Sharifi-Rad et *al.,* 2018). Furthermore, there are no previous reports on the antioxidant and enzyme inhibitory potentials of *A. pubescens*.

The main objectives of the present study were (1) to determine the polyphenolic profile (total phenolic, total flavonoid, benzoates, hydroxycinnamates and flavonols) of different extracts from *A. pubescens*; to reveal (2) antioxidant activity (DPPH, ABTS, GOR, ect.) of *A. pubescens*; and (3) to assess α-amylase inhibitory activity

* Corresponding author. e-mail: chouaib.kandouli@umc.edu.dz.

of the extracts. Six extracts from the aerial parts of *A. pubescens* were evaluated in this study.

2. Materials and Methods

2.1. Chemicals

Folin-Ciocalteu's phenol reagent, 2,2- azino-bis (3-ethylbanzthiazoline-6- sulphonic acid (ABTS), 2,6-Di-tert-butyl-α-(3,5-di-tert-butyl-4-oxo-2,5-cyclohexadien-1-ylidene)-p-tolyloxy (Galvinoxyl), 3-(2-pyridyl)-5,6-bis(4-phenylsulfonic acid)-1,2,4-triazine (Ferrozine), 2,2-Diphenyl-1-Picrylhydrazyl (DPPH) , 2-deoxyribose, ammonium molybdate ferric chloride, neocuproine, Trichloroacetic Acid (TCA), Thiobarbituric Acid (TBA), iodine potassium iodide, rutin, cafeic acid, ascorbic acid, gallic acid , $AlCl_3$ and porcine pancreatic *α*-amylase (EC 3.2.1.1, type VI-B) were obtained from Sigma-Aldrich Chemicals. Solvents and other reagents were of analytical grade.

2.2. Materials

Aerial parts of *A. pubescens* were collected in March 2018 from Ghardaïa, a region in southern Algeria, (Altitude, 450m). After identification, a voucher specimen (LBE 18/03) was deposited at the Herbarium of the Faculty of Natural and Life Sciences at the University of Frères Mentouri, Constantine 1. Aerial parts of *A. pubescens* were air-dried in the laboratory and stored before use in a dry place.

2.3. Preparation of Aqueous lyophilized extract

Twenty grams of dried raw material was immersed in 300 mL of hot distilled water and agitated for 30 min. The extract solution was filtered and lyophilized (LaBconco, FreeZone Benchtop Freeze Dryer) at −80 °C. The aqueous lyophilized extract (AQL; 3 g, 15% w/w) was stored at −20 °C until analysis.

2.4. Preparation of organic extracts

The dried raw material (200g) was immersed in 1000 mL of methanol for 24h at room temperature then filtered. The filtrate was evaporated at 37 °C until dryness to give the methanol extract (MeOH; 33.55 g, 16.7% w/w) then rinsed with a hot water. As previously described by Kandouli *et al.* (2017), the aqueous solution was treated with petroleum ether, ethyl acetate and *n*-butanol in sequence. In this way, the following extracts were produced: petroleum ether extract (PE; 2.13 g, 1.1 % w/w), ethyl acetate extract (EtOAc; 3.2 g, 1.5% w/w) and *n*-butanol extract (*n*-BuOH; 5 g, 2.5% w/w) and aqueous residual fraction (AR; 4 g, 2% w/w). Each fraction was stored at −20 °C until further analysis.

2.5. Determination of phenolic contents

The total phenolic content was determined using Folin–Ciocalteu assay (Singleton *et al.,* 1999). An aliquot of 160 µL extract solution (0.1 mg/mL) was mixed with 800 µL of Folin–Ciocalteu reagent (0.2 N). After 5 min, 640 µL of sodium carbonate (75 %, w/v) was added and incubated for 2h at room temperature. The absorbance was measured at 760 nm against a blank without extract. The TPC was calculated on the basis of the calibration curve of gallic acid and expressed as gallic acid equivalents (GAE), in milligrams per gram of dry weight.

2.6. Determination of flavonoid contents

The total flavonoid content was determined using $AlCl_3$ method (Kandouli *et al.,* 2017). Briefly, 600 µL of extract solution (0.5 mg/mL) was mixed with 600 µL of $AlCl_3$ (2%, w/v) solution in ethanol. The mixture was incubated for 1h at room temperature, and the absorbance was measured at 420 nm. The total flavonoid content was calculated on the basis of the calibration curve of quercetin and expressed as quercetin equivalents (QE), in milligrams per gram of dry weight.

2.7. HPLC Analysis of Phenolic Compounds

The HPLC analysis was conducted on an Agilent Technology HPLC system (Agilent 1260 Infinity Quaternary) and a UV/Vis detector (Diode Array Detector (DAD)) with an analytical column (Stable Bond C18 (Zorbax) (4.6 × 150 mm × 15 µm). The system was controlled by use of Open Lab software (Agilent Technologies). Samples were dissolved in methanol (2 mg/mL) and injected with a volume of 20 µL. The mobile phase was a gradient flow (0.8 mL/min) of Methanol (A) and Water (B) (H3PO4 0.07 %) with multi-step gradient elution conditions and a total run time of 60 min per sample applied as follow: (A) 0 min: 30%; (A) 45 min: 60%; (A) 50 min: 60%; (A) 51-60 min: 30%. For each fraction, amounts of phenolic classes were evaluated on the basis of the calibration curves of standards obtained at the maximum UV absorbances of hydroxycinnamic, flavonols and hydroxybenzoic classes. They were evaluated as caffeic acid equivalents (CAE), rutin equivalents (RUE) and gallic acid equivalents (GAE), in milligrams per gram of dry weight, respectively.

2.8. Antioxidant Activity

2.8.1. DPPH radical scavenging activity

The free radical scavenging activity of *A. pubescens* was assessed using DPPH method (Kandouli *et al.,* 2017). Extracts were dissolved in methanol and water with a range of final concentrations of 0.0125–0.8 mg/mL, then 40 µL of extract solution was added to 160 µL/well of DPPH solution (0.8 mM). The mixture was incubated for 30 min in the dark at room temperature and absorbance was measured at 517 nm using a microplate reader (Perkin Elmer Enspire, Singapore). The ability of the extracts to scavenge DPPH was expressed as a percentage of inhibition calculated using the following equation (1):

$$Inhibition\ (\%) = [100 \times (A_0 - A)/A_0] \quad (1)$$

Where A_0 is the absorbance of the control and A is the absorbance of the test extracts. IC_{50} value (the concentration needed to scavenge 50% of DPPH) was evaluated from a dose-response curve-fitting model.

2.8.2. ABTS radical scavenging activity

The anti-radical activity of different extracts from *A. pubescens* were assessed according to ABTS method reported by (Re *et al.,* 1999). In brief, 160 µL of ABTS (7 mM) was added to 40 µL of each sample prepared in methanol and water at different concentrations (0.0125–0.8 mg/mL, final concentration). The absorbance was measured at 734 nm after 10 min, then the percentage of inhibition was quantified using the previous equation (1). Where A_0 is the absorbance of the control and A is the

absorbance of the test extracts. IC_{50} value (the concentration needed to scavenge 50% of ABTS) was quantified from a dose-response curve-fitting model.

2.8.3. Galvinoxyl radical (GOR) scavenging activity

The Glvinoxyl radical cavenging activity of different extracts from *A. pubescens* were assessed according to the method of (Shi *et al.,* 2001) with slight modifications. In brief, 160 µL of a fresh galvinoxyl radical methanolic solution (0.08 mM) was added to 40 µL of different concentrations of each extract (0.0125–0.8 mg/mL, final concentration). The reaction mixture was kept at ambient temperature for 120 min, then the absorbance was read at 428 nm. The scavenging activity was calculated using equation (1) and IC_{50} value which represents the concentration of the extract needed to scavenge 50% of galvinoxyl radical, it was calculated from a concentration-response curve-fitting model.

2.8.4. Hydroxyl radical scavenging activity

Hydroxyl radical scavenging activity of AQL, *n*-BuOH and AR extracts was evaluated using the colorimetric assay reported by (Aruoma *et al.,* 1987). For this assay, aliquots (100 µL) of the following reagents (deoxyribose, $FeCl_3$, EDTA or buffer, H_2O_2 and ascorbic acid) were added with 500 µL of tested extract (0.025 to 0.25 mg/mL). After 1h of incubation at 37 °C, TBA and acetic acid were added, and the mixture was heated for 15 min at 100 °C. The absorbance was read at 532 nm, and mannitol (1−10 mM) was used as a reference. The inhibition percentage of hydroxyl radical scavenging activity by the extract in the presence or absence of EDTA was calculated using equation (1) mentioned previously; where A_0 is the absorbance of the control and A is the absorbance of the test extracts.

2.8.5. Metal Chelating Capacity

The chelating activity of samples with ferrous ions Fe^{2+} was determined following the ferrous iron–ferrozine complex method (Santos *et al.,* 2017) with some modifications. Briefly, 840 µL of extract solution (0.0125–0.8 mg/mL) was mixed with 80 µL of $FeSO_4$ (0.3 mM) and 40 µL of 0.8 mM of ferrozine. After 10 min, the absorbance was measured at 562 nm, and the MCC was evaluated using the calibration curve of EDTA. The results are expressed as micromoles of EDTA equivalents (ADTAE) per gram of dry weight.

2.8.6. Reducing power

The reducing power ability of the extracts was evaluated according to the method described by (Oyaizu, 1986). In this assay, 0.2 mL of sample solutions at various concentrations, 0.5 mL of phosphate buffer (0.2 M; pH 6.6) and 0.5 mL of potassium ferricyanide (1%) were mixed and incubated at 50 °C for 20 min. Then, 0.50 mL of trichloroacetic acid (10%) was added. After 10 min, 0.5 mL of the supernatant was mixed with 0.5 mL of distilled water and 0.2 mL of ferric chloride (0.1%). The absorbance was read at 700 nm. Increased values of absorbance indicate a high reducing power of the sample.

2.8.7. Cupric ion reducing antioxidant capacity

Cupric ion reducing antioxidant capacity of the extracts was determined using the method developed by (Apak *et al.,* 2007). The reaction consists of mixing 50 ml of copper chloride (10 mM), 50 ml of Neocuproine (7.5 mM) and 60 ml of ammonium acetate (1 M, pH 7.0) with 40 mL of the sample at different concentrations in a microplate of 96 wells. The microplate was allowed to incubate for 1h, and the absorbance was read at 450 nm. Increased values of absorbance indicate a high cupric reducing power of the sample.

2.8.8. Total antioxidant capacity

Total antioxidant capacity of the extracts was determined according to the method of (Prieto *et al.,* 1999). In this assay, 0.3 mL of each tested extract or ascorbic acid (standard) was mixed with 3.0 mL of the reagent solution (0.6 M sulfuric acid, 28 mM sodium phosphate and 4 mM ammonium molybdate). The reaction mixture was incubated at 90 °C for 90 min, and absorbance was measured at 695 nm. The antioxidant capacity was expressed as ascorbic acid equivalent (AAE) in µmol per gram of dry weight.

2.9. α-Amylase inhibitory activity

The capacity of α-amylase inhibition was performed according to the method proposed by (Zengin *et al.,* 2014). In each well of a 96 microplate, 25 µL of the tested extract at different concentrations (0.00625–0.4 mg/mL, final concentration) was added to 50 µL of α-amylase solution prepared in phosphate buffer (pH 6.9 with 6 mM sodium chloride). The mixture was then incubated for 10 min at 37°C. After incubation, 50 µL of soluble starch (0.1%) was added and plates were incubated for 10 min at 37 ◦C. Then, 25 µL of HCl (1M) was added to stop the reaction. The blank was prepared by adding extract solution to all reagents without enzyme solution. Finally, 100 µL of Iodine Potassium Iodide (IKI) solution were added, and the absorbance was measured at 630 nm. The absorbance of the blank was subtracted from that of the extract, and the inhibition percentage of α-amylase was calculated.

2.10. Statistical Analysis

Data Statistical analysis was carried out using GraphPad Prism software. The results are presented as mean ± SD for the indicated number of independent experiments. Evaluation of statistical significance was conducted by one-way analysis of variance (ANOVA), Newman-Keuls or a Pearson's correlation (r^2) coefficients calculations. A $p< 0.05$ was considered statistically significant.

3. Results and discussion

3.1. Extract Yields, TPC and TFC

Plant polyphenols present a several group of phenolic compounds that possess an ideal structural chemistry for radical scavenging activity. Phenolic compounds have been shown to be responsible for the antioxidant activity of plant materials (Rice-Evans *et al.,* 1996).The comparative data of extraction yield, TPC and TFC of different extracts from *A. pubescens* are presented in Table 1. The Extraction yields varied from 1.1% to 16.7% 9 (w/w) with the following order: MeOH ≥ AQL > *n*-BuOH > AR > EtOAc > EP. Broadly speaking, the extraction

yield was strongly influenced by the used solvent, and has significantly increased with the increase of solvent polarity which is consistent with the results of (Zhang *et al.,* 2014). Accordingly, a significant difference in the extraction yield (p<0.05) was recorded. Zhang *et al.* (2014) has also reported that performing different extraction methods for the same tested sample may lead to a significant difference in the extraction yield and antioxidant activity.

The total phenolics content (TPC) of various *A. pubescens* extracts was performed using the regression equation of the calibration curve ($y = 13.41x$, r^2:0.994). The highest TPC value of 335.9 mg GAE/g was detected in EtOAc extract, while PE and AR extracts recorded the lowest values (~70 mg GAE/g dw) which represent approximately 1/5 of EtOAc extract value. The TPC values in *A. pubescens* extracts ranged from 70 to 335.9 mg GAE/g dw (Table 1) in the following descending order: EtOAc > *n*-BuOH > AQL ≥ MeOH > EP ≥ AR (p< 0.05).

The total flavonoids content (TFC) of different *A. pubescens* extracts was quantified using the regression equation ($y = 24.83x$, r^2:0.993). The TFC ranged from 6 mg QE/ g dw, in AR extract to 165.4 mg QE/g dw, in *n*-BuOH extract (Table 1). There was no significant difference in TFC between AQL and MeOH extracts were registered (p>0.05), while *n*-BuOH and EtOAc extracts had the highest TFC with a significant difference (p< 0.05) compared to the other analysed extracts. Our results are significantly different from the findings of (Metrouh *et al.,* 2015), in which TPC and TFC were around ~26 mg GAE/g and ~9 mg QE/g, respectively. These results possibly reflect differences in plant drying procedures, geographical or the genetic background (Kandouli *et al.,* 2017).

Interestingly, TFC showed a low correlation with TPC (r^2= 0.695, p< 0.05), which is consistent with the work of Zou *et al.* (2011), who recorded a low correlation between TPC and TFC values when conducting a study on phenolic profile and antioxidant properties of lentil. Our results were also in correspondence with the literature of Meda *et al.* (2005), who reported that some chemical groups of proteins and amino acids present in plants are also able to react with Folin–Ciocalteu reagent. Several investigations have focused on the medicinal activities of phenolics as they are considered as powerful antioxidants and free radical scavengers. It has been also shown that the antioxidant capacity of phenolics including flavonoids is mainly attributed to their redox characteristics, acting as reducing agents, hydrogen atom donors or singlet oxygen quenchers (Leopoldini *et al.,* 2011; Kumar and Goel, 2019 and Rice-Evans *et al.,* 1996).

Table 1. Extraction Yield, Total Phenolic, Total Flavonoid and Phenolic compounds Contents in *A. pubescens* extracts.

Extract	Phenolic classes					
	Yield (% ,w/w)	TPC (mg GAE / g)	TFC (mg QE / g)	Hydroxycinnamates (mg CAE / g)	Flavonols (mg RUE / g)	Hydroxybenzoates (mg GAE / g)
AQL	14.9	115.6 ± 2.1*	84 ± 39 ‡	10.41 ± 1.72*	26.60 ± 0.59*	1.64 ± 0.04*
MeOH	16.7	121.5 ± 2.0*	79.3 ± 5.5‡	15.43 ± 1.71*	36.7 ± 0.75*	2.66 ± 0.8*
PE	1.1	73.06 ± 3.2§	15.0 ± 3.2*	1.11 ± 0.07§	9.21 ± 0.9§	5.37 ± 0.26‡
EtOAc	1.5	335.9 ± 8.9‡	150.2 ± 2.9#	50.08 ± 4.8‡	95.40 ± 1.38‡	16.71 ± 0.68§
n-BuOH	2.5	198.3 ± 7.3 #	165.4 ± 6.8#	42.46 ± 4.15#	102.31 ± 10.31‡	9.1 ± 0.41#
AR	2.0	70.1 ± 3.1§	6.0 ± 0.3§	4.25 ± 0.41§	nd	2.35 ± 0.19*

Values are represent the mean ± SD of 4–6 in tetraplicate (n=4). AQL, aqueous lyophilized extract; MeOH, methanolic extract; PE, petroleum ether extract; EtOAc, ethyle acetate extract; *n*-BuOH, *n*-butanolic extract; AR, aqueous residual extract. nd: not detected. Results followed by different symbols in the same column are statistically significant difference (p< 0.05) as measured by Newman-Keuls test.

3.2. Phenolic classes content

A. pubescens major components of its phenolic extracts were separated by analytical HPLC-DAD as described in materials and methods. Representative chromatograms are displayed in Figure 1. Since different phenolic classes comprise a considerable number of compounds, UV absorbance is the most common and convenient parameter for the quantitation of phenolic compounds. Table 1 (right panel) presents the three major classes, benzoates, hydroxycinnamates and flavonols of *A. pubescens*. These phenolic classes were identified by comparing retention times (t_R) and UV spectra of gallic acid (t_R = 4.3 min), caffeic acid (t_R = 11.15 min) and rutin (t_R = 25.6 min) at maximal absorption wavelengths of 280, 325 and 365 nm, respectively (Fig. 1). EtOAc and *n*-BuOH extracts revealed a higher content of total phenols, particularly higher absolute levels of flavonols (95.4-102.31 mg RUE/g), and hydroxycinnamates (42.46-52.08 mg CAE/g), but also still found in good yields in AQL and MeOH extracts, unlike PE and AR extracts which were found in weak amounts or even in traces. Small amounts of benzoates (1.64-16.74 mg GAE/g) were also identified in our tested extracts.

.

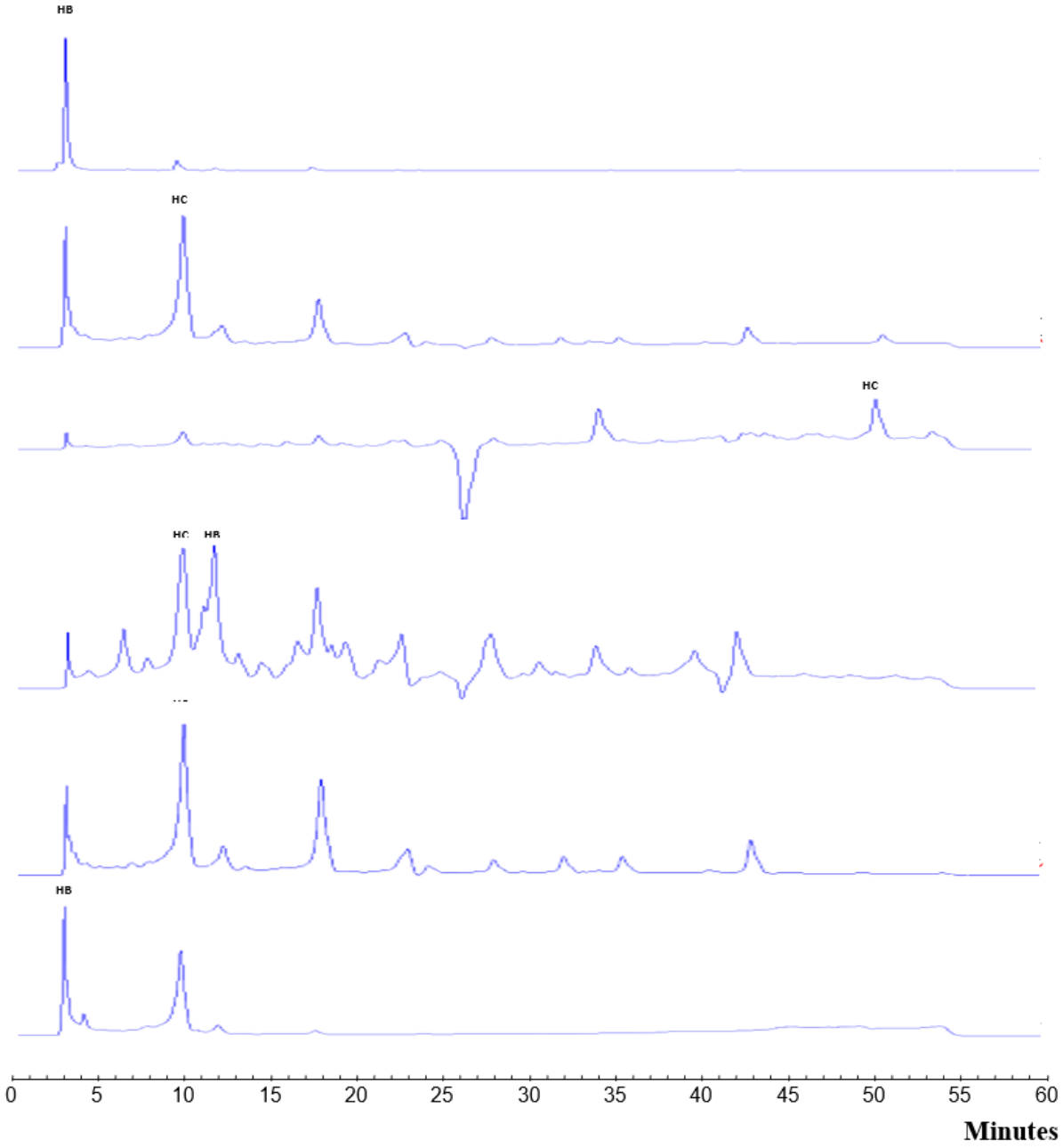

Figure 1. HPLC chromatograms of different extracts from *A. pubescens* recorded at 280 nm. (HB) hydroxybenzoates, (HC) hydroxycinnamates, (F) flavonols.

High correlation levels were registered between TPC and hydroxycinnamates (r^2 = 0.890) and benzoates (r^2 = 0,863), which suggests that hydroxycinnamates and hydroxybenzoates could considerably contribute to the total phenolic content in *A. pubescens*. Hydroxycinnamic acids are important phenolic acids present in plants. Due to their diverse health benefits including antioxidant, antiinflammatory, and anticancer properties, hydroxycinnamic acid derivatives are receiving a growing attention (Zhang *et al.,* 2014). Good correlation values were also rated between TFC and hydroxycinnamic acids (r^2 = 0.870), but also between TFC and flavonols (r^2 = 0.940), whereas benzoates showed an insignificant correlation (p> 0.05).

3.3. Antioxidant activity

A single assay approach is insufficient for assessment of antioxidant activity of polyphenolic compounds. Furthermore, the assay concept and experimental conditions vary between antioxidant assays. Antioxidant capacity may be examined by two main types of assays with various mechanisms, including hydrogen atom transfer (HAT) and electron transfer (ET). In ET-based assays, the capacity of antioxidants to transfer one electron to reduce any oxidant is measurable, while HAT-based assays measure the capacity of antioxidants to quench radicals by hydrogen donation.

3.3.1. DPPH, ABTS and GOR

The DPPH radical scavenging activity assay has been used frequently to evaluate natural antioxidant effects. One of the reasons is that this method is simple and very sensitive. This method depends on the capability of antioxidants to provide a proton or an electron to the DPPH radical (purple) to transform it to the non-radical form (yellow) (Apak *et al.,* 2016 and Foti, 2015). The

reduction ability of DPPH induced by antioxidants was evaluated by a decline in its absorbance at 517 nm. The scavenging ability of the *A. pubescens* extracts was found to increase in a dose dependent manner at a final concentration range of 0.0125-0.8 mg/mL. Figure 2 shows that the scavenging effect of samples on DPPH radical was in the following order: EtOAc ≥ *n*-BuOH ≥ AQL > MeOH > AR> EP. Our results demonstrated that the EtOAc and *n*-BuOH extracts exhibited much stronger scavenging activity with IC_{50} values of 43.3 and 62.2 µg/mL respectively, whereas PE and AR fractions have a weaker activity with IC_{50} values of 693.3 and > 800 µg/mL, respectively. Our values were about 17 to 53 times greater than those of methanol and water extracts reported in the study of (Metrouh *et al.,* 2015).

Furthermore, the extraction process performed in this study for preparing various extracts of *A. pubescens* significantly enhanced DPPH scavenging capacity. Similar studies also reported that *n*-butanol and ethyl acetate fractions of *A. radiata* (Kandouli *et al.,* 2017) and *R. anthopogonoides* (Jing *et al.,* 2015) revealed higher DPPH antioxidant activity than other extracts. In our study, the observed differential free radical scavenging effect of the plant extracts against DPPH process seems related to the occurrence of several compounds in the extract with potential antioxidant properties. Accordingly, the activities of EtOAc and *n*-BuOH extracts might be due to the chemical composition of phenolic compounds and the availability of phenolic hydroxyl groups, which have the capability to provide their electron/ hydrogen, thereby producing stable products.

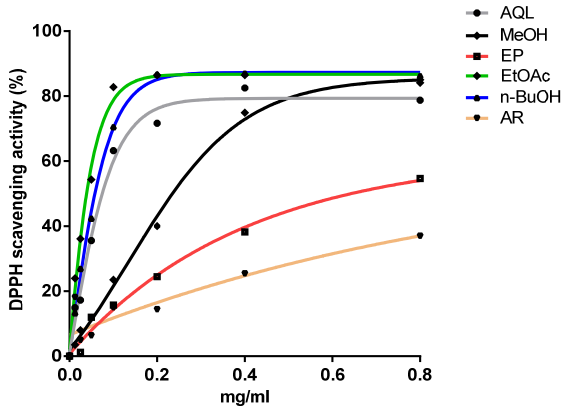

Figure 2. DPPH radical scavenging activity of different extracts from *A. pubescens*. Values represent the mean ± SD made in tetraplicate (*n*=4). AQL, aqueous lyophilized extract; MeOH, methanolic extract; PE, petroleum ether extract; EtOAc, ethyle acetate extract; *n*-BuOH, *n*-butanolic extract; AR, aqueous residual extract

DPPH antioxidant activity of *A. pubescens* extracts correlates significantly in a positive manner with TPC (r^2 = 0.852, $p< 0.01$) and with TFC (r^2 = 0.804, $p< 0.05$), suggesting their contribution in scavenging radicals. Similarly, hydroxycinnamates (r^2 = 0.817, $p< 0.05$) positively correlated with DPPH values. These results are consistent with Mitrevska *et al.* (2020), who demonstrated a good significant correlation between DPPH and phenolic extracts indicating the major contribution of phenolics to DPPH antioxidant activity.

Free radical scavenging process of different extracts from *A. pubescens* was performed using ABTS radical to corroborate the results obtained with DPPH method. ABTS assay is an excellent tool for determining the antioxidant activity of hydrogen-donating antioxidants and of chain-breaking antioxidants (Ozgen *et al.,* 2006). In the absence of antioxidants, the ABTS radical is rather stable, but it reacts actively with an hydrogen atom donor, and by that converted into a noncolored form of ABTS (Sachindra e*t al.,* 2007).

The IC_{50} values of tested extracts varied from 13.2 ± 1.8 to 641.3 ± 11 µg/mL. Figure 3 shows that ABTS radical scavenging activity of different extracts from *A. pubescens* was in the following order: EtOAc > *n*-BuOH ≥ MeOH ≥ AL > EP > AR, with the strongest antioxidant activity for EtOAc fraction and the weaker for the AR fraction. These results suggest that ethyl acetate fraction might contain the most potent free radical scavenger compounds. Our results are in agreement with findings of (Laouini *et al.,* 2016) and our IC_{50} values were 2500 times greater than those of methanol (16.21 mg/mL) and water (15.78 mg/mL) extracts reported in study of (Metrouh *et al.,* 2015). Sachindra *et al.* (2007) and Zou *et al.* (2011), reported that antioxidant compounds scavenging ABTS radical more efficiently compared to DPPH radical scavenging. Tang *et al.* (2010) also reported that ABTS was more sensitive than DPPH for the measurement of antioxidant potential of water-soluble proteins and peptides. These observations may be due to the fact that DPPH radical can be dissolved only in organic media. In contrast, ABTS radical can be solubilized in both aqueous and organic media (Arnao, 2000).

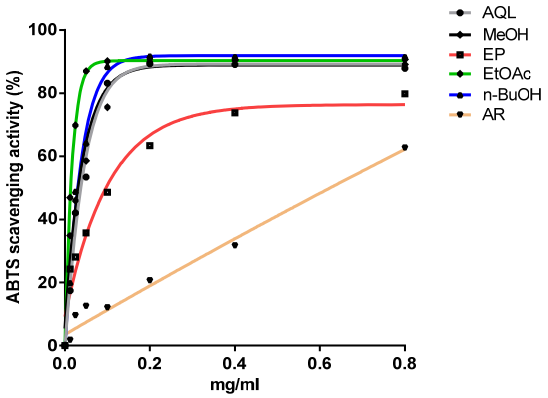

Figure 3. ABTS radical scavenging activity of different extracts from *A. pubescens*. Values represent the mean ± SD made in tetraplicate (*n*=4).

A highly significant correlation was shown between ABTS radical scavenging and TPC (r^2= 0.939, $p< 0.001$), indicating the great contribution of phenolics to radical scavenging capacity, which is consistent with the results of (Metrouh *et al.,* 2015). However, significant correlations were also established between ABTS radical scavenging and TFC, hydroxycinnamates, hydroxybenzoites and flavonols ($0.682 < r^2 < 0.779$, $p< 0.05$), suggesting that the antioxidant activity of tested extracts results mainly from the presence of molecules belonging to different phenolic classes.

Galvinoxyl, another stable phenoxyl radical can be reduced by hydrogen-donating free radical scavengers. Like the DPPH and ABTS results, IC_{50} values of Galvinoxyl radical (GOR) scavenging activity ranged widely from 14.1 to 611.6 µg/mL (Fig. 4). The highest

GOR scavenging activity values were observed in EtOAc and *n*-BuOH fractions with the values of 14.1µg/mL and 29.4µg/mL respectively, whereas the lowest value of 611.6µg/mL was observed in AR extract. However, galvinoxyl radical scavenging activity of *A. pubescens* extracts comparison was shown to be in the same order as ABTS and DPPH radical scavenging activity (EtOAc > *n*-BuOH > AQL > MeOH > EP > AR). According to the findings of this study, DPPH, ABTS and GOR were strongly inhibited by extracts which demonstrated moderate inhibition when compared to the standard compounds, BHT (IC_{50} ranges from 1.55±0.26 to 6, 55±0.59 µg/mL) and BHA (IC_{50} ranges from 5.38 ±0.06 to 15.74 ±0.47 µg/mL).

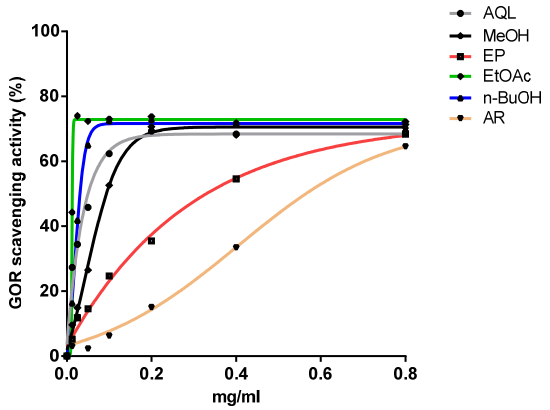

Figure 4. GOR radical scavenging activity of different extracts from *A. pubescens*. Values represent the mean ± SD made in tetraplicate (*n*=4).

This study showed that GOR values of *A. pubescens* extracts correlated significantly with TPC (r^2 = 0.991, p< 0.001), TFC (r^2 = 0.669, p< 0.05) and hydroxycinnamates (r^2 = 0.864, p< 0.01), indicating the contribution of phenolics to galvinoxyl radical scavenging activity and particularly hydroxycinnamates.

3.3.2. Hydroxyl radical scavenging activity

Hydroxyl radical is the most reactive ROS and attacks almost every molecule in the body, resulting in peroxidation of cell membrane lipids and in the formation of malondialdehyde, a mutagenic and carcinogenic product (Basu and Marnett, 1983). The results obtained of hydroxyl radical scavenging from deoxyribose degradation assay are presented in figure 5. In this assay, the radiomimetic method assesses the antioxidant potential of the extracts based on their capacity to compete with deoxyribose for hydroxyl radicals, that were generated free in solution from a Fe^{2+}-EDTA chelate (Halliwell *et al.,* 1987). Our results demonstrated that all of the three soluble extracts showed a concentration dependent radiomimetic hydroxyl scavenging activity. Moreover, the fact that *n*-BuOH (53.51%, 0.5mg/mL), AQL (39.18%, 0.5mg/mL) and AR (33.11%, 0.5mg/mL) extracts demonstrated significantly higher capabilities to prevent deoxyribose degradation compared to D-Mannitol (32.17%) at a concentration of 10 mg/mL (Fig. 5), which suggests the great capacity of *n*-BuOH, AQL and AR extracts to react with ·OH compared to D-Mannitol.

The hydroxyl scavenging activity method performed in the omission of EDTA is important because it evaluates the oxidative deoxyribose damage by site-specific production of hydroxyl radicals and offers information about *A. pubescens* soluble-extracts capability of chelating Fe ions. Thus, Fe chelator reduces the level of thiobarbituric-reactive substances (TBRS) generated from deoxyribose (Aruoma *et al.,* 1987). The activity of *n*-BuOH (30.92%), AR (25.26%) and AQL (24.78%) of inhibiting the site-specific damage to deoxyribose indicates their great capacity of Fe chelation compared to D-Mannitol (19.45%) (Fig. 5). Capacities of extracts in radiomimetic and site-specific indicate their potency as chelating agents as well as their ability to scavenge hydroxyl radicals, which are produced from a Fe^{2+} EDTA chelate (Singh *et al.,* 2007). The strong potency shown by *n*-BuOH extract could be related to its high amount of TPC and TFC. We can suggest that our results might be due to the active hydrogen donating ability of hydroxyl substitutions.

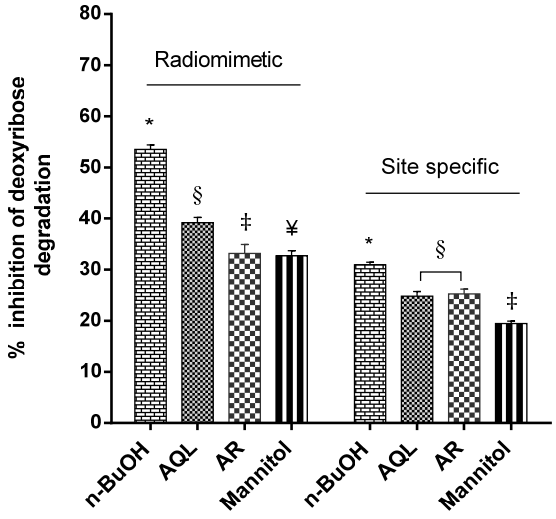

Figure 5. Hydroxyl radical scavenging activity of water soluble extracts of *A. pubescens* in the presence or absence of EDTA. Values represent the mean ± SD made in tetraplicate (*n*=4). Different symbols are statistically significant difference (p< 0.05) as measured by Newman-Keuls test.

3.3.3. MCC, Reducing Power, CUPRAC and TAC

$Fe^{2+/3+}$ and $Cu^{1+/2+}$, are critical biological molecules for normal body function. Dyshomeostasis of these metal ions could increase ROS production via Fenton-like reactions, resulting in increasing oxidative stress. The notion of redox reducing ability as an indicator of antioxidant activity may be used in different methods. There are several tests based on transitional metals (iron and copper), such as those using ferricyanide, ferrozine, or cupric ions. These metal transition assays were widely used in medical investigation, including thiol antioxidants and total antioxidant activity of biological fluids such as plasma, urine, etc (Munteanu and Apetrei, 2021).

Ferrous ion is a key transition metal ion responsible for the initiation of peroxidation in food and biological systems. In MCC assay ferrous ions form a complex with ferrozine, and the intensity of this complex purple color decreases in the presence of chelating agents. Lower absorbance indicates higher metal chelating activity. The MCC of the extracts was determined using the regression equation of the calibration curve ($y = 4.56x$, r^2:0.993), and the results were expressed as µmol EDTA equivalents per gram dry weight (Fig. 6). MCC values varied widely from

26.1 to 78.54 µmol EDTAE/g dw. The highest MCC values of 78.54, 61.93 and 62.8 µmol EDTAE/g, were detected in EP, AL and MeOH extracts respectively, whereas the lowest value of 26.1 µmol of EDTAE/g was observed with *n*-BuOH extract.

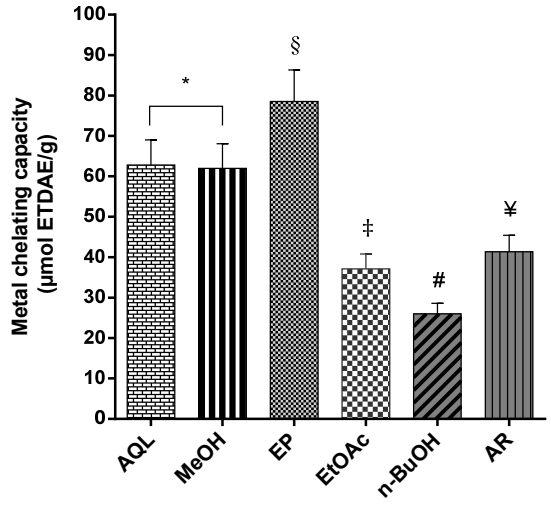

Figure 6. Metal chelating capacity (MCC) of different extracts from *A. pubescens*. Values represent the mean ± SD made in tetraplicate (n=4). Different symbols are statistically significant difference (p< 0.05) as measured by Newman-Keuls test.

Interestingly, MCC of *A. pubescens* correlated neither with TPC and TFC nor with DPPH, ABTS, and GOR (r^2 ranges from 0.181 to 0.404), which is consistent with previous findings which reported that a poor correlation existed between MCC, TPC and other antioxidant activities such as DPPH, ABTS and reducing power (Kandouli *et al.,* 2017 and Zhao *et al.,* 2008). Metal chelating potency of polyphenolic compounds are dependent upon their unique phenolic structure and the number and arrangement of hydroxyl groups (Khokhar *et al.,* 2003). The study conducted by Saiga *et al.,* (2003) showed that some peptides as well as proteins have also been reported to possess the ability to chelate metal ions, which is also believed to be the reason for EP and AQL extracts chelating capacity.

In the reducing power assay, the antioxidants present in a sample reduce the Fe^{3+} to Fe^{2+} by donating an electron and a blue colored Iron (II) complex is formed. We demonstrated that the reducing power ability of different extracts from *A. pubescens* increased in a concentration dependent manner. Values for fractions were in the following order: EtOAc > *n*-BuOH > AQL > MeOH> EP> AR. The increase in absorbance indicated an increase in reducing power due to the high antioxidant potential. The EtOAc and *n*-BuOH fractions showed a good reducing power with values of 0.314 ± 0.004 and 0.256 ± 0.001 at 0.2 mg/mL, respectively (Fig. 7). However, the EP and AR fractions demonstrated lower values. These findings may be explained by the high content of phenolics present in various fractions of *A. pubescens*. It has also been reported that reducing power is associated with antioxidant activity, and may serve as a significant reflection of the antioxidant potential (Oktay *et al.,* 2003).

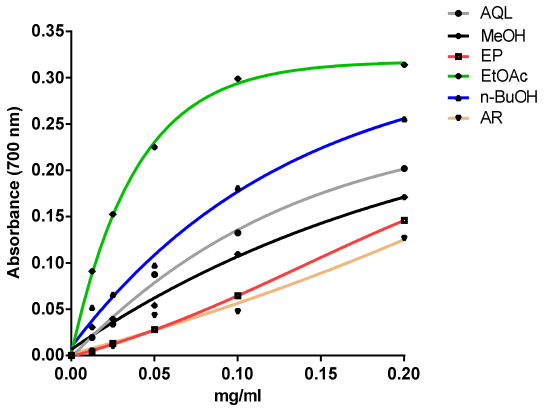

Figure 7. Reducing power activity of different extracts from *A. pubescens*. Values represent the mean ± SD made in tetraplicate (n=4).

The antioxidants donate their electrons in order to stabilize the radicals and also break the free radical chain reaction in the reducing power assay (Shabbir *et al.,* 2013). A positive relationship existed between reducing power and the different phenolic classes of TPC, TFC, hydroxycinnamates, hydroxybenzoites and flavonols ($0.749 < r^2 < 0.929$, p<0.01), suggesting their contribution in reducing power.

CUPRAC antioxidant capacity assay is a stable, rapid, selective and suitable for a wide variety of antioxidant types including both lipophilic and hydrophilic. It utilizes the copper (II)-neocuproine [Cu(II)-Nc] reagent as a chromogenic oxidizing agent at the basis of cupric reducing ability of reducing compounds to cuprous. Our obtained results in CUPRAC assay demonstrated a trend of antioxidant activity similar to the previous tests. As shown in figure 8, CUPRAC antioxidant activity of extracts is in the following order: n-BuOH > EtOAc > AQL≈ MeOH ≈ EP > AR. In this assay, a high absorption indicates high reducing power of cupric ions. The highest CUPRAC antioxidant activity values of 4.27 ± 0.04 and 3.96 ± 0.03 at 0.2 mg/mL, were observed in EtOAc and *n*-BuOH fractions respectively, whereas AR extract showed the lowest value of 0.43 ± 0.02 at 0.8 mg/mL, (Fig 8). Similar findings that reported an increase of cupric reducing ability in a dose dependant manner were demonstrated in different studies (Sharma and Adarsh, 2014).

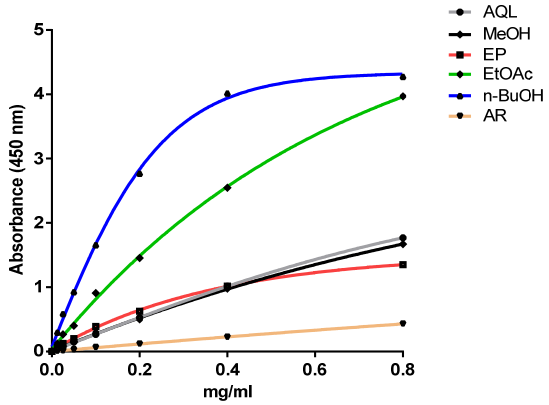

Figure 8. CUPRAC capacity of different extracts from *A. pubescens*. Values represent the mean ± SD made in tetraplicate (n=4).

In this study, CUPRAC assay results showed a significant positive correlation with TPC and TFC, hydroxycinnamates and flavonols ($0.737 < r^2 < 0.974$, $p < 0.01$), which is consistent with the results of (Jin *et al.,* 2012), suggesting that a significant correlation is detectable between CUPRAC and phenolic content levels in plant extracts. A recent report (Apak *et al.,* 2016) demonstrated that some bioactive compounds present in medical plants possessed high antioxidant capacity in the CUPRAC, that was due the number and position of the hydroxyl groups as well as the degree of conjugation of the whole molecule, which are important for easy electron transfer.

Total antioxidant capacity (TAC) of the extracts, expressed as the number of equivalent of ascorbic acid (AA), was obtained from the calibration curve ($y = 0.008x$, r^2:0.994). In this assay, Mo (VI) was reduced to Mo (V) by antioxidant effect of extracts in a concentration dependent manner. Results of TAC of the extracts are shown in figure 9. Total antioxidant capacity of different extracts of *A. pubescens* was in the order of EtOAc ≈ *n*-BuOH > AQL ≈ MeOH > EP ≈ AR. In this assay, high µmol AAE/g value indicates a high total antioxidant capacity. Accordingly, EtOAc and *n*-BuOH extracts demonstrated the highest values of activity (~455µmol AAE/g), while PE extract was 2 times less potent (~240 µmol AAE/g). Similar findings highlighting the potency of EtOAc and *n*-BuOH over methanol extracts in term of TAC have been already observed (Ahmed *et al.,* 2014 and Khatoon *et al.,* 2013).

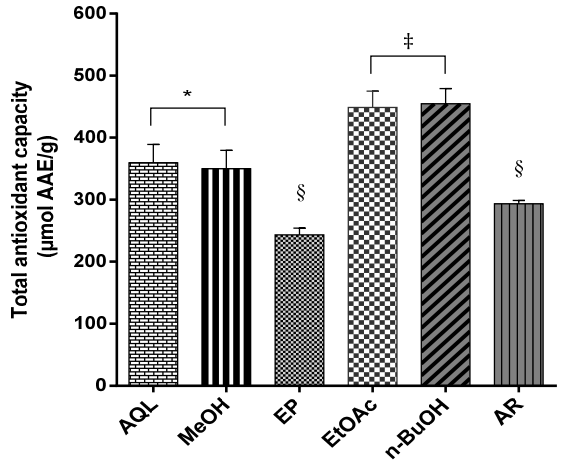

Figure 9. Total antioxidant capacity (TAC) of different extracts from *A. pubescens***.** Values represent the mean ± SD made in tetraplicate (n=4). Different symbols are statistically significant difference ($p < 0.05$) as measured by Newman-Keuls test.

Moreover, a good relationship existed between total antioxidant activity and TPC, TFC, hydroxycinnamates and flavonols ($0.711 < r^2 < 0.943$, $p < 0.01$). Many flavonoids and polyphenolics present in medicinal plants were reported to contribute significantly to the total antioxidant capacity (El Kamari *et al., 2021* and Afsar *et al.,* 2016). Our results are consistent with the research of Tung *et al.,* (2009) who reported that gallic acid, catechin, myricetin along with other polyphenols in *A. confusa* leaves extracts were responsible for the significant antioxidant potential.

3.4. α-Amylase inhibitory activity

Diabetes mellitus is mainly associated with hyperglycemia, which is characterized by high circulating blood glucose levels. α-Amylase inhibitors could retard the rate of maltose released from starch, resulting in delaying maltose conversion to glucose and lowering postprandial plasma glucose concentrations. The inhibitory activity of *A. pubescens* extracts against porcine α-amylase was evaluated in this study. As seen in figure 10, all extracts exhibited α-amylase inhibitory activity at the same concentration (12.5µg/mL). The highest α-amylase inhibitory activity values of 89.8 ± 0.7, 81.7 ± 3.2 and 72.3 ± 1.6 were observed in AQL, *n*-BuOH and EtOAc fractions respectively, whereas the lowest value of 36.8 ± 2.1 was observed with AR extract (Fig. 10). A 12.5 µg/mL concentration of acarbose inhibited enzyme activity by 8.08± 0.3%. α-amylase inhibitory activity of *A. pubescens* extracts was higher than the activity of acarbose at the same concentration. This study suggested that the plant has a very strong inhibition on α -amylase which may contribute to its demonstrated *in vivo* antidiabetic effect. Polyphenolic compounds have been discovered to form complexes with a wide range of proteins. Notably, previous research suggests that polyphenolic compounds, including flavonoids, may interact with amino acid residues in enzyme active sites or interact with amino acid residues near the active site, thereby closing the channel to the active site and inhibiting enzyme activity (Zhu *et al.,* 2020). It has been reported in different studies that phenolic compounds are effective α-glucosidase and α-amylase inhibitors (Dehimat *et al.,* 2021 and Zhu *et al.,* 2020).

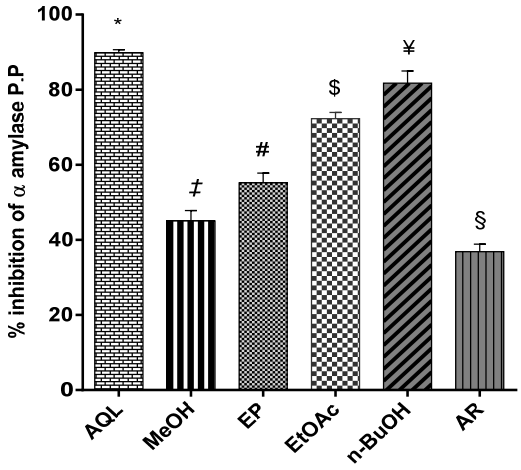

Figure 10. Inhibitory effect of different extracts from *A. pubescens* on α-Amylase**.** Values represent the mean ± SD made in tetraplicate (*n*=4). Different symbols are statistically significant difference ($p < 0.05$) as measured by Newman-Keuls test.

4. Conclusion

In conclusion, it should be emphasized that in the present study, chemical and biological examinations of six *A. pubescens* extracts were undertaken for the first time. The radical scavenging activity of the tested samples is due to flavonoids, phenolic acids and their derivatives. Therefore, *A. pubescens* may be an interesting alternative for the treatment of diabetes mellitus not only by inhibiting

an enzyme that is related to the disorder, but also by improving the antioxidant defenses of patients. The highest antioxidant activity and phenolic contents were exhibited by the EtOAc and *n*-BuOH extracts. These results suggest the use of EtOAc and *n*-BuOH fractions as primary antioxidant therapeutic sources. However, further investigation would be required to study such potential capacities, and to better understand their mechanisms of action related to the chemical composition of these extracts

Acknowledgments

We are grateful to Bensalem M, Boursas D, Cherfia H, Ramli I and Khalfaoui S for their valuable assistance.

Reference

Afsar T, Razak S, Khan MR, Mawash S, Almajwal A , Shabir M and Haq IU. 2016. Evaluation of antioxidant, anti-hemolytic and anticancer activity of various solvent extracts of *Acacia hydaspica* R. Parker aerial parts. *BMC Complement Med Ther*, **16**: 258-274.

Ahmed D, Fatima K and Saeed R. 2014. Analysis of Phenolic and Flavonoid Contents, and the Anti-Oxidative Potential and Lipid Peroxidation Inhibitory Activity of Methanolic Extract of *Carissa opaca* Roots and Its Fractions in Different Solvents. *Antioxidants,* **3**: 671-683.

Apak R, Güçlü K, Demirata B, Ozyürek M, Celik S E, Bektasoglu B, Berker KI and Ozyurt D. 2007. Comparative evaluation of various total antioxidant capacity assays applied to phenolic compounds with the CUPRAC assay. *Molecules,* **12**: 1496-1547.

Apak R, Ozyurek M, Guclu K and Capanoglu E. 2016. Antioxidant Activity/Capacity Measurement. 2. Hydrogen Atom Transfer (HAT)-Based, Mixed-Mode (Electron Transfer (ET)/HAT), and Lipid Peroxidation Assays. *J Agric Food Chem*, **6**4: 1028-1045.

Arnao MB. 2000. Some methodological problems in the determination of antioxidant activity using chromogen radicals: a practical . *Trends Food Sci Technol*, **11**: 419-421.

Aruoma OZ, Grootveld M and Halliwell B. 1987. The role of iron in ascorbate-dependent deoxyribose degradation. Evidence consistent with a site-specific hydroxyl radical generation caused by iron ions bound to the deoxyribose molecule. *J Inorg Biochem*, **29**: 289-299.

Basu AK and Marnett LJ. 1983. Unequivocal Demonstration That Malondialdehyde Is a Mutagen. *Carcinogenesis,* **4**: 331-333.

Benchelah AC, Bouziane H, Maka M and Ouahes C. 2000. Sahara flowers, Voyage ethnobotanique avec les Touaregs du Tassili. Ibis Press, Paris.

Boutaghane N, Kabouche A, Touzani R, Maklad YA, El-Azzouny A, Bruneau C and Kabouche Z. 2011. GC/MS analysis and analgesic effect of the essential oil of *Matricaria pubescens* from Algeria. *Nat Prod Commun*, **6**: 251-252.

Cherif HS, Ferrah R, Tail G, Bennacer A, Saidi F. 2017. Traditional use of *Matricaria pubescens* (Desf.) Schultz in two regions of southern Algeria and contribution to study the antioxidant activity. *IJTK*, **16**: 562-567.

Dehimat A, Azizi I, Baraggan-Montero V and Khettal B. 2*021. In vitro* antioxidant and inhibitory potential of leaf extracts of *Varthemia sericea* against key enzymes linked to type 2 diabetes. *Jordan J of Bio Scie*, **14**(1): 97 – 104.

El Kamari F, Ousaaid D, Taroq A, El Atki Y, Aouam I, Lyoussi B, and Abdellaoui A. 2021. Bioactive ingredients of different extracts of *Vitex agnus-castus L.* Fruits from Morocco and their antioxidant potential. *Jordan J of Bio Scie*, **14**(2): 267 – 270.

Foti MC. 2015. Use and Abuse of the DPPH• Radical. *J Agric Food Chem*, **63**. 8765-8776.

Halliwell B, Gutteridge JMC and Aruoma OI. 1987. The deoxyribose method: A simple "test-tube" assay for determination of rate constants for reactions of hydroxyl radicals. *Anal Biochem*, **165**: 215-219.

Hammiche V and Maiza K. 2006. Traditional medicine in Central Sahara: pharmacopoeia of Tassili N'ajjer. *J Ethnopharmacol*, **105**: 358-367.

Jin L, Zhang Y, Yan L, Guo Y and Niu L. 2012. Phenolic Compounds and Antioxidant Activity of Bulb Extracts of Six Lilium Species Native to China. *Molecules,* **17**: 9361-9378.

Jing L, Ma H, Fan P, Gao R and Jia Z. 2015. Antioxidant potential, total phenolic and total flavonoid contents of *Rhododendron anthopogonoides* and its protective effect on hypoxia-induced injury in PC12 cells. *BMC Complement Altern Med,* **15**: 287-299.

Kancheva VD and Kasaikina OT. 2013. Bio-antioxidants- a chemical base of their antioxidant activity and beneficial effect on human health. *Curr Med Chemi*, **20**: 4784-4805.

Kandouli C, Cassien M, Mercier A, Delehedde C, Ricquebourg E, Stocker P, Mekaouche M, Leulmi Z, Mechakra A, Thetiot-Laurent S, Culcasi M and Pietri S. 2017. Antidiabetic, antioxidant and anti inflammatory properties of water and n-butanol soluble extracts from Saharian *Anvillea radiata* in high-fat-diet fed mice. *J Ethnopharmacol***, 207**: 251-267.

Khatoon M, Islam E, Islam R, Rahman AA, Alam AH, Khondkar P, Rashid M and Parvin S. 2013 Estimation of total phenol and in vitro antioxidant activity of *Albizia procera* leaves. *BMC Res Notes,* **6**: 121-128.

Khokhar S, Richard K and Apenten O. 2003. Iron binding characteristics of phenolic compounds: some tentative structure-activity relations. *Food Chem,* **81**: 133-140.

Laouini SE, Berra D and Ouahrani MR. 2016. Solvent pH Extraction Effect on Phytochemical Composition and Antioxidant Properties of Algerian *Matricaria pubescens*. *J Pharm Res,* **10**: 106-112.

Leopoldini M, Russo N and Toscano M. 2011. The molecular basis of working mechanism of natural polyphenolic antioxidants. *Food Chem*, **125**: 288-306.

Liguori I, Russo G, Curcio F, Bulli G, Aran L, Della-Morte D, Gargiulo G, Testa G, Cacciatore F, Bonaduce D and Abete P. 2018. Oxidative stress, aging, and diseases. *Clin Interv Aging,* **13**: 757-772.

Makhloufi A, BenLarbi L, Moussaoui A, Lazouni HA, Romane A, Wanner J, Schmidt E, Jirovetz L and HÖferle M. 2015. Chemical composition and antifungal activity of *Aaronsohnia pubescens* essential oil from Algeria. *Nat Prod Commun,* **10**: 149-151.

Meda A, Lamien CE, Millog JO and Nacoulma OG. 2005. Determination of the total phenolic, flavonoid and proline contents in Burkina Fasan honey, as well as their radical scavenging activity. *Food Chem,* **91**: 571-577.

Metrouh AH, Duarte MMC and Maiza F. 2015 Solvent effect on total phenolic contents, antioxidant, andantibacterial activities of *Matricaria pubescens* . *Ind Crops Prod*, **67**: 249-256.

Mitrevska K, Grigorakis S, Loupassaki S and Calokerinos A. 2020. Antioxidant Activity and Polyphenolic Content of North Macedonian Wines. *Appl Sci,* **10**: 2010-2021.

Munteanu IG and Apetrei C. 2021. Analytical Methods Used in Determining Antioxidant Activity: A Review. *Int. J. Mol. Sci*, **22** : 3380-3410.

Naresh K and Nidhi G. 2019. Phenolic acids: Natural versatile molecules with promising therapeutic applications. *Biotechnol Rep,* **24**: 1-10.

Oktay M, Gulcin I and Kufrevioglu OI. 2003. Determination of in vitro antioxidant activity of fennel (Foeniculum vulgare) seed extracts. *Lebensm Wiss Technol,* **36**: 263-271.

Oyaizu M. 1986. Studies on products of browning reactions: Antioxidant activities of products of browning reaction prepared from glucosamine. *J Nutr,* **44**: 307-35.

Ozgen M, Reese RN, Tulio AZJ, Scheerens JC and Miller AR. 2006. Modified 2,2-azino-bis-3-ethylbenzothiazoline-6-sulfonic acid (abts) method to measure antioxidant capacity of Selected small fruits and comparison to ferric reducing antioxidant power (FRAP) and 2,2'-diphenyl-1-picrylhydrazyl (DPPH) methods. *J Agric Food Chem,* **54**: 1151-1157.

Prieto P, Pineda M and Aguilar M. 1999 Spectrophotometric quantitation of antioxidant capacity through the formation of a phosphomolybdenum complex: specific application to the determination of vitamin E. *Anal Biochem,* **269**: 337-341.

Ray PD, Huang BW and Tsuji Y. 2012. Reactive oxygen species (ROS) homeostasis and redox regulation in cellular signaling. *Cell Signal,* **24**: 981-990.

Re R, Pellegrini N, Proteggente A, Pannala A, Yang M and Rice-Evans C. 1999. Antioxidant activity applying an improved ABTS radical cation decolorization assay. *Free Radic Biol Med*, **26**: 1231-1237.

Rice-Evans CA, Miller NJ and Paganga G .1996. Structure-antioxidant activity relationships of flavonoids and phenolic acids. *Free Radic Biol Med*, **20**: 933-956.

Sachindra NM, Sato E, Maeda H, Hosokawa M, Niwano Y, Kohno M and Miyashita K. 2007. Radical scavenging and singlet oxygen quenching activity of marine carotenoid fucoxanthin and its metabolites. *J Agric Food Chem,* **55**: 8516-8522.

Saiga A, Tanabe S and Nishimura T. 2003. Antioxidant activity of peptides obtained from porcine myofibrillar proteins by protease treatment. *J Agric Food Chem*, **51**: 3661-3667.

Santos JS, Alvarenga Brizola, VR and Granato D. 2017. High-throughput assay comparison and standardization for metal chelating capacity screening: A proposal and application. *Food Chem,* **214**: 515-522.

Shabbir M, Khan MR and Saeed N. 2013. Assessment of phytochemicals, antioxidant, anti-lipid peroxidation and anti-hemolytic activity of extract and various fractions of Maytenus royleanus leaves. *BMC Complement Altern Med,* **13**: 143-156.

Sharifi-Rad M, Nazaruk J, Polito L, Morais-Braga MFB, Rocha JE, Coutinho HDM, Salehi B, Tabanelli G, Montanari C, Del Mar CM, Yousaf Z, Setzer WN, Verma DR, Martorell M, Sureda A and Sharifi-Rad J. 2018. Matricaria genus as a source of antimicrobial agents: From farm to pharmacy and food applications. *Microbiol Res,* **215**: 76-88.

Sharma S and Adarsh PV. 2014. Preliminary Phytochemical Screening and In Vitro Antioxidant Activities of *Parkinsonia aculeata* Linn. *Biomed Res Int*: 1-8.

Shi H, Noguchi N and Niki E. 2001. Galvinoxyl method for standardizing electron and proton donation activity. *Methods Enzymol,* **335**: 157-166.

Singh R, Singh S, Kumar S and Arora S. 2007. Free radical-scavenging activity of acetone extract/fractions of *Acacia auriculiformis* A. Cunn. *Food Chem,* **103**: 1403-1410.

Singleton VL, Orthofer R and Lamuela-Raventos RM. 1999. Analysis of total phenols and other oxidation substrates and antioxidants by means of FolinCiocalteu reagent. *Methods Enzymol,* **299**: 152-178.

Tang X, He Z, Dai Y, Xiong YL, Xie M and Chen J. 2010. Peptide fractionation and free radical scavenging activity of zein hydrolysate. *J Agric Food Chem*, **58**: 587-593.

Tung YT, Wu JH, Hsieh CT, Chen PS and Chan ST. 2009. Free radical-scavenging phytochemicals of hot water extracts of Acacia confusa leaves detected by an on-line screening method. *Food Chem,* **115**: 1019-1024.

Zengin G, Sarikurkcub C, Aktumseka A, Ceylana R and Ceylan O. 2014. Comprehensive study on phytochemical characterization of Haplophyllum myrtifolium Boiss. endemic to Turkey and its inhibitory potential against key enzymes involved in Alzheimer, skin diseases and type II diabetes. *Ind Crops Prod,* **53**: 244-251 .

Zhang L, Tu ZC, Yuan T, Wang H, Fu Z, Wen QH and Wang XQ. 2014. Solvent optimization, antioxidant activity, and chemicalcharacterization of extracts from *Artemisia selengnesis* Turcz . *Ind Crops Prod*, **56**: 223-230.

Zhao H, Fan W, Dong J, Lu J, Chen J, Shan L, Lin Yand Kong W. 2008. Evaluation of antioxidant activities and total phenolic contents of typical malting barley varieties. *Food Chem*, **107**: 296-304.

Zhu J, Chen C, Zhang B and Huang Q. 2020. The inhibitory effects of flavonoids on α-amylase and α -glucosidase. *Crit Rev Food Sci Nutr,* **60**: 695-708.

Zou Y, Chang SK, Gu Y and Qian SY. 2011. Antioxidant activity and phenolic compositions of lentil (*Lens culinaris* var. Morton) extract and its fractions. *J Agric Food Chem*, **59**: 2268-2276.

JJBS

Volume 15, Number 4,December 2022
ISSN 1995-6673
Pages 709 – 716
https://doi.org/10.54319/jjbs/150420

Jordan Journal of Biological Sciences

The Characteristics of Functional Analog Rice Made from Modified Arrowroot Starch and Corn Flour with Seaweed

Damat Damat[1,*], Roy Hendroko Setyobudi[2], Andalusia Trisna Salsabila[3], Effendi Andoko[4], Desiana Nuriza Putri[1], and Ririn Harini[5]

[1]*Department of Food Technology, Faculty of Agriculture and Animal Science, University of Muhammadiyah Malang, Jl. Raya Tlogomas No 246, Malang 65144, East Java, Indonesia;* [2]*Department of Agriculture Science, Postgraduate Program, University of Muhammadiyah Malang, Malang, 65145, East Java, Indonesia;* [3]*Department of Food Science, Faculty of Agriculture Technology, Postgraduate Program, IPB University, Gedung Fateta, Kampus IPB Darmaga PO Box 220, Bogor 16002, West Java, Indonesia;* [4]*College of Agriculture and Natural Resources, National Chung Hsing University, Agricultural Environment Science Building, South District, Taichung City, Taiwan 402;* [5]*Department of Nursing, Faculty of Health Sciences, University of Muhammadiyah Malang, Jl. Bendungan Sutami No. 188-A, Malang 65145, East Java, Indonesia*

Received: Sep 14, 2022; Revised: Oct 14, 2022; Accepted Oct, 18, 2022

Abstract

The modification of starch with the heat moisture treatment (HMT) method increases the level of type 3 resistant starch, which is used to develop functional foods such as analog rice. Therefore, this study aims to analyze the physicochemicals of analog rice made of modified arrowroot starch (*Maranta arundinacea* L.) and corn flour (*Zea mays* L.) with seaweed (*Gracilaria* sp.). It was conducted using a factorial randomized block design method of two factors. The first factor was the difference in the ratio of the composition of modified arrowroot and corn flour, which consisted of three levels, namely 30:70, 40:60, and 50:50. Meanwhile, the second factor was the concentration of seaweed porridge with three levels, namely 1 %, 2 %, and 3 %. The results showed that increasing the proportion of modified arrowroot starch and the concentration of seaweed porridge reduced water, fat, protein, and ash contents but increased analog rice resistant starch levels. Furthermore, the antioxidant activity of analog rice also increased after steaming. This study has proven that using modified arrowroot starch, corn flour, and the addition of seaweed can improve the functional properties of analog rice.

Keywords: Antioxidant activity, Artificial rice, Fitobentos, Functional food, *Gracilaria* sp., *Maranta arundinacea* L., Modified starch, *Zea mays* L.

1. Introduction

In Indonesia, the Central Statistics Agency stated that rice production decreased from 33.94 × 10^6 t in 2018 to 31.31 × 10^6 t in 2019 (Central Statistics Agency, 2020). This decline was caused by extreme weather in early 2019 and a long mid-year drought. Rice is the staple food for most Indonesians, as its consumption was 29.13 × 10^6 t in 2017 and is expected to increase with the population (Anggraeni, 2020).

The decline in rice production has forced the Indonesian goverment to import the commodity; meanwhile, people are being promoted to diversify their food to reduce importation. A food diversification product that has the potential to be developed is analog rice. It is a product in the form of rice but made from non-rice ingredients, with a carbohydrate content close to or exceeds the rice produced from local food flour and is cooked in the same way as rice (Damat *et al*., 2021; Mishra *et al.*, 2012; Wahjuningsih *et al*., 2018). Analog rice has almost the same or more nutritional content as rice and functional properties according to the raw materials used. On the other hand, it is an artificial product made from non-rice carbohydrate sources with high contents such as sweet potatoes [*Ipomoea batatas* (L.) Lam.], cassava (*Manihot esculenta* Crantz.), sago (*Cycas revoluta* Thunb.), sorghum [*Sorghum bicolor* (L). Moench.], and other ingredients (Sumardiono *et al*., 2014).

Several studies on analog rice that have been carried out include analog rice of composite flour (Sumardiono *et al.*, 2014), sorghum (Budijanto and Yuliana, 2015; Wahjuningsih *et al*., 2018; Wahjuningsih *et al*., 2018), taro [*Colocasia esculenta* (L.) Schott.] and seaweed (Wahjuningsih and Susanti, 2018), from sweet potato and carrot flour [*Daucus carota* subsp. sativus (Hoffm) Schübl. & G. Martens] (Anggraini *et al*., 2016), from sago flour and arrowroot starch (Pudjihastuti *et al*., 2019), from sweet potato flour, avocado (*Persea americana* Mill.) seeds, tofu pulp (Putri and Sumardiono, 2020), from sago and red beans (*Phaseolus vulgaris* L.) (Wahjuningsih *et al*., 2020), and analog rice from corn flour and seaweed grass (*Gracilaria* sp.) (Purwaningsih *et al*., 2020). However, there are no studies on analog rice made from a mixture of modified arrowroot starch using the heat moisture treatment (HMT) method and corn flour with seaweed porridge as a source of antioxidants.

Therefore, this study used modified arrowroot starch to increase resistant starch content in analog rice. Resistant

* Corresponding author. e-mail: damat@umm.ac.id.

starch is the fraction that resists hydrolysis of digestive enzymes and can be approximately 22.56 % in arrowroot starch (Astuti *et al*., 2018). The compact structure of resistant starch molecules also prevents digestive damage by enzymes, namely blood glucose; hence, it is considered suitable for people with diabetes (Damat, 2013; Damat *et al*., 2019; Ferng *et al*., 2016; Joslowski *et al*., 2015; Saari *et al.,* 2017).

Corn flour is added to improve the shape of the rice lost during cooking and reduce the stickiness because of the high content of 4.93 % fat in white corn flour (Hidayat *et al*., 2017). Furthermore, composite components can be added to manufacture artificial rice as needed.

Seaweed is the primary source of hydrocolloids and contains functional components such as high dietary fiber, which absorbs water and binds glucose. Therefore, it reduces glucose availability and stabilizes and lowers blood glucose in the body (Carlson *et al*., 2018). It is also rich in antioxidants, nucleic acids, amino acids, and vitamins A, B, C, D, E, and K (Khan *et al*., 2019; Rocha *et al*., 2019). A previous study showed that seaweed is an abundant source of antioxidants such as carotenoids, pigments, and polyphenols, with various polysaccharides (Sreejamole and Greeshma, 2013). Antioxidants are chemical compounds that play an essential role in protecting cells due to attacks from free radicals that cause damage (Damat *et al*., 2020; Queralt *et al*., 2015; Setyobudi *et al*., 2019; Setyobudi *et al.*, 2022). Therefore, the use of seaweed flour is expected to increase the functional properties of analog rice. The aim of this study is to determine analog rice made from modified arrowroot starch, corn flour, and seaweed porridge as well as analyze the physicochemical of antioxidant-rich.

2. Materials and Methods

2.1. Preparation of study materials

The materials used in the manufacturing of analog rice included arrowroot starch from farmers in Junrejo District, Batu City, East Java, corn flour from CV Makmur Sejati Malang, East Java. Arrowroot starch is made from arrowroot tubers, and prepared using the Damat *et al*., (2019) method. *Gracilaria* sp. type seaweed from CV Agar Sari Jaya Malang, East Java. Glycerol monostearate (GMS) – one stearyl for one glycerol – (Pro Analytic), and water. Other materials used in this study were a solution of H_2SO_4 (Pro Analytic, Merck), Na_2SO_4 (Pro Analytic, Merck), HgO (Pro Analytic, Merck), distilled water, boric acid (Pro Analytic, Smartlab), HCl (Pro Analytic, 37 %, Merck), petroleum benzene (Pro Analytic, Merck), ethanol 96 % (Technical), and DPPH (Pro Analytic, Merck), Bovine serum albumin (BSA) (Sigma-Aldrich), and NaOH.

2.2. Preparation of seaweed porridge

Seaweed (*Gracilaria* sp.) was dried, sorted, and cleaned of dirt such as salt, sand, shellfish, and other impurities by washing, repeatedly. A total of 100 g of seaweed was soaked in 2 L of solution for 24 h, containing whiting (1.5 % w v^{-1}), rice flour (2.5 % w v^{-1}), and lime juice (0.3 % v v^{-1}). Next, the neutralization process was carried out by washing the seaweed in running water, followed by soaking the seaweed in a 25 % alum solution for 4 h to remove the fishy smell.

The size of the seaweed was reduced to one cm after obtaining clean and odorless seaweed. Subsequently, the seaweed was mashed using a Blender Maspion Set MT 1206 with the addition of 1:1 water. Finally, the delicate seaweed was heated for 15 min at a temperature of 50 °C to 60 °C.

2.3. Arrowroot starch modification

Modification of starch using the heat moisture treatment (HMT) was carried out using the method by Liu *et al*. (2016). After adding distilled water, the water content became 30 %, and the sample was left at 4 °C for 24 h in a closed container. Next, the samples were heated at 105 °C for 16 h using the UN-55 Memmert Universal Drying Oven and cooled to room temperature. Furthermore, the samples were dried using a cabinet dryer type AM-TD12 at 40 °C until the water content was less than 10 % (db). After drying, the starch was crushed and sifted using a 100 stainless mesh sieve.

2.4. Preparation of analog rice

The analog rice preparation implemented extrusion technology, where modified arrowroot starch and corn flour were mixed, with the composition according to the treatment. The mixture was added with 1 %, 2 %, and 3 % of seaweed porridge and 20 % (w v^{-1}) water. Subsequently, the mixture was steamed using a Maspion SKU 15448 steamer for 30 min at 80 °C and later molded into rice grains using the Barata Indonesia extruder model BA-05. Finally, the analog rice grains were dried in a Maksindo drying cabinet at 50 °C for 20 h.

Table 1. Formulation of analog rice

Treatment	The proportion of modified arrowroot starch:corn flour	Seaweed porridge (% v w^{-1})
R1C1	30:70	1
R2C1	40:60	1
R3C1	50:50	1
R1C2	30:70	2
R2C2	40:60	2
R3C2	50:50	2
R1C3	30:70	3
R2C3	40:60	3
R3C3	50:50	3

2.5. Analysis of physicochemical properties of analog rice

The physicochemical properties of analog rice included analysis of water content, fat content using Soxhlet, protein content using the Kjeldahl method, and carbohydrate content using the method McCleary *et al.* (2020). In addition, the fiber content of analog rice was analyzed using the Yu *et al*. method (Yu *et al*., 2014). In contrast, the levels of resistant starch were analyzed using the method described by McCleary (McCleary *et al*., 2020).

2.6. Antioxidant activity analysis

The antioxidant activity test was conducted using the Saluri and Tuvikene method (Saluri and Tuvikene, 2020). In this study, 25 g of analog rice was added to 1 mL of 90 % m methanol (MeOH) 0.56 acetic acid and mixed for

1 min on sonication by centrifugation at 3×10^3 rpm for 10 min (1 rpm = 1/60 Hz), which was used as the supernatant. Subsequently, 0.2 mL of the samples from each treatment was taken with a measuring pipette, put in a test tube, and 3.8 mL of previously prepared 500 µM DPPH solution was added. The solution was homogenized with a Vortex Mixer model no. VM-300 and incubated in a dark room for 30 min. The sample was adsorbed using a UV-Vis spectrophotometer Shimadzu UV-1800 with a maximum wavelength of DPPH. Meanwhile, the antioxidant activity of examples that have reacted with free radicals from DPPH is determined using the Equation (1) below:

$$\% \text{ Inhibition} = \frac{\text{Abs.blank} - \text{Abs.sample}}{\text{Abs.blanko}} \times 100 \% \quad (1)$$

Notes:

Abs. Blank = Absorbancy of DPPH 50 µ

Abs. Sample = Absorbancy of the sample

2.7. 4 Resistant starch determination

As described by McCleary *et al.* (2020), the resistant starch was determined using the 2002.02 AOAC method. A sample of 0.50 g was weighed into a screw cap test tube measuring 16 mm × 125 mm, and 4 mL of pancreatic amylase solution (10 mg mL^{-1}) (3 µ mL^{-1} amylo-glucosidases/sodium azide 0.03 %) was added to each sample. The tubes were closed and incubated at 37 °C with continuous shaking at 100 rpm for precisely 16 h to allow the dissolution of non-resistant starch and hydrolysis to D-glucose.

The reaction was stopped by adding 4 mL of absolute ethanol, and the resistant starch was removed by centrifugation (2 000 × *g*, 10 min at room temperature). Furthermore, the pellets were washed twice with 8 mL 50 % ethanol at 4 °C and centrifuged (2 000 × *g,* 10 min at room temperature), which was later dissolved by adding 2 mL of 2 M KOH and stirred evenly. The solution was neutralized with 8 mL of 1.2 M sodium acetate buffer (pH 3.8), and 0.1 mL of amyloglucosidase was immediately added. The sample was incubated at 50 °C and shaken for 60 min, and the content of the tube was diluted at 1:10 with distilled water. The supernatant from each solution was centrifuged (1 500 × *g*, 10 min), and the 40 L supernatant was mixed with a 1.2 mL glucose oxidase-peroxidase-4-amino antipyrine reagent (megazyme resistant starch assay, Megazyme International Ireland Ltd., Co. Wicklow, Ireland) and incubated at 50 °C for 20 min. The supernatant was further calibrated using a spectrophotometer (Shimadzu UV-1800) at a wavelength of 510 nm.

2.8. Study design

This study used a randomized block design with Duncan's follow-up test. Data analysis was performed using SPSS-IBM 18 (Adinurani, 2016). Each experimental treatment was repeated three times.

3. Results and Discussion

3.1. Raw material analysis

In this study, the raw materials used included modified arrowroot starch, corn flour, and seaweed (*Gracilaria* sp.). Based on the proximate analysis of raw materials shown, the moisture content of modified arrowroot starch, corn flour, and seaweed are 7.02 %, 9.18 %, and 87.30 %. Respectively, moisture content plays an essential role in determining the material's shelf life. Since seaweed has a relatively high moisture content, storage was carried out at cold temperatures (5 °C). Therefore, storage at low temperatures can prevent the growth of bacteria and fungi and inhibit metabolism and chemical reactions (Frau *et al*., 2021). Each material's ash content, such as modified arrowroot starch, corn flour, and seaweed, ranged from 0.18 % to 0.65 %. Meanwhile, the highest ash content was discovered in seaweed, which showed that it has the highest mineral content.

The fat content of the ingredients ranged from 1.98 % to 3.46 %, where the corn flour has the highest, which is discovered in many parts of the treatment (Hidayat *et al*., 2017). Protein is among the macronutrients needed in the body, while its content in the material ranged from 0.86 % to 3.55 %, whereas seaweed had the highest. Furthermore, the carbohydrate content in the material ranged from 6.13 % to 91.49 %, and the lowest was in seaweed.

3.2. Proximate composition of analog rice

The results of the proximate analysis of analog rice are shown in Table 2.

Table 2. Proximate analysis of analog rice

Treatment	Water content (%)	Ash content (%)	Fat content (%)	Protein content (%)	Carbohydrate content (%)
R1C1	13.56^{h}	0.51^{c}	0.81^{g}	0.44^{bc}	85.09^{a}
R2C1	10.62^{g}	0.46^{b}	0.73^{de}	0.46^{bcd}	87.80^{b}
R3C1	10.14^{f}	0.48^{bc}	0.66^{c}	0.38^{ab}	88.40^{c}
R1C2	9.85^{e}	0.33^{a}	0.76^{f}	0.44^{bc}	88.70^{d}
R2C2	9.45^{c}	0.52^{d}	0.71^{d}	0.30^{a}	88.94^{e}
R3C2	8.20^{b}	0.52^{d}	0.58^{b}	0.37^{ab}	90.17^{f}
R1C3	9.63^{d}	0.56^{e}	0.75^{ef}	0.49^{cd}	88.58^{c}
R2C3	8.06^{a}	0.52^{d}	0.66^{c}	0.55^{d}	90.03^{f}
R3C3	9.44^{c}	0.51^{cd}	0.40^{a}	0.50^{cd}	88.77^{de}

Note: The average value followed by the same letter showed that it was not significantly different from the 5 % DMRT test.

Water content was one of the essential factors in the manufacture of analog rice because high water content easily damages the analog rice. Based on the analysis of variance, there was an interaction between differences in flour composition and the addition of seaweed porridge. The water content test ranged from 8.06 % to 13.56 %, where the highest was in the proportion of modified arrowroot starch: corn flour, in a ratio of 30:70, with 1 % seaweed porridge. The lowest water content was from the formulation of 40 % modified arrowroot starch, 60 % corn flour, and 3 % seaweed porridge. All treatments applied fulfilled the Indonesian National Standard (SNI 6128-2015), with the maximum water content of milled rice being 14 % (Anggraini, 2020).

Ash content in analog rice was also an indicator of the number of mineral elements (Wahjuningsih and Susanti, 2018). The results showed an interaction between differences in flour composition with the addition of seaweed porridge. The ash content of analog rice ranged from 0.33 % to 0.56 %, where the highest was discovered

in the proportion of modified arrowroot starch:corn flour, in a ratio of 30:70 with seaweed porridge 3 % to 0.56 %. Meanwhile, the lowest was in the proportion of modified arrowroot starch: corn flour, in a ratio of 30:70, with the addition of 2 % seaweed porridge of 0.33 %. Although according to Chan and Matanjun (2017) seaweed (*Gracilaria* sp.) contained an ash content of 8.09 %, another study showed that seaweed had vitamins, amino acids, nucleic acids, and macro minerals such as calcium and iodine (Rocha *et al*., 2019). Meanwhile, it is assumed that seaweed contained minerals, specifical iodine as a trace element, and and also ash content of 3.24 %. Modified arrowroot starch contained 0.21 % ash content (Astuti *et al*., 2018), while in this study its value was 0.65 %.

Fat is a compound that is insoluble in water but soluble in organic solvents. In this study, there was an interaction between differences in flour composition with the addition of seaweed porridge. The fat content of analog rice ranged from 0.40 % to 0.81 %, and the highest content was discovered in the proportion of modified arrowroot starch:cornflour in a ratio of 30:70 with a 2 % seaweed porridge of 0.81 %. Meanwhile, the lowest was in the proportion of modified arrowroot starch: corn flour in a ratio of 50:50 with 1 % seaweed porridge. Corn flour contained fat of 4.93 % (Hidayat *et al*., 2017). In addition, the source of fat in analog rice came from the GMS, which is derived from oil palm and prevents extrudates from sticking to each other (Damat *et al*., 2019). The fat content in corn flour can be used as a lubricant in the extruder, which facilitates the formation of the dough (Hidayat *et al*., 2017).

Protein is one of the crucial macronutrients that the body needs (Setyobudi *et al*., 2019, 2021). In this study, there was an interaction between the differences in flour composition with the addition of seaweed porridge. Furthermore, the protein content of analog rice ranged from 0.30 % to 0.55 %, where the highest was discovered in the proportion of modified arrowroot starch:corn flour in a ratio of 30:70 with 3 % seaweed porridge of 0.55 %. Meanwhile, the lowest was in the proportion of modified arrowroot starch: corn flour in a ratio of 50:50 with an additional 3 % seaweed porridge of 0.30 %. The amount of protein used was 3.55 %, different from the 16.83 %, a study by Zhang *et al*. (2020). A previous study by Chan and Matanjun (2017) suggested that *Gracilaria* sp. contained a minimum of 0.3 % protein. The protein content was much lower than milled rice because the analog rice raw materials of starch and flour were also low in protein.

Carbohydrates are the primary source of energy that the body needs for activity. The results showed that the carbohydrate content of analog rice ranged from 84.57 % to 90.32 %. There was an interaction between differences in flour composition with the addition of seaweed porridge. Furthermore, the carbohydrate content of analog rice ranged from 84.57 % to 90.32 %, with the highest content in the modified arrowroot starch:corn flour in a ratio of 40:60 with 2 % seaweed pulp of 90.32 %. However, the lowest was in the proportion of modified arrowroot starch:corn flour in a ratio of 30:70 with 1 % seaweed porridge of 84.06 %. The carbohydrate content in analog rice was relatively high because of the source, which was the raw materials in starch and flour. All treatments still had carbohydrate levels above milled rice, which is 78.90 % (Anggraini, 2020).

Antioxidants are compounds that counteract free radicals, and in this study the moderate antioxidant activity of pre-cooked rice was lower than cooked rice. Also, there was an interaction between differences in flour composition with the addition of seaweed porridge. Based on the results, the antioxidant activity of pre-cooked rice ranged from 20.18 % to 26.79 %, while cooked rice ranged from 34.38 % to 43.91 %. The highest antioxidant activity of pre-cooked rice was discovered in the proportion of modified arrowroot starch:corn flour in a ratio of 40:60 with 1 % seaweed porridge of 26.79 %. Meanwhile, the lowest was in the proportion of modified arrowroot starch:corn flour in a ratio of 30:70 with the addition of 3 % seaweed pulp of 20.18 %. Similarly, the highest antioxidant activity in cooked rice was in the formulation of modified arrowroot starch: corn flour in a ratio of 30:40 with the 3 % seaweed porridge of 43.91 % while the lowest was in proportion with a ratio of 40:30 with the addition of 1 % seaweed porridge of 34.38 %. The results of the antioxidant activity are shown in Table 3.

Table 3. Antioxidant activity of analog rice, steamed rice from analog rice, and resistant starch (RS) content of analog rice

Treatment	Antioxidant activity (%) of pre-cooked rice	Antioxidant activity (%) of cooked rice	RS Content (%)
R1C1	25.54±0.28^{e}	34.38±0.26^{a}	10.74±0.07^{a}
R2C1	26.79±0.06^{f}	37.57±0.02^{c}	12.23±0.07^{b}
R3C1	26.11±0.12^{ef}	36.39±0.31^{b}	14.23±0.39^{d}
R1C2	22.89±0.26^{bc}	38.65±0.28^{d}	13.55±0.19^{c}
R2C2	23.93±0.36^{d}	38.65±0.18^{d}	14.78±0.78^{e}
R3C2	23.67±0.17^{cd}	40.3±0.211^{f}	16.52±0.18^{g}
R1C3	20.18±0.57^{a}	38.19±0.05^{d}	15.88±0.06^{f}
R2C3	23.46±0.27^{cd}	43.91±0.06^{g}	16.51±0.04^{g}
R3C3	22.37±0.42^{b}	39.74±0.26^{e}	17.81±0.18^{h}

Note: The average value followed by the same letter showed that it was not significantly different from the 5 % DMRT test.

Analog rice becomes a functional food category when it contains active compounds that benefit the body. In addition to beta-carotene, other sources of antioxidants also came from the addition of seaweed, which contained enzymes, pigments, carotenoids, tannins, flavonoids, terpenes, steroids, and polysaccharides in high amounts (Sreejamole and Greeshma, 2013). Meanwhile, a previous study showed that there were 1 776 µg of carotenoids from 100 g of algae (Rocha *et al*., 2019). The antioxidant activity decreased by an increase in the concentration of seaweed since antioxidant compounds such as pigments, carotenoids, and flavonoids were still in the cells and did not come out entirely due to a cell wall in seaweed. The increase in seaweed reduced the proportion of other projected ingredients and also contained antioxidants such as corn flour.

After the gelatinization process occurs, the antioxidant content of seaweed reaches the maximum point. The antioxidant compounds such as phenolic compounds in cell walls ruptured due to heat generated from collisions and friction between material particles (Chan *et al*., 2015; Chan and Matanjun, 2017). The heating process breaks the

cell walls of seaweed for the antioxidants to be maximized due to its hemicellulose degradation (Rocha *et al*., 2019). According to Verni *et al*. (2019), the lowest antioxidant activity was obtained at a temperature of 5 °C at pH 12. Only a small amount of antioxidant compounds was extracted due to the difficulty in penetrating the cell wall. In addition, corn flour used in the manufacturing of analog rice was a source of antioxidants. Corn contains beta-carotene, a type of antioxidant (Setyobudi *et al*., 2019, 2021). Carotenoid pigments can also scavenge peroxyl radicals, be converted into carotenoid peroxide radicals, and are easily decomposed, so they are not harmful to live cells (Sedjati *et al*., 2020).

3.3. Resistant starch (RS) content of analog rice

The body needs resistant starch (RS) to maintain digestive health (Damat *et al*., 2019; Setyobudi *et al*., 2022). Based on the results, there was an interaction between differences in the composition of modified arrowroot starch: cornflour and the addition of seaweed porridge on the levels of analog rice resistant starch. Resistant starch levels in analog rice ranged from 10.74 % to 17.81 % (Table 3), which increased with the increasing proportion of modified arrowroot starch. The highest RS content was discovered in analog rice with the formulation of modified arrowroot starch: cornflour in a ratio of 50:50 and 3 % seaweed porridge. Meanwhile, the lowest was in the formulation with a ratio of 30:70 and 1 % seaweed porridge, which was 10.74 % due to the addition of modified arrowroot starch.

Analog rice with high levels of resistant starch (RS) can be developed into functional food. In the large intestine, it is fermented by lactic acid bacteria (LAB) to produce several types of short-chain fatty acids (SCFA), which have good effects (Damat, 2013; Wahjuningsih and Susanti, 2018). Food products with much resistant starch are digested slowly to reduce postprandial sugar levels (Damat *et al*., 2021).

The modified arrowroot starch granules were of 88 591 µm, which is larger than the natural ones (Damat *et al*., 2021). Meanwhile, changes in the size of starch granules can cause an increase in the content of resistant starch and decrease its digestibility (Pasquale *et al*., 2021). This occurance was due to the incorporation of amylose in the cooling process to form crystals different from natural starch. In addition, starch modified by HMT, followed by cooling, made the surface of the starch grains uneven as an effect of passing through gelatinization and retrogradation, causing changes in structure, viscosity, solubility, and swelling power (Dundar and Gocmen, 2013; Lin *et al*., 2020; Liu *et al*., 2016; Tako *et al*., 2014). Therefore, starch becomes more heat and shear-resistant, which causes a lower viscosity (Dhital *et al*., 2017). In addition, modification of starch by HMT also leads to the formation of type 3 resistant starch (Espinosa-Solis *et al*., 2021).

The use of modified arrowroot starch can cause an increase in the granule size of analog rice. The granule size increases with the proportion of modified arrowroot starch added (Damat *et al*., 2021) due to differences in granule size and resistant starch content in analog rice. Similar results were also described by Ratnaningsih *et al*. (2019) which showed that the ability of enzymes to hydrolyze starch is influenced by amylose, resistant starch, and granule size. Food products with a high resistant starch (RS) content have a hypoglycemic effect and a low glycemic index (Aprianita *et al*., 2014; Vrancheva *et al*., 2020). Aforementioned qualities are why the products are called functional foods.

In analog rice, resistant starch levels increase with the addition of seaweed, a dietary fiber source. It has been discovered that seaweed (*Gracilaria* sp.) contained 9.76 % (% w w^{-1}) dietary fiber and 29.94 mg L^{-1} iodine (Chan and Matanjun, 2017). Dietary fibers in cooked rice are smaller than in raw rice because it contains a higher water content. Furthermore, cooked rice passes through a starch gelatinization process which causes the starch granules to expand due to the entry of water, and the result is irreversible (Astuti *et al*., 2018). Therefore, *Gracilaria* sp. is a source of dietary fiber in analog rice, which contains 54.4 % galactan and 19.7 % (Rosemary *et al*., 2019).

3.4. Shape of analog rice

In general, the appearance of rice from all treatments was relatively the same. The shape of cooked rice is complete and resembles milled rice (Figure 1). Milled rice has a slightly oval shape and is whole when cooked. The addition of *Gracilaria* sp. also functions as a gelling agent so that when the cooking process, the shape of the rice produced is not lost (Figure 2). The addition of *Gracilaria* sp. also affects the appearance of analog rice. Agar cannot dissolve in cold water and, when heated, will form cross-links that affect the gelation process. After cooking, a single helix or double helix bond is formed. The helix bond will occur after folding and cooling (Tako *et al*., 2014). According to Ramadhan and Wini (2017), gelatin can form a triple helix network where the network can simultaneously trap water and reduce fluid flow from the dough so that it can strengthen the gel in a jam.

Figure 1. Analog rice shape

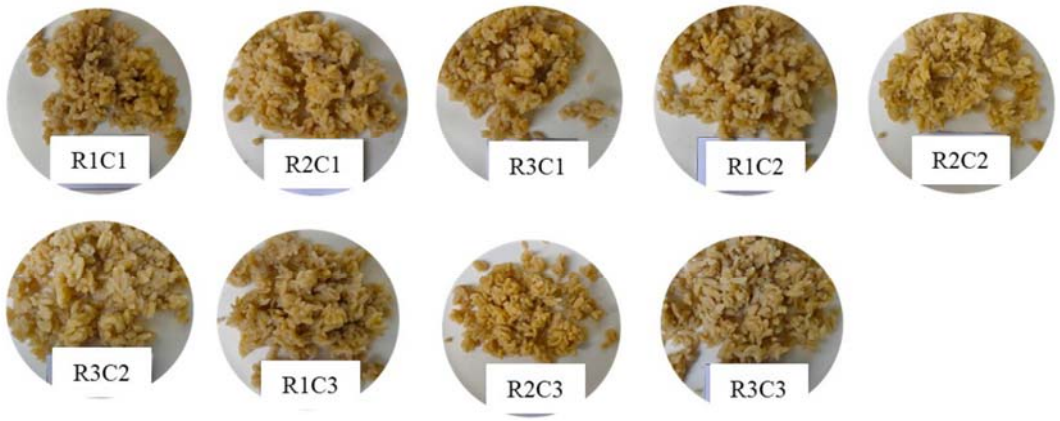

Figure 2. Rice shape from analog rice.

4. Conclusion

The results showed that increasing the proportion of modified arrowroot starch and the concentration of seaweed (*Gracilaria* sp.) porridge can reduce the water, fat, protein, and ash contents. The addition also enhances the resistant starch and allows an increase in antioxidant activity of analog rice after steaming. It is therefore conclusive that using modified arrowroot starch, corn flour, and the addition of *Gracilaria* sp. can improve the functional properties of analog rice.

Acknowledgements

The author would like to thank the Chancellor of the University of Muhammadiyah Malang, who has provided research funding assistance through the 2022 PKID Scheme and through the Rector's Decree number: E.2.a/334/BAA-UMM/IV/2022.

References

Adinurani PG. 2016. **Design and analysis of agrotrial data: Manual and SPSS**. Plantaxia, Yogyakarta, Indonesia

Anggraeni T. 2020. A Comparative study of Indonesian estimated rice production and consumption. *J. Anal. Kebijakan Pelayanan Publik.,* **6(2)** :101–112. https://doi.org/10.31947/jakpp.vi.9279

Anggraini T, Putri VJ, Neswati and Yuliani. 2016. Characteristics of red sweet potato (*Ipomea batatas*) analog rice (SPAR) from the addition of cassava flour (*Manihot utillisima*) and carrot (*Daucus carota*). *Int. J. Adv. Sci. Eng. Inf. Technol.,* **6(5)**, 723–728. http://dx.doi.org/10.18517/ijaseit.6.5.762

Aprianita A, Vasiljevic T, Banniko A and Kasapis S. 2014. Physicochemical properties of flours and starches derived from traditional Indonesian tubers and roots. *J. Food Sci. Technol.*, **51:**3669–3679. https://doi.org/10.1007/s13197-012-0915-5

Astuti RM, Widaningrum, Asiah N, Setyowati A and Fitriawati R. 2018. Effect of physical modification on granule morphology, pasting behavior, and functional properties of arrowroot (*Marantha arundinacea* L.) starch. *Food Hydrocoll.,* **81**:23–30. https://doi.org/10.1016/j.foodhyd.2018.02.029

Budijanto S and Yuliana ND. 2015. Development of rice analog as a food diversification vehicle in Indonesia. *Journal of Developments in Sustainable Agriculture,* **10(1)**:7–14. https://doi.org/10.11178/jdsa.10.7

Carlson JL, Erickson JM, Lloyd BB and Slavin JL. 2018. Health effects and sources of prebiotic dietary fiber. *Current Developments in Nutrition,* **2(3-**nzy005):1–8. https://doi.org/10.1093/cdn/nzy005

Central Bureau of Statistics. 2020. Harvest area, production, and rice productivity by Province 2018–2019. https://www.bps.go.id/indicator/53/1498/1/luas-panen-produksi-danproduktivitas-padi-menurut-provinsi.html.

Chan PT, Matanjun P, Yasir MS, and Tan TS . 2015. Antioxidant activities and polyphenolics of various solvent extracts of red seaweed, *Gracilaria changii*. *J. Appl. Phycol.*, **27(6)**: 2377–2386. https://doi.org/10.1007/s10811-014-0493-1

Chan PT and Matanjun P. 2017. Chemical composition and physicochemical properties of tropical red seaweed, *Gracilaria changii*. *Food Chem.,* **221**:302–310. https://doi.org/10.1016/j.foodchem.2016.10.066

Damat D. 2013. Effect of butyrylated arrowroot starch to the digesta profile and molar ratio SCFA. *J. Food Sci.,* **2(2)**:144–149.

Damat D, Anggriani R, Setyobudi RH and Soni P. 2019. Dietary fiber and antioxidant activity of gluten-free cookies with coffee cherry flour addition. *Coffee Sci.,* **14(4)**:493–500. http://dx.doi.org/10.25186/cs.v14i4

Damat D, Tain A, Handajani H, Chasanah U and Siskawardani DD. 2019. Functional cake characteristics of modified arrowroot starch (MAS) with the gelatinization-retrograde method. *IOP Conf. Ser.: Mater. Sci. Eng.,* **532(012017)**: 1–6. https://doi.org/10.1088/1757-899X/532/1/012017

Damat D, Setyobudi RH, Soni P, Tain A, Handjani H and Chasanah U. 2020. Modified arrowroot starch and glucomannan for preserving physicochemical properties of sweet bread. *Ciência e Agrotecnologia,* **44(014820):**1–9. https://doi.org/10.1590/1413-7054202044014820.

Damat D, Setyobudi RH, Utomo JS, Gaile ZV, Tain A and Siskawardani DD. 2021. The characteristics and predicted of glycemic index of rice analogue from modified arrowroot starch (*Maranta arundinaceae* L.). *Jordan J. Biol. Sci.,* **14(3):**389–393. http://jjbs.hu.edu.jo/vol14.htm

Dhital S, Warren FJ, Butterworth PJ, Ellis PR and Gidley MJ. 2017. Mechanisms of starch digestion by α-amylase—Structural basis for kinetic properties. *Crit. Rev. Food Sci. Nutr.,* **57(5)**:875–892. https://doi.org/10.1080/10408398.2014.922043

Dundar AN and Gocmen D. 2013. Effects of autoclaving temperature and storing time on resistant starch formation and its functional and physicochemical properties. *Carbohydr. Polym.,* **97(2)**:764–771. https://doi.org/10.1016/j.carbpol.2013.04.083

Espinosa SV, Zamudio FPB, Espino DM, Vela GG, RendonVJR, Hernandez GM, Henzandez CF, Lopez DLPHY, Salgado DR and Ortega OA. 2021. Physicochemical characterization of resistant starch type-iii (Rs3) obtained by *Autoclaving Malanga* (*Xanthosoma sagittifolium*) flour and corn starch. *Molecules*, **26(13)**: 1–13. https://doi.org/10.3390/molecules26134006

Ferng L, Liou CM, Yeh, R and Chen SH. 2016. Physicochemical property and glycemic response of chiffon cakes with different rice flours. *Food Hydrocoll.* **53**:172–179. https://doi.org/10.1016/j.foodhyd.2015.02.020

Frau F, Carate JNL, Salinas F and Pece N. 2021. Effect of vacuum packaging on artisanal goat cheeses during refrigerated storage. *Food Sci. Technol.,* **41(2)**. https://doi.org/10.1590/fst.36719

Hidayat B, Akmal S, Muslihudin M and Suhada B. 2017. Assessment of corn-based rice analogues made from modified corn flour and cassava starch which processed by granulation method as functional food. *Food Science and Quality Management,* **61**:19–24.

Joslowski G, Halim J, Goletzke J, Gow M, Ho M, C-Y Louie J, Buyken AE, Cowell CT and Garnett SP. 2015. Dietary glycemic load, insulin load, and weight loss in obese, insulin resistant adolescents: Resist study. *Clin Nutr*, **34(1)**: 89–94. https://doi.org/10.1016/j.clnu.2014.01.015

Khan BM, Mai QH, Wang XF, Liu ZY, Zhang JY, Guo YJ, Chen WZ, Liu Y and Cheong KL. 2019. Physicochemical characterization of Gracilaria chouae sulfated polysaccharides and their antioxidant potential. *Int. J. Biol. Macromol.* **134:** 255–261. https://doi.org/10.1016/j.ijbiomac.2019.05.055

Lin CL, Lin JH, Lin JJ and Chang YH. 2020. Properties of high-swelling native starch treated by heat–moisture treatment with different holding times and iterations. *Molecules*, **25(23)**: 1–12. https://doi.org/10.3390/molecules25235528

Liu H, Iv M, Wang L and Li Y. 2016. Comparative study: How annealing and heat-moisture treatment affect the digestibility, textural, and physicochemical properties of maize starch. *Starke*, **68(11–12)**:1158–1168. https://doi.org/10.1002/star.201500268

McCleary BV, McLoughlin C, Charmier LMJ and McGeough P. 2020. Measurement of available carbohydrates, digestible, and resistant starch in food ingredients and products. *Cereal Chem.*, **97(1)**: 114–137. https://doi.org/10.1002/cche.10208

Mishra A, Mishra HN and Rao PS. 2012. Preparation of rice analogues using extrusion technology. *Int. J. Food Sci. Technol.*, **47(9)**:1789–1797. https://doi.org/10.1111/j.1365-2621.2012.03035.x

Pasquale DI, Verni M, Verardo V, Caravaca AMG and Rizzello CG. 2021. Nutritional and functional advantages of the use of fermented black chickpea flour for semolina-pasta fortification. *Foods*, **10(1)**:1–21. https://doi.org/10.3390/foods10010182

Pudjihastuti I, Sumardiono S, Supriyo E and Kusumayanti H. 2019. Analog rice made from cassava flour, corn and taro for food diversification. *E3S Web Conf.*, **125(03010)**:1–4. https://doi.org/10.1051/e3sconf/201912503010

Purwaningsih S, Santoso J, Handharyani E, Setiawan NP and Deskawati E. 2020. Artificial rice from *Gracillaria* sp. as functional food to prevent diabetes. *IOP Conf. Ser: Earth Environ. Sci.* **414(012017)**: 1–7. https://doi.org/10.1088/1755-1315/414/1/012017

Putri ECJ and Sumardiono S. 2020. Analog rice production of composite materials flour (cassava, avocado seeds, and tofu waste) for functional food. *AIP Conf Proc,* **2197(070005).** https://doi.org/10.1063/1.5140938

Ramadhan W, and Wini T. 2017. Formulation of hydrocolloid-Agar, sucrose, and acidulant on jam leather product development. *Jurnal Pengolahan Hasil Perikanan Indonesia*. **20(1)**:95–108. https://doi.org/10.17844/jphpi.v20i1.16495 .

Ratnaningsih, Nilasari R and Purwani EY. 2019. Bread quality of pre-gelatinized cassava flour with frozen storage. *IOP Conf. Ser.: Earth Environ. Sci.*, **309(012051)**:1–7. https://doi.org/10.1088/1755-1315/309/1/012051

Rocha CMR, Sousa AMM, Kim JK, Magalhaes JMCS, Yarish C and Goncalves MDP. 2019. Characterization of agar from *Gracilaria tikvahiae* cultivated for nutrient bioextraction in open water farms. *Food Hydrocoll.*, **89**:260–271. https://doi.org/10.1016/j.foodhyd.2018.10.048

Rosemary T, Arulkumar A, Paramasivam S, Porticarrero AM and Miranda JM. 2019. Biochemical, micronutrient and physicochemical properties of the dried red seaweeds *Gracilaria edulis* and *Gracilaria corticata*. *Molecules*, **24(12)**:1–14. https://doi.org/10.3390/molecules24122225

Saari H, Fuentes C, Sjoo M, Rayner M and Wahlgren M. 2017. Production of starch nanoparticles by dissolution and non-solvent precipitation for use in food-grade pickering emulsions. *Carbohydr. Polym.*, **157**:558–566. https://doi.org/10.1016/j.carbpol.2016.10.003

Saluri K and Tuvikene R. 2020. Anticoagulant and antioxidant activity of lambda- and theta-carrageenans of different molecular weights. *Bioact. Carbohydr. Diet. Fibre*, **24**: 100243. https://doi.org/10.1016/j.bcdf.2020.100243

Sedjati S, Pringgenies D and Fajri M. 2020. Determination of the pigment content and antioxidant activity of the marine microalga *Tetraselmis suecica*. *Jordan J. Biol. Sci.*, **13(1):**55–58.

Setyobudi RH, Zalizar L, Wahono SK, Widodo W, Wahyudi A, Mel M, Prabowo B, Jani Y, Nugroho YA, Liwang T and Zaebudin A. 2019. Prospect of Fe non-heme on coffee flour made from solid coffee waste: Mini review. *IOP Conf. Ser. Earth Environ. Sci.*, **293 (012035)**:1–24. https://doi.org/10.1088/1755-1315/293/1/012035.

Setyobudi RH, Yandri E, Nugroho YA, Susanti MS, Wahono SK, Widodo W, Zalizar L, Saati EA, Maftuchah M, Atoum MFM, Massadeh MI, Yono D, Mahaswa RK, Susanto H, Damat D, Roeswitawati D, Adinurani PG and Mindarti S. 2021. Assessment on coffee cherry flour of Mengani Arabica Coffee, Bali, Indonesia as iron non-heme source. *Sarhad J. Agric.*, **37(Special issue 1)**: 171–183. https://dx.doi.org/10.17582/journal.sja/2022.37.s1.171.183

Setyobudi HS, Atoum MFM, Damat D, Yandri E, Nugroho YA, Susanti MS, Wahono SK, Widodo W, Zalizar L, Wahyudi A, Saati EA, Maftuchah M, Hussain Z, Yono D, Harsono SS, Mahaswa RK, Susanto H, Adinurani PA, Ekawati I, Fauzi A and Mindarti S. 2022. Evaluation of coffee pulp waste from coffee cultivation areas in Indonesia as iron booster. *Jordan J. Biol. Sci.*, **15(3)**: 475–488. https://doi.org/10.54319/jjbs/150318

Sreejamole KL and Greeshma PM. 2013. Antioxidant and brine shrimp cytotoxic activities of ethanolic extract of red alga *Cracilaria corticata* (J. Agardh). *Indian J Nat Prod Resour*, **4(3)** :233–237.

Sumardiono S, Pudjihastuti I, Poerwoprajitno AR and Suswadi MS. 2014. Physichocemical properties of analog rice from composite flour: Cassava, green bean and hanjeli. *World Appl. Sci. J.,* **32(6)**:1140–1146. http://dx.doi.org/10.5829/idosi.wasj.2014.32.06.708

Tako M, Tamaki Y, Teruya T and Takeda Y. 2014. The principles of starch gelatinization and retrogradation. *Food Sci. Nutr.*, **05(03)**:280–291. https://doi.org/10.4236/fns.2014.53035

Queralt VA, Regueiro J, Alvarenga JFR, Huelamo MM, Leal LN and Raventos PML. 2015. Characterization of the phenolic and antioxidant profiles of selected culinary herbs and spices: caraway,

turmeric, dill, marjoram and nutmeg. *Food Sci. Technol.*. **35(1)**:189–195. https://doi.org/10.1590/1678-457X.6580

Verni M, Verardo V and Rizzello CG. 2019. How fermentation affects the antioxidant properties of cereals and legumes. *Foods*. **8(9):**362–383. https://doi.org/10.3390/foods8090362

Vrancheva R, Popova A, Mihaylova D and Krastanov A. 2020. Phytochemical analysis, in vitro antioxidant activity and germination capability of selected grains and seeds. *Jordan J. Biol. Sci.*, **13(3)**: 337–342.

Wahjuningsih SB, Haslina, Untari S and Wijanarka A. 2018. Hypoglycemic effect of analog rice made from modified cassava flour (Mocaf), arrowroot flour and kidney bean flour on STZ-NA induced diabetic rats. *Asia Pac. J. Clin. Nutr.*, **10(1)**:8–15. http://doi.org/10.3923/ajcn.2018.8.15

Wahjuningsih SB, Marsono Y, Praseptingga D, Haryanto B and Azkia MH. 2020. Organoleptic, chemical, and physical characteristics of sago (*Metroxylon* spp.) analog rice supplemented with red bean (*Phaseolus vulgaris*) flour as a functional food. *Int. J. Adv. Sci. Eng. Inf. Technol.*, **10(3)**:1289–1296. http://dx.doi.org/10.18517/ijaseit.10.3.11098

Wahjuningsih SB and Susanti S. 2018. Chemical, physical, and sensory characteristics of analog rice developed from the mocaf, arrowroof, and red bean flour. *IOP Conf. Ser.: Earth Environ. Sci.*, **102(012015)**: 1–10. https://doi.org/10.1088/1755-1315/102/1/012015

Yu K, Ke MY, Li WH, Zhang SQ and Fang XC. 2014. The impact of soluble dietary fibre on gastric emptying, postprandial blood glucose and insulin in patients with type 2 diabetes. *Asia Pac. J. Clin. Nutr.*, **23(2)**:210–218. https://doi.org/10.6133/apjcn.2014.23.2.01

Zhang K, Jia X, Zhu Z and Xue W. 2020. Physicochemical properties of rice analogs based on multi-level: Influence of the interaction of extrusion parameters. *Int. J. Food Prop.*, **23(1)**:2033–2049. https://doi.org/10.1080/10942912.2020.1840389

Subscription

Jordan Journal of Biological Sciences

An International Peer – Reviewed Research Journal

Published by the Deanship of Scientific Research, The Hashemite University, Zarqa, Jordan

Name: ..... الاسم:

Specialty: ..... التخصص:

Address: ..... العنوان:

P.O. Box: ..... صندوق البريد:

City &Postal Code:..... المدينة: الرمز البريدي:

Country: ..... الدولة:

Phone: ..... رقم الهاتف

Fax No.: ..... رقم الفاكس:

E-mail: ..... البريد الإلكتروني:

Method of payment: ..... طريقة الدفع:

Amount Enclosed: ..... المبلغ المرفق:

Signature: ..... التوقيع:

Cheque should be paid to Deanship of Research and Graduate Studies – The Hashemite University.

I would like to subscribe to the Journal

For

- ☐ One year
- ☐ Two years
- ☐ Three years

One Year Subscription Rates

	Inside Jordan	Outside Jordan
Individuals	JD10	$70
Students	JD5	$35
Institutions	JD 20	$90

Correspondence

Subscriptions and sales:

The Hashemite University
P.O. Box 330127-Zarqa 13115 – Jordan
Telephone: 00 962 5 3903333
Fax no. : 0096253903349
E. mail: jjbs@hu.edu.jo

المجلة الأردنية للعلوم الحياتية
Jordan Journal of Biological Sciences (JJBS)

http://jjbs.hu.edu.jo

المجلة الأردنية للعلوم الحياتية: مجلة علمية عالمية محكمة ومفهرسة ومصنفة، تصدرعن الجامعة الهاشمية وبدعم من صندوق دعم البحث العلمي والإبتكار – وزراة التعليم العالي والبحث العلمي.

ترسل البحوث الى العنوان التالي:

رئيس تحرير المجلة الأردنية للعلوم الحياتية
الجامعة الهاشمية
ص.ب , 330127 , الزرقاء, 13115 , الأردن
هاتف: 0096253903333
E-mail: jjbs@hu.edu.jo, Website: www.jjbs.hu.edu.jo

المملكة الأردنية الهاشمية

المجلة الأردنية

للعلوم الحياتية

مجلة علمية عالمية محكمة

تصدر بدعم من صندوق دعم البحث العلمي و الابتكار

http://jjbs.hu.edu.jo/